Carbon Materials: Chemistry and Physics 6
Series Editors: Franco Cataldo · Paolo Milani

Mircea Vasile Diudea
Csaba Levente Nagy *Editors*

Diamond and Related Nanostructures

Springer

Diamond and Related Nanostructures

CARBON MATERIALS: CHEMISTRY AND PHYSICS

A comprehensive book series which encompasses the complete coverage of carbon materials and carbon-rich molecules from elemental carbon dust in the interstellar medium, to the most specialized industrial applications of the elemental carbon and derivatives. A great emphasis is placed on the most advanced and promising applications ranging from electronics to medicinal chemistry. The aim is to offer the reader a book series which not only consists of self-sufficient reference works, but one which stimulates further research and enthusiasm.

Series Editors

Dr. Prof. Franco Cataldo
Via Casilina 1626/A,
00133 Rome, Italy

Professor Paolo Milani
University of Milan
Department of Physics
Via Celoria, 26
20133, Milan, Italy

VOLUME 6:
DIAMOND AND RELATED NANOSTRUCTURES

Volume Editors

Prof. Dr. Mircea Vasile Diudea
Dr. Csaba Levente Nagy
Faculty of Chemistry and Chemical Engineering
Babes-Bolyai University
Cluj-Napoca
Arany Janos street 11
Romania

For further volumes:
http://www.springer.com/series/7825

Mircea Vasile Diudea • Csaba Levente Nagy
Editors

Diamond and Related Nanostructures

Springer

Editors
Mircea Vasile Diudea
Faculty of Chemistry and Chemical Engineering
Babes-Bolyai University
Cluj-Napoca
Romania

Csaba Levente Nagy
Faculty of Chemistry and Chemical Engineering
Babes-Bolyai University
Cluj-Napoca
Romania

ISSN 1875-0745 ISSN 1875-0737 (electronic)
ISBN 978-94-007-6370-8 ISBN 978-94-007-6371-5 (eBook)
DOI 10.1007/978-94-007-6371-5
Springer Dordrecht Heidelberg New York London

Library of Congress Control Number: 2013938405

Printed on acid-free paper

Springer is part of Springer Science+Business Media (www.springer.com)

Preface

Diamond is renowned for its beauty as well as for its superlative physical qualities. The rigor of its composition determines its exceptional thermal conductivity and hardness, traits that have found numerous industrial applications (e.g., as heatsink in electronics and in cutting, drilling, or polishing) and boosted the demand for diamond and diamond-like carbon.

A diamond crystal is in fact one molecule with macroscopic dimensions. When moving from molecules to materials, the model representing primary atomic arrangements undergoes transformations both in concept and experimental realization, as well as in the computational treatment. Following the latest developments and discoveries in the field, this book provides a thorough description of the diamond (and its relatives) in different hypostases.

Chapter 1 introduces the classical diamond through the eye of a chemist. Here the basic molecular substructures, adamantane and diamantane, are presented when they group together to build the star of materials: the diamond (indicated in our book as D_6).

Chapter 2 examines the synthesis by chemical vapor deposition of diamond (and diamond-like carbon) films deposited on various surfaces and the analysis of these deposits.

Chapter 3 introduces the chemistry of a new diamond, named diamond D_5, which is suggested being seeded by the small cage C_{17}.

Chapter 4 describes some exotic carbon clathrates with sp^3 carbon networks and calculates their electronic structure.

Chapter 5 analyzes the diamond D_5, a hyper-diamond structure with both translational and rotational symmetry, as encountered in quasicrystals.

Chapter 6 presents the fivefold symmetry which dominates the newly discovered world of quasicrystals. Such symmetry is built up by self-assembly of small cages, eventually called fullerenes, that form larger spherical multi-shell cages whose energetics is described.

Chapter 7 is drawn on the seed C_{17} and other substructures of D_5 to evaluate their thermal stability.

Chapter 8 calculates the energetics and topology of lattices built up by nanotube junctions, as observed in diamond-related networks consisting of sp^2 carbon.

Chapters 9 and 10 provide graph theoretical descriptions, in terms of counting polynomials, of the classical diamond and some newer diamondoids.

Chapter 11 describes nanotube junctions that could join to form a hypergraphene.

Chapter 12 presents polybenzenes, diamond-like structures with benzene-patched sp^2 networks.

Chapter 13 analyzes fullerenes with negative curvature that could be involved in the construction of some carbon phases.

Chapter 14 offers an algebraic approach to the design of molecules having non-crystallographic symmetry.

Chapter 15 discusses carbon networks in the solid state, approached by DFT calculations.

Chapter 16 examines the diamond network drawing by using topological coordinates.

Chapter 17 treats the problem of filling the Euclidean space via a higher-dimensional space and non-crystallographic symmetries, as encountered in quasicrystals.

Chapter 18 gives a mathematical approach, in terms of group theory, to the symmetries encountered in the diamond D_5.

Finally, Chapter 19 provides a gallery of new structures, either space filled or spongy ones, possibly populating the quasicrystal world.

This unique volume brings together the major findings on the subject and will therefore be a source of inspiration and understanding for advanced undergraduates, graduates, and researchers with an interest in physics, graph theory, crystallography, and computational and synthetic chemistry.

Cluj-Napoca, Romania
December 11, 2012

Mircea V. Diudea
Csaba L. Nagy

Acknowledgements

We would like to thank Franco Cataldo and Paolo Milani, series editors of "Carbon Materials: Chemistry and Physics" series, for ably identifying the need of a book on Diamond and Related Nanostructures.

We acknowledge Nadia Rojo and Ilaria Tassistro for their technical assistance.

Last but not least, our warmest thanks go to all the respected contributors of this book.

Cluj-Napoca, Romania
December 11, 2012

Mircea V. Diudea
Csaba L. Nagy

Contents

Contributors

A.R. Ashrafi Department of Nanocomputing, Institute of Nanoscience and Nanotechnology, University of Kashan, Kashan, I. R. Iran

Department of Mathematics, Faculty of Mathematical Sciences, University of Kashan, Kashan, I. R. Iran

Alexandru T. Balaban Department of Marine Sciences, Texas A&M University at Galveston, Galveston, TX, USA

Attila Bende Molecular and Biomolecular Physics Department, National Institute for R&D of Isotopic and Molecular Technologies, Cluj-Napoca, Romania

Giorgio Benedek Dipartimento di Scienza dei Materiali, Universitá di Milano-Bicocca, Milan, Italy

Donostia International Physics Center (DIPC), University of the Basque Country (UPV-EHU), Donostia – San Sebastián, Spain

Marco Bernasconi Dipartimento di Scienza dei Materiali, Universitá di Milano-Bicocca, Milan, Italy

Virginia Bucila Department of Chemistry, Faculty of Chemistry and Chemical Engineering, Babes-Bolyai University, Cluj, Romania

Marzio de Corato Dipartimento di Scienza dei Materiali, Universitá di Milano-Bicocca, Milan, Italy

Centro S3, CNR-Istituto Nanoscienze, I-41125 Modena, Italy

Dipartimento di Fisica, Universitá di Modena-Reggio Emilia, Modena, Italy

Michel Deza Ecole Normale Superieure, Paris, France

Mircea V. Diudea Department of Chemistry, Faculty of Chemistry and Chemical Engineering, Babes-Bolyai University, Cluj, Romania

Mahmood Ghoranneviss Plasma Physics Research Center, Science and Research Branch, Islamic Azad University, Tehran, Iran

Aleksandar Ilić Department of Computer Science, Faculty of Sciences and Mathematics, University of Niš, Niš, Serbia

Aneta Jezierska-Mazzarello Faculty of Chemistry, University of Wrocław, Wrocław, Poland

Zahra Khalaj Plasma Physics Research Center, Science and Research Branch, Islamic Azad University, Tehran, Iran

F. Koorepazan-Moftakhar Department of Mathematics, Faculty of Mathematical Sciences, University of Kashan, Kashan, I. R. Iran

Dietmar Kuck Department of Chemistry, Bielefeld University, Bielefeld, Germany

István László Department of Theoretical Physics, Institute of Physics, Budapest University of Technology and Economics, Budapest, Hungary

A.L. Mackay Lanchester Road, London, UK

Birkbeck College, University of London, Bloomsbury, London, England

Mihai Medeleanu Department of Applied Chemistry and Organic and Natural Compounds Engineering, Faculty of Industrial Chemistry and Environmental Engineering, University "Politehnica" Timisoara, Timisoara, Romania

Csaba L. Nagy Department of Chemistry, Faculty of Chemistry and Chemical Engineering, Babes-Bolyai University, Cluj, Romania

Katalin Nagy Department of Chemistry, Faculty of Chemistry and Chemical Engineering, Babes-Bolyai University, Cluj, Romania

Jarosław J. Panek Faculty of Chemistry, University of Wrocław, Wrocław, Poland

Tomaž Pisanski Department of Mathematics, Faculty of Mathematics and Physics, University of Ljubljana, Ljubljana, Slovenia

Oana Ponta Department of Condensed State Physics and Advanced Technologies, Faculty of Physics, Babes-Bolyai University, Cluj, Romania

Davide M. Proserpio Dipartimento di Chimica, Universitá degli Studi di Milano, Milan, Italy

Vladimir R. Rosenfeld Mathematical Chemistry Group, Department of Marine Sciences, Texas A&M University at Galveston, Galveston, USA

Instituto de Ciencias Matematicas (ICMAT) CSIC, Madrid, Spain

Mahboubeh Saheli Department of Mathematics, University of Kashan, Kashan, I. R. Iran

V.Ya. Shevchenko Institute of Silicate Chemistry RAS, Saint-Petersburg, Russia

Mikhail Shtogrin Steklov Mathematical Institute, Demidov Yaroslavl State University, Yaroslavl, Moscow, Russia

Mathieu Dutour Sikirić Department of Marine and Environmental Research, Institut Rudjer Boskovic, Zagreb, Croatia

M. Stefu Department of Chemistry, Faculty of Chemistry and Chemical Engineering, Babes-Bolyai University, Cluj, Romania

Beata Szefler Department of Physical Chemistry, Collegium Medicum, Nicolaus Copernicus University, Bydgoszcz, Poland

Elnaz Vaghri Plasma Physics Research Center, Science and Research Branch, Islamic Azad University, Tehran, Iran

G.V. Zhizhin Institute of Silicate Chemistry RAS, Saint-Petersburg, Russia

Chapter 1
Diamond Hydrocarbons and Related Structures

Alexandru T. Balaban

Abstract Among the two long-known allotropic forms of carbon, sp^2-hybridized multilamellar graphite is the thermodynamic stable form at normal temperature and pressure, whereas the denser sp^3-hybridized diamond becomes favored at very high pressures. Portions of graphene sheets with dangling bonds connected with hydrogen atoms are planar polycyclic benzenoid hydrocarbons (benzenoids). Similarly, portions of the diamond lattice with dangling bonds connected with hydrogen atoms are diamond hydrocarbons (diamondoids). Dualists of benzenoids consist of vertices in the centers of benzenoid rings and of edges connecting vertices corresponding to benzenoid rings sharing CC bonds. Analogously, dualists of diamondoids consist of vertices in the centers of adamantane units and of edges connecting vertices corresponding to adamantane units sharing six-membered rings. The diamond lattice is self-dual, whereas the honeycomb (hexagonal) and the triangular lattices are reciprocally dual. Encoding benzenoid structures can be achieved by using digits 0, 1, and 2, whereas encoding diamondoid structures (ignoring stereoisomers) can be achieved by using digits 1, 2, 3, and 4. The naming and encoding of diamondoid structures according to the Balaban-Schleyer proposal has now been generally accepted. The discovery and isolation of lower diamondoids in petroleum allowed a recent surge of interest in their properties and applications. Successive sections of this chapter are presenting regularities in the diamond lattice, where Cartesian coordinates can be integers. Then dualists of benzenoids followed by dualists of diamondoids are discussed, with similarities and differences. The latter dualists can be conveniently viewed as staggered rotamers of alkanes. By analogy with benzenoid catafusenes, perifusenes, and coronoids, dualists allow the classification of diamondoids into regular/irregular catamantanes

A.T. Balaban (✉)
Department of Marine Sciences, Texas A&M University at Galveston,
Galveston 77553, TX, USA
e-mail: balabana@tamug.edu

M.V. Diudea and C.L. Nagy (eds.), *Diamond and Related Nanostructures*,
Carbon Materials: Chemistry and Physics 6, DOI 10.1007/978-94-007-6371-5_1,

(with acyclic dualists), perimantanes, and coronamantanes (with 6-membered or larger rings, respectively). This analogy allows a simple enumeration of all possible constitutional isomers of diamondoids. Stereoisomers of the chiral diamondoids are also discussed. The history of diamondoids is briefly discussed. A recently proposed partitioned-formula periodic table for diamondoids presents interesting symmetries, especially for regular catamantanes. On the basis of distance matrices for diamondoid dualists, one can obtain molecular invariants characterizing diamondoid structures. With such invariants, it was possible to rationalize HPLC and GC-MS chromatographic data for naturally occurring diamondoids. Finally, the chemical functionalization of diamondoids for various applications carried out by Schreiner and his coworkers is reviewed.

1.1 Introduction: Carbon Allotropes

Instead of the impersonal style that is customary for journal articles leading to awkward phrases in which authors refer to themselves using the 3rd person singular, in this book chapter, I will not shy from using the 1st person singular.

Although the element carbon occupies the 14th place (0.08 %) among other elements on earth's crust, oceans, and atmosphere, its importance for life places it at the top. Its electronegativity and atomic radius are midway between the extremes, so that carbon can combine with itself, forming stable covalent chains irrespective of their length. One other element, namely divalent sulfur, shares this property, but the results are only various allotropic forms of the element sulfur, unlike the infinite variety of organic and inorganic structures based on carbon chains. Alternating Si–O atom pairs also provide a rich assortment of structures characterizing most of the rocks in earth's crust.

The two long-known, naturally occurring carbon allotropes, namely diamond and multilayer graphite, have sp^3- and sp^2-hybridized carbon atoms, respectively. Their properties are in sharp contrast, as seen in Table 1.1. Diamond has a three-dimensional lattice in which each carbon atom has tetrahedral configuration with bond lengths of 1.54 Å and bond angles $\alpha = 109.5°$ ($\cos\alpha = -1/3$; $\mathrm{tg}(\alpha/2) = \sqrt{2}$). Graphite has two-dimensional planar layers of benzenoid rings whose carbon atoms

Table 1.1 Contrasting properties of diamond and multilayer graphite

Property	Diamond	Multilayer graphite
Aspect	Transparent, highly refractive	Opaque, black
Crystalline system	Cubic	Hexagonal
Density ($g \times cm^{-3}$)	3.514	2.266
Hardness (Mohs scale)	10	Between 1 and 2
Electrical conductivity	Low	High
Thermal conductivity	High	Low
Thermodynamic stability	Unstable	Stable

are 1.42 Å apart with bond angles of 120°; the interlayer distance is 3.35 Å. In this context, one should mention that graphite is converted under high pressure into synthetic diamond at temperatures around 2,000 °C. The thermodynamic instability of diamond at room temperature should allow its conversion into graphite (as described in 1884 by Jules Verne and Paschal Grousset in *The Southern Star*), but actually the activation energy is so high that diamonds *are almost* forever; nevertheless, this conversion can be carried out by heating diamond at 1,000 °C in the absence of oxygen. One should be aware that the high energy of dangling bonds at graphite sheet edges can be overcome by inter-sheet forces only for huge numbers and dimensions of sheets; otherwise, for relatively small numbers of carbon atoms (10^3–10^4), the stable forms are the third allotropic forms (fullerene onion-like spheroidal or nanotubular particles).

Because of these superficial dangling bonds that are normally occupied by hydrogen atoms, one can consider that diamond is an "honorary saturated hydrocarbon" and graphite an "honorary peri-condensed aromatic hydrocarbon" with negligibly small hydrogen-to-carbon ratios. By analogy with heavier stable nuclides whose nuclei must contain much larger numbers of neutrons than protons, one can also consider that dwarf neutron stars are "honorary superheavy atomic nuclei" with negligibly small proton-to-neutron ratios.

Natural diamonds are believed to have formed deep in the earth at high pressure and temperature; then tectonic processes have brought them in certain places closer to the surface. Each diamond crystal is one molecule with macroscopic dimensions.

With perfect sp^2-hybridization, a unilayer planar carbon sheet (called *graphene* by Boehm et al. 1962, 1994) was first obtained by Geim and Novoselov (2007), who were awarded the 2010 Nobel Prize for Physics for their studies of this material which is one-atom thick and has numerous applications owing to its amazing properties. Each graphene sheet is also one macromolecule.

The large family of the third allotropic form of carbon known as fullerenes is quasi-spherical polyhedra consisting of benzenoid rings plus 12 pentagons. They were discovered in 1985 by Kroto, Smalley, and Curl who used mass spectrometry and who were awarded the 1996 Nobel Prize for Chemistry (Curl 1997; Kroto 1997; Smalley 1997). All lower fullerenes obey the "isolated pentagon rule" starting with buckminsterfullerene C_{60} (truncated icosahedron, an Archimedean solid or semiregular polyhedron) and followed by C_{70}. Double-capped single-wall nanotubes are fullerenes with oblong structure. After Krätschmer and Huffman extracted fullerenes from soot by appropriate solvents (Krätschmer et al. 1990), research on fullerenes increased immediately.

Open-ended single-wall cylindrical carbon nanotubes (SWNTs, resulting by theoretical folding of graphene sheets) were prepared in 1991 by Ijima (1991) (earlier reports by Russian scientists in 1952 (Radushkevich and Lukyanovich 1952) and by other Japanese scientists (Oberlin et al. 1976) in 1976 were largely ignored). According to Coxeter's vectors m and n on the honeycomb crystal lattice (Coxeter 1971), one can fold graphene sheets to yield a zigzag SWNT when $m = 0$, an armchair SWNT when $m = n$, and a chiral SWNT when $m \neq n$. Differences in

bandgap and electrical conductance between these three types of nanotubes can be correlated with $|m–n|$ values: only when this difference is a multiple of 3 do circles in Clar structures (Clar 1972) overlap in congruent fashion on folding the graphene sheet; other foldings of graphene sheets explain similarly property differences among nanocones or nanotori (Balaban and Klein 2009; Klein and Balaban 2011; Balaban 2011). Whereas many fullerenes such as C_{60} and C_{70} can be prepared as *substances* (pure compounds with identical molecules), so far SWNT are *mixtures* of similar but different molecules, like many natural and synthetic polymers.

In addition to these four classes of carbon allotropes (graphite-graphene, diamond, fullerenes, and nanotubes), one should mention the existence of (1) amorphous carbon; (2) lonsdaleite, found in meteorites (Frondel and Marvin 1967; Pan et al. 2009; Bundy 1967; He et al. 2002), a relative of diamond (whereas in diamond all hexagons are in chair conformation with staggered C–C bonds, in lonsdaleite some 6-membered rings have eclipsed bonds as in wurtzite or iceane); and (3) other predicted carbon nets (Sheng et al. 2011; Zhu et al. 2011), such as Diudea's diamond D_5 (Diudea 2010; Diudea et al. 2011; Diudea and Nagy 2012).

Finally, one should discuss whether we can have a one-dimensional sp-hybridized carbon allotrope (a mythical polyyne allotrope, often mentioned in the literature as carbyne, a long chain of triply bonded carbon atoms, or a long cumulene) (Kroto 2010; Heimann et al. 1999; Baughman 2006; Itzhaki et al. 2005; Chalifoux and Tykwinski 2009; Lagow et al. 1995; Xue et al. 2004; Tobe and Wakabayashi 2005). The detection of interstellar and circumstellar molecules by radio, microwave, or infrared spectroscopy led to the identification of polyynes and their nitrile or dinitrile derivatives. However, one must take into account that these molecules are not in condensed phase. Acetylene is explosive when compressed (therefore it can be stored at higher pressure only in solution) and polyacetylenes even more so. The huge energy release on polymerization of polyynes makes their existence unlikely in condensed phase (Heimann et al. 1999). Several structures $R–(C{\equiv}C)_n–R$ with various bulky or electron-acceptor end-caps R have been synthesized for $n < 45$, but this seems to be the approximate limit.

1.2 The Three-Dimensional Diamond Lattice

Vertices of the diamond lattice can be given integer coordinates by using a cubical unit cell four units across. With these coordinates, the points of the structure have coordinates (x, y, z) in the Euclidean three-dimensional space satisfying the equations

$$x = y = z (\mathrm{mod}\, 2) \text{ and}$$

$$x + y + z = 0 \text{ or } 1 (\mathrm{mod} 4).$$

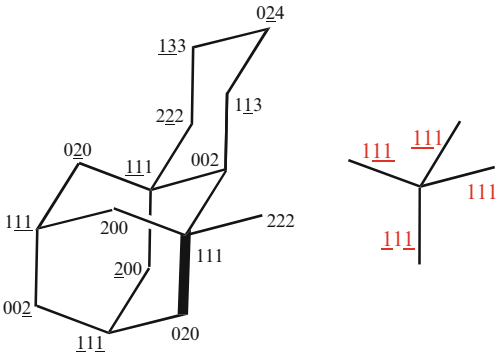

Fig. 1.1 Integer coordinates (*xyz*) for carbon atoms in the diamond lattice. *Left*: carbon atom coordinates for an adamantane unit with a fused 6-membered ring and one attached carbon atom (*minus signs* are represented by underlined digits). *Right*: ongoing from the central vertex to its four neighboring vertices, the *red numbers* indicate changes in the *xyz* coordinates

There are eight points (modulo 4) that satisfy these conditions:

$$(0, 0, 0), (0, 2, 2), (2, 0, 2), (2, 2, 0), (3, 3, 3), (3, 1, 1), (1, 3, 1), \text{and } (1, 1, 3).$$

All of the other points in the integer lattice may be obtained by adding multiples of four to the coordinates x, y, and z of these eight points. In this integer lattice, adjacent points connected by C–C bonds are at distance $\sqrt{3}$ apart. A triplet of even numbers is always connected with a triplet of odd numbers. In Figs. 1.1 and 1.2, one can see this diamond lattice with integer coordinates. For economy of space, minus signs are written under each digit, instead of being placed before each digit. In Fig. 1.2, full red lines delineate adamantane units, and blue dashed lines indicate cubic cells.

The origin of the rectangular Cartesian axes has been arbitrarily selected to coincide with the center of an octahedral "empty" space inside a central adamantane cell, and the coordinate axes are along the directions to the corners of the octahedron.

An interesting feature of the smallest unit (the adamantane scaffold) with its ten carbon atoms is the fact that six of these atoms symbolized by vertices (points) of the lattice form an "empty" regular octahedron, whereas the other four points lie at the centers of four regular tetrahedra fused to four alternant faces of the total of eight octahedron faces. This fusion yields a larger tetrahedron, with doubled linear extensions. It is known that the dihedral angle of the octahedron is α, whereas the dihedral angle of the tetrahedron is $\beta = 180° - \alpha$, so that the three-dimensional space can be filled by an assortment of octahedra and tetrahedra sharing faces, with two octahedra sharing an edge (Fig. 1.3).

In Table 1.2, one may see the coordinates of the carbon atoms at the eight corners of the cube situated on the right side of Fig. 1.2; the two parts of this table are for vertices of virtual tetrahedra within the cube.

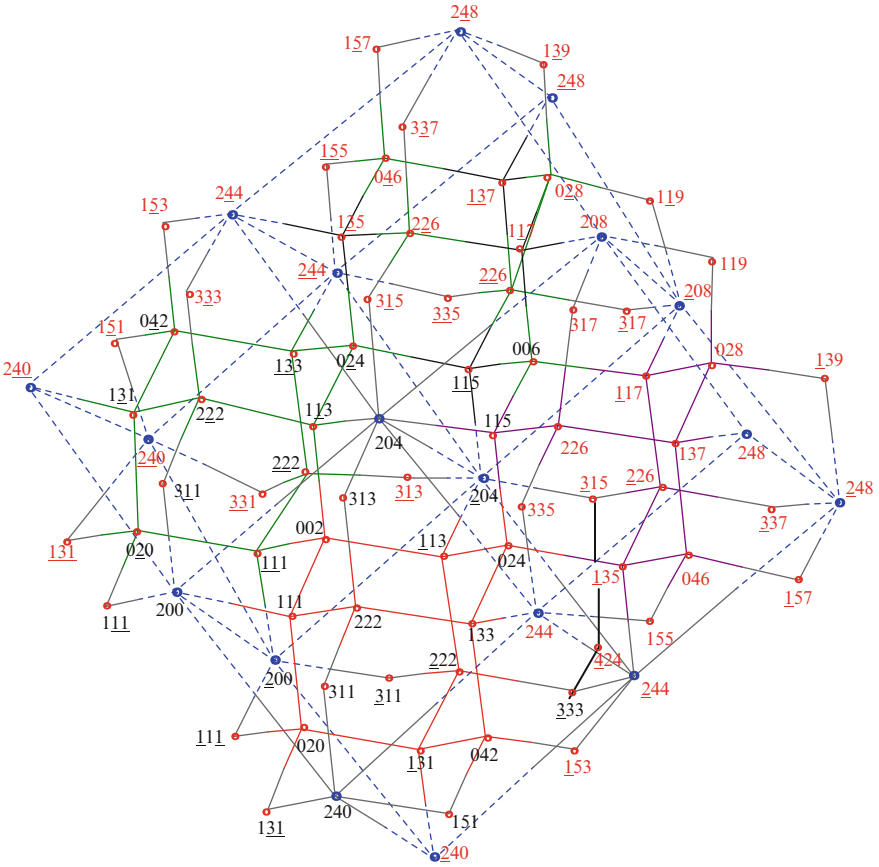

Fig. 1.2 Integer coordinates for the diamond lattice; four cubic cells are shown with *blue dashed lines* and C–C bonds by *red lines*. *Minus signs* are indicated under the corresponding digits

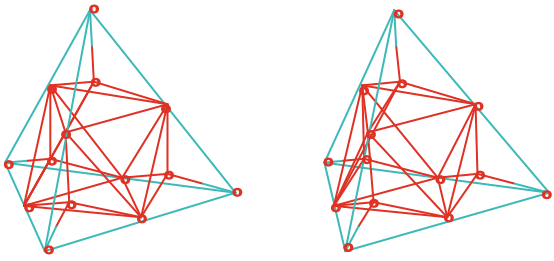

Fig. 1.3 Stereo view of one adamantane cell with an octahedron and four tetrahedra

Table 1.2 Integer coordinates for C atoms at cube corners in Fig. 1.2

x	y	z
−2	0	8
2	4	8
2	0	4
−2	4	4
2	0	8
−2	4	8
−2	0	4
2	4	4

1.3 Dualists of 2D Polycyclic Aromatic Hydrocarbons (Benzenoids)

In 1968, I published with two coworkers a theoretical estimation of possible new two-dimensional and three-dimensional carbon lattices and nets (Balaban et al. 1968). In what started a fruitful collaboration I had with Frank Harary (Balaban and Harary 1968), the dualists of polycyclic benzenoids allowed a rigorous graph-theoretical study of such polycyclic aromatic hydrocarbons. One takes *a portion of an infinite graphene plane or an infinite diamond lattice* and defines a *dualist* of that portion by vertices that are centers of the cyclic cells (benzenoid rings or adamantane units, respectively) and by edges connecting vertices in adjacent cells. Dualists are similar to, but not identical with, graphs because angles between edges do matter (Balaban and Harary 1968; Balaban 1969, 1982).

Historically, benzenoids have been classified as cata-condensed (catafusenes) when all C or CH carbon atoms are on the periphery and as peri-condensed when there exist internal carbon atoms (necessarily without hydrogen). Dualists provide a simpler classification (catafusenes have acyclic dualists, whereas perifusenes have 3-membered rings) and allow an easy definition of a third type of benzenoids, coronoids, having dualists with larger rings. In Fig. 1.4, the isomeric phenanthrene (**1**) and anthracene (**2**) are catafusenes, pyrene (**3**) is a perifusene, and kekulene (**4**) is a coronoid.

For catafusenes, we developed a coding system based on the dualist, as indicated in Fig. 1.5, based on the angles in the dualist longest continuous line (Balaban and Harary 1968; Balaban 1969, 1982). Starting from one end of the dualist, and examining the angle at each vertex, one assigns digit 0 for a straight annelation (angle 180°) and digit 1 or 2 for a kinked annelation (angle 120° or 240°), selecting as the canonical code the smallest number resulted from all digits. This means that one has to compare all endpoints and all kink notations.

For nonbranched catafusenes, it is simple to devise canonical notations for all isomeric catafusenes with four benzenoid rings $C_{18}H_{12}$, as seen in Fig. 1.6. For a branched catafusene such as triphenylene, one selects the longest linear path for the dualist, indicating in round parentheses the code of the branching line; if the branch has only one benzenoid ring as in triphenylene, **10**, a dot denotes this single branching benzenoid ring.

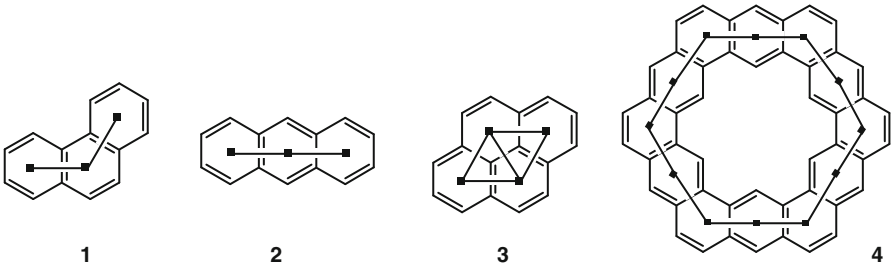

Fig. 1.4 Two isomeric catafusenes $C_{14}H_{10}$ (**1** and **2**), a perifusene $C_{16}H_{10}$ (**3**), and a coronoid $C_{48}H_{24}$ (**4**)

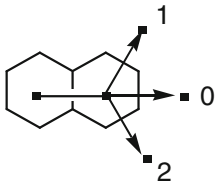

Fig. 1.5 Coding scheme for catafusenes based on dualist angles at each annelation step

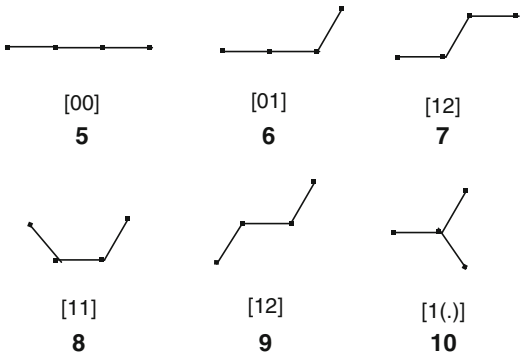

Fig. 1.6 Dualists and codes for all isomeric catafusenes $C_{18}H_{12}$ with four benzenoid rings, **5**–**10**

Interesting correlations for properties of benzenoids were made possible by using dualists: resonance energies (Balaban 1970), electrochemical potentials (Singh et al. 2006), and rates of Diels-Alder cycloaddition with maleic anhydride (Balaban et al. 1985). In collaborations with the Roumanian graph-theorist Tomescu, I introduced the term "isoarithmic" for benzenoids whose codes differ only in permutations between digits 1 and 2 (Balaban and Tomescu 1983) such as **8** and **9**: they have exactly the same numbers of Kekulé resonance structures in one-to-one correspondence and most of their properties are quasi-identical. In other words, on replacing in catafusene codes digits 1 and 2 by lowercase L which looks like digit 1, the catafusenes whose L-transform of 3-digit codes (looking like binary numbers) is identical should have very similar properties (Balaban 1977); similar ideas have been independently developed by Gutman (Balaban and Randić 2011).

In the 1930s, Eric Clar formulated his theory about aromatic sextets in benzenoids (Clar 1972); it can be summarized in postulating that benzenoid rings in cata- or perifusenes compete for π-electron sextets, resulting, for instance, that a sextet in acenes can belong to only one ring, whereas in zigzag catafusenes $C_{4n+2}H_{2n+4}$, there are $n/2$ or $(n+1)/2$ such Clar circles, for instance, one Clar circle in benzene and naphthalene and two Clar circles in phenanthrene (**1**) or in the three tetracatafusenes **7**, **8**, and **9** which have the same L-transform code. In the graphene lattice, Clar circles lie along poly-*para*-phenylene pathways. The dualist of this honeycomb lattice is a triangular lattice and vice versa.

When mathematical chemists started to enumerate all possible benzenoids, an interesting divergence occurred: one could consider benzenoids as being flat portions of the graphene lattice or as being assemblies of benzenoid rings sharing CC bonds, allowing to climb into the 3rd dimension. In the latter case, one could include helicenes, which are normal, stable catafusenes, and in a consolidated report, we pleaded for this approach, which complicates the calculations. Interesting findings were found by Dias who constructed "formula periodic tables" of benzenoids.

Before leaving the benzenoids, I would like to mention collaborations with my lifelong friend Milan Randić (a series of joint publications on numerical characterization of cata- or peri-condensed benzenoids according to partitions of π-electrons among adjacent benzenoid rings) (Randić and Balaban 2008; Balaban and Randić 2008); with Ivan Gutman on related topics for heteroanalogs of benzenoids (Balaban et al. 2007a); with Douglas J. Klein and his coworkers on fullerenes, nanocones, and nanotubes (Balaban et al. 1994a, b; Klein and Balaban 2006); with Roald Hoffmann (Merz et al. 1987) or D. J. Klein for combined sp^2–sp^3 hybridized lattices (Balaban et al. 1994a, b; Balaban and Klein 1997); and with Roger Mallion (Balaban and Mallion 2012), Milan Randić (Randić et al. 2012), or Patrick W. Fowler (Balaban et al. 2010) on ring currents in benzenoids.

1.4 Dualists of 3D Polycyclic Diamondoid Hydrocarbons and Staggered Alkane Rotamers

From two-dimensional dualists, it was easy to think about a similar approach involving three-dimensional polycyclic hydrocarbons (diamond hydrocarbons or diamondoids). Electronic factors and the tetrahedral bond angle $\alpha = 109.5°$ impose staggered conformations of alkanes that allow again an approach based on discrete mathematics, using dualists. In this case, however, there is no climbing to a higher dimension analogous to helicenic structures of benzenoids; on the other hand, one can still distinguish between catamantanes and perimantanes according to whether the dualist is acyclic or cyclic. The diamond lattice is self-dual.

In Fig. 1.7, one can see the single isomers of adamantane (**11**), diamantane (**12**), and triamantane (**13**). The four tetrahedral directions around a vertex are denoted by digits 1–4 as in Fig. 1.8, and again the canonical code for the staggered conformation

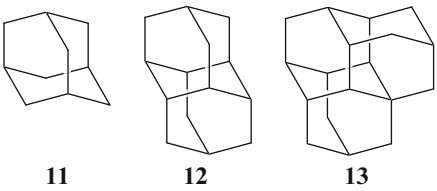

Fig. 1.7 Adamantane (**11**, $C_{10}H_{16}$), diamantane (**12**, $C_{14}H_{20}$), and triamantane (**13**, $C_{16}H_{24}$)

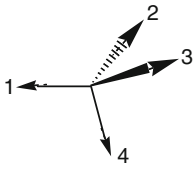

Fig. 1.8 The four tetrahedral directions

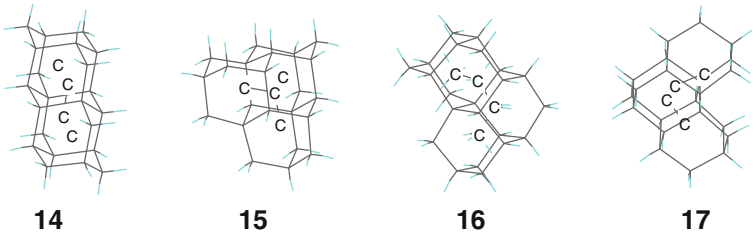

Fig. 1.9 The four possible tetramantanes: the achiral [121]tetramantane, the achiral [1(2)3]tetramantane, and the two chiral enantiomers [123]tetramantane and [124]tetramantane

of an alkane has the minimal number resulting from sequential reading of the directions along the longest linear chain. Their dualists are represented by the carbon scaffolds of methane, ethane, and propane.

When there are branches along the longest linear chain of the dualist, their directions are enclosed in round brackets; as in the case of the benzenoids, codes are enclosed in square brackets.

Starting with C_4 alkanes, isomers and staggered conformational rotamers are possible, with the associated tetramantanes. The two isomers are *n*-butane and isobutane; the staggered conformational rotamers are the *anti*- and *gauche n*-butane. Only the latter is chiral. Figure 1.9 presents the four possible tetramantanes with their dualists indicated by the carbon skeleton of the corresponding alkane.

1.5 Isomers of Diamondoids

Pentanes give rise to three isomers and to seven rotamers (ignoring enantiomerism). Six of the corresponding pentamantanes are regular having molecular formula $C_{26}H_{32}$, with dualists shown as stereo views in Fig. 1.10. The seventh pentamantane

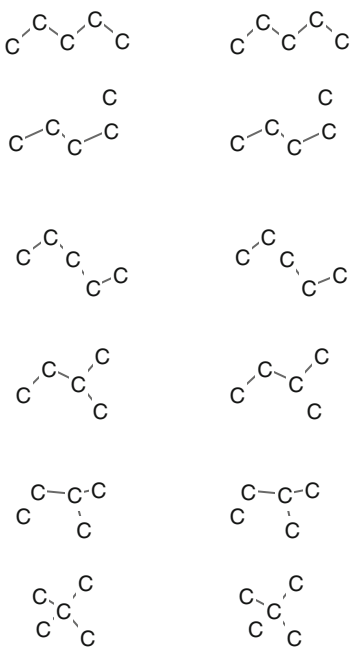

Fig. 1.10 Stereo view of the dualists for regular pentamantanes with codes [1212], [1213], [1234], [12(1)3], [12(3)4], and [1(2,3)4]

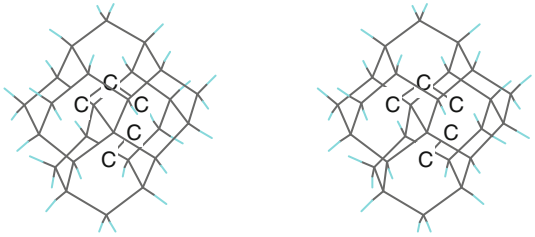

Fig. 1.11 Stereo view of the irregular pentamantane with its dualist [1231]

with dualist code [1231] is irregular having molecular formula $C_{26}H_{30}$, and it is shown as stereo view with its dualist in Fig. 1.11. One can see that the ends of the dualist are close to each other. When the dualist is a chair-shaped hexagon, the corresponding hexamantane is the smallest possible perimantane. In Table 1.3, one can see all possible catamantanes with one to six adamantane cells.

After having enumerated all possible staggered rotamers of alkanes (Balaban 1976a, b; Balaban and Baciu 1978), I have noticed marked similarities with isomers of benzenoids. Since Paul von Ragué Schleyer was the world's authority on adamantane and polymantanes, I wrote to him in 1978 suggesting collaboration, and the result was a paper (Balaban and Schleyer 1978) that used the code I had proposed, which is much simpler than the von Baeyer IUPAC nomenclature (Eckroth 1967). For example, the literature names of the three unique diamondoids with $n = 1$–3 adamantane units are tricyclo[3.3.1.$1^{3,7}$]decane for adamantane; for diamantane pentacyclo[7.3.1.$1^{4,12}$.$0^{2,7}$.$0^{6,11}$]tetradecane; and for triamantane the IUPAC name is heptacyclo[7.7.1.$1^{3,15}$.$0^{1,12}$.$0^{2,7}$.$0^{4,13}$.$0^{5,11}$]octadecane.

Table 1.3 Catamantanes with $n = 1$–6 adamantane units

	Regular					Irregular				
	Linear			Branched		Linear			Branched	
n	Code	Sym	Formula	Code	Sym	Code	Sym	Formula	Code	Sym
1		T_d	$C_{10}H_{16}$							
2	1	D_{3d}	$C_{14}H_{20}$							
3	12	C_{2v}	$C_{18}H_{24}$							
4	121	C_{2h}	$C_{22}H_{28}$	1(2)3	C_{3v}					
	123	C_2								
5	1212	C_{2v}		12(1)3	C_1					
	1213	C_1	$C_{26}H_{32}$	12(3)4	C_s	1231	C_s	$C_{25}H_{30}$		
	1234	C_2		1(2,3)4	T_d					
6	12121	C_{2h}		121(2)3	C_1					
	12123	C_1		12(1)32	C_1					
	12131	C_1		121(3)4	C_s	12132	C_1	$C_{29}H_{34}$	12(1)31	C_s
	12134	C_1	$C_{30}H_{36}$	12(1)34	C_1	12314	C_1		123(1)2	C_1
	12321	C_i		12(1,3)4	C_1				123(1)4	C_1
	12324	C_2		12(3)12	C_s				12(3)41	C_s
	12341	C_2		1(2)3(1)2	C_{2h}					
				1(2)314	C_1					
				12(3)14	C_1					
				1(2)3(1)4	C_{2h}					

1.6 Brief History of Diamondoids

Adamantane (hexamethylene-tetramethine, Fig. 1.1) was first discovered as a constituent of petroleum (Landa and Machacek 1933). Inorganic compounds such as P_4O_6 were also found to have the same geometry as adamantane. Urotropine (hexamethylene-tetramine), which has the same geometry as adamantane, has been known for a long time because it is easily formed from formaldehyde and ammonia. Adamantane was then synthesized by Prelog using a lengthy route (Prelog and Seiwerth 1941a, b); no further progress in the synthesis of higher members was made till Schleyer demonstrated that Lewis-acid catalysis may convert their valence isomers into such "diamondoid hydrocarbons" or polymantanes. Schleyer's synthesis of adamantane (Schleyer 1957, 1990) was based on the fact that all C–H and C–C bonds are staggered, without any angular or conformational strain, so that being the most stable among all isomers, it is formed by the $AlCl_3$-catalyzed rearrangement of any $C_{10}H_{16}$ saturated isomer; Schleyer's synthesis started from the hydrogenated dimer of cyclopentadiene. Analogously, the dimer of norbornene rearranged (Cupas et al. 1965) to diamantane (congressane was its challenging name for the 1963 IUPAC meeting in London), and triamantane was obtained similarly using bis-cyclopropanated polycyclic dimer of cyclooctatetraene with a sludge of $AlBr_3$ and *tert*-BuBr as catalyst (Williams et al. 1966); McKervey used another

hydrocarbon, Binor-S, in a higher-yield reaction (Burns et al. 1976). Among the tetramantane isomers, only the rodlike structure could be made synthetically, also by McKervey and coworkers (McKervey 1980).

The X-ray diffraction of diamantane confirmed its structure and contributed to the award of the 1985 Nobel Prize in Chemistry to Jerome Karle (Karle and Karle 1965). Yet another link to this fascinating field was provided by using my reaction graphs (Balaban et al. 1966; Balaban 1994) for explaining the mechanism of the complicated rearrangements involved in these syntheses of polymantanes (Whitlock and Siefken 1968; Gund et al. 1975; Engler et al. 1973). Two early reviews on diamondoids were published by Fort Jr (Fort and Schleyer 1964; Fort 1976), and a very recent book has been published in 2012 (Mansoori et al. 2012). Since 1986, I have published three reviews on carbon and its nets (Balaban 1986a, b, 1989, 1998).

The recent discovery that mixtures of various diamondoids are found in crude oil and natural gas condensates (at concentrations 1–100 ppm) from offshore stations in the US Norphlet Formation (Gulf of Mexico) makes this class of substances attractive for many uses (Dahl et al. 1999, 2003a, b). The high volatility, high melting points (e.g., 268 °C for adamantane, which sublimes; 237 °C for diamantane; and 221 °C for triamantane), and resistance to oxidation of these compounds provide an explanation for their easy isolation. They may be separated and isolated in pure state. Their formation by catagenesis in oil deposits is due to their high thermodynamic stability, having no steric strain. Because they clogged natural gas pipelines, they were first considered as a nuisance.

Figure 1.12 represents four series of higher diamondoids as successive "adamantane analogs" indicated by four different colored carbon frameworks superimposed on a gray diamond lattice and shown separately with their notation. The yellow diamondoids are regular nonbranched rodlike zigzag catamantanes; the blue diamondoids are regular branched catamantanes; perimantanes are colored green. In the case of the red-colored chiral diamondoids (having primary helicity), enantiomeric pairs are displayed with **P/M** notations. Members of each series have been found and isolated from petroleum (Schreiner et al. 2009).

1.7 Degree Partitions of Dualist Vertices and Carbon Atom Partitions of Diamondoids

An interesting observation was made about isomers of diamondoids with n adamantane units. We recall that such [n]diamondoids are classified as catamantanes with acyclic dualists, perimantanes with dualists having one or more 6-membered rings, and coronamantanes when their dualists have larger rings that are not envelopes of smaller six-membered rings. Catamantanes can be regular when they have molecular formulas $C_{4n+6}H_{4n+12}$ and irregular catamantanes or perimantanes when the number of carbon atoms is lower than $4n + 6$ and as a consequence, the ratio C/H is higher than $n/(n + 6)$. To add one more adamantane unit to a regular diamondoid

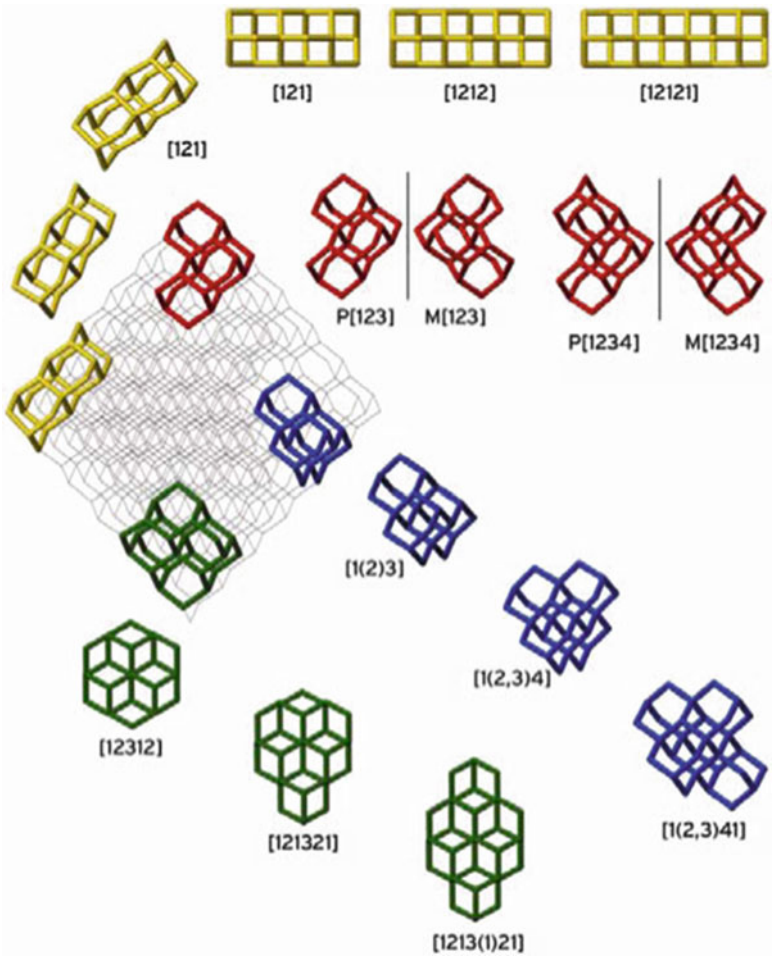

Fig. 1.12 Examples of four structure series of higher diamondoids

in order to form a new regular diamondoid, one needs to replace four C–H bonds by an isobutane $(CH)_4$ fragment. It is important to realize that such a replacement needs to be done properly, because otherwise boat-shaped cyclohexane rings would result, as seen in Fig. 1.13.

Diamondoids having an acyclic dualist where four edges have close-situated extremities (called "proximities") need a smaller fragment to produce a new adamantane unit, and the product is an irregular catamantane or a perimantane. A proximity has a code that includes a sequence of digits containing a repetition of type *abca*. Dualists of irregular catamantanes have five vertices along a chair-shaped hexagon, causing hydrogen atoms of the corresponding repeating adamantane units to approach too closely. Dualists of perimantanes have an even more extended

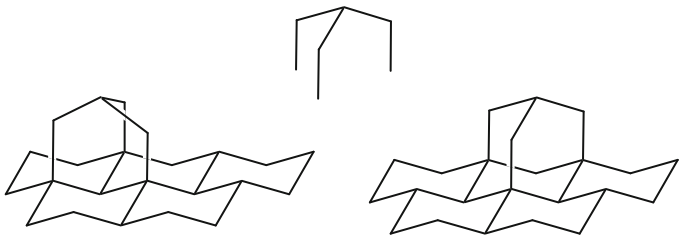

Fig. 1.13 The two possibilities of attaching to "perhydrographene" an isobutane fragment $(CH)_4$ shown above together with four "dangling bonds": only the right-hand possibility is allowed, producing an adamantane unit with chair-shaped 6-membered rings in staggered conformations; the left-hand alternative yields tub-shaped 6-membered rings having bonds in eclipsed conformations

repetition of type *abcab*. As it may be seen in Table 1.3, the smallest irregular [*n*]diamondoid has $n = 5$, and the smallest perimantane has $n = 6$.

Isomers of diamondoids with up to six adamantane units are enumerated in Table 1.3 and those with $n = 7$ adamantane units in Table 1.4. In an earlier paper (Balaban 1986a), I have discussed all 262 possible valence isomers of adamantane, i.e., all molecules having the same partition of four CH and six CH_2 groups. Valence isomers constitute a subclass of isomers characterized by having the same distribution of vertex degrees in the constitutional hydrogen-depleted graph. Interconversions between valence isomers of annulenes have been thoroughly discussed in reviews and a 3-volume book (Balaban et al. 1986).

Recently, applying a more restrictive condition for partitioning the C, CH, and CH_2 groups, we have produced *partitioned-formula periodic tables for diamondoids.* For benzenoids, Dias has published extensively interesting findings in his formula periodic tables (Dias 1982, 1984, 1985, 1987, 1990). A remarkable symmetry can be observed in Table 1.5 displaying regular catamantanes (Balaban 2012). Adamantane, diamantane, and triamantane have a single isomer each, and therefore Table 1.5 starts with triamantane. Rows characterize regular diamondoid isomers with the same *n* sharing the same molecular formula. The partition of the $4n + 6$ carbon atoms is shown by a triplet separated by hyphens (*Q*-*T*-*S* indicating the numbers of quaternary, tertiary, and secondary carbon atoms or C, CH, and CH_2 groups with vertex degrees 4, 3, and 2 of the hydrogen-depleted constitutional formula). Now, looking at the *n* vertices of the dualist, the columns show, under each triplet, a quadruplet separated by commas indicating the numbers of vertices with vertex degrees 1, 2, 3, and 4 (in red). Columns are labeled with a number starting with 1. For columns labeled 3 and 4, the dualist has 0 and 1 branches, respectively. Columns labeled 5 and 6 are for dualists having two branches; the smallest regular catamantane with a dualist having two branches and no degree-4 vertex is a hexamantane.

By means of partitioning the *C* carbon atoms into triplets and the *n* adamantane units into quadruplets according to the vertex degrees, the result is a formula periodic table of diamondoids allowing a better understanding of their topological and geometrical shapes. One should be aware that so far, we have discussed

Table 1.4 Of all 88 possible constitutional isomers of heptamantane

Catamantanes								Perimantanes	
Regular				Irregular					
Formula: $C_{34}H_{40}$				Formula: $C_{33}H_{38}$				$C_{30}H_{34}$	
Linear		Branched		Linear		Branched		Cyclic	
Code	Sym	Code	Sym	Code	Sym	Code	Sym	Code	Sym
121212	C_{2v}	1212(1)3	C_1	121231	C_1	12(12)31	C_1	121321	C_s
121213	C_1	121(2)31	C_1	121323	C_s	121(2)32	C_1	123124	C_s
121232	C_1	1212(3)4	C_s	121324	C_1	1213(1)2	C_1		
121234	C_1	121(2)34	C_1	121341	C_1	12(1)3(1)2	C_1		
121312	C_1	12(12)34	C_s	123132	C_1	12(1)314	C_1		
121314	C_1	121(2,3)4	C_s	123134	C_1	12(1)3(1)4	C_1		
121342	C_1	1213(1)4	C_1	123142	C_1	12(1)321	C_1		
121343	C_2	121(3)21	C_1	123143	C_2	1213(2)4	C_1		
123214	C_1	121(3)23	C_1	123421	C_s	12(1)341	C_1		
123231	C_s	121(3)24	C_1			12(13)41	C_s		
123234	C_2	12(1)324	C_1			12(1,3)41	C_s		
123241	C_1	12(1)3(2)4	C_1			121(3)42	C_1		
123412	C_2	12(13)32	C_3			12(1)342	C_1		
		12(13)34	C_1			12(13)43	C_1		
		121(3)41	C_1			123(1)23	C_1		
		12(1,3)42	C_1			1(2)31(2)3	C_1		
		121(3)43	C_1			123(1)24	C_1		
		12(1,3)43	C_1			1(2)3124	C_1		
		12(3)1(2)3	C_1			123(1,2)4	C_1		
		12(3)124	C_1			1(2)31(2)4	C_1		
		12(3)1(2)4	C_1			12(3)132	C_1		
		1(2)3(1)24	C_1			1231(3)4	C_1		
		1(2)3(1,2)4	C_s			12(31)41	C_{3v}		
		1(2)3132	C_1			123(1)42	C_1		
		12(3)134	C_1			12(3)142	C_1		
		1(2)3134	C_1			1(2)3(1)42	C_1		

constitutional formulas, ignoring chirality. The partition of carbon atoms in diamondoids according to the vertex degrees of their constitutional hydrogen-depleted carbon scaffolds is indicated by the following relationships.

$$\text{Quaternary C groups :} \quad Q = n + b - 2 = S - 6 \tag{1.1}$$

$$\text{Ternary CH groups :} \quad T = 2(n + b + 2) \tag{1.2}$$

$$\text{Secondary } CH_2 \text{ groups :} \quad S = n + b + 4 \tag{1.3}$$

In other words, the above relationships are translated as $C_{n+b-2}(CH)_{2n+2b+4}(CH_2)_{n+b+4}$ for representing the partitioned formula for regular catamantanes, where the parameter b stands for the number of branches plus the number of

Table 1.5 For regular catamantanes, partitions of degrees of carbon atoms (upper row: quaternary-tertiary-secondary carbon atoms) and partitions of vertex degrees of dualists (lower row: numbers of vertices with degree 1, 2, 3, 4)

1	2	3	4	5	6	7	8	9
Cells	Formula	Zero branches	One branch	Two branches		Three branches		Four branches
3	$C_{18}H_{24}$	1-10-7 **2**, 1, 0 0						
4	$C_{22}H_{28}$	2-12-8 **2**, 2, 0, 0	3-10-9 **3**, 0, **1**, 0					
5	$C_{26}H_{32}$	3-14-9 **2**, 3, 0, 0	4-12-10 **3**, 1, **1**, 0		6-8-12 4, 0, 0, **1**			
6	$C_{30}H_{36}$	4-16-10 **2**, 4, 0, 0	5-14-11 **3**, 2, **1**, 0	6-12-12 **4**, 0, **2**, 0	7-10-13 **4**, 1, 0, **1**			
7	$C_{34}H_{40}$	5-18-11 **2**, 5, 0, 0	6-16-12 **3**, 3, **1**, 0	7-14-13 **4**, 1, **2**, 0	8-12-14 **4**, 2, 0, **1**	9-10-15 **5**, 0, **1, 1**		
8	$C_{38}H_{44}$	6-20-12 **2**, 6, 0, 0	7-18-13 **3**, 4, **1**, 0	8-16-14 **4**, 2, **2**, 0	9-14-15 **4**, 3, 0, **1**	10-12-16 **5**, 1, **1, 1**		12-8-18 **6**, 0, 0, **2**
9	$C_{42}H_{48}$	7-22-13 **2**, 7, 0, 0	8-20-14 **3**, 5, **1**, 0	9-18-15 **4**, 3, **2**, 0	10-16-16 **4**, 4, 0, **1**	11-14-17 **5**, 2, **1, 1**		13-10-19 **6**, 1, 0, **2**
10	$C_{46}H_{52}$	8-24-14 **2**, 8, 0, 0	9-22-15 **3**, 6, **1**, 0	10-20-16 **4**, 4, **2**, 0	11-18-17 **4**, 5, 0, **1**	12-16-18 **5**, 3, **1, 1**	13-14-19 **5**, 2, **3**, 0	14-12-20 **6**, 2, 0, **2**

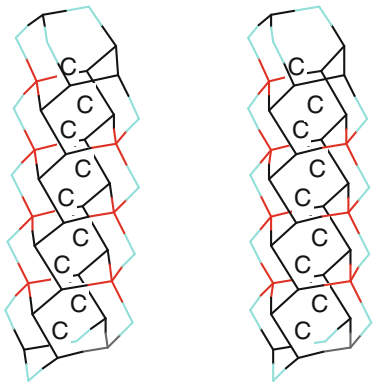

Fig. 1.14 Stereo view of the nonbranched zigzag regular [121212121]nonamantane

degree-4 vertices in the dualist. The two nonbranched regular nonamantanes presented in Figs. 1.14 and 1.15 are isomers with molecular formula $C_{42}H_{48}$ and have completely different geometries (the former is achiral whereas the latter is chiral owing to its helicity), yet their partitions are exactly the same: $C_7(CH)_{22}(CH_2)_{13}$. In both figures, red vertices correspond to quaternary C atoms and blue vertices to secondary CH_2 groups.

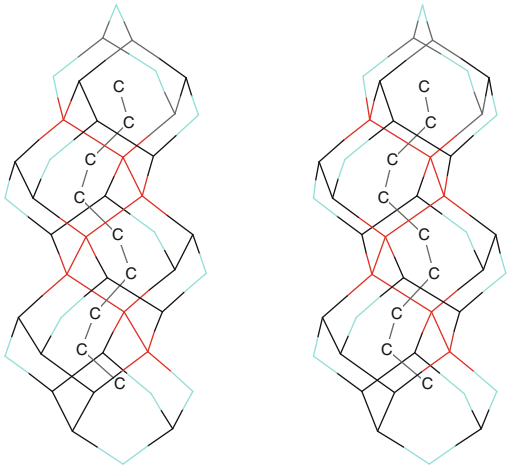

Fig. 1.15 Stereo view of the nonbranched helical regular [123412341]nonamantane

There is a perfect symmetry according to columns, rows, and diagonals in Table 1.5: boldface red numbers show the constant nonzero numbers in each column. The red numbers of degree-2 vertices increase steadily in each column with increasing n. In the triplet of each row, the numbers Q and S of the same parity increase steadily from left to right, whereas the even numbers T decrease steadily from left to right.

There are still some aspects of the partitioned-formula periodic tables that are incompletely understood, especially for the irregular catamantanes and the perimantanes (Balaban 2012).

1.8 Chromatographic Separation and Identification of Diamondoids from Petroleum

In collaboration with Drs. Carlson and Dahl from Chevron and with Professor Klein from Texas A&M University Galveston, graph-theoretical matrices of diamondoid dualists were converted into molecular invariants characterizing diamondoid structures. With the help of these invariants, quantitative structure–property correlations were obtained using the data provided by Chevron (Balaban et al. 2007a, b). In Fig. 1.15, one can see that most tetramantanes and pentamantanes can be separated and identified by a combination of high-performance liquid chromatography (HPLC) and gas chromatography plus the corresponding mass spectra (GC-MS). Regular diamondoids have higher molecular weights than irregular diamondoids with the same number of carbon atoms. Only identified compounds are displayed in Table 1.6, but in the article (Balaban et al. 2007b) and in Fig. 1.16, many other unidentified diamondoids were included.

Table 1.6 Chromatographic data of identified diamondoids from petroleum

Higher diamondoid code	Compound reference number	Molecular formula	M^+ (*m*/*z*) base peak	GC/MS relative retention times*	ODS HPLC relative elution volumes*
[1(2)3]	4;1	$C_{22}H_{28}$	292	1	1
[121]	4;2	$C_{22}H_{28}$	292	1.069	1.055
[123]	4;3	$C_{22}H_{28}$	292	1.126	1.036
[1(2,3)4]	5;1	$C_{26}H_{32}$	344	1.284	1.126
[12(1)3]	5;2	$C_{26}H_{32}$	344	1.473	1.269
[1212]	5;3	$C_{26}H_{32}$	344	1.479	1.431
[1213]	5;4	$C_{26}H_{32}$	344	1.529	1.323
[12(3)4]	5;5	$C_{26}H_{32}$	344	1.543	1.269
[1234]	5;6	$C_{26}H_{32}$	344	1.57	1.287
[12312]	C-6	$C_{26}H_{30}$	342	1.523	1.341
[12121]	6;6	$C_{30}H_{36}$	396	1.868	2.039
[121321]	7;1	$C_{30}H_{34}$	394	1.847	1.743
[123124]	7;2	$C_{30}H_{34}$	394	1.917	1.664
[121212]	7;4B	$C_{34}H_{40}$	448	2.185	2.521
[12312412]	9;1	$C_{34}H_{40}$	444	2.292	2.396
[1231241(2)3]	10;1	$C_{38}H_{43}$	456	2.451	2.503
[123(1,2)42143]	11;1	$C_{39}H_{38}$	508	2.599	2.987

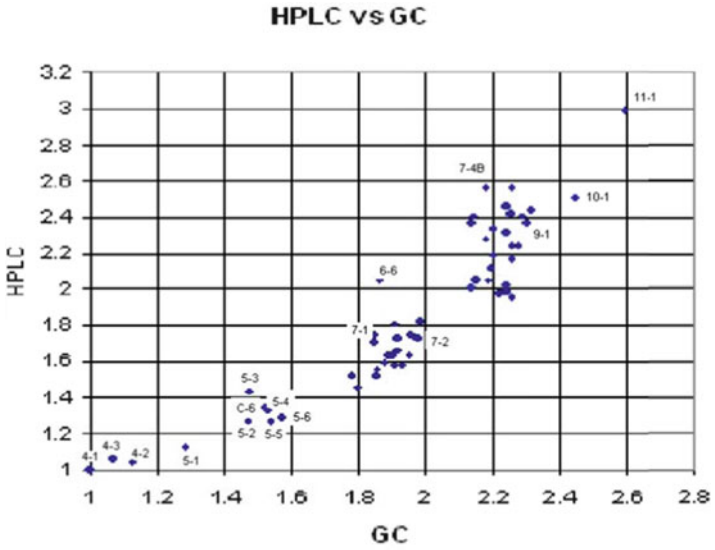

Fig. 1.16 Plot of the HPLC eluent volumes versus the GC retention times of diamondoid

Table 1.7 Molecular invariants (*D*-eigenvalues) and chromatographic data

Diamondoid	*n*	*D*-eigenv.	GC/MS	HPLC	Type
[1(2)3]	4	6.87	1.000	1.000	4-cata
[121]	4	7.79	1.069	1.055	4-rod
[123]	4	7.15	1.126	1.036	4-cata
[1(2,3)4]	5	10.58	1.284	1.126	5-bundle
[12(1)3]	5	11.08	1.473	1.269	5-cata
[1212]	5	12.27	1.479	1.431	5-rod
[1213]	5	11.88	1.529	1.323	5-cata
[12(3)4]	5	10.04	1.543	1.269	5-cata
[1234]	5	10.53	1.570	1.287	5-cata
[12121]	6	17.74	1.868	2.039	6-rod
[12312]	6	12.44	1.523	1.341	6-bundle
[121321]	7	16.89	1.847	1.743	7-bundle
[123124]	7	15.88	1.917	1.664	7-bundle
[121212]	7	24.17	2.185	2.521	7-rod
[12312412]	9	21.84	2.292	2.396	9-bundle
[1231241(2)3]	10	24.74	2.451	2.503	10-bundle
[123(1,2)42143]	11	29.65	2.599	2.987	11-bundle

One may observe that in Fig. 1.16, all three tetramantanes appear at the lower left (GC around 1.1), followed by an isolated spot corresponding to C-6, the peri-hexamantane with a chair hexagon as dualist (GC around 1.3). The next cluster has six points corresponding to the pentamantanes (GC around 1.5); the topmost point (with HPLC around 1.4) is due to the rodlike pentamantane. Catamantanes from the hexamantane group and perimantanes from the heptamantane group form the next cluster between GC 1.75 and 2.0; the topmost point with HPLC 2.04 is the rodlike hexamantane; also two perifused heptamantanes with dualists isomorphic to methylcyclohexane were identified in this cluster: the equatorial [121321]heptamantane with GC around 1.85 and the axial [123124]heptamantane with GC around 1.92. The next cluster with GC between 2.1 and 2.35 contains diamondoids from the octamantane and nonamantane groups, mostly perimantanes, including the nonamantane having a dualist graph isomorphic to bicyclo[3.3.1]nonane. The last two points with GC around 2.5 and 2.6 correspond, respectively, to the decamantane having as its dualist the adamantane skeleton and to its undecamantane homolog having one extra vertex attached to a "tertiary carbon" of the adamantane-like dualist (Table 1.7).

From the distance matrix of the dualist, one can easily obtain the largest eigenvalue, and this is one possible molecular invariant for the corresponding diamondoid (Table 1.6). As seen in Fig. 1.17, a satisfactory correlation ($R^2 = 0.9842$) was obtained for the HPLC elution volumes.

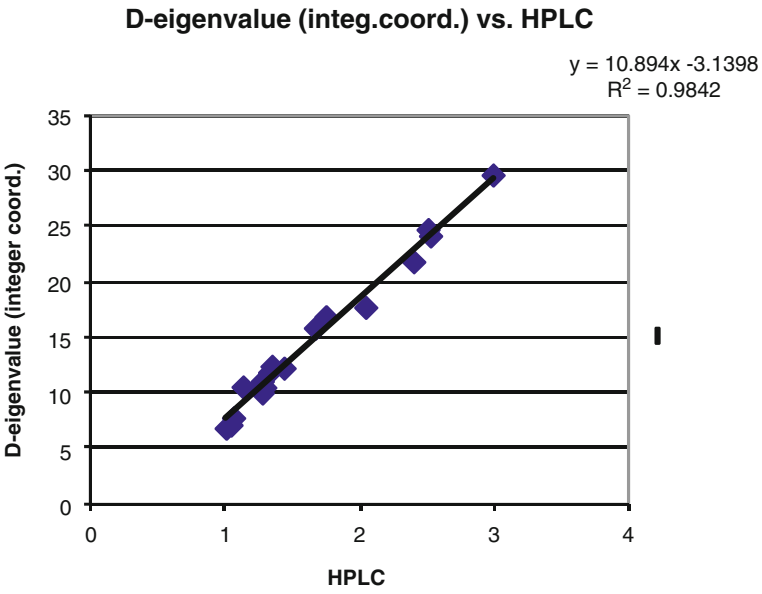

Fig. 1.17 Plot of D-eigenvalues for idealized coordinates vs. HPLC relative elution values

1.9 Applications and Uses of Diamondoids

Lower diamondoids are readily available from petroleum, so that many possible applications are imminent. Prominent among these are applications of rod-shaped molecules functionalized at one or both ends, securing thus exactly fitting distances between functional groups matching protein receptor sites. There are other nanorod-like molecules (Balaban et al. 2007b; Schwab et al. 1999, 2005) such as carbon nanotubes; however, these nanotubes are *mixtures* of similar but not identical molecules. By contrast, one can prepare and functionalize regioselectively diamondoids as *pure substances*. Due to different reactivities of tertiary and secondary C–H bonds in diamondoids, it is possible to achieve a regioselective functionalization. Apical positions in rodlike diamondoids starting with diamantane or [121]tetramantane (with zigzag dualists as in Fig. 1.14) are especially attractive. Grouping diamondoids according to valence-isomeric classes having definite numbers of tertiary (CH) and secondary (CH_2) hydrogen atoms is therefore of highest importance in this regard.

Schreiner and his coworkers (together with Dahl and Carlson who provided the diamondoids from petroleum) investigated thoroughly the regioselectivity of diamondoid functionalization in a series of 30 papers, only a few of which can be mentioned here (Schreiner et al. 2011; Fokin et al. 2005; Schwertfeger et al. 2008, 2009; Fokin et al. 2009a, b, c, d; Dahl et al. 2010; Fokina et al. 2012; Wang et al. 2011; Schreiner et al. 2009; Schwertfeger et al. 2010a, b; Richter et al. 2009; Fokin

and Schreiner 2009; Roth et al. 2010). It has long been known that the tertiary C–H bonds of adamantane can be more readily halogenated than secondary C–H bonds (Schwertfeger et al. 2008). For diamantane, it was observed (Fokin et al. 2005) that alcohol formation by oxidation with *meta*-chloroperbenzoic acid favors medial-tertiary over apical-tertiary attack; higher yields are achieved by nitroxylation by anhydrous nitric acid followed by hydrolysis; interestingly, apical substitution is favored by longer reaction times. For fluorination, AgF halogen exchange and alcohol conversion using $Et_2N–SF_3$ proved to be methods of choice (Schwertfeger et al. 2009). Photoacetylation of diamondoids with diacetyl gives predominantly apical acetyl derivatives owing mainly by polarizability effects, with steric factors playing a minor role (Fokin et al. 2009a). Bis-apical rodlike functionalized diamondoids are the most promising candidates for applications. The global shape of the diamondoid also influences the regioselectivity (Fokin et al. 2009b). A fundamental finding of Schreiner's research group was that the formation of higher diamondoids occurred via a homolytic mechanism involving sequential addition of isobutane fragments to diamondoids (Dahl et al. 2010). Oxa- and thia-diamondoids were also prepared (Fokin et al. 2009d). Bis-apical [121]tetramantane-dicarboxylic acid and its dimethyl ester were prepared in 77 and 69 % yields, respectively, starting from the corresponding diol derivative and converting into the dibromo derivative, which was treated with H_2SO_4 and HCOOH in a Koch-Haaf reaction (Fokina et al. 2012). The influence of type and positions of heteroatoms was studied in order to predict the band gap tuning in nanodiamonds (Fokin and Schreiner 2009). Helical [123]tetramantane [102] (Schreiner et al. 2009) and the smallest perimantane (Fokin et al. 2009b) were isolated and studied for reactivity. Phosphorylated diamondoids and diamondoid-modified DNA were also prepared (Wang et al. 2011; Schwertfeger et al. 2010a, b). A recent paper in *Nature* reports the preparation of dimeric diamondoids with the longest yet reported C–C bond lengths between quaternary carbon atoms; their thermal stability and high melting points are due to attractive dispersion forces [91] (Schreiner et al. 2011). Schreiner's review (Schwertfeger and Schreiner 2010) and Hopf's comments on diamondoids (Hopf 2003) made it clear that some of the diamondoids from petroleum may be considered as nano-jewels, i.e., diamonds of 10^{-20} carats (1 carat = 200 mg).

Small diamond crystals from outer space have been first detected in meteorites (Hopf 2003; Lewis et al. 1987; Anders and Zinner 1993; Jones et al. 2004; Pirali et al. 2007) and then identified in interstellar infrared spectra. At the lower dimensions such nanodiamonds are probably diamondoids with all peripheric "dangling bonds" of the diamond lattice saturated with hydrogen atoms.

References

Anders A, Zinner E (1993) Interstellar grains in primitive meteorites: diamond, silicon carbide, and graphite. Meteoritics 28:490–514

Balaban AT (1969) Chemical graphs. VII. Proposed nomenclature of branched cata–condensed benzenoid polycyclic hydrocarbons. Tetrahedron 25:2949–2956

Balaban AT (1970) Chemical graphs. X. Resonance energies of cata–condensed benzenoid polycyclic hydrocarbons. Rev Roum Chim 15:1243–1250
Balaban AT (1976a) Chemical graphs. XXVII. Enumeration and codification of staggered conformations of alkanes. Rev Roum Chim 21:1049–1071
Balaban AT (1976b) Enumeration of catafusenes, diamondoid hydrocarbons and staggered alkane C–rotamers. MATCH Commun Math Comput Chem 2:51–61
Balaban AT (1977) Chemical graphs. XXVIII. A new topological index for catafusenes: L–transform of their three–digit codes. Rev Roum Chim 22:45–47
Balaban AT (1982) Challenging problems involving benzenoid polycyclics and related systems. Pure Appl Chem 54:1075–1096
Balaban AT (1986a) Chemical graphs. Part 46. Enumeration of valence isomers of adamantane using Pólya's theorem. Rev Roum Chim 31:795–819
Balaban AT (1986b) Symmetry in chemical structures and reactions. Comput Math Appl 12B: 999–1020. Reprinted in: Hargittai I (ed) Symmetry unifying human understanding. Pergamon, New York
Balaban AT (1989) Carbon and its nets. Comput Math Appl 17:397–416. Reprinted in: Hargittai I (ed) Symmetry II. Pergamon, Oxford
Balaban AT (1994) Reaction graphs. In: Bonchev D, Mekenyan O (eds) Graph theoretical approaches to chemical reactivity. Understanding chemical reactivity, vol 9. Kluwer Academic Publishers, Dordrecht
Balaban AT (1998) Theoretical investigation of carbon nets and molecules. In: Parkanyi C (ed) Theoretical organic chemistry. Elsevier, Amsterdam
Balaban AT (2011) Using Clar sextets for two– and three–dimensional aromatic systems. Phys Chem Chem Phys 13:20649–20658
Balaban AT (2012) Partitioned–formula periodic tables for diamond hydrocarbons (diamondoids). J Chem Inf Model 52:2856–2863
Balaban AT, Baciu V (1978) Chemical graphs. XXXV. Application of Polya's theorem to catamantanes. MATCH Commun Math Comput Chem 4:131–159
Balaban AT, Harary F (1968) Chemical graphs. V. Enumeration and proposed nomenclature of benzenoid cata–condensed polycyclic aromatic hydrocarbons. Tetrahedron 24:2505–2516
Balaban AT, Klein DJ (1997) Local interconversions between graphite and diamond structures. Carbon 35:247–251
Balaban AT, Klein DJ (2009) Claromatic carbon nano–structures. J Phys Chem C 113:19123–19133
Balaban AT, Mallion RB (2012) Correlations between topological ring–currents, π–electron partitions, and six–centre delocalisation indices in benzenoid hydrocarbons. Croat Chem Acta 85:37–52
Balaban AT, Randić M (2008) Ring signatures for benzenoids with up to seven rings. Part 2. Pericondensed systems. Intern J Quantum Chem 108:898–926; Erratum, ibid. 3252–3253
Balaban AT, Randić M (2011) Structural approach to aromaticity and local aromaticity in conjugated polycyclic systems. In: Putz MV (ed) Carbon bonding and structures. Advances in physics and chemistry. Springer, Dordrecht, pp 159–204
Balaban AT, Schleyer PR (1978) Systematic classification and nomenclature of diamond hydrocarbons. 1. Graph–theoretical enumeration of polymantanes. Tetrahedron 34:3599–3609
Balaban AT, Tomescu I (1983) Algebraic expressions for the number of Kekulé structures of isoarithmic cata–condensed polycyclic hydrocarbons. MATCH Commun Math Comput Chem 14:155–182
Balaban AT, Farcasiu D, Banica R (1966) Chemical graphs. II. Graphs of multiple 1,2–shifts in carbonium ions and related systems. Rev Roum Chim 11:1205–1227
Balaban AT, Rentea CC, Ciupitu E (1968) Chemical graphs. VI. Estimation of the relative stability of several planar and tridimensional lattices for elementary carbon (Erratum, ibid., p 1233) Rev Roum Chim 13:231–247

Balaban AT, Biermann D, Schmidt W (1985) Chemical graphs. 41. Dualist graph approach for correlating Diels–Alder reactivities of polycyclic aromatic hydrocarbons. Nouv J Chim 9:443–449

Balaban AT, Banciu M, Ciorba V (1986) Annulenes, benzo–, hetero–, homo–derivatives and their valence isomers. CRC Press, Boca Raton

Balaban AT, Klein DJ, Folden CA (1994a) Diamond–graphite hybrids. Chem Phys Lett 217:266–270

Balaban AT, Klein DJ, Liu X (1994b) Graphitic cones. Carbon 32:357–359

Balaban AT, Furtula B, Gutman I, Kovacevic R (2007a) Partitioning of π–electrons in rings of aza–derivatives of polycyclic benzenoid hydrocarbons. Polycyclic Arom Comp 27:51–63

Balaban AT, Klein DJ, Dahl JA, Carlson RMK (2007b) Molecular descriptors for natural diamondoid hydrocarbons and quantitative structure–property relationships for their chromatographic data. Open Org Chem J 1:13–31

Balaban AT, Bean DE, Fowler PW (2010) Patterns of ring current in coronene isomers. Acta Chem Slov 57:507–512

Baughman RH (2006) Dangerously seeking linear carbon. Science 312:1009–1110

Boehm HP, Clauss A, Fischer GO, Hofmann U (1962) Das Adsorptionsverhalten sehr dünner Kohlenstoffolien. Ztschr anorg allgem Chem 316:119–127

Boehm HP, Setton R, Stumpp E (1994) Nomenclature and terminology of graphite intercalation compounds. Pure Appl Chem 66:1893–1901

Bundy FP (1967) Hexagonal diamond – a new form of carbon. J Chem Phys 46:3437

Burns W, Mitchell TRB, McKervey MA, Rooney JJ, Ferguson G, Roberts P (1976) Gas–phase reactions on platinum. Synthesis and crystal structure of anti–tetramantane, a large diamondoid fragment. Chem Commun 21:893–895

Chalifoux WA, Tykwinski RR (2009) Synthesis of extended polyynes: toward carbyne. C R Chim 12:341–358

Clar E (1972) The aromatic sextet. Wiley, London (and further references therein)

Coxeter HSM (1971) Virus macromolecules and geodesic domes. In: Butcher JC (ed) A spectrum of mathematics. Oxford University Press, Oxford, pp 98–107

Cupas CA, P von Schleyer R, Trecker DJ (1965) Congressane. J Am Chem Soc 87:917–918

Curl RF Jr (1997) Dawn of the fullerenes: conjecture and experiment. Angew Chem Int Ed 36:1566–1576

Dahl JE, Moldowan JM, Peters KE, Claypool GE, Rooney MA, Michael GE, Mello MR, Kohnen ML (1999) Diamondoid hydrocarbons as indicators of natural oil cracking. Nature 399:54–57

Dahl JE, Liu SG, Carlson RMK (2003a) Isolation and structure of higher diamondoids, nanometer–sized diamond molecules. Science 299:96–99

Dahl JEP, Moldowan JM, Peakman TM, Clardy JC, Lobkovsky E, Olmstead MM, May PW, Davis TJ, Steeds JW, Peters KE, Pepper A, Ekuan A, Carlson RMK (2003b) Isolation and structural proof of the large diamond molecule, cyclohexamantane ($C_{26}H_{30}$). Angew Chem Int Ed 42:2040–2044

Dahl JEP, Moldowan JM, Wei Z, Lipton PA, Denisevich P, Gat R, Liu S, Schreiner PR, Carlson RMK (2010) Synthesis of higher diamondoids and implication for their formation in petroleum. Angew Chem Int Ed 49:9881–9885

Dias JR (1982) A periodic table for polycyclic aromatic hydrocarbons. Isomer enumeration of fused polycyclic aromatic hydrocarbons. Part I. J Chem Inf Comput Sci 22:15–22

Dias JR (1984) A periodic table of polycyclic conjugated hydrocarbons. Part 2. J Chem Inf Comput Sci 24:124–135

Dias JR (1985) A periodic table for polycyclic aromatic hydrocarbons. Acc Chem Res 18:241–248

Dias JR (1987) Handbook of polycyclic hydrocarbons. Elsevier, Amsterdam

Dias JR (1990) A formula periodic table for benzenoid hydrocarbons and the aufbau and excised internal structure concepts in benzenoid enumerations. J Math Chem 4:17–29

Diudea MV (2010) Diamond D_5, a novel allotrope of carbon. Stud Univ Babes Bolyai Chem 55(4):11–17

Diudea MV, Nagy CL (2012) C_{20}–related structures: diamond D_5. Diam Relat Mater 23:105–108

Diudea MV, Nagy CL, Ilić A (2011) Diamond D_5, a novel class of carbon allotropes. In: Putz MV (ed) Carbon bonding and structures. Advances in physics and chemistry. Springer, Dordrecht

Eckroth D (1967) A method for manual generation of correct von Baeyer names of polycyclic hydrocarbons. J Org Chem 32:3362–3365

Engler EM, Farcasiu M, Sevin A, Cense JM, Schleyer PR (1973) Mechanism of adamantane rearrangement. J Am Chem Soc 95:5769

Fokin AA, Schreiner PR (2009) Band gap tuning in nanodiamonds: first principle computational studies. Mol Phys 107:823–830

Fokin AA, Tkachenko BA, Gunchenko PA, Gusev DV, Schreiner PR (2005) Functionalized nanodiamonds. Part I. An experimental assessment of diamantane and computational predictions for higher diamonds. Chem Eur J 11:7091–7101

Fokin AA, Gunchenko PA, Novikovsky AA, Shubina TE, Chernyaev BV, Dahl JEP, Carlson RMK, Yurchenko AG, Schreiner PR (2009a) Photoacetylation of diamondoids: selectivities and mechanism. Eur J Org Chem pp 5153–5161

Fokin AA, Tkachenko BA, Fokina NA, Hausmann H, Serafin M, Dahl JEP, Carlson RMK, Schreiner PR (2009b) Reactivities of the prism–shaped diamondoids [1(2)3]tetramantane and [12312]hexamantane (cyclohexamantane). Chem Eur J 15:3851–3862

Fokin AA, Merz A, Fokina NA, Schwertfeger H, Liu SL, Dahl JEP, Carlson RMK, Schreiner PR (2009c) Synthetic routes to aminotriamantanes, topological analogues of the neuroprotector Memantine. Synthesis pp 909–912

Fokin AA, Zhuk TS, Pashenko AE, Dral PO, Gunchenko PA, Dahl JEP, Carlson RMK, Koso TV, Serafin M, Schreiner PR (2009d) Oxygen–doped nanodiamonds: synthesis and functionalizations. Org Lett 11:3068–3071

Fokina NA, Tkachenko BA, Dahl JEP, Carlson RMK, Fokin AA, Schreiner PR (2012) Synthesis of diamondoid carboxylic acids. Synthesis 44:259–264

Fort RC Jr (1976) Adamantane. The chemistry of diamond molecules. Marcel Dekker, New York

Fort RC Jr, Schleyer PR (1964) Adamantane: consequences of the diamondoid structure. Chem Rev 64:277–300

Frondel C, Marvin UB (1967) Lonsdaleite, a new hexagonal polymorph of diamond. Nature 214(5088):587–589

Geim AK, Novoselov KS (2007) The rise of graphene. Nat Mater 6:183–191

Gund TM, PvR S, Gund PH, Wipke WT (1975) Computer assisted graph theoretical analysis of complex mechanistic problems in polycyclic hydrocarbons. Mechanism of adamantane formation from various pentacyclotetradecanes. J Am Chem Soc 97:743–751

He H, Sekine T, Kobayashi T (2002) Direct transformation of cubic diamond to hexagonal diamond. Appl Phys Lett 81:610

Heimann RB, Evsyukov SE, Kavan L (eds) (1999) Carbyne and carbynoid structures. Physics and chemistry of materials with low–dimensional structures, vol 21. Kluwer Academic Publishers, Dordrecht

Hopf H (2003) Diamonds from crude oil? Angew Chem Int Ed 42:2000–2002

Ijima S (1991) Helical microtubules of carbon. Nature 354:56–58

Itzhaki L, Altus E, Basch H, Hoz S (2005) Harder than diamond: determining the cross–sectional area and Young's modulus of molecular rods. Angew Chem Int Ed 44:7432–7435

Jones AP, d'Hendecourt LB, Sheu SY, Change HC, Cheng CL, Hill HGM (2004) Surface C–H stretching features on meteoritic nanodiamonds. Astron Astrophys 416:235–241

Karle IL, Karle J (1965) The crystal and molecular structure of congressane. $C_{14}H_{20}$, by X–ray diffraction. J Am Chem Soc 87:918–920

Klein DJ, Balaban AT (2006) The eight classes of positive–curvature graphitic nanocones. J Chem Inf Model 46:307–320

Klein DJ, Balaban AT (2011) Clarology for conjugated carbon nanostructures: molecules, polymers, graphene, defected graphene, fractal benzenoids, fullerenes, nanotubes, nanocones, nanotori, etc. Open Org Chem J 5(suppl 1–M1):27–61

Krätschmer W, Lamb LD, Fostiropoulos K, Huffman DR (1990) Solid C_{60}: a new form of carbon. Nature 347:354–358

Kroto H (1997) Symmetry, space, stars, and C_{60}. Angew Chem Int Ed 36:1578–1593
Kroto H (2010) Carbyne and other myths about carbon. RSC Chem World 7(11):37
Lagow RJ, Kampa JJ, Wei HC, Battle SL, Genge JW, Laude DA, Harper CJ, Bau R, Stevens RC, Haw JF, Munson E (1995) Synthesis of linear acetylenic carbon: the "sp" carbon allotrope. Science 267:362–367
Landa S, Machacek V (1933) Adamantane, a new hydrocarbon extracted from petroleum. Coll Czech Chem Commun 5:1–5
Lewis RS, Ming T, Wacker JF, Anders E, Steel E (1987) Interstellar diamonds in meteorites. Nature 326:160–162
Mansoori GA, de Araujo PLB, de Araujo ES (2012) Diamondoid molecules: with applications in biomedicine, materials science, nanotechnology and petroleum science. World Scientific, Singapore
McKervey MA (1980) Synthetic approaches to large diamond hydrocarbons. Tetrahedron 36:971
Merz KM Jr, Hoffmann R, Balaban AT (1987) 3,4–connected carbon nets: through–space and through–bond interactions in the solid state. J Am Chem Soc 109:6742–6751
Oberlin A, Endo M, Koyama T (1976) Filamentous growth of carbon through benzene decomposition. J Cryst Growth 32:335–349
Pan Z, Sun H, Zhang Y, Chen C (2009) Harder than diamond: superior indentation strength of wurtzite BN and lonsdaleite. Phys Rev Lett 102:055503
Pirali O, Vervloet M, Dahl JE, Carlson RMK, Tielens AGG, Oomens J (2007) Infrared spectroscopy of diamondoid molecules: new insights into the presence of nanodiamonds in the interstellar medium. Astrophys J 661:919–925
Prelog V, Seiwerth B (1941a) Synthesis of adamantane. Ber Dtsch Chem Ges 74:1644–1648
Prelog V, Seiwerth B (1941b) New method for the preparation of adamantane. Ber Dtsch Chem Ges 74:1679–1772
Radushkevich LV, Lukyanovich VM (1952) On the structure of carbon formed by thermal decomposition of carbon monoxide on iron catalyst (in Russian). Zh Fiz Khim 26:88–95
Randić M, Balaban AT (2008) Ring signatures for benzenoids with up to seven rings. Part 1. Catacondensed systems. Intern J Quantum Chem 108:865–897. Erratum, ibid 3252
Randić M, Vukicević D, Balaban AT, Plavsić D (2012) Ring currents in hexabenzocoronene and its derivatives formed by joining proximal carbons. J Comput Chem 33:1111–1122
Richter H, Schwertfeger H, Schreiner PR, Fröhlich, Glorius F (2009) Synthesis of diamantane–derived N–heterocyclic carbenes (IDAd) and applications in catalysis. Synlett pp 193–197
Roth S, Leuenberger D, Osterwalder J, Dahl FE, Carlson BMK, Tkachanko BA, Fokin AA, Schreiner PR, Hengsberger M (2010) Negative–electron–affinity diamondoid monolayers as high–brilliance source for ultrashort electron pulses. Chem Phys Lett 495:102–108
Schleyer PR (1957) A simple preparation of adamantine. J Am Chem Soc 79:3292
Schleyer PR (1990) My thirty years in hydrocarbon cages: from adamantane to dodecahedrane. In: Olah GA (ed) Cage hydrocarbons. Wiley–Interscience, New York
Schreiner PR, Fokin AA, Reisenauer HP, Tkachenko BA, Vass E, Olmstead MM, Bläser D, Boese R, Dahl JEP, Carlson RMK (2009) [123]Tetramantane: parent of a new family of σ–helicenes. J Am Chem Soc 131:11292–11293
Schreiner PR, Chernish LV, Gunchenko PA, Tikhonchuk EY, Hausmann H, Serafin M, Schlecht S, Dahl JE, Carlson RMK, Fokin AA (2011) Overcoming extremely long C–C alkane bond lability through attractive dispersion forces. Nature 477:308–311
Schwab PFH, Levin MD, Michl J (1999) Molecular rods. I. Simple axial rods. Chem Rev 99:1863–1934
Schwab PFH, Levin MD, Michl J (2005) Synthesis and properties of molecular rods. 2. Zig–zag rods. Chem Rev 105:1197–1279
Schwertfeger H, Schreiner PR (2010) Chemie mit Nano-Juwelen. Chem unserer Zeit 44:248–253
Schwertfeger H, Fokin AA, Schreiner PR (2008) Diamonds are a chemist's best friend: diamond chemistry beyond adamantane. Angew Chem Int Ed 47:1022–1036
Schwertfeger H, Würtele C, Hausmann H, Dahl JEP, Carlson RMK, Fokin AA, Schreiner PR (2009) Selective preparation of diamondoid fluorides. Adv Synth Catal 451:1041–1054

Schwertfeger H, Machuy M, Würtele C, Dahl JEP, Carlson RMK, Fokin AA, Schreiner PR (2010a) Diamondoid phosphines – selective phosphorylation of nanodiamonds. Adv Synth Catal 352:609–615

Schwertfeger H, Würtele C, Schreiner PR (2010b) Synthesis of diamondoid nitro compounds from amines with m–chloroperbenzoic acid. Synlett pp 493–495

Sheng XL, Yan QB, Ye F, Zheng QR, Su G (2011) T–carbon: a novel carbon allotrope. Phys Rev Lett 106:155703

Singh J, Singh S, Meer S, Agrawal VK, Khadikar PV, Balaban AT (2006) QSPR correlations of half–wave reduction potentials of cata–condensed benzenoid hydrocarbons. Arkivoc xv:104–109

Smalley RE (1997) Discovering the fullerenes. Angew Chem Int Ed 36:1594–1601

Tobe Y, Wakabayashi T (2005) Carbon–rich compounds: acetylene–based carbon allotropes. In: Diederich F, Stang PJ, Tykwinski RR (eds) Acetylene chemistry: chemistry, biology, and material science. Wiley-VCH Verlag GmbH & Co. KGaA, Weinheim, pp 387–426

Wang Y, Tkachenko BA, Schreiner PR, Marx A (2011) Diamond–modified DNA. Org Biomol Chem 9:7482–7490

Whitlock HW Jr, Siefken MW (1968) Tricyclo[4.4.0.03,8]decane to adamantane rearrangement. J Am Chem Soc 90:4929

Williams VZ Jr, Schleyer PR, Gleicher GJ, Rodewald LB (1966) Triamantane. J Am Chem Soc 88:3862–3863

Xue KH, Tao FF, Shen W, He CJ, Chen QL, Wu LJ, Zhu YM (2004) Linear carbon allotrope – carbon atom wires prepared by pyrolysis of starch. Chem Phys Lett 385:477–480

Zhu Q, Oganov A, Salvadó M, Pertierra P, Lyakhov A (2011) Denser than diamond: Ab initio search for superdense carbon allotropes. Phys Rev B 83:193410

Chapter 2
Diamond and Diamond-Like Carbon

Zahra Khalaj, Mahmood Ghoranneviss, Elnaz Vaghri, and Oana Ponta

Abstract A carbon allotrope is classified as "diamond" according to several parameters including the types of chemical bonds, type of crystal network, or range of crystal dimensionality. This chapter is a review on two major allotropes: diamond and diamond-like carbon, which are mostly produced by CVD technique. A detailed description of these techniques, as experienced by our group, is given. The importance of preparing the support for depositions and monitoring the process parameters is argued by the quality of carbon allotrope deposits, evidenced by a variety of physical measurements and microscopic images.

2.1 Introduction

Carbon is one of the most important natural elements in the periodic table, having more than one million different compounds in different forms. There exist four valance electrons in a carbon atom, two in 2s subshells and two in the 2p subshell. The atomic arrangement makes the carbon to exist with different allotropes such as diamond, diamond-like carbon, graphite, fullerene, carbon nanotubes, and carbon nanowalls and different material properties (Vaghri et al. 2012; Shams et al. 2012). This chapter is a review on two major allotropes, diamond and diamond-like carbon, that can be produced by chemical vapor deposition (CVD) techniques. Nanodiamond films (NDF) and nanocrystalline diamonds (NCD) possess high thermal

Z. Khalaj (✉) • M. Ghoranneviss • E. Vaghri
Plasma Physics Research Center, Science and Research Branch,
Islamic Azad University, Tehran, Iran
e-mail: khalaj.z@gmail.com

O. Ponta
Department of Condensed State Physics and Advanced Technologies, Faculty of Physics,
Babes-Bolyai University, Cluj, Romania

M.V. Diudea and C.L. Nagy (eds.), *Diamond and Related Nanostructures*,
Carbon Materials: Chemistry and Physics 6, DOI 10.1007/978-94-007-6371-5_2,

conductivity, large bandgap, excellent hardness, high electrical resistivity, and low friction coefficient (Takano et al. 2005; Yamazaki et al. 2008a, b). These properties promise outstanding applications of NCDs in electronics, optics, mechanics, etc. (Sharda et al. 2001). In addition, during the last decades, diamond-like carbon films have been intensively studied and utilized in many fields of industry, owing to their remarkable characteristics. Due to the excellent properties, very close to that of diamond, this allotrope was called diamond-like carbon (DLC). These films are extremely hard and mainly consist of sp^2 and sp^3 carbon networks.

2.2 Carbon Allotropes

Carbon is unique among all the elements, having four valence electrons and four vacancies in its outer shell, with an electron ground state $1s^2\ 2s^2\ 2p^2$.

There are three types of hybridization in allotropes of the carbon:

sp-type hybridization: one s-orbital hybridizes with one of the p-orbitals to make two sp-hybridized orbitals. The angle between these new orbitals is 180° and the carbon atom bounds by a diagonal symmetry.

sp^2-type hybridization: one s-orbital is mixed with two of the p-orbitals to form three hybridized orbitals with a trigonal symmetry; the angles between them are 120°.

sp^3-type hybridization: one s-orbital of a carbon atom is hybridized with all the three p-orbitals of the carbon atom to form four new orbitals with a tetrahedral symmetry and with 109.5° angles between them.

Combination of the above hybridized states allows the formation of several allotropic forms such as graphite, diamond, diamond-like carbon, and spherical cages also called fullerenes.

Figures 2.1, 2.2, 2.3, and 2.4 show some types of carbon allotropes produced by the authors using Plasma Enhanced Chemical Vapor Deposition (PECVD) and Hot Filament Chemical Vapor Deposition (HFCVD) techniques.

2.3 History of the Diamond

It is thought that the first diamond has been discovered by human beings more than 3,000 years ago. The word “diamond” comes from ancient Greek word “adamas,” which means “invincible,” referring to the extreme hardness of the material. After scientists discovered that diamond is an allotrope of carbon, many groups attempted to produce this rare and valuable material synthetically. General Electric Company was the first group who succeeded to heat carbon up to 3,000 °C under a very high pressure. After optimization of the growth process, they named it high-pressure high

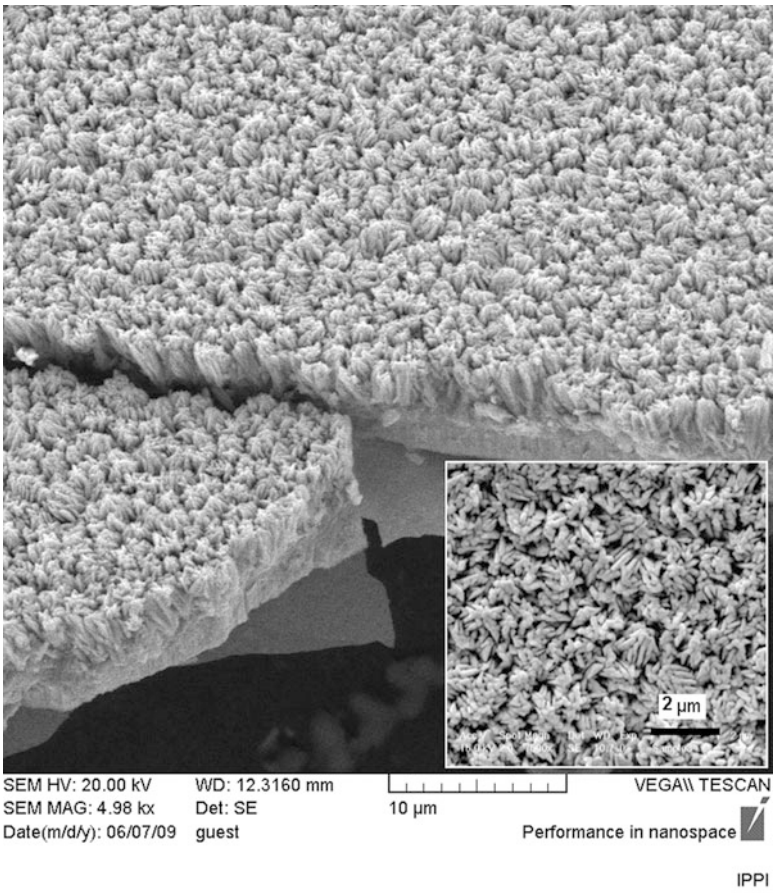

Fig. 2.1 Self-assembled cone-like carbon synthesized on gold coated silicon substrate using ammonia as an annealing gas and a mixture of CH_4/H_2 with 5% flow ratio as a reaction gas by HFCVD technique

temperature (HPHT) method. Scientists tried to grow diamonds as pure as possible. Next, the chemical vapor deposition (CVD) technique was proposed to grow the diamond at lower pressure and temperature.

In diamond lattice, each carbon atom is tetrahedrally coordinated, forming strong bonds to its four neighbors using sp^3 hybridized orbitals, with equal angles of 109.28° to each other. Each tetrahedron combines with four other tetrahedra forming a strongly bonded, uniform, three-dimensional, entirely covalent crystalline structure with the bond length of 0.154 nm. Due to its outstanding properties, diamond is the unique material with various applications in life and technology. It is the hardest of all natural materials and the highest thermal conductivity.

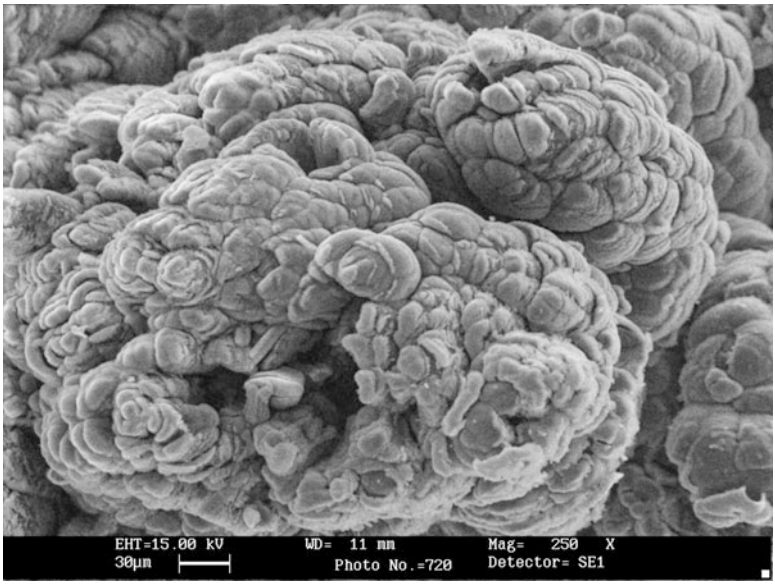

Fig. 2.2 SEM image of the DLC synthesized using PECVD technique

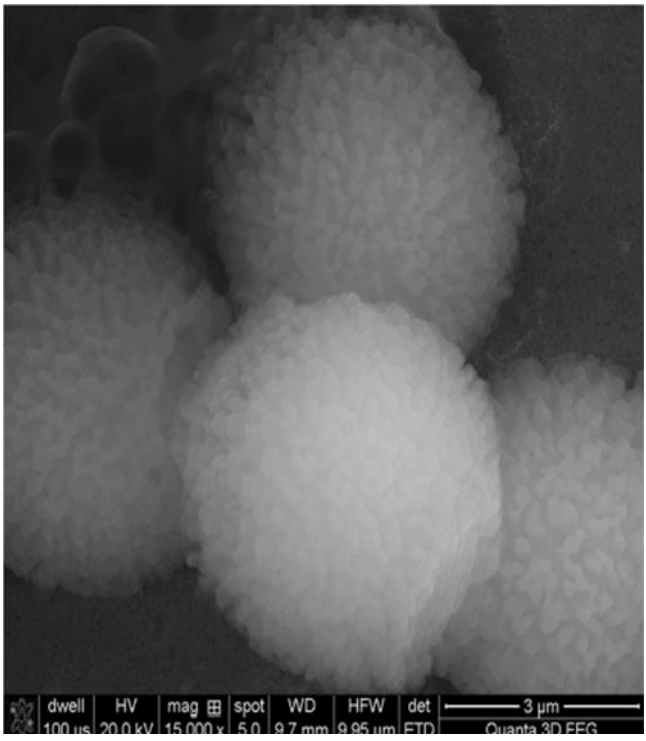

Fig. 2.3 Carbon microspheres synthesized by PECVD technique

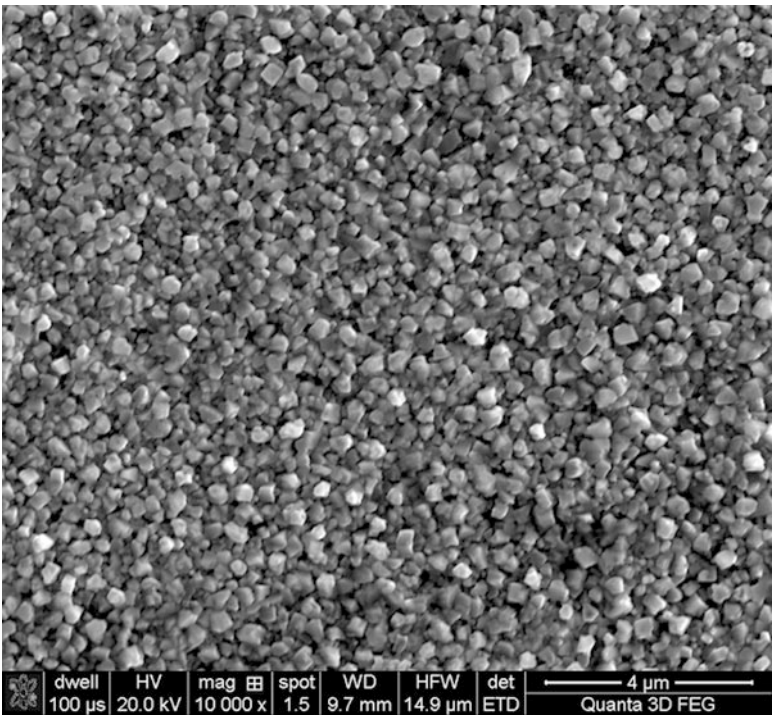

Fig. 2.4 Diamond thin film deposited on high-purity nickel substrate by PECVD technique

2.4 Quality of the Diamond Films

By developing the chemical vapor deposition (CVD), nanocrystalline diamonds (NCDs) and nanocrystalline diamond films (NDFs) became the topic of wide research (Khalaj et al. 2009, 2012; Khalaj and Ghoranneviss 2012; Atefi et al. 2012; Gupta et al. 2002; Yamazaki et al. 2008a, b; Melo et al. 2007; Tallaire et al. 2006; Zhoutong et al. 2008; Arnault et al. 1999; Donato et al. 2001). Nanocrystalline diamond films can be grown in a variety of conditions, using different chemical vapor deposition techniques at relatively low pressures and high nucleation densities. The quality and purity of nanostructures in CVD techniques are very important. There are some ways for increasing the quality and quantity of these deposits. To achieve a high nucleation density, several approaches are available.

2.4.1 Role of Interlayer and Catalyst Layer

The nucleation and growth of diamond coating on non-diamond substrates (e.g., silicon, steel, and Al) can be dramatically improved with different surface treatments (Fu et al. 2000). There are several methods to enhance the diamond nucleation, including mechanical and chemical treatment processes such as using interlayer or catalyst layer. In this case, the interlayer might act as an adhesion layer and makes a good reactive surface for adsorbing the carbon. Furthermore, using a catalyst layer can increase the rate of diamond nucleation and provide a diffusion barrier to increase the carbon concentration for diamond nucleation. Using suitable catalyst (e.g., gold or silver nanoparticles) can enhance the diamond nucleation and, therefore, increase the quality of the films (Khalaj and Ghoranneviss 2012). In addition, a homogenous distribution of the catalyst nanoparticles could lead to a dense film of the diamond.

2.4.2 Role of Etching Treatment

Another effective way to enhance the diamond nucleation is the chemical or physical etching treatment of the substrate (Khalaj et al. 2010). The etching process can be a wet or a dry one, depending on whether the material removed enters the liquid or gas phase, respectively (Ohring 2002). While wet etching techniques dominate in micromechanics, up to micrometer range, dry etching becomes interesting with decreasing structure size and it plays a key role in diamond growth. Due to the dependence on the etching rate (involving the mobile phase, chemical reactions at solid state surface, or removal of reaction products) of the thickness of the diamond deposit, it is important to calculate the etching rate (r_{etch}) for each sample, $r_{\text{etch}} = d_{\text{etch}} / t_{\text{etch}}$, where d_{etch} is the removed thickness of the layer and t_{etch} is the duration of etching (Ohring 2002).

Different research groups have investigated various parameters, treatments, and CVD techniques with the aim of enhancing the diamond nucleation and increasing the deposit quality (Gruen 1999; Buhler and Prior 2000; Liang et al. 2006; Khalaj et al. 2012). Producing a high quality and controllable growth of the diamond is very important for industrial applications. Using different etching gases, such as hydrogen, nitrogen, and ammonia, has different effect on diamond nucleation. By our experience (Khalaj et al. 2010), the quality of the diamond deposits was higher in case we used hydrogen as an etching gas. Depending on the experimental conditions, good quality diamond films or diamond single crystals were obtained.

An example of the morphology and the Energy dispersive X-ray analysis (EDS) from the surface of the high-quality diamond film synthesized on nickel substrate is shown in Fig. 2.5. The substrate is polished with 1μm diamond paste and etching treated by hydrogen before inserting the reaction gases. Hydrogen-etching

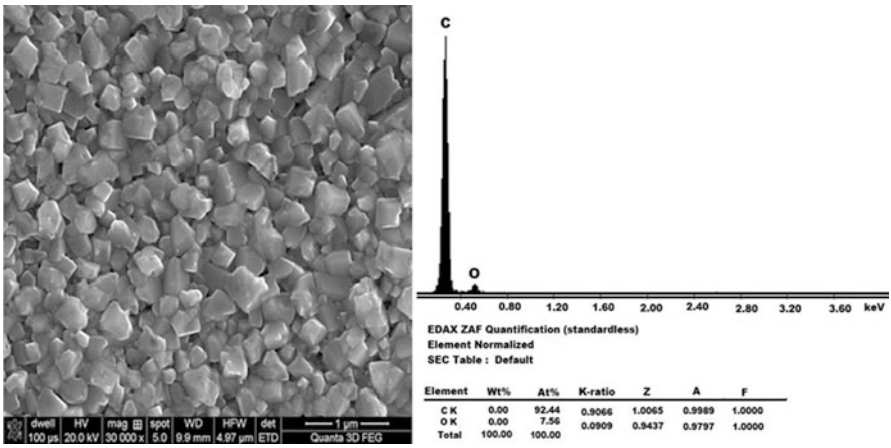

Fig. 2.5 High nucleation density of a diamond film obtained by seeding high-purity nickel (99.99 %) substrate with 1 μm diamond paste. The film was produced by our group using CH_4/H_2 mixture with flow ratio 8 % by plasma-enhanced CVD system

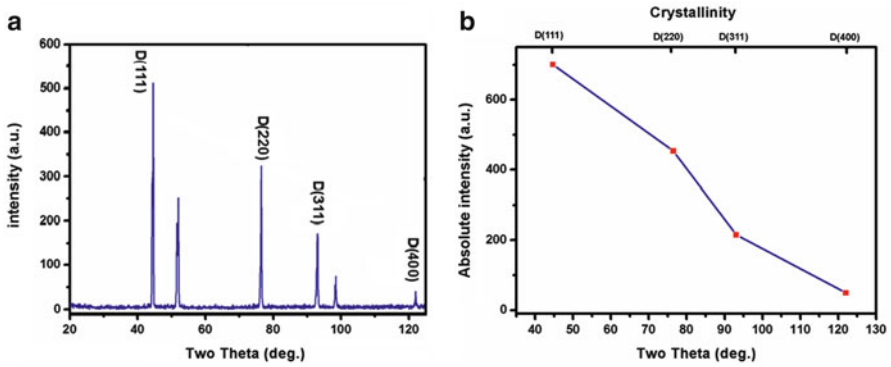

Fig. 2.6 (**a**) The XRD pattern for synthesized diamond film on Ni substrate by PECVD system and (**b**) two-theta diagram versus intensity and crystallinity, respectively

treatment helps to produce dense diamond film with high-purity crystallite structure in comparison with virgin substrate with no etching treatment.

The crystalline structure of this film was measured using X-ray diffraction (XRD). The XRD patterns were recorded with a Shimadzu XRD – 6,000 diffractometer using Cu Kα ($\lambda = 1.5405$ Å) radiation. Crystallographic identification was accomplished by comparing the experimental XRD patterns with standard inorganic crystal structure data JCPDS. Based on the spectra in Fig. 2.6, four diffraction peaks were found in the spectra for the typical SEM image, at different two-theta values. One can observe the spectrum is dominated by $2\Theta = 44.44°$, 76.34°, and 92.91° which could be identified with reflections from (111), (220), and (311) plane of

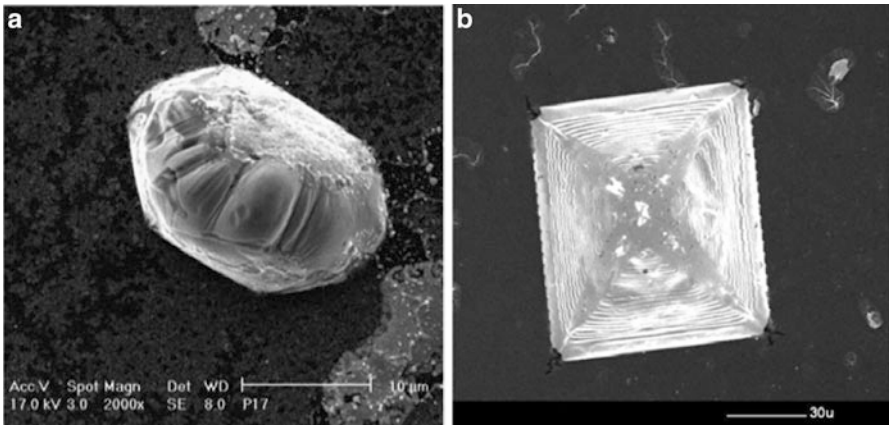

Fig. 2.7 Diamond single crystals grown on selected area: (**a**) gold coated silicon wafer and (**b**) silicon

diamond. The last peak with lower intensity exhibits at 121.70° which is indexed to the diffraction from (400) crystal planes of diamond. The full width half maximum (FWHM) of the diamond peaks shows the sharp peaks with small FWHM which indicate high crystal quality.

In addition, one can see an obvious pattern for two-theta versus absolute intensity and crystallinity. Due to the intensity and FWHM of each peak, the quality of the crystallites varies with changing the two theta. Therefore, it is clearly seen that the quality of the crystallites orientation decreases by increasing the two-theta degree on diamond coated nickel substrate.

2.4.3 Selective Growth

One of the important methods in controllable diamond production is the selective growth method (Khokhryakov and Palyanov 2006; Tran et al. 2010; Li et al. 2003, 2010). A good quality of CVD diamond depends on the controllable growth in selected area that can make the diamond more applicable. Figure 2.7 shows the microcrystalline diamond with different crystallite structure grown on selected area.

2.5 Diamond-Like Carbon Films

A great variety of materials are formed from carbon, ranging from crystalline to amorphous structures. Diamond-like carbon (DLC) films consist of a random network of sp^2 and sp^3 carbon sites with varying amount of hydrogen dispersed

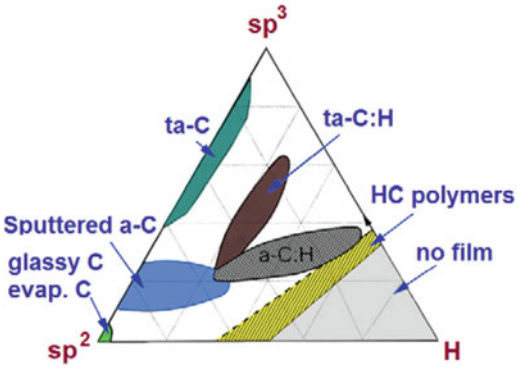

Fig. 2.8 Ternary phase diagram of the C, H system displaying composition of DLC films

within the lattice (Donnet et al. 1999, 2000). The sp^2-bonded carbon controls the optical properties of DLC films like bandgap and infrared refractive index while the sp^3-bonded carbon controls the mechanical properties like hardness, coefficient of fraction, and Young modulus (Robertson 2002).

Aisenberg and Chabot (1971) were the first who prepared DLC films using carbon ions in argon environment. A first model of DLC structure was proposed by Robertson (1986, 2001, 2002). Angus and Jansen (1988) developed a model describing DLC as a dense film phase of a random covalent carbon network. Based on the existence of hydrogen in these films, a material can be categorized as follows:

1. Hydrogenated amorphous carbon (a-C: H) is the common form of DLC; these films contain a moderate content of sp^3carbon and 10–40 % H (Lifshitz 2003). The a-C: H films or DLC films can be divided into two different forms, the hard a-C: H and the soft one. The hard a-C: H consists of a fraction of sp^2 bonds and sp^3 bonds and low hydrogen amount whereas the soft a-C: H has a higher hydrogen amount.
2. Hydrogenated tetrahedral amorphous carbon (ta-C: H) films with a high sp^3 content and relatively low hydrogen content.
3. Hydrogen-free form of amorphous carbon (a-C) film is another important form of DLC; it has a significant fraction of sp^2 bonds.
4. Tetrahedral hydrogen-free amorphous carbon (ta-C) contains up to 90 % sp^3-hybridized bonds (Lifshitz 2003). Figure 2.8 represents various forms of DLC by a ternary diagram.

The three corners of this diagram are related to diamond, graphite, and hydrocarbons. The a-C: H film is located at the center of the phase diagram and shows various amounts of sp^3, sp^2, and H contents. Research on diamond-like carbon films has been devoted to find both optimized conditions and characteristics of the deposited films on various substrates. Depending on the deposition conditions, DLC films can be totally amorphous or include micro- or nanocrystalline diamond. Figure 2.9 shows a sample of DLC structures without crystalline orientation.

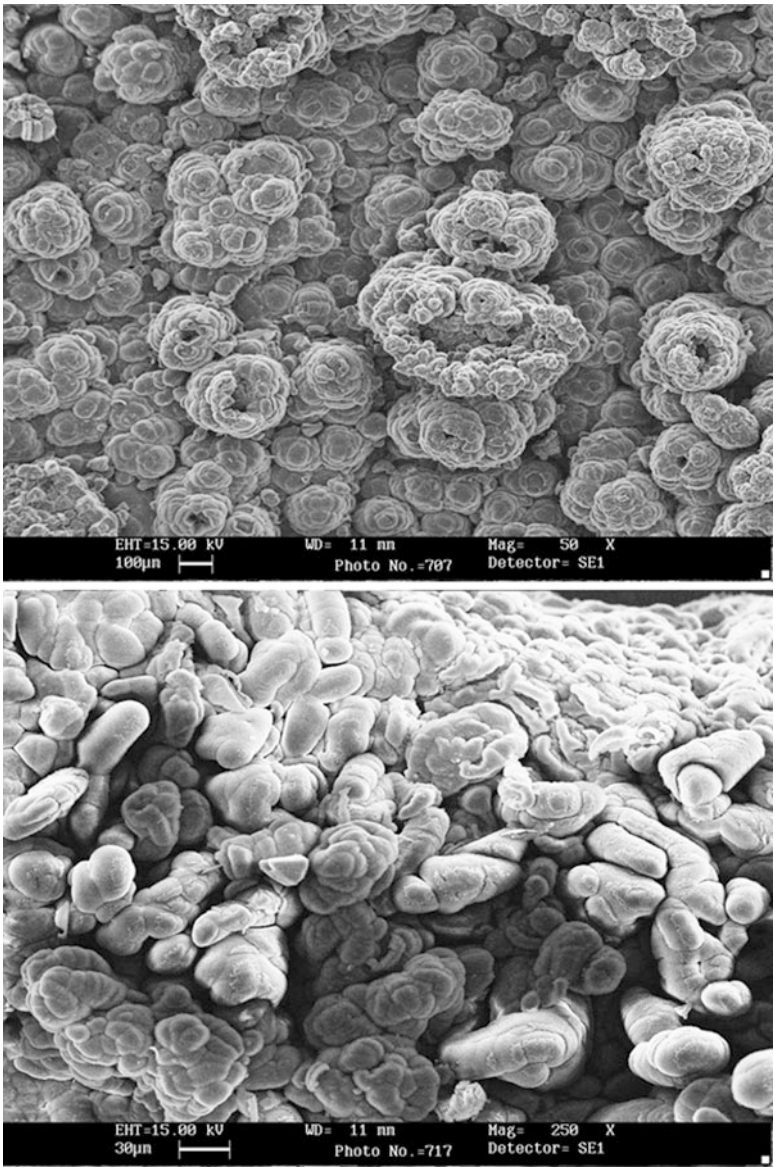

Fig. 2.9 Typically SEM images of diamond-like carbon synthesized by our group

2.6 Properties and Applications

Since their first preparation, in the early 1970s (Aisenberg and Chabot 1971), DLC films have attracted a considerable interest from both academic and industrial communities owing to their extraordinary properties such as: low friction coefficient,

high wear resistance, chemical inertness, optical transparency, high hardness, and biocompatibility (Nakazawa et al. 2010) that make them reliable to use in various fields of science and technology. DLC coatings have found biomedical applications such as contact lenses, medical wires, arterial stents, orthopedic pins, surgical scalpels, and dental instruments (Yin et al. 2008; Robertson 2002; Donnet et al. 1999; Donnet and Grill 1997; McHargue et al. 1991; Shirakura et al. 2006; Morrison et al. 2006; Ishihara et al. 2005). One of the significant properties of DLC is the high mechanical hardness; thus, they are commonly utilized in industry as protective, nonabrasive, and corrosion-resistant coating. Other applications include antireflection optical windows and lubricant coatings in micro-electromechanical devices (Cho et al. 2005; Singh et al. 2006; Piazza et al. 2005; Ferrari 2004; Robertson 2001; Dearnaley and Arps 2005; Grill 1999, 2003; Vaghri et al. 2011). In addition, DLC coating would increase the surface hardness and its longevity, therefore, it can be used for harden the internal wall of the Tokamak reactors (Vaghri et al. 2011). However, adhesion of DLC films to metallic substrates, especially stainless steel, is the major concern related to these films.

2.7 Quality of DLC Films

The presence of a high internal compressive stress in DLC films is the main drawback of these films leading to crack and poor adhesion to the substrate (Grill 1999, 2003; Silva et al. 2011; Chiba and Tada 2012) which results in production of low-quality DLC films with no application. The internal stress of DLC films is composed from the intrinsic stress and thermal stress. The intrinsic stress appears during the growth process while the thermal stress is caused by difference in thermal expansion coefficient between the film and base material (Ji et al. 2008). Many attempts have been made to increase the adherence of diamond-like carbon coatings to the substrate such as incorporation of elements into the film and/or introducing interlayer between films and substrates (Ji et al. 2008; Azzi et al. 2010; Chen and Lin 2009; Ahmed et al. 2009). Dwivedi et al. (2012) investigated the growth and characteristics of Cu-incorporated DLC films. Their experimental results illustrated that copper incorporation into DLC matrix relaxed the residual stress and considerably improved the temperature-dependent electrical transport. Gayathri et al. (2012) reported the growth of DLC films with different transition metal (M = Cr, Ag, Ti, Ni) interlayers. They found that chromium interlayer reduces the internal stress significantly compared to titanium, nickel, and silver. Ban and Hashegawa (2002) found that the incorporation of silicon into DLC films reduced the internal stress. Other parameters influencing on DLC adhesion to the substrates include: chemical bonding between the DLC coating and substrate, contamination, roughness of the substrate, and physical properties (Koski et al. 1996; Morshed et al. 2003). Surface roughness and morphologic variations have direct influence on layer adhesion to the substrate. We can decrease the surface roughness by selecting a suitable intermediate layer and roughness of the coatings. In view to produce a

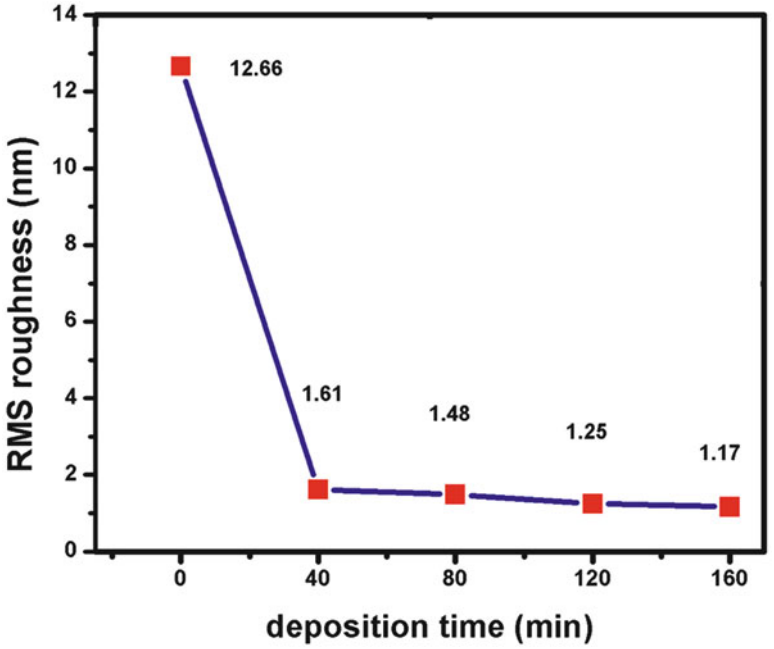

Fig. 2.10 Variation in the roughness of Ni coating on AISI 304L substrates at different deposition times

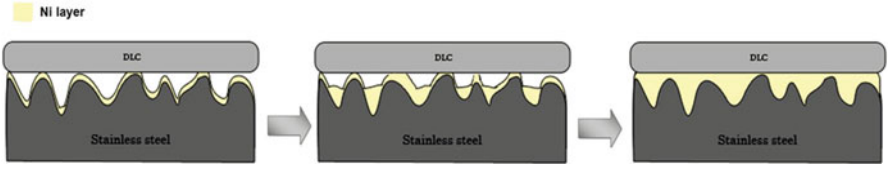

Fig. 2.11 The contact mechanism of a *DLC* sliding on a Ni-coated stainless steel with different surface roughness

high quality of DLC, we used nickel as an intermediate layer (Khalaj et al. 2012) and investigate the effect of surface roughness on the deposit quality. Decreasing in the nickel layer roughness (see Fig. 2.10) resulted in a DLC better adhesion to the stainless steel substrate (probably due to a higher degree of chemical bonding and good friction coefficient of Ni layer which is compatible with the model in Fig. 2.11).

The root-mean-squared roughness (R_{rms}) of surface is one of the most important parameters for the characterization of the surface structure (Eskusson et al. 2008). An illustration of the roughness and morphology of the surface of the stainless steel coated by nickel is given in Fig. 2.12.

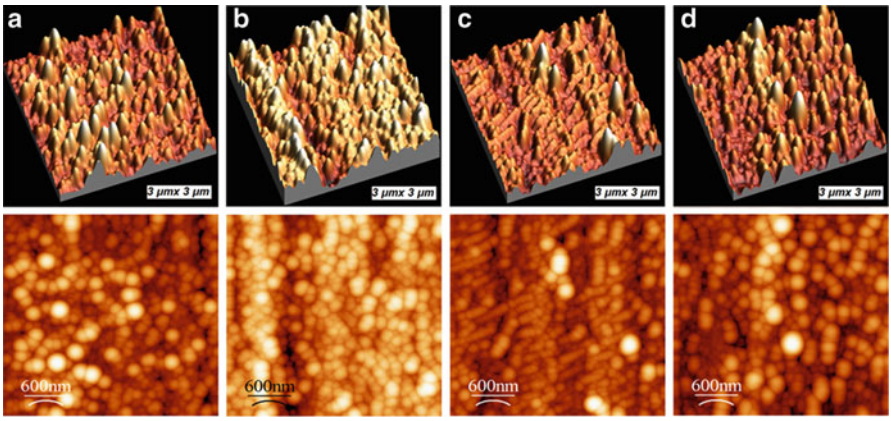

Fig. 2.12 2D and 3D AFM images of the stainless steel coated by Ni at different deposition time: (**a**) 40 min, (**b**) 80 min, (**c**) 120 min, and (**d**) 180 min, respectively

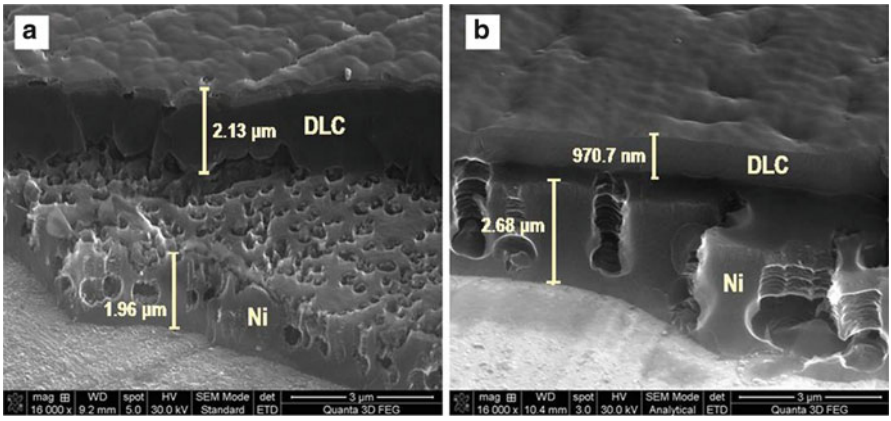

Fig. 2.13 Typical cross-section SEM images of DLC deposits on stainless steel coated by Ni at 40 min (**a**) and 180 min (**b**)

For a more detailed morphological analysis there was performed a cross section using high-current ion column. Quanta 3D FEG's high-current Focused Ion Beam (FIB) enables fast material removal. Automated FIB sectioning recipes enable accurate cross-sectioning and low damage sample cleaning. Figure 2.13 shows the minimum and the maximum thickness of the Ni layer in coatings.

Forming an intermediate layer between the DLC film and substrate releases the thermal stress by diminishing the mismatch of thermal expansion coefficients while incorporation of elements into the film releases the intrinsic stress by adjustment of film composition and structure (Ji et al. 2008).

2.8 Deposition Techniques

A wide variety of chemical and physical vapor deposition methods have been developed for the deposition of the diamond and DLC films. Different types of CVD techniques are used to produce diamond and diamond-like carbon films, and they can be grouped into four main categories based on the activation process: (1) plasma activation, (2) thermal activation, (3) laser ablation, and (4) combustion. Similarly, physical vapor deposition (PVD) techniques have also been attempted in the last years. In this part, we introduced two of the most applicable CVD techniques for producing DLC and diamond films: plasma-enhanced chemical vapor deposition and hot filament chemical vapor deposition, designed by Plasma Physics Research Center (PPRC) engineering group.

2.8.1 PECVD Technique

Two of the most common techniques used for the deposition of DLC films are Dc- and Rf-PECVD methods. Possibility of deposition on a large area and at low temperature is the main advantage of the PECVD technique; it provides using a wide variety of substrate materials, with great industrial importance (Eskusson et al. 2008). The central part of our PECVD system is a cylindrical process chamber with a diameter of about 30 cm consisting of a base and a cap. On the top of the cap, the Dc-/Rf-source is flanged. The chamber can be opened for substrate handling by vertical shifting the aluminum cap on top. The substrate is placed on a furnace right under the anode. The temperature of the substrates is monitored by a thermocouple. Figure 2.14 shows the schematic diagram of our PECVD system.

The PECVD process is based on the disintegration of a carbonaceous gas into species such as ions, radicals, and atoms near the substrate surface. In this way, a wide range of substrate material can be used. Most of the researches used Rf-discharge to produce DLC (Whitmell and Williamson 1976; Bubenzer et al. 1983; Dhawan et al. 2003; Li et al. 2003, 2010). It is generally considered that DLC is not possible with DC discharge due to deposition of dielectric films, the electrode exposed to the plasma gradually becoming covered with an insulator (Angus and Jansen 1988). Although a DC discharge may be initiated, it will quickly extinguish as the electrons accumulate on the insulator and recombine with the available ions. Using hydrogen dilution could avoid covering the target with a hydrocarbon gas. In addition, DC-PECVD is suitable for DLC coating because of the low stress values of deposits in comparison to Rf-PECVD method (Ferrari 2004).

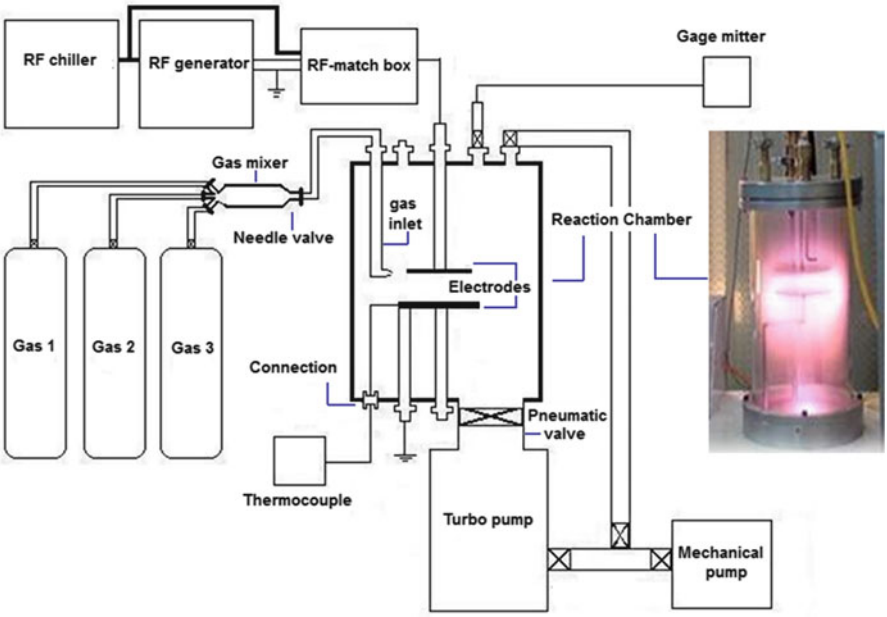

Fig. 2.14 The schematic diagram of the PECVD system designed and fabricated by S. Shams and M. Ghoranneviss (Registered in: State Reg. Org. for Deeds and Real-Estates, Industrial Property General Office, Iran, Serial No: A/89-020594)

2.8.2 HFCVD Technique

The Hot filament chemical vapor deposition (HFCVD) system is used for growing diamond films and other carbon allotropes (Shahsavari et al. 2011; Atefi et al. 2011). This system consists of a horizontal stainless steel (S.S.316) cylinder as a reaction chamber, a furnace, and filament. Figure 2.15 shows the schematic diagram of our HFCVD system. Tungsten wires were used as filaments which electrically heated to over 2,000 °C during the reaction. The substrate is placed on a substrate holder right under the filament, where the distance between the filament and substrate is adjustable. Due to the high degree of ionization occurring by the hot filament, this system is much more suitable for diamond growth. Production of other carbon allotropes is also possible using optimum experimental condition. In order to obtain diamond nano- and microstructures, the substrate is introduced into the reaction chamber and it will evacuate to 10^{-6} Torr as a base pressure. The source gas and dilution gas are fed into the system through a steel nozzle.

Diamond can be deposited from a large variety of precursors including methane, aliphatic, and aromatic hydrocarbons. These compounds generally decompose into stable primary species such as the methyl radical (CH_3) that is considered the dominant species in generating the growth of CVD diamond.

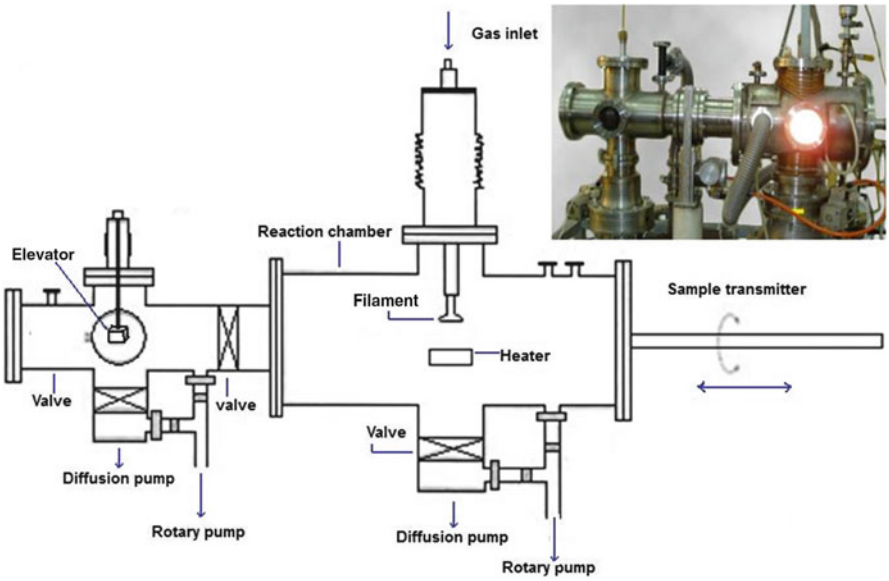

Fig. 2.15 The schematic diagram of the HFCVD system fabricated by Plasma Physics Research Center group

The stable hydrogen diatomic molecule (H_2) dissociates at low pressure and the temperature over 2,000 °C to free atoms. The rate of recombination to diatomic molecule is rapid, the half-life of atomic hydrogen being only 0.3 s (Hugh O. Pierson 1999). Atomic hydrogen plays an essential role in the surface and plasma chemistry of diamond deposition as it contributes to the stabilization of the sp^3 dangling bonds found on the diamond surface plane (Yasuda et al. 1990). Unlike molecular hydrogen, atomic hydrogen is extremely reactive and helps to remove the graphite selectively by etching the deposits. Although the hydrogen etching occurs simultaneously in graphite and diamond, its effect on graphite is 20 times as fast as it etches diamond. This process is very important and sensitive in producing high-quality diamond films.

References

Ahmed SF, Moon M-W, Lee K-R (2009) Effect of silver doping on optical property of diamond like carbon films. Thin Solid Films 517:4035–4038

Aisenberg S, Chabot R (1971) Ion–deposition of thin films of diamond like carbon. Appl Phys 42:2953–2958

Angus J, Jansen F (1988) Dense “diamond like” hydrocarbons as random covalent networks. Vac Sci Technol A 6:1778–1782

Arnault JC, Demuynck L, Speisser C, Le Normand F (1999) Mechanisms of CVD diamond nucleation and growth on mechanically scratched Si (001) surfaces. Eur Phys J B 11:327–343
Atefi H, Ghoranneviss M, Khalaj Z, Diudea MV (2011) Effect of different substrate temperature on growth of nano crystalline diamond by HFCVD technique. Studia Univ Babes-Bolyai Chemia 56:133–140
Atefi H, Khalaj Z, Ghoranneviss M (2012) Deposition and characterization of nano crystalline diamond on different substrates by plasma enhanced CVD technique. Studia Univ Babes-Bolyai, Chemia 57:51–58
Azzi M, Amirault P, Paquette M, Klemberg-Sapieha JE, Martinu L (2010) Corrosion performance and mechanical stability of 316L/DLC coating system: role of interlayers. Surf Coat Technol 204:3986–3994
Ban M, Hasegawa T (2002) Internal stress reduction by incorporation of silicon in diamond–like carbon films. Surf Coat Technol 162:1–5
Bubenzer A, Dischler B, Brandt G, Koidl P (1983) Rf plasma deposited amorphous hydrogenated hard carbon thin films: preparation, properties, and applications. J Appl Phys 54:4590–4595
Buhler J, Prior Y (2000) Study of morphological behavior of single diamond crystals. Cryst Growth 209:779–788
Chen K-W, Lin F-J (2009) The study of adhesion and nanomechanical properties of DLC films deposited on tool steels. Thin Solid Films 517:4916–4920
Chiba K, Tada M (2012) Buffered internal stresses in diamond–like carbon films reinforced with single–walled carbon nanotubes. Thin Solid Films 520:1993–1996
Cho S-J, Chung J-W, Lee K-R (2005) Characterization of the mechanical properties of diamond–like carbon films. Diam Relat Mater 14:1270–1276
Dearnaley G, Arps JH (2005) Biomedical applications of diamond–like carbon (DLC) coatings. A review. Surf Coat Technol 200:2518–2524
Dhawan A, RoyChowdhury S, De PK, Sharma SK (2003) Corrosion behaviour of amorphous Ti48Cu52, Ti50Cu50 and Ti60Ni40 alloys investigated by potentiodynamic polarization method. Bull Mater Sci 26:609–612
Donato MG, Faggio G, Marinelli M, Messina G, Milani E, Paoletti A, Santangelo S, Tucciarone A, Verona Rinati G (2001) High quality CVD diamond: a Raman scattering and photoluminescence study. Eur Phys J B 20:133–139
Donnet C, Grill A (1997) Friction control of diamond–like carbon coatings. Surf Coat Technol 94:456–462
Donnet C, Fontaine J, Le Mogne T, Belin M, Héau C, Terrat JP, Vaux F, Pont G (1999) Diamond–like carbon–based functionally gradient coatings for space tribology. Surf Coat Technol 120:548–555
Donnet C, Fontaine J, Grill A, Le Mogne T (2000) The role hydrogen on the friction mechanism of diamond–like carbon films. Tribol Lett 9:137–142
Dwivedi N, Kumar S, Malik H, Sreekumar C, Dayal S, Rauthan CMS, Panwar OS (2012) Investigation of properties of Cu containing DLC films produced by PECVD process. Phys Chem Solids 73:308–316
Eskusson J, Jaaniso R, Lust E (2008) Synthesis of DLC films by PLD from liquid target and dependence of film properties on the synthesis conditions. Appl Phys A 93:745–749
Ferrari AC (2004) Diamond–like carbon for magnetic storage disks. Surf Coat Technol 180:190–206
Fu Y, Yan B, Nee Lam L (2000) Effects of pre–treatments and interlayers on the nucleation and growth of diamond coatings on titanium substrates. Surf Coat Technol 130:173–185
Gayathri S, Krishnan R, Ravindran TR, Tripura Sundari S, Dash S, Tyagi AK, Raj B, Sridharan M (2012) Spectroscopic studies on DLC/TM (Cr, Ag, Ti, Ni) multilayers. Mater Res Bull 47:843–849
Grill A (1999) Diamond–like carbon: state of the art. Diam Relat Mater 8:428–434
Grill A (2003) Diamond–like carbon coatings as biocompatible materials an overview. Diam Relat Mater 12:166–170
Gruen DM (1999) Nanocrystalline diamond films. Ann Rev Mater Sci 29:211–259

Gupta S, Weiner BR, Morell G (2002) Electron field emission properties of microcrystalline and nanocrystalline carbon thin films deposited by S–assisted hot filament CVD. Diam Relat Mater 11:799–803

Ishihara M, Suzuki M, Watanabe T, Nakamura T, Tanaka A, Koga Y (2005) Synthesis and characterization of fluorinated amorphous carbon films by reactive magnetron sputtering. Diam Relat Mater 14:989–993

Ji L, Li H, Zhao F, Chen J, Zhou H (2008) Adhesion studies of diamond–like carbon films on 202 stainless steel substrate with a silicon interlayer. Eng Mater 373–374:151–154

Khalaj Z, Ghoranneviss M (2012) Investigation of metallic nanoparticles produced by laser ablation method and their catalytic activity on CVD diamond growth. Studia Univ Babes-Bolyai Chemia 57:21–28

Khalaj Z, Taheri SZ, Laheghi SN, Eslami PA (2009) Diamond growth on aluminium substrate by HFCVD using different etching gasses. Iran Phys J 3(1):19

Khalaj Z, Ghoranneviss M, Nasirilaheghi S, Ghorannevis Z, Hatakeyama R (2010) Growth of nanocrystalline diamond on silicon substrate using different etching gases by HFCVD. Chin J Chem Phys 23:689–692

Khalaj Z, Ghoranneviss M, Vaghri E, Saghaleini A, Diudea MV (2012) Deposition of DLC film on stainless steel substrates coated by nickel using PECVD method. Acta Chim Slov 59:338–343

Khokhryakov AF, Palyanov YN (2006) Revealing of dislocations in diamond crystals by the selective etching method. Cryst Growth 293:469–474

Koski K, Hölsä J, Ernoult J, Rouzaud A (1996) The connection between sputter cleaning and adhesion of thin solid films. Surf Coat Technol 80:195–199

Li Y, Li Q, Wang F (2003) The electrochemical corrosion behavior of TiN and (Ti, Al)N coatings in acid and salt solution. Corros Sci 45:1367–1381

Li YS, Pan TJ, Tang Y, Yang Q, Hirose A (2010) Selective synthesis of diamond and CNT nanostructures directly on stainless steel substrates. Diam Relat Mater 20:187–190

Liang X, Wang L, Yang D (2006) The structural evolution of nanocrystalline diamond films synthesized by r.f. PECVD. Mater Lett 60:730–733

Lifshitz Y (2003) Pitfalls in amorphous carbon studies. Diam Relat Mater 12:130–140

McHargue CJ, Tzeng Y, Yoshikawa M, Murakawa M (1991) In: Feldman A (ed) Applications of diamond films and related materials, Materials science monographs. Elsevier, New York, p 113

Melo LL, Moro JR, Castro RM, Corat EJ, Trava Airoldi VJ (2007) A comparative study of diamond growth on tungsten wires by using methane and graphite as the carbon source. Surf Coat Technol 201:7382–7386

Morrison ML, Buchanan RA, Liaw PK, Berry CJ, Brigmon RL, Riester L, Abernathy H, Jin C, Narayan RJ (2006) Electrochemical and antimicrobial properties of diamond like carbon–metal composite films. Diam Relat Mater 15:138–146

Morshed MM, McNamara BP, Cameron DC, Hashmi MSJ (2003) Effect of surface treatment on the adhesion of DLC film on 316L stainless steel. Surf Coat Technol 163–164:541–545

Nakazawa H, Sudoh A, Suemitsu M, Yasui K, Itoh T, Endoh T, Narita Y, Mashita M (2010) Mechanical and tribological properties of boron, nitrogen–coincorporated diamond–like carbon films prepared by reactive radio–frequency magnetron sputtering. Diam Relat Mater 19:503–506

Ohring M (2002) Materials science of thin films: deposition and structure, 2nd edn. Academic Press, USA

Piazza F, Grambole D, Schneider D, Casiraghi C, Ferrari AC (2005) Protective diamond–like carbon coatings for future optical storage disks. Diam Relat Mater 14:994–999

Pierson HO (1999) Principles, technology, and applications, 2nd edn, CVD diamond growth. Noyes, Norwich, pp 93–95

Robertson J (1986) Amorphous carbon. Adv Phys 35:317–374

Robertson J (2001) Ultrathin carbon coatings for magnetic storage technology. Thin Solid Films 383:81–88

Robertson J (2002) Diamond–like amorphous carbon. Mater Sci Eng R 37:129–281

Shahsavari F, Ghoranneviss M, Khalaj Z, Diudea MV (2011) Effect of atalyst layer thickness on growth of CVD diamond. Studia Univ Babes-Bolyai Chemia 56:141–148

Shams S, Khalaj M, Ghoranneviss M (2012) How plasma species affect the structural and morphological properties of mwcnts. Studia Univ Babes-Bolyai Chemia 57:167–176

Sharda T, Rahaman MM, Nukaya Y, Soga T, Jimbo T, Umeno M (2001) Structural and optical properties of diamond and nano–diamond films grown by microwave plasma chemical vapor deposition. Diam Relat Mater 10:561–567

Shirakura A, Nakaya M, Koga Y, Kodama H, Hasebe T, Suzuki T (2006) Diamond–like carbon films for PET bottles and medical applications. Thin Solid Films 494:84–91

Silva WM, Trava-Airoldi VJ, Chung YW (2011) Surface modification of 6150 steel substrates for the deposition of thick and adherent diamond–like carbon coatings. Surf Coat Technol 205:3703–3707

Singh RA, Yoon E-S, Kim HJ, Kong H, Park S-J, Lee K-R (2006) Friction behaviour of diamond–like carbon films with varying mechanical properties. Surf Coat Technol 201:4348–4351

Takano Y, Nagao M, Takenouchi T, Umezawa H, Sakaguchi I, Tachiki M, Kawarada H (2005) Superconductivity in polycrystalline diamond thin films. Diam Relat Mater 14:1936–1938

Tallaire A, Achard J, Secroun A, De Gryse O, De Weerdt F, Barjon J, Silva F, Gicquel A (2006) Multiple growth and characterization of thick diamond single crystals using chemical vapour deposition working in pulsed mode. Cryst Growth 291:533–539

Tran DT, Fansler C, Grotjohn TA, Reinhard DK, Asmussen J (2010) Investigation of mask selectivities and diamond etching using microwave plasma–assisted etching. Diam Relat Mater 19:778–782

Vaghri E, Khalaj Z, Ghoranneviss M (2012) Preparation and characterization of diamond-like carbon films on various substrates by PECVD system. Studia Univ Babes-Bolyai Chemia 57:143–150

Vaghri E, Khalaj Z, Ghoranneviss M, Borghei M (2011) Characterization of diamond: like carbon films synthesized by DC–plasma enhanced chemical vapor deposition. Fusion Energy 30:447–452

Whitmell DS, Williamson R (1976) The deposition of hard surface layers by hydrocarbon cracking in a glow discharge. Thin Solid Films 35:255–261

Yamazaki K, Furuichi K, Tsumura I, Takagi Y (2008a) The large–sized diamond single–crystal synthesis by hot filament CVD. J Cryst Growth 310:1019–1022

Yamazaki K, Furuichi K, Tsumura I, Takagi Y (2008b) The large–sized diamond single–crystal synthesis by hot filament CVD. Cryst Growth 310:1019–1022

Yasuda T, Ihara M, Miyamoto K, Genchi Y, Komiyama H (1990) Gas phase chemistry determining the quality of CVD diamond. In: Spear K, Cullen G (eds) Proceedings of the 11th international conference on CVD. Electrochemical Society in Pennington, Pennington, pp 134–140

Yin Y, Hang L, Xu J, McKenzie DR, Bilek MMM (2008) Surface adsorption and wetting properties of amorphous diamond–like carbon thin films for biomedical applications. Thin Solid Films 516:5157–5161

Zhoutong H, Shumin Y, Qintao L, Dezhang Z, Jinlong G (2008) Selective growth of diamond by hot filament CVD using patterned carbon film as mask. Nucl Sci Technol 19:83–87

Chapter 3
Experimental Access to Centropolycyclic Carbon Compounds Containing the Massive C_{17}-Core: On the Way to D_5 Seeds

Dietmar Kuck

Abstract The construction of complex three-dimensional all-carbon molecular scaffolds from simple indane precursors to centropolycyclic structures bearing a core of 17 quaternary carbon atoms is described. This C_{17}^{q}-core represents the carbon framework of centrohexaindane, a topologically nonplanar $C_{41}H_{24}$ hydrocarbon. Some derivatives of centrohexaindane are also presented. Besides the various experimental routes to centrohexaindane and the congeneric lower centropolyindanes, including benzoannellated propellanes, triquinacenes and fenestrindanes, the quite limited access to partially benzoannellated centrohexaquinanes including (mono-) benzocentrohexaquinane is described. By contrast, the purely alicyclic parent, centrohexaquinane, and the corresponding hexaolefin, centrohexaquinacene, are both still elusive and, thus, challenging targets of organic chemistry, especially in view of their potential role as molecular seeds of D_5-diamond owing to their unique C_{17}^{q}-core.

3.1 Prologue

For a young organic chemist, the 1980s was a particular period in time. The art of synthesis was developed to a great extent. Exercising concepts and designing strategies for synthesis had become that much mature that people in the chemical community started arguing that "everything can be made" by synthesis (Seebach 1990). The synthesis of naturally occurring compounds was one measure to assess the state of the art and the access to non-natural compounds focussed on platonic hydrocarbons was another one (Hopf 2000): Cubane was already invented before

D. Kuck (✉)
Department of Chemistry, Bielefeld University, Universitätsstraße 25, 33615 Bielefeld, Germany
e-mail: dietmar.kuck@uni-bielefeld.de

M.V. Diudea and C.L. Nagy (eds.), *Diamond and Related Nanostructures*,
Carbon Materials: Chemistry and Physics 6, DOI 10.1007/978-94-007-6371-5_3,

(Eaton and Cole 1964), and the synthesis of tetrakis(*tert*-butyl)tetrahedrane (Maier et al. 1978) and, some years later, the two independent and so much different syntheses of dodecahedrane by Paquette (Ternansky et al. 1982) and by Prinzbach (Fessner et al. 1987; Prinzbach and Weber 1994) were outstanding proofs for that statement. The popularity of retrosynthesis as part of the training in organic chemistry had become popular for years already, reflecting at least in part that looking back into the toolbox of organic synthesis was considered more important than looking ahead to what has remained hidden in the wonder-world of organic synthesis (Brückner 1989).

My personal inspiration as an organic mass spectrometrist was fed by my enthusiasm about the fact that chemical reactions occurring in the highly diluted gas phase of a mass spectrometer could be studied very fruitfully and in depth when suitably tailored organic model compounds became accessible in my own hands through self-performed synthesis. Combining the potential of contemporary mass spectrometric techniques and contemporary synthetic methodology provided a special and quite fruitful way of investigating the chemistry of gaseous ions. Deep and generalised insights on the chemistry of both ions and neutrals emerged from this kind of work (Kuck 1990a, 2002).

However – organic chemists may or may not believe it – sometimes reactions in a mass spectrometer run more reliably than those in solution. In fact, whereas a cyclisation reaction in the gas phase may be recognised reliably (Kuck 1992), it may occur unforeseen during a synthetic procedure. This is what happened to me in 1979.

3.2 Inspiration

Five- and six-membered alicyclic rings form easily when a suitably functionalised precursor molecule containing an unsaturated C–C bond is converted to a cationic reactive intermediate. Radical-induced and photo-induced cyclisation reactions of this sort are well known, but cyclisation by classical Brønsted and Lewis acid-induced cyclisations via cationic intermediates are even more widespread.

When 2-benzyl-1-indanol (**1a**) is heated in formic acid solution, a proton-induced elimination of water takes place giving 2-benzylindene (**2a**) as the expected product (Scheme 3.1) (Campbell et al. 1963). The same 1,2-elimination of water occurs starting from the corresponding *para*-methoxy-substituted benzylindanol **1b**; the 2-(*para*-anisylmethyl)indene **2b** is formed in good yield. In contrast, the *meta*-methoxybenzyl isomer **1c** reacts along two competing paths: Dehydration does occur in either way but in part as a ring-forming process, a cyclodehydration (Bradsher 1946). The electron-rich *meta*-methoxy group strongly facilitates the attack of the ionised carbinol carbon (C-1) at one of the *ortho*-positions of the benzyl residue. A major part of the dehydration products obtained from the indanol **1c** is a mixture of the tetrahydroindeno[1,2-*a*]indenes **3a** and **3b**. A new five-membered ring is formed and its fusion to the cyclopentene unit of the starting compound

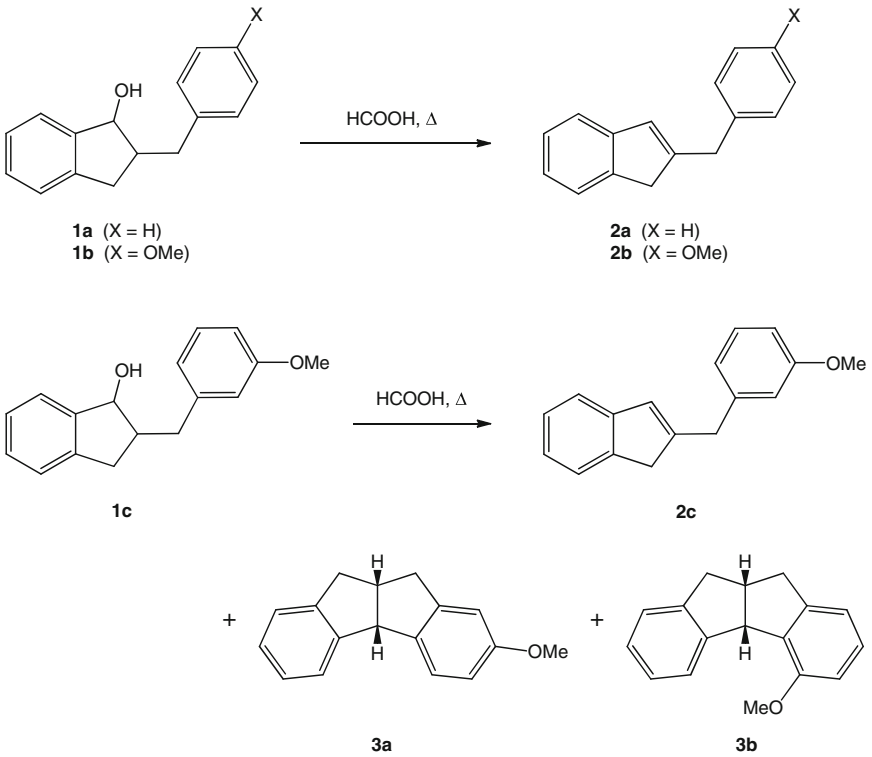

Scheme 3.1 1,2-Dehydration and cyclodehydration of 2-benzyl-1-indanols

1c gives rise to a *cis*-bicyclo[3.3.0]octane core bearing two benzene nuclei in a C_s-symmetrical orientation. Tetrahydroindeno[1,2-*a*]indenes are known for a long time already (Baker et al. 1957).

3.3 Syntheses of Centrohexaindanes and Some Lower Centropolyindane Congeners

This was the start of my thinking on cyclopentane rings or, more precisely, indane units that could be fused in three dimensions (Kuck 1996). Why not subject 1,3-indanediols bearing two benzyl groups the C-2 position, such as **4**, to such cyclodehydration conditions (Fig. 3.1)? Or use 1,3-indanediols of type **5** carrying a diphenylmethyl (benzhydryl) group along with a simple alkyl group at C-2? This should give rise to two novel triindanes of different ring fusion. Maybe even a 1,3-indanedione charged with two benzhydryl groups, such as **6**, would allow us to generate four new five-membered rings in one step? This would lead to a

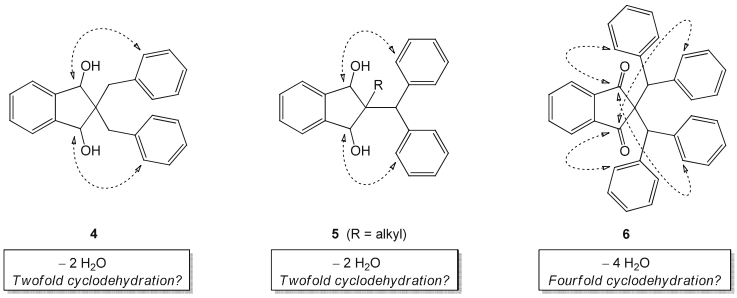

Fig. 3.1 Potential cyclodehydration of 2-benzyl- and 2-benzhydryl-1,3-indanediols and 2-benzhydryl-1,3-indanediones

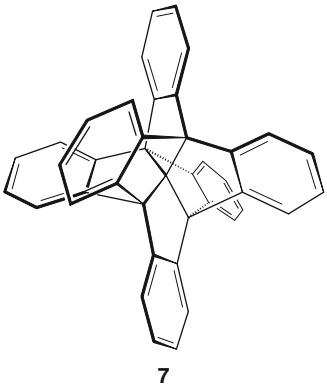

Fig. 3.2 Centrohexaindane, a $C_{29}H_{24}$ hydrocarbon bearing three orthogonally fused spirane units and a core of 17 quaternary carbon atoms

fivefold indane, a "pentaindane"! In this vein, it became quickly obvious that even six indane units could be merged into a common polycyclic carbon framework. The former C-2 carbon atom of the starting indane derivative would be deeply hidden in the centre of a fascinating and highly unusual and truly three-dimensional construction: a hexacyclic C_{17}-core carrying six benzene rings at its rims. Such a structure would be unique and reminiscent of a seed of diamond but consist of cyclopentane instead of cyclohexane rings (Diudea 2010; Diudea et al. 2011)! And, no doubt, its sixfold benzoannellation would render it a very stable organic compound prone to study versatile arene chemistry. For some years, this remained a dream. However, "centrohexaindane" (**7**, Fig. 3.2) was synthesised by us for the first time a few years later (Kuck and Schuster 1988), and its semi-rational name indicates in the same time the type of the constituents, the way they are composed and the fact that centrohexaindane has a set of relatives with fewer indane units, the above-mentioned centropentaindane being only one of them. The family of centropolyindanes emerged (Kuck 1990b, 1996, 1997a, b, 2006a, b).

Looking closer to this set of ideas, it became quickly evident that a simple topological view would be followed (Fig. 3.3): Neopentane (**8**) presents a

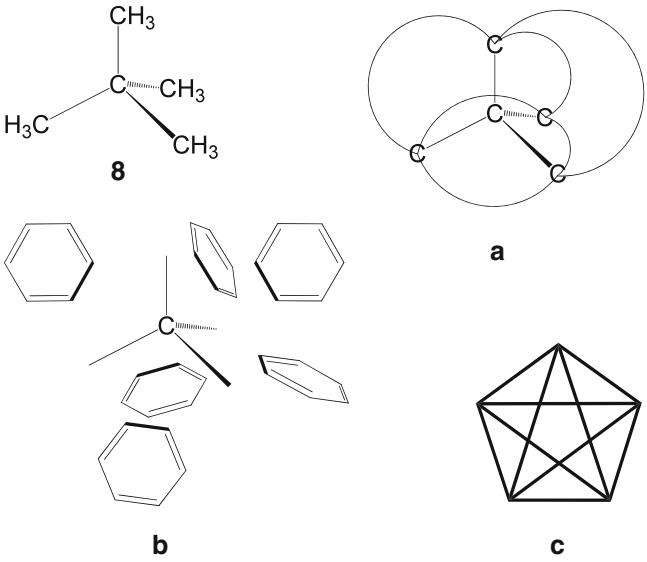

Fig. 3.3 Assembly of centrohexaindane (**7**) from neopentane (**8**) in a centrohexacyclic manner (**a**) using six benzene units (**b**) to generate a topologically nonplanar (K_5) carbon framework (**c**)

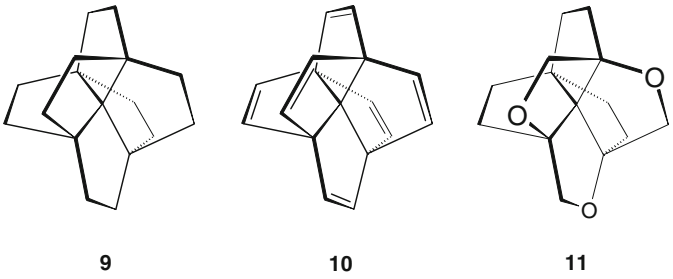

Fig. 3.4 Two experimentally unknown K_5 hydrocarbons, centrohexaquinane (**9**) and centrohexaquinacene (**10**), and the experimentally known centrohexacyclic triether **11**

perfectly tetrahedral nucleus for being fused with six benzene units, each of which bridging one pair of α-carbons of the methyl groups (cf. **a** and **b**). Notably, the resulting carbon network would be topologically nonplanar, since the C_{17}-core would correspond to the complete graph K_5 (**c**) (Kuratowski 1930). In fact, two widely noted short communications appeared in 1981 as back-to-back articles that reported on the efforts to construct the C_{17}-core as the hypothetical fully alicyclic, saturated hydrocarbon, C_{17}-hexaquinane **9** (Fig. 3.4) (Simmons and Maggio 1981; Paquette and Vazeux 1981). Although this compound remained elusive, as did the corresponding fully unsaturated C_{17}-hexaquinacene **10**, the two groups of authors were able to show that a corresponding triether **11**, bearing a topologically nonplanar

$C_{14}O_3$ core, was synthetically accessible. In fact, this trioxa derivative is notable because it was the first K_5-type organic compound known. As pointed out later, the constitution of triether **11** corresponds to a chiral-nonplanar graph, in contrast to the hydrocarbons **9** and **10** being achiral (Chambron et al. 1993). A later full report on the synthesis of triether **11** concluded the futile attempts to synthesise the corresponding homocyclic parent compound (Paquette et al. 1984). However, the idea that such a small hydrocarbon framework could be topologically nonplanar attracted more interest. Early molecular-mechanics calculations were applied to the problem, and the conformational degrees of freedom of centrohexaquinane **9** and centrohexaquinacene **10** were studied during the same time (Ermer 1981). Molecular *T*-symmetry was predicted of the conformational ground state of the saturated hydrocarbon **9**, whereas T_d-symmetry was assigned to that of the fully unsaturated analogue **10**. A systematic study on the so-called centropolycyclanes appeared the same year, entitled "How Many Rings Can Share a Common Carbon Atom?" (Gund and Gund 1981). It was demonstrated that, in principle, up to six three-, four-, five- or/and six-membered rings (cf. **a**, Fig. 3.3) could be fused about a central carbon atom (or neopentane core) and molecular-mechanics calculations revealed what could be easily expected by pencil-and-paper chemistry: Five-membered rings, and cyclopentane rings in particular, would almost perfectly fit into the six C−C−C bond angles of neopentane, and cyclopentene and indane units should do even better. Interestingly, the doctoral thesis of H. E. Simmons III, written under the guidance of R. B. Woodward and completed under supervision of P. Wenders in 1980, concludes at its end with the suggestion to bridge the neopentane nucleus by six benzene rings, instead of ethylene or vinylidene units (Simmons III 1980). A personal visit of the author at DuPont Research Station in Wilmington, DE, in 1990 not only brought a copy of that thesis but also enlightened parts of the background and personal stories associated with the competition to make the elusive centrohexaquinane **9**.

In the early 1980s, we started to investigate systematically the directed construction of what – in reminiscence of Gund and Gund's article about the centropolycyclanes – we later called the centropolyindanes. In the very first attempts already, we found that *trans*-2,2-dibenzyl-1,3-indanediol (**4**), readily accessible from 1,3-indanedione (**12**) via the 2,2-dibenzyl derivative **13**, could be successfully subjected to twofold cyclodehydration to give the C_2-symmetrical centrotriindane **14** (Scheme 3.2) (Kuck 1984). Likewise, the stereoisomeric 2-benzhydryl-2-methyl-1,3-indanediols **5** (R=CH_3) obtained via the indanediones **17** and **18** underwent the analogous reaction giving the C_{3v}-symmetrical centrotriindane **19** in moderate yield. The dehydrating medium used was orthophosphoric acid in refluxing toluene or xylene. Several other acid catalysts did not give such delightful results, for example, use of *para*-toluenesulfonic acid in benzene solution gave rise to fragmentation of the five-membered ring of the starting indanediol unit, rather than generating new rings (Kuck 1984, 1994). This confirmed our early suspicion that 1,3-diols such as **4** and **5** would be prone to undergo Grob fragmentation (Prantz and Mulzer 2010), which in fact they tend to do. It is still a mystery why orthophosphoric acid (H_3PO_4) is that much useful for twofold or, as will be mentioned below,

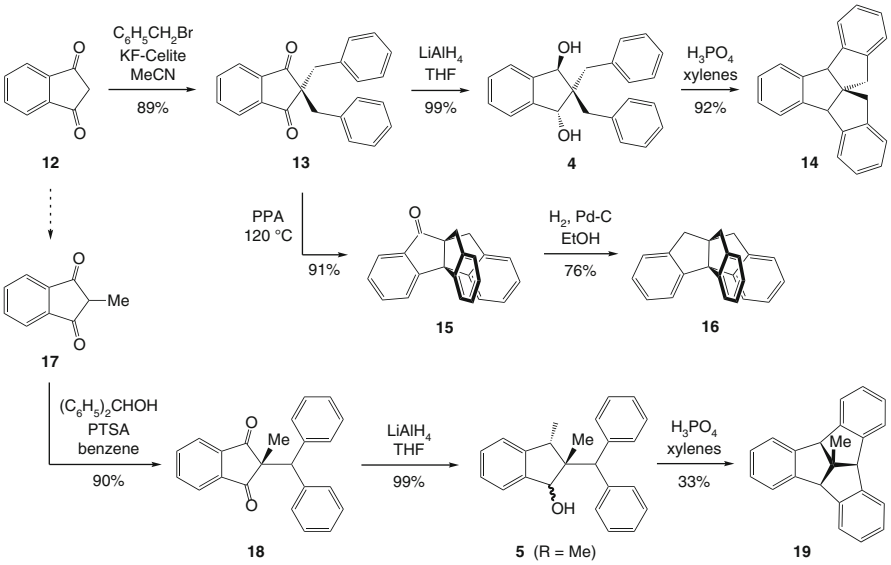

Scheme 3.2 Synthesis of three isomeric centrotriindanes **14**, **16** and **19** by cyclodehydration

even threefold cyclodehydration reactions. This seems to be related to the likewise somewhat magic power of the widely used polyphosphoric acid (PPA), which may actually form under our cyclodehydration conditions (Popp and McEwen 1958). The finding that the two centrotriindanes **14** and **19** were accessible in only very few steps from 1,3-indanedione (**12**) via the respective indanediols **4** and **5** – provided the appropriate Brønsted acid was used – encouraged us to further pursue the idea to annellate even more benzene rings about the neopentane nucleus (Kuck 1984).

Polyphosphoric acid was also the reagent used by H. W. Thompson to prepare another centrotriindane isomer of **14** and **19**, namely, the corresponding propellane-type hydrocarbon **16** (Thompson 1966, 1968). Owing to its structural relation to triptycene (Bartlett et al. 1942), Thompson dubbed his prototypical, C_{3v}-symmetrical tribenzo[3.3.3]propellane "triptindane". Notably, this compound was the only higher congener of the centropolyindane family known before we started our investigations. [*Note*: Besides this, an isomeric C_2-symmetrical centrotriindane that does not belong to the centropolyindane family was described early (Ten Hoeve and Wynberg 1980b) and the formation of a tribenzotriquinacene (cf. **56**) was suspected even much earlier (Baker et al. 1957).] It turned out that, different from Thompson's early synthesis based on electron-rich precursors, the use of polyphosphoric acid in the cyclisation step allowed us to shorten the synthesis of the parent hydrocarbon (Paisdor and Kuck 1991). Much to our surprise, 2,2-dibenzyl-1,3-indanedione (**13**) was found to undergo "bicyclisation" with one of the two carbonyl groups in high yield giving 9-triptindanone **15** in high yield (Scheme 3.2). This finding enabled the synthesis not only of the corresponding centrotriindane hydrocarbon, triptindane (**16**), but also of the corresponding trione **21** (Fig. 3.5)

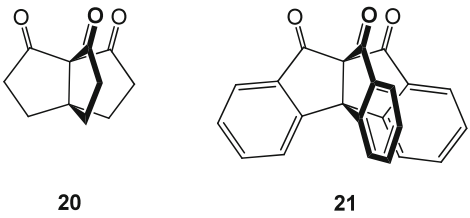

Fig. 3.5 Conia's triketone (**20**) and its threefold benzo analogue, 9,10,11-triptindanetrione (**21**)

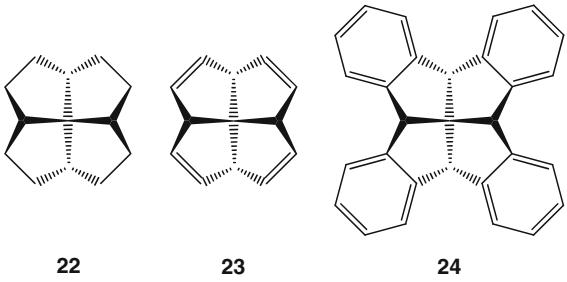

Fig. 3.6 All-*cis*-[5.5.5.5]fenestrane (**22**), all-*cis*-[5.5.5.5]fenestra-2,5,8,11-tetraene (**23**) and the fourfold benzo analogue of both, all-*cis*-fenestrindane (**24**)

that is obtained by stepwise oxidation of triptindane-9-one **15** (Paisdor and Kuck 1991). In fact, triptindane-9,10,11-trione (**21**) is a highly remarkable compound. It represents the tribenzo analogue of Conia's triketone **20** (Prange et al. 1977), which was used as the starting material for the efforts aimed at the preparation of centrohexaquinane (Simmons and Maggio 1981; Paquette and Vazeux 1981; Paquette et al. 1984). Similar to the alicyclic triketone **20**, the aromatic triketone **21** is a non-enolisable and threefold 1,3-dicarbonyl compound that, in fact, turned out to be a key compound for the synthesis of centrohexaindane (**7**) and its derivatives (see below) (Kuck et al. 1994a; Kuck et al. 1995).

Another access to centrohexaindane (**7**) was discovered alongside with the twofold cyclodehydration of the indanediols **4** and **5** but in the context with our first contribution to fenestrane chemistry (Kuck and Bögge 1986). Fenestranes have inspired chemists because of the idea that four rings being mutually fused in a window-like manner, with the central carbon atom being shared by all of them, could open an access to flattened or even planar tetracoordinate carbon in an anti-Van't Hoff-Le Bel coordination. An impressive amount of research has been undertaken to explore the "flatland" of fenestrane chemistry (Keese 2006; Röttger and Erker 1997). Among these efforts, the investigations into [5.5.5.5]fenestranes and their derivatives were of particular importance to us. Two major synthesis routes were published that opened the access to the parent hydrocarbons all-*cis*-[5.5.5.5]fenestrane (**22**) (Luyten and Keese 1984) and all-*cis*-[5.5.5.5]fenestra-2,5,8,11-tetraene (**23**) (Venkatachalam et al. 1985) (Fig. 3.6). In the early 1980s, only very few researchers thought about the possibility to construct fenestranes bearing aromatic rings to stabilise the to-be-flattened [n.m.o.p]fenestrane core. But how about a fully benzoannellated analogue of **21** and **23**, that is, an all-*cis*-tetrabenzo[5.5.5.5]fenestrane, **24**? A highly important impact came from a group in Groningen, the Netherlands (Ten Hoeve and Wynberg 1980a, b). In his

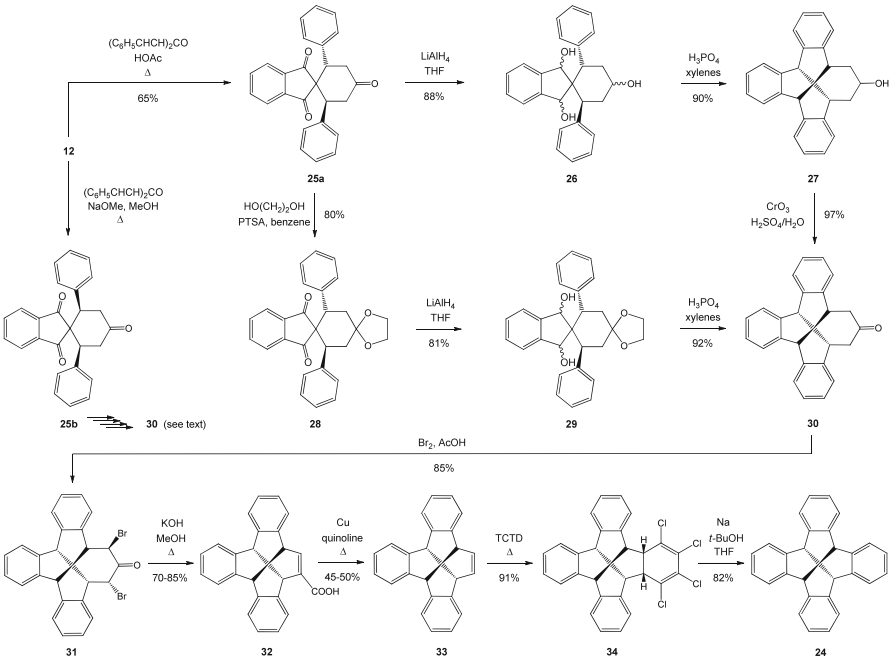

Scheme 3.3 The stereoisomeric spirotriketones **25a** and **25b** and the synthesis of all-*cis*-fenestrindane (**24**)

doctoral thesis entitled "The long and winding road to Planar Carbon", W. ten Hoeve reported on various attempts using diaryl-substituted spirocyclic diketones, including spirocyclic indane-1,3-diones, to generate benzoannellated fenestranes and related aromatic congeners (Ten Hoeve 1979). With the successful twofold cyclodehydration of 2,2-dibenzyl-1,3-indanediol **4** in mind, it was obvious to me that the corresponding spirotriol **26** (Scheme 3.3) would be a promising candidate to generate an all-*cis*-[5.5.5.6]fenestrane framework bearing three annellated benzene nuclei. The *trans*-orientation of the two phenyl residues in the spirotriketone **25a** was considered ideal for this purpose.

In fact, this idea turned out to be particularly constructive (Scheme 3.3). Twofold Michael addition of dibenzylideneacetone to 1,3-indanedione **12** was known to give either the *trans*- or the *cis*-diphenylspirotriketones **25a** or **25b**, respectively, as the products of kinetic or thermodynamic control, depending on the reactions conditions (Shternberga and Freimanis 1968; Popelis et al. 1972; Ten Hoeve and Wynberg 1979, 1980a). Reduction to the corresponding triol **26**, obtained as a mixture of stereoisomers, followed by cyclodehydration under the approved conditions using orthophosphoric acid in xylene or, alternatively, protection of the cyclohexanone functionality giving **28**, subsequent reduction to the dispiroindanediols **29**, again obtained as a mixture of stereoisomers, followed by cyclodehydration furnished the desired all-*cis*-tribenzo[5.5.5.6]fenestranone

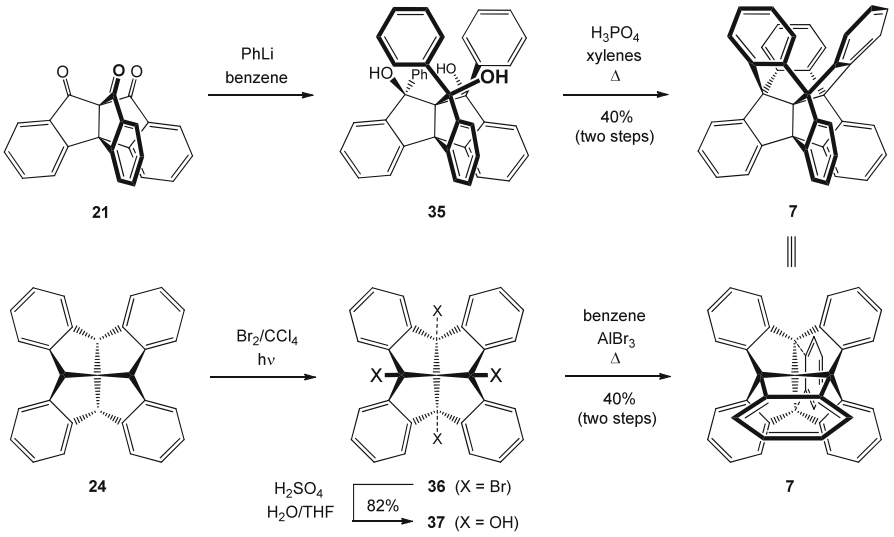

Scheme 3.4 The last two steps of the two major syntheses of centrohexaindane (**7**) along the propellane route (*top*) and along the fenestrane route (*bottom*)

30 in good overall yields (Kuck 1994). Later, we learnt that, counter-intuitively, the *cis*-diphenyl isomer **25b** also represents a suitable starting point for the construction of the tribenzo[5.5.5.6]fenestrane skeleton, albeit with the strained *cis*,*cis*,*cis*,*trans*-configuration (Bredenkötter et al. 1999, 2001). Most interestingly, epimerisation of the *cis*,*cis*,*cis*,*trans*-tribenzo[5.5.5.6]fenestrane framework to the all-*cis*-configuration is possible. Nevertheless, the all-*cis*-stereochemistry of [5.5.5.6]fenestranone **30** was found to be a prerequisite for the subsequent ring contraction via the dibromo derivative **31** which readily undergoes Favorskii rearrangement to the all-*cis*-tribenzo-[5.5.5.5]fenestrene carboxylic acid **32**. Decarboxylation to the corresponding [5.5.5.5]fenestrene hydrocarbon **33** followed by a two-step benzoannellation procedure using tetrachlorothiophene-*S*,*S*-dioxide (TCTD) via **34** and eventual dissolving-metal reduction afforded the desired product **24**. As the parent hydrocarbon of all fully benzoannellated [5.5.5.5]fenestranes, we named this compound **24** "fenestrindane" – or, more precisely, all-*cis*-fenestrindane (Kuck and Bögge 1986; Kuck 1994).

In retrospect, triptindane-9,10,11-trione (**21**) and fenestrindane (**24**) represent the very two key compounds to construct centrohexaindane (**7**) and its derivatives (Scheme 3.4). Both of these centropolyindanes are only two steps off the final goal. Whereas the triketone **21** can be readily extended by reaction with various carbon nucleophiles to produce the corresponding 9,10,11-substituted triptindane-9,10,11-triols, including 9,10,11-triaryl derivatives such as **35**, hydrocarbon **24** requires functionalisation of the four bridgehead positions first, for example, by halogenation. In spite of steric hindrance, fourfold bromination of **24** occurs easily, giving 4b,8b,12b,16b-tetrabromofenestrindane **36**, another important key

intermediate for [5.5.5.5]fenestrane chemistry (Kuck et al. 1991). The two very last steps of the two independent syntheses of centrohexaindane consist of either a threefold or even fourfold C–C bond forming processes: On the one hand, 9,10,11-triphenyltriptindane-9,10,11-triol (**35**), generated by enforced addition of three equivalents of phenyllithium to triketone **21**, undergoes a threefold cyclodehydration giving centrohexaindane (**7**) if, once again, orthophosphoric acid in xylene is used as the catalyst. On the other hand, tetrabromofenestrindane **36** reacts with two equivalents of benzene used as a solvent, if the fourfold Friedel-Crafts-type condensation is induced by Lewis acid catalysts, such as aluminium bromide, to give centrohexaindane (**7**) as well. In both these ways, the six indane units required for **7** were assembled from a centrotriindane derivative, namely, triol **35**, incorporating three additional benzene rings, or a centrotetraindane, namely, tetrabromide **36**, incorporating two more benzene rings (Kuck et al. 1995).

In a total view, the two most viable synthesis routes to centrohexaindane (**7**) start both from 1,3-indanedione (**12**) and comprise either 6 or 11 steps. Clearly, the so-called propellane route, running through several propellane intermediates such as **21**, is the more attractive one since it enables the synthesis of the hydrocarbon in gram amounts in an overall yield of 25%. By contrast, the so-called fenestrane route, winding through a landscape of several benzoannellated [5.5.5.6]- and [5.5.5.5]fenestranes including tetrabromofenestrindane **36**, is quite tedious and gives a total yield of 8%. However, both routes deserve more comparison. No surprise, the longer route was discovered first (Kuck and Schuster 1988) and represented the major breakthrough. Besides the access to the parent hydrocarbon **7**, several centrohexaindane derivatives, such as the (achiral or chiral) tetraethers **38**–**40**, were synthesised along the fenestrane route by introducing substituents in the last step of the sequence (Fig. 3.7) (Tellenbröker et al. 2005). In this case, tetrabromide **36** was hydrolysed first to give the corresponding fenestrindanetetrol **37** (Scheme 3.4) because this fourfold benzhydrol proved to be a useful intermediate for the condensation with electron-rich arenes under Brønsted acid catalysis. In principle, other substituents could be introduced from the very beginning of the sequence, but there are also quite some more limitations. In this respect, the propellane route appears to be more variable because it allows substituents to be incorporated either into the propellane framework or only in the second-last step, to produce methyl-substituted centrohexaindane derivatives such as **41** and **42** (Kuck et al. 2007). The propellane route proved to be also viable for the synthesis of centrohexaindanes bearing 12 residues at the outer periphery of the polycyclic framework. Unfortunately, however, the dodecamethoxy derivative **43** (Fig. 3.8) has remained the only example of this kind to date, and the yields were low (Harig and Kuck 2006). Nevertheless, this chemistry should be developed further and is certainly extendable to generate centrohexaindanes bearing appropriate functionalisation in the six directions of the Cartesian space. Independently, the fenestrane route should also allow one to construct various unusual three-dimensional molecular scaffolds. As an example, formation of the twofold crown ether **44** was observed in relatively low yield when benzo-18-crown-6 was reacted with fenestrindanetetrol **37** mentioned above under catalysis with Brønsted acids [unpublished results].

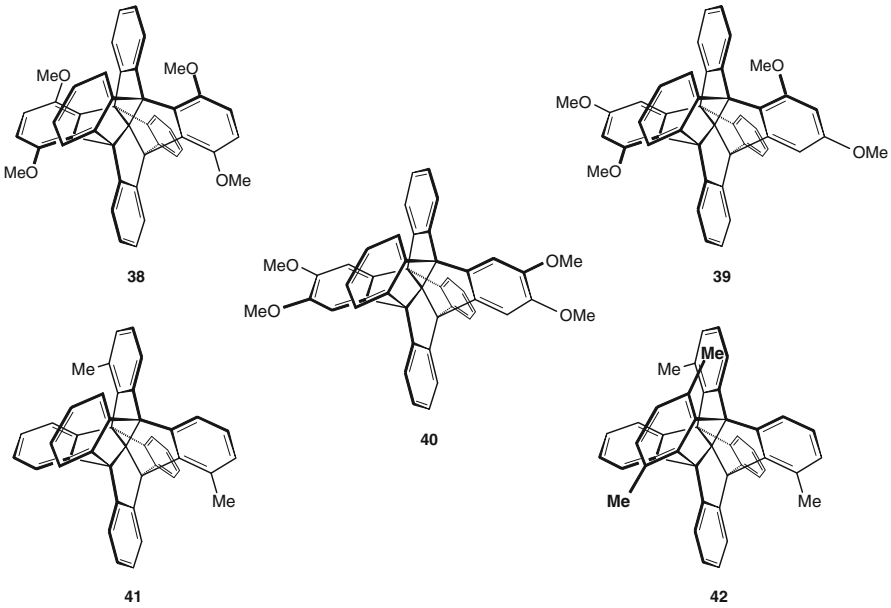

Fig. 3.7 Five centrohexaindane derivatives synthesised along the fenestrane route (**38**–**40**) and along the propellane route (**41** and **42**)

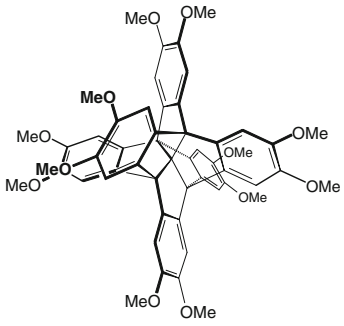

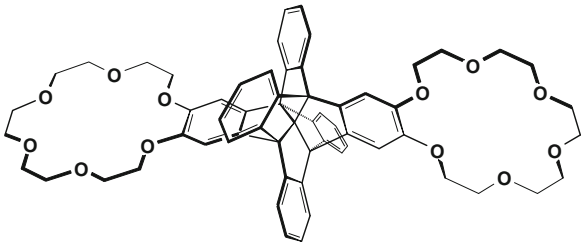

Fig. 3.8 Dodecamethoxy-centrohexaindane **43** synthesised along the propellane route and the twofold crown ether **44** synthesised along the fenestrane route

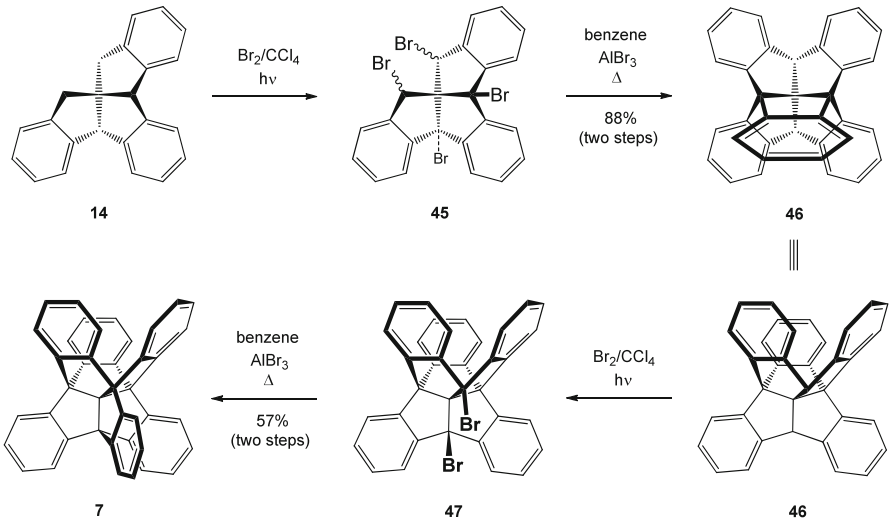

Scheme 3.5 Synthesis of centrohexaindane (**7**) from centrotriindane **14**, a "broken fenestrane", via centropentaindane (**46**) – the last four steps of the broken-fenestrane route

Still more routes to centrohexaindane (**7**) have been explored, but these are viable only with considerable efforts, risks and losses (Kuck et al. 1995). The "broken fenestrane route" (Scheme 3.5) runs through the triindane **14**, an incomplete (or "broken") [5.5.5.5]fenestrane, and its conversion to **7** requires four further and in part quite delicate steps, including the preparation of centropentaindane (**46**) via the mixture of tetrabromides **45**. It is obvious that hydrocarbon **46**, as a rigidified fenestrindane (cf. **24**), is conformationally as rigid as centrohexaindane (**7**). Therefore, functionalisation at the two remaining methyne bridgehead positions of **46** is particularly difficult and the dibromide **47** obtained from **46** under careful control of the reaction conditions proved to be a rather reactive compound. Nevertheless, Friedel-Crafts reaction with benzene under Lewis acid catalysis furnished the highest centropolyindane (**7**) in remarkably high (ca. 50%) yield (Kuck et al. 1994b, 1995, 1996). The aforementioned rigidity of the centropenta- and centrohexacyclic framework was nicely demonstrated by the near-to-planar conformation of the related 1,2-diketone **48** (Fig. 3.9), the X-ray crystal structure analysis of which revealed a torsional angle of only 7° between the two carbonyl groups. Several other derivatives of centropentaindane were synthesised, including the remarkably crowded phenylcentropentaindane **49** (a *seco*-centrohexaindane) as well as the endoperoxide **50** and the disulfide **51** (Kuck et al. 1995, 1996, 1998).

The last route to centrohexaindane (**7**) appeared rather promising in the beginning but turned out to be a dead-end alley (Scheme 3.6) (Kuck et al. 1995). We called that hoped-for approach "triquinacene route" for quite obvious reasons. As shown above, 12d-methyltribenzotriquinacene (**19**) is easily accessible (Kuck 1984; Kuck et al. 1992), and its threefold bridgehead brominated derivative **51**,

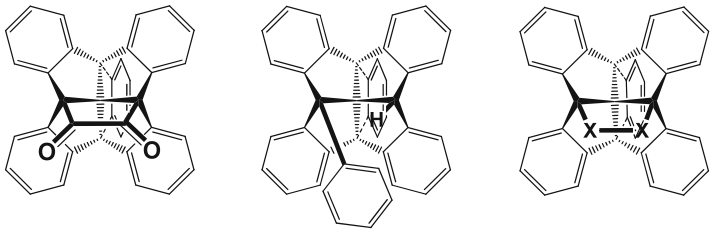

Fig. 3.9 A particularly rigid centrohexacyclic 1,2-diketone **48**, a *seco*-centrohexaindane **49** and two centrohexa-heterocyclic congeners, endoperoxide **50** and disulfide **51**

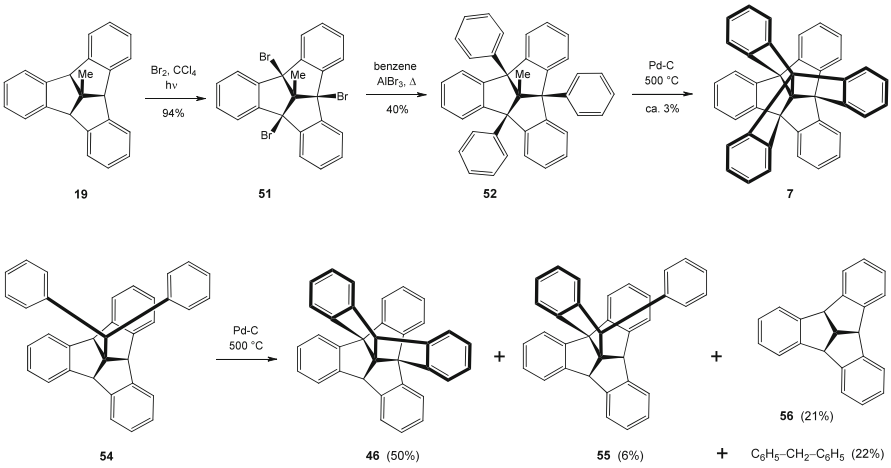

Scheme 3.6 The synthesis of centrohexaindane (**7**) along the triquinacene route, including an almost non-productive cyclodehydrogenation step, as compared to a similar approach leading to centropentaindane (**46**)

which can be also produced in large amounts, represents a key intermediate for the development of TBTQ chemistry (Kuck et al. 2001). 4b,8b,12b-Triphenyl-12d-methyltribenzotriquinacene (**52**) synthesised from **51** by threefold Friedel-Crafts reaction contains all elements of the target hydrocarbon **7** and formally requires the removal of six hydrogen atoms under catalytic dehydrogenation conditions (Kuck et al. 1995). Unfortunately, all our attempts to perform threefold cyclodehydrogenation proved practically unsuccessful. Enforced dehydrogenation conditions at 500 °C in the presence of a large excess of an intimately powdered mixture of palladium-on-charcoal furnished only minute amounts of the desired product hydrocarbon **7**. By contrast, a formally similar, twofold cyclodehydrogenation of 12d-benzhydryltribenzotriquinacene **54** was comparably successful: Heating of this

sterically crowded hydrocarbon under the same conditions afforded centropentaindane **46** in relatively high yield (50%) along with the singly cyclodehydrogenated product **55** and the two products of hydrogenolysis, namely, the parent tribenzotriquinacene (**56**) and diphenylmethane (Kuck et al. 1996).

There is no doubt that the success to build up the centropolyindane family and to have a good handle to construct centrohexaindane (**7**) and a (yet limited) number of its derivatives is encouraging. With a sizeable amount of experimental investment, twelvefold functionalised derivatives should become accessible, and truly three-dimensional networks consisting of centrohexaindane cores and large voids should become into reach. However, our hope to generate the neat C_{17}-core of centrohexaquinane (**9**) or even that of the sixfold unsaturated centrohexaquinacene (**10**), that is, to avoid the presence of benzene units for stabilising and protecting the centrohexacyclic hydrocarbon, has not been fulfilled so far. Nevertheless, some remarkable stages of the race have been reached. In fact, since the *Aufbau* strategy to the alicyclic hydrocarbons **9** and **10** appeared, and still appears, to be experimentally "forbidden", we focused our attention on the controlled dismantling ("Abbau") of the benzoannellation of the C_{17}-core. The course and the results of these attempts will be described below.

3.4 Partially Benzoannellated Centrohexaquinanes: A Long Way, Still, to the C_{17}-Core

Conceptually, there exists a whole family of partially benzoannellated centrohexaquinanes, comprising one single pentabenzocentrohexaquinane (**57**) and one single (mono-) benzocentrohexaquinane **65** (Fig. 3.10). In between these extremal cases, two structurally different tetrabenzocentrohexaquinane congeners, **58** and **59**, are conceivable, as are three different tribenzocentrohexaquinane congeners, **60**, **61** and **62**, as well as two dibenzocentrohexaquinanes, **63** and **64**. It is obvious that the conceptual variability of the family of partially benzoannellated centrohexaquinanes corresponds to that of the centropolyindanes discussed above. Moreover, beyond the benzocentrohexaquinanes, there should be the parallel world of the partially benzoannellated centrohexaquinacenes (not shown here), each member of which would bear one or more cyclopentene rings in place of the cyclopentane rings of the centropolycyclanes **57**–**65**. The conformational flexibility of the members of the benzoannellated centropolyquinanes **57**–**65** and the corresponding benzoannellated centropolyquinacenes can be predicted on the basis of that of the centropolyindanes (Kuck 2006b). Thus, wherever a tribenzotriquinacene subunit (cf. **19** or **56**) would be present in a partially benzoannellated centrohexaquinane, the molecules would have a rigid framework with one single conformation only. This holds true for hydrocarbons **57**, **58** and **61**. Probably, the presence of a non-benzoannellated triquinacene unit would add conformational rigidity on its own. Thus, the situation for the benzoannellated

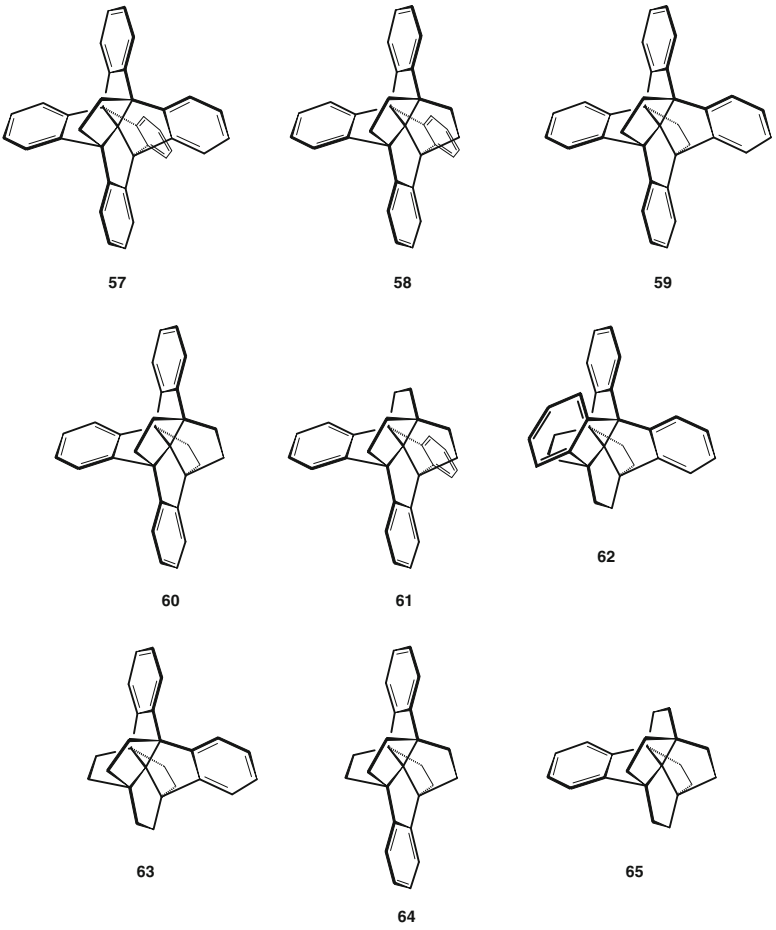

Fig. 3.10 The complete family of the partially benzoannellated centrohexaquinanes, **57**–**65**

centrohexaquinacenes would be different; within this family, all members would exist in only one single conformer, as does the parent centrohexaquinacene **10**, too (Ermer 1981). The chemical stability of the partially benzoannellated centrohexaquinanes would be similar to those of the centropolyindanes, whereas the partially benzoannellated centrohexaquinacenes would suffer enhanced reactivity due to the presence of one or several olefinic double bonds.

A mixed situation between quite limited *Aufbau* and *Abbau* strategies has evolved through our work (Scheme 3.7). A viable construction of the polycyclic framework of pentabenzocentrohexaquinane **57** was accomplished based on the experience with similar approaches in the centropolyindane series discussed above. Catalytic hydrogenation of the isolated double bond of tribenzo[5.5.5.5]fenestrene **33** leads to the corresponding [5.5.5.5]fenestrane **66** (Kuck 1994), which can be subjected

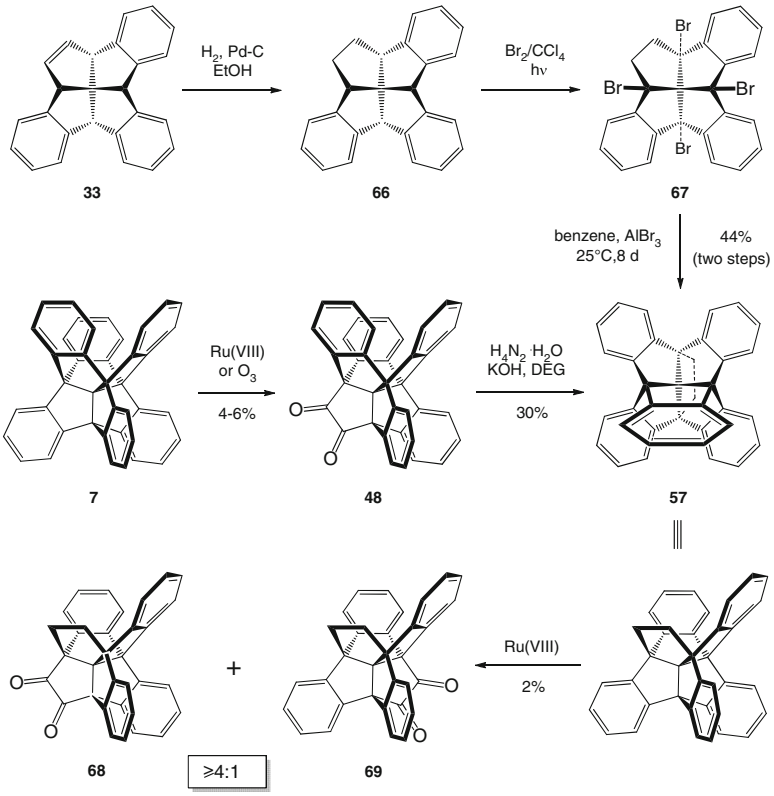

Scheme 3.7 Synthesis of pentabenzocentrohexaquinane (**57**) by *Aufbau* (from **33**) and generation of this hydrocarbon by *Abbau* (from **7**) strategies and attempts to dismantle another benzene unit

to an essentially fourfold bromination at its benzylic and benzhydrylic bridgehead positions to give compound **67** (Kuck et al. 1998). In this case, functionalisation has to be carried out with special care in order to avoid over-bromination via dehydrobrominated intermediates. Subsequent fourfold Friedel-Crafts reaction using benzene as the solvent affords pentabenzocentrohexaquinane **57** in acceptable yield (44%). In contrast to this *Aufbau* route, disassembly of one or even two benzene units of centrohexaindane (**7**) was also studied (Gestmann et al. 1996). Unfortunately, however, this strategy does not lead very far (Scheme 3.7).

Careful ozonolysis of **7** in dichloromethane in the presence of pyridine at −10 °C gives rise to 1,2-diketone **48**, a beautiful red-coloured crystalline solid, albeit in 7% yield only. Subsequent Wolff-Kishner reduction gives the hydrocarbon **57** in moderate yield. This was the first hint to the fact that, in line with general experience, oxidative dismantling of the aromatic periphery of the benzoannellated centrohexaquinanes would be highly uneconomic. This turned out to be evidently true when pentabenzocentrohexaquinane **57** was subjected to oxidation (Gestmann et al. 1996). Ruthenium(VIII) oxide, generated in situ from ruthenium(III) chloride and

sodium periodate, was used as the oxidative agent. As expected, a reddish product indicating the formation of the 1,2-diketone chromophore was obtained. However, the product was formed in minute yield (2% only) and, as also anticipated, turned out to be a mixture of the two isomeric diketones **68** and **69**. The unsymmetrical isomer **68** was found to predominate by far, in line with both the both sterical and statistical preconditions for the attack of the oxidant at the framework of pentabenzocentrohexaquinane (**59**) (Gestmann et al. 1996). Due to the extremely low efficiency and yield of the dismantling approach, original plans to reduce the dicarbonyl functions of the diketones **68** and **69** to generate the corresponding tetrabenzocentrohexaquinanes **58** and **59**, respectively, had to be abandoned.

A fortunate finding made upon our attempts to use tripindanetrione **21** as a starting point for the construction of C_3-symmetrical propellanes opened the door to a group of lower partially benzoannellated centrohexaquinanes (Kuck et al. 1994a). In particular, the access to the propellane-type tribenzo congener **62** turned out to be remarkable, and this eventually enabled the synthesis of the unique single benzoannellated benzocentrohexaquinane **65**. As mentioned above, tripindanetrione **21** can be reacted threefold with various metalorganic nucleophiles, including alkyl and aryl reagents (Paisdor and Kuck 1991; Kuck et al. 2007; Hackfort and Kuck 1999). Recently, alkenyllithium reagents were found to react as well (unpublished results). When we tried to add three equivalents of lithium acetylide or lithium phenylacetylide to the triketone **21**, we found to our great surprise that all of the three acetylenic synthons were added across the propellane bays. The centrohexacyclic compounds **70** and **72** were formed and isolated in 25 and 27% yields, respectively. Thus, during the formation of these compounds, not only were the three new C–C bonds formed in a C_3-symmetrical orientation, as expected, but also nucleophilic addition of the lithium alkoxide groups to the acetylenic moieties occurred in this manner. Actually, the threefold enol ethers **70** and **72** represented (and still represent) the first derivatives of the parent centrohexacyclic triether **11**. The discovery of this one-pot "tricyclisation", clearly representing quite an efficient *Aufbau* step that turns centrotricyclic into a centrohexacyclic (albeit heterocyclic) framework, was limited since we found that highly alkyllithium reagents such as *n*-hexynyllithium did not give the corresponding analogue (Kuck et al. 1994a).

Nevertheless, the formation of the tris-enol ethers **70** and **72** turned out to be very exciting. In fact, we found that triether **70** undergoes a clean thermally induced rearrangement (300 °C in decaline) of all of its three enol ether groupings to give the isomeric carbocyclic triketone **71** in 30% yield (Kuck et al. 1994a). Although the experimental procedure is quite tedious – use of sealed glass tubes on small scales is required – and various other reaction conditions proved to be unproductive, this reaction enabled, for the very first time, an access to a centrohexacyclic framework bearing as few as only three annellated benzene rings. Similar to the rearrangement of triether **70**, the triphenyl derivative **72** obtained from propellanetrione **21** and phenylethynyllithium was isomerised at 300 °C to give the corresponding centrohexacyclic triphenylketone **73** in good yield (60%). Interestingly, only one single diastereomer was found. Closer inspection by ^{1}H NMR spectroscopy revealed that each of the three phenyl groups is oriented into

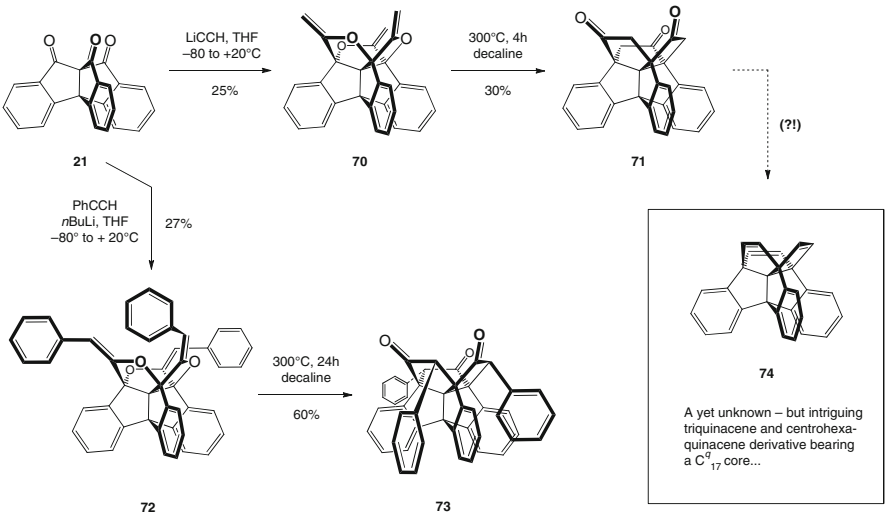

Scheme 3.8 Construction of the tribenzocentrohexaquinane framework from 9,10,11-triptindanetrione (**21**) and access to the experimentally unknown tribenzocentrohexaquinacene **74**, a shielded triquinacene derivative with a potential for the "globular" dimerisation to a dodecahedrane

one of the three bays of the triptindane framework, that is, in *anti*-position with respect to the triquinanetrione "bowl" fused to the propellane moiety in **73** (Kuck et al. 1994a). Both the triphenyltriketone **73** and, in particular, triketone **71** deserve more investigation. Most excitingly, the latter compound should be converted into the corresponding tribenzocentrohexaquinacene **74**, a still unknown hydrocarbon (Scheme 3.8). Maybe this particular triquinacene derivative represents the best candidate to date to undergo a head-to-head dimerisation of the concave 1,4,7-cyclononatriene unit to generate, eventually, a dodecahedrane skeleton bearing two bulky – and thus strongly shielding – triptindane scaffolds in their convex backsides. In this way, famous but never fulfilled dreams (Woodward et al. 1964) disclosed alongside with the publication of the first synthesis of triquinacene would become reality. Moreover, triketone **71** appears to be another good candidate to render new life into Serratosa's idea (Carceller et al. 1986) to condense two such concave triquinanetriones into the dodecahedrane framework.

From the discussion presented above, it is obvious that the chemistry of centrohexacyclic compounds is unusual, exciting and quite demanding in the same time. In fact, there is ample motivation to continue our efforts towards the still elusive polycyclic targets, such as centrohexaquinane (**9**) and centrohexaquinacene (**10**) – beside the challenge to make a dodecahedrane. The last part of the experimentally achieved research presented here again concerns our efforts to remove the residual benzene units from the "half-way" dismantled hydrocarbon, tribenzocentrohexaquinane **62** (Gestmann et al. 1996). In fact, this hydrocarbon was obtained with relative ease when triketone **71** was subjected to Wolff-Kishner

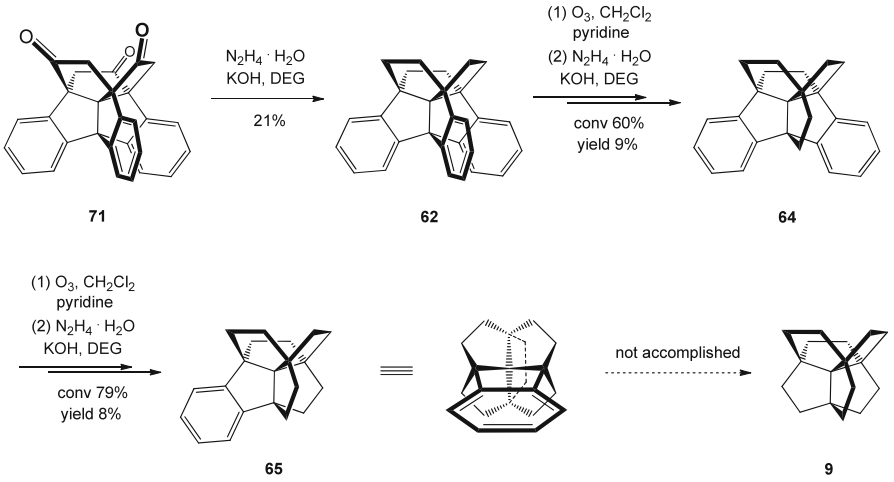

Scheme 3.9 Synthesis of tribenzocentrohexaquinane **62** and subsequent access to dibenzocentrohexaquinane **64** and benzocentrohexaquinane **65** by ozonolytic dismantling of further benzene units

reduction (Scheme 3.9). Similar to the procedures employed before for 1,2-diketone **48** discussed above, we obtained the C_{3v}-symmetrical tribenzocentrohexaquinane **62** in 42% yield as colourless crystals from methanol (Kuck et al. 1994a). In a *parforce* effort, we subjected this hydrocarbon to a sequence of ozonolysis under most careful controlled conditions and subsequent Wolff-Kishner reduction of the expected 1,2-diketone (Gestmann et al. 1996). In this way, the C_s-symmetrical dibenzocentrohexaquinane **64** was obtained as a colourless oil in 9% overall yield based on the conversion of the starting tribenzo-annellated precursor **62**. Although the latter hydrocarbon was recovered in part, the efficiency of this two-step de-annellation sequence was discouraging. Starting from **62** on a 500-mg scale, only 22 mg of the product **64** were obtained (Gestmann et al. 1996). Nevertheless, repeated conversions **62** → **64** furnished the dibenzocentrohexaquinane hydrocarbon in amounts that allowed us to perform the next step – and with utmost possible thoroughness. A total amount of 95 mg of hydrocarbon **64** was used for the same two-step sequence of ozonolysis and Wolff-Kishner reduction described above. In contrast to the preceding degradation step, no reddish colour was observed that would have indicated the formation of the 1,2-diketone. However, reduction of the material that was assumed to contain the 1,2-diketone followed by careful workup including chromatographic separation did afford the monobenzocentrohexaquinane **65**, again as a colourless oil. Electron-impact mass spectrometry (EI-MS) including an accurate mass measurement as well as proton nuclear resonance (^{1}H NMR) spectroscopy clearly proved its identity as a centrohexacyclic $C_{21}H_{24}$ hydrocarbon – probably the most unusual indane derivative ever made (Gestmann et al. 1996). The yield of compound **65** based on the converted precursor **64** was again very low (8%); the absolute yield was only 5 mg. It may be worth being noted that

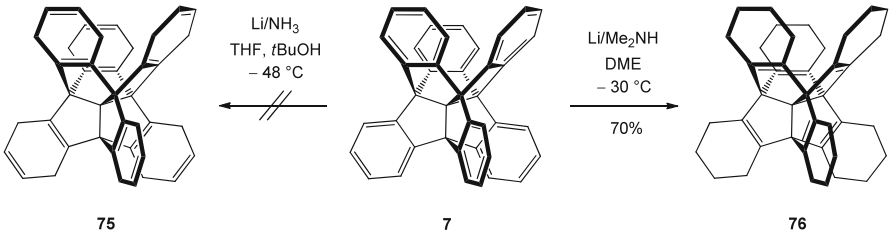

Scheme 3.10 Futile attempts of Birch reduction of centrohexaindane (**7**) and successful Benkeser reduction, leading to the first experimentally known (nonaromatic) centrohexaquinacene **76**

inspection of the ^{1}H NMR spectrum of this sample of **65** recorded at 300 MHz at the time suggested two details: (1) The ground-state structure of **65** appears to be C_2-symmetrical and may suffer a relatively low conformational interconversion of the equivalent conformers. This follows from the fact that the aromatic protons do not reflect an AA′BB′ spin system but rather give rise to two more complex 2H-multiplets at δ 7.02 and δ 6.92. (2) The ^{1}H NMR spectrum of the very same sample exhibits the resonances of 20 alicyclic protons in the range δ 1.31–1.94 as complex multiplets. However, a very narrow singlet was found at δ 1.61 (but with a low fraction of the overall integral). This signal was tentatively assigned to a minor component present as a very special impurity: the elusive centrohexaquinane (**9**). In fact, this hydrocarbon should exhibit its 24 equivalent protons in this very range as a singlet, and its presence may have been the result of an ozonolytic over-degradation of the precursor hydrocarbon **64**. Hence there is reason to believe that the elusive centrohexaquinane did exist in our laboratory – but never in isolated form (Gestmann et al. 1996).

Finally, it may be noted that one single and truly olefinic, nonaromatic derivative of centrohexaquinacene **10** does exist (Scheme 3.10). Hexakis(cyclohexano)-centrohexaquinacene (**76**) was prepared by Benkeser reduction of centrohexaindane (**7**) in good yield. In contrast, unfortunately and as another telling result, hexakis(cyclohexa-2,4-dieno)centrohexaquinacene (**75**) was not obtained, when the same starting hydrocarbon **7** was subjected to Birch reduction (Eckrich and Kuck 1993). No doubt the latter hydrocarbon would be the more interesting product. Whereas it is obvious that considerable limits of solubility prevent the Birch reduction of **7**, more experience in directed dismantling of the aromatic units about the C_{17}-core of suitable centrohexaindane precursors is highly desired!

3.5 Conclusions

A wealth of novel chemistry has been developed during the past three decades as a result of our research into the chemistry of the centropolyindanes. Whereas centrohexaindane (**7**), a large and stable hydrocarbon bearing six benzene units

oriented along the six directions of the Cartesian space, can be prepared in gram amounts via several routes, most of the corresponding partially benzoannellated congeners are difficult to access or even still unknown. This holds true, in particular, for the nonaromatic parent hydrocarbons bearing the same C_{17} of quaternary carbon atoms, centrohexaquinane (**9**) and centrohexaquinacene (**10**). Since the experimental approaches to the partially benzoannellated centrohexaquinanes are low-yielding or even dead-end alleys, as demonstrated in this chapter, further research should be invested based on the results obtained to date, and maybe new and independent routes to these elusive C_{17}-hydrocarbons can be explored. There is no doubt that the motif of D_5-diamond would deserve such efforts.

Acknowledgements The author is grateful to all his students, co-workers and colleagues who contributed to this research over the many years by their enthusiasm, skill, ideas and hard work.

References

Baker W, McOmie JFW, Parfitt SD, Watkins DAM (1957) Attempts to prepare new aromatic systems. Part VI. 1:2–5:6-Dibenzopentalene and derivatives. J Chem Soc 4026–4037

Bartlett PD, Ryan MJ, Cohen SG (1942) Triptycene (9,10-o-benzenoanthracene). J Am Chem Soc 64:2649–2653

Bradsher CK (1946) Aromatic cyclodehydration. Chem Rev 38:447–499

Bredenkötter B, Barth D, Kuck D (1999) Synthesis and based-induced epimerization of cis,cis,cis,trans-Tribenzo[5.5.5.6]fenestranes. J Chem Soc Chem Commun 847–848

Bredenkötter B, Flörke U, Kuck D (2001) Benzoannelated cis, cis, cis, trans-[5.5.5.6]Fenestranes. Syntheses, base lability and flattened molecular structure of strained epimers of the all-cis series. Chem Eur J 7:3387–3400

Brückner R (1989) Organisch-chemischer Denksport. Vieweg, Braunschweig, pp 35–36

Campbell N, Davison PS, Heller HG (1963) The interaction of diphenylketene and 2-benzylideneindan-1-one. J Chem Soc 993–998

Carceller E, García ML, Moyano A, Pericàs MA, Serratosa F (1986) Synthesis of triquinacene derivatives: new approach towards the synthesis of dodecahedrane. Tetrahedron 42:1831–1839

Chambron JC, Dietrich-Buchecker C, Sauvage JP (1993) From classical chirality to topologically chiral catenands and knots. Top Curr Chem 165:131–162

Diudea MV (2010) Diamond D_5, a novel allotrope of carbon. Studia Univ Babes-Bolyai Chemia 55:11–17

Diudea MV, Nagy CL, Ilić A (2011) Diamond D_5, a novel class of carbon allotropes. In: Putz MV (ed) Carbon bonding and structures. Springer, Heidelberg; chapter 11

Eaton PE, Cole TW Jr (1964) Cubane. J Am Chem Soc 86:3157–3158

Eckrich R, Kuck D (1993) Multiple Birch and Benkeser reduction of centropolyindanes. Synthesis of a Hexakis(cyclohexano)centrohexaquinacene. Synlett 4:344–347

Ermer O (1981) Aspekte von Kraftfeldrechnungen. Wolfgang Baur Verlag, München

Fessner WD, Murty BARC, Wörth J, Hunkler D, Fritz H, Prinzbach H, Roth WR, Schleyer PR, McEwen AB, Maier WF (1987) Die Pagodan-Route zu Dodecahedranen – thermische, reduktive und oxidative Pagodan-Umwandlungen. Angew Chem 99:484–486, Angew Chem Int Ed Engl 26:452–454

Gestmann D, Pritzkow H, Kuck D (1996) Partially benzoanellated centrohexaquinanes: oxidative degradation of centropolyindanes using ruthenium(VIII) oxide and ozone. Liebigs Ann 1349–1359

Gund P, Gund TM (1981) How many rings can share a quaternary atom? J Am Chem Soc 103:4458–4465

Hackfort T, Kuck D (1999) Phenanthro[1.10]-annelated [3.3.3]Propellanes by cyclodehydrogenation reactions of mono-, di- and tribenzylidenetriptindanes. Eur J Org Chem 2867–2878

Harig M, Kuck D (2006) The first centrohexaindane bearing twelve functional groups at its outer molecular periphery and related lower veratrole-derived centropolyindanes. Eur J Org Chem 1647–1655

Hopf H (2000) Classics in hydrocarbon chemistry. Syntheses, concepts, perspectives. Wiley-VCH, Weinheim

Keese R (2006) Carbon flatland: planar tetracoordinate carbon and fenestranes. Chem Rev 106:4787–4808

Kuck D (1984) Ein einfacher Zugang zu benzoanellierten Centropolyquinanen. Angew Chem 96:515–516; Angew Chem Int Ed 23:508–509

Kuck D (1990a) Mass spectrometry of alkylbenzenes and related compounds. Part II: gas phase ion chemistry of protonated alkylbenzenes (alkylbenzenium ions). Mass Spectrom Rev 9:583–630

Kuck D (1990b) Centropolyindanes. Multiply fused benzoannelated cyclopentane hydrocarbons with a central carbon atom. In: Hargittai I (ed) Quasicrystals, networks, and molecules of fivefold symmetry. VCH Publishers, New York; chapter 19

Kuck D (1992) Gaseous $[M-H]^+$ Ions of α, ω-diphenylalkanes: cyclization to $[M+H]^+$ type ions of benzocycloalkanes as recognized by chain-length dependent proton exchange. Int J Mass Spectrom Ion Process 117:441–455

Kuck D (1994) Benzoanellated Centropolyquinanes, 15. Benzoannelated Fenestranes with [5.5.5]-, [5.5.5.6]- and [5.5.5.5]-frameworks: The route from 1,3-Indandione to Fenestrindane. Chem Ber 127:409–425

Kuck D (1996) By cyclodehydration to centropolyindanes: development of a novel class of indane hydrocarbons with three-dimensional molecular frameworks using a classical synthetic tool. Synlett 949–965

Kuck D (1997a) The centropolyindanes and related centro-fused polycyclic organic compounds. Polycycles between neopentane $C(CH_3)_4$ and the carbon nucleus $C(CC_3)_4$. Top Curr Chem 196:167–220

Kuck D (1997b) Centrohexacyclic or 'K_5' molecules – development of a growing class of topologically nonplanar organic compounds. Liebigs Ann/Rec 1043–1057

Kuck D (2002) Half a century of scrambling in organic ions: complete, incomplete, progressive and composite atom interchange. Int J Mass Spectrom 213:101–144

Kuck D (2006a) Functionalized aromatics aligned with the three cartesian axes: extension of centropolyindane chemistry. Pure Appl Chem 78:749–775

Kuck D (2006b) Three-dimensional hydrocarbon cores based on multiply fused cyclopentane and indane units: the centropolyindanes. Chem Rev 106:4885–4925

Kuck D, Bögge H (1986) Benzoannelated Centropolyquinanes. 2. all-cis-Tetrabenzotetracyclo[5.5.1.04,13.010,13]tridecane, "Fenestrindane". J Am Chem Soc 108:8107–8109

Kuck D, Schuster A (1988) Die Synthese von Centrohexaindan – dem ersten Kohlenwasserstoff mit topologisch nicht-planarer Molekülstruktur. Angew Chem 100:1222–1224; Angew Chem Int Ed 27:1192–1194

Kuck D, Schuster A, Krause RA (1991) Synthesis and conformational behavior of fenestrindanes (Tetrabenzo[5.5.5.5]fenestranes) with four bridgehead substituents. J Org Chem 56:3472–3475

Kuck D, Lindenthal T, Schuster A (1992) Benzoanellated centropolyquinanes, 11. The synthesis of tribenzotriquinacene and some centro-substituted derivatives. Chem Ber 125:1449–1460

Kuck D, Paisdor B, Gestmann D (1994a) Synthese centrohexacyclischer Kohlenwasserstoffe über die 'Propellan-Route': Centrohexaindan und Tribenzocentrohexaquinan. Angew Chem 106:1326–1328; Angew Chem Int Ed Engl 33:1251–1253

Kuck D, Schuster A, Gestmann D (1994b) Centropentaindane: synthesis and some bridgehead transformations of a novel regular centropolyindane. J Chem Soc Chem Commun 609–610

Kuck D, Schuster A, Paisdor B, Gestmann D (1995) Centrohexaindane: three complementary syntheses of the highest member of the centropolyindane family. J Chem Soc Perkin Trans 1:721–732

Kuck D, Schuster A, Gestmann D, Posteher F, Pritzkow H (1996) Centropentaindane, a novel fenestrindane bearing an additional ortho-phenylene bridge. Independent syntheses, molecular structure, and bridgehead substitution. Chem Eur J 2:58–67

Kuck D, Krause RA, Gestmann D, Posteher F, Schuster A (1998) Polycyclic compounds beyond the propellanes and fenestranes: [m.n.o.p.q]centropenta- and [m.n.o.p.q.r]centrohexa-cyclanes. Tetrahedron 54:5247–5258

Kuck D, Schuster A, Krause RA, Tellenbröker J, Exner CP, Penk M, Bögge H, Müller A (2001) Multiply bridgehead- and periphery-substituted tribenzotriquinacenes – highly versatile rigid molecular building blocks with C_{3v} or C_3 symmetry. Tetrahedron 57:3587–3613

Kuck D, Hackfort T, Neumann B, Stammler HG (2007) Centrohexaindanes bearing methyl groups in their molecular propellane cavities. Pol J Chem 81:875–892

Kuratowski C (1930) Sur le problème des courbes gauches en topologie. Fund Math 15:271–283

Luyten M, Keese R (1984) all-cis-[5.5.5.5]Fenestran. Angew Chem 96:358–359; Angew Chem Int Ed Engl 23:390–391

Maier G, Pfriem S, Schäfer U, Mattusch R (1978) Tetra-tert-butyltetrahedran. Angew Chem 90:552–553; Angew Chem Int Ed Engl 17:520–521

Paisdor B, Kuck D (1991) Synthesis and reactions of 9,10,11-triptindantrione and some other functionalized tribenzo[3.3.3]propellanes (9H,10H-4b,9a-([1,2]benzenomethano)indeno [1,2-a]indenes). J Org Chem 56:4753–4759

Paquette LA, Vazeux M (1981) Threefold transannular epoxide cyclization. Synthesis of a heterocyclic C_{17}-hexaquinane. Tetrahedron Lett 22:291–294

Paquette LA, Williams RV, Vazeux M, Browne AR (1984) Factors conducive to the cascade rearrangement of sterically congested and geometrically restricted three-membered rings. Facile synthesis of a topologically nonplanar heterocycle. J Org Chem 49:2194–2197

Popelis YY, Pestunovich VA, Shternberga IY, Freimanis YF (1972) Spiroketones based on β-diketones. VI. NMR spectra and structure of 1,3-diaryl-2,2-spirophthaloylcyclohexan-5-ones. Zh Org Khim 8:1860–1864; J Org Chem USSR 8:1907–1910

Popp FD, McEwen WE (1958) Polyphosphoric acids as a reagent in organic chemistry. Chem Rev 58:321–401

Prange T, Drouin J, Leyendecker F, Conia JM (1977) X-ray molecular structure of a highly symmetrical triketone: [3.3.3]propellane-2,8,9-trione. J Chem Soc Chem Commun 1977: 430–431

Prantz K, Mulzer J (2010) Synthetic applications of the carbonyl generating grob fragmentation. Chem Rev 110:3741–3766

Prinzbach H, Weber K (1994) Vom Insektizid zu Platons Universum – die Pagodan-Route zu Dodecahedranen: Neue Wege und neue Ziele. Angew Chem 106:2329–2348; Angew Chem Int Ed Engl 33:2239–2258

Röttger D, Erker G (1997) Verbindungen mit planar tetrakoordiniertem Kohlenstoff. Angew Chem 109:840–856; Angew Chem Int Ed Engl 36:813–827

Seebach D (1990) Organische synthese – wohin? Angew Chem 102:1363–1409; Angew Chem Int Ed Engl 29:1320–1367

Shternberga IY, Freimanis YF (1968) Spiroketones based on β-diketones. II. Synthesis and properties of 1,3-diaryl-2,2-phthaloylcyclohexanones-5. Zh Org Khim 4:1081–1086; J Org Chem USSR 4:1044–1048

Simmons HE III (1980) The synthesis, structure and reactions of some theoretically interesting propellanes: the synthesis of the first topologically non-planar organic molecule. PhD thesis, Harvard University, Cambridge, MA

Simmons HE III, Maggio JE (1981) Synthesis of the first topologically non-planar molecule. Tetrahedron Lett 22:287–290

Tellenbröker J, Barth D, Neumann B, Stammler HG, Kuck D (2005) Methoxy-substituted centrohexaindanes through the fenestrane route. Org Biomol Chem 3:570–571

Ten Hoeve W (1979) The long and winding road to planar carbon, proofschrift. Doctoral thesis, Rijksuniversiteit te Groningen
Ten Hoeve W, Wynberg H (1979) Chiral spiranes. Optical activity and nuclear magnetic resonance spectroscopy as a proof for stable twist conformations. J Org Chem 44:1508–1514
Ten Hoeve W, Wynberg H (1980a) Synthetic approaches to planar carbon, 1. J Org Chem 45: 2925–2930
Ten Hoeve W, Wynberg H (1980b) Synthetic approaches to planar carbon, 2. J Org Chem 45: 2930–2937
Ternansky RJ, Balogh DW, Paquette LA (1982) Dodecahedrane. J Am Chem Soc 104:4503–4504
Thompson HW (1966) Synthesis of a tricyclo[3.3.3.01,5]undecane system. Tetrahedron Lett 7:6489–6494
Thompson HW (1968) Synthesis of triptindane. J Org Chem 33:621–625
Venkatachalam M, Kubiak G, Cook U, Weiss U (1985) General approach for the synthesis of polyquinanes. Tetrahedron Lett 26:4863–4866
Woodward RB, Fukunaga T, Kelly RC (1964) Triquinacene. J Am Chem Soc 86:3162–3164

Chapter 4
Two C_{28} Clathrates

Marzio de Corato, Davide M. Proserpio, Marco Bernasconi, and Giorgio Benedek

Abstract Although carbon fullerenic clathrates, characterized by eclipsed bonds, have not been synthesized yet, their structure may be reflected in the assembly of tetrahedral diamondoid clusters (hollow diamonds) due to their assembling into the eclipsed configuration. The detection by El Goresy et al. (Lunar Planetary Sci 34:art. No. 1016, 2003a; C R Geosci 335:889–898, 2003b; Meteorit Planet Sci 39:A36, 2004) in highly shocked meteoritic rocks of a cubic diamond-like polymorph with almost 400 atoms per unit cell stimulated the present investigation on hypothetical small carbon clathrates with 4-membered rings on which hollow diamonds can be constructed via a cluster assembly. Two polytypes of a novel C_{28} clathrate, one body-centered orthorhombic (bco) and the other simple cubic (sc), are proposed, with a detailed ab initio characterization of the electronic and zero-wave-vector vibrational structures of the bco phase. The assembly of C_{14} diamondoid clusters

M. de Corato (✉)
Dipartimento di Scienza dei Materiali, Universitá di Milano-Bicocca,
Via R. Cozzi 53, 20125 Milan, Italy
e-mail: marzio.decorato@unimore.it

Centro S3, CNR-Istituto Nanoscienze, I-41125 Modena, Italy

Dipartimento di Fisica, Università di Modena e Reggio Emilia, I-41125 Modena, Italy

D.M. Proserpio
Dipartimento di Chimica, Universitá degli Studi di Milano, Via Golgi 19, 20133 Milan, Italy

M. Bernasconi
Dipartimento di Scienza dei Materiali, Universitá di Milano-Bicocca,
Via R. Cozzi 53, 20125 Milan, Italy

G. Benedek
Dipartimento di Scienza dei Materiali, Universitá di Milano-Bicocca,
Via R. Cozzi 53, 20125 Milan, Italy

Donostia International Physics Center (DIPC), University of the Basque Country (UPV-EHU),
P.M. de Lardizábal 4, 20018 Donostia – San Sebastián, Spain
e-mail: giorgio.benedek@unimib.it

M.V. Diudea and C.L. Nagy (eds.), *Diamond and Related Nanostructures*,
Carbon Materials: Chemistry and Physics 6, DOI 10.1007/978-94-007-6371-5_4,

into the sc-C_{28} array is briefly discussed in comparison with the above polymorph in order to illustrate a viable method of topological analysis of complex crystalline structures.

4.1 Introduction

While large diamond crystals are regarded as the most precious of all gemstones, at the molecular and nanocrystalline levels, diamond-like carbon is largely diffused in the Earth's crust, especially in the various forms of diamondoids present in fossil fuel reservoirs (Mansoori et al. 2012). The comparatively large abundance of carbon in the solar system is also signaled by the detection of crystalline sp^3 carbon polymorphs in shocked meteoritic materials (El Goresy et al. 2003a, b, 2004; Ferroir et al. 2010). These findings have stimulated several theoretical investigations (Mackay and Terrones 1991; Hirai and Kondo 1991; Gogotsi et al. 1998; Ribeiro et al. 2006; Scandolo et al. 1996; Serra et al. 1998; Pickard et al. 2001; Li et al. 2009; Selli et al. 2011) suggesting novel forms of sp^3 carbon crystals having cohesive energy and bulk modulus and hardness comparable to those of diamond and lonsdaleite. The phase diagrams of these hypothetical diamond-like forms indicate in many cases their possible formation under unusual pressure and temperature conditions, as occurring in meteoritic shocks or cosmic environments, but also as synthetic products from the conversion of sp^2 carbon, notably graphite or fullerenes, into sp^3 carbon under very large pressures (Kozlov et al. 1995, 1996; Mao et al. 2003).

The synthesis of novel forms of sp^3 carbon crystals with a clathrate structure originating from the coalescence of fullerenic cages (Diudea and Nagy 2007; Benedek and Colombo 1996; Benedek et al. 1995, 1997; Blase et al. 2010), where all bonds are in the eclipsed configuration, has been also attempted with softer approaches like cluster beam deposition and laser-ablation methods. An example of the latter method is the synthesis of a novel periodic carbon structure obtained from assembling the smallest fullerenic cages, C_{20} (Iqbal et al. 2003). The assembling of the C_{20} molecules occurs through eight covalent bonds per molecule, eight being the smallest magic valence number of C_{20} (Milani et al. 1996). This structure is an example of *incomplete* fullerenic clathrate, because only 8 of the 20 dangling bonds of C_{20} are used to coordinate the neighbor molecules, the remaining 12 bonds being either passivated by hydrogen or paired in distorted π-bonds. As discussed in the present chapter, a complete clathrate with 28 atoms in the unit cell may be obtained from a simple cubic assembly of C_{20} at the cost, however, of introducing 4-membered carbon rings.

Indeed the predicted variety of possible sp^3 carbon lattices of high stability and superior mechanical properties is virtually infinite when, starting from the basic fullerenic clathrates (with only 5- and 6-membered rings), structures of increasing complexity are generated through topological multiplication algorithms, where, for example, either eclipse-bonded clusters or staggered-bonded diamondoid clusters

(Benedek and Colombo 1996; Blase et al. 2010) substitute the atoms of the original structure. When the bonding structure, for example, the eclipsed one, is preserved in the replacement process, the multiplication can be iterated, so as to lead to topological fractals and, when integer dimensions are preserved via relaxation, to topological quasicrystals (Benedek and Colombo 1996; Blase et al. 2010). On the other hand, the replacement of diamondoid clusters yields mixed eclipsed-staggered bonding configurations, eventually generating a class of lattices called *hollow diamonds* (Benedek and Colombo 1996). Even more plausible structures are possible when also 4-membered or/and rings larger than hexagons are admitted. In particular clathrates with square rings form a fairly stable wide class of clathrates not yet explored as thoroughly as the fullerenic ones, apart from the very interesting and compact hex-C_{16} (Benedek et al. 2003).

The frequent occurrence of diamondoids in nature (Mansoori et al. 2012) suggests that hollow diamond structures, eventually assembled in a clathrate with square rings, may also be found in nature, as argued later in connection with a superhard cubic diamond-like form of carbon with about 396 atoms per unit cell reported a few years ago by El Goresy et al. (2003a). In this connection, we discuss in the next sections two isomers of a novel clathrate C_{28}, which are more compact than the smallest fullerenic clathrate, having the face-centered-cubic (fcc) structure with 34 atoms in the rhombohedric unit cell. One of these isomers is the above-mentioned simple cubic (sc) assembly of C_{20} fullerenes connected through cycloadditions and saturated with cubane clusters. This form, multiplied by 14 through the substitution of C_{14} diamondoid clusters, gives just a sc clathrate with a number (392) of atoms close to the cubic cell of El Goresy et al. (2003a) sample. The other isomer is a novel body-centered orthorhombic (bco) clathrate. It also includes squared rings and is thoroughly characterized via an ab initio calculation of its electronic bands and its $q = 0$ phonon spectrum, with a favorable comparison to the smallest fullerenic clathrates.

4.2 Topological Properties of Clathrate with Squared Rings

There are several carbon structures which include square rings. The simplest three-dimensional structure is the sp^3cubane molecule C_8H_8 (Fig. 4.1) (Eaton and Cole 1964; Eaton 1992).

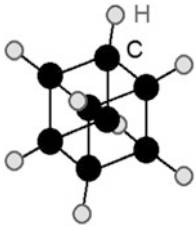

Fig. 4.1 The C_8H_8 cubane molecule

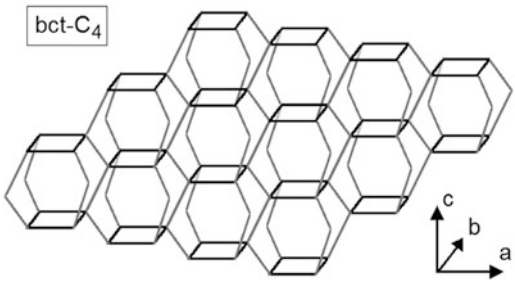

Fig. 4.2 The bct-C_4 crystal showing the presence of 4-membered rings connecting distorted graphenic layers and a pseudo-clathrate structure; the projection on a plane normal to the *c*-axis shows a tiling of squares and distorted octagons (Umemoto et al. 2010)

Among the carbon lattices with 4-membered rings, it has been proposed, on the basis of ab initio calculations, as a new type of crystal with only four atoms per unit cell, the body-centered tetragonal bct-C_4 (Umemoto et al. 2010), which may be obtained from graphenic sheets interlinked by 4- and 8-membered rings. This net is known in solid-state chemistry as the net of the boron atoms in CrB_4, the underlying net of zeolite BCT, and named **crb** according to the database RCSR (O'Keeffe et al. 2008). It has been shown later by means of ab initio molecular dynamics that this phase can be obtained in principle from graphite under a pressure of 20 GPa (Zhou et al. 2010). These works underline the important fact that this structure is endowed with a high stability, comparable to that of graphite and diamond. As appears from the perspective, top, and lateral views of the bct-C_4 lattice (Fig. 4.2), the interlayer bonds yield cages organized in a sort of clathrate crystal.

In this section, it is worth reminding the topological equations governing the sp^3 clathrates, previously discussed for fullerenic clathrates (Blase et al. 2010), in order to include clathrates with also 4-membered rings. Assuming first a fullerenic carbon clathrate lattice with three-dimensional periodic boundary condition and a unit cell containing N atoms and V_h fullerenic cages made of 12 pentagons and h hexagons, the following equation holds as a consequence of Euler theorem (Blase et al. 2010):

$$\sum_h \left(5 + \frac{1}{2}h\right) V_h = N \tag{4.1}$$

Clathrates including, besides the 6- and 5-membered rings of ordinary fullerenic clathrates, also 4-membered rings are viewed as formed by the coalescence of polyhedra denoted by

$$6^h 5^{12-2s} 4^s, \tag{4.2}$$

where s is the number of 4-membered rings in a given cage. Note that the insertion of a square in a cage implies the elimination of two 5-membered rings. Thus, the extreme case of no 5-membered and no 6-membered rings requires $s = 6$ and corresponds to the cube. In this case, Eq. (4.1) is readily extended to:

$$N = \sum_h \left(5 + \frac{1}{2}h\right) V_h + \sum_s \left(5 + \frac{1}{2}h_s - \frac{1}{2}s\right) v_s \tag{4.3}$$

where v_s is the number of cages with 4-membered rings and h_s hexagons. The smallest clathrate of this family is hex-C_{16}: it is obtained from the coalescence of one C_{36} fullerene and two C_{14} non-fullerenic cages per unit cell and has been characterized by ab initio methods in a previous work (Benedek et al. 2003). This clathrate net has been named **alb-x-d** in RCSR (O'Keeffe et al. 2008). Larger members of the family with 28 atoms per unit cell are described in the next sections as novel structures.

4.3 A Simple-Cubic C_{28} Clathrate

The smallest fullerenic cage, the dodecahedral C_{20}, can be assembled in a complete sp^3-bonded clathrate through a simple-cubic polymerization via the formation of cycloaddition 4-membered rings linking six identical dodecahedra in the orthogonal directions. This implies the saturation of 12 dangling bonds, corresponding to the second magic valence number (12) of the C_{20} molecule (Milani et al. 1996). The remaining eight dangling bonds per cage could then by passivated by hydrogen atoms. Alternatively the leftover empty spaces can host exactly a cubane cluster each, with a complete saturation of the dangling bonds.

The resulting structure is a complete clathrate with several 4-membered rings; the structure is depicted in Fig. 4.3, where for purpose of clarity, the cycloaddition bonds connecting the dodecahedra and the saturating bonds connecting the dodecahedra to

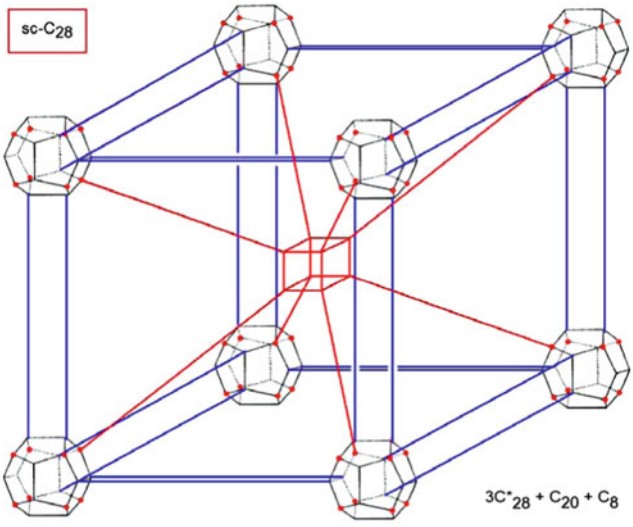

Fig. 4.3 The schematic structure of the simple-cubic clathrate C_{28}. For purpose of clarity, the cycloaddition bonds connecting the dodecahedra and the saturating bonds connecting the dodecahedra to the cubane have been elongated by a factor 7. The lattice unit cell includes one fullerene C_{20}, one cubane C_8, and three C_{28}* cages

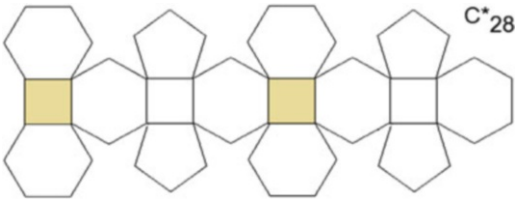

Fig. 4.4 The C_{28}* polyhedron, here shown developed into its 16 faces, is made of 8 hexagons, 4 pentagons, and 4 squares, of which two belong to a cubane and two to cycloaddition rings

the cubane have been elongated by a factor 7. The unit cell of this sc lattice includes one fullerene C_{20}, one cubane C_8, and three cages of 28 atoms, here denoted by C_{28}* in order to distinguish them from the well-known tetrahedral fullerene C_{28}. The C_{28}* polyhedron, developed in Fig. 4.4, is made of 8 hexagons, 4 pentagons, and 4 squares, of which two belong to a cubane and two to cycloaddition rings.

There does not seem to be in the literature a description of this comparatively simple clathrate. A first-principle study of its ground-state cohesive energy, mechanical and hardness properties, as well as of its electronic and vibrational structure would be in order. This structure will be discussed below as a possible candidate for a hollow diamond obtained by a replacement algorithm with the diamondoid cluster C_{14}.

4.4 The Body-Centered Orthorhombic C_{28} Clathrate

4.4.1 Structure

An interesting isomer of the clathrate introduced in the above section has a body-centered orthorhombic (bco) lattice and can be obtained from the coalescence of one dodecahedral fullerene C_{20} (5^{12}), two fullerenes C_{30} ($5^{12}6^5$) with C_{2v} symmetry, and two cages C_{16} (4^25^8) made of eight pentagons and two squares, also known as square truncated trapezohedra (Fig. 4.5). This crystal, whose structure is shown in Figs. 4.6 and 4.7, belongs to the space group *Immm*. It contains much less square rings than its simple-cubic isomer and should be more stable, albeit the two C_{30} cages are subject to appreciable strains. Indeed the ab initio calculations of the cohesive energy per atom place this structure among the ordinary fullerenic clathrates.

The optimized geometry of this new clathrate has been obtained from ab initio calculations within the density functional theory (DFT), with the generalized-gradient approximation proposed by Perdew, Burke, and Ernzerhof (PBE) (1996). Ultrasoft pseudopotentials have been used with Kohn-Sham orbitals expanded in plane waves up to a kinetic cutoff of 30 Ry (charge density cutoff up to 240 Ry) as implemented in Quantum Espresso programs (Giannozzi et al. 2009). A Monkhorst-Pack (Monkhorst and Pack 1976) $4 \times 4 \times 4$ mesh that corresponds

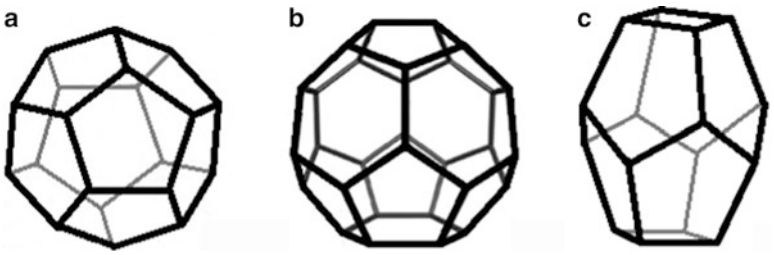

Fig. 4.5 The three cages composing the carbon clathrate bco-C_{28}: (**a**) the dodecahedral fullerene C_{20} (5^{12}), (**b**) the C_{2v} isomer of the fullerene C_{30} ($5^{12}6^5$), and (**c**) the square truncated trapezohedron C_{16} ($4^2 5^8$)

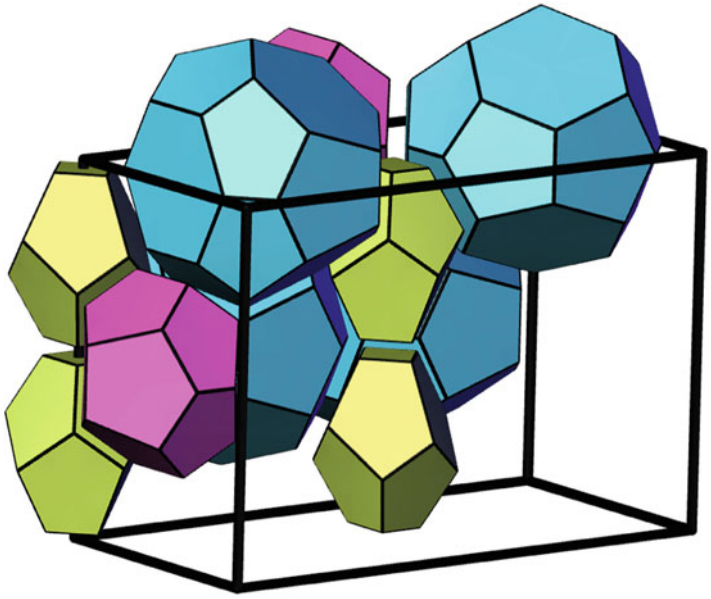

Fig. 4.6 A pictorial representation of the tiling $2(4^2.5^8) + (5^{12}) + 2(5^{12}.6^5)$ with the three different polyhedra constituting the unit cell of the carbon bco-C_{28} clathrate (space group *Immm*). The tiling has been computed with TOPOS (Blatov 2006) and plotted with *3dt* part of the GAVROG project (Delgado-Friedrichs 2008)

to eight k-points in the irreducible Brillouin zone (BZ) has been used in BZ integrations. The b/a and c/a ratios of the bco lattice were optimized at each volume with a residual non-hydrostatic pressure below 1 kbar. The energy per atom calculated as a function of the volume V has been interpolated with a Murnaghan equation of state (Murnaghan 1944):

$$E = \frac{V_0 B_0}{b}\left\{\frac{1}{b-1}\left(\frac{V_0}{V}\right)^{b-1} + \frac{V}{V_0}\right\} + \text{const}, \tag{4.4}$$

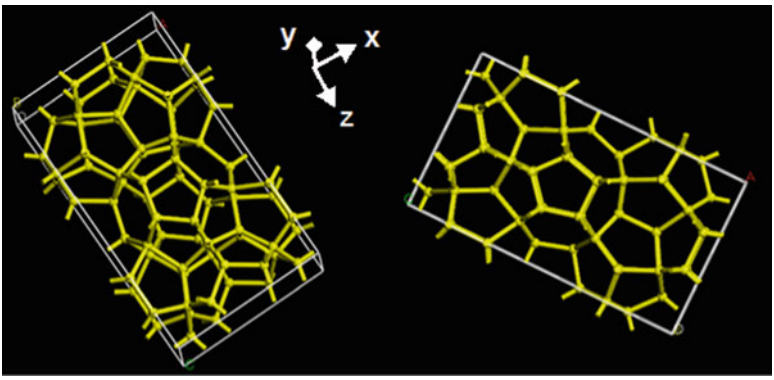

Fig. 4.7 Two *ball-and-stick side views* of the carbon bco-C_{28} lattice

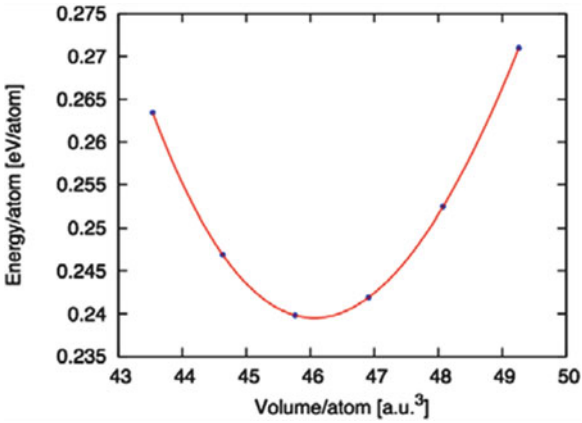

Fig. 4.8 Equation of state of bco-C_{28} carbon clathrate. The energy per atom is relative to the ground-state energy per atom of diamond

Table 4.1 The ground-state energy per atom and the equilibrium bulk modulus relative to that of diamond (second column) of bco-C_{28} (last column) and of other clathrates (Blase et al. 2010), with the RCSR name in bold (O'Keeffe et al. 2008)

	Diamond	Fcc-C_{34}	hex-C_{40}	sc-C_{46}	hex-C_{16}	
	Dia	mtn	zra-d	mep	alb-x-d	bco-C_{28}
$E - E_d$ (eV/atom)	0	0.134	0.170	0.144	0.547	0.239
B_0 (GPa)	443	364	365	364	319	341

where B_0 is the bulk modulus, b its derivative with respect to pressure at equilibrium, and V_0 is the equilibrium volume. The interpolated energy per atom is plotted in Fig. 4.8 and allows to derive the values of the ground state per atom energy and bulk modulus at equilibrium. The values of bco-C_{28} are compared to those of diamond (ground-state energy per atom $E_d = -8.36$ eV) and of other carbon fullerenic and non-fullerenic clathrates in Table 4.1.

Table 4.2 The three equilibrium lattice constants of bco-C_{28} as derived from an ab initio DFT calculation and the equilibrium position of the seven independent atoms in the unit cell of the bco-C_{28} lattice in units of the respective lattice constants for the space group *Immm*

$A = 6.840$ Å	$b = 5.070$ Å	$c = 11.022$ Å
0.68947	0.75330	0.38200
0.69672	0.64987	0.00000
0.50000	0.35228	0.56943
0.80842	0.50000	0.33023
0.87389	0.50000	0.19549
0.00000	0.50000	0.59823
0.50000	0.21467	0.00000

The bco-C_{28} crystal appears to be more stable than the other non-fullerenic clathrate C_{16} but slightly less stable than the fullerenic clathrates. Also the bulk modulus reflects this tendency, classifying however bco-C_{28} as a very stiff and presumably super-hard material. The optimized lattice constant and the crystallographic coordinates of the seven atoms which are independent by symmetry are reported in Table 4.2.

4.4.2 The Electronic Band Structure

The DFT electronic band structure of bco-C_{28} (Fig. 4.9) appears to be rather similar to that of the other clathrates, though the indirect gap of 3.3 eV in this non-fullerenic clathrate is considerably smaller than those obtained from tight-binding calculations for the fullerenic clathrates and even of that of diamond (shown for comparison in Fig. 4.10). This difference may certainly be attributed to a drawback of the present DFT approach which generally yields smaller gaps in insulators. A fairly flat band occurs near the top of the valence band, which contributes a very sharp peak in the electronic density of states (DOS) just below the edge (Fig. 4.10). This feature is common to all the other carbon clathrates so far investigated but is absent in diamond. This is indeed related to the occurrence of fairly localized states peculiar of the eclipsed bonding structure and has been associated in silicon clathrates to possible optical and photoluminescent properties (Galvani et al. 1996).

4.4.3 Phonons

The phonon spectrum of bco-C_{28} at zero-wave vector ($\mathbf{q} = 0$) has been calculated by means of the density functional perturbation theory (DFPT) (Baroni et al. (2001)).

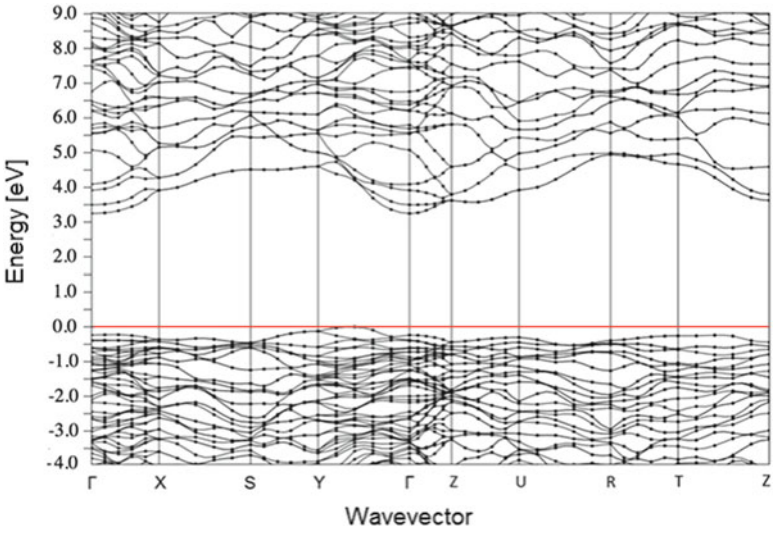

Fig. 4.9 The electronic band structure and the electronic density of states (DOS) of bco-C_{28}. Note the indirect bandgap of 3.3 eV and the flat band on the top of the valence states

To this propose that the kinetic cutoff of the plane-waves expansion of Kohn-Sham orbitals has been increased up to 40 Ry while the charge density cutoff has been increased up to 400 Ry. Similarly to the electronic band structure, the phonon density of states of this clathrate has some resemblance to that of the other fullerenic clathrates, though the latter have been calculated with a dynamical matrix derived from the Tersoff interatomic potential. The comparison between the $\mathbf{q} = 0$ phonon spectra is shown in Fig. 4.11. The upper edge of the spectrum is around 1,350 cm^{-1} for all the clathrates and is approximately 75 cm^{-1} lower that the upper edge of the phonon spectrum of diamond (1,425 cm^{-1} from a DFPT calculation). This softening with respect to diamond is well consistent with the smaller bulk modulus and is currently associated with the occurrence of the eclipsed bonding structure.

4.5 Hollow Diamonds from C_{28} Clathrates

Hollow diamonds were introduced (Benedek and Colombo 1996) as mixed eclipsed-staggered diamond-like structures generated from a clathrate through a topological multiplication algorithm where each atom of the clathrate is replaced by a given tetrahedral diamondoid cluster (Fig. 4.12), so that the diamondoid clusters can be joined together through the dangling bonds of the triangular faces. While the connections between parallel faces of cluster pairs are eclipsed in character, the bonds inside each cluster are staggered. The elements of the diamondoid cluster

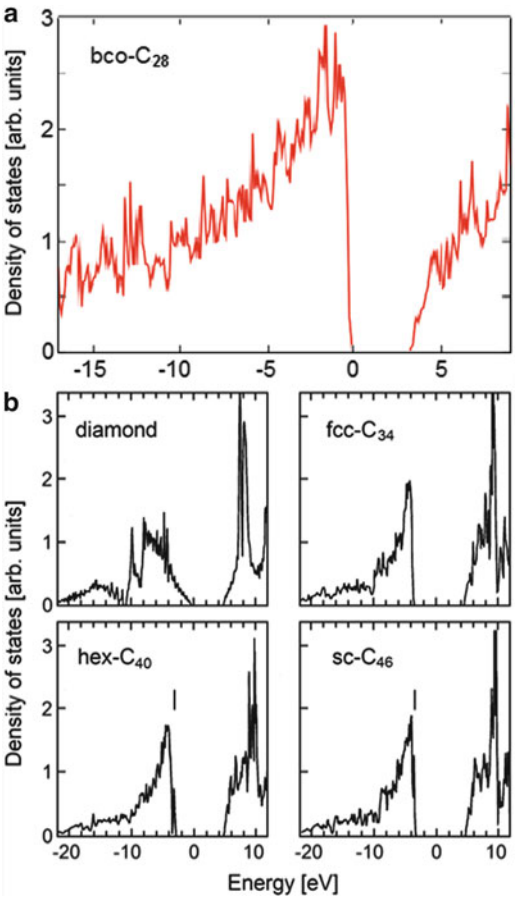

Fig. 4.10 DFT electronic density of states of bco-C_{28} (*top*) as compared to those of diamond and of the fullerenic clathrates fcc-C_{34}, hex-C_{40}, and sc-C_{46} (*bottom*), previously calculated with the tight-binding method (Blase et al. 2010)

series (Fig. 4.12) have $n(n+1)(2n+1)/6$ atoms with $n = 1, 2, 3, \ldots$; these numbers are the multiplication factors generating the series of hollow diamonds associated to a given clathrate.

Were the eclipsed bond of 1.0768 times longer than the ordinary staggered diamond bond (Dodziuk 2009), the replacement algorithm would not change the density of the original clathrate. Note that the replacement of the vertex atoms with a hydrogen atom and the passivation with hydrogen of the remaining dangling bonds transform the diamondoid clusters into the ordinary diamondoid hydrocarbons. In particular the $n = 2$ cluster C_{14} becomes the well-known adamantane $C_{10}H_{14}$ (Mansoori et al. 2012).

The hollow diamond generated from the sc-C_{28} clathrate by replacing the atoms with the clusters C_{14} would have $28 \times 14 = 392$ atoms. We note incidentally that this number is close to about 396 atoms contained in the cubic super-hard diamond-like polymorph described by El Goresy et al. (2003a). This polymorph is reported to have a cubic cell with a lattice parameter $a = 14.6970$ Å and a density of 2.49 g/cm^3

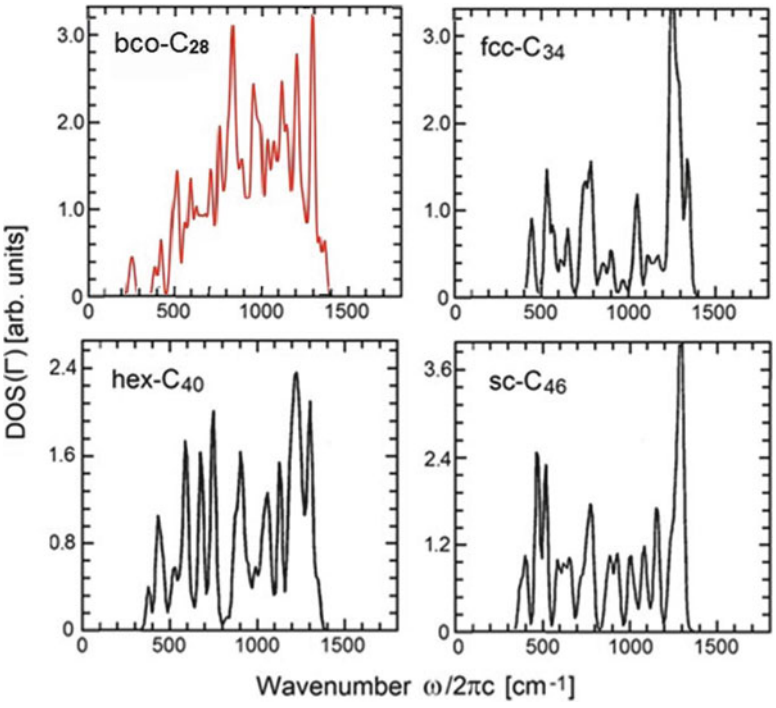

Fig. 4.11 Phonon density of states (DOS) of the bco-C_{28} carbon clathrate and of the smallest fullerenic carbon clathrates at zero-wave vector ($\mathbf{q} = 0$, Γ-point). The upper edge of the spectrum is around 1,350 cm^{-1} for all the clathrates as compared to that of cubic diamond (1,425 cm^{-1}) calculated with the same potential. The phonon DOS for bco-C_{28} is calculated with DFPT whereas those for the fullerenic clathrates are obtained from classical molecular dynamics and the Tersoff interatomic potential (Adapted from Blase et al. 2010)

to be compared with the lattice constant of 13.5 Å for the ideal sc-C_{28} clathrate. By ideal it is meant that all bonds length inside each diamondoid cluster are those of cubic diamond, while the eclipsed bonds are slightly longer so as to preserve the density as explained above. However, if all bonds are slightly elongated as a consequence of relaxation so as to equate the length of the eclipsed bonds, the lattice constant of the hollow diamond sc cell practically coincides with that of the observed polymorph.

Of course a simple approximate numeric correspondence, although between two fairly big numbers, does not allow to consider the simple-cubic hollow diamond described above as a possible candidate for the exotic structure identified by El Goresy et al. (2003a, 2004). Apart from the difficulty to figure out a cluster assembling process under extreme impact conditions, a structure identification requires a close comparison between theory and experiment of physical properties such as Raman frequencies and intensities. The search of numerical correspondences based on geometrical arguments is only a first step, and the present analysis based

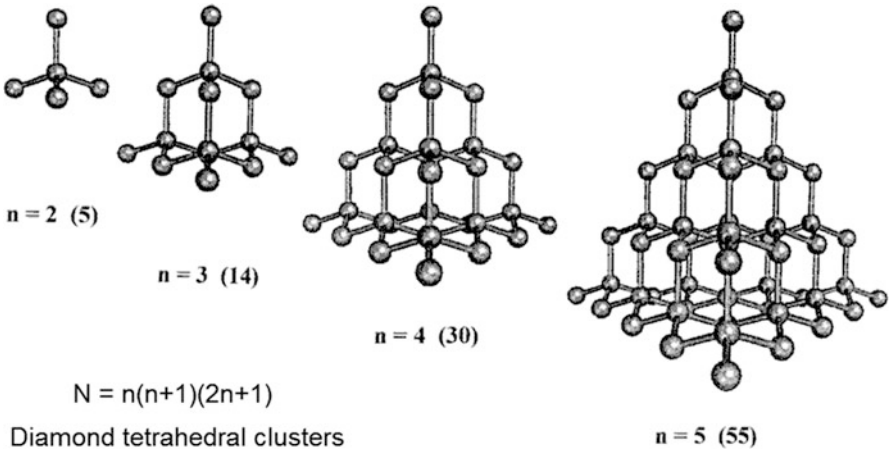

Fig. 4.12 The series of the diamond tetrahedral clusters (diamondoid clusters) having $n(n+1)(2n+1)/6$ atoms with n as any positive integer number (Benedek and Colombo 1996). The substitution of the four vertex atoms with hydrogen and the passivation with hydrogen of the remaining dangling bonds lead to a series of diamondoid hydrocarbons (Mansoori et al. 2012)

on replacement algorithms should be regarded as purely illustrative of a method for the topological generation of complex lattices which may eventually occur in nature.

4.6 Conclusions

There is a virtually infinite variety of sp^3 diamond-like carbon crystals with any mixture of staggered or eclipsed bonds and a cohesive energy not far from that of cubic diamond. In particular an infinite series of hollow diamonds can be theoretically generated from an elementary clathrate through a topological multiplication algorithm. Despite the immense number of hypothetical allotropic forms, the identification of experimental super-hard polymorphs of exotic origin, occurring either in meteorites or produced by meteoritic impacts, remains particularly challenging when the number of atoms per unit cell is large.

In this chapter, two polytypes of a novel clathrate with 28 atoms per unit cell and the presence of 4-membered rings have been presented, and a detailed description of the electronic band structure and the $\mathbf{q} = 0$ vibrational spectrum has been given for the body-centered orthorhombic isomer bco-C_{28}. When the $n = 2$ hollow diamonds are constructed from these isomers, sp^3 diamond-like crystals with 392 atoms per unit cell are obtained. The correspondence of this number to the approximate number of carbon atoms found in the novel super-hard transparent diamond-like structure identified by El Goresy et al. (2003a, 2004) in shocked meteoritic rocks,

as intriguing it may be, has been mentioned as a pure illustration of a method for the topological generation of complex structures which might be eventually found in nature under extreme conditions.

Acknowledgments We thank Prof. Mircea Diudea for many illuminating discussions on the beauty of exotic carbon structures and the power of topological analysis. One of us (GB) acknowledges the support of the Alexander-von-Humboldt Stiftung, and thanks Drs. Igor Baburin, Yanming Ma, and Artem Oganov for useful discussions.

References

Baroni S, de Gironcoli S, Dal Corso A, Giannozi P (2001) Phonons and related crystal properties from density-functional perturbation theory. Rev Mod Phys 73:515–562

Benedek G, Colombo L (1996) Hollow diamonds from fullerenes. In: Sattler K (ed) Cluster assembled materials. Trans Tech Publications Ltd, Zürich, pp 247–274

Benedek G, Galvani E, Sanguinetti S (1995) Hollow diamonds: stability and elastic properties. Chem Phys Lett 244:339–344

Benedek G, Colombo L, Gaito S, Serra S (1997) Exotic diamonds from topology and simulation. In: Paoletti A, Tucciarone A (eds) The physics of diamond. Ios Press, Amsterdam, pp 575–598

Benedek G, Bernasconi M, Gambirasio A (2003) The carbon clathrate hex-C_{16}. Phys Status Solidi (b) 237:296–300

Blase X, Benedek G, Bernasconi M (2010) Structural, mechanical, and superconducting properties of clathrates. In: Colombo L, Fasolino AL (eds) Computer-based modeling of novel carbon systems and their properties. Carbon materials: chemistry and physics 3. Chapter 6. Springer, Berlin/Heidelberg

Blatov VA (2006) IUCr CompComm newsletter 7:4–38. Available at http://www.topos.samsu.ru. Accessed Mar 2013

Delgado-Friedrichs O (2008) The gavrog project. Available at http://gavrog.sourceforge.net. Accessed Mar 2013

Diudea MV, Nagy CL (2007) Periodic nanostructures. Springer, Dordrecht

Dodziuk H (ed) (2009) Strained hydrocarbons. Wiley-VCH Verlag, Weinheim

Eaton PE (1992) Cubanes: starting materials for the chemistry of the 1990s and the new century. Angew Chem 104:1421–1436

Eaton PE, Cole TW (1964) Cubane. J Am Chem Soc 86:962–964

El Goresy A, Dubrovinsky LS, Gillet Ph, Mostefaoui S, Graup G, Drakonopoulos M, Simionovici AS, Swamy V, Masaitis VL (2003a) A novel cubic, transparent and super-hard polymorph of carbon from the Ries and Popigai craters: implications to understanding dynamic-induced natural high-pressure phase transitions in the carbon systems. Lunar Planetary Sci 34:art. No. 1016

El Goresy A, Dubrovinsky LS, Gillet P, Mostefaoui S, Graup G, Drakopoulos M, Simionovici AS, Swamy V, Masaitis VL (2003b) A new natural, super-hard, transparent polymorph of carbon from the Popigai impact crater, Russia. C R Geosci 335:889–898

El Goresy A, Gillet P, Dubrovinsky L, Chen M, Nakamura T (2004) A super-hard, transparent carbon form, diamond, and secondary graphite in the Havero ureilite: a fine-scale micro-Raman and synchrotron tomography. Meteorit Planet Sci 39:A36

Ferroir T, Dubrovinsky L, El Goresy A, Simionovici A, Nakamura T, Gillet P (2010) Carbon polymorphism in shocked meteorites: evidence for new natural ultrahard phases. Earth Planet Sci Lett 290:150–154

Galvani G, Onida G, Serra S, Benedek G (1996) First principles study of a new large-gap nonoporous silicon crystal: hex-Si_{40}. Phys Rev Lett 77:3573–3576

Giannozzi P et al (2009) Quantum Espresso: a modular and open-source software project for quantum simulations of materials. J Phys Condens Matter 21:395502

Gogotsi YG, Kailer A, Nickel KG (1998) Pressure-induced phase transformation in diamond. J Appl Phys 84:1299–1304

Hirai H, Kondo K (1991) Modified phases of diamond formed under shock compression and rapid quenching. Science 253:772–774

Iqbal Z, Zhang Y, Grebel H, Vijayalakshmi S, Lahamer A, Benedek G, Bernasconi M, Cariboni J, Spagnolatti I, Sharma R, Owens KJ, Kozlov ME, Rao KV, Muhammed M (2003) Evidence for a solid phase of dodecahedral C_{20}. Eur Phys J B 31:509–515

Kozlov ML, Hirabayashi M, Nozaki K, Tukumoto M, Ihara H (1995) Transformation of C_{60} fullerenes into a superhard form of carbon at moderate pressure. Appl Phys Lett 66:1199–1201

Kozlov ML, Yase K, Minami N, Fons P, Durand H-A, Obraztsov AN, Nozaki K, Tokumoto M (1996) Observation of diamond crystallites in thin films prepared by laser ablation of hard fullerene-based carbon. J Phys D Appl Phys 29:929–933

Li Q, Ma Y, Oganov AR, Wang H, Xu Y, Cui T, Mao H-K, Zou G (2009) Superhard monoclinic polymorph of carbon. Phys Rev Lett 102:175506 (1–4); The progress in the search of novel structures by means of ab-initio evolutionary algorithms is well illustrated in the recent comprehensive paper by Zhu Q, Zeng Q, Oganov AR (2012) Systematic search for low-enthalpy sp(3) carbon allotropes using evolutionary metadynamics. Phys Rev B 85:201407

Mackay AL, Terrones H (1991) Diamond from graphite. Nature 352:762

Mansoori SA, de Araujo PLB, de Araujo ES (2012) Diamondoid molecules. World Scientific, Singapore

Mao WL, Mao HK, Eng PJ, Trainor TP, Newville M, Kao CC, Heinz DL, Shu JF, Meng Y, Hemley RJ (2003) Bonding changes in compressed superhard graphite. Science 302:425–427

Milani C, Giambelli C, Roman HE, Alasia F, Benedek G, Broglia RA, Sanguinetti S, Yabana K (1996) The valence of small fullerenes. Chem Phys Lett 258:554–558

Monkhorst HJ, Pack JD (1976) Special points for Brillouin-zone integrations. Phys Rev B 13:5188–5192

Murnaghan FD (1944) The compressibility of media under extreme pressures. Proc Natl Acad Sci 30:244–247

O'Keeffe M, Peskov MA, Ramsden SJ, Yaghi OM (2008) The Reticular Chemistry Structure Resource (RCSR) database of, and symbols for, crystal nets. Acc Chem Res 41:1782–1789

Perdew JP, Burke K, Ernzerhof M (1996) Generalized gradient approximation made simple. Phys Rev Lett 77:3865–3868

Pickard CJ, Milman V, Winkler B (2001) Is there theoretical evidence for a metallic carbon polymorph with space group symmetry Fm(3)over-barm at ambient conditions? Diam Relat Mater 10:2225–2227

Ribeiro FJ, Tangney P, Louie SG, Cohen ML (2006) Hypothetical hard structures of carbon with cubic symmetry. Phys Rev B 74:172101

Scandolo S, Chiarotti GL, Tosatti E (1996) A metallic phase of carbon at terapascal pressures. Phys Rev B 54:5051–5054

Selli D, Baburin IA, Martoňák R, Leoni S (2011) Superhard sp^3 carbon allotropes with odd and even ring topologies. Phys Rev B 84:161411

Serra S, Benedek G, Facchinetti M, Miglio L (1998) Possible high-pressure phase of diamond. Phys Rev B 57:5661–5667 (The new structure described in this paper was originally assigned to a triclinic form of diamond. Igor Baburin (private communication) recognized the base-centred monoclinic structure for this lattice)

Umemoto K, Wentzcovitch RM, Saito S, Miyake T (2010) Body-centered tetragonal C4: a viable sp^3 carbon allotrope. Phys Rev Lett 104:125504 (1–4), and references therein

Zhou X-F, Qian G-R, Dong X, Zhang L, Tian Y, Wang H-T (2010) Ab initio study of the formation of transparent carbon under pressure. Phys Rev B 82:134126

Chapter 5
Diamond D_5

Csaba L. Nagy and Mircea V. Diudea

Abstract Carbon allotropes, built up as hyper-structures of the classical diamond and having a high percentage of sp^3 carbon atoms and pentagons, are generically called diamond D_5. Four allotropes are discussed in this chapter: a spongy net; a dense hyper-diamond D_5, with an "anti"-diamantane structure; the corresponding hyper-lonsdaleite; and a quasi-diamond which is a fivefold symmetry quasicrystal with "sin"-diamantane structure. Substructures of these allotropes are presented as possible intermediates in a lab synthesis, and their energetics evaluated at Hartree-Fock, DFT, and DFTB levels of theory. A topological description of these networks is also given.

5.1 Introduction

Nano-era, a period starting since 1985 with the discovery of C_{60}, is dominated by the carbon allotropes, studied for applications in nanotechnology. Among the carbon structures, fullerenes (zero dimensional), nanotubes (one dimensional), graphenes (two dimensional), diamonds, and spongy nanostructures (three dimensional) were the most studied (Diudea and Nagy 2007). Inorganic compounds also attracted the attention of scientists. Recent articles in crystallography promoted the idea of topological description and classification of crystal structures (Blatov et al. 2004, 2007, 2009; Delgado-Friedrichs and O'Keeffe 2005).

Dendrimers are hyper-branched nanostructures, made by a large number of (one or more types) substructures called monomers, synthetically joined within a rigorously tailored architecture (Diudea and Katona 1999; Newkome et al. 1985;

C.L. Nagy (✉) • M.V. Diudea (✉)
Department of Chemistry, Faculty of Chemistry and Chemical Engineering, Babes-Bolyai University, Arany Janos street 11, Cluj RO-400028, Romania
e-mail: nc35@chem.ubbcluj.ro; diudea@chem.ubbcluj.ro

M.V. Diudea and C.L. Nagy (eds.), *Diamond and Related Nanostructures*, Carbon Materials: Chemistry and Physics 6, DOI 10.1007/978-94-007-6371-5_5,

Tomalia 1993). They can be functionalized at terminal branches, thus finding a broad pallet of applications in chemistry, medicine, etc. (Tang et al. 1996; Pan et al. 2007).

Multi-tori are structures of high genera (Diudea 2005b, 2010b; Diudea and Nagy 2007), consisting of more than one tubular ring. Such structures can appear in spongy carbon or in zeolites (DeCarli and Jamieson 1961; Aleksenski et al. 1997; Krüger et al. 2005). Spongy carbon has recently been synthesized (Benedek et al. 2003; Barborini et al. 2002).

There are rigid monomers that can self-assemble in dendrimers, but the growing process stops rather at the first generation. At a second generation, yet the endings of repeat units are not free, they fit to each other, thus forming either an infinite lattice, if the monomer symmetry is octahedral, or a spherical multi-torus, if the symmetry is tetrahedral. The last one is the case of structures previously discussed by Diudea and Ilic (2011).

A detailed study on a multi-torus (Diudea 2010a; Diudea and Ilic 2011), built up by a tetrapodal monomer designed by $Trs(P_4(T))$ sequence of map operations (Diudea 2005a, b; Diudea et al. 2006) and consisting of all pentagonal faces, revealed its dendrimer-like structure (given as the number of monomer units added at each generation, in a dendrimer divergent synthesis, up to the 5th one): 1; 4; 12, 24, 12, 4. Starting with the second generation (i.e., the stage when first 12 monomers were added), pentagonal super-rings appear, leading finally to the multi-torus. The above sequence will be used to suggest a synthetic way to the multi-cage C_{57}, which is the reduced graph of the above multi-torus and one of the main substructures of the diamond D_5.

This chapter is organized as follows: after a short introduction, the main substructures of the D_5 diamonds are presented in Sect. 5.2, while the networks structure is detailed in Sect. 5.3. The next section provides a topological description of the nets, and computational details are given in Sect. 5.5. The chapter ends with conclusions and references.

5.2 Main Substructures of D_5

Carbon allotropes, built up as hyper-structures of the classical diamond and having a high percentage of sp^3 carbon atoms and pentagons, are generically called *diamond D_5* (Diudea 2010a, b; Diudea and Nagy 2012; Diudea et al. 2012). The most important substructures, possible intermediates in the synthesis of D_5, are detailed in the following.

5.2.1 Structure C_{57}

Structure C_{57}, above mentioned, can be "composed" by condensing four C_{20} cages so that they share a common vertex. Starting from a tetrahedral configuration,

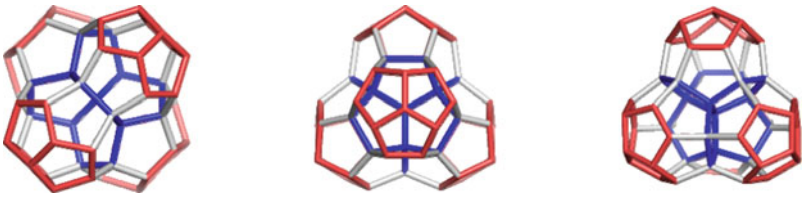

C_2 axe view C_3 axe view side view

Fig. 5.1 C_{57} multi-cage in different views

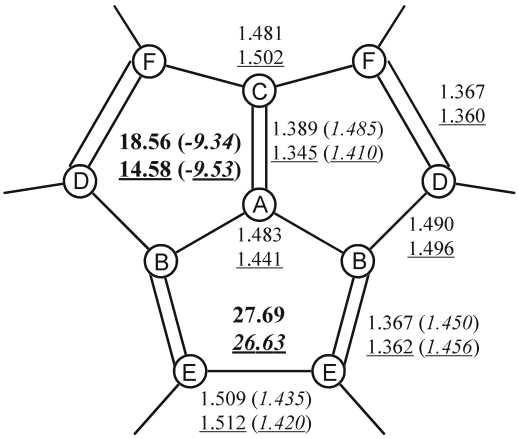

Fig. 5.2 Bond lengths and NICS values (*boldface*) in the acepentalene fragment for C_{57}-D_{2d} and C_{57}^{8-}-T_d (*italics*) and in $C_{10}H_6$-C_s (*underlined*) and $C_{10}H_6^{2-}$-C_{3v} (*italics*) obtained at the B3LYP/6-311G(2d,p) level of theory

geometry optimization of C_{57}, without symmetry constraints, leads to a structure with D_{2d} symmetry. The deformation occurs because of the degeneracy of the frontier orbitals. Maximal symmetry can be achieved by an *octa*-anionic form. This can be explained if we consider C_{57} consisting of two fragments: the core (in blue, Fig. 5.1), i.e., the centrohexaquinane C_{17} (Fig. 5.4 – Paquette and Vazeux 1981; Kuck 2006) which is capped by four acepentalene (Haag et al. 1996) fragments (consisting of only three-valence carbon atoms – marked in red, Fig. 5.1). A theoretical study (Zywietz et al. 1998) has shown the ground state of acepentalene $C_{10}H_6$ with 10π electrons has C_s symmetry. Since in C_{57} the four acepentalene fragments are isolated from each other, their local geometry is close to the isolated acepentalene molecule. The dianion of acepentalene, with 12π electrons, is a stable and aromatic structure ($C_{10}H_6^{2-}$-C_{3v}) and has been isolated as salts (Haag et al. 1998). If two electrons are added for each acepentalene fragment, the geometry optimization resulted in a structure with tetrahedral symmetry C_{57}^{8-}-T_d.

Figure 5.2 summarizes the geometry and local ring aromaticity in the acepentalene fragments of C_{57} and its anion (in italics) compared to that of acepentalene (underlined values) and its dianion (in italics). It can be seen that in C_{57} the bonds are in general slightly longer than in its octa-anionic form, where the bond

Table 5.1 Local strain energies (kcal mol^{-1}) according to POAV theory, computed for the three-coordinated carbon atoms in the acepentalene fragment

	C_{57}-D_{2d}	$C_{10}H_6$-C_s	C_{57}^{8-}-T_d	$C_{10}H_6^{2-}$-C_{3v}
A	37.359	17.974	42.695	8.233
B	25.778	8.506	18.792	6.118
C	17.198	3.161	18.792	6.118
D	19.458	0.003	22.654	0.072
E	19.703	1.246	22.654	0.072
F	22.032	0.002	22.654	0.072

Labeling of the atoms position corresponds to that in Fig. 5.1

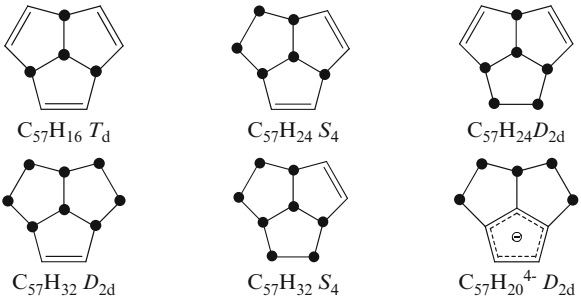

Fig. 5.3 Patterns of the partially hydrogenated C_{57} structure. The *black dots* correspond to the linking position of the hydrogen atoms in the acepentalene fragment

lengths are nearly uniform, ranging from 1.43 to 1.48 Å. Notice the central bonds (AB = AC = 1.48) are much longer in C_{57} than in $C_{10}H_6^{2-}$, with implications in the pyramidalization of the central atom "A" (see below).

The NICS study revealed that, in C_{57}^{8-}, the fragment is aromatic and nearly the same as the acepentalene dianion. However these rings are more antiaromatic in C_{57} than in $C_{10}H_6$-C_s.

The local strain energy of the three-coordinated atoms, induced by deviation from planarity, was evaluated by the POAV theory (Haddon 1987, 1990) and is presented in Table 5.1. Notice that both in C_{57} and its anionic form there is a big strain on each atom compared to the isolated acepentalene. The central atom "A" has the largest strain and becomes a reactive site, particularly in case of C_{57}^{8-}; this polar atom is then pushed away from the molecule, and therefore the C_{20} moieties have an elongated shape.

Strain relief could be achieved by partial or total hydrogenation (in general, exohedral derivatization). There are known examples of non-IPR fullerenes that are stabilized by hydrogenation/halogenation of their pentagon double/triple substructures (Wahl et al. 2006; Prinzbach et al. 2006; Chen et al. 2004; Fowler and Heine 2001; Han et al. 2008). Patterns appearing in the partially hydrogenated C_{57} structure are illustrated in Fig. 5.3.

All possible isomers in the addition of hydrogen to C_{57} were checked: an even number of hydrogen atoms (with one exception) were added to each acepentalene fragment, from four up to ten (i.e., complete reduced species), only the lowest energy isomers being illustrated in Fig. 5.3. Exception was the case when added

Table 5.2 Single-point calculation results (HOMO-LUMO gap in eV and total energy E_{tot} in a.u.) for the C_{57} multi-cage and the hydrogenated $C_{57}H_n$ derivatives, calculated at the HF/6-31G(d,p) and B3LYP/6-31G(d,p) levels of theory

		HF			B3LYP		
Structure	PG	Gap	E_{tot} (au)	E_{tot}/C	Gap (eV)	E_{tot} (au)	E_{tot}/C
C_{57}	D_{2d}	7.57	−2,156.98	−37.84	1.89	−2,196.27	−38.53
C_{57}^{8-}	T_d	7.91	−2,154.27	−37.79	3.12	−2,168.24	−38.04
$C_{57}H_{16}$	T_d	11.55	−2,167.19	−38.02	4.84	−2,181.06	−38.26
$C_{57}H_{20}^{4-}$	D_{2d}	10.43	−2,169.01	−38.05	4.37	−2,183.13	−38.30
$C_{57}H_{24}$	D_{2d}	11.31	−2,172.15	−38.11	4.78	−2,186.15	−38.35
$C_{57}H_{24}$	S_4	11.44	−2,172.15	−38.11	4.83	−2,186.15	−38.35
$C_{57}H_{32}$	D_{2d}	12.10	−2,177.08	−38.19	5.27	−2,191.22	−38.44
$C_{57}H_{32}$	S_4	12.11	−2,177.08	−38.19	5.32	−2,191.22	−38.44
$C_{57}H_{40}$	T_d	14.27	−2,181.99	−38.28	7.37	−2,170.67	−38.08

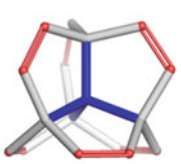

$C_{17}H_{12}$-T_d (1,4,12)

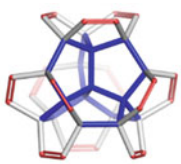

$C_{41}H_{24}$-T_d (1,4,12,24)

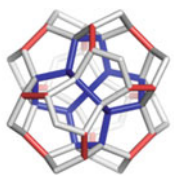

$C_{53}H_{24}$-C_{2v} (1,4,12,24,12)

Fig. 5.4 Structures in the pathway to C_{57} (1; 4; 12, 24, 12, 4); the number of atoms added shell by shell is given in *brackets*

five hydrogen atoms and one electron, thus resulting an isomer with one aromatic pentagon in each acepentalene fragment. Both $C_{57}H_{24}$ and $C_{57}H_{32}$ have two isomers, with symmetries D_{2d} and S_4, respectively, and very close stability (the difference in their total energy is only 0.01 kcal/mol, while in the HOMO-LUMO gap is 0.05 eV). In the totally reduced species $C_{57}H_{40}$, the bond lengths are in the range of 1.52 (core)–1.56 Å (periphery) compared to 1.55 Å in the dodecahedrane, so that the C_{20} fragments regain a quasi-spherical shape. Single-point calculations for hydrogenated $C_{57}H_n$ derivatives are listed in Table 5.2.

The stabilization by hydrogenation is more pregnant in case of C_{20}; while dodecahedrane $C_{20}H_{20}$ was synthesized in amounts of grams, the efforts of scientists to prove the existence of the smallest fullerene C_{20} are well-known (Paquette and Balogh 1982; Prinzbach et al. 2006).

Possible intermediates in the pathway to C_{57} molecule, starting from C_{17} considered the "seed" of D_5, are presented in Fig. 5.4, while the single-point calculation data are shown in Table 5.3. These species could be used as derivatives (e.g., halogenated and hydrogenated ones) in the building of further structures. Their stability was evaluated as partially hydrogenated species, the red bonds in Fig. 5.4 being kept as double bonds. The vibrational spectra of these molecules evidenced a very rigid carbon skeleton, only the hydrogen atoms presenting intense signals.

Table 5.3 Single-point calculation results (HOMO-LUMO gap in eV and total energy E_{tot} in a.u.) for intermediate structures leading to C_{57} multi-cage, calculated at the HF/6-31G(d,p) and B3LYP/6-31G(d,p) levels of theory

		HF			B3LYP		
Structure	PG	Gap	E_{tot} (au)	E_{tot}/C	Gap	E_{tot} (au)	E_{tot}/C
$C_{17}H_{12}$	T_d	12.99	−650.66	−38.27	6.04	−654.92	−38.52
$C_{41}H_{24}$	T_d	12.59	−1,566.40	−38.20	5.75	−1,576.58	−38.45
$C_{53}H_{24}$	T_d	11.62	−2,020.50	−38.12	4.97	−2,033.59	−38.37
$C_{65}H_{24}$	T_d	10.15	−2,474.64	−38.07	3.78	−2,490.58	−38.32
$C_{81}H_{40}$	T_d	12.99	−3,090.56	−38.16	6.03	−3,110.51	−38.40

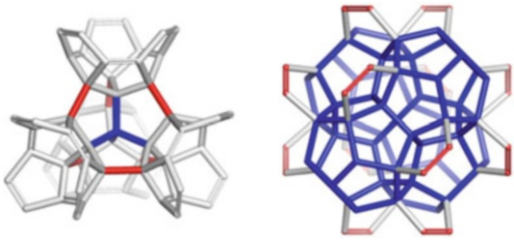

$C_{65}H_{24}$-T_d $C_{81}H_{40}$-T_d

Fig. 5.5 Intermediate structures to D_5 network

Of particular interest are the outer (red) bonds in C_{17}, the length of which varying by the structure complexity. As the structure grows, an increase in their strain appears provoking an elongation of the mentioned bond. This can be observed in the increase of the total energy per carbon atom (and decrease of the gap energy) in the order $C_{17} > C_{41} > C_{53}$. However, with further addition of C_1/C_2 fragments, finally leading to a periodic network (see below), the considered bonds are shortened progressively.

A way from C_{57} to D_5 could include C_{65} and C_{81} intermediates (see Fig. 5.5). The stability of these structures was evaluated as hydrogenated species (Table 5.3, the last two rows). The structure C_{81} (with a C_{57} core and additional 12 flaps) is the monomer of spongy D_5 network (see below). Its stability is comparable to that of the reduced C_{17} seed (Table 5.3, first row) and also to that of the fully reduced C_{57} (Table 5.2, last row), thus supporting the viability of the spongy lattice.

5.2.2 Hyper-Adamantane

Other substructures/intermediates, related to D_5, could appear starting from C_{17}. The seed C_{17} can dimerize (probably by a cycloaddition reaction) to $C_{34}H_{12}$ (Fig. 5.6), a C_{20} derivative bearing 2×3 pentagonal wings in opposite polar disposition. The dimer can further form an angular structure C_{51} (Fig. 5.6, right).

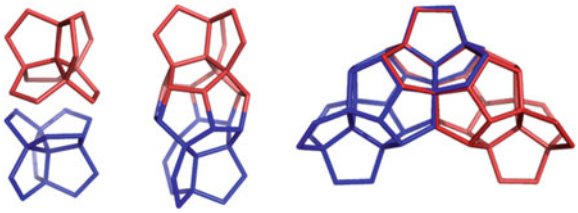

Fig. 5.6 Steps to ada_20: C_{17} (*left*) dimerizes to $C_{34}H_{12}$ (*middle*) and trimerizes to $C_{51}H_{14}$ (*right*)

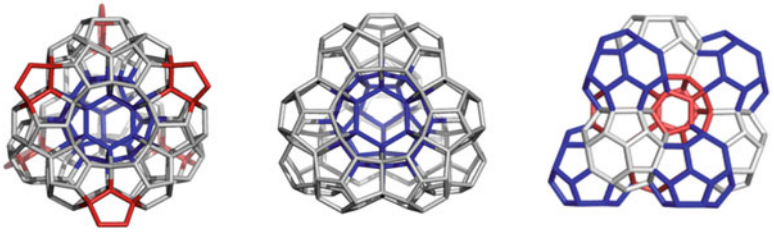

Fig. 5.7 Adamantane-like structures: ada_20_170 (*left*), ada_20_158 (*central*), and ada_28_213 (*right*)

Table 5.4 Single-point calculation results (HOMO-LUMO gap in eV and total energy E_{tot} in a.u.) at the B3LYP/6-31G(d,p) level of theory for some substructures of D_5

Formula	Symmetry	GAP (eV)	E_{tot}/N (a.u.)
$C_{17}H_{12}$	T_d	6.04	−38.52
$C_{34}H_{12}$	D_{3d}	3.236	−38.305
$C_{51}H_{14}$	C_{2v}	3.340	−38.257
$C_{57}H_{18}$	D_{3h}	2.969	−38.282
$C_{170}H_{12}$	T_d	3.171	−38.136
$C_{158}H_{12}(D_5\_20)$	T_d	3.236	−38.139
$C_{213}H_{28}(D_5\_28)$	T_d	3.696	−38.180
$C_{250}H_{30}$ (L_5_28)	D_{3h}	0.333	−38.172
$C_{134}H_{20}$	D_{3d}	3.738	−38.188

A linear analogue is energetically also possible. The angular tetramer C_{51} will compose the six edges of a tetrahedron in forming an adamantane-like **ada_20_170**, with six pentagonal wings (in red – Fig. 5.7, left) or without wings, as in **ada_20_158** (Fig. 5.7, central). Energetic data for these intermediates are given in Table 5.4. The unit ada_20_158 consist of $12 \times C_{20}$ cages, the central hollow of which exactly fitting the structure of fullerene C_{28}. A complete tetrahedral ada_20_196 consist of $16 \times C_{20}$ or $4 \times C_{57}$ units. The hyper-adamantane is the repeating unit of the dense diamond D_5 (see below). A corresponding ada_28_213 can be conceived starting from C_{28} (Fig. 5.7, right).

In the above symbols, "20" refers to C_{20}, as the basic cage in the frame of dense diamond D_5 (see below), while the last number counts the carbon atoms in the structures.

5.3 Diamond D_5 Allotropes

Four different allotropes can be designed, as will be presented in the following.

5.3.1 Spongy Diamond D_5

In spongy diamond D_5 (Fig. 5.8), the nodes of the network consist of alternating oriented (colored in red/blue) C_{57} units; the junction between two nodes recalls a C_{20} cage. The translational cell is a cube of eight C_{57} entities. This network is a decoration of the P-type surface; it is a new 7-nodal 3,3,4,4,4,4,4-c net, group *Fm*-3*m*; point symbol for net: $(5^3)16(5^5.8)36(5^6)17$; stoichiometry (3-c)4(3-c)12(4-c)24(4-c)12(4-c)12(4-c)4(4-c).

The density of the net varies around an average of $d = 1.6$ g/cm^3, in agreement with the "spongy" structure illustrated in Fig. 5.8.

5.3.2 Diamond D_5

The ada_20 units can self-arrange in the net of dense diamond D_5 (Fig. 5.9, left). As any net has its co-net, the diamond D_5_20 net has the co-net D_5_28 (Fig. 5.9, right), with its corresponding **ada_28_213** unit (Fig. 5.7, right). In fact it is one and the same *triple periodic* D_5 network, built up basically from C_{20} and having as hollows the fullerene C_{28}.

This dominant pentagon-ring diamond (Fig. 5.8) is the *mtn* triple periodic, three-nodal net, namely, ZSM-39, or clathrate II, of point symbol net: {5^5.6}12{5^6}5 and $2[5^{12}]$; $[5^{12}.6^4]$ tiling, and it belongs to the space group: *Fd*-3*m*. For all the crystallographic data, the authors acknowledge Professor Davide Proserpio, University of Milan, Italy.

Domains of this diamond network, namely, D_5_20_3,3,3_860 and D_5_28_3,3,3_1022 co-net, were optimized at the DFTB level of theory (Elstner et al. 1998).

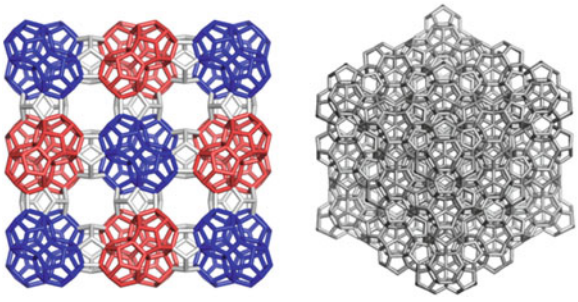

top view corner view

Fig. 5.8 Spongy D_5 (C_{57}) triple periodic network

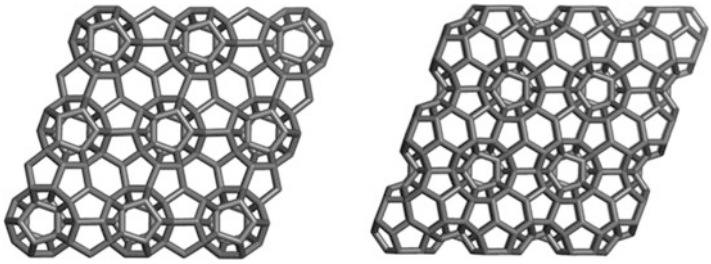

Fig. 5.9 Diamond D_5_20 net and its co-net D_5_28 represented as (*k*,*k*,*k*)-cubic domains: D_5_20_3,3,3_860 (*left*) and D_5_28_3,3,3_1022 (*right*); "*k*" is the number of repeating units on each edge of the domain

Hydrogen atoms were added to the external carbon atoms of the network structures, in order to keep the charge neutrality and the sp^3 character of the C–C bonds at the network surface. Energetically stable geometry structures were obtained in both cases, provided the same repeating unit was considered.

Identification of the equivalent carbon atoms in the neighboring units of the $3 \times 3 \times 3$ super-cell along the main symmetry axes, envisaged a well-defined triclinic lattice, with the following parameters: $a = b = c = 6.79$ Å and $\alpha = 60°$, $\beta = 120°$, $\gamma = 120°$, even the most symmetrical structure is *fcc* one. Density of the D_5 network was calculated to be around 2.8 g/cm^3.

Analyzing the C–C bond distances in these carbon networks, the values vary in a very narrow distance domain of 1.50–1.58 Å, suggesting all carbon atoms are sp^3 hybridized. Considering the one-electron energy levels of the HOMO and LUMO, a large energy gap could be observed for both D_5_20_860 net ($E_{HOMO} = -5.96$ eV, $E_{LUMO} = +2.10$ eV, $\Delta E_{HOMO-LUMO} = 8.06$ eV) and D_5_28_1022 co-net ($E_{HOMO} = -6.06$ eV, $E_{LUMO} = +2.45$ eV, $\Delta E_{HOMO-LUMO} = 8.51$ eV) structures, which indicates an insulating behavior for this carbon network.

Structural stability of substructures related to the D_5 diamond was evaluated both in static and dynamic temperature conditions by molecular dynamics MD (Kyani and Diudea 2012; Szefler and Diudea 2012). Results show that C_{17} is the most temperature resistant fragment. For a detailed discussion, see Chap. 7.

Note that the hypothetical diamond D_5 is also known as *fcc*-C_{34} because of its face-centered cubic lattice (Benedek and Colombo 1996). Also note that the corresponding clathrate structures are known in silica synthetic zeolite ZSM-39 (Adams et al. 1994; Meier and Olson 1992; Böhme et al. 2007) and in germanium allotrope Ge(*cF*136) (Guloy et al. 2006; Schwarz et al. 2008) as real substances.

5.3.3 *Lonsdaleite L_5*

Alternatively, a hyper-lonsdaleite L_5_28 network (Fig. 5.10, left) can be built (Diudea et al. 2011, 2012) from hyper-hexagons L_5_28_134 (Fig. 5.10, right), of

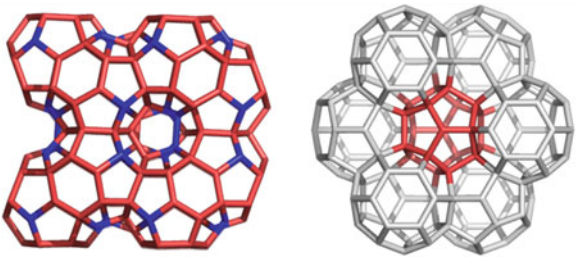

Fig. 5.10 Lonsdaleite L_5_28 net represented as L_5_28_250 (side view – *left*); the substructure L_5_28_134 is a hyper-hexagon of which nodes are C_{28} with additional two C atoms, thus forming a C_{20} core (*top view – central*); the L_5_20 co-net (in *red*) superimposes partially over the net of D_5_20 (*side view – right*) in the domain (*k*,*k*,2)

which nodes represent C_{28} fullerenes, joined by identifying the four tetrahedrally oriented hexagons of neighboring cages. The lonsdaleite L_5_28/20 is a triple periodic network, partially superimposed to the D_5_20/28 net. Energetic data for the structures in Fig. 5.10 are given in Table 5.4.

5.3.4 Quasi-Diamond D_5

A fourth allotrope of D_5 was revealed by Diudea (Chap. 19) as D_5_*sin* quasicrystal diamond (Fig. 5.11), clearly different from the "classical" D_5, named here D_5_*anti*. The quasi-diamond D_5_*sin* is a quasicrystal 27 nodal 3,4-c net, of the *Pm* group, with the point symbol: $\{5^3\}18\{5^5.6\}18\ \{5^5.8\}16\{5^6\}13$. Substructures of this new allotrope are shown in the top of Fig. 5.11.

5.4 Topological Description

Topology of diamond D_5, namely, spongy D_5 (Fig. 5.8) and D_5_*anti* (Fig. 5.9), is presented in Tables 5.5 and 5.6, respectively: formulas to calculate the number of atoms, number of rings *R*, and the limits (at infinity) for the ratio of sp^3 C atoms over the total number of atoms and also the ratio *R*[5] over the total number of rings are given function of *k* that is the number of repeating units in a cuboid (*k*,*k*,*k*). One can see that, in an infinitely large net, the content of sp^3 carbon approaches 0.77 in case of spongy net while it is unity in case of dense diamond D_5.

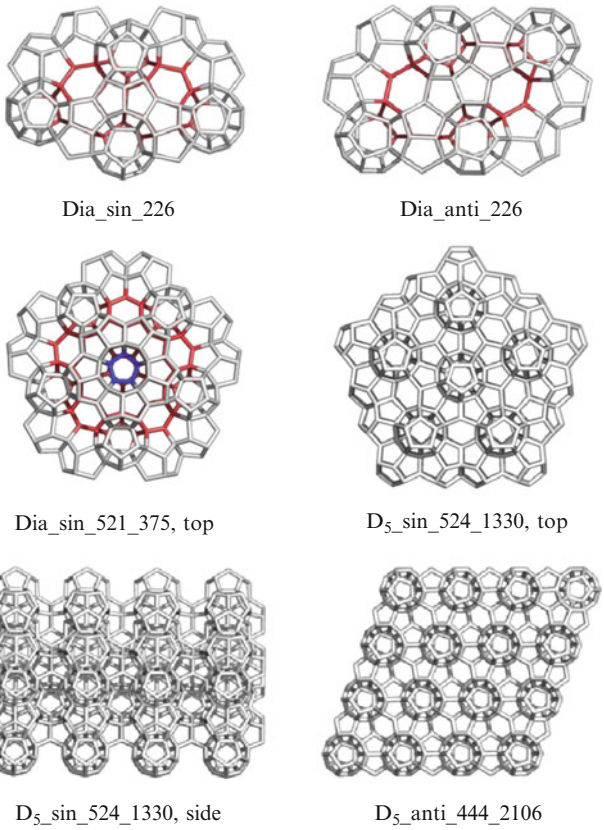

Fig. 5.11 Diamond D_5-related structures

Table 5.5 Topological description (sp^2/sp^3 carbon percentage) of the spongy SD_5 diamond network as function of the number of monomers k

	Formulas: C_{57} net
1	$v(D_5) = 3k^2[19 + 23(k-1)] = 69k^3 - 12k^2$ $e(D_5) = 2k^2(65k - 18); m(D_5) = k^3; k = 1,2,\ldots$
2	$C(sp^2) = 16k^3 - 24k + 48$
3	$C(sp^3) = 53k^3 - 12k^2 + 24k - 48$
4	$C(sp^2\&sp^3) = 69k^3 - 12k^2$
5	$C(sp^3\%) = (53k^3 - 12k^2 + 24k - 48)/(69k^3 - 12k^2)$ $\lim_{k\to\infty}(C(sp^3\%)) = 53/69 \simeq 0.768116$ $\text{Rings}[5] = 6k^2(11k - 4)$
6	$\lim_{k\to\infty}(C(sp^2)/C(sp^3)) = 16/53 \simeq 0.301887$

Table 5.6 Topological description of diamond D_5_20 net function of $k = 1, 2, \ldots$ number of ada_20 units along the edge of a (k,k,k) cuboid

	D_5_20; R[6]; formulas
1	$v(D_5 20a) = -22 - 12k + 34k^3$
2	$\text{Atoms}(sp^3) = -10 - 36k^2 + 34k^3$
3	$R[5] = -18 - 6k - 18k^2 + 36k^3$
4	$R[6] = -1 + 6k - 9k^2 + 4k^3$
5	$R[5] + R[6] = -19 - 27k^2 + 40k^3$
6	$\lim_{k\to\infty} \frac{R[5]}{R[6]} = 9;\ \lim_{k\to\infty} \frac{R[5]}{R[5]+R[6]} = \frac{9}{10}$
7	$\lim_{k\to\infty} \left[\frac{\text{Atoms}(sp^3)}{v(G)} = \frac{-10 - 36k^2 + 34k^3}{-22 - 12k + 34k^3} = \frac{-(10/k^3) - (36/k) + 34}{-(22/k^3) - (12/k^2) + 34} \right] = 1$

5.5 Computational Methods

Geometry optimizations were performed at the Hartree-Fock (HF) and density functional (DFT) levels of theory using the standard polarized double-zeta 6-31G(d,p) basis set. For DFT calculations, the hybrid B3LYP functional was used. Harmonic vibrational frequencies were calculated for all optimized structures at the same level of theory to ensure that true stationary points have been reached. Symmetry was used to simplify calculations after checking the optimizations without symmetry constraints resulted in identical structures. The following discussion only considers the singlet states.

To investigate the local aromaticity, NICS (nucleus-independent chemical shift) was calculated on the DFT optimized geometries. NICS was measured in points of interest using the GIAO (Gauge-Independent Atomic Orbital) method at GIAO-B3LYP/6-311G(2d,p)//B3LYP/6-311G(2d,p). Calculations were performed using the Gaussian 09 package (Gaussian 09 2009).

For larger structures, geometry optimization was performed at SCC-DFTB level of theory (Elstner et al. 1998) by using the DFTB+ program (Aradi et al. 2007) with the numerical conjugated gradient method.

Strain energy, induced by deviation from planarity, appearing in such nanostructures, was evaluated by the POAV theory (Haddon 1987, 1990), implemented in our JSChem software (Nagy and Diudea 2005).

Topological data were calculated by our NanoStudio software (Nagy and Diudea 2009).

5.6 Conclusions

Four allotropes of the diamond D_5 were discussed in this chapter: a spongy net; a dense hyper-diamond D_5, with an "anti"-diamantane structure; the corresponding hyper-lonsdaleite; and a quasi-diamond which is a fivefold symmetry quasicrystal

with "sin"-diamantane structure. The main substructures of these allotropes were presented as possible intermediates in a lab synthesis on the ground of their energetics, evaluated at Hartree-Fock, DFT, and DFTB levels of theory. A topological description of these networks, made in terms of the net parameter *k*, supports the generic name diamond D_5 given to these carbon allotropes; among these, the spongy and quasi-diamond represent novel networks of D_5.

Acknowledgments CL Nagy acknowledges the financial support of the Sectorial Operational Programme for Human Resources Development 2007–2013, cofinanced by the European Social Fund, under the project number POSDRU 89/1.5/S/60189 with the title "Postdoctoral Programs for Sustainable Development in a Knowledge Based Society."

References

Adams GB, O'Keeffe M, Demkov AA, Sankey OF, Huang Y-M (1994) Wide-band-gap Si in open fourfold-coordinated clathrate structures. Phys Rev B 49(12):8048–8053

Aleksenski AE, Baidakova MV, Vul' AY, Davydov VY, Pevtsova YA (1997) Diamond-graphite phase transition in ultradisperse-diamond clusters. Phys Solid State 39:1007–1015

Aradi B, Hourahine B, Frauenheim T (2007) DFTB+, a sparse matrix-based implementation of the DFTB method. J Phys Chem A 111:5678–5684

Barborini E, Piseri P, Milani P, Benedek G, Ducati C, Robertson J (2002) Negatively curved spongy carbon. Appl Phys Lett 81:3359–3361

Benedek G, Colombo L (1996) Hollow diamonds from fullerenes. Mater Sci Forum 232:247–274

Benedek G, Vahedi-Tafreshi H, Barborini E, Piseri P, Milani P, Ducati C, Robertson J (2003) The structure of negatively curved spongy carbon. Diam Relat Mater 12:768–773

Blatov VA, Carlucci L, Ciani G, Proserpio DM (2004) Interpenetrating metal-organic and inorganic 3D networks: a computer-aided systematic investigation. Part I. Analysis of the Cambridge structural database. CrystEngComm 6:377–395

Blatov VA, Delgado-Friedrichs O, O'Keeffe M, Proserpio DM (2007) Three-periodic nets and tilings: natural tilings for nets. Acta Crystallogr Sect A Found Crystallogr 63(5):418–425

Blatov VA, O'Keeffe M, Proserpio DM (2009) Vertex-, face-, point-, Schläfli-, and Delaney-symbols in nets, polyhedra and tilings: recommended terminology. CrystEngComm 12(1): 44–48

Böhme B, Guloy A, Tang Z, Schnelle W, Burkhardt U, Baitinger M, Grin Y (2007) Oxidation of M_4Si_4 (M = Na, K) to clathrates by HCl or H2O. J Am Chem Soc 129:5348–5349

Chen Z, Heine T, Jiao H, Hirsch A, Thiel W, Schleyer PVR (2004) Theoretical studies on the smallest fullerene: from monomer to oligomers and solid states. Chem Eur J 10(4):963–970

DeCarli PS, Jamieson JC (1961) Formation of diamond by explosive shock. Science 133:1821–1822

Delgado-Friedrichs O, O'Keeffe M (2005) Crystal nets as graphs: terminology and definitions. J Solid State Chem 178(8):2480–2485

Diudea MV (ed) (2005a) Nanostructures, novel architecture. NOVA Scientific Publishers, New York

Diudea MV (2005b) Nanoporous carbon allotropes by septupling map operations. J Chem Inf Model 45:1002–1009

Diudea MV (2010a) Diamond D_5, a novel allotrope of carbon. Studia Univ Babes Bolyai Chemia 55(4):11–17

Diudea MV (2010b) Nanomolecules and nanostructures-polynomials and indices, MCM, No. 10. University of Kragujevac, Serbia

Diudea MV, Ilić A (2011) All-pentagonal face multi tori. J Comput Theor Nanosci 8:736–739
Diudea MV, Katona G (1999) Molecular topology of dendrimers. In: Newkome GA (ed) Adv Dendritic Macromol 4(1999):135–201
Diudea MV, Nagy CL (2007) Periodic nanostructures. Springer, Dordrecht
Diudea MV, Nagy CL (2012) C_{20}-related structures: diamond D_5. Diam Relat Mater 23:105–108
Diudea MV, Ştefu M, John PE, Graovac A (2006) Generalized operations on maps. Croat Chem Acta 79:355–362
Diudea MV, Nagy CL, Ilic A (2011) Diamond D_5, a novel class of carbon allotropes. In: Putz MV (ed) Carbon bonding and structures. Carbon materials: chemistry and physics, vol 5. Springer, Dordrecht, pp 273–289
Diudea MV, Nagy CL, Bende A (2012) On diamond D_5. Struct Chem 23:981–986
Elstner M, Porezag D, Jungnickel G, Elsner J, Haugk M, Frauenheim T, Suhai S, Seifert G (1998) Self-consistent-charge density-functional tight-binding method for simulations of complex materials properties. Phys Rev B 58:7260–7268
Fowler PW, Heine T (2001) Stabilisation of pentagon adjacencies in the lower fullerenes by functionalization. J Chem Soc Perkin Trans 2:487–490
Gaussian 09 Rev. A.1, Frisch MJ, Trucks GW, Schlegel HB, Scuseria GE, Robb MA, Cheeseman JR, Scalmani G, Barone V, Mennucci B, Petersson GA, Nakatsuji H, Caricato M, Li X, Hratchian HP, Izmaylov AF, Bloino J, Zheng G, Sonnenberg JL, Hada M, Ehara M, Toyota K, Fukuda R, Hasegawa J, Ishida M, Nakajima T, Honda Y, Kitao O, Nakai H, Vreven T, Montgomery JA, Peralta JE, Ogliaro F, Bearpark M, Heyd JJ, Brothers E, Kudin KN, Staroverov VN, Kobayashi R, Normand J, Raghavachari K, Rendell A, Burant JC, Iyengar SS, Tomasi J, Cossi M, Rega N, Millam NJ, Klene M, Knox JE, Cross JB, Bakken V, Adamo C, Jaramillo J, Gomperts R, Stratmann RE, Yazyev O, Austin AJ, Cammi R, Pomelli C, Ochterski JW, Martin RL, Morokuma K, Zakrzewski VG, Voth GA, Salvador P, Dannenberg JJ, Dapprich S, Daniels AD, Farkas Ö, Foresman JB, Ortiz JV, Cioslowski J, Fox DJ (2009) Gaussian Inc, Wallingford
Guloy A, Ramlau R, Tang Z, Schnelle W, Baitinger M, Grin Y (2006) A quest-free germanium clathrate. Nature 443:320–323
Haag R, Schröder D, Zywietz T, Jiao H, Schwarz H, Von Schleyer PR, de Meijere AT (1996) The long elusive acepentalene – experimental and theoretical evidence for its existence. Angew Chem 35:1317–1319
Haag R, Schüngel F-M, Ohlhorst B, Lendvai T, Butenschön H, Clark T, Noltemeyer M, Haumann T, Boese R, de Meijere A (1998) Syntheses, structures, and reactions of highly strained dihydro- and tetrahydroacepentalene derivatives. Chem Eur J 4:1192–1200
Haddon RC (1987) Rehybridization and π-orbital overlap in nonplanar conjugated organic molecules: π-orbital axis vector (POAV) analysis and three-dimensional hückel molecular orbital (3D-HMO) theory. J Am Chem Soc 109:1676–1685
Haddon RC (1990) Measure of nonplanarity in conjugated organic molecules: which structurally characterized molecule displays the highest degree of pyramidalization? J Am Chem Soc 112:3385–3389
Han X, Zhou S-J, Tan Y-Z, Wu X, Gao F, Liao Z-J, Huang R-B, Feng Y-Q, Lu X, Xie S-Y, Zheng L-S (2008) Crystal structures of saturn-like $C_{50}Cl_{10}$ and pineapple-shaped $C_{64}Cl_4$: geometric implications of double- and triple-pentagon-fused chlorofullerenes. Angew Chem Int Ed 47:5340–5343
Krüger A, Kataoka F, Ozawa M, Fujino T, Suzuki Y, Aleksenskii AE, Vul' AYA, Ōsawa E (2005) Unusually tight aggregation in detonation nanodiamond: identification and disintegration. Carbon 43:1722–1730
Kuck D (2006) Functionalized aromatics aligned with the three Cartesian axes: extension of centropolyindane chemistry. Pure Appl Chem 78:749–775
Kyani A, Diudea MV (2012) Molecular dynamics simulation study on the diamond D_5 substructures. Central Eur J Chem 10(4):1028–1033
Meier WM, Olson DH (1992) Atlas of zeolite structure types, 3rd edn. Butterworth-Heinemann, London

Nagy CL, Diudea MV (2005) JSChem. Babes–Bolyai University, Cluj
Nagy CL, Diudea MV (2009) NANO-Studio software. Babes-Bolyai University, Cluj
Newkome GR, Yao Z, Baker GR, Gupta VK (1985) Micelles. Part 1. Cascade molecules: a new approach to micelles. A [27]-arborol. J Org Chem 50:2003–2004
Pan BF, Cui DX, Xu P, Huang T, Li Q, He R, Gao F (2007) Cellular uptake enhancement of polyamidoamine dendrimer modified single walled carbon nanotubes. J Biomed Pharm Eng 1:13–16
Paquette LA, Balogh DW (1982) An expedient synthesis of 1,16-dimethyldodecahedrane. J Am Chem Soc 104:774–783
Paquette LA, Vazeux M (1981) Threefold transannular epoxide cyclization. Synthesis of a heterocyclic C_{17}-hexaquinane. Tetrahedron Lett 22:291–294
Prinzbach H, Wahl F, Weiler A, Landenberger P, Wörth J, Scott LT, Gelmont M, Olevano D, Sommer F, Issendoef B (2006) C_{20} carbon clusters: fullerene-boat-sheet generation, mass selection, photoelectron characterization. Chem Eur J 12:6268–6280
Schwarz U, Wosylus A, Böhme B, Baitinger M, Hanfland M, Grin Y (2008) A 3D network of four-bonded germanium: a link between open and dense. Angew Chem Int Ed 47:6790–6793
Szefler B, Diudea MV (2012) On molecular dynamics of the diamond D_5 seed. Struct Chem 23(3):717–722
Tang MX, Redemann CT, Szoka FC Jr (1996) In vitro gene delivery by degraded polyamidoamine dendrimers. Bioconjug Chem 7:703–714
Tomalia DA (1993) Starburst™/cascade dendrimers: fundamental building blocks for a new nanoscopic chemistry set. Aldrichim Acta 26:91–101
Wahl F, Weiler A, Landenberger P, Sackers E, Voss T, Haas A, Lieb M, Hunkler D, Worth J, Knothe L, Prinzbach H (2006) Towards perfunctionalized dodecahedranes – en route to C_{20} fullerene. Chem Eur J 12:6255–6267
Zywietz TK, Jiao H, Schleyer PR, de Meijere A (1998) Aromaticity and antiaromaticity in oligocyclic annelated five-membered ring systems. J Org Chem 63:3417–3422

Chapter 6
Energetics of Multi-shell Cages

Attila Bende and Mircea V. Diudea

Abstract Fullerene aggregation can follow a well-defined geometry of which energy trends to a minimal value. The pattern of space filling differs function of the dimensions and shapes of composing small fullerenes. An attempt of building and stability evaluation of several fullerene aggregates was made. The results show these aggregates as multi-shell covalently bonded structures with a stability comparable to that of C_{60}, the reference fullerene in nanoscience. The calculations were made at the DFTB+ level of theory.

6.1 Introduction

Among the 1,812 topological isomers of C_{60}, the buckminsterfullerene with I_h symmetry is the lowest-energy isomer and the only one prepared by Krätschmer et al. (1990) arc discharge method. The classical fullerenes already synthesized all fulfill the isolated pentagon rule, IPR (i.e., pentagons must be separated by each other by surrounding hexagons, Kroto 1987), C_{60} being the smallest one and the best studied. Several fullerenes larger than C_{60} have been isolated and characterized (Hennrich et al. 1996).

Classical fullerenes smaller than C_{60} are also possible (Fowler and Manolopoulos 1995); however, such cages must have at least two adjacent pentagons. These obey no more IPR and are denoted as non-IPR fullerenes.

A. Bende
Molecular and Biomolecular Physics Department, National Institute for R&D of Isotopic and Molecular Technologies, Donath Street, No. 65-103, RO-400293 Cluj-Napoca, Romania
e-mail: bende@itim-cj.ro

M.V. Diudea (✉)
Department of Chemistry, Faculty of Chemistry and Chemical Engineering, Babes-Bolyai University, Arany Janos Str., 400028 Cluj, Romania
e-mail: diudea@chem.ubbcluj.ro

M.V. Diudea and C.L. Nagy (eds.), *Diamond and Related Nanostructures*, Carbon Materials: Chemistry and Physics 6, DOI 10.1007/978-94-007-6371-5_6,

Nonclassical fullerenes, containing other rings (e.g., squares, heptagons) in addition to pentagons and hexagons, have been considered (Taylor 1992). Often, nonclassical cages are energetically competitive with the lowest-energy classical fullerene isomers.

Despite some unsuccessful attempts to isolate non-IPR C_n cages from fullerene soots (Piskoti et al. 1998), such fullerenes have been obtained in experiment by derivatization (either exohedral or endohedral – Koshio et al. 2000; Löffler et al. 2010; Tan et al. 2009): $C_{20}H_{10}$ (Scott et al. 1991), $C_{36}H_6$, $C_{36}H_6O$ (Koshio et al. 2000), $C_{50}Cl_{10}$ (Xie et al. 2004), $C_{58}F_{18}$ (a nonclassical fullerene with a heptagon, 13 pentagons, and 17 hexagons – Troshin et al. 2005), $C_{64}H_4$ (Wang et al. 2006), and $Sc_2@C_{66}$ (Wang et al. 2000). It seems that functionalization stabilizes (not necessarily) the most stable (i.e., lowest-energy) structural isomers, eventually by saturating the reactive C–C bonds shared by two adjacent pentagons (Lu et al. 2004; Gao and Zhao 2007; Yan et al. 2007).

The group of Kappes (Böttcher et al. 2004, 2005; Löffler et al. 2006, 2009, 2010) used the low-energy (mass-selected cluster) ion-beam deposition to produce solid films of small non-IPR fullerenes, C_n ($n = 48, 50, 52, 54, 56, 58, 62, 64, 66,$ and 68), onto HOPG (highly oriented pyrolytic graphite). Such non-isolated-pentagon-ring (non-IPR) fullerene materials are not accessible to standard fullerene preparation methods. The films of non-IPR fullerenes grow via formation of covalently bonded dendritic C_n aggregates, whereas deposition of IPR fullerenes under analogous conditions (e.g., C_{60} or C_{70}) leads to compact islands (governed by weak van der Waals cage–cage interactions). The film topographies, thermal stabilities, and the general electronic properties (e.g., HOMO–LUMO gaps) can be rationalized in terms of formation of covalent inter-cage bonds involving reactive non-IPR sites (comprising adjacent pentagon pairs).

The chapter is organized as follows. After an introductory part, some concepts related to the spongy and filled multi-shell structures are presented, and the main classes of structures are presented in the second section. The third section is devoted to the discussion about the stability of these multi-shell structures, while the forth section gives computational details. The chapter ends with conclusions and references.

6.2 Spongy and Filled Structures

In the synthesis of fullerenes, it is well-known that a mixture of nanostructures appears: single- and multiwalled nanotubes, nanotubes capped by fullerene halves, onion-fullerenes, and others. It is expected that, in the experimental conditions, fullerenes can be spanned, thus resulting in open cages, of which open faces (i.e., windows) can fit to the eventually present nanotubes of various chirality and tessellation (most probably being the graphitic hexagonal structures). Such spanned fullerenes, joined with nanotubes consisting of 0, 1, . . . , n rows of atoms, can be assimilated to the nanotube junctions. According to their symmetry, tetrahedral, octahedral, and icosahedral junctions can be distinguished (Diudea and Nagy 2007).

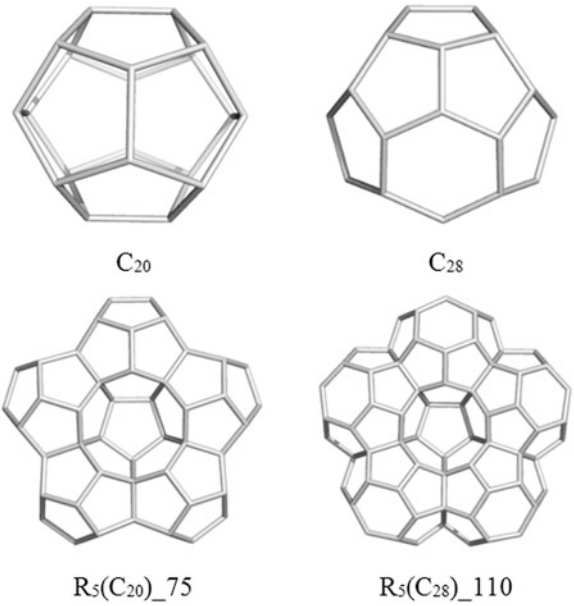

Fig. 6.1 Small cages/units (*top row*) used in the building of pentagonal hyper-rings R_5 (*bottom row*)

Graphitic structures, with rings larger than the hexagon, which induce the negative Gaussian curvature, have been proposed since the early papers published 20 years ago, (Schoen 1970; Mackay and Terrones 1991, 1993; Townsend et al. 1992; Lenosky et al. 1992; O'Keeffe et al. 1992; Vanderbilt and Tersoff 1992). These have been called schwarzites, in honor of H. A. Schwarz (1865, 1890), who first investigated the differential geometry of such surfaces. Next, the molecular junctions have been "in silico" assembled in various networks, and experimental evidences for such junctions have been reported (Ricardo-Chavez et al. 1997; Terrones and Mackay 1997; Terrones et al. 2002; Terrones and Terrones 1997, 2003; Ceulemans et al. 1999; Romo-Herrera et al. 2007).

Schwarzites' associate graphs are assumed to be embedded in triply periodic minimal surfaces and are related to labyrinth graphs, also involving nanotube junctions.

6.2.1 Structures Including C_{20} and C_{28} Fullerenes

Here, we present the design of (both spongy and dense) structures with icosahedral symmetry, as appear in quasicrystals.

Starting from units, like the smallest fullerenes, C_{20} and C_{28} a hyper-pentagon can be designed (Fig. 6.1). The number of atoms is given at the end of structure name.

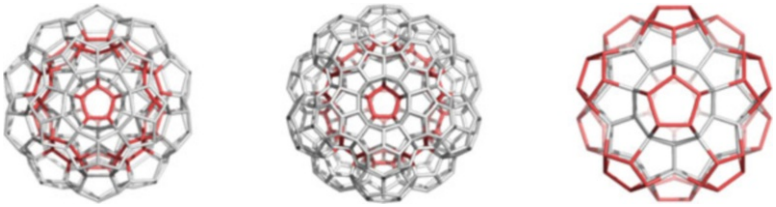

Fig. 6.2 Spongy hyper-dodecahedra: **20**(20)_250 (*left*); **28**(20)_380 (*middle*) and their common core, the 110-keplerate, designed by map operation sequence DoP_4TRS (*right*)

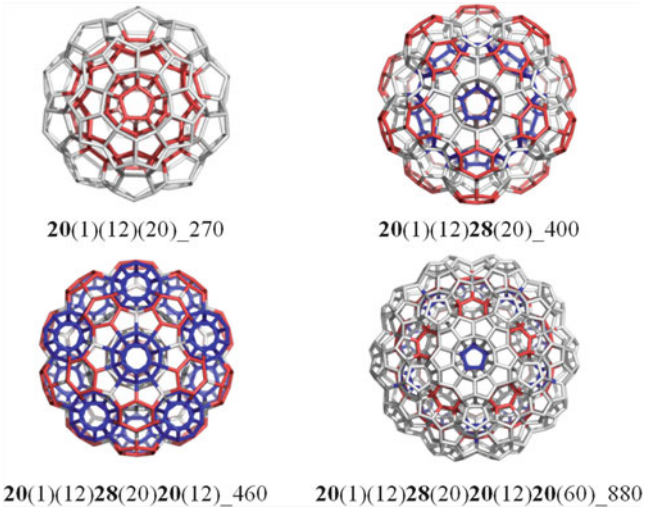

Fig. 6.3 Radial space filling by C_{20} and C_{28} fullerenes

Next, 12 such hyper-faces will complete a dodecahedron, as a spongy structure (Fig. 6.2). Note that both these hyper-dodecahedra **20**(20)_250 and **28**(20)_380 have the same hollow core: DoP_4TRS_110, designed by applying the P_4 map operation on the dodecahedron, followed by the selective truncation "TRS" of the five connected vertices (see Chap. 19, this book). The structure DoP_4TRS_110, known as the 110-vertex icosahedral keplerate, is the "envelope" of 12 dodecahedra, having as the core a 13th dodecahedron, denoted as **20**(1)(12)_130 (also 13Do_130), a structure consisting of $20 + 110$ atoms. For more details on these structures, the reader is invited to consult Chap. 19, this book.

Filling the space can be achieved eventually by self-assembling of nanoparticles. Figure 6.3 gives examples of filled cages in the series of C_{20} and C_{28} fullerenes. One can see that C_{28} is aggregated with C_{20} in filling the radial space, analogously to their complementarity in filling the translational space, as realized in the diamond D_5 (also known as clathrate of type II) structure.

The name of the above multi-shell cages includes the type of cages (the occurrence, in brackets), shell by shell, and the number of atoms, as a suffix.

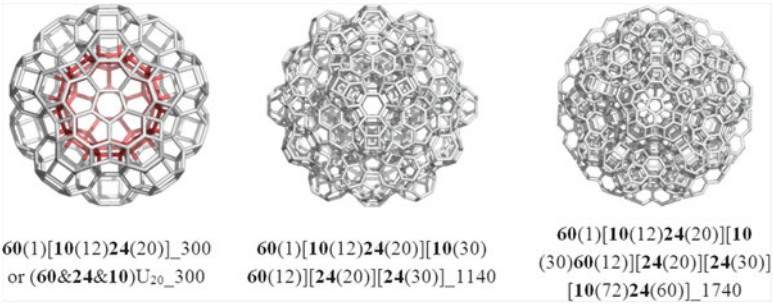

Fig. 6.4 Radial aggregation by **60**&**24**&**10**

Multi-shell icosahedral/dodecahedral structures have been designed earlier by several authors (Dandoloff et al. 1980; Zeger and Kaxiras 1993; Shevchenko 2011).

6.2.2 Structures Including Fullerene C_{60}

By applying the map/net operations on dodecahedral filled structures like 20(1)(12)_130 (and others), a mixed tiling system can be generated.

C_{60} can aggregate with itself and some additional carbon atoms, disposed in a radial geometry as follows: (1) truncated octahedron C_{24} shares hexagons with itself and the fullerene C_{60} while the pentagonal prism C_{10} keeps the distance between the pentagonal faces of fullerene, and (2) fullerene shares with itself a pentagon while the hexagons are all covered by truncated tetrahedra C_{12}. Figure 6.4 illustrates the radial multi-shell aggregates by **60**&**24**&**10** while Fig. 6.5 shows **60**&**12** structures. Note that the first shell in these structures is again a hyper-dodecahedron U_{20}, as those presented in Fig. 6.2, possibly resulting by self-arranging of C_{24} cages.

Radial aggregation of **60**&**12** can be easily designed by applying the map operations, e.g., *Le*, on the multi-shell structures (Fig. 6.5, bottom).

Linear aggregation is also possible (Fig. 6.6). It was found that oxomolybdate clusters can form rodlike structures (Müller and Roy 2003; Shevchenko 2011).

To check the consistency of an assumed structure, one can use the Schläfli (1901) formula for a convex polytope in four dimensions: $f_0 - f_1 + f_2 - f_3 = 0$, with f_i being vertices, edges, rings, and cages, respectively. For the series **60**&**24**&**10**, the radial space filling is given in Table 6.1.

6.3 Energetics of Multi-shell Cages

The energy of carbon structures herein discussed have been computed by the DFTB+ method (Aradi et al. 2007), a method swallowing more than 1,500 atoms; a relative stabilization by aggregation (reference molecule C_{60} – see below) was

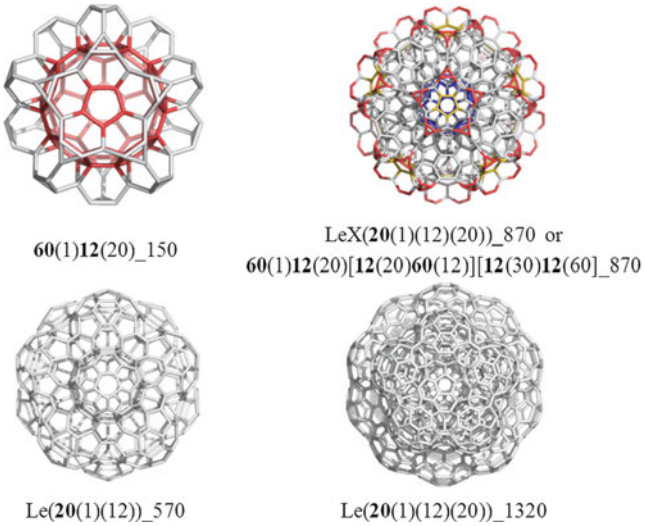

Fig. 6.5 Radial aggregation by **60**&**12**, within leapfrog *Le* map operation

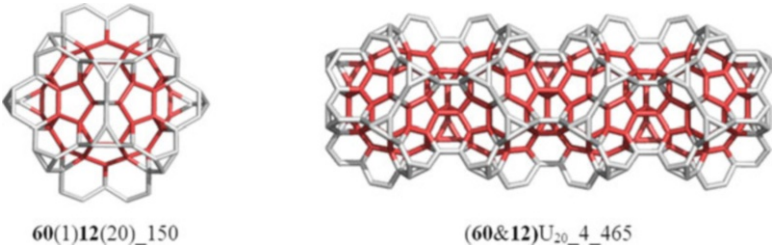

Fig. 6.6 Linear aggregation by **60**&**12**

evidenced. As mentioned in Introduction, several non-IPR fullerenes have been isolated rather as derivatives, the most frequent being exohedrally passivated by hydrogen or halogen atoms. Our calculations have shown a clear passivation by full hydrogenation (the full hydrocarbon having a far deeper gap, as expected – see Table 6.2, cases **20**(20)_250_40H and **20**(20)_250_100H). The reference structure was also calculated as the hydrocarbon $C_{60}H_{60}$. To mark the hydrogenated species, a capital H will suffix the name of structures.

Data are given as total energy and total energy per carbon atom, E_{tot}/C and the HOMO–LUMO gap, all in atomic units.

From Tables 6.2 and 6.3, it seems that structures consisting of C_{20} and C_{28} cages, as well as their precursors/substructures, could be searched in real experiments, basically as hydrocarbons (see data at the bottom of these tables). The only structures that show a clear energetic gain by aggregation are those made by combination **60**&**24**&**10.** The hyper-dodecahedron (**60**&**24**&**10**) U_{20}_300 (Table 6.4, shell 1)

Table 6.1 Radial space filling by **60**&**24**&**10**

Shell	Space filling	v	e	r_4	r_5	r_6	r	24	10	c	c_{60}	c_{sum}	f
–	60	60	90	0	12	20	32	0	0	0	1	2	0
1	60(1)[10(12)24(20)]	300	540	120	24	130	274	20	12	32	1	34	0
2	60(1)[10(12)24(20)] [10(30)60(12)]	780	1,380	210	156	310	676	20	42	62	13	76	0
3	60(1)[10(12)24(20)] [10(30)60(12)][24(20)]	900	1,620	270	156	390	816	40	42	82	13	96	0
4	60(1)[10(12)24(20)][10(30) 60(12)][24(20)][24(30)]	1,140	2,100	420	156	510	1,086	70	42	112	13	126	0
5	60(1)[10(12)24(20)] [10(30)60(12)] [24(20)][24(30)] [10(72)24(60)]	1,740	3,300	780	228	810	1,818	130	114	244	13	258	0

Table 6.2 Data for the **20** series

Structure	No C	E_{tot}(au)	E_{tot}/C (au)	GAP (eV)
C_{60}	60	−103.292	−1.722	1.798
$R_5(20)\_75$	75	−127.802	−1.704	0.022
DoP_4TRS_110	110	−186.513	−1.696	0.343
20(1)(12)_130	130	−222.256	−1.710	0.033
20(1)(12)(20)_270	270	−458.618	−1.699	0.054
$R_5(20)\_75H$	75	−148.552	−1.981	8.900
DoP_4TRS_110H	110	−219.994	−2.000	7.904
20(1)(12)_130H	130	−247.251	−1.902	7.723
20(20)_250_40H	250	−438.870	−1.755	0.122
20(20)_250_100H	250	−465.370	−1.861	5.474
20(1)(12)(20)_270_80H	270	−491.660	−1.821	4.736
60H	60	−125.584	−2.093	10.412

Table 6.3 Data for the **20**&**28** series

Structure	Atoms	E_{tot} (au)	E_{tot}/C(au)	GAP (eV)
C_{60}	60	−103.292	−1.722	1.798
20(1)(12)_130	130	−222.256	−1.710	0.033
$R_5(28)\_110$	110	−188.084	−1.710	0.019
28(20)_380	380	−650.780	−1.713	0.011
20(1)(12)28(20)_400	400	−686.690	−1.717	0.001
20(1)(12)28(20)20(12)_460	460	−791.948	−1.722	0.061
20(1)(12)28(20)20(12) 20(60)_880	880	−1,513.795	−1.720	0.362
20(1)(12)_130H	130	−247.251	−1.902	7.723
$R_5(28)\_110H$	110	−220.185	−2.002	9.27
28(20)_380H	380	−732.468	−1.928	8.059
20(1)(12)28(20)_400H	400	−758.894	−1.897	4.561
20(1)(12)28(20)20(12)_460H	460	−864.167	−1.879	7.95
20(1)(12)28(20)20(12) 20(60)_880H	880	−1,615.295	−1.836	7.424
60H	60	−125.584	−2.093	10.412

appears the most stable, with a gain in gap of about 1 au, in comparison to C_{60}. Next stable is the structure of 900 atoms (Table 6.4, shell 3), having 1+12 C_{60} units inside. These multi-cages show the C_{60} fullerene not coalesced with itself but separated by means of smaller cages C_{24} and C_{10}.

Data in Table 6.4 suggest a clear stabilization by covalent aggregation of C_{60}. The smaller cages can be seen as "ordered" additional carbon atoms, possibly present in experiment, surrounding the C_{60} cages. However, the building of U_{20}_300 (and its series) can eventually be achieved by only C_{24} (either available substance or appearing *in situ*), the other cages resulting by self-assembly of this small cage.

Aggregation of **60**&**12** cages is also conceivable, as this combination appears in leapfrog *Le* map operation transforms of multi-shell structures (see Table 6.5).

Table 6.4 Data for **60**&**24**&**10** structures

Shell	Structure	Atoms	E_{tot} (au)	E_{tot}/C(au)	GAP (eV)
0	C_{60}	60	−103.292	−1.722	1.798
–	$R_5(24)$	90	−153.200	−1.702	1.827
1	60(1)[10(12)24(20)] or (60&24&10)U_{20}	300	−512.794	−1.709	2.845
2	60(1)[10(12)24(20)][10(30)60(12)]	780	−1,340.01	−1.718	1.024
3	60(1)[10(12)24(20)][10(30)60(12)][24(20)]	900	−1,545.56	−1.717	2.452
4	60(1)[10(12)24(20)][10(30)60(12)] [24(20)][24(30)]	1,140	−1,950.76	−1.711	1.613
5	60(1)[10(12)24(20)][10(30)60(12)] [24(20)][24(30)] [10(72)24(60)]	1,740	−2,972.53	−1.708	1.519

Table 6.5 Data for leapfrog transforms

	Structure	Atoms	E_{tot} (au)	E_{tot}/C(au)	GAP (eV)
1	C_{60}	60	−103.292	−1.722	1.798
2	Le(20(1)(12))	570	−980.894	−1.721	1.474
3	Le(20(1)(12)(20))	1,320	−2,260.391	−1.712	0.021
4	LeX(20(1)(12)(20))[a]	870	−1,479.293	−1.7003	0.022
5	Le(20(20))	1,050	−1,803.205	−1.717	0.009

[a]a **60**&**12** structure

Table 6.6 Data for linear (**60**&**12**) U_{20}_k and other hydrogenated structures

	Structure	Atoms	E_{tot} (au)	E_{tot}/C(au)	GAP (eV)
1	C_{60}	60	−103.292	−1.722	1.798
2	(60&12)U_{20}_1	150	−279.799	−1.865	7.34
3	(60&12)U_{20}_2	255	−471.215	−1.848	7.05
4	(60&12)U_{20}_3	360	−662.630	−1.841	6.93
5	(60&12)U_{20}_4	465	−854.045	−1.837	6.88
6	12(1)60(4)[12(16)12(40)]T[a]	402	−734.636	−1.827	6.87
7	60(1)12(20)[12(20)60(12)][12(30)12(60)]	870	−1,556.774	−1.789	2.490
8	**60H**	60	−125.584	−2.093	10.412

[a]Tetrahedral structure

Stable enough appears to be only *Le*(**20**(1)(12))_570, the transform by leapfrog of 20(1)(12)_130 cage. It contains 13 C_{60} units, coalesced to each other by a pentagonal face and filling the radial space by sharing a hexagonal face with the truncated tetrahedron C_{12} cage (existent there as an empty space). The last row in Table 6.5 is a hyper-dodecahedron made only by C_{60} units, appearing not enough stabilized by aggregation.

A better stabilization is obtained by hydrogenation of **60**&**12** structures; compare the cage of 870 atoms in Tables 6.5 and 6.6, respectively. Hydrogenation could enable the realization of rodlike structures like those illustrated in Fig. 6.6 (see data in Table 6.6).

Table 6.7 Comparing methods for C_{60} and C_{24} reference structures

Structure	Theory level	Atoms	E_{tot} (au)	E_{tot}/C(au)	GAP (eV)
C_{60}	DFT/M06-2x/6-31G(d,p)	60	−2,285.46	−38.091	4.544
$C_{60}H_{60}$	DFT/M06-2x/6-31G(d,p)	120	−2,321.05	−38.684	9.115
C_{60}	HF/6-31G(d,p)	60	−2,271.83	−37.864	19.673
C_{60}	DFTB	60	−103.292	−1.722	1.798
$C_{60}H_{60}$	DFTB	120	−125.584	−2.093	10.412
C_{24}	DFT/M06-2x/6-31G(d,p)	24	−913.51	−38.063	4.517
$C_{24}H_{24}$	DFT/M06-2x/6-31G(d,p)	48	−928.47	−38.686	9.034
C_{24}	DFTB	24	−40.60	−1.692	1.464
$C_{24}H_{24}$	DFTB	48	−50.26	−2.094	10.811

At the same number of C_{60} units (e.g., 4), the linear structure (Table 6.6, entry 5) is more stable than a tetrahedral one (Table 6.6, entry 6), maybe due to a higher hydrogenation ratio (0.322 vs. 0.298, respectively).

Finally, we stress that even the DFTB+ method gives different result in comparing the more reliable methods HF and DFT (see Table 6.7). It is a good tool in investigating series of structures containing large number of atoms, still keeping a good relative ordering of their stability, as compared with the C_{60} fullerene, the reference structure in nanoscience.

6.4 Computational Details

Due to the large number of atoms, we limited here to calculate the total energy at the density functional-based tight-binding level of theory. This method, combined with the self-consistent charge technique (SCC-DFTB, Elstner et al. 1998), can provide a solution in treating large nanoscaled molecular materials, with nearly good accuracy (Elstner et al. 2000, 2001a, b) compared to some higher-level theoretical methods. The SCC-DFTB-optimized geometries were performed using the DFTB+ program (DFTB+; Aradi et al. 2007). The results were presented in Tables 6.2, 6.3, 6.4, 6.5, 6.6, and 6.7. As regarding the C–C bonds and C–C–C bond angles, they are in a good agreement with the known results.

6.5 Conclusions

Fullerene aggregation was shown to follow a well-defined geometry within multi-shell nanostructures. The way of space filling is different, function of dimensions and shape of composing small fullerenes. The design of structures was made by using map operations as implemented in our CVNET (Stefu and Diudea 2005) and by Nano Studio (Nagy and Diudea 2009) software packages. The stability of the

studied structures was evaluated at the DFTB+ level of theory. The results revealed some multi-shell structures, as aggregates of C_{60} units not coalesced to each other (i.e., remained separated), as the most stable ones, with a clear gain in stability, in comparison to the non-aggregated C_{60} fullerene. The stabilization by hydrogenation, a way of exohedral derivatization, was also proved. This study was an attempt to explore the possible stabilization by aggregation of some fullerenes, including C_{60}, C_{24} and some smaller ones (the last being seen as additional carbon atoms).

References

Aradi B, Hourahine B, Frauenheim T (2007) DFTB+, a sparse matrix-based implementation of the DFTB method. J Phys Chem A 111(26):5678–5684

Böttcher A, Weis P, Bihlmeier A, Kappes MM (2004) C_{58} on HOPG: soft-landing adsorption and thermal desorption. Phys Chem Chem Phys 6:5213–5217

Böttcher A, Weis P, Jester SS, Bihlmeier A, Kloppe W, Kappes MM (2005) Solid C_{58} films. Phys Chem Chem Phys 7:2816–2820

Ceulemans A, King RB, Bovin SA, Rogers KM, Troisi A, Fowler PW (1999) The heptakisoctahedral group and its relevance to carbon allotropes with negative curvature. J Math Chem 26:101–123

Dandoloff R, Döhler G, Bilz H (1980) Bond charge model of amorphous tetrahedrally coordinated solids. J Non-Cryst Solids 35–36:537–542

Diudea MV, Nagy CL (2007) Periodic nanostructures. Springer, Dordrecht

Elstner M, Porezag D, Jungnickel G, Elsner J, Haugk M, Frauenheim T, Suhai S, Seifert G (1998) Self-consistent-charge density-functional tight-binding method for simulations of complex materials properties. Phys Rev B 58:7260–7268

Elstner M, Jalkanen K, Knapp-Mohammady M, Frauenheim T, Suhai S (2000) DFT studies on helix formation in N-acetyl-(L-alanyl)n-N-methylamide for n = 1–20. Chem Phys 256:15–27

Elstner M, Jalkanen KJ, Knapp-Mohammady M, Frauenheim T, Suhai S (2001a) Energetics and structure of glycine and alanine based model peptides: approximate SCC-DFTB, AM1 and PM3 methods in comparison with DFT, HF and MP2 calculations. Chem Phys 263:203–219

Elstner M, Hobza P, Frauenheim T, Suhai S, Kaxiras E (2001b) Hydrogen bonding and stacking interactions of nucleic acid base pairs: a density-functional-theory based treatment. J Chem Phys 114:5149–5155

Fowler PW, Manolopoulos DE (1995) An atlas of fullerenes. Oxford University Press, Oxford

Gao X, Zhao Y (2007) The way of stabilizing non-IPR fullerenes and structural elucidation of C(54)Cl(8). J Comput Chem 28:795–801

Hennrich FH, Michel RH, Fischer A, Richard-Schneider S, Gilb S, Kappes MM, Fuchs D, Bürk M, Kobayashi K, Nagase S (1996) Isolation and characterization of C_{80}. Angew Chem 35: 1732–1734

Koshio A, Inakuma M, Sugai T, Shinohara H (2000) A preparative scale synthesis of C_{36} by high-temperature laser-vaporization: purification and identification of $C_{36}H_6$ and $C_{36}H_6O$. J Am Chem Soc 122:398–399

Krätschmer W, Lamb LD, Fostiropoulos K, Huffman DR (1990) Solid C_{60}: a new form of carbon. Nature 347:354–358

Kroto HW (1987) The stability of the fullerenes Cn (n = 24, 28, 32, 50, 60 and 70). Nature 329:529–531

Lenosky T, Gonze X, Teter M, Elser V (1992) Energetics of negatively curved graphitic carbon. Nature 355:333–335

Löffler D, Jester SS, Weis P, Böttcher A, Kappes MM (2006) Cn films (n = 50, 52, 54, 56, and 58) on graphite: cage size dependent electronic properties. J Chem Phys 124:054705-3
Löffler D, Bajales N, Cudaj M, Weis P, Lebedkin S, Bihlmeier A, Tew DP, Klopper W, Böttcher A, Kappes MM (2009) Non-IPR C60 solids. J Chem Phys 130:164705
Löffler D, Ulas S, Jester S-S, Weis P, Bottcher A, Kappes MM (2010) Properties of non-IPR fullerene films versus size of the building blocks. Phys Chem Chem Phys 12:10671–10684
Lu X, Chen Z, Thiel W, Schleyer PR, Huang R, Zheng L (2004) Properties of fullerenes[50] and D5h decachlorofullerene[50]: a computational study. J Am Chem Soc 126:14871–14878
Mackay AL, Terrones H (1991) Diamond from graphite. Nature 352:762–762
Mackay AL, Terrones H (1993) Hypothetical graphite structures with negative Gaussian curvature. Philos Trans R Soc A 343:113–127
Müller A, Roy S (2003) En route from the mystery of molybdenum blue via related manipulatable building blocks to aspects of materials science. Coord Chem Rev 245:153–166
Nagy CL, Diudea MV (2009) NANO-studio software. Babes-Bolyai University, Cluj
O'Keeffe M, Adams GB, Sankey OF (1992) Predicted new low energy forms of carbon. Phys Rev Lett 68:2325–2328
Piskoti C, Yarger J, Zettl A (1998) C_{36}, a new carbon solid. Nature 393:771–773
Ricardo-Chavez JL, Dorantes-Dávila J, Terrones M, Terrones H (1997) Electronic properties of fullerenes with nonpositive Gaussian curvature: finite zeolites. Phys Rev B 56:12143–12146
Romo-Herrera JM, Terrones M, Terrones H, Dag S, Meunier V (2007) Covalent 2D and 3D networks from 1D nanostructures: designing new materials. Nano Lett 7:570–576
Schläfli L (1901) Theorie der vielfachen Kontinuität Zürcher und Furrer. Zürich (Reprinted in: Schläfli L 1814–1895 (1950) Gesammelte Mathematische Abhandlungen, Band 1:167–387, Verlag Birkhäuser, Basel)
Schoen AH (1970) Infinite periodic minimal surfaces without self-intersections. NASA Technical note D-5541
Schwarz HA (1865) Über minimalflächen. Monatsber Berlin Akad, Berlin
Schwarz HA (1890) Gesammelte Matematische Abhandlungen. Springer, Berlin
Scott LT, Hashemi MM, Meyer DT, Warren HB (1991) Corannulene. A convenient new synthesis. J Am Chem Soc 113:7082–7084
Shevchenko VY (2011) Search in chemistry, biology and physics of the nanostate. Lema, St Petersburg
Stefu M, Diudea MV (2005) CageVersatile_CVNET. Babes-Bolyai University, Cluj
Tan YZ, Xie SY, Huang RB, Zheng L (2009) The stabilization of fused-pentagon fullerene molecules. Nat Chem 1:450–460
Taylor R (1992) Rationalization of the most stable isomer of a fullerene C_n. Perkin Trans 2 J Chem Soc 3–40
Terrones M, Banhart F, Grobert N, Charlier J-C, Terrones H, Ajayan PM (2002) Molecular junctions by joining single–walled carbon nanotubes. Phys Rev Lett 89(1–4):075505
Terrones H, Mackay AL (1997) From C_{60} to negatively curved graphite. Prog Cryst Growth Character 34:25–36
Terrones H, Terrones M (1997) Quasiperiodic icosahedral graphite sheets and high-genus fullerenes with nonpositive Gaussian curvature. Phys Rev B 55:9969–9974
Terrones H, Terrones M (2003) Curved nanostructured materials. New J Phys 5:1261–12637
Townsend SJ, Lenosky TJ, Muller DA, Nichols CS, Elser V (1992) Negatively curved graphite sheet model of amorphous carbon. Phys Rev Lett 69:921–924
Troshin PA, Avent AV, Darwisch AD, Martsinovich N, Abdul-Sada AK, Street JM, Taylor R (2005) Isolation of two seven-membered ring C_{58} fullerene derivatives: $C_{58}F_{17}CF_3$ and C58F18. Science 309:278–281
Vanderbilt D, Tersoff J (1992) Negative-curvature fullerene analog of C_{60}. Phys Rev Lett 68: 511–513
Wang CR, Kai T, Tomiyama T, Yoshida T, Kobayashi Y, Nishibori E (2000) C66, fullerene encaging a scandium dimmer. Nature 408:426–427

Wang CR, Shi ZQ, Wan LJ, Lu X, Dunsch L, Shu CY, Tang YL, Shinohara H (2006) $C_{64}H_4$: production, isolation and structural characterizations of a stable unconventional fulleride. J Am Chem Soc 128:6605–6610

Xie SY, Gao F, Lu X, Huang RB, Wang CR, Zhang X, Liu ML, Deng SL, Zheng SL (2004) Capturing the labile fullerene[50] as $C_{50}Cl_{10}$. Science 304:699–699

Yan QB, Zheng QR, Su G (2007) Theoretical study on the structures, properties and spectroscopies of fullerene derivatives $C_{66}X_4$ (X = H, F, Cl). Carbon 45:1821–1827

Zeger L, Kaxiras E (1993) New model for icosahedral carbon clusters and the structure of collapsed fullerite. Phys Rev Lett 70:2920–2923

Chapter 7
On Molecular Dynamics of the Diamond D_5 Substructures

Beata Szefler

Abstract Diamond D_5 is a hyperdiamond, with the rings being mostly pentagonal and built up on the frame of *mtn* structure, appearing in type II clathrate hydrates. The centrohexaquinane C_{17} was proposed as the seed of D_5 (Diudea, Studia Univ Babes-Bolyai Chemia, 55(4):11–17, 2010a; Diudea, Nanomolecules and nanostructures – polynomials and indices. University of Kragujevac, Kragujevac, 2010b). In this chapter, we present some results on molecular dynamics (MD) of four structures based on C_{17} skeleton, as all-carbon or partly oxygenated derivatives. The results are discussed in terms of structural stability as given by DFT calculations as well as by the stable fluctuations of root-mean-square deviations (*RMSD*) and total, potential, and kinetic energies provided by MD calculations. Within D_5, several other substructures are discussed in this chapter. The structural stability of such intermediates/fragments appearing in the construction/destruction of D_5 net is also discussed in terms of molecular dynamics simulation. The calculations herein discussed have been done using an empirical many-body potential energy function for hydrocarbons. It has been found that, at normal temperature, the hexagonal hyper-rings are more stable, while at higher temperature, the pentagonal ones are relatively stronger against the heat treatment.

7.1 Introduction

In the nano-era, a period starting with the discovery of $C_{60,}$ in 1985, the carbon allotropes played a dominant role. Among the carbon structures, fullerenes (zero dimensional), nanotubes (one dimensional), graphene (two dimensional), diamond,

B. Szefler (✉)
Department of Physical Chemistry, Collegium Medicum, Nicolaus Copernicus University, Kurpińskiego 5, 85-950 Bydgoszcz, Poland
e-mail: beata.szefler@cm.umk.pl

M.V. Diudea and C.L. Nagy (eds.), *Diamond and Related Nanostructures*, Carbon Materials: Chemistry and Physics 6, DOI 10.1007/978-94-007-6371-5_7,

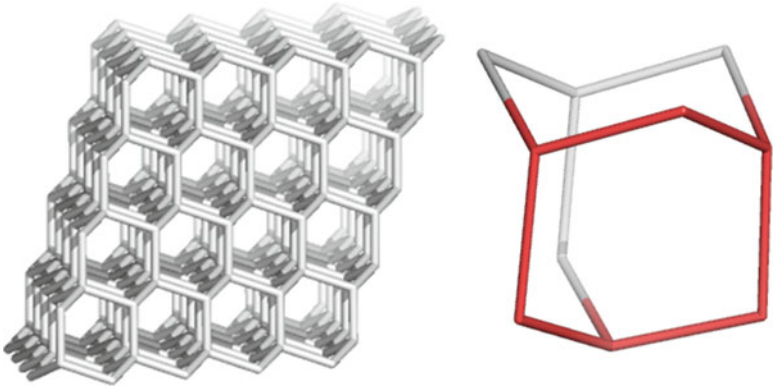

Fig. 7.1 Diamond D_6 (*left*) and its repeating unit, adamantane (*right*)

and spongy carbon (three dimensional) were the most studied (Diudea 2005, 2010a; Diudea and Nagy 2007), both from theoretical reasons and applications perspective.

Diamond D_6, the beautiful classical diamond, with all-hexagonal rings of sp^3 carbon atoms (Fig. 7.1), crystallized in the face-centered cubic *fcc* network (space group *Fd*-3*m*), has kept its leading interest among the carbon allotropes, in spite of the "nano" varieties (Decarli and Jamieson 1961; Aleksenskiĭ et al. 1997; Osawa 2007, 2008; Williams et al. 2007; Dubrovinskaia et al. 2006). Its aesthetical appeal and mechanical characteristics are of great importance in jewelry and industry. Synthetic diamonds are currently produced by a variety of methods, including high pressure-high temperature (HPHT), chemical vapor deposition (CVD), and ultrasound cavitation (Khachatryan et al. 2008).

However, the diamond D_6 is not unique: a hexagonal network called lonsdaleite (space group $P6_3/mmc$) (Frondel and Marvin 1967) was discovered in a meteorite in the Canyon Diablo, Arizona, in 1967. Several diamond-like networks have also been proposed (Diudea et al. 2010; Hyde et al. 2008).

In a previous study, Diudea and Ilić (2011) described some multi-tori (i.e., structures showing multiple hollows (Diudea and Petitjean 2008)); one of them is illustrated in Fig. 7.2, left.

The reduced graph of this multi-torus provided the structure for the seed of diamond D_5: C_{17} (Fig. 7.2, right) consisting of a tetravalent atom surrounded by six pentagons, the maximum possible number of pentagons around an sp^3 carbon atom. According to the chemical nomenclature, C_{17} is a centrohexaquinane, a class of structures previously studied by Gund and Gund (1981), Paquette and Vazeux (1981), and more recently by Kuck (1984, 2006) and Kuck et al. (1995).

Diamond D_5 is the name given by Diudea to diamondoids consisting mostly of pentagonal rings (Diudea 2010a, b; Diudea and Ilić 2011). D_5 is a hyperdiamond built up in the frame of the trinodal *mtn* structure, while its seed is eventually the centrohexaquinane C_{17}. However, D_5 belongs to the family of Clathrates with the point symbol net {5^5.6}12{5^6}5 and $2[5^{12}] + [5^{12} \times 6^4]$ tiling and belongs to the

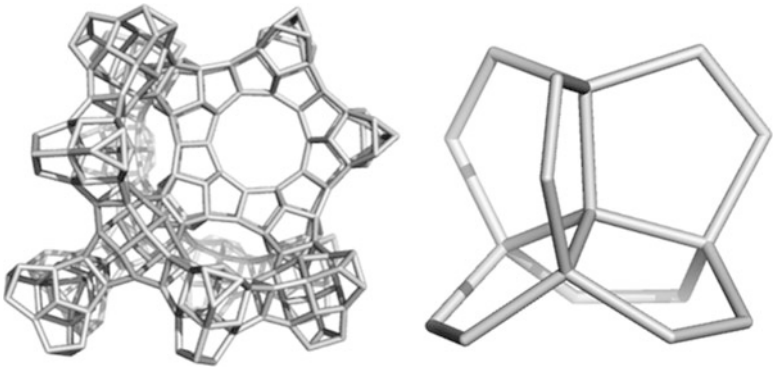

Fig. 7.2 A multi-torus (*left*) and its reduced graph C_{17} (*right*), the seed of diamond D_5

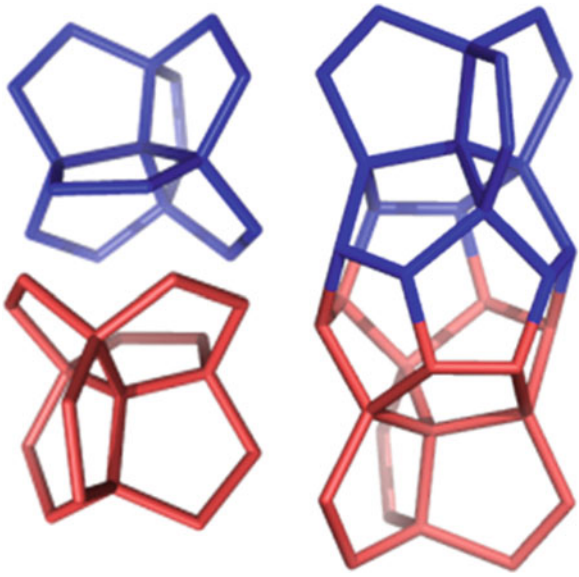

Fig. 7.3 A joint of two C17 units (*left*) to give a dimer C34 (*right*), the repeat unit (in crystallographic terms) of the diamond D_5 network

space group *Fd*3*m* (Delgado-Friedrichs et al. 2005). It is precisely type II clathrate, also called C_{34} (Blasé et al. 2010), of which Si_{34}-analogue was already synthesized.

C_{17} can dimerize to $2 \times C_{17} = C_{34}$ (Fig. 7.3), the repeating unit, in crystallographic terms, of the diamond D_5 network. Thus, D_5 (Fig. 7.4) and *fcc*-C_{34} are herein synonyms (Fig. 7.5).

In a chemist's view, the building of D_5 network may start with the seed C_{17} and continue with some intermediates, the adamantane- and diamantane-like ones included (Figs. 7.6, 7.7, and 7.8). The structure ada_20_158 (Fig. 7.7, left) corresponds to adamantane (Fig. 7.5, left) in the classical diamond D_6. In crystallochemical terms, an adamantane-like structure, as ada_20_158, is the

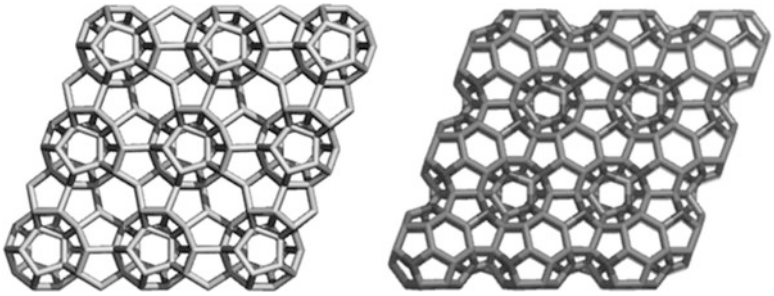

Fig. 7.4 Diamond D_5_20_860 net (*left*) and D_5_28_1022 co-net (*right*)

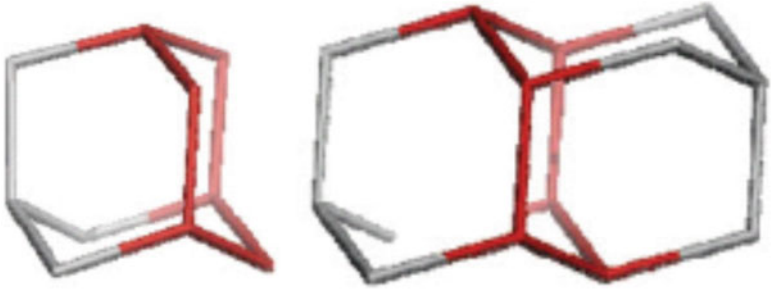

Fig. 7.5 Diamond D_6: adamantane (*left*), diamantane (*right*)

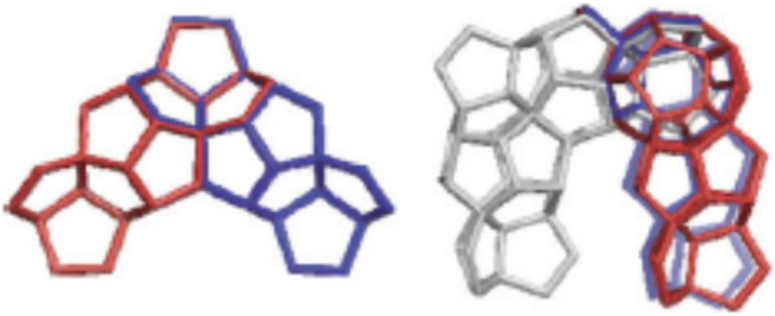

Fig. 7.6 Intermediate structures originating in C_{34} unit: C_{51} (*left*) and $3 \times C_{51}$ (*right*)

monomer which will probably condense to form the D_5 network (Fig. 7.4). The ada-like structure, starting from C_{28} can be seen in Fig. 7.7, right. Diamantane-like units can also be modeled, as in Fig. 7.8 (compare with the diamantane, Fig. 7.5, right). In fact, there is one and the same triple periodic D_5 network, built up basically from C_{20} and having as hollows the fullerene C_{28}. The co-net D_5_28 cannot be derived from C_{28} alone since the hollows of such a net consist of C_{57} units (a C_{20}-based

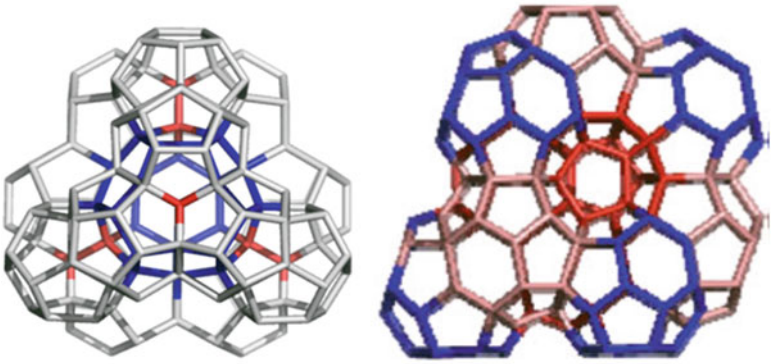

Fig. 7.7 Adamantane-like structures: ada_20_158 (*left*) and ada_28_213 (*right*)

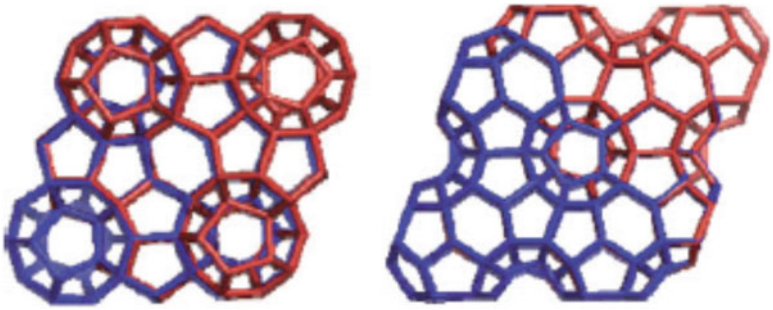

Fig. 7.8 Diamantane-like structures: dia_20_226 net (*left*) and dia_28_292 co-net (*right*)

structure, see above) or higher tetrahedral arrays of C_{20}, thus needing extra C atoms per ada-unit. It is worthy to note the stabilizing effect of the wings in case of C_{34} (Fig. 7.3, right) in comparison to C_{20}.

Remark the efforts made by a series of bright scientists (Prinzbach et al. 2006; Paquette et al. 1981; Saito and Miyamoto 2001; Eaton 1979) to reach the dodecahedral cage C_{20}, either as fullerene or hydrogenated species. Also remark the endeavor to synthesize the centrohexaquinane C_{17}, both as oxygen-containing heterocycle (Simmons and Maggio 1981; Paquette and Vazeux 1981) or all-carbon structure (Gestmann et al. 2006; Kuck 2006). Thus, the hyperdiamond D_5_20/28 mainly consists of sp^3 carbon atoms building ada-type repeating units (including C_{28} as hollows). The ratio C-sp^3/C-total trends to one in a large enough network. As the content of pentagons R[5] (Aleksenskiĭ et al. 1997; Williams et al. 2007) per total rings trend to 90 %, this network was named the diamond D_5 (Diudea 2010a, b).

In the above symbols, "20" refers to C_{20} and "28" refers to C_{28}, while the last number counts the carbon atoms in structures.

7.2 Method

In a study of structural stability, performed by Szefler and Diudea (2012), ab initio calculations and molecular dynamics have been used. The four structures (Figs. 7.9 and 7.12) based on C_{17} skeleton, as all-carbon or partly oxygenated derivatives, were optimized at the Hartree-Fock (HF) (HF/6-31G**) and DFT (B3LYP/6-311+G**) levels of theory and submitted to molecular dynamics (MD) procedure. All calculations were performed in gas phase by Gaussian 09 (Gaussian 09 software package 2009) while MD calculations were done in vacuum, using Amber 10.0 software (Case et al. 2005). The single-point energy minima obtained for the investigated structures are shown in Table 7.1. Before MD, the atomic charges were calculated according to Merz-Kollmann scheme via the RESP (Wang et al. 2000) procedure, at HF/6-31G** level. The AMBER force field (Wang et al. 2004) was used for dynamic trajectory generation. There were several steps of molecular dynamics. After stabilization of energies and RMSD values during run, the actual molecular dynamics were performed, in a cascade way. Each tested system was heated by 20 ps while MD simulations were 100 ns long. The visualizations were prepared in the GaussView program. After MD run, the values of RMSD and energies of analyzed structures were recorded: total energy (E_{tot}), kinetic energy (E_{kin}), and potential energy (E_{pot}). In the analysis, averaged values of all generated points of energies and values of RMSD in every 1 ps of MD were used.

The stability of 12 other substructures was investigated by Kyani and Diudea (2012) by performing a molecular dynamics (MD) computer simulation, using an empirical many-body adaptive intermolecular reactive empirical bond-order (AIREBO) potential energy function. All the diamond D_5 substructures are fully

Fig. 7.9 C_{17}_hexaquinane trioxo derivatives: Paquette P_1 (*left*) and Diudea, D_1 (*middle*) and D_2 (*right*)

Table 7.1 The single-point energies of the optimized structures at DFT (B3LYP/6-311+G**) level of theory

B3LYP	C_{17}	D_1	D_2	P_1
B3LYP (a.u)	−655.058	−766.491	−766.480	−766.479
B3LYP_Gap (eV)	5.868	6.461	6.264	6.274

hydrogenated ones. The studied structures were optimized at the semiempirical PM3 level of theory and then submitted to the MD simulation procedure. Canonical ensemble molecular dynamics was used for this simulation. Within this ensemble, the number of atoms N, the volume V, and the temperature T are considered constants while velocities are scaled with respect to T, ensuring that the total kinetic energy, and hence the temperature, is constant (isokinetic MD). The initial velocities follow the Maxwell distribution. The AIREBO potential energy function (PEF) developed for hydrocarbons (Stuart et al. 2000), as provided by LAMMPS software (Plimpton 1995), was used to investigate the stability of nanostructures at increasing temperatures. This parameterized potential adds Lennard-Jones and torsional contributions to the many-body REBO potential (Brenner 2000; Brenner et al. 2000). It is similar to a pairwise dispersion-repulsion potential, while adding a bond-order function modulates the dispersion term and incorporates the influence of the local atomic environment. Through this interaction, individual atoms are not constrained to remain attached to specific neighbors, or to maintain a particular hybridization state or coordination number. Thus, at every stage of the simulation, the forming and breaking of the bonds is possible. This potential is derived from ab initio calculations, and therefore, it is well adapted to classical molecular simulations of systems containing a large number of atoms such as carbon nanostructures. The equations of particle motion were solved using the Verlet algorithm (Verlet 1967, 1968), and the temperature was gradually increased by 100 K at each run. One time step was taken to be 10–16 s and at each run a relaxation with 5,000 time steps was performed. The root-mean-square deviation (RMSD) of the atoms was used as criterion for examining the stability of the simulated structures.

7.3 Results and Discussion

Stability evaluation was performed on four hypothetical seeds of D_5, the all-carbon structure C_{17} (Fig. 7.2, right) and three trioxa derivatives of C_{17}. The isomer in Fig. 7.9, left, was synthesized by Paquette and Vazeux (1981) and is hereafter denoted as P_1. Other two structures, denoted as D_1 and D_2 (Fig. 7.9, middle and right), were proposed (Szefler and Diudea 2012), as possibly appearing in rearrangements of the Paquette's P_1 structure. The last two structures would be the appropriate ones in the next step of dimerization to C_{34}, in fact the repeating unit of D_5 (Blasé et al. 2010).

The stability of molecules was evaluated both in static and dynamic temperature conditions. The isomer D_1 seems the most stable among all studied structures, as given by optimization in gas phase at DFT level (Table 7.1). In a decreasing order of stability, it follows P_1 and D_2. However, at MD treatment, the all-carbon C_{17} appears the most stable, even at DFT level is the last one. This is probably because the C–C bond is more stable at temperature variations (see Fig. 7.12, below).

In MD, C_{17} keeps its structure up to about 1,800 K, while its destruction starts at 2,000 K (Tables 7.2 and 7.4, Figs. 7.10 and 7.11). Kuck has reported a

Table 7.2 The average total energy (E_{tot}) values estimated, by MD, on geometries in the gas phase

C_{17}							
TEMP (K)	300	600	900	1,200	1,400	1,600	1,800
E_{tot} (kcal/mol)	127.405	180.379	233.358	286.460	322.227	357.665	393.123
δ	5.789	11.585	17.373	23.121	27.070	30.932	34.938
D_1							
TEMP (K)	300	600	900	1,200	1,400	1,600	
E_{tot} (kcal/mol)	144.996	197.907	250.689	303.114	337.947	373.136	
δ	5.782	11.593	17.273	23.106	26.739	30.745	
D2							
TEMP (K)	300	600	900				
E_{tot} (kcal/mol)	116.45	169.266	222.049				
δ	5.783	11.542	17.363				
P1							
TEMP (K)	300	600	900	1,200	1,400	1,600	
E_{tot} (kcal/mol)	142.574	195.448	247.889	300.329	335.524	370.602	
δ	5.798	11.535	17.300	23.076	26.931	30.678	

The averaged values were calculated on all the generated points of energies in every 1 ps of molecular dynamics
Symbol δ means the standard deviation

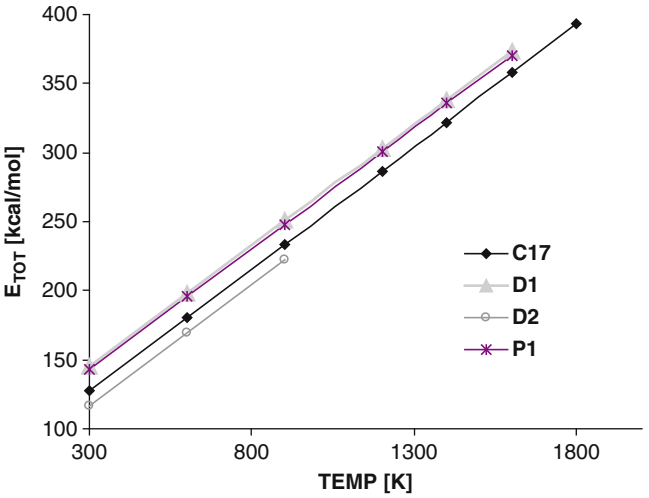

Fig. 7.10 The plot of total energy (E_{tot}) versus temperature (TEMP)

centrohexaindane as the most symmetric structure in this series but also a benzo-centrohexaquinane (Kuck et al. 1995; Kuck 2006) as the last step structure in the synthesis of a nonplanar 3D structure, designed according to mathematical rules. However, in the synthesis of centrohexaquinane derivatives, C_{17} remained yet elusive.

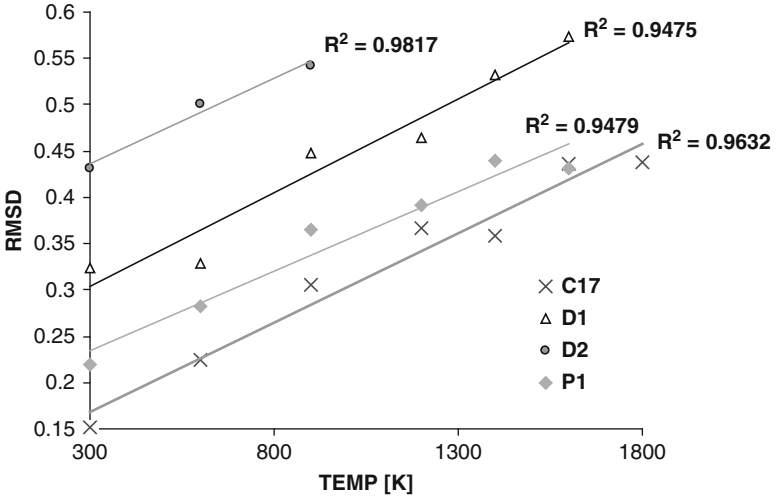

Fig. 7.11 The plot of RMSD versus temperature (TEMP)

Very close to C_{17} behaves the oxygen-containing isomer D_1, as expected from its highest stability at DFT level.

Despite, in molecular dynamics, a very long time (100ns) was leaded, it is believed that prolonged annealing at 1,800 K for both P_1 and D_1 isomers finally resulted in the destruction of these molecules. Thus, P_1 and D_1 isomers behave similarly in MD conditions. The isomer D_2 was the least stable one, as the largest RMSD values were recorded for this isomer.

According to molecular dynamics, it is clear that increasing the temperature resulted in higher values of energy and RMSD of all the analyzed structures, with high values of correlation. The plots of E_{tot} versus temperature for all tested systems are given in Fig. 7.10, while for RMSD, the plots are given in Fig. 7.11. As expected, the correlations in the RMSD plot are a little lower than those for E_{tot}. The MD calculations, listed in Tables 7.2, 7.3, and 7.4, show the following.

As can be seen from Tables 7.2 and 7.3, the values of standard deviations of the averaged values of E_{tot} are closely correlated with the values of temperature, in the range the molecular dynamics simulations were done. The values of these standard deviations at a given temperature are similar for all four studied structures, due to their structural relatedness. The smallest values of the RMS deviation are observed for C_{17}, with the lowest values of standard deviation (δ) at all the studied values of temperature (Table 7.4).

In the case of P_1, one can see a similar behavior but somewhat with larger values of RMSD, compared to the all-carbon structure C_{17} (Table 7.4). It confirms the structural stability of the above structures. The largest values of the RMS deviation were recorded for D_2 isomer (Table 7.4 and Fig. 7.11). Visualization of the structural changes (first step destruction, the right column) is presented in Fig. 7.12.

Table 7.3 The values of standard deviations of E_{tot} at a given temperature (see the center of each slide) for the four investigated structures

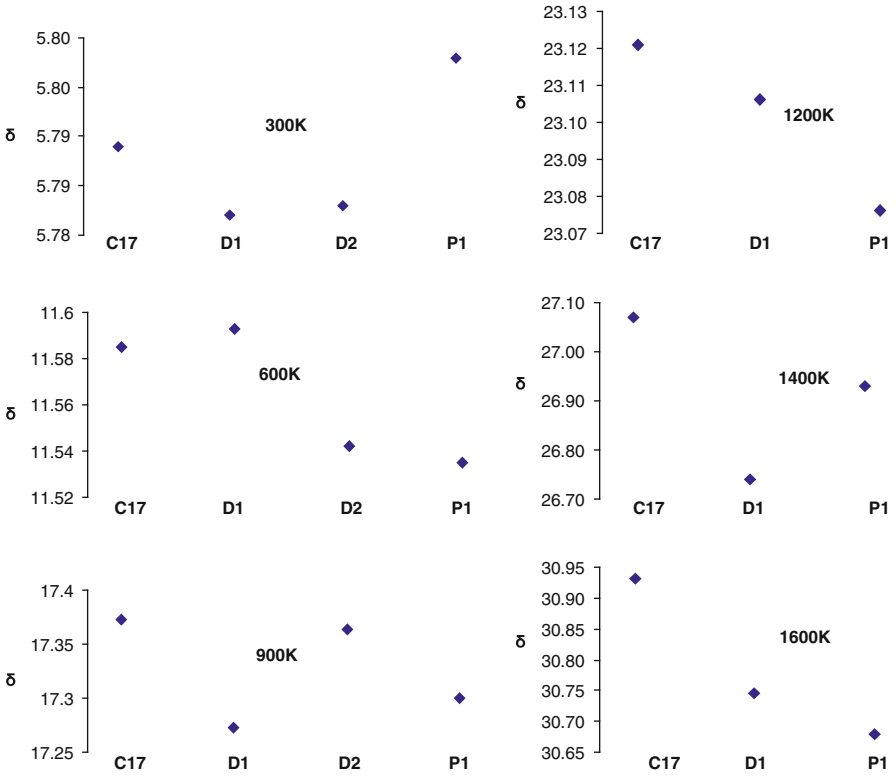

When discussing about diamonds, we consider structures consisting mostly of sp^3 hybridized carbon atom. The molecular dynamic with formulation and parametrization intended for carbon system is REBO (Tersoff 1988a, b; Abell 1985). The Tersoff's and Brenner's (Brenner 1990, 1992) models could describe single-, double-, and triple-bond energies in carbon structures such as hydrocarbons and diamonds, where extended Tersoff's potential function is extended to radical and conjugated hydrocarbon bonds by introducing two additional terms into the bond-order function. Compared to the classical first-principle and semiempirical approaches, the REBO model is less time-consuming. In recent years, the REBO model has been widely used in studies concerning mechanical and thermal properties of carbon nanotubes (Ruoff et al. 2003; Rafii-Tabar 2004).

Molecular dynamic MD calculations using the REBO model were performed by Kyani and Diudea (2012) on the structures listed in Figs. 7.13 and 7.14. The last number in the symbol of structures refers to the number of carbon atoms.

Table 7.4 The averaged RMSD values estimated by molecular dynamics (MD) on the geometries in the gas phase

C_{17}							
TEMP (K)	300	600	900	1,200	1,400	1,600	1,800
RMSD	0.151	0.224	0.305	0.366	0.358	0.437	0.438
δ	0.024	0.032	0.045	0.056	0.054	0.054	0.062
D_1							
TEMP (K)	300	600	900	1,200	1,400	1,600	
RMSD	0.324	0.328	0.448	0.465	0.532	0.574	
δ	0.134	0.088	0.079	0.086	0.091	0.118	
D_2							
TEMP (K)	300	600	900				
RMSD	0.432	0.500	0.542				
δ	0.257	0.245	0.208				
P_1							
TEMP (K)	300	600	900	1,200	1,400	1,600	
RMSD	0.220	0.283	0.365	0.392	0.440	0.431	
δ	0.062	0.069	0.092	0.070	0.093	0.070	

The averaged values were calculated on all the generated points of RMSD in every 1 ps of MD
Symbol δ represents the standard deviation

The main reason for doing calculations on hydrogenated species, although the fragments can appear as non-hydrogenated ones, is the sp^3 hybridization of carbon atoms in the diamond structures. Thus, the four-valence state is preserved.

PM3 calculations show the hexagonal hyper-rings more stable than the pentagonal ones, either with a hollow or filled one as in case of lens-like structures (Table 7.5, entries 5, 6 and 10). There is one exception; the empty hexagon of C_{28} fullerenes (entry 9) is less stable than the corresponding empty pentagon (entry 7). The hexagonal filled ring structures are more stable than the empty ones, except the empty hexagon $20^6\_H_{60}$ (entry 5), made from C_{20}, which seems to be the most stable, as isolated structure, herein discussed. Similarly, $C_{20}H_{20}$ (entry 1) is the stabilized form of the most reactive/unstable fullerene C_{20}. The stabilizing effect of ring filling is a reminiscence of the infinite crystal lattice, whose substructures are $20^6\_28^2H_{68}$ (diamond D_5 net) and $28^6\_20^2H_{92}$ (lonsdaleite L_5 net).

As in studies of the stability of hypothetical seeds of the diamond D_5 by using Amber 10.0 for MD, also here we could see that with increasing temperature, the energy of the systems increases, what would be expected. The total energy versus temperature for three of the considered systems is illustrated in (Fig. 7.15).

MD simulations on increasing temperature evolution show that the studied structures are stable up to 2,000 K, for the C_{20}-based structures (Fig. 7.13), and up to 1,500–2,000 K, for the C_{28}-based structures (Fig. 7.14). The three numbers at the figure bottom represent temperatures, in K degree, for: geometry modifications, topology changes, and major destruction of the structure. Where there are only two data, the topological changes were not observed.

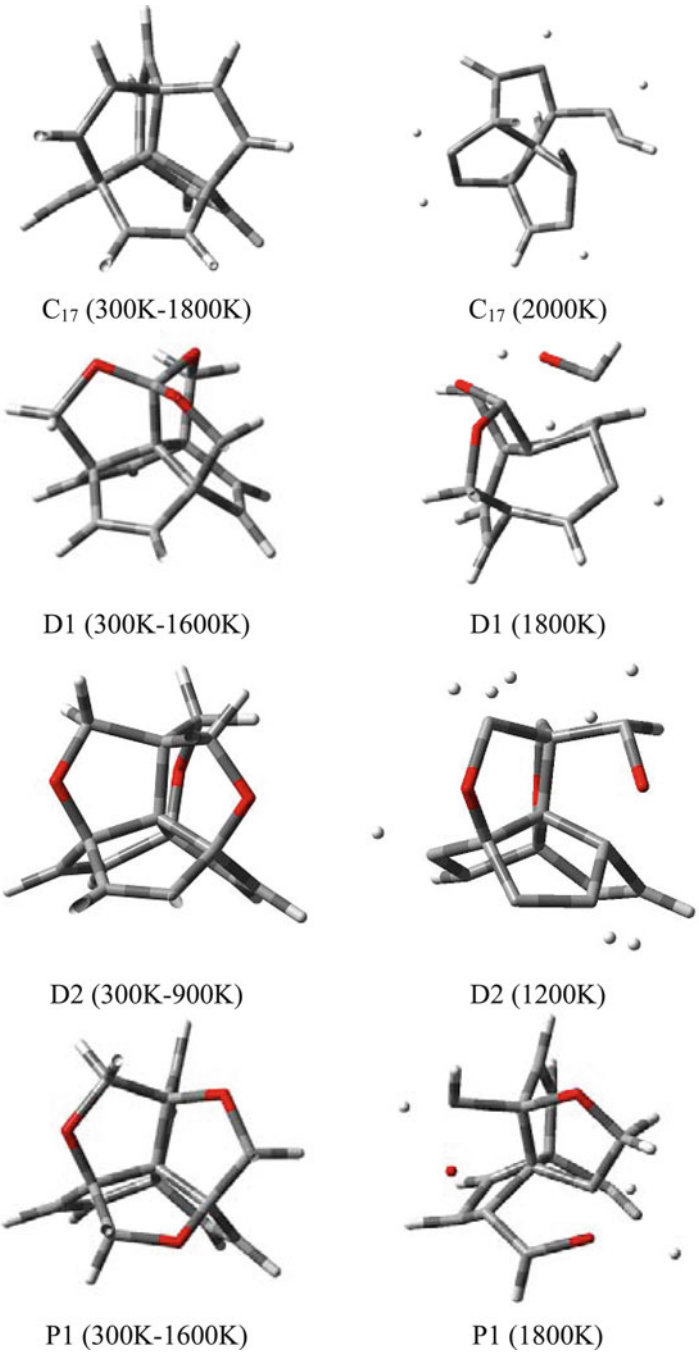

Fig. 7.12 The structure of the tested hypothetical seeds of the diamond D_5 during molecular dynamics

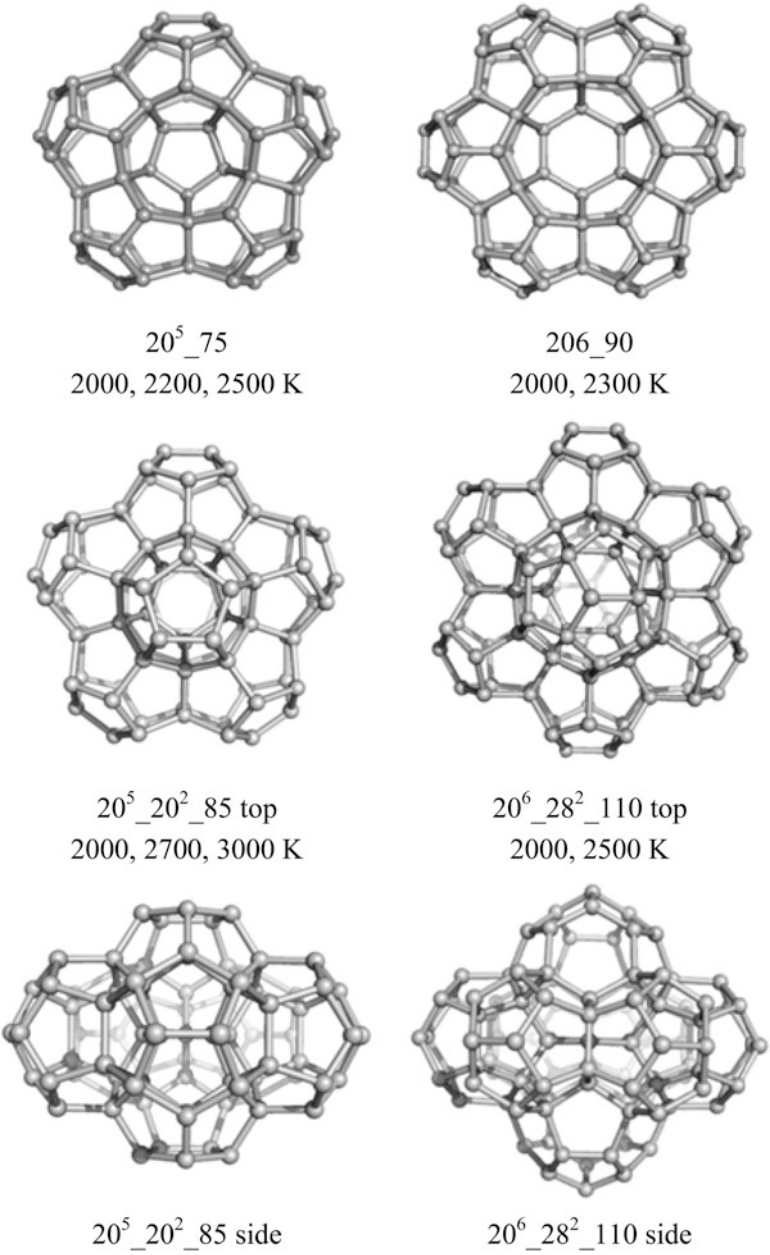

Fig. 7.13 C_{20}-based structures; $20^6\_28^2\_110$ a substructure of $D_5\_20/28$ (Reproduced from Central European Journal of Chemistry 2012, 10(4), 1028–1033)

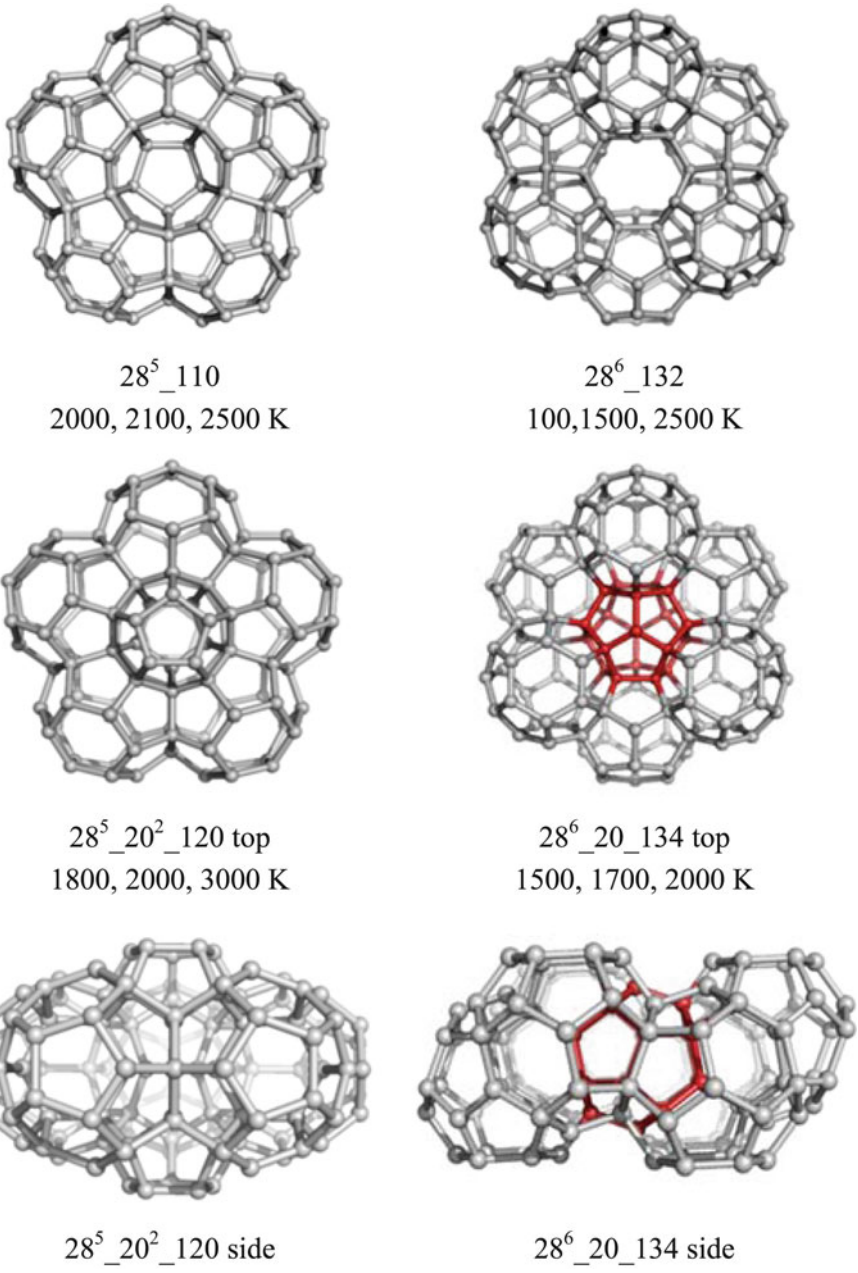

Fig. 7.14 C_{28}-based structures; 286_20_134 a substructure of L5_28/20. The *red* lines show the core substructure, that is C_{20} the smallest fullerene (Reproduced from Central European Journal of Chemistry 2012, 10(4), 1028–1033)

Table 7.5 PM3 energies calculated on fully hydrogenated species

	Structure	Total energy (a.u.)	Gap (eV)
1	$C_{20}H_{20}$	−0.0620	13.905
2	$C_{28}H_{28}$	−0.0035	13.769
3	$20^5\_H_{50}$	0.0045	12.953
4	$20^5\_20^2H_{50}$	0.0432	12.898
5	$20^6\_H_{60}$	−0.1215	13.198
6	$20^6\_28^2H_{68}$	−0.0167	13.061
7	$28^5\_H_{80}$	0.1564	13.034
8	$28^5\_20^2H_{80}$	0.1648	13.061
9	$28^6\_H_{60}$	0.3432	12.490
10	$28^6\_20^2H_{92}$	0.1353	13.034

Reproduced from Central European Journal of Chemistry 2012, 10(4), 1028–1033

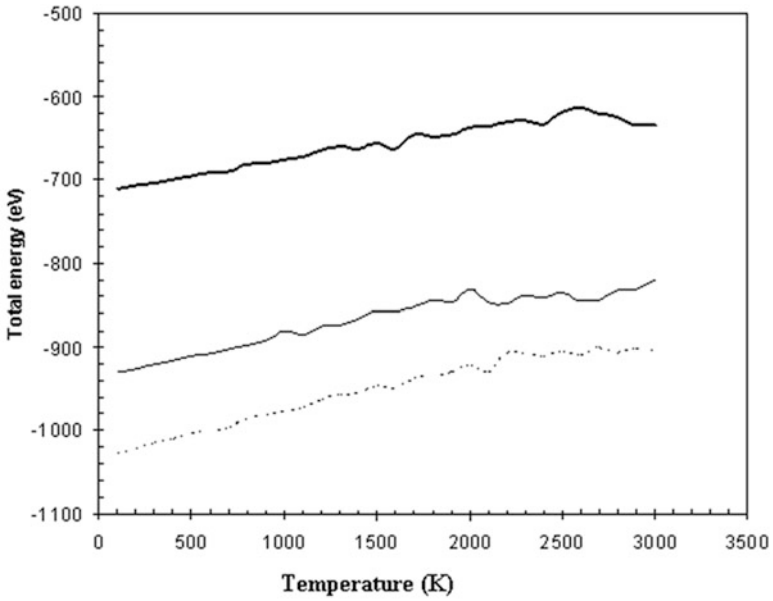

Fig. 7.15 Total energy versus temperature of some of the diamond D_5 substructures: $20^5\_20^2H_{50}$ (*solid line*, Table 7.5, entry 4), $20^6\_28^2H_{68}$ (*simple line*, Table 7.5, entry 6), and $28^5\_20^2H_{80}$ (*dotted line*, Table 7.5, entry 8) (Reproduced from Central European Journal of Chemistry 2012, 10(4), 1028–1033)

The structures in Fig. 7.16 show elongated bonds (i.e., broken bonds, marked by orange color) at temperatures above 2,000 K. Question about structure preserving must be addressed when more than one broken bond will appear (see the bottom row, Fig. 7.16). Above 2,500 K, the complete destruction is expected for all the three structures shown in Fig. 7.16; for two structures (those with only two temperatures on their bottom) the topological changes were not observed. In case of the basic fullerenes, the data are: $C_{20}H_{20}$, 2,700 and 3,000 K, and $C_{28}H_{28}$, 2,500, 2,600,

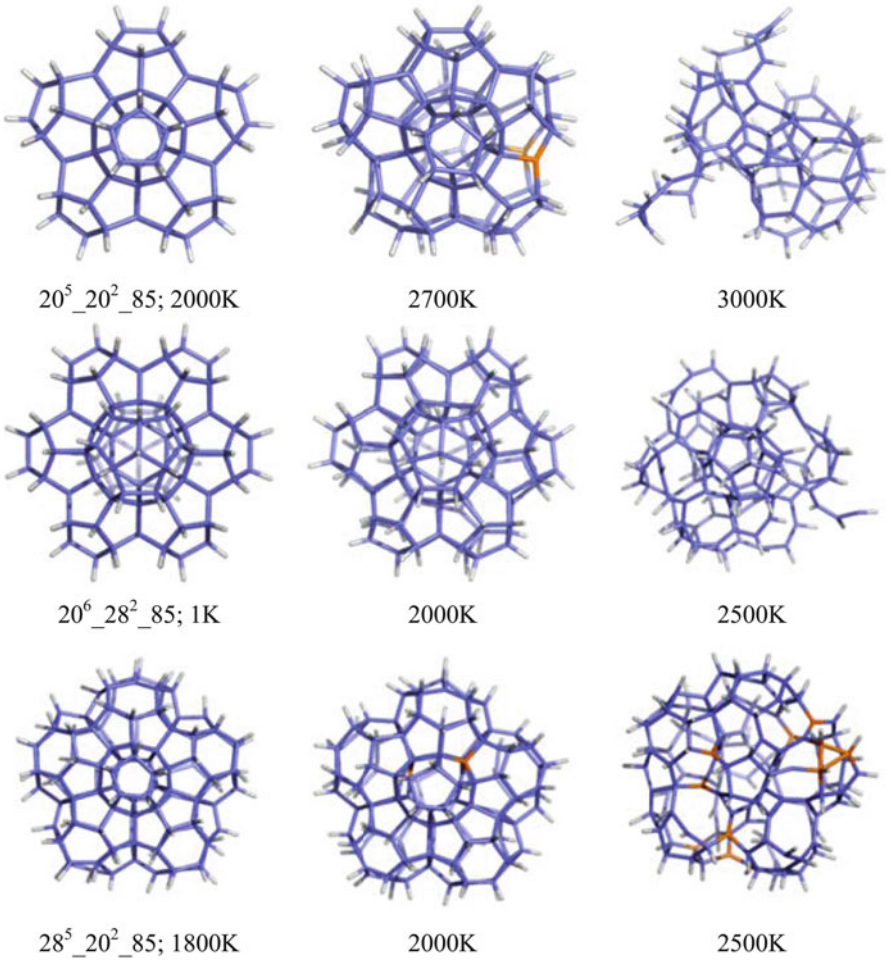

Fig. 7.16 Relaxed structures of $20^5\_20^2\_85$, $20^6\_28^2\_85$ and $28^5\_20^2\_85$ at various temperatures. The *orange* colors mark the broken/formed bonds (Reproduced from Central European Journal of Chemistry 2012, 10(4), 1028–1033)

and 3,000 K. Among the frequent topological changes, the most important is the expansion of two pentagons sharing an edge to octagon and also the apparition of trigons, squares, or larger rings before the structure dramatically decomposes. It is obvious that the structural changes will affect the energetics of the system.

The MD data agree with the PM3 data; in fact, the C_{20}-based structures are more stable than the C_{28}-ones, which corresponds to the higher stability of diamond D_5 compared to lonsdaleite L_5 (Aste and Weaire 2008). At higher temperature, the five-fold hyper-rings seem to be more stable, at least in the isolated fragments (see Figs. 8.13 and 8.14). Remind that such fragments can appear either in synthesis of D_5

or in its destruction, their knowledge thus being of real interest. It is important to know the limit temperature, e.g., in the annealing process of repeating unit C_{34} in the possible synthesis of D_5. Conversely, in the analysis of such diamondoids, the possible fragments appearing in the destruction of their lattice must be known.

7.4 Conclusions

In this chapter, structural stability of four seeds of the diamond D_5 and several substructures/fragments related to the D_5 diamond were investigated. In the first case, it was evaluated both in static and dynamic temperature conditions by molecular dynamics (MD). During MD, the all-carbon C_{17} appeared the most resistant to changes in temperature. Structural and energetic stability of the other three seeds of D_5 vary both with the values of temperature and evolution time in molecular dynamics and the arrangement of oxygen atoms in the molecules. Among all the studied structures, the D_2 isomer is the most sensitive to changes in temperature. After optimization by B3LYP, D_1 isomer seemed to be the most stable one. The structure stability of D_1 and P_1 isomers in MD are similar. These two isomers are only slightly more sensitive to temperature as compared with the all-carbon C_{17}.

Other substructures/fragments related to the D_5 diamond (and its relative L5 lonsdaleite) were constructed and investigated for stability, by both static PM3 calculation and molecular dynamics simulation procedures as well. The results show a good stability of several hyper-rings made from the small fullerenes C_{20} and C_{28}, modulated function of the central hollow, and the type consisting of small cages. At normal temperature, the hexagonal hyper-rings are more stable (as given by PM3 data), while at higher temperature, the pentagonal ones appear more stable, at least as isolated fragments. The substructures belonging to D_5 and L_5 showed a pertinent stability, possibly increased in the infinite corresponding lattice. The actual study employed the molecular dynamics simulation in finding the temperature limits for the most important events in a molecule: changes in topology and next its destruction.

These results could be useful in guiding further reactions, e.g., the dimerization to C_{34} and condensation to adamantane-like structures, finally leading to the diamond D_5 or, in general, in the design and synthesis of new strong structures, with possible applications in nanotechnology.

References

Abell G (1985) Empirical chemical pseudopotential theory of molecular and metallic bonding. Phys Rev B 31:6184–6196

Aleksenskiĭ AE, Baĭdakova MV, Vul AY, Davydov VY, Pevtsova YA (1997) Diamond-graphite phase transition in ultradisperse-diamond clusters. Phys Solid State 39:1007–1015

Aste T, Weaire D (2008) The pursuit of perfect packing, 2nd edn. Taylor & Francis, London
Blasé X, Benedek G, Bernasconi M (2010) Structural, mechanical and supraconducting properties of clathrates. In: Colombo L, Fasolino A (eds) Computer-based modeling of novel carbon systems and their properties. Beyond nanotubes. Springer, Dordrecht, Chapter 6, pp 171–206
Brenner D (1990) Empirical potential for hydrocarbons for use in simulating the chemical vapor deposition of diamond films. Phys Rev B 42:9458–9471
Brenner D (1992) Empirical potential for hydrocarbons for use in simulating the chemical vapor deposition of diamond films. Phys Rev B 46:1948–1992
Brenner DW (2000) The art and science of an analytic potential. Phys Stat Sol 217:23–40
Brenner DW, Shenderova OA, Harrison JA, Stuart SJ, Ni B, Sinnott SB (2000) Second generation reactive empirical bond order (REBO) potential energy expression for hydrocarbons. J Phys Condens Matter 14:783–802
Case DA, Cheatham TE III, Darden T, Gohlke H, Luo R, Merz KM, Onufriev AJ, Simmerling C, Wang B, Woods R (2005) The Amber biomolecular simulation programs. J Comput Chem 26:1668–1688
Decarli PS, Jamieson JC (1961) Formation of diamond by explosive shock. Science 133: 1821–1822
Delgado-Friedrichs O, Foster MD, O'Keeffe M, Proserpio DM, Treacy MMJ, Yaghi OM (2005) What do we know about three-periodic nets? J Solid State Chem 178:2533–2554
Diudea MV (ed) (2005) Nanostructures, novel architecture. NOVA, New York
Diudea MV (2010a) Diamond D_5, a novel allotrope of carbon. Studia Univ Babes-Bolyai Chemia 55(4):11–17
Diudea MV (2010b) Nanomolecules and nanostructures – polynomials and indices. University of Kragujevac, Kragujevac
Diudea MV, Ilić A (2011) All-pentagonal face multi tori. J Comput Theor Nanosci 8:736–739
Diudea MV, Nagy CL (2007) Periodic nanostructures. Springer, Dordrecht
Diudea MV, Petitjean M (2008) Symmetry in multi tori. Symmetry Cult Sci 19(4):285–305
Diudea MV, Bende A, Janežič D (2010) Omega polynomial in diamond-like networks. Fuller Nanotub Carbon Nanostruct 18:236–243
Dubrovinskaia N, Dub S, Dubrovinsky L (2006) Superior wear resistance of aggregated diamond nanorods. Nano Lett 6:824–826
Eaton PE (1979) Towards dodecahedrane. Tetrahedron 35(19):2189–2223
Frondel C, Marvin UB (1967) Lonsdaleite a hexagonal polymorph of diamond. Nature 214: 587–589
Gaussian 09 (2009) Revision A.1, Frisch MJ, Trucks GW, Schlegel HB, Scuseria GE, Robb MA, Cheeseman JR, Scalmani G, Barone V, Mennucci B, Petersson GA, Nakatsuji H, Caricato M, Li X, Hratchian HP, Izmaylov AF, Bloino J, Zheng G, Sonnenberg JL, Hada M, Ehara M, Toyota K, Fukuda R, Hasegawa J, Ishida M, Nakajima T, Honda Y, Kitao O, Nakai H, Vreven T, Montgomery JA, Peralta JE, Ogliaro F, Bearpark M, Heyd JJ, Brothers E, Kudin KN, Staroverov VN, Kobayashi R, Normand J, Raghavachari K, Rendell A, Burant JC, Iyengar SS, Tomasi J, Cossi M, Rega N, Millam NJ, Klene M, Knox JE, Cross JB, Bakken V, Adamo C, Jaramillo J, Gomperts R, Stratmann RE, Yazyev O, Austin AJ, Cammi R, Pomelli C, Ochterski JW, Martin RL, Morokuma K, Zakrzewski VG, Voth GA, Salvador P, Dannenberg JJ, Dapprich S, Daniels AD, Farkas Ö, Foresman JB, Ortiz JV, Cioslowski J, Fox DJ, Gaussian Inc, Wallingford
Gestmann D, Kuck D, Pritzkow H (2006) Partially benzoannelated centro-hexaquinanes: oxidative degradation of centropolyindanes by using ruthenium (VIII) oxide and ozone. Liebigs Ann 1996:1349–1359
Gund P, Gund TM (1981) How many rings can share a quaternary atom? J Am Chem Soc 103:4458–4465
Hyde ST, Keeffe MO, Proserpio DM (2008) A short history of an elusive yet ubiquitous structure in chemistry, materials, and mathematics. Angew Chem Int Ed 47:7996–8000

Khachatryan AK, Aloyan SG, May PW, Sargsyan R, Khachatryan VA, Baghdasaryan VS (2008) Graphite-to-diamond transformation induced by ultrasound cavitation. Diam Relat Mater 17:931–936

Kuck D (1984) A facile route to benzoannelated centrotriquinanes. Angew Chem Int Ed 23: 508–509

Kuck D (2006) Three-dimensional hydrocarbon cores based on multiply fused cyclopentane and indane units: centropolyindanes. Chem Rev 106:4885–4925

Kuck D, Schuster A, Paisdor B, Gestmann D (1995) Benzoannelated centropolyquinanes. Part 21. Centrohexaindane: three complementary syntheses of the highest member of the centropolyindane family. J Chem Soc Perkin Trans 1 Org Bio-Org Chem 6:721–732

Kyani A, Diudea MV (2012) Molecular dynamics simulation study on the diamond D_5 substructures. Central Eur J Chem 10(4):1028–1033

Osawa E (2007) Recent progress and perspectives in single-digit nanodiamond. Diam Relat Mater 16:2018–2022

Osawa E (2008) Monodisperse single nanodiamond particulates. Pure Appl Chem 80:1365–1379

Paquette LA, Balogh DW, Usha R, Kountz D, Christoph GG (1981) Crystal and molecular structure of a pentagonal dodecahedrane. Science 211:575–576

Paquette LA, Vazeux M (1981) Threefold transannular epoxide cyclization: synthesis of a heterocyclic C_{17}-hexaquinane. Tetrahedron Lett 22:291–294

Plimpton SJ (1995) Fast parallel algorithms for short-range molecular dynamics. Comp Phys 117:1–19

Prinzbach H, Wahl F, Weiler A, Landenberger P, Wörth J, Scott LT, Gelmont M, Olevano D, Sommer F, Bv I (2006) C_{20} carbon clusters: fullerene-boat-sheet generation, mass selection, photoelectron characterization. Chem Eur J 12:6268–6280

Rafii-Tabar H (2004) Computational modelling of the thermo-mechanical and transport properties of carbon nanotubes. Phys Rep 390:235–452

Ruoff R, Qian D, Liu W (2003) Mechanical properties of carbon nanotubes: theoretical predictions and experimental measurements. C R Phys 4:993–1008

Saito M, Miyamoto Y (2001) Theoretical identification of the smallest fullerene, C_{20}. Phys Rev Lett 87:035503

Simmons HE III, Maggio JE (1981) Synthesis of the first topologically non-planar molecule. Tetrahedron Lett 22:287–290

Stuart SJ, Tutein AB, Harrison JA (2000) A reactive potential for hydrocarbons with intermolecular interactions. J Chem Phys 112:6472–6486

Szefler B, Diudea MV (2012) On molecular dynamics of the diamond D5 seeds. Struct Chem 23(3):717–722

Tersoff J (1988a) New empirical approach for the structure and energy of covalent systems. Phys Rev B 37:6991–7000

Tersoff J (1988b) Empirical interatomic potential for carbon, with applications to amorphous carbon. Phys Rev Lett 61:2879–2882

Verlet L (1967) Computer "experiments" on classical fluids. I. Thermodynamical properties of Lennard-Jones molecules. Phys Rev 159:98–103

Verlet L (1968) Computer "experiments" on classical fluids II. Equilibrium correlation functions. Phys Rev 165:201–214

Wang J, Cieplak P, Kollman PA (2000) How well does a restrained electrostatic potential (RESP) model perform in calculating conformational energies of organic and biological molecules? J Comput Chem 21:1049–1074

Wang J, Wolf RM, Caldwell JW, Kollamn PA, Case DA (2004) Development and testing of a general amber force field. J Comput Chem 25:1157–1174

Williams OA, Douhéret O, Daenen M, Haenen K, Osawa E, Takahashi M (2007) Enhanced diamond nucleation on monodispersed nanocrystalline diamond. Chem Phys Lett 445:255–258

Chapter 8
P-Type and Related Networks: Design, Energetics, and Topology

Mahboubeh Saheli, Katalin Nagy, Beata Szefler, Virginia Bucila, and Mircea V. Diudea

Abstract A P-type network is an embedding of an sp^2 carbon net in a triply periodic minimal surface with the symmetry of uninodal simple cubic Bravais lattice. Construction of P-type and some related networks, by using map operations, is described. The stability of the repeating units and some small domains of these networks are discussed in terms of single-point total energy, and HOMO-LUMO gap computed, on the optimized, hydrogenated species, at the Hartree-Fock level of theory. Their topology is described in terms of Omega polynomial.

8.1 Introduction to P-Type Networks

A triply periodic minimal surface TPMS possesses a translational symmetry in three independent directions. It belongs to one of the 230 symmetry groups of the Euclidean space. If no self-intersections, it partitions the space into two disjoint labyrinthine regions. A carbon lattice, having all sp^2 atoms, can be embedded in a TPMS, with a negative (saddle-shaped) Gaussian curvature. Such carbon allotropes are called (periodic) schwarzites (Terrones and Mackay 1997; Benedek et al. 2003). P-type schwarzites represent decorations of the uninodal simple cubic Bravais

M. Saheli
Department of Mathematics, University of Kashan, Kashan 87317-51167, I.R. Iran
e-mail: mahboubeh.saheli@gmail.com

K. Nagy (✉) • V. Bucila • M.V. Diudea
Department of Chemistry, Faculty of Chemistry and Chemical Engineering, Babes-Bolyai University, 400028 Cluj, Romania
e-mail: knagy@chem.ubbcluj.ro; diudea@chem.ubbcluj.ro

B. Szefler
Department of Physical Chemistry, Collegium Medicum, Nicolaus Copernicus University, Kurpińskiego 5, 85-950 Bydgoszcz, Poland
e-mail: beata.szefler@cm.umk.pl

M.V. Diudea and C.L. Nagy (eds.), *Diamond and Related Nanostructures*, Carbon Materials: Chemistry and Physics 6, DOI 10.1007/978-94-007-6371-5_8,

lattice. The P-type surface can be decorated with a variety of (repeating) patches in addition to a number of polygonal faces larger than the hexagon, needed to produce the negative Gaussian curvature.

An example of decorated P-type surface is the embedding of (7,3) tessellation, also called Klein tessellation (Klein 1884, 1923; Ceulemans et al. 1999). It can be achieved by applying one of the two septupling map operations on the Cube, $Op(S_1(C))$ and $Op_{2a}(S_2(C))$ (Diudea 2005, 2010a). The P-(7,3) network was registered in the Topos system by Benedek: *kgn* net, space group *P*432, point symbol for net: (7^3); trinodal 3,3,3-c net, with stoichiometry (3-c)(3-c)3(3-c)3.

Another famous tessellation of the P-surface is the P-(8,3) network, known as the Dyck tessellation (Dyck 1880; Ceulemans et al. 1999); it was registered by Topo Group Cluj: diu8 = CQOp2a, group *Fm*-3*c*, point symbol for net: (8^3), 3,3-c net with stoichiometry (3-c)3(3-c); 2-nodal net.

Some experiments inferred that junctions of carbon nanotubes can be obtained by "nano-welding" of crossing tubes in an electron beam (Terrones et al. 2002). The porosity of the spongy carbon could be explained by the presence of such nanotube junctions (Benedek et al. 2003; Diudea and Nagy 2007).

Lattices of this type have been modeled by Mackay and Terrones (1991), Lenosky et al. (1992), Terrones and Mackay (1997), Vanderbilt and Tersoff (1992), and O'Keeffe et al. (1992).

Within this chapter, P-type networks and some related, by their map operation design, hypothetical or real structures are described about their energetics and topology, in terms of Hartree-Fock calculations and Omega polynomial, respectively. All the crystallographic data herein presented have been provided by Professor Davide Proserpio, University of Milan, Italy, and one of the co-authors (Virginia Bucila).

8.2 Omega Polynomial

A counting polynomial (Diudea 2010a, b) is a representation of a graph $G(V,E)$, with the exponent k showing the extent of partitions $p(G)$, $\cup p(G) = P(G)$ of a graph property $P(G)$, while the coefficient $p(k)$ is related to the number of partitions of extent k:

$$P(x) = \sum_k p(k) \cdot x^k \tag{8.1}$$

Let G be a connected graph, with the vertex set $V(G)$ and edge set $E(G)$. Two edges $e = (u,v)$ and $f = (x,y)$ of G are said to be *codistant* (briefly: $e\ co\ f$) if they fulfill the relation (John et al. 2007)

$$d(v,x) = d(v,y) + 1 = d(u,x) + 1 = d(u,y) \tag{8.2}$$

where d is the usual shortest-path distance function. The above relation *co* is reflexive (e *co* e) and symmetric (e *co* f) for any edge e of G but in general is not transitive. A graph is called a *co-graph* if the relation *co* is also transitive and thus an equivalence relation.

Let $C(e) := \{f \in E(G);\ f\ co\ e\}$ be the set of edges in G, codistant to $e \in E(G)$. The set $C(e)$ can be obtained by an orthogonal edge-cutting procedure: take a straight line segment, orthogonal to the edge e, and intersect it and all other edges (of a polygonal plane graph) parallel to e. The set of these intersections is called an *orthogonal cut* (*oc* for short) of G, with respect to e. If G is a *co-graph*, then its orthogonal cuts $C_1, C_2, \ldots, C_k$ form a partition of $E(G)$: $E(G) = C_1 \cup C_2 \cup \cdots \cup C_k$, $C_i \cap C_j = \emptyset$, $i \neq j$.

A subgraph $H \subseteq G$ is called *isometric*, if $d_H(u, v) = d_G(u, v)$, for any $(u, v) \in H$; it is *convex* if any shortest path in G between vertices of H belongs to H. The relation *co* is related to $\sim$ (Djoković 1973) and Θ (Winkler 1984) relations (Klavžar 2008; Diudea and Klavžar 2010).

Two edges e and f of a plane graph G are in relation *opposite, e op f,* if they are opposite edges of an inner face of G. Then e *co* f holds by the assumption that faces are isometric. The relation *co* is defined in the whole graph while *op* is defined only in faces/rings. Note that John et al. (2007) implicitly used the "*op*" relation in defining the Cluj-Ilmenau index *CI*. Relation *op* will partition the edges set of G into *opposite* edge *strips ops*, as follows: (1) Any two subsequent edges of an *ops* are in *op* relation; (2) any three subsequent edges of such a strip belong to adjacent faces; (3) in a plane graph, the inner dual of an *ops* is a path, an open or a closed one (however, in 3D networks, the ring/face interchanging will provide *ops* which are no more paths); and (4) the *ops* is taken as maximum possible, irrespective of the starting edge. The choice about the maximum size of face/ring, and the face/ring mode counting, will decide the length of the strip. Note that *ops* are *qoc* (quasi orthogonal cuts), meaning the transitivity relation is, in general, not obeyed.

The Omega polynomial $\Omega(x)$ (Diudea 2006; Diudea et al. 2008, 2009) is defined on the ground of opposite edge strips *ops* $S_1, S_2, \ldots, S_k$ in the graph. Denoting by m, the number of *ops* of cardinality/length $s = |S|$, then we can write

$$\Omega(x) = \sum_s m \cdot x^s \tag{8.3}$$

The first derivative (in $x = 1$) can be taken as a graph invariant or a topological index:

$$\Omega'(1) = \sum_s m \cdot s = |E(G)| \tag{8.4}$$

An index, called Cluj-Ilmenau CI(G), was defined on $\Omega(x)$:

$$\mathrm{CI}(G) = \left\{[\Omega'(1)]^2 - [\Omega'(1) + \Omega''(1)]\right\} \tag{8.5}$$

In tree graphs, the Omega polynomial simply counts the non-opposite edges, being included in the term of exponent $s = 1$.

On the ground of strips s, the Sadhana polynomial (Ashrafi et al. 2008) and corresponding index (Khadikar et al. 2002, 2004) can be defined:

$$Sd(x) = \sum_s m \cdot x^{e-s} \tag{8.6}$$

$$\mathrm{Sd}'(G,1) = \sum_s m \cdot (e-s) = \mathrm{Sd}(G) \tag{8.7}$$

Omega polynomial was thought to describe the covering of polyhedral nanostructures or the tiling of crystal-like lattices, as a complementary description of the crystallographic one.

8.3 Crystal Networks Designed by Leapfrog and Chamfering

In this section, we present four infinitely periodic networks, of which repeating units can be designed by applying leapfrog *Le* and chamfering *Q* map operations (Diudea 2004, 2005; Diudea et al. 2003, 2005, 2006, 2011, also Chap. 19, this book) on the Cube C. The units are the small cages C_{24} and C_{32}, with vertex symbol (4.6^2) and $(4.6^2)(6^3)$, respectively.

The lattice CLe_4 (Fig. 8.1) is a triple periodic net built up from $C_{24} = CLe\_24$, by identifying the (4,4) faces. It is the well-known sodalite *sod* net, a uninodal 4-c net, belonging to the *Im*-3*m* group and having the net symbol $(4^2.6^4)$ and topological type sod/SOD; 4/4/c1; sqc970 (www.Topos). Note the repeating unit CLe_24 is just the truncated Octahedron.

Applying the chamfering *Q* operation on the Cube results in the repeating unit CQ_32. Next, by identifying (4,4), (4,6), or (6,6) faces it results in different

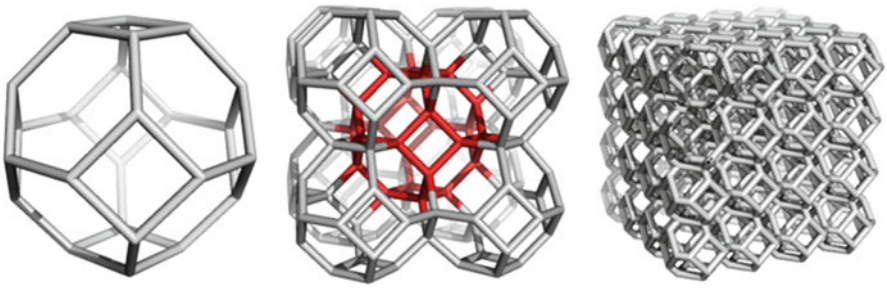

Fig. 8.1 $CLe_4 =$ *sod*, a triple periodic lattice, belonging to the *Im*-3*m* group, designed by Le(C) and identifying (4,4) faces: the unit CLe_24 (vertex symbol 4.6^2) (*left*) and two cubic domains of the net, 2,2,2_144 (*middle*) and 4,4,4_960 (*right*); the last number counts the atoms in a given domain

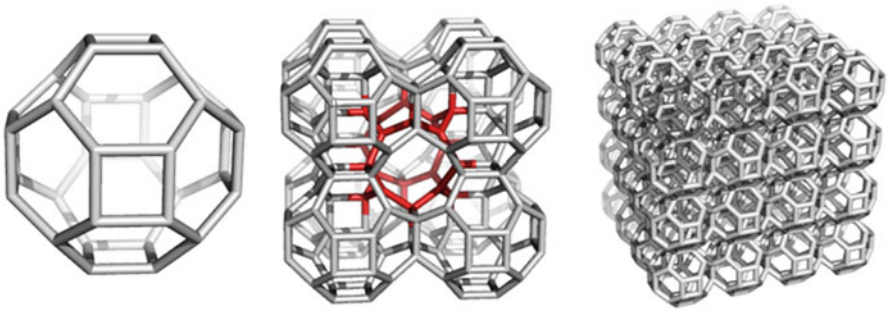

Fig. 8.2 $CQ_4 = tfg$, sqc9223, group *Pm*-3*m*, a triple periodic lattice designed by *Q*(C) and identifying (4,4) faces: the unit CQ_32, vertex symbol $(4.6^2)(6^3)$ (*left*), and two cubic domains, 2,2,2_208 (*middle*) and 4,4,4_1472 (*right*)

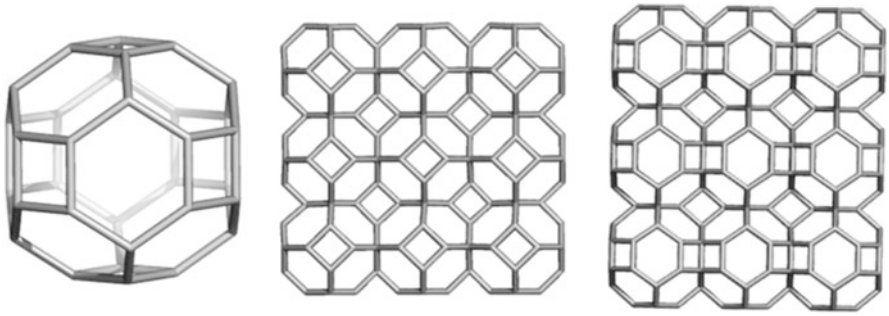

Fig. 8.3 $CQ_{4,6}$ = sqc8121, group *P*4/*mmm*, a triple periodic net designed by *Q*(C(*a*,*b*,*c*)) and identifying (4,6) faces: the unit CQ_32 (*left*) and two cubic domains, 3,3,3_576 (**a**) (*middle*) and 3,3,3_576 (**b**, **c**) (*right*)

networks: CQ_4, $CQ_{4,6}$, or CQ_6; even the starting object is one and the same. Figure 8.2 shows the net CQ_4 (known as *tfg* or sqc9223), a triple periodic 2-nodal lattice of the group *Pm*-3*m* (http://epinet.anu.edu.au); its net point symbol is $(4.6^4.8)3(6^3)2$, 3,4-c net with stoichiometry (3-c)2(4-c)3.

The net $CQ_{4,6}$ (Fig. 8.3) is a 3-nodal 4,4,4-c net of the group *P*4/*mmm*, with stoichiometry (4-c)2(4-c)(4-c) and point symbol for net: $(4.6^5)(4^2.6^4)(4^3.6^3)2$. Its topological specification is sqc8121 (epinet.anu.edu.au).

Finally, the net CQ_6 (Fig. 8.4) is also known as *ast* net, group *Fm*-3*m*; it is a triple periodic 4,4-c, 2-nodal net, built up by identifying (6,6) faces of C_{32} unit. The point symbol for net is $(4^3.6^3)4(6^6)$ and stoichiometry (4-c)4(4-c); its topological type is: ast/octadecasil/AST; sqc3869.

Analytical formulas to calculate the Omega polynomial were developed for either incomplete (*a*,*b*,*c*), $a \geq b \geq c$ or complete (*a*,*a*,*a*) cubic domains; other net parameters like number of vertices, edges, and rings are given, function of *a* that is the number of repeating units on one direction in a cubic domain (Diudea et al. 2011).

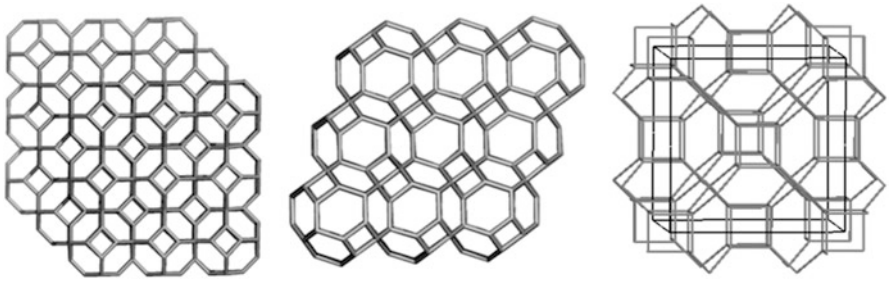

Fig. 8.4 CQ_6 net = ast, group *Fm*-3*m*, a triple periodic net designed by *Q*(C) and identifying f_6 faces: DP_333_492 domain (*left*); TP_333_484 domain (*middle*) and the unit cell (*right*) (Saheli et al. 2012)

Net	Formulas
$G = CLe_4(a,b,c)$; $a \geq b \geq c$:	
$\Omega(G,X) = 4\sum_{i=1}^{c-1} X^{4ai+2i} + 2(b-c+1)X^{(4a+2)c}$	
	$+ 4\sum_{i=1}^{c-1} X^{4bi+2i} + 2(a-c+1)X^{(4b+2)c}$
	$+ 4\sum_{i=1}^{b-1} X^{4ci+2i} + 2(a-b+1)X^{(4c+2)b}$
$G = CLe_4$ (a,a,a):	
$\Omega(G,X) = 12\sum_{i=1}^{a-1} X^{2i(2a+1)} + 6X^{2a(2a+1)}$	
$\Omega'(G,1) = 12a^2(2a+1)$	
$G = CQ_4(a,b,c)$; $a \geq b \geq c$:	
$\Omega(G,X) = 4abcX^6 + aX^{4bc+2b+2c} + bX^{4ac+2a+2c} + cX^{4ab+2a+2b}$	
$G = CQ_4$ (a,a,a):	
$\Omega(G,X) = 4a^3X^6 + 3aX^{4a(a+1)}$	
$\Omega'(G,1) = 12a^2(3a+1) = e(G) = \lvert E(G)\rvert$	
$v(G) = \lvert V(CQ_4)\rvert = 4a^2(3+5a)$	
$R_4 = 3a^2(1+3a)$; $R_6 = 12a^3$	
$G = CQ_{4,6}(a,b,c)$; $a \geq b \geq c$:	
$\Omega(G,X) = 4\sum_{i=1}^{b-1} X^{2(3c+1)i} + 2(a-b+1)X^{2(3c+1)b}$	
	$+ 4\sum_{i=1}^{c-1} X^{2(2a+1)i} + 2(b-c+1)X^{2(2a+1)c}$
	$+ 4\sum_{i=1}^{c-1} X^{2(2b+1)i} + 2(a-c+1)X^{2(2b+1)c} + cX^{4ab+2a+2b}$
$G = CQ_{4,6}$ (a,a,a):	

(continued)

(continued)

Net	Formulas
	$\Omega(G,X)=4\sum_{i=1}^{a-1} X^{2i(3a+1)}+8\sum_{i=1}^{a-1} X^{2i(2a+1)}+2X^{2a(3a+1)}+4X^{2a(2a+1)}+aX^{4a(a+1)}$
	$\Omega'(G,1)=16a^2(2a+1)=e(G)=\lvert E(G)\rvert$
	$v(G)=\lvert V(\mathrm{CQ}_{4,6})\rvert=16a^2(1+a)$
	$R_4=a(4-7a+9a^2)$; $R_6=2a(2-3a+7a^2)$
	$G=\mathrm{CQ}_6$ (a,a,a) DP:
	$\Omega(x)=2\left[\sum_{i=1}^{a-1} x^{(2a-2)+(4a+4)i}+\sum_{i=1}^{a} x^{2i^2+6i}+2\sum_{i=1}^{a-1} x^{2a+(2a+2)i}+\sum_{i=1}^{\frac{2a-7-(-1)^a}{4}a} x^{(2a^2+6a)+4(a-1-i)i}\right]+(2a+2)\,x^{2a(a+2)}+a\,x^{4a(a+1)}+\frac{3+(-1)^a}{2}\,x^{\left(3a^2+4a+\frac{1-(-1)^a}{2}\right)}+1\,x^{4a^2+6a-2}$
	$\mathrm{CI}(G)=400a^6+\frac{7,756}{5}a^5+\frac{2,648}{3}a^4-\frac{3,532}{3}a^3+\frac{2,384}{6}a^2-\frac{1,408}{15}a+8$
	$e(G)=\lvert E(G)\rvert=\Omega'(G,1)=20a^3+40a^2-14a+2$
	$v(G)=\lvert \mathrm{V(CQ6\_DP)}\rvert=10a^3+26a^2-4a$
	$R(4)=6a^3+20a^2+18a+6$; $R(6)=10a^3+36a^2+33a+12$
	$\mathrm{G}=\mathrm{CQ}_6$ (a,a,a) TP:
	$\Omega(x)=2\left[\sum_{i=1}^{a} x^{i^2+4i+1}+3\sum_{i=1}^{a-1} x^{2a+(4a+2)i}+\sum_{i=1}^{\frac{2a-7-(-1)^a}{4}} x^{a^2+4a+1+2(a-1)i-2i^2}\right]+\frac{3+(-1)^a}{2}x^{\frac{6a^2+12a+5-(-1)^a}{4}}+3ax^{2a(a+2)}+3x^{4a(a+1)}$
	$\mathrm{CI}(G)=400a^6+\frac{6,969}{5}a^5+917a^4-650a^3-116a^2+\frac{86}{5}a+6$
	$e(G)=\lvert E(G)\rvert=\Omega'(G,1)=20a^3+36a^2-6a-2$
	$v(G)=\lvert \mathrm{V(CQ6\_TP)}\rvert=10\mathrm{a}^3+24a^2-2$
	$R(4)=6\mathrm{a}^3$; $R(6)=10\mathrm{a}^3+3a^2-3a+2$

Data in this section refer to $R_{\max}$[6]. If faces instead of rings are considered, the polynomial is different. Data were calculated by the original program Nano Studio (Nagy and Diudea 2009) developed at the Topo Group Cluj. Examples are given for each discussed lattice, both for polynomials and indices, in Tables 8.1, 8.2, 8.3, 8.4, 8.5, and 8.6.

Table 8.1 Examples for $CLe_4(a,b,c)$ lattice

$CLe_4(a,b,c)$_atoms	Omega polynomial	CI_Index
111_24	$6x^6$	1,080
222_144	$12x^{10} + 6x^{20}$	54,000
422_272	$4x^{10} + 4x^{14} + 4x^{18} + 6x^{20} + 6x^{28} + 2x^{36} + 2x^{44}$	363,408
442_512	$4x^{14} + 8x^{18} + 4x^{28} + 12x^{36} + 4x^{42} + 2x^{56} + 2x^{80}$	1,353,664
444_960	$12x^{18} + 12x^{36} + 12x^{54} + 6x^{72}$	2,900,448
	Sadhana polynomial	Sd_Index
111_24	$6x^{30}$	180
222_144	$6x^{220} + 12x^{230}$	4,080
422_272	$2x^{572} + 2x^{580} + 6x^{588} + 6x^{596} + 4x^{598} + 4x^{602} + 4x^{606}$	16,632
442_512	$2x^{1104} + 2x^{1128} + 4x^{1142} + 12x^{1148} + 4x^{1156} + 8x^{1166} + 4x^{1170}$	41,440
444_960	$6x^{1656} + 12x^{1674} + 12x^{1692} + 12x^{1710}$	70,848

Table 8.2 Examples for $CQ_4(a,b,c)$ lattice

$CQ_4(a,b,c)$_atoms	Omega polynomial		CI_Index
111_32	$4x^6 + 3x^8$		1,968
222_208	$32x^6 + 6x^{24}$		108,288
331_240	$36x^6 + 6x^{20} + 1x^{48}$		141,456
332_444	$72x^6 + 6x^{34} + 2x^{48}$		521,688
333_648	$108x^6 + 9x^{48}$		1,141,776
444_1472	$256x^6 + 12x^{80}$		6,144,000
	Sadhana polynomial		Sd_Index
111_32	$3x^{40} + 4x^{42}$		288
222_208	$6x^{312} + 32x^{330}$		12,432
331_240	$x^{336} + 6x^{364} + 36x^{378}$		16,128
332_444	$2x^{684} + 6x^{698} + 72x^{726}$		57,828
333_648	$9x^{1032} + 108x^{1074}$		125,280
444_1472	$12x^{2416} + 256x^{2490}$		666,432
CQ_4 (a,a,a)	e(G)	$v(G)$	CI_Index
111	48	32	1,968
222	336	208	108,288
333	1,080	648	1,141,776
444	2,496	1, 472	6,144,000

8.3.1 Quantum Computations on CQ_6_DP/TP Networks

With the aim of giving a rational support to our topological investigation, we performed quantum calculations at Hartree-Fock (HF) level of theory on some small hydrocarbon precursors of CQ_6 network. The structures were optimized with the set HF/6-31G**, on totally hydrogenated structures (in the aim of preserving the sp^3 hybridization of C atoms, as in the infinite network) in gas phase by Gaussian 09 (2009). The single-point energy minima obtained for the investigated structures

Table 8.3 Examples for $CQ_{4,6}(a,b,c)$ lattice

$CQ_{4,6}(C(a,b,c))$_atoms	Omega polynomial	CI_Index
222_192	$8x^{10} + 4x^{14} + 4x^{20} + 2x^{24} + 2x^{28}$	96,496
422_360	$4x^{10} + 4x^{14} + 4x^{18} + 6x^{20} + 6x^{28} + 2x^{36} + 2x^{44}$	363,408
442_672	$4x^{14} + 8x^{18} + 4x^{28} + 12x^{36} + 4x^{42} + 2x^{56} + 2x^{80}$	1,353,664
444_1280	$8x^{18} + 4x^{26} + 8x^{36} + 4x^{52} + 8x^{54} + 4x^{72} + 4x^{78} + 4x^{80} + 2x^{104}$	5,166,304
	Sadhana polynomial	Sd_Index
222_192	$2x^{292} + 2x^{296} + 4x^{300} + 4x^{306} + 8x^{310}$	6,080
422_360	$2x^{572} + 2x^{580} + 6x^{588} + 6x^{596} + 4x^{598} + 4x^{602} + 4x^{606}$	16,632
442_672	$2x^{1104} + 2x^{1128} + 4x^{1142} + 12x^{1148} + 4x^{1156} + 8x^{1166} + 4x^{1170}$	41,440
444_1280	$2x^{2200} + 4x^{2224} + 4x^{2226} + 4x^{2232} + 8x^{2250} + 4x^{2252} + 8x^{2268} + 4x^{2278} + 8x^{2286}$	103,680

$CQ_{4,6}$			
111	48	32	1,968
222	320	192	96,496
333	1,008	576	979,056
444	2,304	1,280	5,166,304

Table 8.4 Examples for $CQ_6(a,a,a)$ _DP lattice

a	Omega polynomial: examples	e(G)	v(G)	CI(G)
2	$2x^8 + 4x^{10} + 2x^{14} + 6x^{16} + 2x^{20} + 2x^{24} + 1x^{26}$	294	176	81,352
3	$2x^8 + 4x^{14} + 4x^{20} + 4x^{22} + 8x^{30} + 4x^{36} + 1x^{40} + 3x^{48} + 1x^{52}$	860	492	711,552
4	$2x^8 + 4x^{18} + 2x^{20} + 2x^{26} + 4x^{28} + 2x^{36} + 4x^{38} + 2x^{46} + 10x^{48} + 2x^{56} + 2x^{64} + 2x^{66} + 4x^{80} + 1x^{86}$	1,866	1,040	3,383,432
5	$2x^8 + 2x^{20} + 4x^{22} + 2x^{32} + 4x^{34} + 2x^{36} + 4x^{46} + 4x^{56} + 4x^{58} + 12x^{70} + 4x^{80} + 2x^{92} + 1x^{96} + 2x^{104} + 5x^{120} + 1x^{128}$	3,432	1,880	11,511,472
6	$2x^8 + 2x^{20} + 4x^{26} + 2x^{36} + 2x^{38} + 4x^{40} + 4x^{54} + 2x^{56} + 2x^{66} + 4x^{68} + 2x^{80} + 4x^{82} + 2x^{94} + 14x^{96} + 2x^{108} + 2x^{122} + 2x^{124} + 2x^{132} + 2x^{150} + 6x^{168} + 1x^{178}$	5,678	3,072	31,627,912

are shown in Table 8.7. The C_{60} structure was added as the reference structure in nanoscience, even no direct comparison can be made between non-hydrogenated and hydrogenated structures. Clearly, these structures appear passivated by hydrogenation. Such a stabilization procedure can be done in real experiments in view of performing a synthesis of CQ_6 crystals (Saheli et al. 2012).

Table 8.5 Examples for $CQ_6(a,a,a)$_TP lattice

a	Omega polynomial: examples	e(G)	v(G)	CI(G)
2	$2x^6 + 2x^{13} + 6x^{14} + 6x^{16} + 3x^{24}$	290	174	79,250
3	$2x^6 + 2x^{13} + 6x^{20} + 2x^{22} + 1x^{24} + 9x^{30} + 6x^{34} + 3x^{48}$	844	484	686,034
4	$2x^6 + 2x^{13} + 2x^{22} + 6x^{26} + 2x^{33} + 2x^{37} + 6x^{44} + 12x^{48} + 6x^{62} + 3x^{80}$	1,830	1,022	3,257,022
5	$2x^6 + 2x^{13} + 2x^{22} + 6x^{32} + 2x^{33} + 2x^{46} + 2x^{52} + 7x^{54} + 15x^{70} + 6x^{76} + 6x^{98} + 3x^{120}$	3,368	1,848	11,094,692
6	$2x^6 + 2x^{13} + 2x^{22} + 2x^{33} + 6x^{38} + 2x^{46} + 2x^{61} + 6x^{64} + 2x^{69} + 2x^{73} + 6x^{90} + 18x^{96} + 6x^{116} + 6x^{142} + 3x^{168}$	5,578	3,022	30,544,554

Table 8.6 Number of rings in CQ_6_DP and CQ_6_TP networks

	CQ_6_DP		CQ_6_TP	
a	R[4]	R[6]	R[4]	R[6]
2	50	91	48	88
3	170	302	162	290
4	402	705	384	678
5	782	1, 360	750	1, 312
6	1, 346	2, 327	1, 296	2, 252

Table 8.7 Quantum calculations on some small precursors of CQ_6_DP/TP networks

	Structure	E_{HF} (au)	E_{HF}/C (au)	HL gap (eV)
1	CQ_6_111_32 = C_{32}	−1,230.158	−38.442	13.214
2	CQ_6_222_176_DP	−6,729.831	−38.238	11.864
3	CQ_6_222_174_TP	−6,654.016	−38.241	11.932
4	C_{60}	−2,271.830	−37.864	7.418

8.4 Lattices Built Up by *Op*(*Trs*(*P*$_4$(*Oct*)))

The lattices below are constructed by using the units designed with the sequence *Op*(*Trs*(P_4(*Oct*))), where Oct is the Octahedron. The net in the top row of Fig. 8.5 was made by identifying ("Id"-net) the opposite faces of non-optimized units, thus appearing as a more "mathematical" network. The net in the bottom of this figure is realized by joining ("Jn"-net) energetically optimized structures, the net being a more "chemical" one (Diudea and Ilić 2010). These networks show only hexagonal faces/rings and have large hollows, as those encountered in zeolites, natural alumino-silicates widely used in synthetic chemistry as catalysts.

Omega polynomial was evaluated on a cubic domain, the analytical formulas being listed below. Examples are given in Tables 8.8 and 8.9.

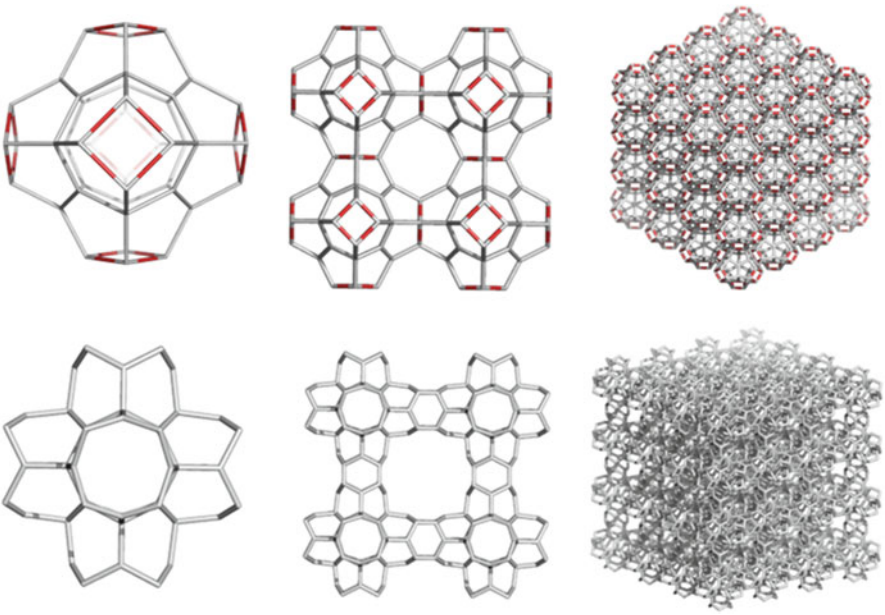

Fig. 8.5 *Top row*: Unit designed by $Op(Trs(P_4(Oct)))$ and the net constructed by identifying ("Id"-net) the opposite faces of non-optimized units, thus being a "mathematical" network. *Bottom row*: a more "chemical" network constructed by joining ("Jn"-net) the energetically optimized units; the right column shows these hypothetical networks in the corner view of a cubic domain *a*,*a*,*a* where *a* is the number of repeating units on a given dimension of 3D space

Table 8.8 Examples of Omega polynomial in *Op*(*Trs*(*P*4(Oct)))_*Id* crystal-like network

a	Omega polynomial; $R_{\max}[6]$	*v*	*e*	CI
1	$24x^3 + 6x^4$	68	96	8,904
2	$48x^3 + 48x^4 + 48x^5 + 12x^8$	448	672	448,416
3	$72x^3 + 162x^4 + 144x^5 + 72x^8$	1,404	2,160	4,654,152
4	$96x^3 + 384x^4 + 288x^5 + 216x^8$	3,200	4,992	24,892,032
5	$120x^3 + 750x^4 + 480x^5 + 480x^8$	6,100	9,600	92,104,200
6	$144x^3 + 1{,}296x^4 + 720x^5 + 900x^8$	10,368	16,416	269,387,424

Omega polynomial in $Op(Trs(P_4(Oct)))\_Id$ crystal-like network

$\Omega\,(R_{\max}[6]; \mathrm{Id}, x) = a_3x^3 + a_4x^4 + a_5x^5 + a_8x^8$
$a_3 = 24a;\ a_4 = 6a^3;\ a_5 = 24a(a-1);\ a_8 = 6a(a-1)^2$
$\Omega\,(R_{\max}[6]; \mathrm{Id}, x) = 24ax^3 + 6a^3x^4 + 24a(a-1)x^5 + 6a(a-1)^2x^8$
$\Omega'\,(R_{\max}[6]; \mathrm{Id}, 1) = |E(G)| = e(G) = 24a^2(3a+1)$
$\Omega''\,(R_{\max}[6]; \mathrm{Id}, 1) = 24a^2(17a-8)$
$\mathrm{CI}\,(R_{\max}[6]; \mathrm{Id}) = 24a^2(216a^4 + 144a^3 + 24a^2 - 20a + 7)$
$v(\mathrm{Id}) = 44a^3 + 24a^2$

Table 8.9 Examples of Omega polynomial in $Op(Trs(P_4(Oct)))\_Jn$ crystal-like network

a	Omega polynomial; $F_{\max}[6]$	v	e	CI
1	$24x^3 + 6x^4$	68	96	8,904
2	$48x^3 + 60x^4 + 48x^9$	544	816	660,576
3	$72x^3 + 216x^4 + 72x^9 + 72x^{15}$	1,836	2,808	7,858,728
4	$96x^3 + 528x^4 + 96x^9 + 96x^{15} + 96x^{21}$	4,352	6,720	45,077,376
5	$120x^3 + 1{,}050x^4 + 120x^9 + 120x^{15} + 120x^{21} + 120x^{27}$	8,500	13,200	174,045,000
6	$144x^3 + 1{,}836x^4 + 144x^9 + 144x^{15} + 144x^{21} + 144x^{27} + 144x^{33}$	14,688	22,896	523,826,784

Omega polynomial in $Op(Trs(P_4(Oct)))\_Jn$ crystal-like network

$$\Omega\left(F_{\max}[6];\mathrm{Jn},x\right) = a_3x^3 + a_4x^4 + a_3\sum_{i=2}^{a} x^{3(2i-1)}$$

$$a_3 = 24a;\ a_4 = 6a[a(a-1)/2 + a^2]$$

$$\Omega\left(F_{\max}[6];\mathrm{Jn},x\right) = 24ax^3 + 6a\left[a(a-1)/2 + a^2\right]x^4 + 24a\sum_{i=2}^{a} x^{3(2i-1)}$$

$$\Omega'\left(F_{\max}[6];\mathrm{Jn},1\right) = |E(G)| = e(G) = 12a^2(9a-1)$$

$$\Omega''\left(F_{\max}[6];\mathrm{Jn},1\right) = 36a^2(8a^2 + a - 3)$$

$$\mathrm{CI}\left(F_{\max}[6];\mathrm{Jn}\right) = 24a^2(486a^4 - 108a^3 - 6a^2 - 6a + 5)$$

$$v(\mathrm{Jn}) = 68a^3$$

8.5 Dyck Graph-Based Networks

The networks making the subject of this section were built up by units that are representations of the celebrate Dyck graph (Dyck 1880). This graph consists of 32 vertices of valence 3, it has 48 edges, 12 octagons $R[8]$, girth 6, diameter 5, and the chromatic number 2; it is nonplanar and has the genus $g = 1$ (i.e., there exists an embedding of the graph on the torus). Cycle counting on the finite representation revealed 12 octagons and 16 hexagons. As a unit of the infinite lattice, it shows 12 octagons and the genus (Harary 1969) is $g = 3$.

The Dyck graph units are designed as the zigzag isomer Z-56 (Fig. 8.6, left) by the sequence $Op(Q(\mathrm{C}))$, performed on the Cube C, while the armchair isomer A-56 (Fig. 8.6, middle), by the sequence $Op_{2a}(Q(\mathrm{C}))$. There is a third unit that makes co-net with the above A-isomer, designed by $Op_{2a}(Ca(\mathrm{C}))$ and denoted A-104 (Fig. 8.6, right). All these units have the genus $g = 3$, the last one being a chiral unit, made by

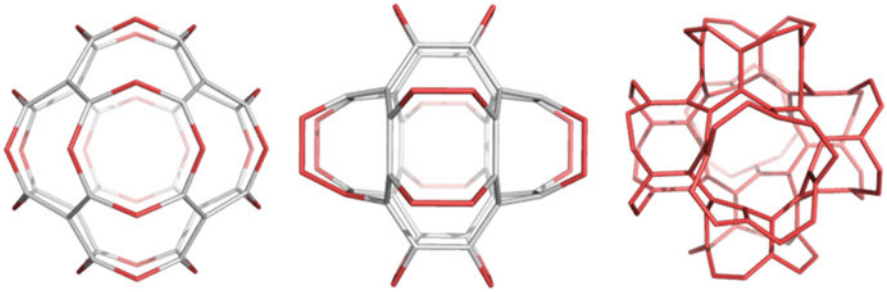

Fig. 8.6 Dyck graph units: zigzag Z-56, $R[8] = 12$ (*left*); armchair A-56, $R[8] = 12$ (*middle*); armchair A-104, $R[8] = 24$ (*right*)

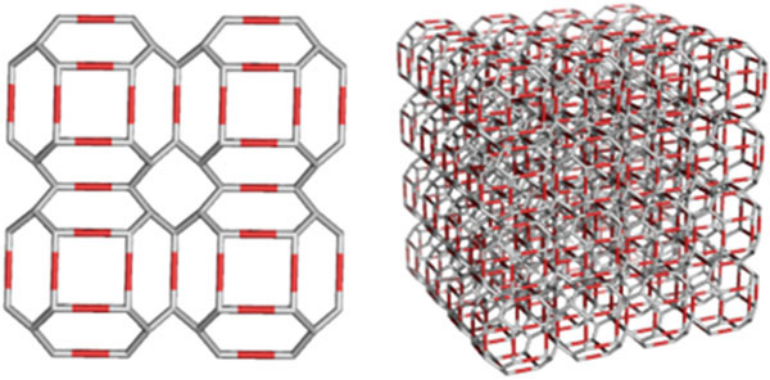

Fig. 8.7 Dyck Z-56 based network as a "mathematical" non-optimized "Id"-lattice: 222_352 (*left*) and 444_2432 (*right*)

the pro-chiral operation *Ca* = "Capra" (Rom) = Goat (Eng). The chirality induced by *Ca*-operation approaches the unity, according to Petitjean theory (Diudea and Petitjean 2008).

8.5.1 Networks of Dyck Z-56 Unit

The *Op*(*Q*(C)) sequence of map operations was used to provide the unit Dyck Z-56 (in non-optimized form) and next the "mathematical" Dyck Z-56_Id network (Fig. 8.7) (Diudea and Ilić 2010).

Formulas for the calculation of Omega polynomial in Dyck Z-56 lattice is given below while examples are given in Table 8.10.

Table 8.10 Omega polynomial in Dyck Z-56_Id crystal-like network (unit designed by $Op(Q(C))$)

	Examples (a = odd)			
a	Omega	v	e	CI
3	$8x^6 + 18x^{48} + 4x^{72} + 4x^{78}$	1,080	1,512	2,199,312
5	$8x^6 + 30x^{120} + 4x^{366} + 4x^{372}$	4,600	6,600	42,038,352
7	$8x^6 + 42x^{224} + 4x^{1020} + 4x^{1026}$	12,152	17,640	300,689,616
	Examples (a = even)			
a	Omega	v	e	CI
4	$8x^6 + 24x^{80} + 2x^{168} + 6x^{192}$	2,432	3,456	11,512,416
6	$8x^6 + 36x^{168} + 2x^{624} + 6x^{648}$	7,776	11,232	121,843,296
8	$8x^6 + 48x^{288} + 2x^{1512} + 6x^{1536}$	17,920	26,112	659,126,880

Omega polynomial in Dyck Z-56_Id crystal-like network; unit designed by $Op(Q(C))$

$$\Omega\left(R_{\max}[8]; \mathrm{Id}, a = \text{odd}, x\right) = a_1 x^{e1} + a_2 x^{e2} + a_3 x^{e3} + a_4 x^{e4}$$
$$a_1 = 8;\ a_2 = 6a;\ a_3 = 4;\ a_4 = 4$$
$$e_1 = 6;\ e_2 = 4a(a+1);\ e_3 = 3(a^3-3);\ e_4 = 3(a^3-1)$$
$$\Omega\left(R_{\max}[8]; \mathrm{Id}, a = \text{odd}, x\right) = 8x^6 + 6ax^{4a(a+1)} + 4x^{3(a^3-3)} + 4x^{3(a^3-1)}$$
$$\Omega'\left(R_{\max}[8]; \mathrm{Id}, a = \text{odd}, 1\right) = |E(G)| = e(G) = 24a^2(2a+1)$$
$$\Omega''\left(R_{\max}[8]; \mathrm{Id}, a = \text{odd}, 1\right) = 72a^6 + 96a^5 + 192a^4 - 240a^3 - 24a^2 + 648$$
$$\mathrm{CI}\left(R_{\max}[8]; \mathrm{Id}, a = \text{odd}\right) = 2,232a^6 + 2,208a^5 + 384a^4 + 192a^3 - 648$$
$$v\,(\text{Dyck Z-56\_Id}) = 32a^3 + 24a^2$$
$$\Omega\left(R_{\max}[8]; \mathrm{Id}, a = \text{even}, x\right) = a_1 x^{e1} + a_2 x^{e2} + a_3 x^{e3} + a_4 x^{e4}$$
$$a_1 = 8;\quad a_2 = 6a;\quad a_3 = 2;\quad a_4 = 6$$
$$e_1 = 6;\ e_2 = 4a(a+1);\ e_3 = 3(a^3-8);\ e_4 = 3a^3$$
$$\Omega\left(R_{\max}[8]; \mathrm{Id}, a = \text{even}, x\right) = 8x^6 + 6ax^{4a(a+1)} + 2x^{3(a^3-8)} + 6x^{3a^3}$$
$$\Omega'\left(R_{\max}[8]; \mathrm{Id}, a = \text{even}, 1\right) = |E(G)| = e(G) = 24a^2(2a+1)$$
$$\Omega''\left(R_{\max}[8]; \mathrm{Id}, a = \text{even}, 1\right) = 72a^6 + 96a^5 + 192a^4 - 240a^3 - 24a^2 + 1440$$
$$\mathrm{CI}\left(R_{\max}[8]; \mathrm{Id}, a = \text{odd}\right) = 2,232a^6 + 2,208a^5 + 384a^4 + 192a^3 - 1,440$$
$$\mathrm{CI}\left(R_{\max}[8]; \mathrm{Id}, a = \text{odd}\right) = \mathrm{CI}\left(R_{\max}[8]; \mathrm{Id}, a = \text{even}\right) + 792$$

The unit Dyck Z-56 was also used to build other two networks: one by the identification procedure, Dyck Z-56_Id_spiro (Fig. 8.8, left and middle), and one by joining the points/atoms of lower connectivity/valence, Dyck Z-56_Jn (Fig. 8.8, right) (Diudea et al. 2010).

The "spiro" net (the name reminds two chemical cycles sharing one tetravalent carbon atom) is a new net: CQOpSpD1 = diu21; group P4/mmm; point symbol for net: $(4.8^2)2(4^2.8^4)(8^3)6(8^6)(8)2$; a 2,3,3,3,4,4-c net with stoichiometry (2-c)2(3-c)2(3-c)4(3-c)2(4-c)(4-c); 6-nodal net.

The last net, Dyck Z-56_Jn, is the known lattice *sqc*13204, of the group *Pm*-3*m*, a 3-nodal 3,3,3-c net, with point symbol for net: $(6.8^2)3(6^2.8)3(8^3)$. Omega polynomial formulas for these two networks are given below. Examples are given in Table 8.11.

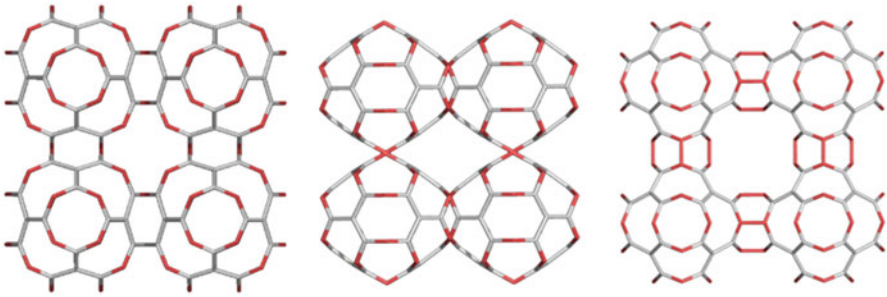

Fig. 8.8 The Dick Z-56 unit in lattices built by identification (Dyck Z-56_Id_spiro, *left* and *middle*) and junction (Dyck Z-56_Jn, *right*)

Table 8.11 Omega polynomial in Dyck Z-56_Id_spiro and Dyck Z-56_Jn networks; examples

a	Dyck Z-56_Id_spiro; Omega ($R_{\max}[8]$)	v	e	CI
3	$18x^{36} + 18x^{48} + 3x^{144}$	1,368	1,944	3,652,128
4	$32x^{48} + 32x^{64} + 4x^{256}$	3,200	4,608	20,766,720
5	$50x^{60} + 50x^{80} + 5x^{400}$	6,200	9,000	79,700,000
a_{even}	Dyck Z-56_Jn; Omega ($R_{\max}[8]$)	v	e	CI
2	$12x^4 + 32x^6 + 8x^{48}$	448	624	369,600
4	$144x^4 + 256x^6 + 8x^{384}$	3,584	5,184	25,682,688
6	$540x^4 + 864x^6 + 8x^{1296}$	12,096	17,712	300,238,272
a_{odd}	Dyck Z-56_Jn; Omega ($R_{\max}[8]$)	v	e	CI
3	$54x^4 + 108x^6 + 2x^{144} + 6x^{168}$	1,512	2,160	4,450,032
5	$300x^4 + 500x^6 + 2x^{720} + 6x^{760}$	7,000	10,200	99,514,800
7	$882x^4 + 1{,}372x^6 + 2x^{2016} + 6x^{2072}$	19,208	28,224	762,643,056

Omega polynomial in Dyck Z-56_Id_spiro net; $R_{\max}[8]$; unit designed by $Op(Q(\text{C}))$

$$\Omega\,(\text{Id, spiro}, x) = 2a^2 \cdot x^{12a} + 2a^2 \cdot x^{16a} + a \cdot x^{16a^2}$$
$$\Omega'(G,1) = e(G) = |E(G)| = 72a^3$$
$$\Omega''(G,1) = 8a^3(32a^2 + 100a - 9)$$
$$\text{CI}(G) = 32a^4(162a^2 - 8a - 25)$$
$$v(G) = a^2(104 + 48(a-2)) = 8a^2(6a+1)$$

Omega polynomial in Dyck Z-56_Jn net; $R_{\max}[8]$; unit designed by $Op(Q(\text{C}))$

Jn_a_{even}	$\Omega\,(\text{Jn\_}a_{\text{even}}, x) = 3a^2(a-1)x^4 + 4a^3x^6 + 8x^{6a^3}$
	$\Omega'(G,1) = e(G) = \lvert E(G)\rvert = 12a^2(7a-1)$
	$\Omega''(G,1) = 288a^6 + 108a^3 - 36a^2$
	$\text{CI}(G) = 48a^2(141a^4 - 42a^3 + 3a^2 - 4a + 1)$
Jn_a_{odd}	$\Omega\,(\text{Jn\_}a_{\text{odd}}, x) = 3a^2(a-1)x^4 + 4a^3x^6 + 2x^{6a(a^2-1)} + 6x^{6(6a^2+2)}$
	$\Omega'(G,1) = e(G) = \lvert E(G)\rvert = 12a^2(7a-1)$
	$\Omega''(G,1) = 288a^6 + 108a^3 + 60a^2$
	$\text{CI}(G) = 48a^2(141a^4 - 42a^3 + 3a^2 - 4a - 1)$
Jn	$v(\text{Dyck Z-56\_Jn}) = 56a^3$

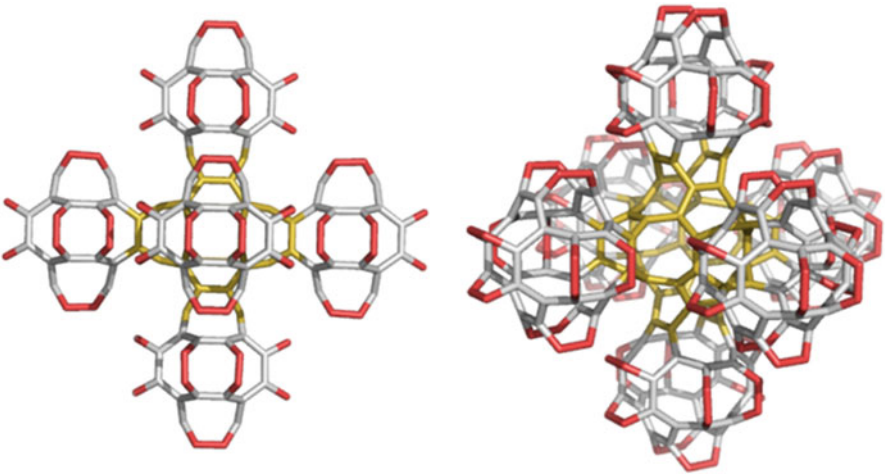

Fig. 8.9 A dendrimer built up from Dyck A-56 unit; $u(\mathrm{D}) = 7$; $v = 344$

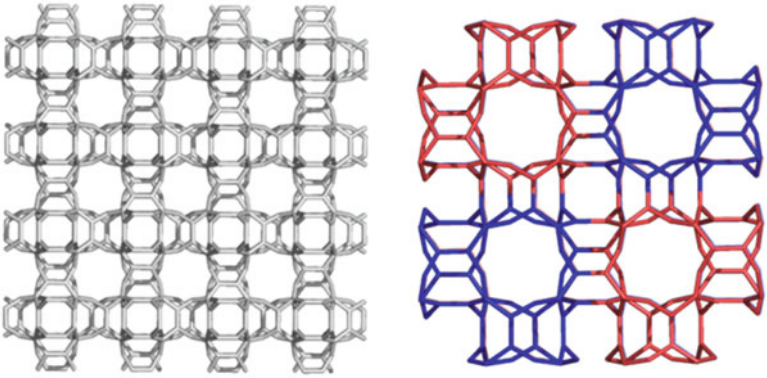

Fig. 8.10 Dyck graph network: A-(56&104)_444_2432 lattice (*left*) and A-(104&56)_222_544, *R/L mezzo* net

8.5.2 Networks of Dyck A-56 Unit

The unit Dyck A-56 can be assembled in a dendrimer (Diudea et al. 1997; Diudea and Katona 1999) (Fig. 8.9). The growth of such a dendrimer goes up to the first generation (with the number of vertices $v = 344$). At a second generation, the endings of the units are no more free, they fit to each other thus superimposing to the lattice A-(56&104) (see Fig. 8.10).

The number of units in the ath orbit (i.e., that located at distance a from the center) of a regular dendrimer can be expressed as a function vertex degree d:

$$u_a = d\,(d-1)^{a-1} \tag{8.8}$$

By using the progressive degree $p = d - 1$, relation (8.1) becomes

$$u_a = (p+1)\,p^{a-1} \tag{8.9}$$

The total number of units u(D) in dendrimer is obtained by summing the populations on all orbits (up to the radius/generation r) and the core

$$u(\mathrm{D}) = 1 + (p+1)\sum_{a=1}^{r} p^{a-1} \tag{8.10}$$

By developing the sum in (8.10) one obtains (Diudea and Katona 1999)

$$u(\mathrm{D}) = \frac{2\left(p^{r+1}-1\right)}{p-1} - p^r \tag{8.11}$$

In case of Fig. 8.9, one obtains: $p = 5$; $r = 1$; $u(\mathrm{D}) = 7$.

The units of lattice A-(56&104) or A-(104&56) fit only right/left *R*/*L* to form an alternating, non-chiral, *mezzo* net (Fig. 8.10, right) (Diudea 2010b). The two above lattices are one and the same, irrespective which one is called the net or co-net (i.e., the complement); only the boundaries are different. Accordingly, the Omega polynomial description takes into account the two different boundaries and the formulas will also differ (Diudea 2010b).

Note that A-(56&104) is a new network (diu8 = CQOp2a) belonging to the space group *Fm*-3*c* (topos: http://www.toposssusamararu/index.html); it is a 2-nodal 3,3-c net, with the point symbol for net: (8^3) and stoichiometry (3-c)3(3-c).

8.5.2.1 Omega Polynomial in Dyck A-(56&104) Lattice

Omega polynomial in the Dyck A-(56&104) lattice is calculated on two maximal rings $R_{\max}[8]$ and $R_{\max}[12]$, according to the lattice structure. The polynomial consists of two terms: the first term refers to the "oblique" *ops* while the second one to the "orthogonal" *ops*. Examples are given in Table 8.9.

Omega polynomial in Dyck A-(56&104) lattice; $R_{\max}[8]$, unit designed by $Op_{2a}(Q(\mathrm{C}))$:

$$\Omega(\text{A-(56\&104)}, x) = c_1 x^{e_1} + c_2 x^{e_2} = 6a^2 \cdot x^{6a+2} + 3a \cdot x^{4a(a+1)}$$
$$v(G) = 24a^2 + 32a^3$$
$$\Omega'(G,1) = e(G) = |E(G)| = 24a^2 + 48a^3;$$
$$\Omega''(G,1) = 144a^3 + 312a^4 + 48a^5$$
$$\mathrm{CI}(G) = -24a^2 - 192a^3 + 264a^4 + 2,256a^5 + 2,304a^6$$
$$R[8] = 18a^3 - 3(a-1)a^2 = 3a^2(5a+1);\ R[12] = 6a(2a^2 - a + 1)$$

Table 8.12 Omega polynomial in Dyck A-(56&104) network; examples ($G =$ Dyck A-(56&104); lattice (a,a,a); $R_{\max}[8]$)

CI: ($a = 1$) = 4,608; ($a = 2$) = 222,240; ($a = 3$) = 2,243,808; ($a = 8$) = 678,885,888.
v(G): ($a = 1$) = 56; ($a = 2$) = 352; ($a = 3$) = 1,080; ($a = 8$) = 17,920.
R[8]: ($a = 1$) = 18; ($a = 2$) = 132; ($a = 3$) = 432; ($a = 8$) = 7,872.

Table 8.13 Examples of Omega polynomial in Dyck A-(104&56) lattice

Examples: G = Dyck A-(104&56) lattice; $R_{\max}[8]$
CI: ($a = 1$) = 17,004; ($a = 2$) = 513,864; ($a = 3$) = 4,185,828; ($a = 8$) = 894,907,728.
$v(G)$: ($a = 1$) = 104; ($a = 2$) = 544; ($a = 3$) = 1,512; ($a = 8$) = 20,992.
R[8]: ($a = 1$) = 24; ($a = 2$) = 150; ($a = 3$) = 468; ($a = 8$) = 8,088.
Examples: $G =$ Dyck A-(104&56) lattice; $R_{\max}[12]$
CI: ($a = 2$) = 128,640; ($a = 3$) = 838,944; ($a = 8$) = 89,647,104.

Omega polynomial in Dyck A-(56&104) lattice; $R_{\max}[12]$, unit designed by $Op_{2a}(Q(\mathrm{C}))$:

$$\Omega(\text{A-(56\&104)}, x) = x^e = x^{24a^2(2a+1)}$$
$$\Omega'(G,1) = e(G) = |E(G)| = 24a^2(2a+1) = 24a^2 + 48a^3$$
$$\Omega''(G,1) = 24a^2(2a+1)(48a^3 + 24a^2 - 1)$$
$$\mathrm{CI}(G) = [(24a^2(2a+1)]^2 - [24a^2(2a+1) + 24a^2(2a+1)(48a^3 + 24a^2 - 1)] = 0$$

In formulas for the number of vertices $v(G)$ and edges $e(G)$ (see above), the terms at highest exponent remind of the parameters of Duck graph. At $R_{\max}[12]$, the polynomial has only one term, and because there is only one *ops*, CI = 0. Examples are given in Table 8.12.

8.5.2.2 Omega Polynomial in Dyck A-(104&56) Lattice

In case of A-(104&56) lattice, the polynomial, calculated at $R_{\max}[8]$, shows five terms. The highest exponent term in calculating CI in both lattices is the same: $2{,}304a^6$, also supporting the fact that there is a single lattice with two different boundaries. At $R_{\max}[12]$, the polynomial has only two terms. Observe Ω' has the same form as in case of $R_{\max}[8]$, its meaning being the number of edges in the graph. Examples are given in Table 8.13 (Diudea 2010b).

Omega polynomial in Dyck A-(104&56) lattice; $R_{\max}[8]$, unit designed by $Op_{2a}(Ca(C))$:

$$\Omega(\text{A-(104\&56)}, x) = \sum_{i=1}^{5} c_i x^{e_i}$$
$$\Omega(G, x) = 36a \cdot x^3 + 6(3a^2 + 2a - 4) \cdot x^4 + 12(a-1)^2 \cdot x^6 + 6(a-1)^2 \cdot x^{6a+4} + 3(a-1) \cdot x^{4a^2}$$
$$\Omega'(G, 1) = 84a^2 + 48a^3$$
$$\Omega''(G, 1) = 144 - 252a + 372a^2 - 192a^3 + 168a^4 + 48a^5$$
$$\text{CI}(G) = -144 + 252a - 456a^2 + 144a^3 + 6,888a^4 + 8,016a^5 + 2,304a^6$$
$$v(\text{G}) = 8a^2\,(13 + 4(a-1))$$
$$R[8](G) = 24a^3 - 3a(a(3a-2)-1) = 3a(5a^2 + 2a + 1)$$

Omega polynomial in Dyck A-(104&56) lattice; $R_{\max}[12]$

$$\Omega(\text{A-(104\&56)}, x) = c_1 x^4 + x^{e_2}$$
$$\Omega(G, x) = 6a^2 x^4 + x^{12a^2[4(a-2)+13]}$$
$$\Omega'(G, 1) = 84a^2 + 48a^3$$
$$\Omega''(G, 1) = 12a^2(1 - 4a + 300a^2 + 480a^3 + 192a^4)$$
$$\text{CI}(G) = 96a^2(36a^2 + 24a^3 - 1)$$

Numerical evaluation of Omega polynomial was made by our software program Nano Studio.

8.6 Networks Patched by Tripentylene and Triphenylene

Two repeating units, embeddable in the P-surface, have been designed: Z-Pen, bearing the "tripentylene," and A-Phe with the "triphenylene" patches, respectively (Fig. 8.11, top); their crystal-like networks are shown at the bottom of Fig. 8.11. The polynomials are calculated at $F_{\max}[8]$ as follows (Stefu et al. 2010).

In the Z-Pen structure, the term at exponent 1 counts the edges in odd faces not counted in even faces. The exponent 2 refers to isolated even rings, the exponent 4 represents strips of three even-membered faces while exponent 8 counts the large hollows, ordered as in zeolites, natural alumino-silicates used as molecular sieves.

In the A-Phe net, there are no odd faces so the polynomial has no terms at exponent 1. Formulas to calculate Omega polynomial in the two networks are listed below while some numerical examples are given in Table 8.14. The count of atoms is given in Table 8.15.

Omega polynomial in Z_Pen network; $F_{\max}[8]$:

$$\Omega(\text{Z-Pen}, x]) = 48a^2x^1 + 12a(4a^2 - 2a + 1)x^2 + 3a(5a^2 + 3a - 4)x^4 + 3a(a-1)^2x^8$$
$$\Omega'(G, 1) = 48a^2 + 2{\cdot}12a(4a^2 - 2a + 1) + 4{\cdot}3a(5a^2 + 3a - 4) + 8{\cdot}3a(a-1)^2 = 12a^2(15a - 1)$$
$$\Omega''(G, 1) = 12a(37a^2 - 23a + 4)$$
$$\text{CI}(G) = 48a(675a^5 - 90a^4 + 3a^3 - 13a^2 + 6a - 1)$$

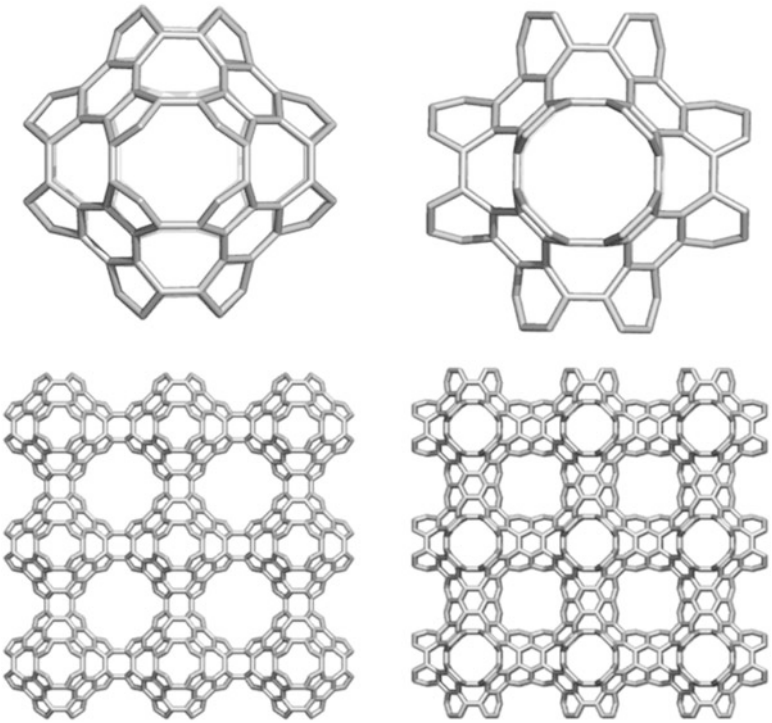

Fig. 8.11 Units Z-Pen_120 ($f_8 = 12$; $f_6 = 8$; $f_5 = 24$, *top*, *left*) and A-Phe_144 ($f_8 = 12$; $f_6 = 32$, *top*, *right*) and the corresponding crystal-like structures: Z-Pen_3240 (*bottom*, *left*) and A-Phe_3456 (*bottom*, *right*)

Omega polynomial in A_Phe network; $F_{\max}[8]$:

$$\Omega(\text{A-Phe}, x) = 12ax^2 + 12a(a+1)x^4 + 3a(a-1)^2x^8 + 12a^2x^{5a+1} + 24a\sum_{i=2}^{a} x^{4(2i-1)}$$
$$\Omega'(G,1) = 12a^2(15a+1)$$
$$\Omega''(G,1) = 4a(203a^3 + 33a^2 - 80a + 12)$$
$$\text{CI}(G) = 4a(8,100a^5 + 1,080a^4 - 167a^3 - 78a^2 + 77a - 12)$$

Zeolites (Baerlocher et al. 2007) are natural or synthetic alumino-silicates with an open three-dimensional crystal structure. Zeolites are microporous solids known as "molecular sieves." The term molecular sieve refers to the property of these materials to selectively sort molecules, based primarily on a size exclusion process. This is due to a regular structure of pores, of molecular dimensions, forming channels. The rigorous and often aesthetically appealing architecture of zeolites attracted the interest of scientists in a broad area, from crystallographers, to chemists and mathematicians.

Table 8.14 Omega polynomial in Z-Pen and A-Phe networks: examples

a	F_{max}[8], Z_Pen network	CI
1	$48x + 36x^2 + 12x^4$	27,840
2	$192x + 312x^2 + 132x^4 + 6x^8$	1,933,728
3	$432x + 1{,}116x^2 + 450x^4 + 36x^8$	22,567,104
4	$768x + 2{,}736x^2 + 1056x^4 + 108x^8$	128,288,064
5	$1{,}200x + 5{,}460x^2 + 2{,}040x^4 + 240x^8$	492,768,960
6	$1{,}728x + 9{,}576x^2 + 3{,}492x^4 + 450x^8$	1,478,124,000
a	F_{max}[8] A_Phe network	CI
1	$12x^2 + 24x^4 + 12x^6$	36,000
2	$24x^2 + 72x^4 + 6x^8 + 48x^{11} + 48x^{12}$	2,199,792
3	$36x^2 + 144x^4 + 36x^8 + 72x^{12} + 108x^{16} + 72x^{20}$	24,609,456
4	$48x^2 + 240x^4 + 108x^8 + 96x^{12} + 96x^{20} + 192x^{21} + 96x^{28}$	136,947,840
5	$60x^2 + 360x^4 + 240x^8 + 120x^{12} + 120x^{20} + 300x^{26} + 120x^{28} + 120x^{36}$	519,300,960
6	$72x^2 + 504x^4 + 450x^8 + 144x^{12} + 144x^{20} + 144x^{28} + 432x^{31} + 144x^{36} + 144x^{44}$	1,544,324,400
7	$84x^2 + 672x^4 + 756x^8 + 168x^{12} + 168x^{20} + 168x^{28} + 756x^{36} + 168x^{44} + 168x^{52}$	3,882,737,712

Table 8.15 Number of atoms $v = |V(G)|$ in Z-Pen and A-Phe networks

Z-Pen network $v_a = 120 \cdot a^3$			A-Phe network $v_a = 144 \cdot a^3 - 24 \cdot a^2(a-1)$			
a	1	2	3	4	5	6
v (Z-Pen)	120	960	3,240	7,680	15,000	25,920
v (A-Phe)	144	1,056	3,456	8,064	15,600	26,784

8.7 Networks Patched by Sumanene Units

The hypothetical carbon networks herein discussed were built up either by identifying two opposite open faces of a unit (Sum-CA_216, Fig. 8.12, left), or by joining the opposite atoms (Sum-S_2Lex, Fig. 8.12, middle and Sum-CZ_192, Fig. 8.12, right), by the aid of Nano Studio software, (Nagy and Diudea 2009). This program also enabled the embedding of these units in the P-type surface, the networks belonging to the space group *Pm*-3*m*. The topological characterization was done on cubic (*a*,*a*,*a*) domains (Szefler et al. 2012).

The three networks, representing decorations of the P-type surface are new networks, designed at Topo Group Cluj, by the aid of CVNET (Stefu and Diudea 2005) and Nano Studio (Nagy and Diudea 2009); their crystallographic data are listed in Table 8.16.

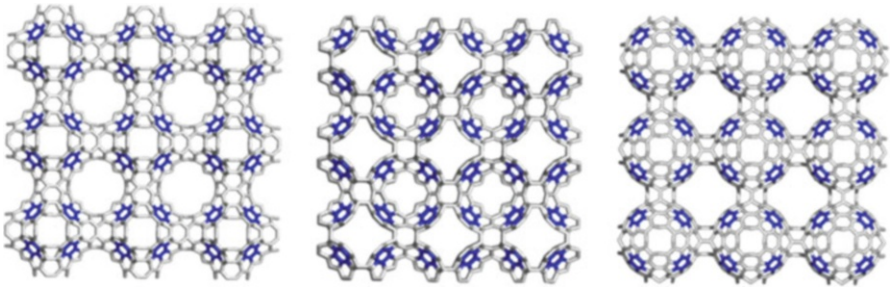

Fig. 8.12 Sumanene-patched networks: Sum-CA_216 (*left*), Sum-S_2Le*x*_168 (*middle*), Sum-CZ_192 (*right*)

Table 8.16 Crystallographic data for the Sumanene-patched networks

Sum-A_216: diu9; point symbol for net: (5.6.8)2(5.6^2)2(5.8^2)(6.8^2)(6^2.8)2; 3,3,3,3,3-c net; stoichiometry (3-c)2(3-c)(3-c)2(3-c)(3-c)2; 5-nodal net
Sum-S_2Lex_168; diu11; point symbol for net: (5.6.7)2(5.6^2)2(5.7^2)(6.7.8)2(7.8^2), 3,3,3,3,3-c net; stoichiometry (3-c)2(3-c)(3-c)(3-c)2(3-c)2; 5-nodal net
Sum-CZ_192; diu10; point symbol for net: (5.10^2)(5.6.9)2(5.6^2)2(6^2.10), 3,3,3,3-c net; stoichiometry (3-c)2(3-c)(3-c)(3-c)2; 4-nodal net

Table 8.17 Total energy E_{tot} per atom (kcal/mol) and HOMO-LUMO (HL) gap, at Hartree-Fock (HF) (HF/6-31G**) level of theory for some Sumanene-patched units

	Structure	No. C atoms	HF/6-31G(d,p) (au)	E_{tot}/C (au/mol)	HF gap (eV)
1	C_{60}	60	−2,271.830	−37.864	7.418
2	Sum-TA_108	108	−4,103.136	−37.992	7.259
3	Sum-T_84	84	−3,194.384	−38.028	7.562
4	Sum-CZ_192	192	−7,298.367	−38.012	6.044
5	Sum-CA_216	216	−8,206.401	−37.993	6.442
6	Sum-S_2Lex_168	168	−6,389.018	−38.030	6.637

8.7.1 Stability of P-Type Surface Network Units

Stability of some units of P-type surface network and related small structures was evaluated on optimized geometries at Hartree-Fock (HF) (HF/6-31G**) level of theory. The calculations were performed, on hydrogen-ended structures, in gas phase by Gaussian 09 (2009). As a reference structure, we considered C_{60}, the most referred structure in Nanoscience. Table 8.17 lists the total energy obtained after optimization, the total energy per Carbon atom, E_{tot}/C and HOMO-LUMO HL gap. This test of stability was done to support the idea that sumanene, a real molecule, can be used to synthesize structural units (Fig. 8.13): Sum_T_A_108 (middle); Sum_T_84 for dendrimers while Sum_CZ_192, Sum_CA_216 and Sum_S_2Le*x*_168, for more

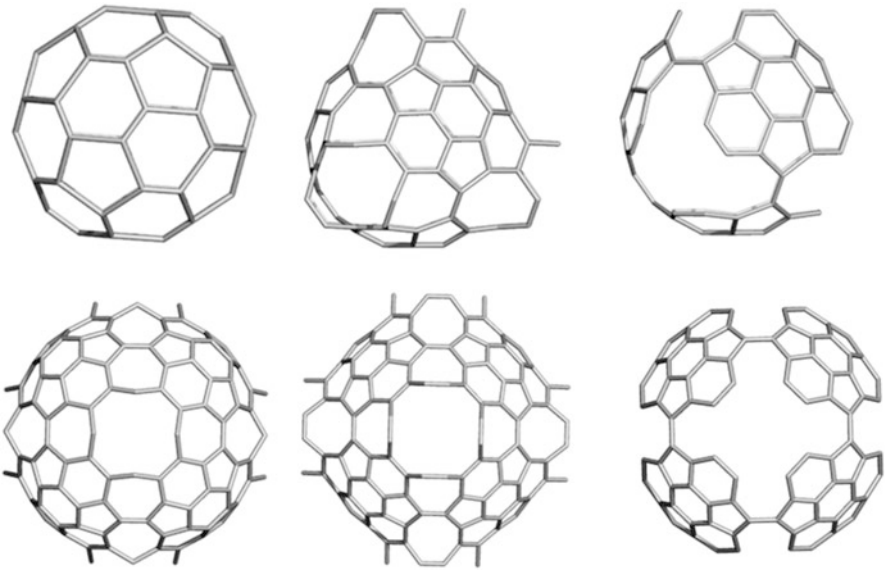

Fig. 8.13 *Top row*: C_{60} (*left*), Sum-TA_108 (*middle*); Sum-T_84 (*right*). *Bottom row*: Sum-CZ_192 (*left*); Sum-CA_216 (*middle*); Sum-S_2Le*x*_168 (*right*)

elaborated nanostructures, such as ordered Schwarzites, embedded in the P-surface. From Table 8.14 it is clear that such units show a stability comparable to that of the well-known C_{60} reference structure (even partially hydrogenated structures cannot be directly compared with all carbon fullerenes); Sum_T_84 and Sum_S_2Le*x*_168 are the most simple and stable units, possible candidates for laboratory synthesis (Szefler et al. 2012).

8.7.2 Omega Polynomial in Sumanene-Based Networks

Omega polynomial is herein calculated at various $R_{\max}$. Formulas were derived by numerical analysis and are presented below. Examples of CI index are given in Table 8.18, the number of vertices are listed in Table 8.19, while the faces/rings in Table 8.20, all function of the number of repeating units a, in a cubic domain (a,a,a) along a chosen direction of the Euclidean space (Szefler et al. 2012).

Omega polynomials in Sum-CA_216; $R_{\max}[6]$:

$$\Omega(G,x)=\left[a^2\,(72a+60)\right]\,x^1+\left[a^2\,(72a-24)\right]\,x^2+24a^2\,x^3+\left[12a^2\,(a-1)\right]\,x^6$$
$$\Omega'(G,1)=|E(G)|=288a^3+12a^2=12a^2(24a+1)$$
$$\mathrm{CI}(G)=82,944\,a^6+6,912\,a^5+144\,a^4-792\,a^3+252a^2$$

Omega polynomials in Sum-CA_216, $R_{\max}[8]$:

$$\begin{aligned}\Omega(G,x) =& 48a^2x^2 + [12a\,(2a+1)]\ x^3 + \left[24a^2\,(2a-1)\right]\ x^4 + [12a\,(a-1)]\ x^5 \\ &+ \left[12a^2\,(a-1)\right]\ x^6 + \left[3a(a-1)^2\right]\ x^8 \\ \Omega'(G,1) &= |E(G)| = 288a^3 + 12a^2 = 12a^2(24a+1) \\ \mathrm{CI}(G) &= 82,944\ a^6 + 6,912\ a^5 + 144\ a^4 - 1,392\ a^3 + 492a^2\end{aligned}$$

Omega polynomials in Sum_S_2Lex_168, $R_{\max}[6] = R_{\max}[8]$:

$$\begin{aligned}\Omega(G,x) &= 60a^3x + 48a^3\ x^2 + 24a^2\ x^3 + 12a^2(a-1)\ x^5 \\ \Omega'(G,1) &= |E(G)| = 216a^3 + 12a^2 = 12a^2(18a+1) \\ \mathrm{CI}(G) &= 46,656\ a^6 + 5,184\ a^5 + 144a^4 - 552\ a^3 + 84a^2\end{aligned}$$

Omega polynomials in Sum_S_2Lex_168, $R_{\max}[10]$:

$$\begin{aligned}\Omega(G,x) =& \left[a\left(48a^2 + 88a - 17\right)\right]\ x^1 + \left[30a^3 - 9a^2 + 4a + 2\right]\ x^2 \\ &+ \left[2a\left(10a^2 - 11a + 7\right)\right]\ x^3 \\ &+ \left[a\left(3a^2 + a - 3\right)\right]\ x^4 + \left[a\left(3a^2 - a - 2\right)\right]\ x^5 \\ &+ \left[a(a-1)^2\right]\ x^6 + \left[a\left(a^2 - 2a + 2\right)\right]\ x^7 \\ &+ \left[a^3 + a^2 - 3a + 2\right]\ x^8 + [3a\,(a-1)]\ x^9 + [2\,(a-1)]\ x^{10} \\ \Omega'(G,1) &= |E(G)| = 216a^3 + 12a^2 = 12a^2(18a+1) \\ \mathrm{CI}(G) &= 46,656\ a^6 + 5,184\ a^5 + 144\ a^4 - 620\ a^3 + 18a^2 + 74a + 64\end{aligned}$$

Omega polynomials in Sum_CZ_192, $R_{\max}[6]$:

$$\begin{aligned}\Omega(G,x) &= \left[12a^2\,(10a-1)\right]\ x + 48a^3\ x^2 + 24a^3x^3 \\ \Omega'(G,1) &= |E(G)| = 288a^3 - 12a^2 = 12a^2(24a-1) \\ \mathrm{CI}(G) &= 46,656\ a^6 + 5,184\ a^5 + 144\ a^4 - 552\ a^3 + 84a^2\end{aligned}$$

Omega polynomials in Sum_CZ_192, $R_{\max}[8]$:

$$\begin{aligned}\Omega(G,x) =& \left[12a^2\,(5a+4)\right]\ x + \left[24a^2\,(3a-1)\right]\ x^2 + 24a^2x^3 \\ &+ \left[3a^2\,(a-1)\right]\ x^4 + \left[12a^2\,(a-1)\right]\ x^6 \\ \Omega'(G,1) &= |E(G)| = 288a^3 - 12a^2 = 12a^2(24a-1) \\ \mathrm{CI}(G) &= 82,944\ a^6 - 6,912\ a^5 + 144\ a^4 - 828\ a^3 + 312a^2\end{aligned}$$

Number of atoms in Sum-CA_216 = N, Sum_S_2Lex_168 = x, and Sum_CZ_192 = Z:

$$v(N) = 8a^2[27 + 24(a-1)]; \quad v(X) = 8a^2[21 + 18(a-1)]; \quad v(Z) = 192a^3;$$

Number of rings in Sumanene-patched networks (symbols as above):

$$\begin{aligned}&R[5](N) = 24a^3; \quad R[6](N) = 4a^2[8 + 11(a-1)]; \quad R[8](N) = 26a^3 \\ &R[5](X) = 24a^3; \quad R[6](X) = 32a^3; \quad R[8](X) = 2a^3 \\ &R[5](Z) = 24a^3; \quad R[6](Z) = 32a^3; \quad R[8](Z) = 2a^2[8 + 7(a-2)]\end{aligned}$$

Table 8.18 Omega polynomial in Sumanene-patched networks: examples

a	Sum-CA_216; $R_{\max}[6]$	e(G)	CI(G)
1	$132x^1 + 48x^2 + 24x^3$	300	89,460
2	$816x^1 + 480x^2 + 96x^3 + 48x^6$	2,352	5,526,576
3	$2{,}484x^1 + 1{,}728x^2 + 216x^3 + 216x^6$	7,884	62,138,340
4	$5{,}568x^1 + 4{,}224x^2 + 384x^3 + 576x^6$	18,624	346,806,720
5	$10{,}500x^1 + 8{,}400x^2 + 600x^3 + 1{,}200x^6$	36,300	1,317,597,300
6	$17{,}712x^1 + 14{,}688x^2 + 864x^3 + 2{,}160x^6$	62,640	3,923,607,600
a	Sum-CA_216, $R_{\max}[8]$	e(G)	CI(G)
1	$48x^2 + 36x^3 + 24x^4$	300	89,100
2	$192x^2 + 120x^3 + 288x^4 + 24x^5 + 48x^6 + 6x^8$	2,352	5,522,736
3	$432x^2 + 252x^3 + 1{,}080x^4 + 72x^5 + 216x^6 + 36x^8$	7,884	62,124,300
4	$768x^2 + 432x^3 + 2{,}688x^4 + 144x^5 + 576x^6 + 108x^8$	18,624	346,772,160
5	$1{,}200x^2 + 660x^3 + 5{,}400x^4 + 240x^5 + 1{,}200x^6 + 240x^8$	36,300	1,317,528,300
6	$1{,}728x^2 + 936x^3 + 950x^4 + 360x^5 + 2{,}160x^6 + 450x^8$	62,640	3,923,486,640
a	Sum_S_2Lex_168; $R_{\max}[6]$	e(G)	CI(G)
1	$60x^1 + 48x^2 + 24x^3$	228	51,516
2	$480x^1 + 384x^2 + 96x^3 + 48x^5$	1,776	3,150,096
3	$1{,}620x^1 + 1{,}296x^2 + 216x^3 + 216x^5$	5,940	35,269,452
4	$3{,}840x^1 + 3{,}072x^2 + 384x^3 + 576x^5$	14,016	196,414,272
5	$7{,}500x^1 + 6{,}000x^2 + 600x^3 + 1{,}200x^5$	27,300	745,223,100
6	$12{,}960x^1 + 10{,}368x^2 + 864x^3 + 2{,}160x^5$	47,088	2,217,163,536
a	Sum_S2Lex_168, $R_{\max}[10]$	e(G)	CI(G)
1	$119x^1 + 27x^2 + 12x^3 + 1x^4 + 1x^7 + 1x^8$	228	51,520
2	$702x^1 + 214x^2 + 100x^3 + 22x^4 + 16x^5 + 2x^6 + 4x^7 + 8x^8 + 6x^9 + 2x^{10}$	1,776	3,149,500
3	$2{,}037x^1 + 743x^2 + 384x^3 + 81x^4 + 66x^5 + 12x^6 + 15x^7 + 29x^8 + 18x^9 + 4x^{10}$	5,940	35,267,308
4	$4{,}412x^1 + 1{,}794x^2 + 984x^3 + 196x^4 + 168x^5 + 36x^6 + 40x^7 + 70x^8 + 36x^9 + 6x^{10}$	14,016	196,409,224
5	$8{,}115x^1 + 3{,}547x^2 + 2{,}020x^3 + 385x^4 + 340x^5 + 80x^6 + 85x^7 + 137x^8 + 60x^9 + 8x^{10}$	27,300	745,213,384
6	$3{,}434x^1 + 6{,}182x^2 + 3{,}612x^3 + 666x^4 + 600x^5 + 150x^6 + 156x^7 + 236x^8 + 90x^9 + 10x^{10}$	47,088	2,217,146,980
a	Sum_CZ_192, $R_{\max}[6]$	e(G)	CI(G)
1	$108x^1 + 48x^2 + 24x^3$	276	75,660
2	$912x^1 + 384x^2 + 192x^3$	2,256	5,085,360
3	$3{,}132x^1 + 1{,}296x^2 + 648x^3$	7,668	58,784,076
4	$7{,}488x^1 + 3{,}072x^2 + 1{,}536x^3$	18,240	332,664,000
5	$14{,}700x^1 + 6{,}000x^2 + 3{,}000x^3$	35,700	1,274,424,300
6	$25{,}488x^1 + 10{,}368x^2 + 5{,}184x^3$	61,776	3,816,160,560

(continued)

Table 8.18 (continued)

a	Sum_CZ_192, $R_{\max}$[8]	e(G)	CI(G)
1	$18x^1 + 48x^2 + 24x^3$	276	75,660
2	$672x^1 + 480x^2 + 96x^3 + 12x^4 + 48x^6$	2,256	5,084,160
3	$2{,}052x^1 + 1{,}728x^2 + 216x^3 + 54x^4 + 216x^6$	7,668	58,778,676
4	$4{,}608x^1 + 4{,}224x^2 + 384x^3 + 144x^4 + 576x^6$	18,240	332,649,600
5	$8{,}700x^1 + 8{,}400x^2 + 600x^3 + 300x^4 + 1{,}200x^6$	35,700	1,274,394,300
6	$14{,}688x^1 + 14{,}688x^2 + 864x^3 + 540x^4 + 2{,}160x^6$	61,776	3,816,106,560

Table 8.19 Number of atoms $v = |V(G)|$ in Sumanene-patched networks

a	$v(N)$	$v(x)$	$v(Z)$
1	216	168	192
2	1,632	1,248	1,536
3	5,400	4,104	5,184
4	12,672	9,600	12,288
5	24,600	18,600	24,000
6	42,336	31,968	41,472

Table 8.20 Number of faces $F(n)$ in Sumanene-patched networks

Structure	N			x			Z		
a	F[5]	F[6]	F[8]	F[5]	F[6]	F[8]	F[5]	F[6]	F[8]
1	24	32	26	24	32	–	24	32	–
2	192	304	208	192	256	16	192	256	64
3	648	1,080	702	648	864	54	648	864	270
4	1,536	2,624	1,664	1,536	2,048	128	1,536	2,048	704
5	3,000	5,200	3,250	3,000	4,000	250	3,000	4,000	1,450
6	5,184	9,072	5,616	5,184	6,912	432	5,184	6,912	2,592

8.8 Networks Patched by Hexagons and Heptagons

At the final, two other networks are presented:

1. C-3Hex (Fig. 8.14, left), patched with hexagons. It is a new net, diu4, group *Pm*-3*m*, point symbol for net: $\{6.8^2\}3\{6^2.8\}6\{6^3\}4$, a 4-nodal 3,3,3,3-c net with stoichiometry (3-c)3(3-c)6(3-c)(3-c)3.
2. C-3Hep (Fig. 8.15, left), patched with heptagons, within the (7,3) Klein tessellation (Klein 1884, 1923). It is the known *kgn* net, group *P*432, point symbol for net (7^3), a 3-nodal 3,3,3-c net, with the net unit C-3HepA_104 (designed by sequence $Op_{2a}(S_2(\mathrm{C}))$ – Fig. 8.15, middle) and co-net C-3HepZ_80 (designed by $Op(S_1(\mathrm{C}))$ – Fig. 8.15, right), both units having the genus $g = 3$.

The units of the above networks were optimized at Hartree-Fock (HF) (HF/6-31G**) and DFT (B3LYP/6-311+G**) levels of theory. The calculations were performed in gas phase by Gaussian 09 (2009). The single-point energy minima obtained for the investigated structures are shown in Table 8.21. Our interest was

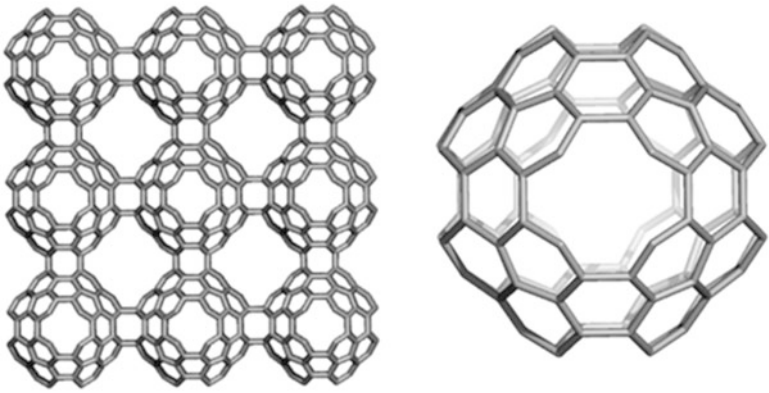

Fig. 8.14 A P-type network, C-3Hex_3,3,3_2808, tessellated by hexagons (*left*) and its unit, C_3HexZ_104 ($f_6 = 36$; $g = 3$ – *right*)

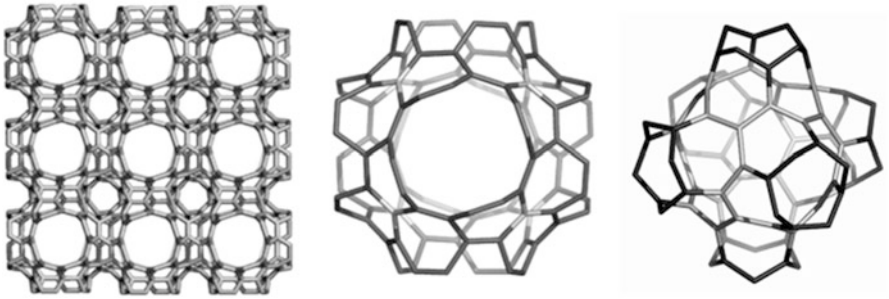

Fig. 8.15 A P-type network, C-3Hep_3,3,3_1944, tessellated by heptagons (*left*) and its net unit (C-3HepA_104; $f_7 = 24$; $g = 3$ – *middle*) and co-net (C-3HepZ_80; $f_7 = 24$; $g = 3$ – *right*)

Table 8.21 Energies (total energy per carbon atom) TE/C (au), HOMO-LUMO gap (eV), strain energy per carbon atom (kcal/mol)

Structure	Theory level	TE/C (au)	Gap (eV)	Strain/C (kcal/mol)	C_{60} relative strain
C_{60}	HF	−37.864	7.418	8.256	1.000
C_3HexZ_104	HF	−37.999	5.342	2.329	0.282
C_3HepA_104	HF	−38.127	6.942	0.240	0.029
C_{60}	DFT	−38.110	2.724	8.256	1.000
C_3HexZ_104	DFT	−38.244	1.658	2.352	0.285
C_3HepA_104	FDT	−38.376	1.354	0.192	0.023

related to the stability of these units, as they show a lower strain (by POAV theory – Haddon 1990, 2001) in comparison to C_{60}, the reference structure in Nanoscience. The open structures were calculated as hydrogen-ended ones. The total energy per carbon atom TE/C and HOMO-LUMO gap values are close to the reference while the strain is relaxed, from C_{60} to C-3Hex and C-3Hep (lower, by

two orders of magnitude, see the last column in Table 8.21). These data give the hope of possible synthesis of such ordered structures in the future experiments in laboratory.

8.9 Conclusions

A network embedded in the P-type surface can be considered a decoration of this surface; basically, it belongs to the space group *Pm*-3*m*. Among many such P-networks there are some ones (having as repeating units) representations of celebrate structures, e.g., P-(7,3) network represents the Klein tessellation (Klein 1884, 1923) while P-(8,3) network is the representation of Dyck graph (Dyck 1880), the last one being registered by Topo Group Cluj (as diu8; Topos). Construction of these networks/decorations was made by using sequences of map operations implemented in the CVNET software (Stefu and Diudea 2005) for the repeating units while their assembly/embedding was done by the aid of Nano Studio program (Nagy and Diudea 2009), both of them developed at Topo Group Cluj. Topology of these networks was described by Omega polynomial (also developed in Cluj), as a complement to the crystallographic classical description. Quantum computations, at Hartree-Fock level of theory, have shown pertinent stability for some repeating units and small related structures, encouraging future researches in experimental realization of such exciting structures with unexpected properties.

References

Ashrafi AR, Ghorbani M, Jalali M (2008) Computing Sadhana polynomial of V-phenylenic nanotubes and nanotori. Indian J Chem A 47:535–537

Baerlocher C, Meier WH, Olson DH (2007) Atlas of zeolite framework types, 6th edn. Elsevier, Amsterdam

Benedek G, Vahedi-Tafreshi H, Barborini E, Piseri P, Milani P, Ducati C, Robertson J (2003) The structure of negatively curved spongy carbon. Diam Relat Mater 12:768–773

Ceulemans A, King RB, Bovin SA, Rogers KM, Troisi A, Fowler PW (1999) The heptakisoctahedral group and its relevance to carbon allotropes with negative curvature. J Math Chem 26:101–123

Diudea MV (2004) Covering forms in nanostructures. Forma (Tokyo) 19:131–163

Diudea MV (2005) Nanoporous carbon allotropes by septupling map operations. J Chem Inf Model 45:1002–1009

Diudea MV (2006) Omega polynomial. Carpath J Math 22:43–47

Diudea MV (2010a) Nanomolecules and nanostructures – polynomials and indices, MCM, No. 10. University of Kragujevac, Kragujevac

Diudea MV (2010b) Omega polynomial in all_R[8] lattices. Iran J Math 1:69–77

Diudea MV, Ilić A (2010) Omega polynomial in crystal-like single-type face/ring networks. Int J Chem Model 3:65–71

Diudea MV, Katona G (1999) Molecular topology of dendrimers. In: Newkome G.A. (ed) Adv Dendritic Macromol 4(1999):135–201

Diudea MV, Klavžar S (2010) Omega polynomial revisited. Acta Chem Slov 57:565–570
Diudea MV, Nagy CL (2007) Periodic nanostructures. Springer, Dordrecht
Diudea MV, Petitjean M (2008) Symmetry in multi tori. Symmetry Cult Sci 19(4):285–305
Diudea MV, Katona G, Pârv B (1997) Delta number, DΔ, of dendrimers. Croat Chem Acta 70: 509–517
Diudea MV, John PE, Graovac A, Primorac M, Pisanski T (2003) Leapfrog and related operations on toroidal fullerenes. Croat Chem Acta 76:153–159
Diudea MV, Ştefu M, John PE (2005) Composite operations on maps. Studia Univ Babes Bolyai 50:165–174
Diudea MV, Ştefu M, John PE, Graovac A (2006) Generalized operations on maps. Croat Chem Acta 79:355–362
Diudea MV, Cigher S, John PE (2008) Omega and related counting polynomials. MATCH Commun Math Comput Chem 60:237–250
Diudea MV, Cigher S, Vizitiu AE, Florescu MS, John PE (2009) Omega polynomial and its use in nanostructure description. J Math Chem 45:316–329
Diudea MV, Nagy K, Pop ML, Gholami-Nezhaad F, Ashrafi AR (2010) Omega and PI_v polynomial in Dyck graph-like Z(8)-unit networks. Int J Nanosci Nanotechnol 6:97–103
Diudea MV, Vizitiu AE, Cigher S (2011) Omega and related polynomials in crystal-like structures. MATCH Commun Math Comput Chem 65:131–142
Djoković DŽ (1973) Distance preserving subgraphs of hypercubes. Comb J Theory Ser B 14: 263–267
Dyck W (1880) Ueber Aufstellung und Untersuchung von Gruppe und Irrationalität regulärer Riemann'sher Flächen. Mathematische Ann 17:473–509
Gaussian 09, Revision A.1, Frisch MJ, Trucks GW, Schlegel HB, Scuseria GE, Robb MA, Cheeseman JR, Scalmani G, Barone V, Mennucci B, Petersson GA, Nakatsuji H, Caricato M, Li x, Hratchian HP, Izmaylov AF, Bloino J, Zheng G, Sonnenberg JL, Hada M, Ehara M, Toyota K, Fukuda R, Hasegawa J, Ishida M, Nakajima T, Honda Y, Kitao O, Nakai H, Vreven T, Montgomery JA, Peralta JE, Ogliaro F, Bearpark M, Heyd JJ, Brothers E, Kudin KN, Staroverov VN, Kobayashi R, Normand J, Raghavachari K, Rendell A, Burant JC, Iyengar SS, Tomasi J, Cossi M, Rega N, Millam NJ, Klene M, Knox JE, Cross JB, Bakken V, Adamo C, Jaramillo J, Gomperts R, Stratmann RE, Yazyev O, Austin AJ, Cammi R, Pomelli C, Ochterski JW, Martin RL, Morokuma K, Zakrzewski VG, Voth GA, Salvador P, Dannenberg JJ, Dapprich S, Daniels AD, Farkas Ö, Foresman JB, Ortiz JV, Cioslowski J, Fox DJ (2009) Gaussian Inc, Wallingford
Haddon RC (1990) Measure of nonplanarity in conjugated organic molecules: which structurally characterized molecule displays the highest degree of pyramidalization? J Am Chem Soc 112:3385–3389
Haddon RC (2001) Comment on the relationship of the pyramidalization angle at a conjugated carbon atom to the σ bond angles. J Phys Chem A 105:4164–4165
Harary F (1969) Graph theory. Addison-Wesley, Reading
John PE, Vizitiu AE, Cigher S, Diudea MV (2007) CI index in tubular nanostructures. MATCH Commun Math Comput Chem 57:479–484
Khadikar PV, Agrawal VK, Karmarkar S (2002) Prediction of lipophilicity of polyacenes using quantitative structure-activity relationships. Bioorg Med Chem 10:3499–3507
Khadikar PV, Joshi S, Bajaj AV, Mandloi D (2004) Correlations between the benzene character of acenes or helicenes and simple molecular descriptors. Bioorg Med Chem Lett 14:1187–1191
Klavžar S (2008) Some comments on Co graphs and CI index. MATCH Commun Math Comput Chem 59:217–222
Klein F (1884) Vorlesungen über das Ikosaeder. Teubner, Leipzig: Part I, chapter II
Klein F (1923) Gesammelten Mathematischen Abhandlungen, vol 3. Springer, Berlin, pp 90–136
Lenosky T, Gonze X, Teter M, Elser V (1992) Energetics of negatively curved graphitic carbon. Nature 355:333–335
Mackay AL, Terrones H (1991) Diamond from graphite. Nature 352:762–762
Nagy CL, Diudea MV (2009) Nano studio software. Babes-Bolyai University, Cluj

O'Keeffe M, Adams GB, Sankey OF (1992) Predicted new low energy forms of carbon. Phys Rev Lett 68:2325–2328

Saheli M, Mehtari-Arani M, Szefler B (2012) Omega polynomial in ast-crystal structure. Studia Univ Babes Bolyai Chemia 57(3):000–000

Stefu M, Diudea MV (2005) CageVersatile_CVNET. Babes-Bolyai University, Cluj

Stefu M, Bucila V, Diudea MV (2010) Omega polynomial in P-type surface networks. Studia Univ Babes-Bolyai Chemia 55(4):211–214

Szefler B, Saheli M, Diudea MV (2012) Sumanene units in P-type surface networks. Acta Chim Slov 59:177–182

Terrones H, Mackay AL (1997) From C_{60} to negatively curved graphite. Prog Crystal Growth and Character 34:25–36

Terrones M, Banhart F, Grobert N, Charlier J-C, Terrones H, Ajayan PM (2002b) Molecular junctions by joining single-walled carbon nanotubes. Phys Rev Lett 89(1–4):075505

Vanderbilt D, Tersoff J (1992) Negative-curvature fullerene analog of C_{60}. Phys Rev Lett 68: 511–513

Winkler PM (1984) Isometric embedding in products of complete graphs. Discrete Appl Math 8:209–212

Chapter 9
Omega Polynomial in Hyperdiamonds

Mircea V. Diudea, Aleksandar Ilić, and Mihai Medeleanu

Abstract Hyperdiamonds are covalently bonded carbon phases, more or less related to the diamond network, having a significant amount of sp^3 carbon atoms and similar physical properties. Many of them have yet a hypothetical existence but a well-theorized description. Among these, the diamond D_5 was studied in detail, as topology, at TOPO GROUP CLUJ, Romania. The theoretical instrument used was the Omega polynomial, also developed in Cluj. It was computed in several 3D network domains and analytical formulas have been derived, not only for D_5 but also for the well-known diamond D_6 and other known networks.

9.1 Introduction

Diamond D_6 (Fig. 9.1), the beautiful classical diamond, with all-hexagonal rings of sp^3 carbon atoms crystallized in a face-centered cubic *fcc* network (space group *Fd3m*), has kept its leading interest among the carbon allotropes, even many "nano" varieties appeared (Decarli and Jamieson 1961; Aleksenskiĭ et al. 1997; Osawa 2007, 2008; Williams et al. 2007; Dubrovinskaia et al. 2006). Its mechanical

M.V. Diudea (✉)
Department of Chemistry, Faculty of Chemistry and Chemical Engineering, "Babes-Bolyai" University, Arany Janos Str. 11, 400028 Cluj, Romania
e-mail: diudea@chem.ubbcluj.ro

A. Ilić
Department of Computer Science, Faculty of Sciences and Mathematics, University of Niš, Višegradska 33, 18000 Niš, Serbia

M. Medeleanu
Department of Applied Chemistry and Organic and Natural Compounds Engineering, Faculty of Industrial Chemistry and Environmental Engineering, University "Politehnica" Timisoara, P-ta Victoriei, nr. 2, RO-300006 Timisoara, Romania

M.V. Diudea and C.L. Nagy (eds.), *Diamond and Related Nanostructures*, Carbon Materials: Chemistry and Physics 6, DOI 10.1007/978-94-007-6371-5_9,

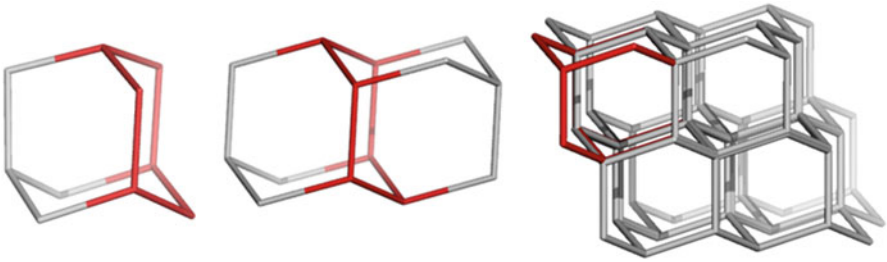

Fig. 9.1 Diamond D_6: adamantane D_6_10 (*left*), diamantane D_6_14 (*middle*), and diamond D_6_52 (a 222 net – *right*)

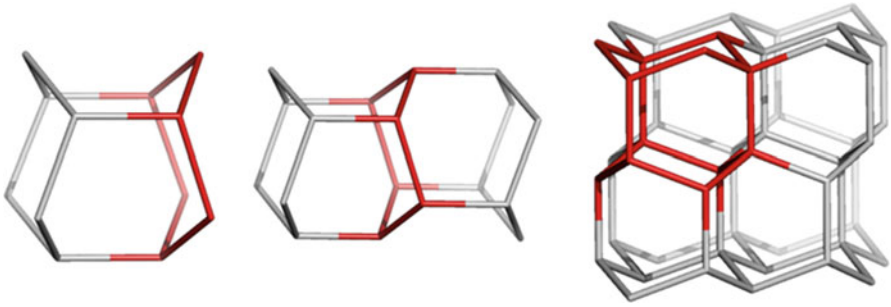

Fig. 9.2 Lonsdaleite: L_6_12 (*left*), L_6_18 (*middle*), and L_6_48 (a 222 net – *right*)

characteristics are of great importance, and composites including diamonds may overpass the resistance of steel or other metal alloys. Synthetic diamonds can be produced by a variety of methods, including high pressure-high temperature HPHT, static or detonation procedures, chemical vapor deposition CVD (Lorenz 1995), ultrasound cavitation (Khachatryan et al. 2008), or mechano-synthesis (Tarasov et al. 2011), under electronic microscopy.

A relative of the diamond D_6, called lonsdaleite L_6 (Frondel and Marvin 1967), with a hexagonal network (space group $P6_3/mmc$ – Fig. 9.2), was discovered in a meteorite in the Canyon Diablo, Arizona, in 1967. Several diamond-like networks have also been proposed (Diudea and Nagy 2007; Diudea et al. 2010a; Hyde et al. 2008).

Hyperdiamonds are covalently bonded carbon phases, more or less related to the diamond network, having a significant amount of sp^3 carbon atoms. Their physical properties are close to that of the classical diamond, sometimes with exceeding hardness and/or endurance.

Design of several hypothetical crystal networks was performed by using our software programs (Diudea 2010a) CVNET and NANO-STUDIO. Topological data were provided by NANO-STUDIO, Omega, and PI programs.

This chapter is structured as follows. After the introductory part, the main networks, diamond D_5 and lonsdaleite L_5, are presented in detail. Next, two

other nets, the uninodal net, called rhr, and the hyper boron nitride, are designed. Two sections with basic definitions in Omega polynomial and in Omega-related polynomials, respectively, are developed in the following. The topology of the discussed networks will be presented in the last part. Conclusions and references will close the chapter.

9.2 Structures Construction

9.2.1 Diamond D_5 Network

Diamond **D_5**, recently theorized by Diudea and collaborators (Diudea and Ilić 2011; Diudea 2010b; Diudea and Nagy 2012; Diudea et al. 2012), is a hyperdiamond, whose seed is the centrohexaquinane C_{17} (Fig. 9.3). D_5 is the *mtn* crystal 4,4,4-c trinodal network, appearing in type II clathrate hydrates; it belongs to the space group Fd-3m and has point symbol net: {5^5.6}12{5^6}5 (Dutour Sikirić et al. 2010; Delgado-Friedrichs and O'Keeffe 2006, 2010). The hyper-structures, from ada- to dia- and a larger net are illustrated in Fig. 9.4, viewed both from C_{20} (left column) and C_{28} (right column) basis, respectively (Diudea et al. 2012).

The hyperdiamond D_5_20/28 mainly consists of sp^3 carbon atoms building ada-like repeating units (C_{20} cages including C_{28} as hollows). The ratio C-sp^3/C-total trends to 1 in a large enough network. As the content of pentagons *R*[5] per total rings trends to 90 % (see Table 9.3, entry 9), this yet hypothetical carbon allotrope is called the diamond D_5.

Energetic data, calculated at various DFT levels (Diudea and Nagy 2012; Diudea et al. 2012), show a good stability of the start and intermediate structures. Limited cubic domains of the D_5 networks have also been evaluated for stability, data proving a pertinent stability of D_5 diamond.

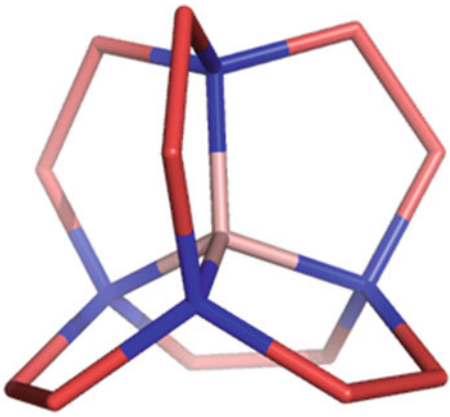

Fig. 9.3 The seed of diamond D_5: C_{17}

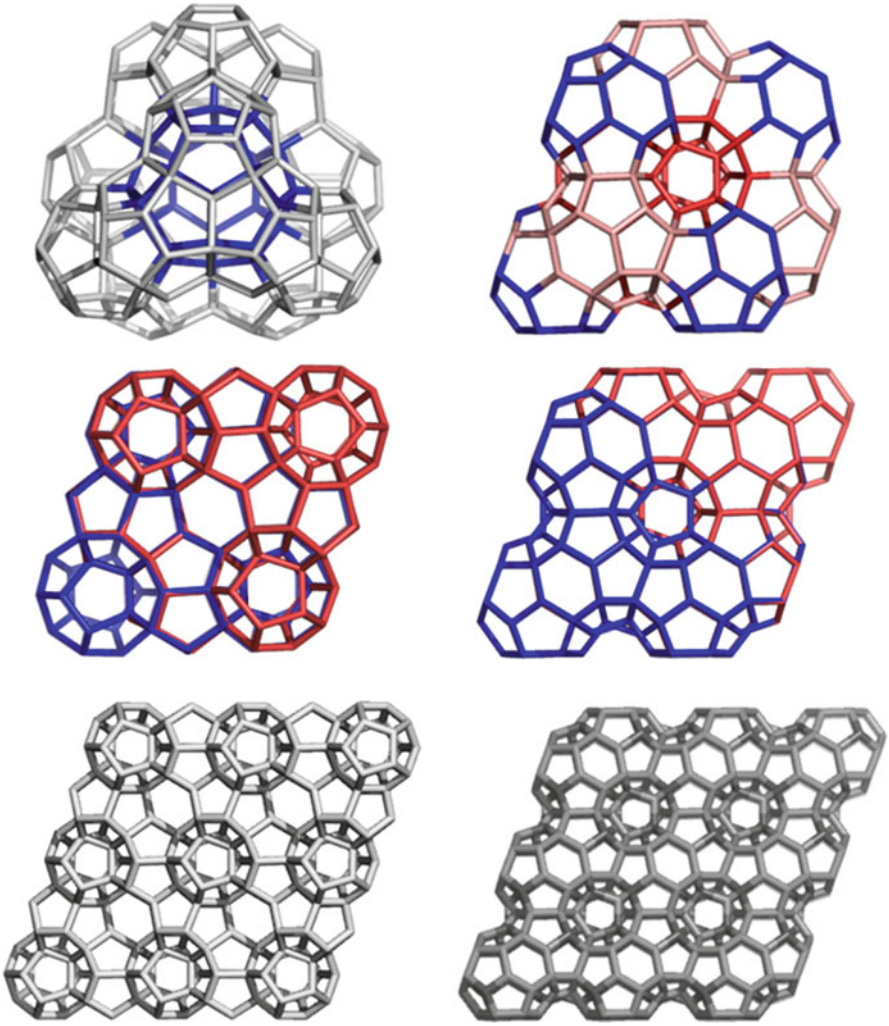

Fig. 9.4 Hyper-adamantane: ada_20_158 and ada_28_213 (*top*), diamantane: dia_20_226_222 and dia_28_292_222 (*middle*), and diamond D_5_20_860_333 and D_5_28_ 1022_333 co-net (*bottom*)

9.2.2 Lonsdaleite L_5 Network

By analogy to D_5_20/28, a lonsdaleite-like net was proposed (Diudea et al. 2012) (Fig. 9.5). The hyper-hexagons L_5_28_134 (Fig. 9.5, middle and right), whose nodes represent the C_{28} fullerene, was used as the monomer (in the chair conformation). Its corresponding co-net L_5_20 was also designed. The lonsdaleite L_5_28/20 is partially

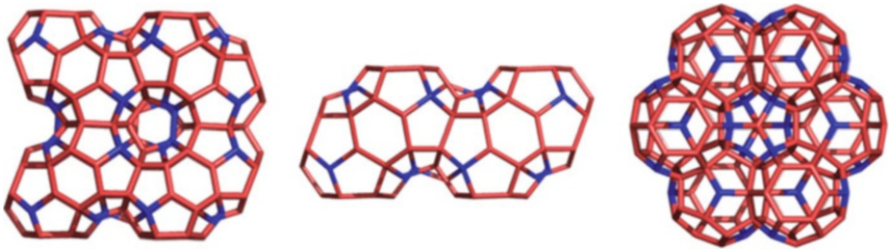

Fig. 9.5 Lonsdaleite: L_5_28_250 (*side view*, *left*), L_5_28_134 (*side view*, *middle*), and L_5_28_134 (*top view*, *right*)

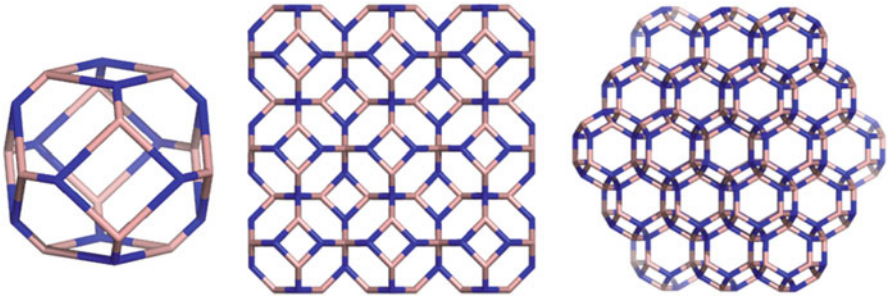

Fig. 9.6 Boron nitride $B_{12}N_{12}$: truncated octahedron (*left*), a cubic (3,3,3)_432 domain built up from truncated octahedra joined by identifying the square faces (*middle*), and a corner view (*right*)

superimposed on D_5_20/28 net. In crystallography, L_5 is known as the 7-nodal mgz-x-d net, with the point symbol: {5^5.6}12{5^6}5.

9.2.3 Hyper Boron Nitride

Boron nitride is a chemical crystallized basically as the carbon allotropes: graphite (**h-BN**), cubic-diamond D_6 (**c-BN**), and lonsdaleite L_6 (wurtzite **w-BN**). Their physicochemical properties are also similar, with small differences.

Fullerene-like cages have been synthesized and several theoretical structures have been proposed for these molecules (Soma et al. 1974; Stephan et al. 1998; Jensen and Toftlund 1993; Mei-Ling Sun et al. 1995; Fowler et al. 1999; Oku et al. 2001; Narita and Oku 2001).

Based on $B_{12}N_{12}$ unit, with the geometry of truncated octahedron, we modeled three 3D arrays: a cubic domain, Fig. 9.6; a dual of cuboctahedron domain, Fig. 9.7; and an octahedral domain, Fig. 9.8.

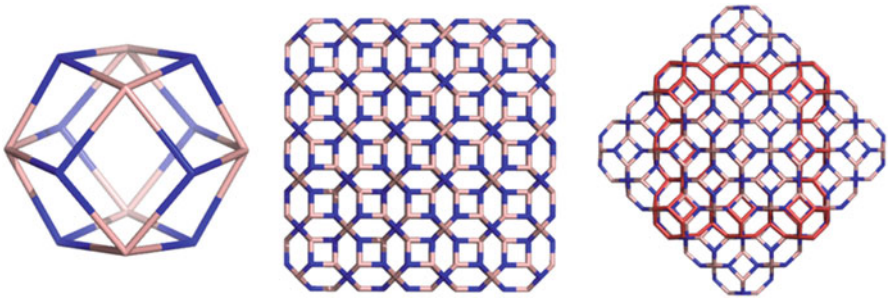

Fig. 9.7 Boron nitride $B_{12}N_{12}$: dual of cuboctahedron (*left*), a (3,3,3)_648 dual of cuboctahedron domain, constructed from truncated octahedra by identifying the square and hexagonal faces, respectively (*middle*), and its superposition with the cubic (3,3,3)_432 domain (*right*)

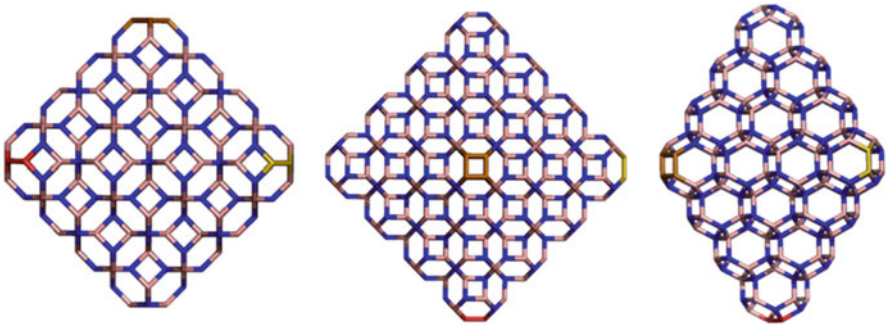

Fig. 9.8 Boron nitride $B_{12}N_{12}$: an octahedral (4,4,4)_480 domain: (1,1,0-*left*), (0,0,1-*central*), and (2,1,1-*right*) constructed from truncated octahedra by identifying the square and hexagonal faces, respectively

The topology of the above hyperdiamonds will be described by using the net parameter *k*, meaning the number of repeat units along the chosen 3D direction, and by the formalism of several counting polynomials, the largest part being devoted to Omega polynomial.

9.2.4 rhr Network

A uninodal 4-c net with a point $\{4^2.6^2.8^2\}$ was named *rhr* or sqc5544. In topological terms, its unit cell is a homeomorphic of cuboctahedron, one of the semi-regular polyhedra (Fig. 9.9). It can be obtained by making the medial operation on the cube or octahedron (Diudea 2010a). The net can be constructed by identifying the vertices of degree 2 in two repeating units, thus the resulting net will have all points of degree 4, as in the classical diamond D_6 (but the rings are both six- and eight-membered ones).

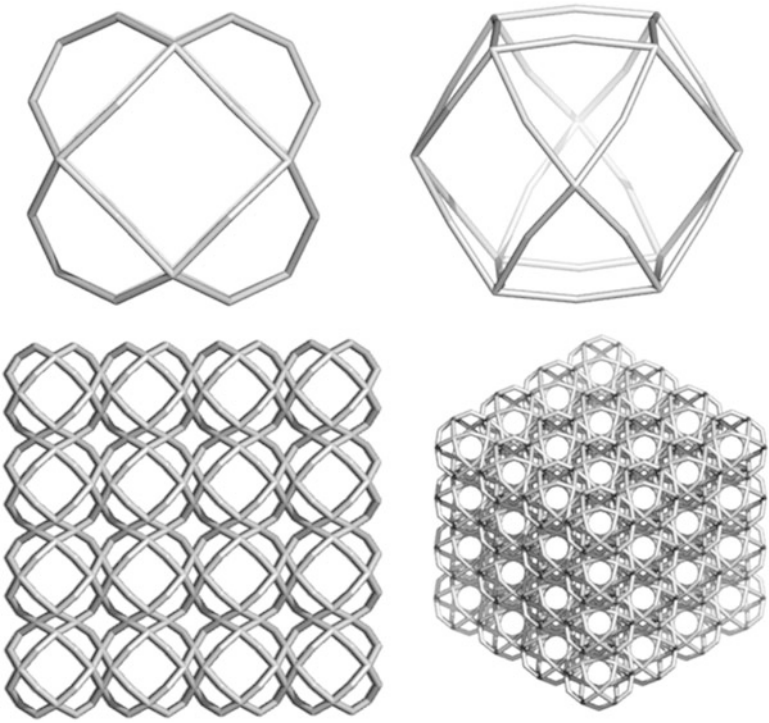

Fig. 9.9 The *rhr* unit (*top*) and network (444_1728, *bottom*: top view (*left*) and corner view (*right*))

9.3 Omega Polynomial

9.3.1 Relations co and op

Let $G = (V(G),E(G))$ be a connected graph, with the vertex set $V(G)$ and edge set $E(G)$. Two edges $e = (u,v)$ and $f = (x,y)$ of G are called *co-distant* (briefly: $e\ co\ f$) if the notation can be selected such that (Diudea 2010a; John et al. 2007; Diudea and Klavžar 2010)

$$e\ co\ f \Leftrightarrow d(v,x) = d(v,y) + 1 = d(u,x) + 1 = d(u,y) \tag{9.1}$$

where d is the usual shortest-path distance function. Relation *co* is reflexive, that is, $e\ co\ e$ holds for any edge e of G and it is also symmetric: if $e\ co\ f$, then also $f\ co\ e$. In general, *co* is not transitive.

For an edge $e \in E(G)$, let $c(e) := \{f \in E(G);\ f\ co\ e\}$ be the set of edges co-distant to e in G. The set $c(e)$ is called an *orthogonal cut* (*oc* for short) of G, with respect to e. If G is a *co*-graph then its orthogonal cuts $C(G) = c_1,\ c_2, \ldots, c_k$ form a partition:

$$E(G) = c_1 \cup c_2 \cup \cdots \cup c_k, \quad c_i \cap c_j = \emptyset,\ \ i \neq j$$

A subgraph $H \subseteq G$ is called *isometric* if $d_H(u, v) = d_G(u, v)$, for any $(u, v) \in H$; it is *convex* if any shortest path in G between vertices of H belongs to H. The n-cube Q_n is the graph whose vertices are all binary strings of length n, two strings being adjacent if they differ in exactly one position (Harary 1969). A graph G is called a *partial cube* if there exists an integer n such that G is an isometric subgraph of Q_n.

For any edge $e = (u,v)$ of a connected graph G, let n_{uv} denote the set of vertices lying closer to u than to v: $n_{uv} = \{w \in V(G) | d(w, u) < d(w, v)\}$. By definition, it follows that $n_{uv} = \{w \in V(G) | d(w, v) = d(w, u) + 1\}$. The sets (and subgraphs) induced by these vertices, n_{uv} and n_{vu}, are called *semicubes* of G; these semicubes are *opposite* and disjoint (Diudea and Klavžar 2010; Diudea et al. 2008; Diudea 2010c).

A graph G is *bipartite* if and only if, for any edge of G, the opposite semicubes define a partition of G: $n_{uv} + n_{vu} = v = |V(G)|$.

The relation *co* is related to the $\sim$ (Djoković 1973) and Θ (Winkler 1984) relations:

$$e\ \Theta\ f \Leftrightarrow d(u, x) + d(v, y) \neq d(u, y) + d(v, x) \tag{9.2}$$

Lemma 9.1 *In any connected graph, co* $= \sim$.

In general graphs, we have $\sim \subseteq \Theta$ and in bipartite graphs $\sim = \Theta$. From this and the above lemma, it follows (Diudea and Klavžar 2010)

Proposition 9.1 *In a connected graph, co* $= \sim$; *if G is also bipartite, then co* $= \sim = \Theta$.

Theorem 9.1 *In a bipartite graph, the following statements are equivalent* (Diudea and Klavžar 2010):

(i) G is a *co*-graph.
(ii) G is a partial cube.
(iii) All semicubes of G are convex.
(iv) Relation Θ is transitive.

Equivalence between (i) and (ii) was observed in Klavžar (2008), equivalence between (ii) and (iii) is due to Djoković (1973), while the equivalence between (ii) and (iv) was proved by Winkler (1984).

Two edges e and f of a plane graph G are in relation *opposite*, $e\ op\ f$, if they are opposite edges of an inner face of G. Then $e\ co\ f$ holds by assuming the faces

are isometric. Note that relation *co* involves distances in the whole graph while *op* is defined only locally (it relates face-opposite edges). A partial cube is also a *co*-graph but the reciprocal is not always true. There are *co*-graphs which are non-bipartite (Diudea 2010d), thus being non-partial cubes.

Relation *op* partitions the edge set of G into *opposite* edge *strips ops*: any two subsequent edges of an *ops* are in *op*-relation, and any three subsequent edges of such a strip belong to adjacent faces.

Lemma 9.2 *If G is a co-graph, then its opposite edge strips ops $\{s_k\}$ superimpose over the orthogonal cuts ocs $\{c_k\}$.*

Proof Recall the *co*-relation is defined on parallel equidistant edges relation (9.1). The same is true for the *op*-relation, with the only difference (9.1) is limited to a single face. Suppose e_1*and* e_2 are two consecutive edges of *ops*; by definition, they are topologically parallel and also *co*-distant (i.e., belong to *ocs*). By induction, any newly added edge of *ops* will be parallel to the previous one and also *co*-distant. Because, in *co*-graphs, c*o*-relation is transitive, all the edges of *ops* will be *co*-distant, thus *ops* and *ocs* will coincide.

Corollary 9.1 *In a co-graph, all the edges of an ops are topologically parallel.*

Observe that the relation *co* is a particular case of the edge *equidistance eqd* relation. The equidistance of two edges $e = (uv)$ and $f = (xy)$ of a connected graph G includes conditions for both (i) topologically parallel edges (relation (9.1)) and (ii) topologically perpendicular edges (in the Tetrahedron and its extensions – relation (9.3)) (Diudea et al. 2008; Ashrafi et al. 2008a):

$$e\ eqd\ f(ii) \Leftrightarrow d(u,x) = d(u,y) = d(v,x) = d(v,y) \tag{9.3}$$

The *ops* strips can be either cycles (if they start/end in the edges e_{even} of the same even face f_{even}) or paths (if they start/end in the edges e_{odd} of the same or different odd faces f_{odd}).

Proposition 9.2 *Let G be a planar graph representing a polyhedron with the odd faces insulated from each other. The set of ops strips $S(G) = \{s_1, s_2, \ldots, s_k\}$ contains a number of op paths opp which is exactly half of the number of odd face edges $e_{\text{odd}}/2$.*

Proof of Proposition 9.2 was given in Diudea and Ilić (2009).

Corollary 9.2 *In a planar bipartite graph, representing a polyhedron, all ops strips are cycles.*

The *ops* is maximum possible, irrespective of the starting edge. The choice is about the maximum size of face/ring searched, and mode of face/ring counting, which will decide the length of the strip.

Definitions 9.1 *Let G be an arbitrary connected graph and $s_1, s_2, \ldots, s_k$ be its op strips. Then ops form a partition of $E(G)$ and the* Ω*-polynomial* (Diudea 2006) *of G is defined as*

$$\Omega(x) = \sum_{i=1}^{k} x^{|s_i|} \tag{9.4}$$

Let us now consider the set of edges *co*-distant to edge e in G, $c(e)$. A Θ-polynomial (Diudea et al. 2008), counting the edges equidistant to every edge e, is written as

$$\Theta(x) = \sum_{e \in E(G)} x^{|c(e)|} \tag{9.5}$$

Suppose now G is a *co*-graph, when $|c_k| = |s_k|$, then (Diudea and Klavžar 2010)

$$\Theta(x) = \sum_{e \in E(G)} x^{|c(e)|} = \sum_{i=1}^{k} \sum_{e \in S_i} x^{|c(e)|} = \sum_{e} |c(e)| x^{|c(e)|} = \sum_{i=1}^{k} |s_i| x^{|s_i|} \tag{9.6}$$

Let us simplify a little the above notations: note by $m(s)$ or simply m the number of *ops* of length $s = |s_k|$ and rewrite the Omega polynomial as (Diudea 2010a; Ashrafi et al. 2008b; Khadikar et al. 2002; Diudea et al. 2010b)

$$\Omega(x) = \sum_{s} m \cdot x^{s} \tag{9.7}$$

Next we can write Theta and other two related polynomials, as follows:

$$\Theta(x) = \sum_{s} ms \cdot x^{s} \tag{9.8}$$

$$\Pi(x) = \sum_{s} ms \cdot x^{e-s} \tag{9.9}$$

$$\mathrm{Sd}(x) = \sum_{s} m \cdot x^{e-s} \tag{9.10}$$

The polynomial $\Theta(x)$ counts equidistant edges while $\Pi(x)$ counts non-equidistant edges. The Sadhana polynomial, proposed by Ashrafi et al. (2008b) in relation with the Sadhana index $\mathrm{Sd}(G)$ proposed by Khadikar et al. (2002), counts non-opposite edges in G. Their first derivative (in $x = 1$) provides single-number topological descriptors also termed topological indices (Diudea 2010a):

$$\Omega'(1) = \sum_{s} m \cdot s = e = |E(G)| \tag{9.11}$$

$$\Theta'(1) = \sum_{s} m \cdot s^2 = \theta(G) \tag{9.12}$$

$$\Pi'(1) = \sum_{s} ms \cdot (e - s) = \Pi(G) \tag{9.13}$$

$$\mathrm{Sd}'(1) = \sum_s m \cdot (e - s) = e(\mathrm{Sd}(1) - 1) = \mathrm{Sd}(G) \tag{9.14}$$

Note $\mathrm{Sd}(1) = \Omega(1)$, then the first derivative given in (9.14) is the product of the number of edges $e = |E(G)|$ and the number of strips $\Omega(1)$ less one.

On Omega polynomial, the Cluj-Ilmenau index (Ashrafi et al. 2008a) $\mathrm{CI} = \mathrm{CI}(G)$ was defined as

$$\mathrm{CI}(G) = \left\{[\Omega'(1)]^2 - [\Omega'(1) + \Omega''(1)]\right\} \tag{9.15}$$

A polynomial related to $\Pi(x)$ was defined by Ashrafi et al. (2008b) as

$$\mathrm{PI}_e(x) = \sum_{e \in E(G)} x^{n(e,u)+n(e,v)} \tag{9.16}$$

where $n(e,u)$ is the number of edges lying closer to the vertex u than to the v vertex. Its first derivative (in $x = 1$) provides the $\mathrm{PI}_e(G)$ index proposed by Khadikar (2000) and developed by Ashrafi et al. (2006).

Proposition 9.3 *In any bipartite graph,* $\Pi(G) = \mathrm{PI}_e(G)$.

Proof Ashrafi defined the equidistance of edges by considering the distance from a vertex z to the edge $e = uv$ as the minimum distance between the given point and the two endpoints of that edge (Ashrafi et al. 2006, 2008a):

$$d(z, e) = \min\{d(z, u), d(z, v)\} \tag{9.17}$$

Then, for two edges $e = (uv)$ and $f = (xy)$ of G,

$$e \; eqd \; f(iii) \Leftrightarrow d(x, e) = d(y, e) \quad \text{and} \quad d(u, f) = d(v, f) \tag{9.18}$$

In bipartite graphs, relations (9.1) and (9.3) superimpose over relations (9.17) and (9.18), then in such graphs, $\Pi(G) = \mathrm{PI}_e(G)$. In general graphs, this is, however, not true.

Proposition 9.4 *In co-graphs, the equality* $\mathrm{CI}(G) = \Pi(G)$ *holds.*

Proof By definition, one calculates

$$\begin{aligned} \mathrm{CI}(G) &= \left(\sum_{i=1}^{k} |s_i|\right)^2 - \left(\sum_{i=1}^{k} |s_i| + \sum_{i=1}^{k} |s_i|(|s_i| - 1)\right) \\ &= |E(G)|^2 - \sum_{i=1}^{k} (|s_i|)^2 = \Pi'(G, 1) = \Pi(G) \end{aligned} \tag{9.19}$$

Relation (9.19) is valid only when assuming $|c_k| = |s_k|$, $k = 1,2,\ldots$, thus providing the same value for the exponents of Omega and Theta polynomials; this is precisely achieved in *co*-graphs. In general graphs, however, $|s_i| \neq |c_k|$ and as a consequence, $CI(G) \neq \Pi(G)$ (Diudea 2010a).

In partial cubes, which are also bipartite, the above equality can be expanded to the triple one:

$$CI(G) = \Pi(G) = PI_e(G) \tag{9.20}$$

a relation which is not obeyed in all *co*-graphs (e.g., in non-bipartite ones).

There is also a vertex-version of PI index, defined as (Nadjafi-Arani et al. 2009; Ilić 2010)

$$PI_v(G) = PI'_v(1) = \sum_{e=uv} n_{u,v} + n_{v,u} = |V| \cdot |E| - \sum_{e=uv} m_{u,v} \tag{9.21}$$

where $n_{u,v}$, $n_{v,u}$ count the non-equidistant vertices with respect to the endpoints of the edge $e = (u,v)$ while $m(u,v)$ is the number of equidistant vertices *vs* u and v. However, it is known that, in bipartite graphs, there are no equidistant vertices *vs*. any edge, so that the last term in (9.21) will miss. The value of $PI_v(G)$ is thus maximal in bipartite graphs, among all graphs on the same number of vertices; this result can be used as a criterion for checking whether the graph is bipartite (Diudea 2010a).

9.3.2 Omega Polynomial of Diamond D_6 and Lonsdaleite L_6

Topology of the classical diamond D_6 and lonsdaleite L_6 is listed in Table 9.1 (Diudea et al. 2011). Along with Omega polynomial, formulas to calculate the number of atoms in a cuboid of dimensions (k,k,k) are given. Above, k is the number of repeating units along the edge of such a cubic domain. One can see that the ratio $C(sp^3)/v(G)$ approaches the unity; this means that in a large enough net almost all atoms are tetra-connected, a basic condition for a structure to be diamondoid. Examples of calculus are given in Table 9.2.

9.3.3 Omega Polynomial of Diamond D_5 and Lonsdaleite L_5

Topology of diamond D_5 and lonsdaleite L_5, in a cubic (k,k,k) domain, is presented in Tables 9.3, 9.4, 9.5, 9.6, 9.7, and 9.8 (Diudea et al. 2011). Formulas to calculate Omega polynomial, number of atoms, number of rings, and the limits (to infinity) for the ratio of sp^3 C atoms over total number of atoms and also the ratio $R[5]$ over the total number of rings as well as numerical examples are given.

Table 9.1 Omega polynomial in diamond D_6 and lonsdaleite L_6 nets, function of the number of repeating units along the edge of a cubic (*k*,*k*,*k*) domain

	Network
A	Omega(D_6); *R*[6]
1	$\Omega(D_6\_k_{\text{odd}}, x) = \left(\sum_{i-1}^{k} 2x^{\frac{(i+1)(i+2)}{2}}\right) + \left(\sum_{i-1}^{(k-1)/2} 2x^{\frac{(k+1)(k+2)}{2} + \frac{k\times k-1}{4} - i(i-1)}\right) + 3kx^{(k+1)^2}$
2	$\Omega(D_6\_k_{\text{even}}, x) = \left(\sum_{i-1}^{k} 2x^{\frac{(i+1)(i+2)}{2}}\right) + \left(\sum_{i-1}^{k/2} 2x^{\frac{(k+1)(k+2)}{2} + \frac{k\times k}{4} - (i-1)(i-1)}\right) - x^{\frac{(k+1)(k+2)}{2} + \frac{k\times k}{4}} + 3kx^{(k+1)^2}$
3	$\Omega'(1) = e(G) = -1 + 6k + 9k^2 + 4k^3$
4	$\text{CI}(G) = 2 - 187k/10 - k^2/4 + 305k^3/4 + 457k^4/4 + 1,369k^5/20 + 16k^6$
5	$v(G) = 6k + 6k^2 + 2k^3$
6	$\text{Atoms}(sp^3) = -2 + 6k + 2k^3$
7	$R[6] = 3k^2 + 4k^3$
8	$\lim_{k\to\infty}\left[\frac{\text{Atoms}(sp^3)}{v(G)} = \frac{-2 + 6k + 2k^3}{6k + 6k^2 + 2k^3}\right] = 1$
B	Omega(L_6); *R*[6]
1	$\Omega(L_6, x) = k \cdot x^{k(k+2)} + x^{(k+1)(3k^2+4k-1)}$
2	$\Omega'(1) = e(G) = -1 + 3k + 9k^2 + 4k^3$
3	$\text{CI}(G) = k^2(k + 2)(7k^3 + 15k^2 + 4k - 2)$
4	$v(G) = 2k(k + 1)(k + 2) = 4k + 6k^2 + 2k^3$
5	$\text{Atoms}(sp^3) = 2(k - 1) \cdot k \cdot (k + 1) = 2k(k^2 - 1)$
6	$R[6] = -2k + 3k^2 + 4k^3$
7	$\lim_{k\to\infty}\left[\frac{\text{Atoms}(sp^3)}{v(G)} = \frac{2k(k^2 - 1)}{4k + 6k^2 + 2k^3}\right] = 1$

9.3.4 Omega Polynomial of Boron Nitride Nets

Topology of boron nitride nets is treated similarly to that of D_5 and L_5 and is presented in Tables 9.9, 9.10, 9.11, 9.12, 9.13, 9.14, 9.15, 9.16, 9.17, and 9.18 (Diudea et al. 2011). Formulas to calculate Omega polynomial, number of atoms, number of rings, and the limits (to infinity) for the ratio of sp^3 C atoms over total number of atoms are given, along with numerical examples. Formulas for Omega polynomial are taken as the basis to calculate the above four related polynomials in these bipartite networks. Formulas are derived here not only for a cubic domain (in case of c_$B_{12}N_{12}$) but also for a dual of cuboctahedron domain (case of COD_$B_{12}N_{12}$) and for an octahedral domain (case of Oct_$B_{12}N_{12}$).

Table 9.2 Examples, Omega polynomial in diamond D_6 and lonsdaleite L_6 nets

k	Polynomial (Net) Omega(D_6); R[6]	Atoms	sp^3 atoms (%)	Bonds	CI(G)	R[6]
1	$2x^3 + 3x^4$ (diamantane)	14	–	18	258	7
2	$2x^3 + 2x^6 + 1x^7 + 6x^9$	52	26 (50.00)	79	5,616	44
3	$2x^3 + 2x^6 + 2x^{10} + 2x^{12} + 9x^{16}$	126	70 (55.56)	206	39,554	135
4	$2x^3 + 2x^6 + 2x^{10} + 2x^{15} + 2x^{18} + 1x^{19} + 12x^{25}$	248	150 (60.48)	423	169,680	304
5	$2x^3 + 2x^6 + 2x^{10} + 2x^{15} + 2x^{21} + 2x^{25} + 2x^{27} + 15x^{36}$	430	278 (64.65)	754	544,746	575
6	$2x^3 + 2x^6 + 2x^{10} + 2x^{15} + 2x^{21} + 2x^{28} + 2x^{33} + 2x^{36} + 1x^{37} + 18x^{49}$	684	466 (68.13)	1,223	1,443,182	972
	Omega(L_6); R[6]					
1	$1x^3 + x^{12}$	12	–	15	72	5
2	$2x^8 + x^{57}$	48	12 (25.00)	73	1,952	40
3	$3x^{15} + x^{152}$	120	48 (40.00)	197	15,030	129
4	$4x^{24} + x^{315}$	240	120 (50.00)	411	67,392	296
5	$5x^{35} + x^{564}$	420	240 (57.14)	739	221,900	565
6	$6x^{48} + x^{917}$	672	420 (62.50)	1,205	597, 312	960

Table 9.3 Omega polynomial in diamond D_5_20 net function of $k =$ no. ada_20 units along the edge of a cubic (k,k,k) domain

	Omega(D_5_20a); R[6]: formulas
1	$\Omega(D_5\_20a, x) = (32 - 54k + 36k^2 + 44k^3) \cdot x + (-3 + 18k - 27k^2 + 12k^3) \cdot x^2$
2	$\Omega'(1) = e(G) = -38 - 18k - 18k^2 + 68k^3$
3	$\mathrm{CI}(G) = 1,488 + 1,350k + 1,764k^2 - 4,612k^3 - 2,124k^4 - 2,448k^5 + 4,624k^6$
4	$v(D_5\_20a) = -22 - 12k + 34k^3$
5	$\mathrm{Atoms}(sp^3) = -10 - 36k^2 + 34k^3$
6	$R[5] = -18 - 6k - 18k^2 + 36k^3$
7	$R[6] = -1 + 6k - 9k^2 + 4k^3$
8	$R[5] + R[6] = -19 - 27k^2 + 40k^3$
9	$\lim_{k\to\infty} \frac{R[5]}{R[6]} = 9$; $\lim_{k\to\infty} \frac{R[5]}{R[5]+R[6]} = \frac{9}{10}$
10	$\lim_{k\to\infty} \left[\frac{\mathrm{Atoms}(sp^3)}{v(G)} = \frac{-10 - 36k^2 + 34k^3}{-22 - 12k + 34k^3} = \frac{-(10/k^3) - (36/k) + 34}{-(22/k^3) - (12/k^2) + 34} \right] = 1$

Table 9.4 Examples, Omega polynomial in D_5_20 net

k	Omega(D_5_20a); R[6]	Atoms	sp^3 atoms (%)	Bonds	CI	R[5]	R[6]
2	$356\,x^1 + 21\,x^2$	226	118 (52.21)	398	157,964	186	7
3	$1{,}318\,x^1 + 132\,x^2$	860	584 (67.91)	1,582	2,500,878	774	44
4	$3{,}144\,x^1 + 405\,x^2$	2,106	1,590 (75.50)	3,954	15,629,352	1,974	135
5	$6{,}098\,x^1 + 912\,x^2$	4,168	3,340 (80.13)	7,922	62,748,338	4,002	304
6	$10{,}444\,x^1 + 1{,}725\,x^2$	7,250	6,038 (83.28)	13,894	193,025,892	7,074	575
7	$16{,}446\,x^1 + 2{,}916\,x^2$	11,556	9,888 (85.57)	22,278	496,281,174	11,406	972

Table 9.5 Omega polynomial in D_5_28 co-net function of $k =$ no. ada_20 units along the edge of a cubic (*k*,*k*,*k*) domain

	Omega (D_5_28a); *R*[6]; formulas
1	$\Omega(D_5\_28a, x) = (-26 - 12k - 6k^2 + 44k^3) \cdot x + (-18 + 9k^2 + 12k^3) \cdot x^2$
2	$\Omega'(1) = e(G) = -62 - 12k + 12k^2 + 68k^3$
3	$\mathrm{CI}(G) = 3,942 + 1,500k - 1,374k^2 - 8,812k^3 - 1,488k^4 + 1,632k^5 + 4,624k^6$
4	$v(D_5\_28a) = -40 - 6k + 18k^2 + 34k^3$
5	$\mathrm{Atoms}(sp^3) = -4 - 6k - 30k^2 + 34k^3$
6	$R[5] = -18 - 18k^2 + 36k^3$
7	$R[6] = -1 + 6k - 9k^2 + 4k^3$
8	$\lim_{k\to\infty}\left[\frac{\mathrm{Atoms}(sp^3)}{v(G)} = \frac{-4 - 6k - 30k^2 + 34k^3}{-40 - 6k + 18k^2 + 34k^3}\right] = 1$

Table 9.6 Examples, Omega polynomial in D_5_28 co-net

k	Omega(D_5_28a); *R*[6]	Atoms	sp^3 atoms (%)	Bonds	CI	*R*[5]	*R*[6]
2	$278\,x^1 + 114\,x^2$	292	136 (46.58)	506	255,302	198	38
3	$1{,}072\,x^1 + 387\,x^2$	1,022	626 (61.25)	1,846	3,405,096	792	129
4	$2{,}646\,x^1 + 894\,x^2$	2,400	1,668 (69.50)	4,434	19,654,134	1,998	298
5	$5{,}264\,x^1 + 1{,}707\,x^2$	4,630	3,466 (74.86)	8,678	75,295,592	4,032	569
6	$9{,}190\,x^1 + 2{,}898\,x^2$	7,916	6,224 (78.63)	14,986	224,559,414	7,110	966
7	$14{,}688\,x^1 + 4{,}539\,x^2$	12,462	10,146 (81.41)	23,766	564,789,912	11,448	1,513

Table 9.7 Omega polynomial in Lonsdaleite-like L_5_28 and L_5_20 nets function of $k =$ no. repeating units along the edge of a cubic (*k*,*k*,*k*) domain

	Formulas
1	$v(c\_B_{12}N_{12}) = 4k^2\big[6 + 3(-1 + k)\big]$
2	$e(G) = 12k^2(1 + 2k)$
3	$\Theta(c\_B_{12}N_{12}, x) = 6 \cdot k(4k + 2) \cdot x^{k(4k+2)} + 12\sum_{i=1}^{k-1} i(4k + 2) \cdot x^{i(4k+2)}$
4	$\Theta'(1) = 6 \cdot \big[k(4k + 2)\big]^2 + 12\sum_{i=1}^{k-1}\big[i(4k + 2)\big]^2 = 8k(2k^2 + 1)(2k + 1)^2$
5	$\Pi(c\_B_{12}N_{12}, x) = 6 \cdot k(4k+2) \cdot x^{12k^2(2k+1)-k(4k+2)} + 12\sum_{i=1}^{k-1} i(4k+2) \cdot x^{12k^2(2k+1)-i(4k+2)}$
6	$\Pi'(1) = 6 \cdot \big[k(4k + 2)\big]\big[12k^2(2k + 1) - k(4k + 2)\big] + 12\sum_{i=1}^{k-1}\big[i(4k+2)\big]\big[12k^2(2k+1) - i(4k+2)\big] = 8k(18k^3 - 2k^2 - 1)(2k+1)^2$
7	$\mathrm{Sd}(c\_B_{12}N_{12}, x) = 6 \cdot x^{12k^2(2k+1)-k(4k+2)} + 12\sum_{i=1}^{k-1} x^{12k^2(2k+1)-i(4k+2)}$
8	$\mathrm{Sd}'(1) = 6 \cdot \big[12k^2(2k + 1) - k(4k + 2)\big] + 12\sum_{i=1}^{k-1}\big[12k^2(2k + 1) - i(4k + 2)\big] = 12k^2(12k - 7)(2k + 1)$
9	$\mathrm{PI}_v = e \cdot x^v$
10	$\mathrm{PI}_v'(1) = e \cdot v = (12k^2)^2(2k + 1)(k + 1) = 144k^4 + 432k^5 + 288k^6$

Table 9.8 Examples, Omega polynomial in L_5_28 and L_5_20 nets

k	Polynomial (Net)						
A	Omega(L_5_28); R[6]	Atoms	sp^3 atoms (%)	Bonds	CI(G)	R[5]	R[6]
1	$232\,x + 99\,x^2$	250	110 (44.00)	430	184,272	165	33
2	$1{,}284\,x + 468\,x^2$	1,224	768 (62.75)	2,220	4,925,244	957	156
3	$3{,}684\,x + 1{,}251\,x^2$	3,330	2,382 (71.53)	6,186	38,257,908	2,809	417
4	$7{,}960\,x + 2{,}592\,x^2$	6,976	5,360 (76.83)	13,144	172,746,408	6,153	864
5	$14{,}640\,x + 4{,}635\,x^2$	12,570	10,110 (80.43)	23,910	571,654,920	11,421	1,545
6	$24{,}252\,x + 7{,}524\,x^2$	20,520	17,040 (83.04)	39,300	1,544,435,652	19,045	2,508
B	Omega(L_5_20); R[6]						
2	$356\,x + 21\,x^2$	226	118 (52.21)	398	157,964	186	7
3	$1{,}303\,x + 132\,x^2$	852	578 (67.84)	1,567	2,453,658	766	44
4	$3{,}114\,x + 405\,x^2$	2,090	1,578 (75.50)	3,924	15,393,042	1,958	135
5	$6{,}053\,x + 912\,x^2$	4,144	3,322 (80.16)	7,877	62,037,428	3,978	304
6	$10{,}384\,x + 1{,}725\,x^2$	7,218	6,014 (83.32)	13,834	191,362,272	7,042	575

Table 9.9 Omega polynomial in c_$B_{12}N_{12}$ net, (designed by *Le*(C_n)_all) function of k = no. repeating units along the edge of a cubic (k,k,k) domain

	Omega (c_$B_{12}N_{12}$); R[4,6]; formulas
1	$\Omega(\text{c\_B}_{12}\text{N}_{12}, x) = 6 \cdot x^{k(4k+2)} + 12 \sum_{i=1}^{k-1} x^{i(4k+2)}$
2	$\Omega'(1) = e(G) = 12k^2(1 + 2k)$
3	$\text{CI}(G) = -8k - 32k^2 - 48k^3 + 80k^4 + 512k^5 + 576k^6$ $= -8k(1 + 2k)^2(1 + 2k^2 - 18k^3)$
4	$v(\text{c\_B}_{12}\text{N}_{12}) = 4k^2[6 + 3(-1 + k)]$
5	$\text{Atoms}(sp^3) = 12k^2(-1 + k)$
6	$R[4] = 3(1 - k + 2k^2)$
7	$R[6] = 8k^3$
8	$m(\text{c\_B}_{12}\text{N}_{12}) = k^3$; m = no. monomer
9	$\lim_{k\to\infty}\left[\frac{\text{Atoms}(sp^3)}{v(G)} = \frac{12k^2(-1+k)}{4k^2[6+3(-1+k)]}\right] = 1$

Table 9.10 Examples, Omega polynomial in c_$B_{12}N_{12}$ cubic (k,k,k) net

k	Omega(c_$B_{12}N_{12}$) R[4,6]	Atoms	sp^3 Atoms (%)	Bonds	CI(G)	R[4]	R[6]
1	$6x^6$	24	110 (44.00)	36	1,080	6	8
2	$12x^{10} + 6x^{20}$	144	768 (62.75)	240	54,000	42	64
3	$12x^{14} + 12x^{28} + 6x^{42}$	432	2,382 (71.53)	756	549,192	144	216
4	$12x^{18} + 12x^{36} + 12x^{54} + 6x^{72}$	960	5,360 (76.83)	1,728	2,900,448	348	512
5	$12x^{22} + 12x^{44} + 12x^{66} + 12x^{88} + 6x^{110}$	1,800	10,110 (80.43)	3,300	10,643,160	690	1,000
6	$12^{26} + 12x^{52} + 12x^{78} + 12x^{104} + 12x^{130} + 6x^{156}$	3,024	17,040 (83.04)	5,616	30,947,280	1,206	1,728

Table 9.11 Theta Θ, Pi Π, Sadhana Sd, and PI_v polynomials in c_$B_{12}N_{12}$ cubic (*k*,*k*,*k*) net

	Formulas
1	$v(\text{c\_B}_{12}\text{N}_{12}) = 4k^2[6 + 3(-1 + k)]$
2	$e(G) = 12k^2(1 + 2k)$
3	$\Theta(\text{c\_B}_{12}\text{N}_{12}, x) = 6 \cdot k(4k + 2) \cdot x^{k(4k+2)} + 12\sum_{i=1}^{k-1} i(4k + 2) \cdot x^{i(4k+2)}$
4	$\Theta'(1) = 6 \cdot [k(4k + 2)]^2 + 12\sum_{i=1}^{k-1} [i(4k + 2)]^2 = 8k(2k^2 + 1)(2k + 1)^2$
5	$\Pi(\text{c\_B}_{12}\text{N}_{12}, x) = 6 \cdot k(4k+2) \cdot x^{12k^2(2k+1)-k(4k+2)} + 12\sum_{i=1}^{k-1} i(4k+2) \cdot x^{12k^2(2k+1)-i(4k+2)}$
6	$\Pi'(1) = 6 \cdot [k(4k + 2)][12k^2(2k + 1) - k(4k + 2)] + 12\sum_{i=1}^{k-1} [i(4k+2)][12k^2(2k+1) - i(4k+2)] = 8k(18k^3 - 2k^2 - 1)(2k+1)^2$
7	$\text{Sd}(\text{c\_B}_{12}\text{N}_{12}, x) = 6 \cdot x^{12k^2(2k+1)-k(4k+2)} + 12\sum_{i=1}^{k-1} x^{12k^2(2k+1)-i(4k+2)}$
8	$\text{Sd}'(1) = 6 \cdot [12k^2(2k + 1) - k(4k + 2)] + 12\sum_{i=1}^{k-1} [12k^2(2k + 1) - i(4k + 2)] = 12k^2(12k - 7)(2k + 1)$
9	$PI_v = e \cdot x^v$
10	$PI'_v(1) = e \cdot v = (12k^2)^2(2k + 1)(k + 1) = 144k^4 + 432k^5 + 288k^6$

Table 9.12 Examples, Theta Θ, Pi Π, Sadhana Sd, and PI_v indices in c_$B_{12}N_{12}$ cubic (*k*,*k*,*k*) net

k	Θ′(1)	Π′(1)	Sd′(1)	$PI'_v(1)$	Ω′(1)=*e*(*G*)	*v*(*G*)
4	85,536	2,900,448	70,848	1,658,880	1,728	960
5	246,840	10,643,160	174,900	5,940,000	3,300	1,800
6	592,176	30,947,280	365,040	16,982,784	5,616	3,024

Table 9.13 Omega polynomial in $B_{12}N_{12}$ net function of $k =$ no. repeating units along the edge of a Du(Med(Cube)) COD (*k*_all) domain

	Omega(COD_$B_{12}N_{12}$); *R*[4,6]; formulas
1	$\Omega(\text{COD\_B}_{12}\text{N}_{12}, x) = 12\sum_{i=0}^{k-2} x^{[2k(k+2)+4ki]} + 6x^{6k^2}$
2	$\Omega'(1) = e(G) = 12k^2(4k - 1)$
3	$\text{CI}(G) = 8k^3(2k - 1)(144k^2 - 13k + 4) = 2,304k^6 - 1,360k^5 + 168k^4 - 32k^3$
4	$v(\text{COD\_B}_{12}\text{N}_{12}) = 24k^3$
5	$\text{Atoms}(sp^3) = 24k^2(k - 1) = 24k^3 - 24k^2$
6	$R[4] = -6k^2 + 12k^3$
7	$R[6] = 4k - 12k^2 + 16k^3$
8	$\lim_{k\to\infty}\left[\frac{\text{Atoms}(sp^3)}{v(G)} = \frac{24k^2(k-1)}{24k^3}\right] = 1$

Table 9.14 Examples, Omega polynomial in COD_$B_{12}N_{12}$ (*k*_all) net

k	Omega(COD_$B_{12}N_{12}$) *R*[4,6]	Atoms	sp^3 atoms (%)	Bonds	CI(G)	*R*[4]	*R*[6]
2	$12x^{16} + 6x^{24}$	192	96 (50.00)	336	106,368	72	88
3	$12x^{30} + 12x^{42} + 6x^{54}$	648	432 (66.67)	1,188	1,361,880	270	336
4	$12x^{48} + 12x^{64} + 12x^{80} + 6x^{96}$	1,536	1,152 (75.00)	2,880	8,085,504	672	848
5	$12x^{70} + 12x^{90} + 12x^{110} + 12x^{130} + 6x^{150}$	3,000	2,400 (80.00)	5,700	31,851,000	1,350	1,720
6	$12x^{96} + 12x^{120} + 12x^{144} + 12x^{168} + 12x^{192} + 6x^{216}$	5,184	4,320 (83.33)	9,936	97,130,880	2,376	3,048

Table 9.15 Theta, Pi, Sadhana, and PI_v polynomials in COD_$B_{12}N_{12}$ (*k*_all) net

	Formulas
1	$v(\text{COD\_B}_{12}\text{N}_{12}) = 24k^3$
2	$\Omega'(1) = e(G) = 12k^2(4k-1)$
3	$\Theta(\text{COD\_B}_{12}\text{N}_{12}, x) = 12\sum_{i=0}^{k-2}[2k(k+2)+4ki]\cdot x^{[2k(k+2)+4ki]} + 36k^2x^{6k^2}$
4	$\Theta'(1) = 12\sum_{i=0}^{k-2}[2k(k+2)+4ki]^2 + 6^3k^4 = 32k^3 - 24k^4 + 208k^5$
5	$\Pi(\text{COD\_B}_{12}\text{N}_{12}, x) = 12\sum_{i=0}^{k-2}[2k(k+2)+4ki]\cdot x^{12k^2(4k-1)-[2k(k+2)+4ki]} + 36k^2x^{12k^2(4k-1)-6k^2}$
6	$\Pi'(1) = 12\sum_{i=0}^{k-2}[2k(k+2)+4ki]\cdot[12k^2(4k-1)-[2k(k+2)+4ki]] + 36k^2[12k^2(4k-1)-6k^2] = -32k^3 + 168k^4 - 1,360k^5 + 2,304k^6$
7	$\text{Sd}(\text{COD\_B}_{12}\text{N}_{12}, x) = 12\sum_{i=0}^{k-2}x^{12k^2(4k-1)-[2k(k+2)+4ki]} + 6x^{12k^2(4k-1)-6k^2}$
8	$\text{Sd}(1) = 12\sum_{i=0}^{k-2}12k^2(4k-1)-[2k(k+2)+4ki]+6[12k^2(4k-1)-6k^2] = 12k^2(4k-1)(12k-7) = 84k^2 - 480k^3 + 576k^4$
9	$PI_v = e\cdot x^v$
10	$PI'_v(1) = e\cdot v = 288k^5(4k-1)$

Table 9.16 Examples, Theta, Pi, Sadhana, and PI_v polynomials in COD_$B_{12}N_{12}$ (*k_all*) net

k	$\Theta'(1)$	$\Pi'(1)$	$\text{Sd}'(1)$	$PI'_v(1)$	$\Omega'(1) = e(G)$	$v(G)$
4	208,896	8,085,504	118,080	4,423,680	2,880	1,536
5	639,000	31,851,000	302,100	17,100,000	5,700	3,000
6	1,593,216	97,130,880	645,840	51,508,224	9,936	5,184

9.3.5 *Omega Polynomial of rhr Network*

Formulas for Omega polynomial are derived here for a cubic domain (*k*,*k*,*k*) of the *rhr* network. The results are listed in Table. 9.19.

Table 9.17 Omega polynomial in $B_{12}N_{12}$ net function of $k =$ no. repeating units along the edge of an octahedral Oct (k_all) domain

	Omega(Oct_$B_{12}N_{12}$); R[4,6]; formulas
1	$\Omega(\text{Oct\_B}_{12}\text{N}_{12}, x, k_{\text{even}}) = \sum_{i=1}^{k-1} 4x^{2i(i+2)} + \sum_{i=1}^{k/2} 8x^{1+2i-2i^2+3k(k+2)/2} + 2x^{2k(k+2)}$
2	$\Omega(\text{Oct\_B}_{12}\text{N}_{12}, x, k_{\text{odd}}) = \sum_{i=1}^{k-1} 4x^{2i(i+2)} + \sum_{i=1}^{(k-1)/2} 8x^{3/2-2i^2+3k(k+2)/2} + 4x^{3/2+3k(k+2)/2} + 2x^{2k(k+2)}$
3	$\Omega'(1) = e(G) = 4k(k+2)(2k+1)$
4	$\text{CI}(G) = 64k^6 + 1,548k^5/5 + 480k^4 + 240k^3 + 8k^2 - 108k/5$
5	$v(\text{Oct\_B}_{12}\text{N}_{12}) = 8k + 12k^2 + 4k^3$
6	$\text{Atoms}(sp^3) = -8k + 4k^2 + 4k^3$
7	$R[4] = 1 - k + 4k^2 + 2k^3$
8	$R[6] = 4k/3 + 4k^2 + 8k^3/3$
9	$\lim_{k\to\infty}\left[\frac{\text{Atoms}(sp^3)}{v(G)} = \frac{-8k + 4k^2 + 4k^3}{8k + 12k^2 + 4k^3}\right] = 1$

Table 9.18 Examples, Omega polynomial in Oct_$B_{12}N_{12}$ (k_all) net

k	Omega(Oct_$B_{12}N_{12}$) R[4,6]	Atoms	sp^3 (%)	Bonds	CI(G)	R[4]	R[6]
2	$4x^6 + 8x^{13} + 2x^{16}$	96	32 (33.33)	160	23,592	31	40
3	$4x^6 + 4x^{16} + 8x^{22} + 4x^{24} + 2x^{30}$	240	120 (50.00)	420	167,256	88	112
4	$4x^6 + 4x^{16} + 4x^{30} + 8x^{33} + 8x^{37} + 2x^{48}$	480	288 (60.00)	864	717,456	189	240
5	$4x^6 + 4x^{16} + 4x^{30} + 8x^{46} + 4x^{48} + 8x^{52} + 4x^{54} + 2x^{70}$	840	560 (66.67)	1,540	2,297,592	346	440
6	$4x^6 + 4x^{16} + 4x^{30} + 4x^{48} + 8x^{61} + 8x^{69} + 4x^{70} + 8x^{73} + 2x^{96}$	1,344	960 (71.43)	2,496	6,067,512	571	728

Table 9.19 Omega polynomial in the *rhr* net function of k

	Omega (x, rhr); $R_{\max} = 6$					
	$\Omega(x) = 24k\sum_{i=0}^{k-1} x^{(4i+2)}$					
	$\text{CI} = 32k^2(72k^4 - 4k^2 + 1)$					
	$e = \lvert E(G)\rvert = 48k^3$					
	$v = \lvert V(G)\rvert = 12k^2(2k+1)$					
	Examples					
k	Omega polynomial; $R_{\max} = 6$	CI	e	v	r4	r6
1	$24x^2$	2,208	48	36	–	8
2	$48x^2 + 48x^6$	145,536	384	240	48	64
3	$72x^2 + 72x^6 + 72x^{10}$	1,669,536	1,296	756	216	216
4	$96x^2 + 96x^6 + 96x^{10} + 96x^{14}$	9,404,928	3,072	1,728	576	512
5	$120x^2 + 120x^6 + 120x^{10} + 120x^{14} + 120x^{18}$	35,920,800	6,000	3,300	1,200	1,000

9.4 Conclusions

Design of several hypothetical crystal networks was performed by using original software programs CVNET and NANO-STUDIO, developed at TOPO GROUP CLUJ. The topology of the networks was described in terms of the net parameters by several counting polynomials, calculated by our NANO-STUDIO, Omega and PI software programs.

Hyperdiamonds are structures related to the classical diamond, having a significant amount of sp^3 carbon atoms and covalent forces to join the consisting fullerenes in crystals. Design of several hypothetical crystal networks was performed by using original software programs CVNET and NANO-STUDIO, developed at TOPO GROUP CLUJ. The topology of the networks was described in terms of the net parameters and several counting polynomials, calculated by our NANO-STUDIO, Omega, and PI software programs.

Acknowledgments Authors acknowledge Professor Davide Proserpio for crystallographic data.

References

Aleksenskiĭ AE, Baĭdakova MV, Vul AY, Davydov V, Pevtsova YA (1997) Diamond-graphite phase transition in ultradisperse-diamond clusters. Phys Solid State 39:1007–1015

Ashrafi AR, Manoochehrian B, Yousefi-Azari H (2006) On the PI polynomial of a graph. Util Math 71:97–108

Ashrafi AR, Ghorbani M, Jalali M (2008a) Computing Sadhana polynomial of V-phenylenic nanotubes and nanotori. Indian J Chem A 47:535–537

Ashrafi AR, Jalali M, Ghorbani M, Diudea MV (2008b) Computing PI and omega polynomials of an infinite family of fullerenes. MATCH Commun Math Comput Chem 60:905–916

Decarli PS, Jamieson JC (1961) Formation of diamond by explosive shock. Science 133:1821–1822

Delgado-Friedrichs O, O'Keeffe M (2006) On a simple tiling of Deza and Shtogrin. Acta Cryst A 62:228–229

Delgado-Friedrichs O, O'Keeffe M (2010) Simple tilings by polyhedra with five- and six-sided faces. Acta Cryst A 66:637–639

Diudea MV (2006) Omega polynomial. Carpath J Math 22:43–47

Diudea MV (2010a) Nanomolecules and nanostructures – polynomials and indices, MCM No. 10. University of Kragujevac, Kragujevac

Diudea MV (2010b) Diamond D_5, a novel allotrope of carbon. Studia Univ Babes-Bolyai Chemia 55:11–17

Diudea MV (2010c) Counting polynomials in partial cubes. In: Gutman I, Furtula B (eds) New molecular structure descriptors – theory and applications I. University of Kragujevac, Kragujevac, pp 191–215

Diudea MV (2010d) Counting polynomials and related indices by edge cutting procedures. MATCH Commun Math Comput Chem 64:569–590

Diudea MV, Ilić A (2009) Note on omega polynomial. Carpath J Math 25:177–185

Diudea MV, Ilić A (2011) All-pentagonal face multi tori. J Comput Theor Nanosci 8:736–739

Diudea MV, Klavžar S (2010) Omega polynomial revisited. Acta Chim Slov 57:565–570

Diudea MV, Nagy CL (2007) Periodic nanostructures. Springer, Dordrecht

Diudea MV, Nagy CL (2012) C_{20}-related structures: diamond D_5. Diam Relat Mater 23:105–108
Diudea MV, Ştefu M, John PE, Graovac A (2006) Generalized operations on maps. Croat Chem Acta 79:355–362
Diudea MV, Cigher S, John PE (2008) Omega and related counting polynomials. MATCH Commun Math Comput Chem 60:237–250
Diudea MV, Bende A, Janežič D (2010a) Omega polynomial in diamond-like networks. Fuller Nanotub Carbon Nanostruct 18:236–243
Diudea MV, Vizitiu AE, Mirzargar M, Ashrafi AR (2010b) Sadhana polynomial in nano-dendrimers. Carpath J Math 26:59–66
Diudea MV, Ilić A, Medeleanu M (2011) Hyperdiamonds: a topological view. Iran J Math Chem 2:7–29
Diudea MV, Nagy CL, Bende A (2012) On diamond D_5. Struct Chem 23:981–986
Djoković DŽ (1973) Distance preserving subgraphs of hypercubes. J Comb Theory Ser B 14:263–267
Dubrovinskaia N, Dub S, Dubrovinsky L (2006) Superior wear resistance of aggregated diamond nanorods. Nano Lett 6:824–826
Dutour Sikirić M, Delgado-Friedrichs O, Deza M (2010) Space fullerenes: a computer search for new Frank–Kasper structures. Acta Cryst A 66:602–615
Fowler PW, Rogers KM, Seifert G, Terrones M, Terrones H (1999) Pentagonal rings and nitrogen excess in fullerene-based BN cages and nanotube caps. Chem Phys Lett 299:359–367
Frondel C, Marvin UB (1967) Lonsdaleite, a hexagonal polymorph of diamond. Nature 214:587–589
Harary F (1969) Graph theory. Addison-Wesley, Reading
Hyde ST, O'Keeffe M, Proserpio DM (2008) A short history of an elusive yet ubiquitous structure in chemistry, materials, and mathematics. Angew Chem Int Ed 47:7996–8000
Ilić A (2010) Note on PI and Szeged indices. Math Comput Model 52:1570–1576
Jensen F, Toftlund H (1993) Structure and stability of C_{24} and $B_{12}N_{12}$ isomers. Chem Phys Lett 211:89–96
John PE, Vizitiu AE, Cigher S, Diudea MV (2007) CI index in tubular nanostructures. MATCH Commun Math Comput Chem 57:479–484
Khachatryan AK, Aloyan SG, May PW, Sargsyan R, Khachatryan VA, Baghdasaryan VS (2008) Graphite-to-diamond transformation induced by ultrasound cavitation. Diam Relat Mater 17:931–936
Khadikar PV (2000) On a novel structural descriptor PI. Natl Acad Sci Lett 23:113–118
Khadikar PV, Agrawal VK, Karmarkar S (2002) Prediction of lipophilicity of polyacenes using quantitative structure-activity relationships. Bioorg Med Chem 10:3499–3507
Klavžar S (2008) Some comments on co graphs and CI index. MATCH Commun Math Comput Chem 5:217–222
Lorenz HP (1995) Investigation of TiN as an interlayer for diamond deposition on steel. Diam Relat Mater 4:1088–1092
Nadjafi-Arani MJ, Fath-Tabar GH, Ashrafi AR (2009) Extremal graphs with respect to the vertex PI index. Appl Math Lett 22:1838–1840
Narita I, Oku T (2001) Effects of catalytic metals for synthesis of BN fullerene nanomaterials. Diam Relat Mater 12:1146–1150
Oku T, Kuno M, Kitahara H, Narita I (2001) Formation, atomic structures and properties of boron nitride and carbon nanocage fullerene materials. Int J Inorg Mater 3:597–612
Osawa E (2007) Recent progress and perspectives in single-digit nanodiamond. Diam Relat Mater 16:2018–2022
Osawa E (2008) Monodisperse single nanodiamond particulates. Pure Appl Chem 80:1365–1379
Soma T, Sawaoka A, Saito S (1974) Characterization of wurtzite type boron nitride synthesized by shock compression. Mater Res Bull 9:755–762
Stephan O, Bando Y, Loiseau A, Willaime F, Shramchenko N, Tamiya T, Sato T (1998) Formation of small single-layer and nested BN cages under electron irradiation of nanotubes and bulk material. Appl Phys A 67:107–111

Sun M-L, Slanina Z, Lee S-L (1995) Square/hexagon route towards the boron-nitrogen clusters. Chem Phys Lett 233:279–283

Tarasov D, Izotova E, Alisheva D, Akberova N, Freitas RA Jr (2011) Structural stability of clean, passivated, and partially dehydrogenated cuboid and octahedral nanodiamonds up to 2 nanometers in size. J Comput Theor Nanosci 8:147–167

Williams OA, Douhéret O, Daenen M, Haenen K, Osawa E, Takahashi M (2007) Enhanced diamond nucleation on monodispersed nanocrystalline diamond. Chem Phys Lett 445:255–258

Winkler PM (1984) Isometric embedding in products of complete graphs. Discrete Appl Math 8:209–212

Chapter 10
Cluj and Other Polynomials of Diamond D_6 and Related Networks

Mahboubeh Saheli and Mircea V. Diudea

Abstract Carbon is the unique element forming complex structures both in mineral and biological state. Its fascinating structures can be described by a variety of descriptors and properties. In this chapter, we use the topological parameters to describe, in terms of Cluj, Omega, and other polynomial, the classical diamond D_6 and two novel-related structures that are decorations of the cuboctahedron, which is the medial between the cube and octahedron. Construction of these networks was achieved by using the Nano Studio software developed at Topo Group Cluj.

10.1 Introduction

Several new carbon allotropes have been discovered and studied for applications in nanotechnology, in the last 20 years, which can be assigned as the "nano-era." The impact of the nano-science resulted in reduction of dimensions of electronic devices and increasing their performances, at a lower cost of energy and money. Among the new carbon structures, fullerenes (zero dimensional), nanotubes (one dimensional), graphene (two dimensional), and spongy carbon (three dimensional) are the most studied (Diudea 2005; Diudea and Nagy 2007). The attention of scientists was also focused to inorganic compounds, a realm where almost any metal atom can form clusters, tubules, or crystal networks, very ordered structures at the nano-level. Recent articles in crystallography promoted the idea of topological description and

M. Saheli
Department of Mathematics, University of Kashan, Kashan 87317-51167, I. R. Iran

M.V. Diudea (✉)
Department of Chemistry, Faculty of Chemistry and Chemical Engineering,
Babes-Bolyai University, 400028 Cluj, Romania
e-mail: diudea@gmail.com; diudea@chem.ubbcluj.ro

M.V. Diudea and C.L. Nagy (eds.), *Diamond and Related Nanostructures*,
Carbon Materials: Chemistry and Physics 6, DOI 10.1007/978-94-007-6371-5_10,

classification of crystal structures (Baburin et al. 2005; Blatov et al. 2004, 2007; Carlucci et al. 2003a, b; Delgado-Friedrichs and O'Keeffe 2005). They present data on real but also hypothetical lattices designed by computer.

This chapter deals with the topological characterization of three networks, one is the classical diamond D_6 and the other two are related, hypothetical networks; topology is presented in terms of Cluj, Omega, and other counting polynomials.

10.2 Cluj Polynomials and Indices

A Cluj fragment/subgraph $CJ_{i,j,p}$ (Diudea 1997a, b, 1999; Diudea et al. 1997; Diudea et al. 2002) collects vertices v lying closer to i than to j, the end points of a path $p(i,j)$. Such a fragment collects the vertex proximities of i against any vertex j, joined by the path p, with the distances measured in the subgraph $D_{(G-p)}$, as shown in the following equation:

$$CJ_{i,j,p} = \left\{ v \,\middle|\, v \in V(G);\ D_{(G-p)}(i,v) < D_{(G-p)}(j,v) \right\} \tag{10.1}$$

In graphs containing rings, a pair (i, j) can be joined by more than one path, thus resulting more than one fragment related to i (with respect to j and a given path p). The entries in the Cluj matrix are taken, by definition, as the maximum cardinality among all such fragments:

$$\left[\mathbf{UCJ}\right]_{i,j} = \max_{p} \left| CJ_{i,j,p} \right| \tag{10.2}$$

In trees, there is only one path between any two vertices so that $CJ_{i,j,p}$ represents the set of paths going to j through i. In this way, the path $p(i,j)$ is characterized by a single end point, which is sufficient to calculate the nonsymmetric matrix **UCJ**. When the path p belongs to the set of distances DI(G), the suffix DI is added to the name of matrix, as in **UCJDI**. When path p belongs to the set of detours DE(G), the suffix is DE. When the matrix symbol is not followed by a suffix, it is implicitly DI. The Cluj matrices are defined in any graph and, except for some symmetric graphs, are nonsymmetric.

To calculate Cluj polynomials, we will use the nonsymmetric matrices **UCJ**, defined on distances and calculated on path $\mathbf{UCJ}_p$ or on edges $\mathbf{UCJ}_e$, which can be obtained by the Hadamard multiplication $\mathbf{A} \cdot \mathbf{UCJ_p}$.

The Cluj polynomials, defined (Diudea 2009; Diudea et al. 2007, 2010a, b) on the basis of Cluj matrices, are written as

$$CJ(x) = \sum_{k} m(k) \cdot x^k \tag{10.3}$$

where $m(k)$ is the vertex proximity of the vertex i with respect to any vertex j in G, joined to i by an edge (the Cluj-edge polynomial $CJ_e(x)$) or by a path (the Cluj-path polynomial $CJ_p(x)$), taken as the shortest (i.e., distance DI) or the longest (i.e., detour DE) paths. In (10.3), the coefficients $m(k)$ can be calculated from the entries of nonsymmetric Cluj matrices by the TOPOCLUJ software program (Ursu and Diudea 2005). The summation runs over all $k = |\{p\}|$ in the graph G.

In bipartite graphs, the coefficients of CJ polynomial can be calculated by an orthogonal edge-cut procedure (Diudea et al. 2010a, b; Gutman and Klavžar 1995; Klavžar 2008a).

Let us define the *partial cube* as a graph embeddable in the n-cube Q_n, which is a regular graph whose vertices are all binary strings of length n, two strings being adjacent if they differ in exactly one position (Harary 1969). The distance function in the n-cube is the Hamming distance. A hypercube can be expressed as the Cartesian product: $Q_n = \square_{i=1}^{n} K_2$ where K_2 is the complete graph with two vertices.

For any edge $e = (u,v)$ of a connected graph G, let n_{uv} denote the set of vertices lying closer to u than to v: $n_{uv} = \{w \in V(G) | d(w,u) < d(w,v)\}$. It follows that $n_{uv} = \{w \in V(G) | d(w,v) = d(w,u) + 1\}$. The sets (and subgraphs) induced by these vertices, n_{uv} and n_{vu}, are called *semicubes* of G; they are *opposite semicubes* and are disjoint ones (Diudea and Klavžar 2010; Diudea et al. 2008).

A graph G is bipartite if and only if, for any edge of G, the opposite semicubes define a partition of G: $n_{uv} + n_{vu} = v = |V(G)|$. These semicubes are just the vertex proximities of (the end points of) edge $e = (u,v)$, on which CJ polynomial is defined. In partial cubes, the semicubes can be estimated by an orthogonal edge-cutting procedure. The orthogonal cuts form a partition of the graph edges:

$$E(G) = c_1 \cup c_2 \cup \cdots \cup c_k, \quad c_i \cap c_j = \emptyset, \quad i \neq j$$

To perform an orthogonal cut, take a straight line segment, orthogonal to the edge e, and intersect e and all its parallel edges (in a plane graph). The set of these intersections is called an *orthogonal cut* $c_k(e)$, $k = 1,2,\ldots,k_{max}$. An example is given in Fig. 10.1. To any orthogonal cut c_k, two numbers can be associated: (1) *number of edges* e_k intersected (i.e., cutting cardinality $|c_k|$) and (2) v_k or the number of points lying to the left hand with respect to c_k (in round brackets, in Fig. 10.1).

There are other polynomials, out than CJ polynomial, that count the (cardinality of) semicubes in G (i.e., the polynomial exponents), they differing only in the mathematical operation used to recompose the edge contributions to the global graph property. Because in bipartite graphs, the opposite semicubes define a partition of vertices, it is easy to identify the two semicubes: $n_{uv} = v_k$ and $n_{vu} = v - v_k$ or vice versa.

The coefficients of these descriptors are calculated (with some exceptions) as the product of three numbers (in the front of brackets – right-hand column of Fig. 10.1) with the meaning (1) symmetry of G, (2) occurrence of c_k (in the whole structure), and (3) e_k.

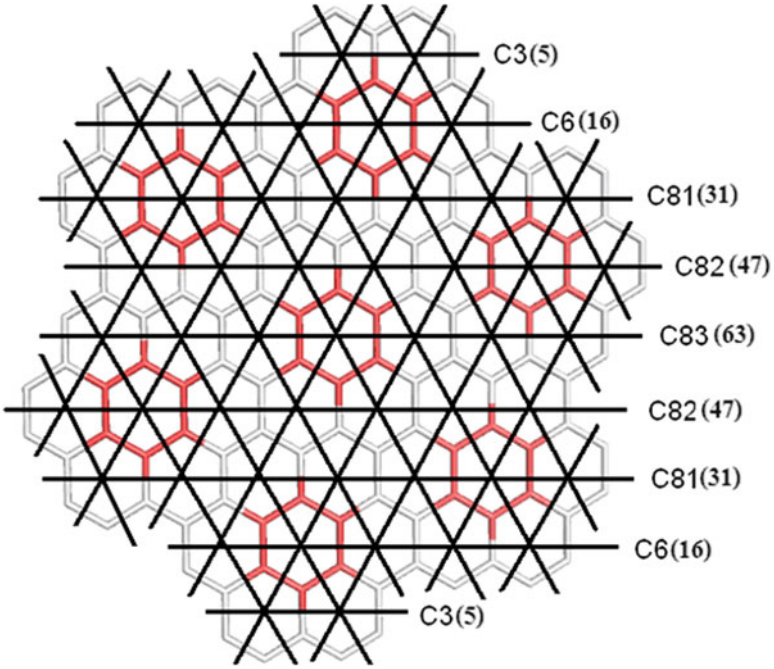

Fig. 10.1 Cutting procedure in calculating several topological descriptors

Resuming to the mathematical operations used in recomposing the edge contributions, four polynomials can be defined (Diudea 2010b):

1. *Summation* polynomial, named *Cluj-Sum* and symbolized *CJS* (Diudea 2009; Diudea et al. 2007, 2010a, b)

$$\mathrm{CJS}(x) = \sum_e (x^{v_k} + x^{v-v_k}) \tag{10.4}$$

2. *Pair-wise summation* polynomial, called PI_v (Khadikar 2000; Ashrafi et al. 2008; Khalifeh et al. 2008a, b)

$$\mathrm{PI}_v(x) = \sum_e x^{v_k+(v-v_k)} \tag{10.5}$$

3. *Pair-wise product* polynomial, called *Cluj-Product* (and symbolized *CJP* – Diudea 1997a, b, 1999; Diudea et al. 1997) or also *Szeged* (and symbolized *SZ*- Khalifeh et al. 2008b; Ashrafi et al. 2008; Mansour and Schork 2009)

$$\mathrm{CJP}(x) = \mathrm{SZ}(x) = \sum_e x^{v_k(v-v_k)} \tag{10.6}$$

4. *Single-edge pair-wise product* polynomial, called *Wiener* and symbolized *W* (Diudea 2010b)

$$\mathrm{W}(x) = \sum_k x^{v_k \cdot (v - v_k)} \tag{10.7}$$

The first derivative (in $x = 1$) of a (graph) counting polynomial provides single numbers, often called topological indices.

It is not difficult to see that the first derivative (in $x = 1$) of the first two polynomials gives one and the same value; however, their second derivative is different, and the following relations hold in any graph (Diudea 2010b; Diudea et al. 2010b):

$$\mathrm{CJS}'(1) = \mathrm{PI}'_v(1); \quad \mathrm{CJS}''(1) \neq \mathrm{PI}''_v(1) \tag{10.8}$$

The number of terms, given by P(1), is $\mathrm{CJS}(1) = 2e$, while $\mathrm{PI}_v(1) = e$ because, in the last case, the two endpoint contributions are pair wise summed for any edge in a bipartite graph (see (10.4) and (10.5)).

In bipartite graphs, the first derivative (in $x = 1$) of $\mathrm{PI}_v(x)$ takes the maximal value, according to

$$\mathrm{PI}'_v(1) = e \cdot v = |E(G)| \cdot |V(G)| \tag{10.9}$$

It can also be found by considering the definition of the corresponding index (Ilić 2009):

$$\mathrm{PI}_v(G) = \mathrm{PI}'_v(1) = \sum_{e=uv} n_{u,v} + n_{v,u} = |V| \cdot |E| - \sum_{e=uv} m_{u,v} \tag{10.10}$$

where $n_{u,v}$ and $n_{v,u}$ count the non-equidistant vertices with respect to the end points of the edge $e = (u,v)$, while $m(u,v)$ is the number of equidistant vertices *vs*. u and v. However, it is known that, in bipartite graphs, there are no equidistant vertices, so that the last term in (10.10) will miss. The value of $\mathrm{PI}_v(G)$ is thus maximal in bipartite graphs, among all graphs on the same number of vertices; the result of (10.9) can be used as a criterion for the "bipatity" of a graph (Diudea et al. 2007).

The third polynomial (10.6) uses the pair-wise product and is called Cluj-Product CJP(x); it is precisely the (vertex) Szeged polynomial $\mathrm{SZ}_v(x)$ (Ashrafi et al. 2008; Khalifeh et al. 2008a, b; Mansour and Schork 2009). This comes out from the relations between the basic Cluj (Diudea 1997a, 1999) and Szeged (Gutman 1994) indices:

$$\mathrm{CJP}'(1) = \mathrm{CJDI}(G) = \mathrm{SZ}(G) = \mathrm{SZ}'_v(1) \tag{10.11}$$

All the three polynomials (and their derived indices) do not count the equidistant vertices, an idea introduced in Chemical Graph Theory by Gutman (1994). We call these *polynomials of vertex proximity*.

We call the last polynomial (10.7) Wiener, because it is calculated as Wiener performed the index W(G) in tree graphs – multiply the number of vertices lying to the left and to the right of each edge (actually read orthogonal cut c_k):

$$\mathrm{W}(G) = \mathrm{W}'(1) = \sum_k v_k \cdot (v - v_k) \tag{10.12}$$

where v_k and $v - v_k$ are the disjoint semicubes forming a partition with respect to each edge in c_k taken, however, as a "single edge" (as in trees).

A last remark on W(x): in partial cubes, its exponents are identical to those in CJP(x) = SZ(x) while the coefficients are those in the above polynomials, divided by e_k.

10.3 Omega Polynomial

Let $G(V,E)$ be a connected graph, with the vertex set $V(G)$ and edge set $E(G)$. Two edges $e = uv$ and $f = xy$ of G are called *codistant e co f* if they obey the following relation (John et al. 2007):

$$d(v, x) = d(v, y) + 1 = d(u, x) + 1 = d(u, y) \tag{10.13}$$

which is reflexive, that is, $e\ co\ e$ holds for any edge e of G, and symmetric, if $e\ co\ f$ then $f\ co\ e$. In general, relation co is not transitive; an example showing this fact is the complete bipartite graph $K_{2,n}$. If "co" is also transitive, thus an equivalence relation, then G is called a *co-graph* and the set of edges $C(e) := \{f \in E(G);\ f\ co\ e\}$ is called an *orthogonal cut oc* of G, $E(G)$ being the union of disjoint orthogonal cuts:

$$E(G) = C_1 \cup C_2 \cup \cdots \cup C_k,\ \ C_i \cap C_j = \emptyset,\ i \neq j$$

Klavžar (2008a, b) has shown that relation co is a theta Djoković (1973) and Winkler (1984) relation.

We say that edges e and f of a plane graph G are in relation *opposite, e op f,* if they are opposite edges of an inner face of G. Note that the relation co is defined in the whole graph while op is defined only in faces. Using the relation op, we can partition the edge set of G into *opposite* edge *strips, ops.* An *ops* is a quasi-orthogonal cut *qoc*, since *ops* is not transitive.

Let G be a connected graph and $S_1, S_2, \ldots S_k$ be the *ops* strips of G. Then the *ops* strips form a partition of $E(G)$. The length of *ops* is taken as maximum. It depends on the size of the maximum fold face/ring $F_{\max}/R_{\max}$ considered, so that any result on Omega polynomial will have this specification.

Denote by $m(G,s)$ the number of *ops* of length s. The Omega polynomial (Diudea 2006; Diudea et al. 2008, 2009) is defined as

$$\Omega(G,x) = \sum_s m(G,s) \cdot x^s \tag{10.14}$$

Its first derivative (in $x = 1$) equals the number of edges in the graph:

$$\Omega'(G,1) = \sum_s m(G,s) \cdot s = e = |E(G)| \tag{10.15}$$

On Omega polynomial, the Cluj-Ilmenau index (John et al. 2007), $CI = CI(G)$, was defined:

$$CI(G) = \{[\Omega'(G,1)]^2 - [\Omega'(G,1) + \Omega''(G,1)]\} \tag{10.16}$$

Data were calculated by an original program called Nano Studio (Nagy and Diudea 2009), developed at the TOPO Group Cluj.

10.4 Lattice Building

The networks herein discussed have been constructed by using the Nano Studio software developed at Topo Group Cluj. In the following, k refers to the number of repeating units on a row, in a cubic domain (k,k,k).

The first network is the classical diamond D_6 (a 4-c uninodal net, belonging to the group *Fd*-3*m* and having the point symbol (6^6)), presented in Fig. 10.2 with its basic units, adamantane and diamantane (Fig. 10.3).

The next two networks represent decorations on a cuboctahedron (the medial of the two Platonics, the cube and octahedron) network; they both are new networks, registered in the TOPOS databases.

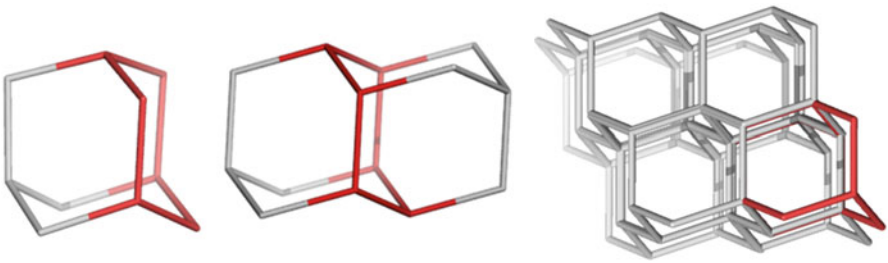

Fig. 10.2 Diamond D_6: adamantane D_6_10 (*left*), diamantane D_6_14 (*middle*), and diamond D_6_52 (a 222 net – *right*)

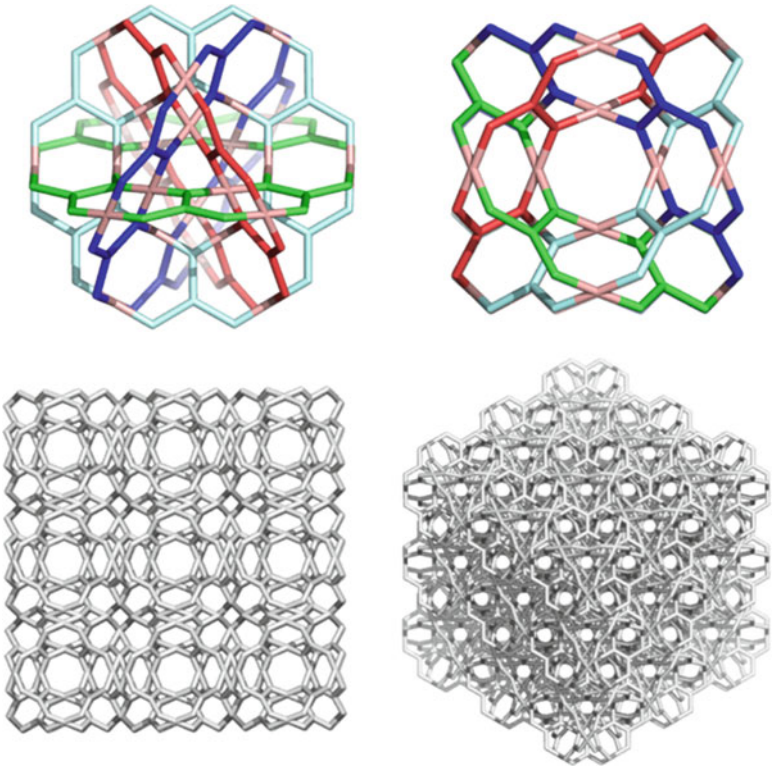

Fig. 10.3 CQS1SpD3, a 5-nodal network; CQS1SpD3_111_120 (*top*); CQS1SpD3_333_2808 (*bottom*)

CQS1SpD3 is a new 5-nodal 3,3,4,4,4-c net, belonging to the group Pm-3m and having the point symbol $\{4.8^2\}2\{4^2.8^4\}3\{6.8^2\}2\{6^2.8^4\}$ and stoichiometry (3-c)2(3-c)2(4-c)2(4-c)(4-c).

CQS1D35 is a new 3-nodal 3,3,5-c network that belongs to the group Fm-3m and has the point symbol $\{5^2.6\}6\{5^3\}2\{5^4.6^2.8^4\}3$ and stoichiometry (3-c)6(3-c)2(5-c)3. The crystallographic data are provided by Professor Davide Proserpio, University of Milan, Italy, and TOPOS databases (Fig. 10.4).

10.5 Main Results

Formulas for calculating the Cluj (cf. 10.4) and related polynomials of vertex proximity are presented in Tables 10.1, 10.2, 10.3, and 10.4 along with some numerical examples.

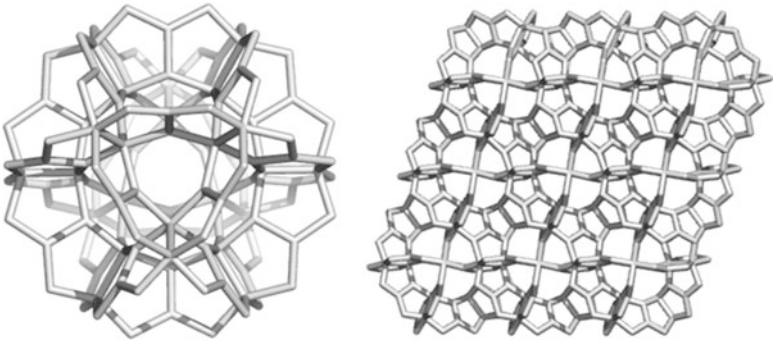

Fig. 10.4 CQS1D35, a 3-nodal network; CQS1D35_111_120 (*left*); CQS1D35_333_1972 (*right*)

Table 10.1 Cluj and related polynomials in Diamond D_6

	PI_v, PI_v', and PI_v'' (D_6)
1	$PI_v = \left(4k^3 + 9k^2 + 6k - 1\right) x^{2k\left(k^2+3k+3\right)}$
2	$PI_v' = 8k^6 + 42k^5 + 90k^4 + 88k^3 + 30k^2 - 6k$
3	$PI_v'' = 16k^9 + 132k^8 + 480k^7 + 760k^6 + 1,086k^5 + 606k^4 + 56k^3 - 66k^2 + 6k$
	Cluj polynomial
5	$CJ = \sum_{i=1}^{k} \left(i^2 + 3i + 2\right) \left[x^{\frac{1}{6}i\left(2i^2+9i+13\right)} + x^{2k\left(k^2+3k+3\right)-\frac{1}{6}i\left(2i^2+9i+13\right)}\right] + \sum_{i=1}^{\lfloor \frac{k}{2} \rfloor} \left[(k+1)(k+2) + 2i(k-i)\right] \left[x^{\frac{1}{6}k\left(2k^2+9k+13\right)+ik(3+i+k)+\frac{i}{3}\left(5-2i^2\right)}\right] + \sum_{i=1}^{\lfloor \frac{k}{2} \rfloor - 1} \left[(k+1)(k+2) + 2i(k-i)\right] \left[x^{\frac{1}{6}k\left(10k^2+27k+23\right)-ik(3+i+k)-\frac{i}{3}\left(5-2i^2\right)}\right] + \left[\frac{1-(-1)^k}{4}\right] \left(3k^2 + 6k + 3\right) x^{\left(k^3+\frac{15}{4}k^2+\frac{9}{2}k+\frac{3}{4}\right)} + 6(k+1)^2 \sum_{i=1}^{k} x^{2k\left(k^2+3k+3\right)-2i(k+1)^2+1}$
6	$CJ'(1) = 8k^6 + 42k^5 + 90k^4 + 88k^3 + 30k^2 - 6k$
7	$CJ''(1) = \frac{32}{3}k^9 + 84k^8 + \frac{10,212}{35}k^7 + \frac{2,772}{5}k^6 + 577k^5 + 245k^4 - \frac{351}{5}k^3 - \frac{397}{5}k^2 + \frac{142}{21}k$
	Szeged polynomial

(continued)

Table 10.1 (continued)

	PI_v, PI_v', and PI_v'' (D_6)
8	$SZ = \frac{8}{3}k^9 + 24k^8 + \frac{3,294}{35}k^7 + \frac{1,014}{5}k^6 + \frac{509}{2}k^5 + \frac{361}{2}k^4 + \frac{631}{10}k^3 + \frac{67}{10}k^2 - \frac{8}{21}k$
9	PIe, $PIe'(1)$, and $PIe''(1)$ $PIe = \sum_{i=1}^{k}\left(i^2+3i+2\right)x^{\left(4k^3+9k^2+6k-4-\frac{(i-1)(i+4)}{2}\right)} + \sum_{i=1}^{\lfloor\frac{k-1}{2}\rfloor}\left[k^2+5k+2(i-1)(k-i-1)\right]x^{\left(4k^3+\frac{17}{2}k^2+\frac{7}{2}k-1-(i-1)(k-i-1)\right)} + \left[\frac{1+(-1)^k}{2}\right]\left(\frac{3}{4}k^2+\frac{3}{2}k+1\right)x^{\left(4k^3+\frac{33}{4}k^2+\frac{9}{2}k-2\right)} + 3k(k+1)^2\,x^{\left(4k^3+8k^2+4k-2\right)}$ $PIe'(1) = 16k^6 + \frac{1,369}{20}k^5 + \frac{457}{4}k^4 + \frac{305}{4}k^3 - \frac{1}{4}k^2 - \frac{187}{10}k + 2$ $= \frac{1}{20}\left(320k^6 + 1,369k^5 + 2,285k^4 + 1,525k^3 - 5k^2 - 374k + 40\right)$ $PIe''(1) = 64k^9 + \frac{2,018}{5}k^8 + \frac{75,701}{70}k^7 + \frac{14,833}{10}k^6 + \frac{18,293}{20}k^5 - \frac{1,867}{20}k^4 - \frac{7,921}{20}k^3 - \frac{1,551}{20}k^2 + \frac{4,897}{70}k - 6$ $= \frac{1}{140}\begin{pmatrix} 8,960k^9 + 5,6504k^8 + 151,402k^7 + 207,662k^6 + 128,051k^5 \\ -13,069k^4 - 5,5447k^3 - 10,857k^2 + 9,794k - 840 \end{pmatrix}$

Table 10.2 Examples of PI_v, PI'_v, PI''_v, and SZ in diamond D_6 net

k	Polynomial (net)	PI'_v	PI''_v	SZ
1	$18x^{14}$	252	3,276	828
2	$79x^{52}$	4,108	209,508	44,098
3	$206x^{126}$	25,956	3,244,500	641,848
4	$423x^{248}$	104,904	25,911,288	4,955,512
5	$754x^{430}$	324,220	139,090,380	26,020,940
6	$1{,}223x^{684}$	836,532	571,351,356	105,219,242

Table 10.3 Examples of Cluj polynomial in diamond D_6 net

k	Polynomial (net)	CJ′(1)	CJ″(1)
1	$6x^{10} + 24x^7 + 6x^4$	252	1,620
2	$6x^{48} + 12x^{39} + 54x^{35} + 14x^{26} + 54x^{17} + 2x^{13} + 6x^4$	4,108	121,312
3	$6x^{122} + 12x^{113} + 20x^{97} + 96x^{95} + 24x^{75} + 96x^{63} + 24x^{51} + 96x^{31} + 20x^{29} + 12x^{13} + 6x^4$	25,956	1,960,804
4	$6x^{244} + 12x^{235} + 20x^{219} + 150x^{199} + 30x^{194} + 36x^{161} + 150x^{149} + 38x^{124} + 150x^{99} + 36x^{87} + 30x^{54} + 150x^{49} + 20x^{29} + 12x^{13} + 6x^4$	104,904	16,000,264
5	$6x^{426} + 12x^{417} + 20x^{401} + 30x^{376} + 216x^{359} + 42x^{340} + 50x^{294} + 216x^{287} + 54x^{242} + +216x^{215} + 54x^{188} + 216x^{143} + 50x^{136} + 42x^{90} + 216x^{71} + 30x^{54} + 20x^{29} + 12x^{13} + 6x^4$	324,220	87,048,500
6	$6x^{680} + 12x^{671} + 20x^{655} + 30x^{630} + 42x^{594} + 294x^{587} + 56x^{545} + 294x^{489} + 66x^{484} + 72x^{415} + 294x^{391} + 74x^{342} + 294x^{293} + 72x^{269} + 66x^{200} + 294x^{195} + 56x^{139} + 294x^{97} + 42x^{90} + 30x^{54} + 20x^{29} + 12x^{13} + 6x^4$	836,532	360,912,872

Table 10.4 Examples of PIe, PI$e'(1)$, and PI$e''(1)$ in diamond D_6 net

k	Polynomial	PI$e'(1)$	PI$e''(1)$
1	$6x^{15} + 12x^{14}$	258	3,444
2	$6x^{76} + 12x^{73} + 7x^{72} + 54x^{70}$	5,616	393,876
3	$6x^{203} + 12x^{200} + 20x^{196} + 24x^{194} + 144x^{190}$	39,554	7,557,684
4	$6x^{420} + 12x^{417} + 20x^{413} + 30x^{408} + 36x^{405} + 19x^{404} + 300x^{398}$	169,680	67,907,892
5	$6x^{751} + 12x^{748} + 20x^{744} + 30x^{739} + 42x^{733} + 50x^{729} + 54x^{727} + 540x^{718}$	544,746	393,069,372
6	$6x^{1220} + 12x^{1217} + 20x^{1213} + 30x^{1208} + 42x^{1202} + 56x^{1195} + 66x^{1190} + 72x^{1187} + 37x^{1186} + 882x^{1174}$	1,443,182	1,701,708,606

Formulas for calculating the Omega polynomial and CI index, as well as the ring polynomial for the net CQS1SpD3 are presented in Table 10.5 while for the net CQS1D35 data are collected in Table 10.6.

Table 10.5 Omega polynomial in CQS1SpD3 network

	Atoms	Omega; $R_{\max}[8]$	CI	e	R_4	R_6	R_8
1	120	$1x^{72} + 1x^{96}$	13,824	168	−	8	78
2	864	$1x^{576} + 1x^{768}$	884,736	1,344	96	64	816
3	2,808	$1x^{1,944} + 1x^{2,592}$	10,077,696	4,536	432	216	3,114
4	6,528	$1x^{4,608} + 1x^{6,144}$	56,623,104	10,752	1,152	512	7,872
5	12,600	$1x^{9,000} + 1x^{12,000}$	216,000,000	21,000	2,400	1,000	15,990
6	21,600	$1x^{15,552} + 1x^{20,736}$	644,972,544	36,288	4,320	1,728	28,368

$\Omega(x, G) = 1x^{72k^3} + 1x^{96k^3}$; CI $= 1,3824 \cdot k^6$; $v = 24k^2(1 + 4k)$; $e = 168 \cdot k^3$; $G =$ CQS1SpD3
$R(x) = ax^4 + bx^6 + cx^8$; $a = 24 \cdot k^2(k - 1)$; $b = 8 \cdot k^3 c = 6k(25k^2 - 20k + 8)$

Table 10.6 Omega polynomial in CQS1D35 network

	Omega; $R\max = 6$	CI	e	v	R_5	R_6
1	$132x^1 + 24x^2$	32,172	180	120	48	8
2	$684x^1 + 210x^2$	1,217,292	1,104	692	312	70
3	$1,794x^1 + 720x^2$	10,454,082	3,234	1,972	936	240
4	$8,642x^1 + 1,698x^2$	49,523,010	7,038	4,224	2,064	566
5	$6,408x^1 + 3,288x^2$	168,564,696	12,984	7,712	3,840	1,096

$\Omega(x) = (30k^3 + 99k^2 + 45k - 42)x + (24k^3 + 18k^2 - 36k + 18)x^2$
CI $= 6,084k^6 + 21,060k^5 + 14,013k^4 - 8,352k^3 - 1,062k^2 + 423k + 6$
$e = |E(G)| = 78k^3 + 135k^2 - 27k - 6$
$v = |V(G)| = 44k^3 + 90k^2 - 6k - 8$
$R_5 = 12k(2k^2 + 3k - 1)$
$R_6 = 8k^3 + 6k^2 - 12k + 6$

10.6 Conclusions

Carbon nanostructures can be described by a variety of descriptors and properties. We used here the topological parameters of the nets, namely, the number of repeating units on a row in a cubic domain (*k*,*k*,*k*) to describe, in polynomial terms, the classical diamond D_6 and two related structures that are decorations of the cuboctahedron network. Analytical formulas, function of *k*, are given along with some examples.

References

Ashrafi A, Ghorbani M, Jalali M (2008) The vertex PI and Szeged indices of an infinite family of fullerenes. J Theor Comput Chem 7:221–231

Baburin I, Blatov V, Carlucci L, Ciani G, Proserpio D (2005) Interpenetrating metal-organic and inorganic 3D networks: a computer-aided systematic investigation. Part II. Analysis of the Inorganic Crystal. Structure Database (ICSD). J Solid State Chem 178:2452–2474

Blatov V, Carlucci L, Ciani G, Proserpio D (2004) Interpenetrating metal-organic and inorganic 3D networks: a computer-aided systematic investigation. Part I. Analysis of the Cambridge structural database. Cryst Eng Commun 6:377–395

Blatov V, Delgado-Friedrichs O, O'Keeffe M, Proserpio D (2007) Three-periodic nets and tilings: natural tilings for nets. Acta Cryst A63:418–425

Carlucci L, Ciani G, Proserpio D (2003a) Polycatenation polythreading and polyknotting in coordination network chemistry. Coord Chem Rev 246:247–289

Carlucci L, Ciani G, Proserpio D (2003b) Borromean links and other non-conventional links in "polycatenated" coordination polymers: re-examination of some puzzling networks. Cryst Eng Commun 5:269–279

Delgado-Friedrichs O, O'Keeffe M (2005) Crystal nets as graphs: terminology and definitions. J Solid State Chem 178:2480–2485

Diudea MV (1997a) Cluj matrix invariants. J Chem Inf Comput Sci 37:300–305

Diudea MV (1997b) Cluj matrix CJ_u: source of various graph descriptors. MATCH Commun Math Comput Chem 35:169–183

Diudea MV (1999) Valencies of property. Croat Chem Acta 72:835–851

Diudea MV (ed) (2005) Nanostructures, novel architecture. NOVA, New York

Diudea MV (2006) Omega polynomial. Carpath J Math 22:43–47

Diudea MV (2009) Cluj polynomials. J Math Chem 45:295–308

Diudea MV (2010a) Counting polynomials in partial cubes. In: Gutman I, Furtula B (eds) Novel molecular structure descriptors – theory and applications I. University of Kragujevac, Kragujevac, pp 191–215

Diudea MV (2010b) Counting polynomials and related indices by edge cutting procedures. In: Gutman I, Furtula B (eds) Novel molecular structure descriptors-theory and applications II. University of Kragujevac, Kragujevac, pp 57–78

Diudea MV, Klavžar S (2010) Omega polynomial revisited. Acta Chim Slov 57:565–570

Diudea MV, Parv B, Gutman I (1997) Detour-Cluj matrix and derived invariants. J Chem Inf Comput Sci 37:1101–1108

Diudea MV, Gutman I, Jäntschi L (2002) Molecular topology. Nova, New York

Diudea MV, Vizitiu A, Janežič D (2007) Cluj and related polynomials applied in correlating studies. J Chem Inf Model 47:864–874

Diudea MV, Cigher S, John P (2008) Omega and related counting polynomials. MATCH Commun Math Comput Chem 60:237–250

Diudea MV, Cigher S, Vizitiu A, Florescu M, John P (2009) Omega polynomial and its use in nanostructures description. J Math Chem 45:316–329

Diudea MV, Dorosti N, Iranmanesh A (2010a) Cluj CJ polynomial and indices in a dendritic molecular graph. Studia Univ Babes-Bolyai Chemia 55(4):247–253

Diudea MV, Ilić A, Ghorbani M, Ashrafi A (2010b) Cluj and PI_v polynomials. Croat Chem Acta 83:283–289

Djoković D (1973) Distance preserving subgraphs of hypercubes. Comb J Theory Ser B 14: 263–267

Gutman I (1994) A formula for the Wiener number of trees and its extension to graphs containing cycles. Graph Theory Notes N Y 27:9–15

Gutman I, Klavžar S (1995) An algorithm for the calculation of the Szeged index of benzenoid hydrocarbons. J Chem Inf Comput Sci 35:1011–1014

Harary F (1969) Graph theory. Addison-Wesley, Reading

Ilić A (2009) On the extremal graphs with respect to the vertex PI index. Appl Math Lett 23(10):1213–1217

John P, Vizitiu A, Cigher S, Diudea M (2007) CI index in tubular nanostructures. MATCH Commun Math Comput Chem 57:479–484

Khadikar P (2000) On a novel structural descriptor. Proc Natl Acad Sci Lett 23:113–118

Khalifeh M, Yousefi-Azari H, Ashrafi A (2008a) A matrix method for computing Szeged and vertex PI indices of join and composition of graphs. Linear Algebra Appl 429:2702–2709

Khalifeh M, Yousefi-Azari H, Ashrafi A (2008b) Vertex and edge PI indices of Cartesian product graphs. Discrete Appl Math 156:1780–1789
Klavžar S (2008a) A bird's eye view of the cut method and a survey of its applications in chemical graph theory. MATCH Commun Math Comput Chem 60:255–274
Klavžar S (2008b) MATCH some comments on co graphs and CI index. Commun Math Comput Chem 59:217–222
Mansour T, Schork M (2009) The vertex PI index and Szeged index of bridge graphs. Discrete Appl Math 157:1600–1606
Nagy C, Diudea M (2009) Nano studio software. Babes-Bolyai University, Cluj
Ursu O, Diudea M (2005) TOPOCLUJ software program. Babes-Bolyai University, Cluj
Winkler P (1984) Isometric embedding in products of complete graphs. Discrete Appl Math 8: 209–212

Chapter 11
Hypergraphene from Armchair Nanotube Y Junctions

Katalin Nagy and Csaba L. Nagy

Abstract Since their discovery, Y carbon nanojunctions have attracted broad attention for future electron device applications, such as three-terminal transistors, amplifiers, and switches. In this study we have investigated the structure and stability of the theoretically proposed Y-shaped junctions. The structures are constructed from single-wall armchair carbon nanotubes. To construct series of objects, the tube length is increased. The change of stability with the tube length and diameter is discussed. The geometry optimization and single-point computations (heat of formation, total energy, molecular orbital energy levels) are performed using the PM3 and PM6 semiempirical quantum-chemical method.

11.1 Introduction: Structural Models of Y Junctions

The first structural models for symmetric carbon nanotube Y junctions based on theoretical calculations (Scuseria 1992; Chernozatonskii 1992) were proposed shortly after the discovery of multiwall carbon nanotubes by Iijima (Fig. 11.1). Both models are based on the insertion of non-hexagonal rings (according to the Euler formula, it needs at least six heptagons) in the hexagonal network in the region where the three branches of the Y are joined together. All the subsequent structural models (Terrones and Terrones 2003; Zsoldos et al. 2004, 2005; Zsoldos and Kakuk 2007; Dimitrakakis et al. 2008; Tylianakis et al. 2011) follow the same construction principle of conserving the sp^2 hybridization of the carbon network, differing only in the kind, number, and placement of the n-H rings. These variations make possible the constructions of various symmetric (Fig. 11.1 left) and asymmetric

K. Nagy (✉) • C.L. Nagy
Department of Chemistry, Faculty of Chemistry and Chemical Engineering,
Babes-Bolyai University, 400028 Cluj, Romania
e-mail: knagy@chem.ubbcluj.ro

M.V. Diudea and C.L. Nagy (eds.), *Diamond and Related Nanostructures*,
Carbon Materials: Chemistry and Physics 6, DOI 10.1007/978-94-007-6371-5_11,

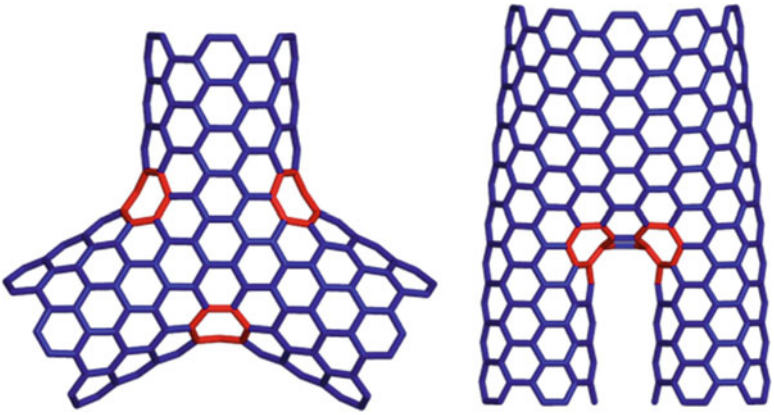

Fig. 11.1 Structural models of carbon nanotube Y junctions: symmetrical type built from one armchair-type nanotube with chirality (6,6) (*left*), asymmetrical type built from two armchair-type nanotubes with chirality (10, 10), and (5,5) (*right*)

(Fig. 11.1 right) model junctions and various angles from Y to T shapes. A Y junction is named symmetric if the three carbon nanotubes joining each other in the Y have identical chirality and the distribution of the n-H rings around the Y is symmetric. Such a junction will be constituted from identical branches oriented at 120°. Whenever one of the above conditions is not fulfilled, the junction will be asymmetric. The case of asymmetric junctions is somewhat more complex as in this case, various combinations of metallic and semiconductor tubes can be built.

A method for constructing junctions between single-wall nanotubes of any chirality and diameter was presented, suitable for junctions where the new nanotube branches are attached to already developed ones (László 2005a, b). A method used for the connection of two arbitrary nanotubes was extended for three and more terminal junctions (László 2008).

11.2 Growth Methods of Y Junctions

The first observation of carbon nanotube Y junctions (Biró et al. 2002a, b, 2004) was reported in an electric arc experiment (Zhou and Seraphin 1995). The junctions found by transmission electron microscopy (TEM) were short-branched, multiwall ones.

The quality of the junctions grown by the catalytic vapor deposition (CVD) method shows wide scattering. Using microwave plasma-enhanced catalytic vapor deposition and Pd catalyst, partially Pd-filled multiwall carbon nanotubes were grown on a porous Si support, in methane-hydrogen atmosphere. Some of the tubes

show Y junctions (Márk et al. 1998). The authors propose a root growth mechanism for the formation of Y junctions in which the molten catalyst particles on the top of two neighboring carbon nanotubes are fused together and the growth continues like a single tube.

The formation of Y-branched carbon nanotubes and of multiple branchings in a proportion of 70 % is reported by Satishkumar et al. (2000). Nickelocene is used as both catalyst source and carbon feedstock in combination with hydrogen bubbled through thiophene in argon-carrying gas. Identical carbon nanotube Y junctions have been successfully synthesized by pyrolysis of methane over cobalt supported on magnesium oxide (Li et al. 2001). Some carbon nanotubes branched several times to form multiple Y junctions, which still keep their arms straight.

The first experiment (Li et al. 1999) achieving the controlled growth of carbon nanotube Y junctions was based on the use of alumina templates with branching nanochannels. Multibranched junctions were grown in nanochannels which were purposely etched in way that gives multibranched structure (Sui et al. 2001a, b).

Experiments carried out in situ at high temperatures (800 °C) in a high acceleration voltage TEM show that it is possible to weld together crossing single-wall carbon nanotubes and to produce Y, X, T, and H junctions (Terrones et al. 2002a, b, 2003). The tubes were welded together under the influence of electron irradiation and annealing at their contact region. The ready-formed X junctions can be manipulated in order to create Y- and T-like molecular connections. By using careful conditions of irradiation, it is possible to remove one of the arms of an X junction in order to create a Y or T junction. In order to understand the formation mechanism of these molecular junctions (Terrones et al. 2002a), the tight-binding molecular dynamics simulation of two crossing tubes under irradiation at 1,000 °C revealed the nanotube merging process, resulting in an almost perfect molecular junction.

11.3 Computational Study of Armchair Yj(*n*,*n*) Junctions

To study the effect of attached carbon nanotube on the stability of the Y junction, several series of structures were built with the help of Nano Studio program (Nagy and Diudea 2009) where the length of the nanotube varies. Both opened, with hydrogenated openings, and closed (by nanotube caps) Y junctions were considered. For the closed structures, two different nanotube caps were used. Only armchair symmetric junctions were studied, where the chirality of the opening is (4,4), (6,6), and (8,8), respectively (Fig. 11.2). Each studied junction includes six heptagons, needed for the negative curvature where two tubes are joined; they are distributed in a symmetric way, and each structure has D_{3h} symmetry.

In the case of Yj(6,6) nanotube junctions, three different junction topologies were studied, which are different by the position of heptagons and also by the number of carbon atoms. All heptagons are isolated, surrounded only by hexagons.

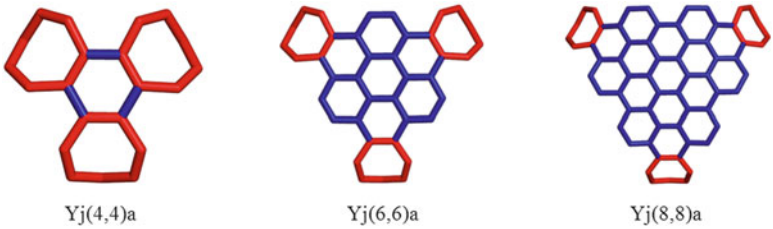

Fig. 11.2 Symmetric armchair Y junctions with D_{3h} symmetry and opening chirality: (4,4), (6,6), and (8,8), respectively. Each junction has the same heptagon position; pairs of heptagons are positioned at the corners where two nanotubes connects

11.4 Opened Symmetrical Armchair Yj(*n*,*n*) Junctions

In Fig. 11.3 the symmetric armchair Y junctions are shown, with the opening chirality being (6,6) and an armchair nanotube of length 3 is attached. As it can be observed, the heptagon positions are different which give the junction a different geometry. In the figures, the optimized geometries are presented (hydrogen atoms are not shown); according to the junction geometry, the shape of the attached nanotube changes; in one case, it preserves its original circular shape, while in the other two cases, the nanotube has an elliptic shape.

The Y junctions related to Yj(6,6)a are shown in Fig. 11.4, they have (4,4) and (8,8) armchair chirality. Only in the case of Yj(6,6)a, the attached nanotube preserves the circular shape; the other two junctions deform it into an elliptical geometry.

The geometry optimization and single-point energy calculations were performed at the PM6 semiempirical level of theory using Gaussian 09 package. As stability criterion, two parameters were followed: the total energy divided by the number of carbon atoms and the HOMO-LUMO energy gap.

The results obtained for the three series of Y junctions Yj(4,4)a, Yj(6,6)a, and Yj(8,8)a are presented in Figs. 11.5, 11.6, and 11.7, respectively. It can be observed that with the increment of the attached nanotube, both the total energy and the gap energy oscillate with a periodicity of three. There is a good correlation between the kinetic and thermodynamic parameter, along the series both parameters sort order matches. In every case, the gap energy decreases; however, the total energy per atom in the case of Yj(4,4)a increases with the length of the tube. In the other two cases, the tube length increases the stability of the structure.

In Fig. 11.8 the total energy per atom between the three series is compared. The highest values correspond to the Yj(4,4)a series, while the lowest on to the Yj(8,8)a junction series. It can be concluded that the nanotube diameter contributes to the stability of the junction; therefore, the junction with the attached nanotube with largest diameter (8,8) is the most stable one.

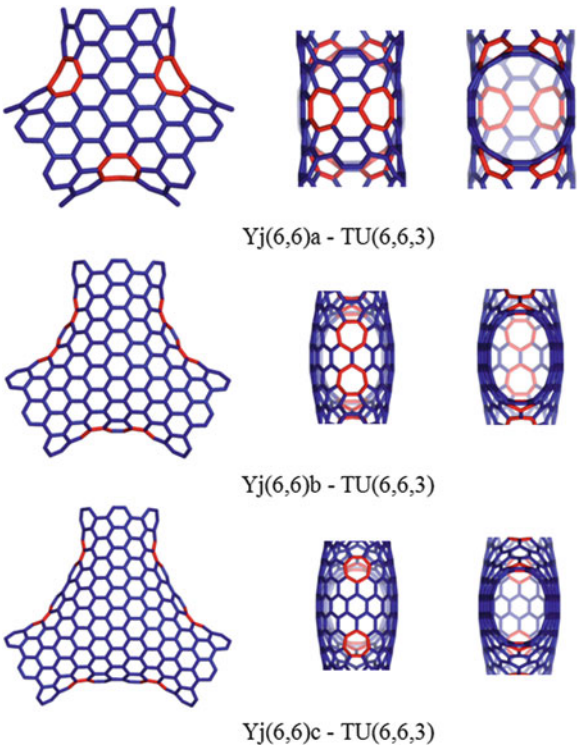

Fig. 11.3 Three symmetric Y-type junctions with D_{3h} symmetry with (6,6) armchair openings, at each opening an armchair nanotube of length 3 is connected. The structures are viewed along the threefold axe C_3 (*left*), twofold axe C_2 top (*center*), and twofold axe C_2 bottom (*right*), respectively

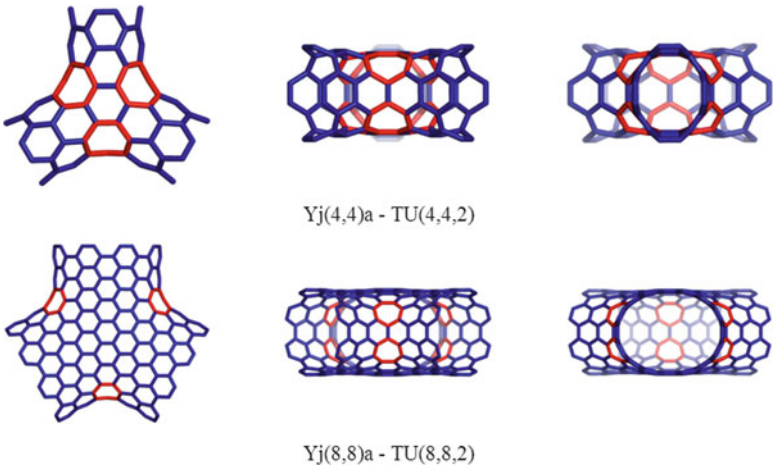

Fig. 11.4 Symmetric Y-type armchair junctions with D_{3h} symmetry Yj(4,4)a (*top*) and Yj(8,8)a (*bottom*), with chirality (4,4) and (8,8), respectively. To each junction an armchair nanotube of length 2 with matching chirality is attached, the structures are viewed along the threefold axe C_3 (*left*), twofold axe C_2 top (*center*), and twofold axe C_2 bottom (*right*)

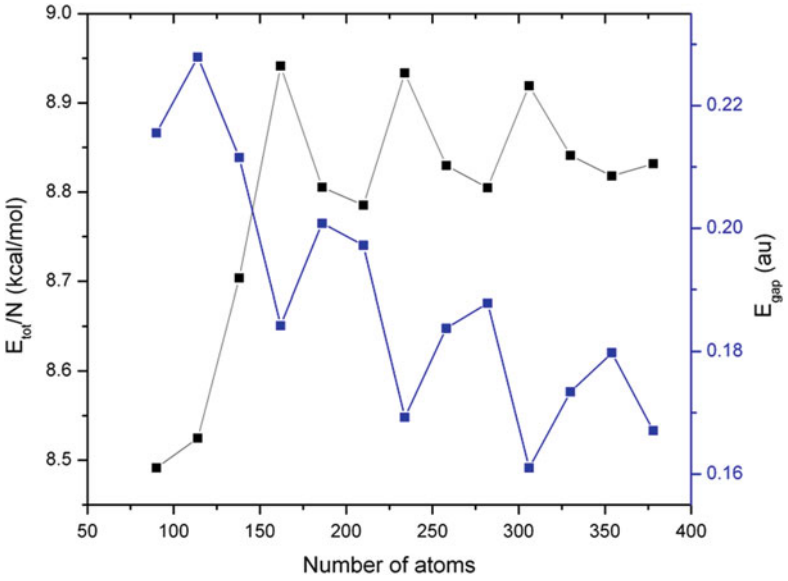

Fig. 11.5 Plot of the total energy (kcal/mol) per number of carbon atoms (E_{tot}/N) and the HOMO-LUMO gap energy (E_{gap} in au) as function of the number of atoms, obtained with the PM6 semiempirical method for the series of opened Y-type junction Yj(4,4)a

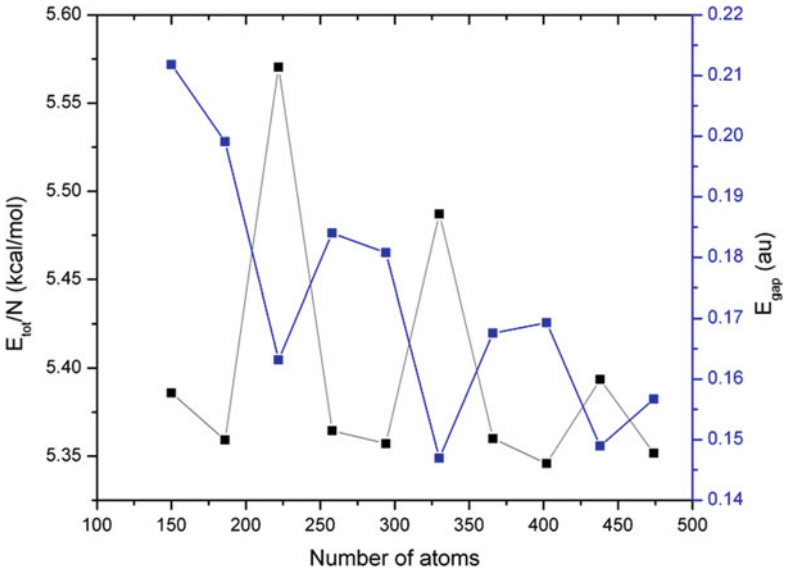

Fig. 11.6 Plot of the total energy (kcal/mol) per number of carbon atoms (E_{tot}/N) and the HOMO–LUMO gap energy (E_{gap} in au) as function of the number of atoms, obtained at the PM6 semiempirical level of theory for the series of opened Y-type junction Yj(6,6)a

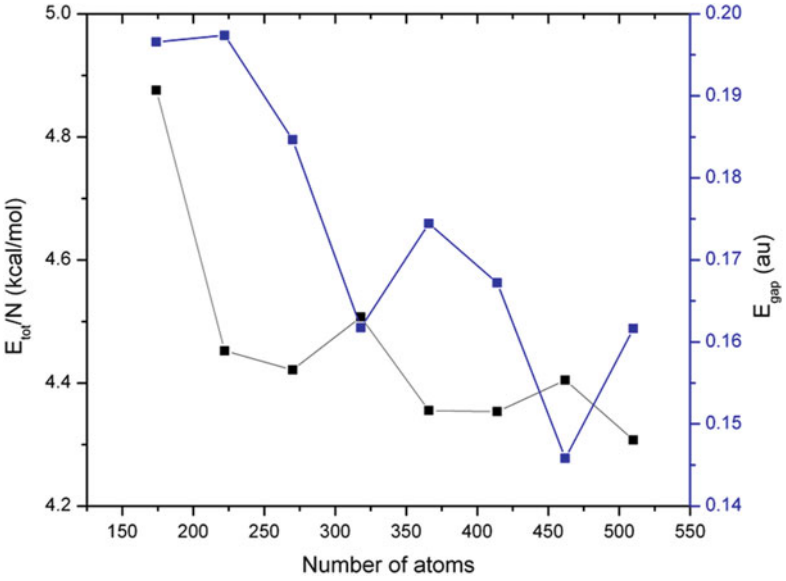

Fig. 11.7 Plot of the total energy (kcal/mol) per number of carbon atoms (E_{tot}/N) and the HOMO-LUMO gap energy (E_{gap} in au) as function of the number of atoms, obtained with the PM6 semiempirical method for the series of opened Y-type junction Yj(8,8)a

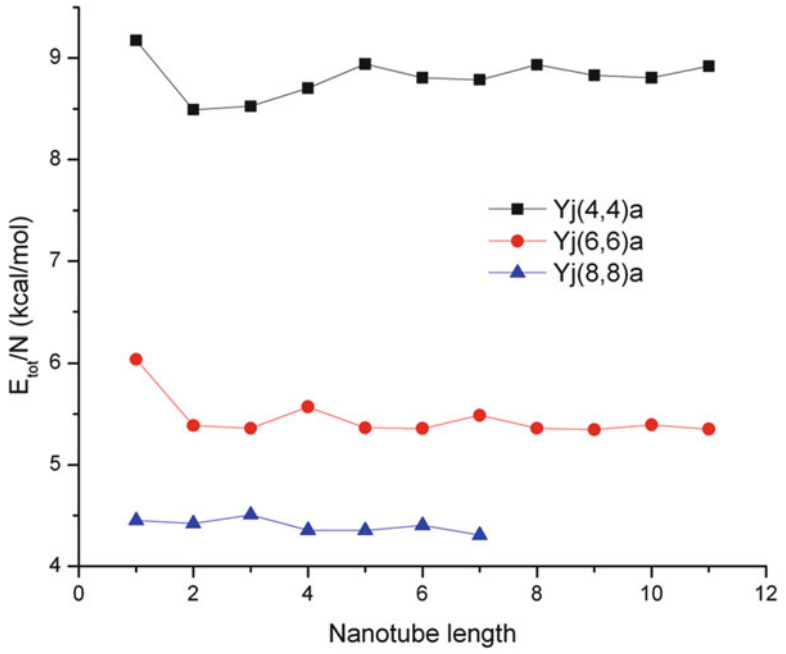

Fig. 11.8 Plot of the total energy (kcal/mol) per number of carbon atoms (E_{tot}/N) as function of the attached nanotube length, obtained with the PM6 semiempirical method for the three series of opened Y-type junction Yj(4,4)a, Yj(6,6)a, and Yj(8,8)a, respectively

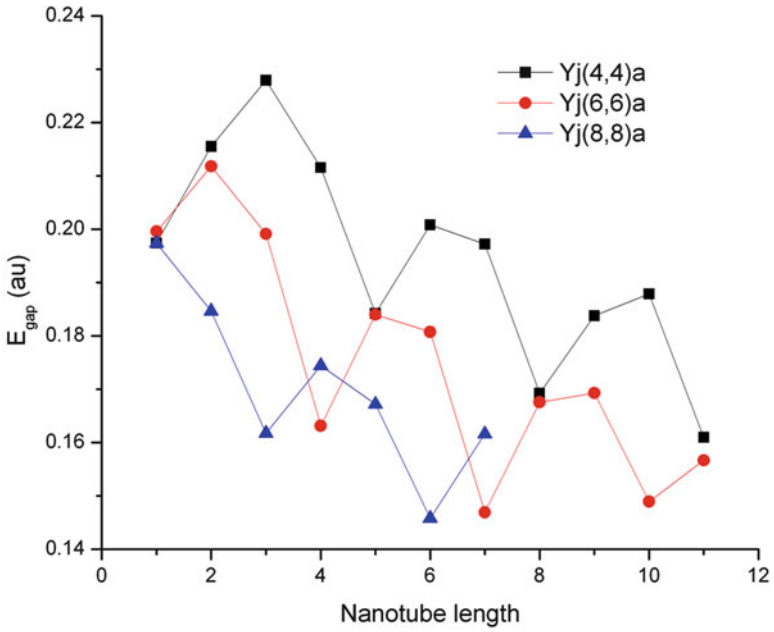

Fig. 11.9 Plot of the HOMO-LUMO energy gap (E_{gap} in au) as function of the nanotube length, obtained at the PM6 semiempirical level of theory, for the three series of opened Y-type junctions: Yj(4,4)a, Yj(6,6)a, and Yj(8,8)a, respectively

This sort order however is not preserved when comparing gap values between the series as it can be seen in Fig. 11.9. Notice however that along one series, the sort order cannot be related to the nanotube length. It can be observed that in each series the most stable structures correspond to a different nanotube length.

The periodic oscillation in the gap energy with the nanotube length was observed in case of opened or closed armchair nanotubes (Rochefort et al. 1999; Yumura et al. 2004a, b, 2005; Reich et al. 2005; Lair et al. 2006; Stobinski et al. 2003; Cioslowski et al. 2002; Sato et al. 1999; Yaguchi and Ando 2002; Matsuo et al. 2003). However, no oscillation in the values of the total energy per atoms was observed.

The three opened armchair Yj(6,6) junction stability is compared in Figs. 11.10 (gap energy) and 11.11 (total energy), respectively. The gap energy oscillation is almost identical along the three series, and the Yj(6,6)a has the highest gap values. This stability ordering is contradicted by the next plot; however, the total energy per atom values is very close at a given nanotube length. Notice that only in the case of Yj(6,6)a the total energy decreases with the tube length, at least in the structured considered in this study. It is possible that with a longer attached nanotube, the tube contributes more to the stability of the structure. The increase in energy can be attributed to the fact that the geometry of this short nanotube is distorted, and strain is introduced. The Y junction series Yj(6,6)b and Yj(6,6)c stability is presented in Figs. 11.12 and 11.13, respectively.

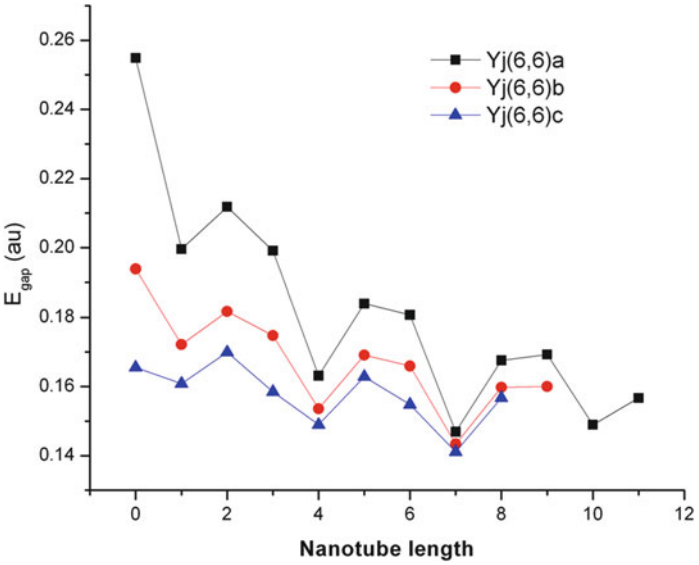

Fig. 11.10 Plot of the HOMO-LUMO energy gap (E_{gap} in au) as function of the nanotube length, obtained at the PM6 semiempirical level of theory, for the three series of opened Y-type junctions: Yj(6,6)a, Yj(6,6)b, and Yj(6,6)c, respectively

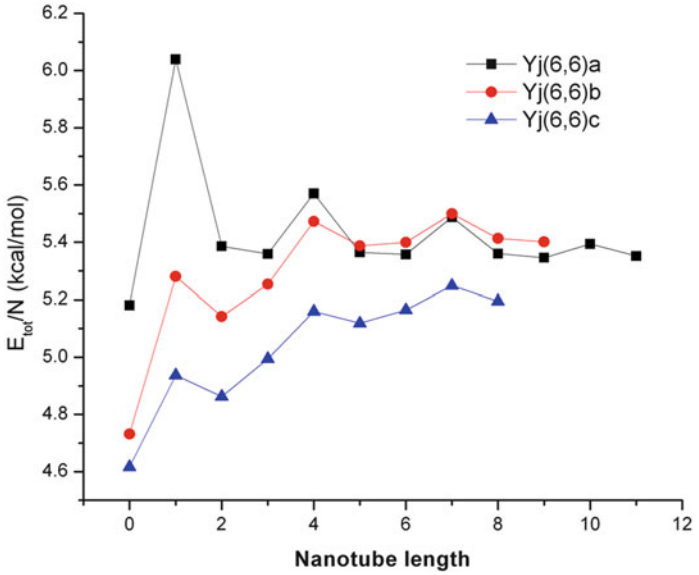

Fig. 11.11 Plot of the total energy (kcal/mol) per number of carbon atoms (E_{tot}/N) as function of the attached nanotube length, obtained with the PM6 semiempirical method for the three series of opened Y-type junctions: Yj(6,6)a, Yj(6,6)b, and Yj(6,6)c, respectively

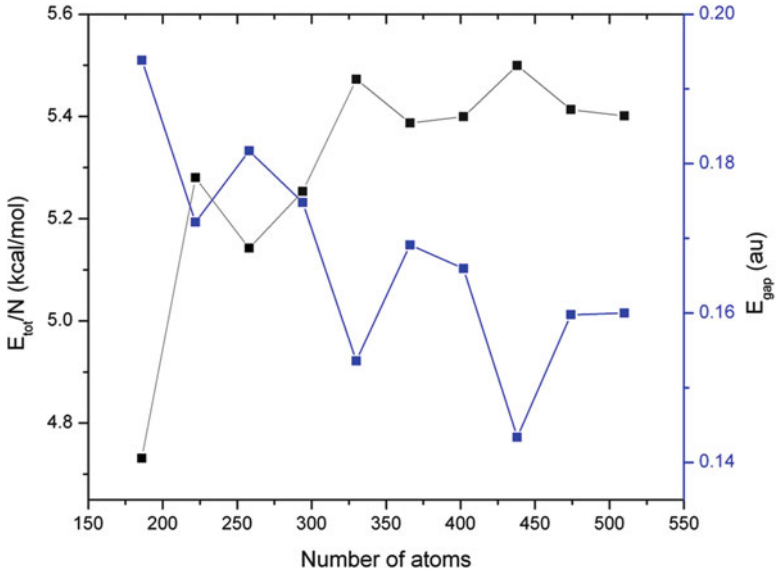

Fig. 11.12 Plot of the total energy (kcal/mol) per number of carbon atoms (E_{tot}/N) and the HOMO-LUMO gap energy (E_{gap} in au) as function of the number of atoms, obtained at the PM6 semiempirical level of theory for the series of opened Y-type junction Yj(6,6)b

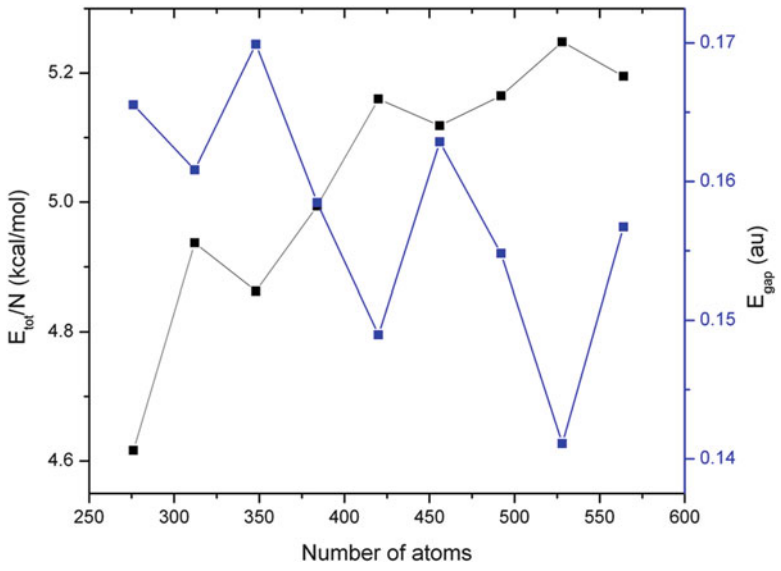

Fig. 11.13 Plot of the total energy (kcal/mol) per number of carbon atoms (E_{tot}/N) and the HOMO-LUMO gap energy (E_{gap} in au) as function of the number of atoms, obtained at the PM6 semiempirical level of theory for the series of opened Y-type junction Yj(6,6)c

11.5 Symmetric Capped Yj(*n*,*n*) Armchair Junctions

To study the cap effect on the stability of the junction, the three armchair junction series Yj(6,6)a, Yj(6,6)b, and Yj(6,6)c were closed at the opposing end of the nanotube with respect to the junction (Fig. 11.14). The nanotube cap is a half fullerene, which includes six pentagons and has a positive curvature. One nanotube cap can fit to only one kind of nanotube; however, a nanotube can be enclosed by more than one cap (depends on the size of the opening) (Lair et al. 2006; Brinkmann et al. 1999, 2002; Diudea and Nagy 2007). To preserve the junction high symmetry, only two symmetrical caps were chosen to close the structure, their structure viewed along the symmetry axe can be seen in Fig. 11.15.

Series were constructed by increasing the length of the tube between the junction and the cap. Depending on the length of the nanotube (even or odd number of rows of atoms), the cap changes its position relative to the junction. Figure 11.16 presents the Yj(6,6)a capped with both nanotube caps, while Fig. 11.17 shows the geometry of the Yj(6,6)b and Yj(6,6)c closed with cap 1.

The plot of the total energy per atom as function of the nanotube length is presented in Fig. 11.18. The stability ordering corresponds to that of the opened Y junctions. The only difference is that in all cases the total energy decreases with the increase of the attached nanotube.

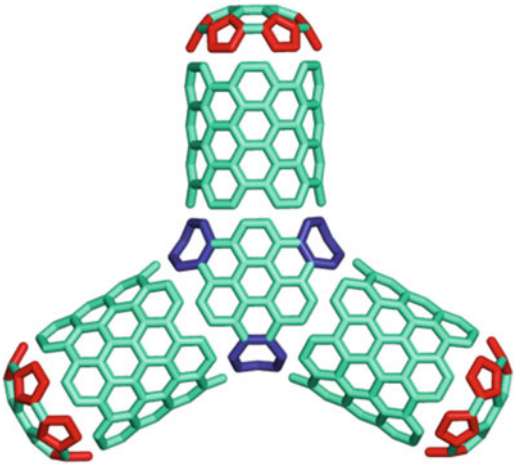

Fig. 11.14 Construction of a closed Y-type junction Yj(6,6) from three fragments: the junction region (*central*) is characterized by negative curvature introduced by the heptagons, the three attached armchair nanotubes to the openings of the junction, and the nanotube caps that enclose the opposite end of the nanotube with respect to the junction and which are characterized by the positive curvature introduced by the pentagons. The chirality of each structural element must be the same

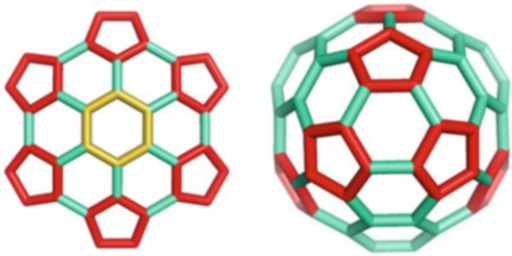

Fig. 11.15 Armchair (6,6) carbon nanotube caps (half fullerenes), with sixfold C_6 (*left*) – cap 1, and threefold C_3 (*right*) – cap 2 rotational symmetry axe, respectively. Each cap contains 6 pentagons which gives a positive curvature to the structure

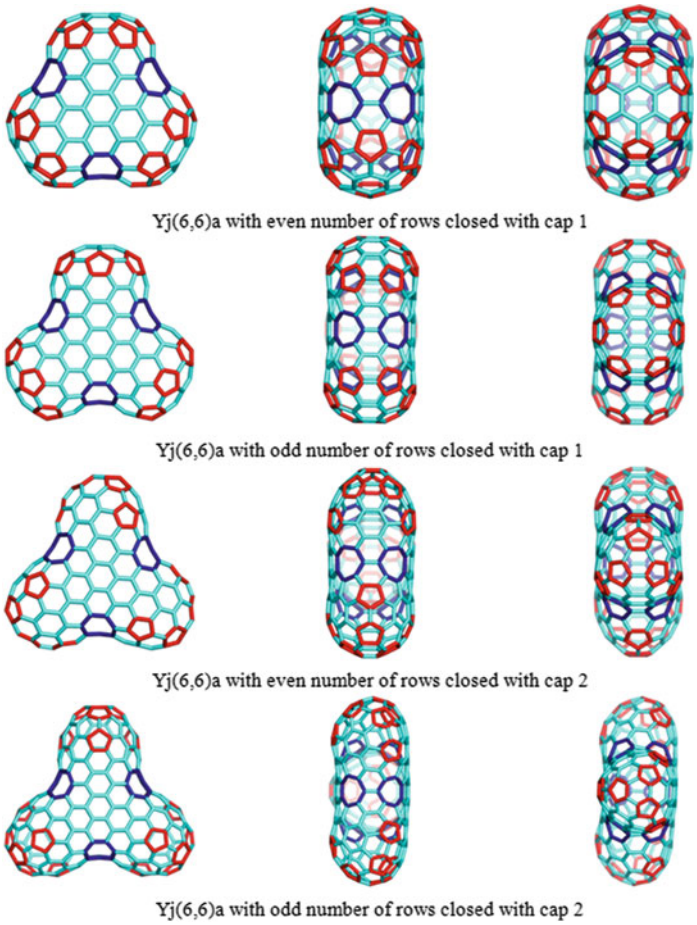

Fig. 11.16 Y-type junction Yj(6,6)a closed at each end with the same nanotube cap. Depending on the attached nanotube length (odd or even), the cap changes its position relative to the junction

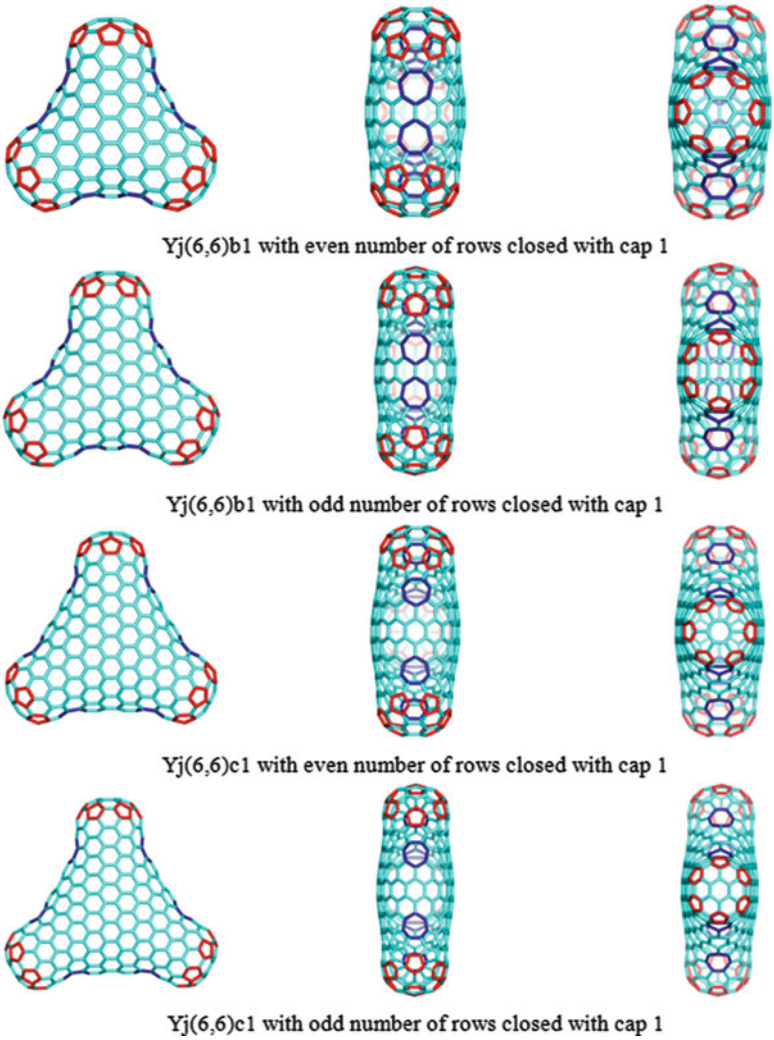

Fig. 11.17 Closed symmetric Y junctions, Yj(6,6)b and Yj(6,6)c, capped at each opening using the same cap. The cap position varies depending on the length of the nanotube between the junction and cap (even and odd number of atom rows)

As in the previous study, the ordering of the three series changes in the case of the energy gap, as it can be seen in Fig. 11.19. Once again, the three curves are almost parallel; the structures with the largest gap correspond to the Yj(6,6)a series.

In Figs. 11.20 and 11.21, the total energy per atom and the gap energy are plotted versus the nanotube length, respectively, in the case of the two series of closed Yj(6,6)a junctions capped with cap 1 and 2. It can be seen that although there is

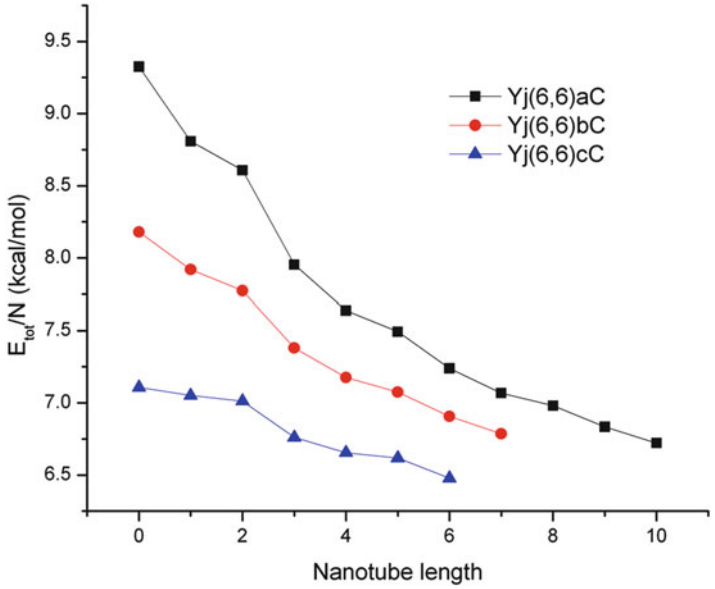

Fig. 11.18 Plot of the total energy (kcal/mol) per number of carbon atoms (E_{tot}/N) as function of the length of the (6,6) armchair nanotube attached to the junction obtained with the PM6 semiempirical method for the series of closed Y junctions: Yj(6,6)aC, Yj(6,6)bC, and Yj(6,6)cC

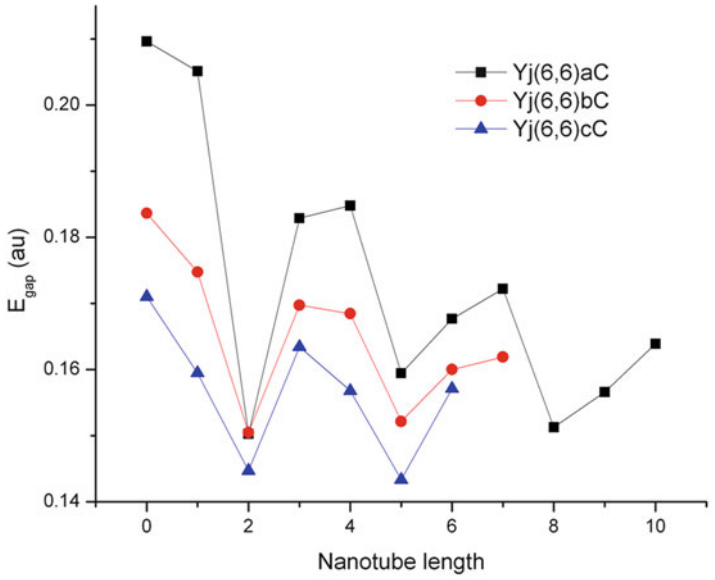

Fig. 11.19 Plot of the HOMO-LUMO energy gap (E_{gap} in au) as function of the nanotube length, obtained at the PM6 semiempirical level of theory, for the three series of closed Y-type junctions: Yj(6,6)aC, Yj(6,6)bC, and Yj(6,6)cC

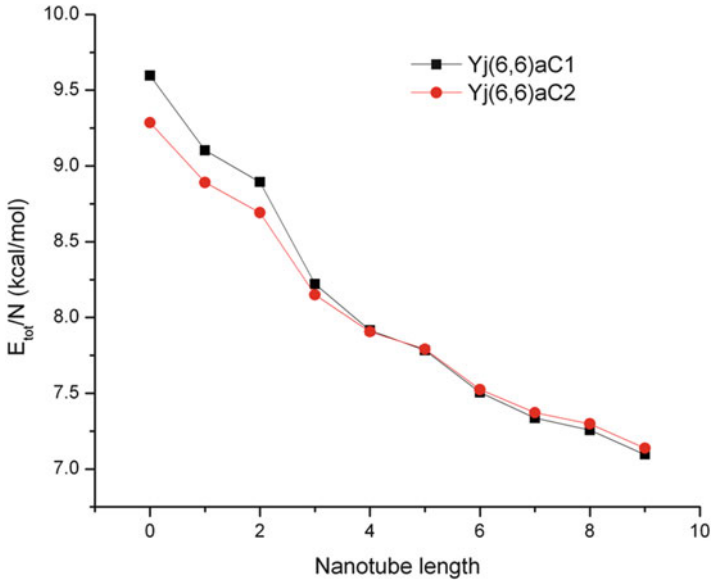

Fig. 11.20 Plot of the total energy (kcal/mol) per number of carbon atoms (E_{tot}/N) as function of the attached (6,6) nanotube length, obtained with the PM3 semiempirical method for the two series of closed Y junctions: Yj(6,6)aC1 and Yj(6,6)aC2, respectively

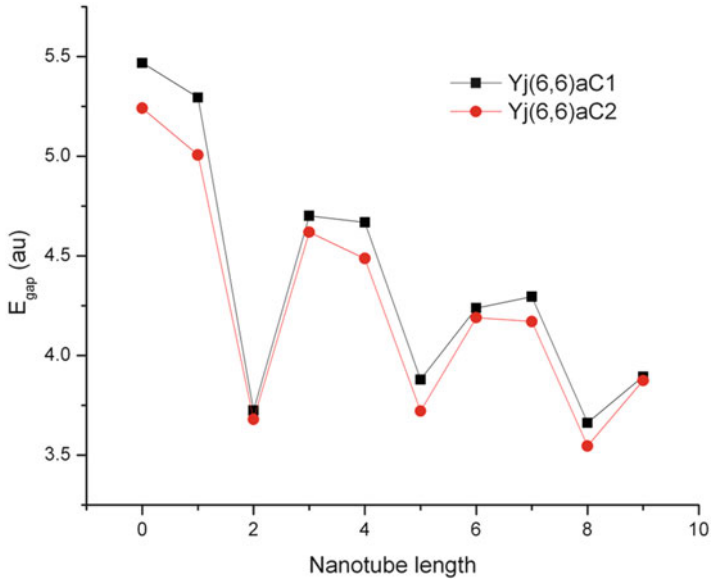

Fig. 11.21 Plot of the HOMO-LUMO energy gap (E_{gap} in au) as function of the nanotube length, obtained at the PM3 semiempirical level of theory, for the two series of capped Y junctions: Yj(6,6)aC1 and Yj(6,6)aC2, respectively

some minor energy difference, however, they have almost the same stability. The periodicity in the gap values is present; the series closed with the higher symmetry cap is somewhat more stable.

11.6 Closed Asymmetric Yj(*n*,*n*) Armchair Junctions

Starting from the Yj(6,6)a junction, four series of junctions were constructed by keeping constant two of the arms of the junctions and increasing only one of the attached nanotube's length. Each nanotube was closed at the end with cap 1. An example is given in Fig. 11.22 where two arms are of length 3, while the third nanotube is of length 8. The geometries were optimized with the PM3 semiempirical method using Gaussian 09 package (Frisch et al. 2009).

Calculation results obtained at the same theoretical level are presented in Figs. 11.23 and 11.24, where the total energy per atom and the HOMO-LUMO gap energy are plotted as the function of the tube length, respectively. The first plot gives a similar answer as was previously observed in the case of closed Y junctions, which is the energy decreases with the tube length in all four series.

Notice however that in the second plot, not all series have the same stability ordering. Only the structures where the length of the tubes was zero and three show a periodicity in the energy gap values. The two series stability is almost the same, with the exception of the first two members of the series. This could be explained by the fact that every third member of these two series is a leapfrog structure (Fowler and Steer 1987; Fowler 1990; Fowler and Pisanski 1994; Rogers and Fowler 2001).

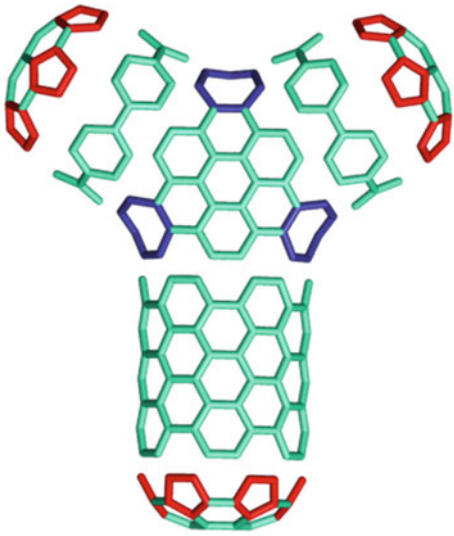

Fig. 11.22 An example of asymmetric junction Yj(*n*,*n*): all attached nanotubes have the same chirality, but the length of one arm is different from the others

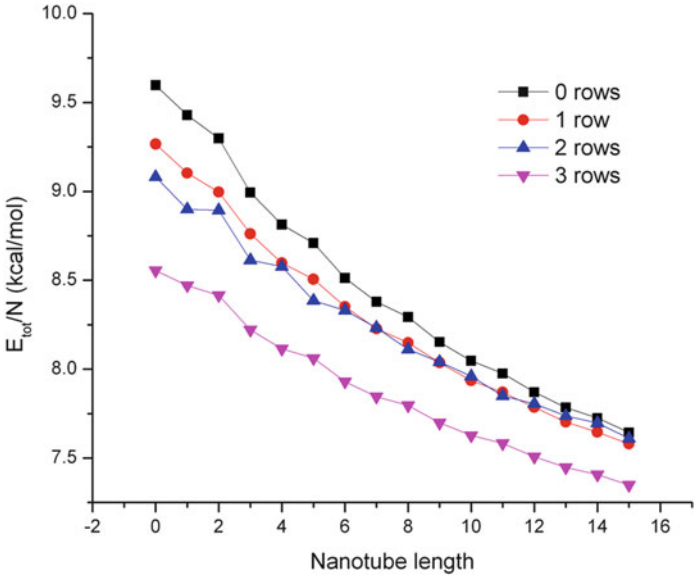

Fig. 11.23 Plot of the total energy (kcal/mol) per number of carbon atoms (E_{tot}/N) as function of the attached (6,6) nanotube length, obtained with the PM3 semiempirical method for the four series of closed asymmetric Y junctions

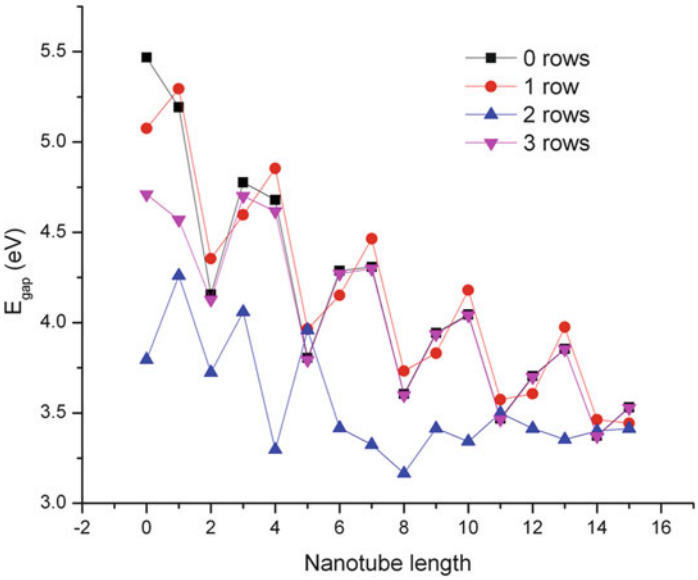

Fig. 11.24 Plot of the HOMO-LUMO energy gap (E_{gap} in au) as function of the nanotube length, obtained at the PM3 semiempirical level of theory, for the four series of closed and asymmetric Y junctions

11.7 Nanodendrimer and Hyperhexagonal Structures

Dendrimers of carbon nanotube junctions are structures where the nodes represent opened fullerene-like units while the edges are nanotubes. One possible way to construct such structures is by using Y armchair junctions as units and connecting them in an orthogonal fashion, as illustrated in Fig. 11.25 at first, second, and third generation.

Hyperhexagonal molecules can be obtained by connecting armchair Y junction; the examples are given in case where Y(4,4) and Y(6,6) were used as building blocks. Carbon nanotube caps (half fullerenes) with sixfold rotational symmetry C_6 were used to close the open hyperhexagonal molecule to obtain finite structures (see Fig. 11.26).

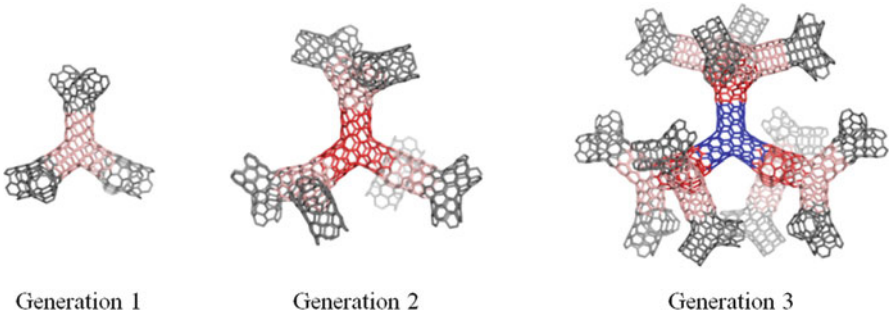

Fig. 11.25 Dendrimers built from Y(4,4) armchair junctions

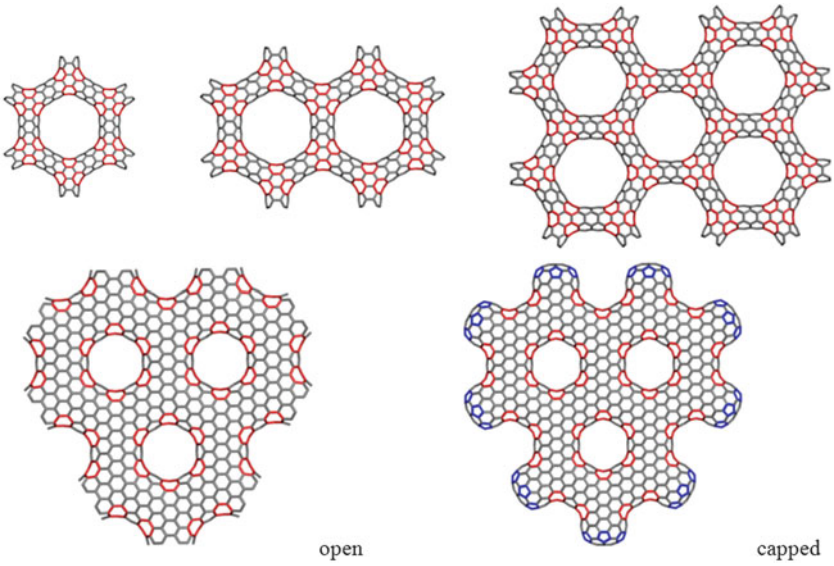

Fig. 11.26 Hyperhexagonal structures build from Y(4,4) and Y(6,6) armchair junctions

11.8 Conclusions

To study the effect of the attached nanotubes on the stability of Y junctions, several series were modeled, where the nanotube length is increased. Also the opened junctions were closed by a nanotube cap, to study the cap effect. Geometry optimizations followed by single-point energy calculations at the PM3 and PM6 semiempirical level of theory showed that the nanotube length and diameter has a big influence on the stability. The closing cap did not alter the stability sort order.

Similar to the armchair-opened and armchair-closed nanotubes, an oscillating periodicity can be observed in the gap values of each series as function of the tube length. No direct relationship could be found between the stability and nanotube length; however, the increase of the tube diameter decreases the total energy.

Acknowledgments CL Nagy acknowledges the financial support of the Sectoral Operational Programme for Human Resources Development 2007–2013, cofinanced by the European Social Fund, under the project number POSDRU 89/1.5/S/60189 with the title "Postdoctoral Programs for Sustainable Development in a Knowledge Based Society."

References

Biró LP, Ehlich R, Osváth Z, Koós A, Horváth ZE, Gyulai J, Nagy JB (2002a) From straight carbon nanotubes to Y-branched and coiled carbon nanotubes. Diam Relat Mater 11(3–6):1081–1085

Biró LP, Ehlich R, Osváth Z, Koós A, Horváth ZE, Gyulai J, Nagy JB (2002b) Room temperature growth of single-wall coiled carbon nanotubes and Y-branches. Mater Sci Eng C 19(1–2):3–7

Biró LP, Horváth ZE, Márk GI, Osváth Z, Koós AA, Benito AM, Maser W, Lambin P (2004) Carbon nanotube Y junctions: growth and properties. Diam Relat Mater 13(2):241–249

Brinkmann G, Fowler PW, Manolopoulos DE, Palser AHR (1999) A census of nanotube caps. Chem Phys Lett 315(5–6):335–347

Brinkmann G, Nathusius UV, Palser AHR (2002) A constructive enumeration of nanotube caps. Discrete Appl Math 116:55–71

Chernozatonskii LA (1992) Carbon nanotube connectors and planar jungle gyms. Phys Lett A 172(3):173–176

Cioslowski J, Rao N, Moncrieff D (2002) Electronic structures and energetics of [5,5] and [9,0] single-walled carbon nanotubes. J Am Chem Soc 124(28):8485–8489

Dimitrakakis GK, Tylianakis E, Froudakis GE (2008) Pillared graphene: a new 3-D network nanostructure for enhanced hydrogen storage. Nano Lett 8(10):3166–3170

Diudea MV, Nagy CL (2007) Periodic nanostructures. Springer, Dordrecht

Fowler PW (1990) Carbon cylinders: a class of closed-shell clusters. J Chem Soc Faraday Trans 86(12):2073–2077

Fowler PW, Pisanski T (1994) Leapfrog transformations and polyhedra of clar type. J Chem Soc Faraday Trans 90(19):2865–2871

Fowler PW, Steer JI (1987) The leapfrog principle: a rule for electron counts of carbon clusters. J Chem Soc Chem Commun 1403–1405

Frisch MJ, Trucks GW, Schlegel HB, Scuseria GE, Robb MA, Cheeseman JR, Scalmani G, Barone V, Mennucci B, Petersson GA, Nakatsuji H, Caricato M, Li X, Hratchian HP, Izmaylov AF, Bloino J, Zheng G, Sonnenberg JL, Hada M, Ehara M, Toyota K, Fukuda R, Hasegawa J, Ishida M, Nakajima T, Honda Y, Kitao O, Nakai H, Vreven T, Montgomery JJA, Peralta JE, Ogliaro

F, Bearpark M, Heyd JJ, Brothers E, Kudin KN, Staroverov VN, Kobayashi R, Normand J, Raghavachari K, Rendell A, Burant JC, Iyengar SS, Tomasi J, Cossi M, Rega N, Millam JM, Klene M, Knox JE, Cross JB, Bakken V, Adamo C, Jaramillo J, Gomperts R, Stratmann RE, Yazyev O, Austin AJ, Cammi R, Pomelli C, Ochterski JW, Martin RL, Morokuma K, Zakrzewski VG, Voth GA, Salvador P, Dannenberg JJ, Dapprich S, Daniels AD, Farkas Ö, Foresman JB, Ortiz JV, Cioslowski J, Fox DJ (2009) Gaussian 09, revision A.02. Gaussian, Inc, Wallingford

Lair SL, Herndon WC, Murr LE, Quinones SA (2006) End cap nucleation of carbon nanotubes. Carbon 44:447–455

László I (2005a) Topological description and construction of single wall carbon nanotube junctions. Croat Chem Acta 78(2):217–221

László I (2005b) A possible topological arrangement of carbon atoms at nanotube junctions. Fuller Nanotub Carbon Nanostruct 13(suppl 1):535–541

László I (2008) Construction of carbon nanotube junctions. Croat Chem Acta 81(2):267–272

Li J, Papadopoulos C, Xu J (1999) Growing Y-junction carbon nanotubes. Nature 402(6759): 253–254

Li WZ, Wen JG, Ren ZF (2001) Straight carbon nanotube Y junctions. Appl Phys Lett 79(12):1879–1881

Márk GI, Biró LP, Gyulai J (1998) Simulation of STM images of three-dimensional surfaces and comparison with experimental data: carbon nanotubes. Phys Rev B 58(19):12645–12648

Matsuo Y, Tahara K, Nakamura E (2003) Theoretical studies on structures and aromaticity of finite-length armchair carbon nanotubes. Org Lett 5(18):3181–3184

Nagy CL, Diudea MV (2009) Nano Studio software. Babes-Bolyai University, Cluj

Reich S, Li L, Robertson J (2005) Structure and formation energy of carbon nanotube caps. Phys Rev B 72:165423(1–8)

Rochefort A, Salahub DR, Avouris P (1999) Effects of finite length on the electronic structure of carbon nanotubes. J Phys Chem B 103:641–646

Rogers KM, Fowler PW (2001) Leapfrog fullerenes, Hückel bond order and Kekulé structures. J Chem Soc Perkin Trans 2:18–22

Satishkumar BC, Thomas PJ, Govindaraj A, Rao CNR (2000) Y-junction carbon nanotubes. Appl Phys Lett 77(16):2530–2532

Sato T, Tanaka M, Yamabe T (1999) Size-dependent HOMO-LUMO gap oscillation of carbon nanotube with a finite length. Synth Met 103:2525–2526

Scuseria GE (1992) Negative curvature and hyperfullerenes. Chem Phys Lett 195(5–6):534–536

Stobinski L, Peszke J, Lin H-M (2003) Computational studies of SWCNTs capped by hemispheres of C_{60} fullerene, based on semiempirical methods. Rev Adv Mater Sci 5(4):363–370

Sui YC, Acosta DR, González-León JA, Bermúdez A, Feuchtwanger J, Cui BZ, Flores JO, Saniger JM (2001a) Structure, thermal stability, and deformation of multibranched carbon nanotubes synthesized by CVD in the AAO template. J Phys Chem B 105(8):1523–1527

Sui YC, González-León JA, Bermúdez A, Saniger JM (2001b) Synthesis of multi branched carbon nanotubes in porous anodic aluminum oxide template. Carbon 39(11):1709–1715

Terrones H, Terrones M (2003) Curved nanostructured materials. New J Phys 5:126.1–126.37

Terrones M, Banhart F, Grobert N, Charlier JC, Terrones H, Ajayan PM (2002a) Molecular junctions by joining single-walled carbon nanotubes. Phys Rev Lett 89(7):075505/1–075505/4

Terrones M, Charlier JC, Banhart F, Grobert N, Terrones H, Ajayan PM (2002b) Towards nanodevice fabrication: joining and connecting single-walled carbon nanotubes. New Diam Front Carbon Technol 12(5):315–323

Terrones M, Banhart F, Hernández E, Grobert N, Charlier JC, Terrones H, Ajayan PM (2003) In-situ welding of single-walled carbon nanotubes and melting of encapsulated metal clusters in carbon shells: theory and experiment. Microsc Microanal 9:320–321

Tylianakis E, Dimitrakakis GK, Melchor S, Dobado JA, Froudakis GE (2011) Porous nanotube network: a novel 3-D nanostructured material with enhanced hydrogen storage capacity. Chem Commun 47(8):2303–2305

Yaguchi T, Ando T (2002) Study of cap states in carbon nanotubes. Physica B 323:209–210

Yumura T, Bandow S, Yoshizawa K, Iijima S (2004a) The role of fullerene hemispheres in determining structural features of finite-length carbon nanotubes. J Phys Chem B 108: 11426–11434

Yumura T, Hirahara K, Bandow S, Yoshizawa K, Iijima S (2004b) A theoretical study on the geometrical features of finite-length carbon nanotubes capped with fullerene hemisphere. Chem Phys Lett 386:38–43

Yumura T, Nozaki D, Bandow S, Yoshizawa K, Iijima S (2005) End-cap effects on vibrational structures of finite-length carbon nanotubes. J Am Chem Soc 127(33):11769–11776

Zhou D, Seraphin S (1995) Complex branching phenomena in the growth of carbon nanotubes. Chem Phys Lett 238(4–6):286–289

Zsoldos I, Kakuk G (2007) New formations of carbon nanotube junctions. Model Simul Mater Sci Eng 15(7):739–745

Zsoldos I, Kakuk G, Réti T, Szasz A (2004) Geometric construction of carbon nanotube junctions. Model Simul Mater Sci Eng 12(6):1251–1266

Zsoldos I, Kakuk G, Janik J, Pék L (2005) Set of carbon nanotube junctions. Diam Relat Mater 14:763–765

Chapter 12
Energetics and Topology of Polybenzenes

Beata Szefler and Mircea V. Diudea

Abstract Polybenzene 6.8^2D was described by O'Keeffe et al. (Phys Rev Lett 68:2325–2328, 1992) as a uninodal embedding of a 6.8^2 net in the infinite periodic minimal *D*-surface and was predicted to have a substantially lower energy per atom in comparison to C_{60}, the reference structure in nanoscience. The authors also described the lattice 6.8^2P, an embedding of the 6.8^2 net in the periodic minimal *P*-surface. Two other polybenzenes: a binodal $(6.8^2)(6^2.8)P$ and a uninodal 6.9^2D ones are discussed here, being related to the above nets both by the presence of benzene patch (motif for the generic name "polybenzenes") and construction procedure.

Polybenzene "armchair"-ended unit BTA_48 can form three different dimers: (1) $R[8_{fcc}](BTA\_48)_{2fcc}\_88$ to provide next the diamond-like net $6.8^2D = BTA_{fcc}$, (2) $R[12_{int}](BTA\_48)_2\_84$ that gives next dendrimers, and (3) $R[12_{ecl}](BTA\_48)_2\_90$ which can form further multi-tori. Polybenzene "zigzag"-ended unit BTZ_24 forms two dimers: $(BTZ\_24)_2\_48$, suitable to build multi-tori, and $(BTZ\_24)_2\_42$ that provides the translational network 6.9^2D.

The energetics of these units and some small substructures of polybenzenes, relative to C_{60}, have been evaluated at the Hartree-Fock level of theory. The results confirmed the previous evaluation of polybenzene stability and support these structures for laboratory preparation. In the hope of their experimental synthesis, vibrational spectra of the most important monomers and dimers have been simulated.

B. Szefler
Department of Physical Chemistry, Collegium Medicum, Nicolaus Copernicus University, Kurpińskiego 5, 85-950 Bydgoszcz, Poland
e-mail: beata.szefler@cm.umk.pl

M.V. Diudea (✉)
Department of Chemistry, Faculty of Chemistry and Chemical Engineering, Babes-Bolyai University, A. Janos 11, 00028 Cluj, Romania
e-mail: diudea@chem.ubbcluj.ro

M.V. Diudea and C.L. Nagy (eds.), *Diamond and Related Nanostructures*, Carbon Materials: Chemistry and Physics 6, DOI 10.1007/978-94-007-6371-5_12,

In this chapter, a rational structure construction, based on topological map operations, for the polybenzene and related networks, is given. A building assay for the $BTA_{fcc}/6.8^2D$ net is here provided. A graph-theoretical description, in terms of Omega polynomial, of the infinite polybenzene networks is also presented.

12.1 Introduction

O'Keeffe et al. (1992) have published about 20 years ago a letter describing two 3D networks of benzene: the first one, called 6.8^2D (also polybenzene, *pbz*), belongs to the space group *Pn*-3*m* and has the topology of the fcc-diamond (point symbol for net: $\{6.8^2\}$; uninodal 3-c net; topological type: pbz; 3/6/c2; sqc9271 – Fig. 12.1,

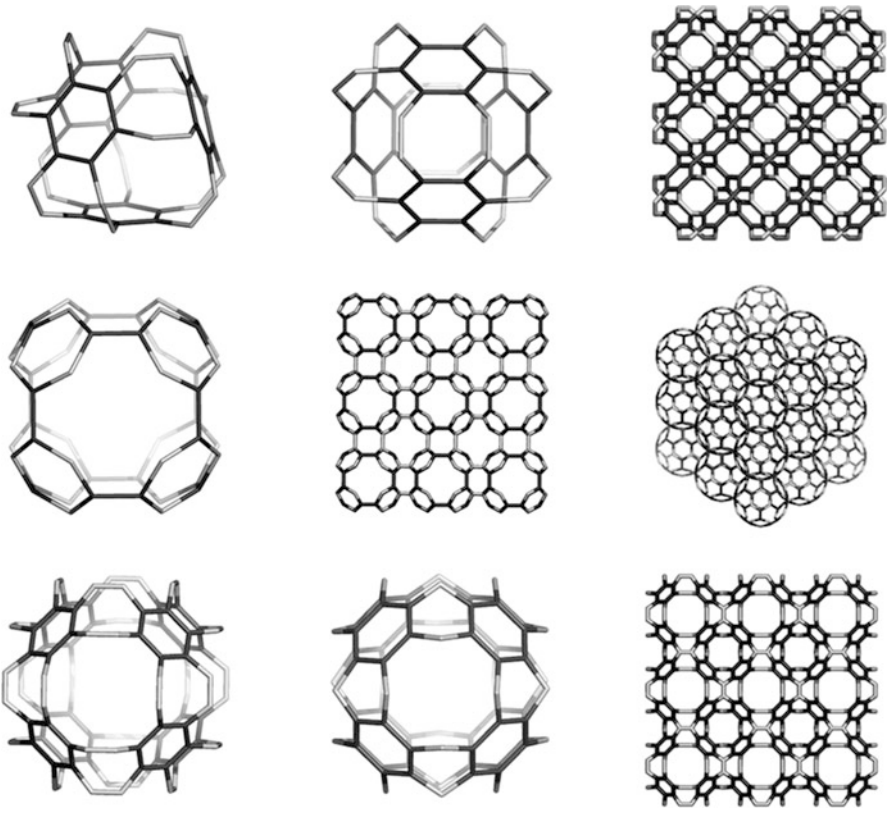

Fig. 12.1 Polybenzenes. *Top*: BTA_48 unit (*left* and *middle*); the face-centered network $6.8^2D = BTA_{fcc}$; symbol for net $\{6.8^2\}$; 3-c uninodal net (a cubic (*k*,*k*,*k*)-domain BTA_{fcc}_(3,3,3)_864, $k = 3$, *right*). *Middle*: BCZ_48 unit (*left*); network $6.8^2P = (BCZ\_48)P$; symbol for net $\{6.8^2\}$; 3-c uninodal net ((BCZ_48)*P*_(3,3,3)_1296, top view (*middle*) and corner view (*right*)). *Bottom*: units BCA_96 (*left*) and BCZ_72 (*middle*); network $(6.8^2)(6^2.8)P = (BCA\_96\&BCZ\_72)P$; symbol for net $(6.8^2)(6^2.8)2$; 3,3-c bimodal net ((BCA_96&BCZ_72)_2160, top view-*right*)

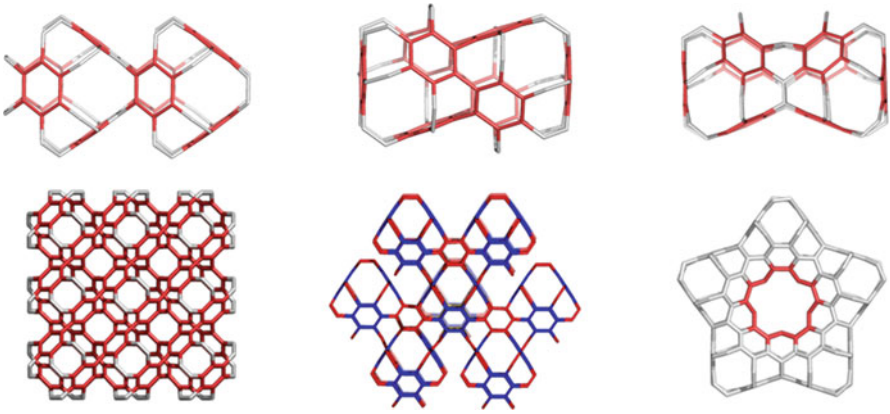

Fig. 12.2 Three different dimers of BTA_48 (*top*): R[8_{fcc}](BTA_48)$_2$_88 (*left*); R[12_{int}](BTA_48)$_2$_84 (*middle*); and R[12_{ecl}](BTA_48)$_2$_90 (*right*) and their networks (*bottom*): BTA$_{fcc}$_(3,3,3)_864 (*left*); BTA$_{17}$_624 (*middle*); and BTA$_{5cy}$_210 (*right*); the last number in their name is the atom count (Reproduced from Central European Journal of Chemistry 2012, 10(6), 1779–1785)

top). The second structure was called 6.8^2P (also pbp) and belongs to the space group *Im*-3*m*, corresponding to the *P*-type surface (point symbol for net: $\{6.8^2\}$; uninodal 3-c net; topological type: pbp; 3/6/c4; sqc9265 – Fig. 12.1, middle). In fact, these are embeddings of the benzene/hexagon patch in the two surfaces of negative curvature, *D* and *P*, respectively. More about these periodic surfaces, the reader can find in Diudea (2005) and Diudea and Nagy (2007).

According to the authors, the two above networks show a stability comparable, or even higher, to that of C_{60} fullerene, the reference structure in nanoscience. The structure 6.8^2D was predicted to be insulator, while 6.8^2P is metallic. Of interest in chemistry is their spongy structure (Barborini et al. 2002; Benedek et al. 2003; Valencia et al. 2003); the large ordered hollows could host alkali metal ions, as in natural zeolites (Baerlocher et al. 2007). These structures was hoped to be synthesized as 3D carbon solids; however, in our best knowledge, no such a synthesis was reported so far. Our intention was to wake up the interest of scientists to the molecular realization of such exciting nanostructures of carbon, as much as graphenes gained a second Nobel Prize, after C_{60}, and the direct synthesis of fullerenes is now a reality (Scott 2004; Amsharov and Jansen 2008).

Polybenzene unit BTA_48 was shown (Szefler and Diudea 2012a, b) to dimerize either by identification of octagons R[8] to provide a R[8_{fcc}](BTA_48)$_2$_88 dimer and next the diamond-like $6.8^2D = \text{BTA}_{fcc}$-net (Fig. 12.2 left column) or by identifying the "windows" rings R[12] when an "intercalated" dimer R[12_{int}](BTA_48)$_2$_84 is formed (Fig. 12.2 middle, top); this second dimer grows next to form dendrimers, for example, dendrimer.

BTA$_{17}$_624 (Fig. 12.2 middle, bottom) at the second generation. A further growing of the dendritic net will complete the diamond-like network over

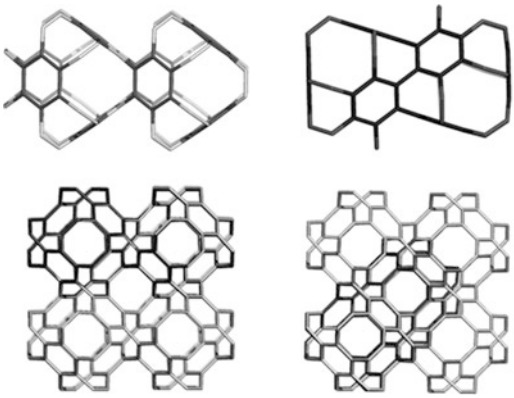

Fig. 12.3 Dimers $R[8_{fcc}](BTA\_48)_2\_88$ (top, *left*) and $R[12_{int}](BTA\_48)_2\_84$ (top, *right*) and their embedding in the $6.8^2D/BTA_{fcc}$ network (*bottom*). In the name of structures, the subscript number indicates the repeating units composing the structure, while the last number counts the C atoms

which the dendrimer is superimposed (Fig. 12.3). In a third way, an "eclipsed"-dimer $R[12_{ecl}](BTA\_48)_2\_90$ can be formed, of which oligomers, for example, BTA_{5cy}_210 (Fig. 12.2, right column), show angles suitable to grow structures of fivefold symmetry, eventually called multi-tori (Diudea and Petitjean 2008; Diudea 2010a).

In the name of structures, the subscript number indicates the repeating units composing the structure, while the last number counts the C atoms.

12.2 Design of Networks

12.2.1 Triple Periodic Nets

The design of units of the considered structures was made by using some operations on maps (Diudea 2004, 2005, 2010a; Diudea et al. 2006), applied to the Platonic solids. For example, the structure BTA_48 (Fig. 12.1 top) was designed by spanning the cage obtained by the sequence of operations denoted $Le(P_4(M))$, M = T (tetrahedron), while BCZ_48 (Fig. 12.1 middle) was designed by spanning the cage provided by $S_2(Oct)$, Oct = octahedron (Szefler and Diudea 2012a). The spanned cages are illustrated in Fig. 12.4. In the name of structures, B represents the "benzene patch" of tessellation; T or C indicates the Platonic solid to which the transformed map is related.

A/Z comes from "armchair" and "zigzag" nanotube ending, respectively, while the last number denotes the number of carbon atoms in structures.

The networks 6.8^2D and 6.8^2P (Fig. 12.1) were constructed either by identifying or joining the common faces in the corresponding repeating units. In case of BTA_48, the face identification is possible either by octagons R[8] or by dodecagons R[12] to provide the 6.8^2D net (denoted here BTA_{fcc}) and corresponding dendrimer (Fig. 12.2).

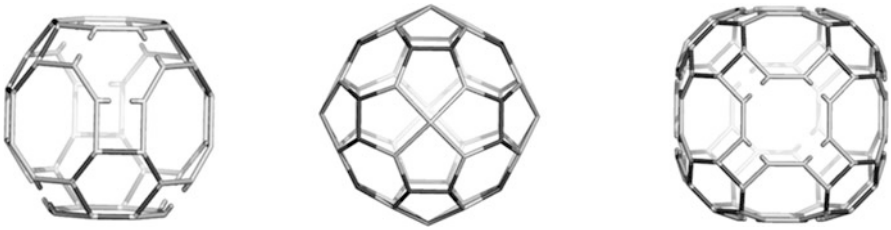

Fig. 12.4 Spanned cages in the design of BTA_48 ($Le(P_4(M))$; M = T, *left*); BCZ_48 (S_2(Oct), *middle*) and BCA_96 ($Le(P_4(M))$, M = C, *right*)

A third network, $(6.8^2)(6^2.8)P$, related to 6.8^2D by the map operation used to design the repeating unit BCA_96 (Fig. 12.4, right) while to 6.8^2P by the embedding surface, was included in Fig. 12.1 bottom. Its crystallographic description is crystal network name sqc13776; group *Pm*-3*m*; point symbol for net: $(6.8^2)(6^2.8)2$; 2-nodal 3,3-c net, with stoichiometry (3-c)(3-c)2; topological type: sqc13776 (epinet: http://epinetanueduau/about; topos: http://www.toposssusamararu/index.html). In our notation, it is a (BCA_96&BCZ_72)*P* net, where BCZ_72 represents the co-net unit; both units bear the benzene/hexagon patch.

Since our calculations confirmed the previous evaluation of polybenzene network stability (O'Keeffe et al. (1992)), thus supporting these structures for laboratory preparation, we focus attention on a possible route for the synthesis of $6.8^2D/\mathrm{BTA}_{\mathrm{fcc}}$ network (see Fig. 12.5). The main idea is to find a complementary structure to be connected to the repeating unit BTA_48. Such a structure could be a substructure of the main unit, for example, BTAX_40 (Fig. 12.5 top, left) that eventually adds to BTA_48, according to the XYZ coordinates, in a progressive growing of the net (see $(\mathrm{BTA_48})_{\mathrm{XYZ}}$_288; $(\mathrm{BTA_48})_{\mathrm{XYZ}}$_672; $((\mathrm{BTA_48})_{\mathrm{XYZ}})_2$_1344, Fig. 12.5). While the connections (following the bisectors of the right coordinates) between the blocks $(\mathrm{BTA_48})_{\mathrm{XYZ}}$_672 are established, the R[12] face identification is involved, in the manner the dendritic dimer $\mathrm{R}[12_{\mathrm{int}}](\mathrm{BTA_48})_2$_84 is embedded in the $\mathrm{BTA}_{\mathrm{fcc}}$ network (see Fig. 12.3).

12.2.2 Single Periodic Nets

There is another cage bearing the benzene patch, even simpler than BTA_48, in which all atoms belong to a hexagon/benzene. It is BTZ_24 and can result by spanning the small fullerene C_{28}, obtained by applying the septupling S_2 map operation on the tetrahedron. BTZ_24 can be designed by opening the leapfrog transform of the tetrahedron, $Op(Le(T))$. This zigzag-opened cage can form two dimers: one "intercalated" $\mathrm{R}[6_{\mathrm{int}}](\mathrm{BTZ_24})_2$_42 (by identifying hexagons R[6] in BTZ_24) and the other "eclipsed" $\mathrm{R}[9_{\mathrm{ecl}}](\mathrm{BTZ_24})_2$_48 (by joining the R[9] windows of BTZ_24). Further, these dimers self-assemble in the hyper-hexagon $\mathrm{BTZ}_{6\mathrm{cy}}$_108 and hyper-pentagon, $\mathrm{BTZ}_{5\mathrm{cy}}$_120, respectively (Fig. 12.6).

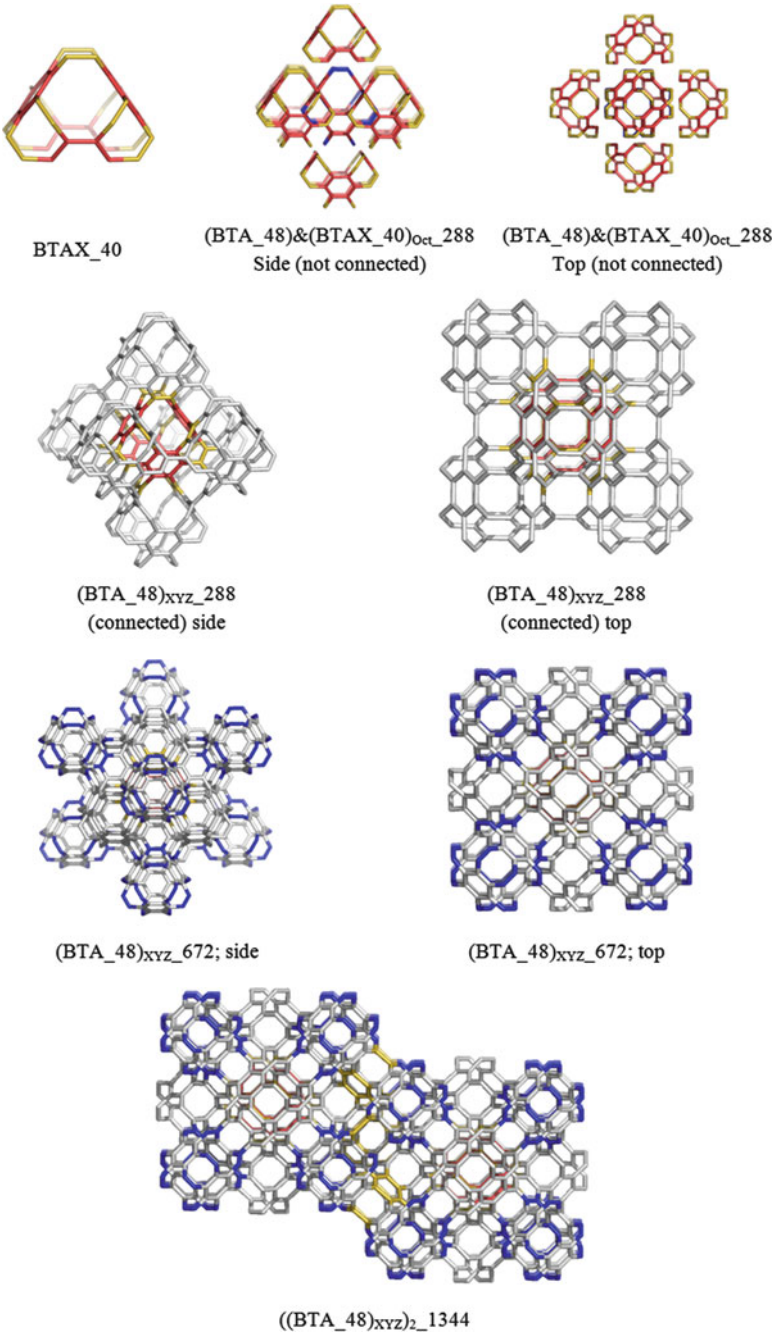

Fig. 12.5 An assay of BTA_{fcc} building

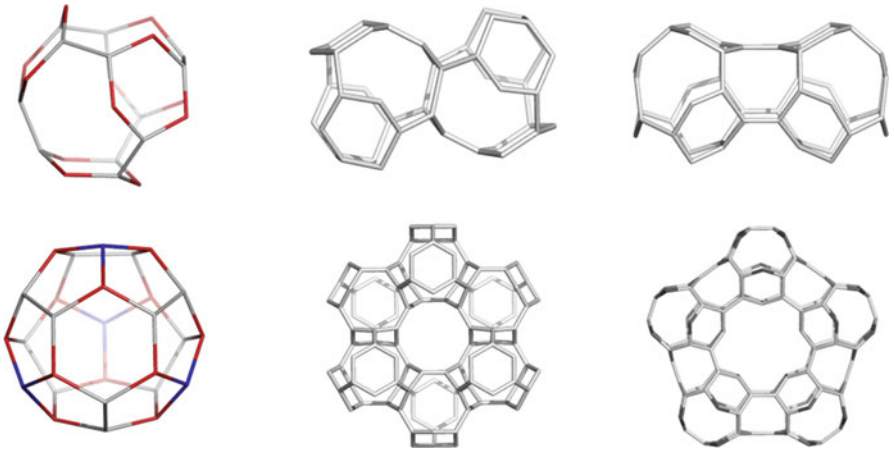

Fig. 12.6 BTZ_24, designed by spanning the cage C28 = S2(T)_28, by deleting the four blue points located at the center of pentagon triples (*left*); the intercalated dimer R[6int](BTZ_24)2_42 and the hyper-hexagon BTZ6cy_108 (*middle*); R[9_{ecl}](BTZ_24)2_48 and the hyper-pentagon BTZ5cy_120 (*right*)

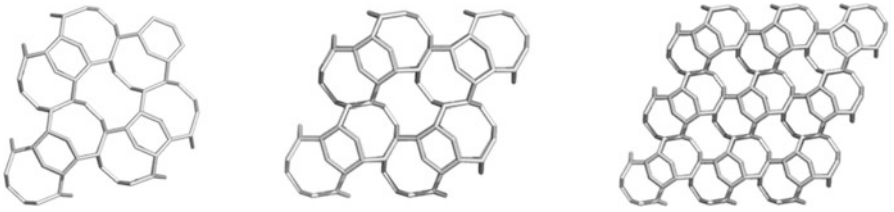

Fig. 12.7 BTZ_24 triply periodic network. Adamantane-like (BTZ_24)ada_168 (*left*); diamantane-like (BTZ_24)dia_228 (*middle*); and the translational net 6.92D, in triclinic appearance, (BTZ_24)_333_774 (*right*)

The hyper-hexagon BTZ_{6cy}_108 provides a decoration (by BTZ_24) of the classical diamond D_6 (a 4-connected net of the group *Fd*-3*m*), with the net symbol (6^6). This hyper-diamond, symbolized 6.9^2D, shows the basic adamantane- and diamantane-decorated substructures (Fig. 12.7). The crystallographic specification of this 3-connected uninodal net is *uta*; 3/6/c-3/sqc9270; group *Fd*-3*m*; and point symbol for net {6.9^2}.

In the following, we focus on the hyper-pentagons of both of BTZ_24 and BTA_48 units (BTZ_{5cy}_120 – Fig. 12.6 and BTA_{5cy}_210 – Fig. 12.2, respectively) that can provide structures of fivefold symmetry, eventually called multi-tori.

Multi-tori are complex structures consisting of more than one single torus (Diudea 2010a; Diudea and Nagy 2007). They include negatively curved substructures (Mackay and Terrones 1991; Hyde and Ramsden 2000), termed schwarzites,

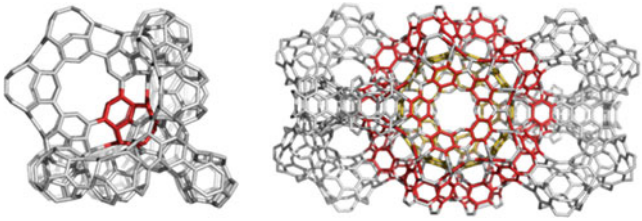

Fig. 12.8 BTZ_{17}_408 (*left*) and BTA_{34}_1332 (*right*)

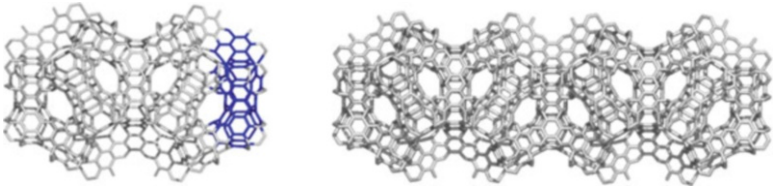

Fig. 12.9 *Top row*: multi-torus BTA20_780 (*top*, *left*) and its core, BDoA_180 (*top*, *right*). *Bottom row*: the repeating unit BTA20_2_1350 (*bottom*, *left*) and a rodlike BTA20_4_2490 (*bottom*, *right*)

in the honor of H. A. Schwarz (1865, 1890), who firstly investigated the differential geometry of this kind of surfaces. Multi-tori probably result by self-assembly of some repeating units/monomers, formed by spanning of cages/fullerenes and can appear in spongy carbon and in natural zeolites, as well. Multi-tori can grow providing either spherical-shaped or linearly periodic structures, of various complexities (Diudea and Petitjean 2008). The high porosity of these materials found applications in catalysis, in gas and energy storage, in gas and liquid purification, as thermal insulators, or in electrochemistry.

Multi-tori can be designed by appropriate map operations (Diudea 2004, 2005, 2010a; Diudea et al. 2006), as implemented in our original software CVNET (Stefu and Diudea 2005) and Nano Studio (Nagy and Diudea 2009).

The hyper-rings BTX_{5cy}; X = A; Z can self-assemble to build the multi-torus BTX_{17} (Fig. 12.8, left), the reduced graph of which is C_{17}, the structure proposed by Diudea (2010b; Diudea et al. 2011; Diudea and Nagy 2012) as the seed for the diamond D_5. A dimer of BTX_{17}, named BTX_{34} (Fig. 12.8, right), corresponding to C_{34}, the repeating unit (Blasé et al. 2010) in the structure of D_5, can be also designed. Thus, these benzene-patched units are expected to form 3D networks similar to that of D_5. The spherical multi-tori BTX_{20} (see Figs. 12.8 and 12.9, top, left and also the middle part of BTA_{34}, Fig. 12.8, right) are structures of genus $g = 21$, with cores also well defined by map operations: core(BTA_{20}) = BDoA_180 = ($-f_5(Le_{2,2}(Do))$) (Fig. 12.9); core (BTZ_{20}) = ($-d_5(S_2(Ico))$) = BDoZ_120 (Fig. 12.10). In the above, ($-f_5$) means deletion of all pentagonal faces in the transformed by leapfrog (2,2) $Le_{2,2}$ of the dodecahedron Do, while ($-d_5$) is deletion of vertices of degree $d = 5$, in the transform of icosahedron = Ico by the septupling S_2 operation. Also,

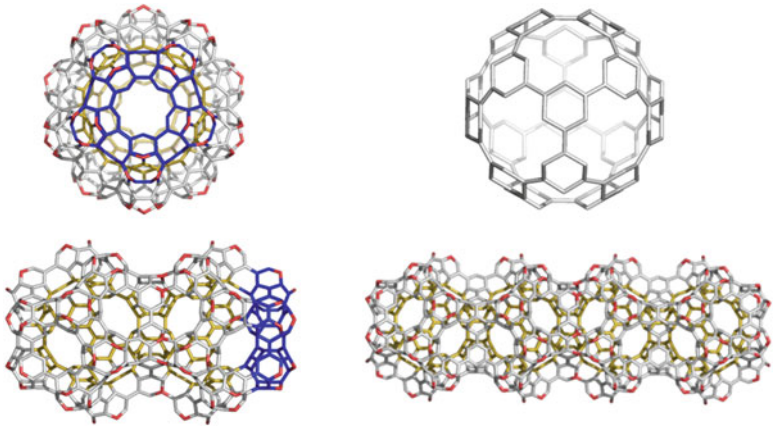

Fig. 12.10 *Top*: multi-torus BTZ20_480 (*left*) and its core BDoZ_120 (*right*). *Bottom*: the repeating unit BTZ20_2_840 (*left*) and a rodlike BTZ20_4_1560 (*right*)

$(-d_5(S_2(\text{Ico}))) = Op(Le(\text{Ico}))$. Recall, g is the genus of the surface on which the graph of a structure is embedded and accounts for the number of simple tori consisting that graph (Harary 1969).

The units BTX_{20} can form linear arrays BTX_{20}_k, of which repeating units consist of two units sharing one pentagonal hyper-face, rotated to each other by pi/5 as in the "dimer" BTX_{20}_2 (Figs. 12.9 and 12.10, bottom, left). Next, the structure can evolve, with one-dimensional periodicity, as shown in BTX_{20}_4 (Figs. 12.9 and 12.10, bottom, right). Twelve units of BTX_{20} can self-arrange in spherical (icosahedral) structure (e.g., BTZ_{130Sph}_3120, not seen here), of which core is just the unit BTX_{20}.

The crystallographic description of the two rodlike 1-periodic (new) nets is as follows:

1. BTA_{20}_k: 27 nodal, 3-c/(also 2-c); group $P21/m$; point symbol for net: $\{6.8^2\}11\{6^2.8\}26\{6^3\}14$
2. BTZ_{20}_k: 20 nodal, 3-c/(also 2-c); group $Pmc21$; point symbol for net: $\{5.6.8\}2\{5.8^2\}3\{6.8^2\}6$

For the crystallographic data, the authors are highly indebted to Professor Davide Proserpio, University of Milan, Italy.

12.3 Computational Details

The structures, as finite hydrogen-ended ones, were optimized at the Hartree-Fock HF (HF/6-31G**) level of theory. The calculations were performed in gas phase by Gaussian 09 (2009). The single-point energies of the optimized structures are

tabulated. Strain energy, according to POAV Haddon's theory (1990, 2001), and HOMA index (Krygowski and Ciesielski 1995; Krygowski and Cyranski 1996) were computed by the JSChem program (Nagy and Diudea 2004). Operations on maps were made by CVNET program (Stefu and Diudea 2005) while the network building and Omega polynomial were performed by Nano Studio software package (Nagy and Diudea 2009).

12.4 Energetics of Polybenzenes

Stability evaluation was performed (Szefler and Diudea 2012a, b; Szefler et al. 2012) on the finite hydrogen-ended structures. As a reference, we considered C_{60}, the most used reference structure in nanoscience. Table 12.1 lists the total energy per carbon atom, E_{tot}/atom, HOMO-LUMO HL gap, strain energy according to POAV theory, and HOMA index for the benzene patch R[6].

Among the considered structures, the most stable appears to be BTA_48, with the tetrahedral embedding of benzene patch (Fig. 12.1, Table 12.1, entry 1), followed by BCA_96 (Table 12.1, entry 3). The last structure makes a co-net with BCZ_72 (Table 12.1, entry 4) which is the least stable structure herein discussed. The BCZ_48 structure (Table 12.1, entry 2) shows the highest value of HOMA geometry-based index of aromaticity; even the benzene patch is less planar in comparison to the same patch in BTA_48, and the structure is most strained among all ones in Table 12.1. This put a question mark on the HOMA index, as the C-C bond length is not the only parameter reflecting the pi-electron conjugation. Looking at the data in Table 12.1, the reference fullerene C_{60} appears the least stable among all the considered structures. For BTA_48, and BCZ_48 and their dimers, the simulated vibrational spectra (Szefler and Diudea 2012a; Szefler et al. 2012) are given in Appendix A.

Comparison of BTA_{fcc} network with the diamonds D_6 and D_5 (Diudea 2010a, b, c, d; Diudea et al. 2011; Diudea and Nagy 2012) was made (see Table 12.2) because of their face-centered cubic lattice, all of them belonging to the space group *Fd*-3*m*.

Table 12.1 Total energy E_{tot} per atom (kcal/mol) and HOMO-LUMO HL gap, at Hartree-Fock HF level of theory, strain according to POAV theory and HOMA index in benzene-based structures vs. C_{60} taken as the reference structure

	Structure	E_{tot} (au)	E_{tot}/atom (au)	HL gap (eV)	Strain/C (kcal/mol)	HOMA *R*[6]
1	BTA_48	−1,831.484	−38.156	11.285	0.083	0.951
2	BCZ_48	−1,831.097	−38.148	8.134	3.395	0.989
3	BCA_96	−3,662.991	−38.156	10.253	0.124	0.939
4	BCZ_72	−2,740.025	−38.056	7.558	2.749	0.812
5	C_{60}	−2,271.830	−37.864	7.418	8.256	0.493

Table 12.2 Total energy E_{tot} per atom (kcal/mol) and HOMO-LUMO HL gap, at Hartree-Fock HF level of theory, in fcc networks

	Structure	No C atoms	E_{tot} (au)	E_{tot}/C (au)	HL gap (eV)
1	BTA_{fcc}_222_288	288	−1,0961.473	−38.061	10.343
2	D_6_444_248	248	−9,478.180	−38.218	12.898
3	D_5_222_226	226	−8,621.954	−38.150	13.333
4	C_{60}	60	−2,271.830	−37.864	7.418

Reproduced with permission from Szefler and Diudea (2012). Copyright (2012), Slovenian Chemical Society

Table 12.3 Total energy E_{tot} and HOMO-LUMO HL gap, at Hartree-Fock HF level of theory, Strain by POAV and HOMA index in benzene-patched oligomers and C_{60} taken as the reference structure

	Structure	No units	E_{tot} (au)	E_{tot}/C atom (au)	HL gap (eV)	Strain/C atom (kcal/mol)	HOMA R[6]
1	BTA_48	1	−1,831.484	−38.156	11.285	0.083	0.951
2	$(BTA_48)_{2dendr}$_84	2	−3,201.679	−38.115	10.895	0.061	0.975
3	$(BTA_48)_{3dendr}$_120	3	−4,571.874	−38.099	10.771	0.056	0.978
4	$(BTA_48)_{4dendr}$_156	4	−5,942.070	−38.090	10.684	0.054	0.978
5	$(BTA_48)_{5dendr}$_192	5	−7,312.265	−38.085	10.594	0.055	0.988
6	$(BTA_48)_{2fcc}$_88	2	−3,355.431	−38.130	10.970	0.074	0.972
8	$(BCA_96)_2$_184	2	−7,013.828	−38.119	9.805	0.180	0.936
9	$(BTZ_24)_2$_48	2	−1,826.768	−38.058	6.194	6.487	−1.350
10	$(BTZ_24)_2$_42	2	−1,599.67	−38.087	6.190	7.650	−1.214
11	BTZ_24	1	−915.092	−38.129	8.221	7.614	0.969

Note the diamond D_5 is also known as the C_{34fcc} net (Blasé et al. 2010). One can see that the stability (E_{tot}/C and HOMO-LUMO HL gap) of polybenzene (Table 12.2, entry 1) immediately follows to that of the diamond networks (Table 12.2, entries 2 and 3) and is above to that of C_{60} fullerene, even the fullerene cannot be directly compared to the hydrogenated above structures (Table 12.2, entry 4), as was also noticed by O'Keeffe et al. (1992).

The stability of dendrimers of BTA_48 (Table 12.3, entries 2–5) decreases monotonically with increasing the number of atoms, as suggested by the total energy per carbon atom and HOMO-LUMO gap. The strain of these dendrimers decreases with the increase in the number of their carbon atoms. This is reflected in the values of HOMA: the benzene patch seems to be few distorted from the ideal planar geometry (thus, showing the unity value), with the maximum at the dendrimer with a complete first generation (Table 12.3, entry 5, last column).

The fcc-dimer $(BTA_48)_{2fcc}$_88 (Table 12.3, entry 6) appears more stable than the dendritic dimer $(BTA_48)_{2dendr}$_84 (Table 12.3, entry 2); however, after the second generation (see Fig. 12.3, bottom, right), the dendritic structure completely superimposes over the BTA_{fcc}-net, so that it is no matter which way the building process has followed. A lower stability shows the dimer $(BCA_96)_2$_184, Table 12.3,

Table 12.4 Energies in polybenzene multi-tori substructures

Structure	Level of theory	E_{tot} (au)	E_{tot}/C atom (au)	HL gap (eV)
BTA_48	B3LYP	−1,843.743	−38.411	5.052
BTA_{2ecl}_90	6-311+G(d,p)	−3,450.946	−38.344	4.200
BTA_{5cy}_210	HF; 6-31G(d,p)	−7,986.806	−38.032	9.545
BTZ_24	B3LYP	−921.359	−38.390	2.753
BTZ_{2ecl}_48	6-311+G (d,p)	−1,839.181	−38.316	1.124
BTZ_{5cy}_120	HF; 6-31G(d,p)	−4,558.826	−37.990	7.178
C_{60}	B3LYP; 6-311+G(d,p)	−2,286.610	−38.110	2.724

entry 8. The unit BTZ_24 and its dimers are presented at the bottom of Table 12.3 (entries 9–11). One can see, they have less favorable energetics, probably due of their strain (comparable, however, with that of C_{60}). The bond length (much larger than in the reference benzene) in the distorted hexagon is counted as "antiaromatic" by the HOMA index. Table 12.4 lists the energetics of some polybenzene multi-tori substructures. The stability of hyper-pentagons BTX_{5cy} (evaluated at HF level of theory) is good enough, even not directly comparable with the data for the others structures in Table 12.4, obtained by dft calculations; these hyper-rings represent the first step in building multi-tori, fascinating spongy structures.

12.5 Omega Polynomial in Polybenzenes

In a connected graph $G(V,E)$, with the vertex set $V(G)$ and edge set $E(G)$, two edges $e = uv$ and $f = xy$ of G are called *codistant e co f* if they obey the relation

$$d(v,x) = d(v,y) + 1 = d(u,x) + 1 = d(u,y)$$

which is reflexive, that is, *e co e* holds for any edge e of G, and symmetric, if *e co f* then *f co e*. In general, relation *co* is not transitive; if "*co*" is also transitive, thus it is an equivalence relation, then G is called a *co-graph* and the set of edges $C(e) := \{f \in E(G);\ f\ co\ e\}$ is called an *orthogonal cut oc* of G, $E(G)$ being the union of disjoint orthogonal cuts: $E(G) = C_1 \cup C_2 \cup \cdots \cup C_k,\ C_i \cap C_j = \emptyset,\ i \neq j$. Klavžar (2008) has shown that relation *co* is a theta Djoković-Winkler relation (Djoković 1973; Winkler 1984).

We say that edges e and f of a plane graph G are in relation *opposite, e op f*, if they are opposite edges of an inner face of G. Note that the relation *co* is defined in the whole graph while *op* is defined only in faces. Using the relation *op*, we can partition the edge set of G into *opposite* edge *strips, ops*. An *ops* is a quasi-orthogonal cut qoc, since ops is not transitive.

Let G be a connected graph and $S_1, S_2, \ldots, S_k$ be the *ops* strips of G. Then the *ops* strips form a partition of $E(G)$. The length of ops is taken as maximum.

It depends on the size of the maximum fold face/ring F_{max}/R_{max} considered, so that any result on Omega polynomial will have this specification.

Denote by $m(G,s)$ the number of ops of length s and define the Omega polynomial as (Diudea 2006, 2010a, c; Diudea and Klavžar 2010)

$$\Omega(G,x) = \sum_s m(G,s) \cdot x^s$$

Its first derivative (in $x = 1$) equals the number of edges in the graph:

$$\Omega'(G,1) = \sum_s m(G,s) \cdot s = e = |E(G)|$$

On Omega polynomial, the Cluj-Ilmenau index,[23] $CI = CI(G)$, was defined:

$$CI(G) = \{[\Omega'(G,1)]^2 - [\Omega'(G,1) + \Omega''(G,1)]\}$$

12.5.1 Omega Polynomial in 3-Periodic Polybenzenes

Formulas to calculate Omega polynomial and CI index in three triply periodic infinite networks, designed on the ground of BTA_48, BCZ_48 and BCA_96 units (see Fig. 12.1), are presented in Table 12.5. Formulas were derived (Szefler and Diudea 2012a) from the numerical data calculated on cuboids of (k,k,k) dimensions by the Nano Studio software (Nagy and Diudea 2009). Omega polynomial was calculated at $R_{max}(8)$ and $R_{max}(12)$, respectively; examples are given in view of an easy verification of the general formulas. Also, formulas for the number of atoms, edges, and rings ($R(6)$, $R(8)$, and $R(12)$) are included in this table. Note that Omega polynomial description is an alternative to the crystallographic description and can be useful in understanding the topology of these networks.

12.5.2 Omega Polynomial in 1-Periodic Polybenzenes

Formulas to calculate Omega polynomial and CI index in the two infinite 1-periodic networks $BTA_{20}k$ and $BTZ_{20}k$, designed on the ground of BTA_48 and BTZ_24 units (Figs. 12.9 and 12.10), are presented in Table 12.6. Formulas were derived (Diudea and Szefler 2012) from the numerical data calculated on rods consisting of k units BTX_{20}. Omega polynomial was calculated at $R_{max} = R(8)$; examples are given in view of an easy verification of the general formulas. Formulas for the number of atoms, edges, and rings (R_6, R_8, and R_{15}, the last one being the simple ring of the hyper-ring BTX_{5Cy}) are included in Table 12.6.

Table 12.5 Omega polynomial and net parameters in polybenzene networks

Net	Omega polynomial
BTA_48	$R_{\max}(8)$
	$\Omega(\text{BTA\_48}) = 18k^2x^2 + 6k(k-1)x^{2k} + 6kx^{4k} + \sum_{s=1}^{k-1} 12kx^{4s}$
	$\Omega'(1) = 12k^2(3k+2) = \lvert E(G)\rvert$ = edges
	$\text{CI}(G) = 8k^2(162k^4 + 216k^3 + 61k^2 + 3k - 13)$
	atoms $= 24k^2(k+1) = \lvert V(G)\rvert$
	$R(6) = 4k^3$; $R(8) = 6k^3 - 3k^2 + 3k$
	$R_{\max}(12)$
	$\Omega(\text{BTA\_48}) = 6x^{2k(2k+1)} + 3x^{4k^2(k+1)} + \sum_{s=1}^{k-1} 12x^{2s(2k+1)}$
	$\Omega'(1) = 12k^2(3k+2) = \lvert E(G)\rvert$ = edges
	$\text{CI}(G) = 8k(6k^2 + 2k - 1)(26k^3 + 24k^2 + 6k + 1)$
	$R(12) = 4k^3$
Examples	$R_{\max}(8)$
	$k = 5$; $\Omega(G) = 450x^2 + 60x^4 + 60x^8 + 120x^{10} + 60x^{12} + 60x^{16} + 30x^{20}$;
	CI = 25,955,400; atoms = 3,600; edges = 5,100; $R(6) = 500$; $R(8) = 690$
	$k = 6$; $\Omega(G) = 648x^2 + 72x^4 + 72x^8 + 252x^{12} + 72x^{16} + 72x^{20} + 36x^{24}$;
	CI = 74,536,992; atoms = 6,048; edges = 8,640; $R(6) = 864$; $R(8) = 1,206$
	$R_{\max}(12)$
	$k = 5$; $12x^{22} + 12x^{44} + 12x^{66} + 12x^{88} + 6x^{110} + 3x^{600}$;
	CI = 24,683,160; $R(12) = 500$.
	$k = 6$; $12x^{26} + 12x^{52} + 12x^{78} + 12x^{104} + 12x^{130} + 6x^{156} + 3x^{1008}$;
	CI = 71,009,232; $R(12) = 864$.
BCZ_48	$R_{\max}(8)$
	$\Omega(\text{BCZ\_48}) = 12kx + 12k(k+1)x^2 + 3k(k-1)(2k-1)x^4 + \sum_{s=1}^{k-1} 24kx^{(2+4s)}$
	$\Omega'(1) = 12k^2(6k-1) = \lvert E(G)\rvert$ = edges
	$\text{CI}(G) = 4k(1,296k^5 - 432k^4 + 4k^3 - 24k^2 + 32k - 3)$
	atoms $= 48k^3 = \lvert V(G)\rvert$
	$R(6) = (2k)^3$; $R(8) = 12k^2(k-1)$
	$R_{\max}(12)$
	$\Omega(\text{BCZ\_48}) = (6k-3)x^{(2k)^2} + 6x^{(2k)^3}$
	$\Omega'(1) = 12k^2(6k-1) = \lvert E(G)\rvert$ = edges
	$\text{CI}(G) = 96k^4(50k^2 - 19k + 2)$
	$R(12) = 6k(2k^2 - 2k + 1)$
Examples	$R_{\max}(8)$
	$k = 5$; $60x + 360x^2 + 540x^4 + 120x^6 + 120x^{10} + 120x^{14} + 120x^{18}$
	CI = 75,601,140; atoms = 6,000; edges = 8,700; $R(6) = 1,000$; $R(8) = 1,200$.
	$k = 6$; $72x + 504x^2 + 990x^4 + 144x^6 + 144x^{10} + 144x^{14} + 144x^{18} + 144x^{22}$
	CI = 228,432,312; atoms = 10,368; edges = 15,120; $R(6) = 1,728$; $R(8) = 2,160$.
	$R_{\max}(12)$
	$k = 5$; $27x^{100} + 6x^{1000}$; CI = 69,420,000; $R(12) = 1,230$.
	$k = 6$; $33x^{144} + 6x^{1728}$; CI = 210,014,208; $R(12) = 2,196$.

(continued)

Table 12.5 (continued)

Net	Omega polynomial
BCA_96	$R_{\max}(8)$
	$\Omega(\text{BCA\_96}) = 36kx^2 + 12k(k-1)x^3 + 3(k-1)(k^2-k+8)x^4 + 24(k-1)x^8 + 12k^2x^{4k} + \sum_{s=0}^{k-3} 24(k-s-2)(x^{10+6s} + x^{14+6s})$
	$\Omega'(1) = 12k^2(9k+1) = \lvert E(G)\rvert$ = edges
	$\text{CI}(G) = 12k(972k^5 + 216k^4 - 16k^3 - 4k^2 + 3k + 1)$
	atoms $= 24k^2(3k+1) = \lvert V(G)\rvert$
	$R(6) = 4k(5k-3)$; $R(8) = 12k^3$; $R(12) = 6k(k-1)^2$
Examples	$R_{\max}(8)$
	$k = 5$; $\Omega(G) = 180x^2 + 240x^3 + 336x^4 + 96x^8 + 72x^{10} + 72x^{14} + 48x^{16} + 348x^{20} + 24x^{22} + 24x^{26}$
	CI $= 190,224,960$; atoms=9, 600; edges=13, 800; $R(6)$=2, 200; $R(8) = 1,500$.
	$k = 6$; $\Omega(G) = 216x^2 + 360x^3 + 570x^4 + 120x^8 + 96x^{10} + 96x^{14} + 72x^{16} + 72x^{20} + 48x^{22} + 432x^{24} + 48x^{26} + 24x^{28} + 24x^{32}$
	CI $= 564,093,144$; atoms $= 16,416$; edges $= 23,760$; $R(6) = 3,888$; $R(8) = 2,592$

Reproduced with permission from Szefler and Diudea (2012). Copyright (2012), Slovenian Chemical Society

Table 12.6 Formulas for Omega polynomial and net parameters in linear periodic BTX_{20}_k network

BTA_{20}_k	$R_{\max}(8)$; $\Omega(\text{BTA}_{20}\_k\_R_8) = 10(k+2)x^3 + 5(k-1)x^4 + (11k+1)x^5 + 20(k+3)x^8 + 10(k-1)x^{10} + 15(k-1)x^{12} + (11k+1)x^{20} + 10x^{2(3k+1)}$
	$\Omega'(1) = 825k + 285 = \lvert E(G)\rvert$ = edges;
	$\text{CI}(G) = 15(45,351k^2 + 30,715k + 5,332)$;
	atoms $= 10(57k+21) = \lvert V(G)\rvert$;
	$R_6 = 5(27k+7)$; $R_8 = 30(3k+1)$; $R_{15} = 11k+1$;
	$u_{48} = 20k - 5(k-1) = 5(3k+1) = R_8/6$;
	$g = 1 + u_{48}$
Examples	$k = 5$;
	CI = 19,390,230; atoms = 3,060; edges = 4,410; $R_6 = 710$; $R_8 = 480$; $R_{15} = 56$; $u_{48} = 80$; $g = 81$.
	$k = 6$;
	CI = 27,333,870; atoms = 3,630; edges = 5,235; $R_6 = 845$; $R_8 = 570$; $R_{15} = 67$; $u_{48} = 95$; $g = 96$.
BTZ_{20}_k	$R_{\max}(8)$
	$\Omega(\text{BTZ}_{20}\_k\_R_8) = 10(k+2)x^2 + 30kx^3 + (11k+1)x^5 + 10(k+5)x^6 + 10(k-1)x^8 + 10(k-1)x^{10} + 6kx^{20}$
	$\Omega'(1) = 525k + 165 = \lvert E(G)\rvert$ = edges
	$\text{CI}(G) = 5(55,125k^2 + 33,653k + 5,392)$

(continued)

Table 12.6 (continued)

	atoms $= 120(3k + 1) = \|V(G)\| = 24u_{24} = 6R_6$ $R_6 = 20(3k + 1) = \|V(G)\|/6$; $R_8 = 15(5k + 1)$; $R_{15} = 11k + 1$ $u_{24} = 20k - 5(k - 1) = 5(3k + 1) = R_6/4$; $g = 1 + u_{24}$
Examples	$k = 5$; $70x^2 + 150x^3 + 56x^5 + 100x^6 + 40x^8 + 40x^{10} + 30x^{20}$ CI = 7,758,910; atoms = 1,920; edges = 2,790; $R_6 = 320$; $R_8 = 390$; $R_{15} = 56$; $u_{24} = 80$; $g = 81$. $k = 6$; $80x^2 + 180x^3 + 67x^5 + 110x^6 + 50x^8 + 50x^{10} + 36x^{20}$ CI = 10,959,050; atoms = 2,280; edges = 3,315; $R_6 = 380$; $R_8 = 465$; $R_{15} = 67$; $u_{24} = 95$; $g = 96$.

Reprinted with permission from Diudea and Szefler (2012). Copyright (2012), Academic Center for Education, Culture and Research at Tarbiat Modares University

12.6 Conclusions

O'Keeffe et al. (1992) have described the polybenzene 6.8^2D as a uninodal embedding of a 6.8^2 net in the infinite periodic minimal D-surface and predicted to have a substantially lower energy per atom in comparison to C_{60}, the reference structure in nanoscience. The authors also described the lattice 6.8^2P, an embedding of the 6.8^2 net in the periodic minimal P-surface. Two other networks: a binodal $(6.8^2)(6^2.8)$ P and a uninodal 6.9^2D ones were added here, being related to the above nets both by the presence of benzene patch and construction procedure. We called "polybenzenes" all other structures bearing the benzene ring as a covering patch. Their construction was done by the aid of topological map operations.

Polybenzene "armchair"-ended unit BTA_48 can form three different dimers: (1) $R[8_{fcc}](BTA\_48)_{2fcc}\_88$ to provide next the diamond-like net $6.8^2D = BTA_{fcc}$, (2) $R[12_{int}](BTA\_48)_2\_84$ that gives next dendrimers, and (3) $R[12_{ecl}](BTA\_48)_2\_90$ which can form further multi-tori. Polybenzene "zigzag"-ended unit BTZ_24 forms two dimers: $(BTZ\_24)_2\_48$, suitable to build multi-tori, and $(BTZ\_24)_2\_42$ that provides the translational network 6.9^2D.

The energetics of these units and some small substructures of polybenzenes have been evaluated at the Hartree-Fock level of theory. The results confirmed the previous evaluation of polybenzene stability and support these structures for laboratory preparation. In the hope of their experimental synthesis, vibrational spectra of the most important monomers and dimers have been simulated.

A building assay for the $BTA_{fcc}/6.8^2D$ net was provided. A graph-theoretical description, in terms of Omega polynomial, of the infinite polybenzene networks was also presented.

Appendix A

1. Vibrational spectra of BTA_48 and BCZ_48 units

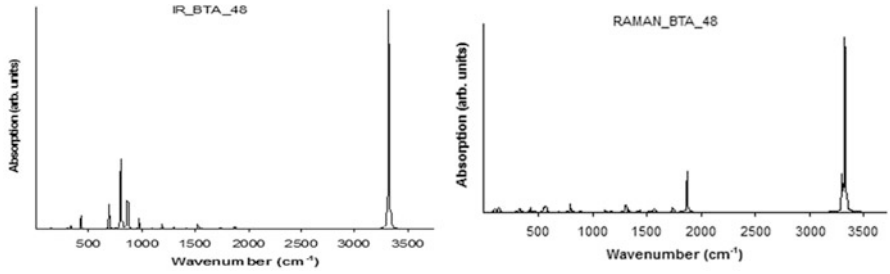

Fig. A.1 IR and Raman spectra of BTA_48 unit

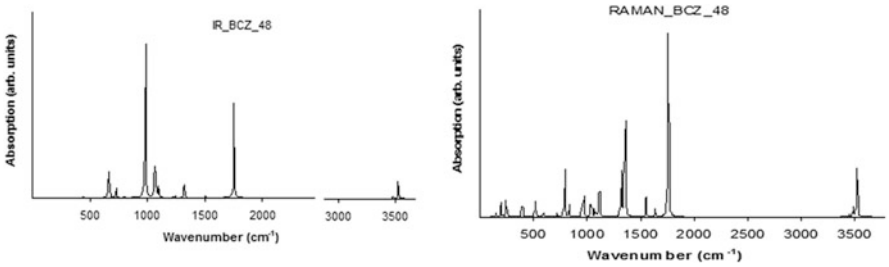

Fig. A.2 IR and Raman spectra of BCZ_48 unit

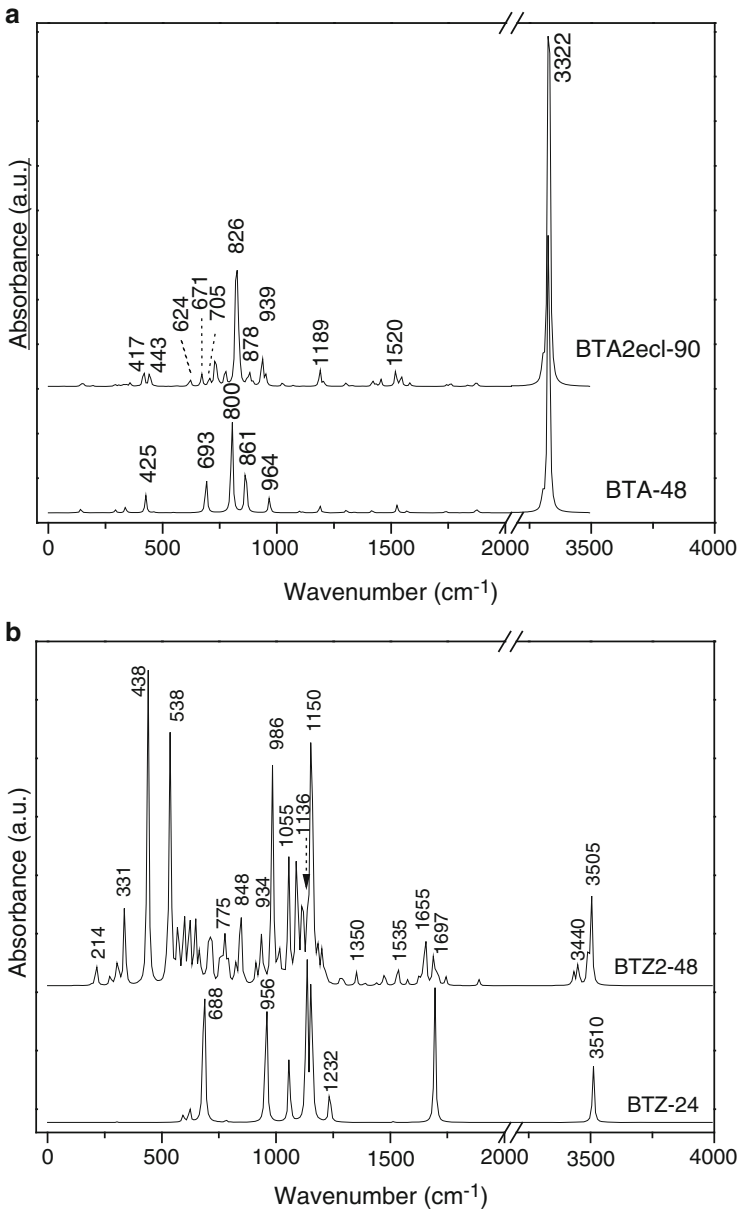

Fig. A.3 IR spectra of polybenzene monomers and "eclipsed" ecl-dimers: (**a**) BTA series (*top*) and (**b**) BTZ series (*bottom*)

2. Vibrational spectra of dimers

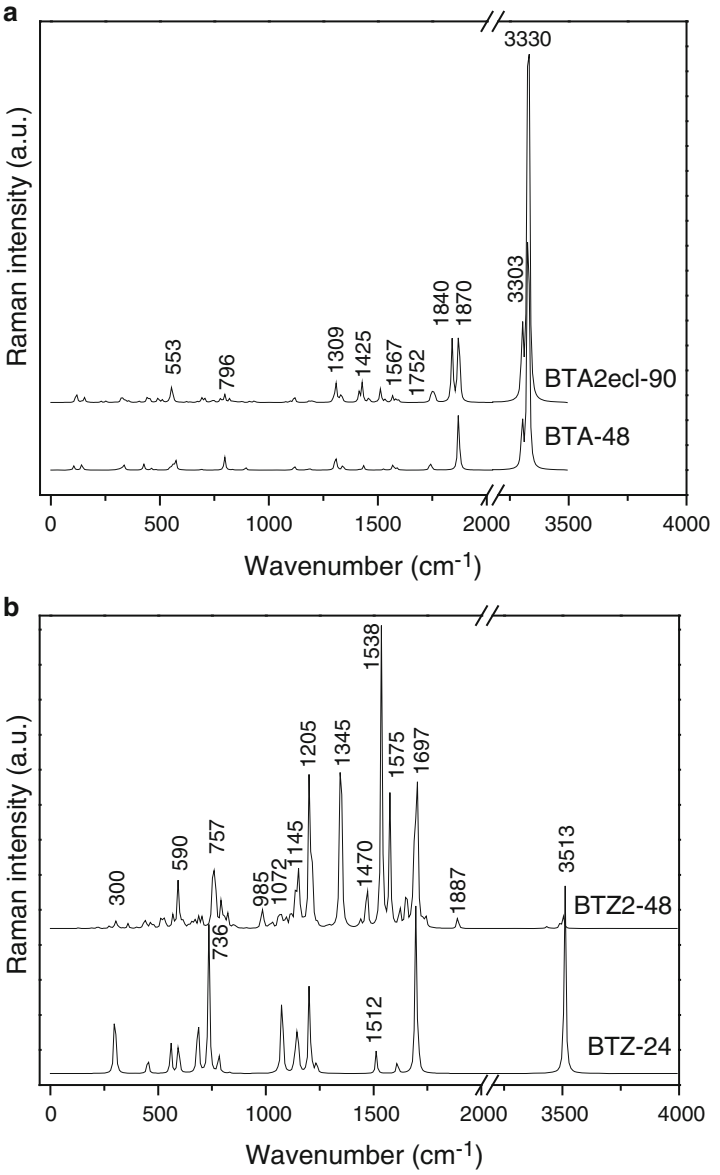

Fig. A.4 Raman spectra of polybenzene monomers and "eclipsed" ecl-dimers: (**a**) BTA series (*top*) and (**b**) BTZ series (*bottom*)

References

Amsharov KY, Jansen M (2008) A C_{78} fullerene precursor: toward the direct synthesis of higher fullerenes. J Org Chem 73:2931–2934

Baerlocher C, Meier WH, Olson DH (2007) Atlas of zeolite framework types, 6th edn. Elsevier, Amsterdam

Barborini E, Piseri P, Milani P, Benedek G, Ducati C, Robertson J (2002) Negatively curved spongy carbon. Appl Phys Lett 81:3359–3361

Benedek G, Vahedi-Tafreshi H, Barborini E, Piseri P, Milani P, Ducati C, Robertson J (2003) The structure of negatively curved spongy carbon. Diam Relat Mater 12:768–773

Blase X, Benedek G, Bernasconi M (2010) In: Colombo L, Fasolino A (eds) Computer-based modeling of novel carbon systems and their properties beyond nanotubes, vol 6. Springer, New York, pp 171–206

Diudea MV (2004) Covering forms in nanostructures. Forma (Tokyo) 19(3):131–163

Diudea MV (ed) (2005a) Nanostructures, novel architecture. NOVA, New York

Diudea MV (2005b) Nanoporous carbon allotropes by septupling map operations. J Chem Inf Model 45:1002–1009

Diudea MV (2006) Omega polynomial. Carpath J Math 22:43–47

Diudea MV (2010a) Nanomolecules and nanostructures – polynomials and indices, MCM10. University of Kragujevac, Kragujevac

Diudea MV (2010b) Diamond D_5, a novel allotrope of carbon. Studia Univ Babes Bolyai Chemia 55(4):11–17

Diudea MV (2010c) Counting polynomials in partial cubes. In: Gutman I, Furtula B (eds) New molecular structure descriptors – theory and applications I, MCM8. University of Kragujevac, Kragujevac, pp 191–215

Diudea MV (2010d) Counting polynomials and related indices by edge cutting procedures. MATCH Commun Math Comput Chem 64:569–590; also in: I Gutman, B Furtula (eds) New molecular structure descriptors – theory and applications II, MCM9. University of Kragujevac, Kragujevac, pp 57–78

Diudea MV, Klavžar S (2010) Omega polynomial revisited. Acta Chem Slov 57:565–570

Diudea MV, Nagy CL (2007) Periodic nanostructures. Springer, Dordrecht

Diudea MV, Nagy CL (2012) C_{20}-related structures: diamond D_5. Diam Relat Mater 23:105–108

Diudea MV, Petitjean M (2008) Symmetry in multi tori. In: Diudea MV (ed) Symmetry. Cult Sci 19(4):285–305

Diudea MV, Szefler B (2012) Omega polynomial in polybenzene multi-tori. Iran J Math Sci Inform 7:67–74

Diudea MV, Ştefu M, John PE, Graovac A (2006) Generalized operations on maps. Croat Chem Acta 79:355–362

Diudea MV, Nagy CL, Ilić A (2011) In: Putz MV (ed) Carbon bonding and structures. Springer, Dordrecht, pp 273–289

Djoković DŽ (1973) Distance preserving subgraphs of hypercubes. J Comb Theory Ser B 14:263–267

EPINET: http://epinetanueduau/about; Topos: http://www.toposssusamararu/index.html

Gaussian 09 (2009) Revision A.1, Frisch MJ, Trucks GW, Schlegel HB, Scuseria GE, Robb MA, Cheeseman JR, Scalmani G, Barone V, Mennucci B, Petersson GA, Nakatsuji H, Caricato M, Li X, Hratchian HP, Izmaylov AF, Bloino J, Zheng G, Sonnenberg JL, Hada M, Ehara M, Toyota K, Fukuda R, Hasegawa J, Ishida M, Nakajima T, Honda Y, Kitao O, Nakai H, Vreven T, Montgomery JA, Peralta JE, Ogliaro F, Bearpark M, Heyd JJ, Brothers E, Kudin KN, Staroverov VN, Kobayashi R, Normand J, Raghavachari K, Rendell A, Burant JC, Iyengar SS, Tomasi J, Cossi M, Rega N, Millam NJ, Klene M, Knox JE, Cross JB, Bakken V, Adamo C, Jaramillo J, Gomperts R, Stratmann RE, Yazyev O, Austin AJ, Cammi R, Pomelli C,

Ochterski JW, Martin RL, Morokuma K, Zakrzewski VG, Voth GA, Salvador P, Dannenberg JJ, Dapprich S, Daniels AD, Farkas Ö, Foresman JB, Ortiz JV, Cioslowski J, Fox DJ, Gaussian Inc, Wallingford

Haddon RC (1990) Measure of nonplanarity in conjugated organic molecules: which structurally characterized molecule displays the highest degree of pyramidalization? J Am Chem Soc 112:3385–3389

Haddon RC (2001) Comment on the relationship of the pyramidalization angle at a conjugated carbon atom to the σ bond angles. J Phys Chem A 105:4164–4165

Harary F (1969) Graph theory. Addison-Wesley, Reading

http://www.toposssusamararu/index.html

Hyde ST, Ramsden S (2000) Chemical frameworks and hyperbolic tilings. In: Hansen P, Fowler P, Zheng M (eds) Discrete mathematical chemistry, vol 51, DIMACS series in discrete mathematics and theoretical computer science., pp 203–224

Klavžar S (2008) Some comments on co graphs and CI index. MATCH Commun Math Comput Chem 5:217–222

Krygowski TM, Ciesielski A (1995) Aromatic character in the benzene ring present in various topological environments in benzenoid hydrocarbons. Nonequivalence of indices of aromaticity. J Chem Inf Comput Sci 35:203–210

Krygowski TM, Cyranski M (1996) Separation of the energetic and geometric contributions to the aromaticity. Part IV. A general model for the pi-electron systems. Tetrahedron 52:10255–10264

Mackay AL, Terrones H (1991) Diamond from graphite. Nature 352:762–768

Nagy CL, Diudea MV (2004) JSCHEM software program. "Babes-Bolyai" University, Cluj

Nagy CL, Diudea MV (2009) Nano studio software program. "Babes-Bolyai" University, Cluj

O'Keeffe M, Adams GB, Sankey OF (1992) Predicted new low energy forms of carbon. Phys Rev Lett 68:2325–2328

Schwarz HA (1865) Über minimalflächen. Monatsber Berlin Akad, Berlin

Schwarz HA (1890) Gesammelte Matematische Abhandlungen. Springer, Berlin

Scott LT (2004) Methods for the chemical synthesis of fullerenes. Angew Chem Int Ed 43:4994–5007

Stefu M, Diudea MV (2005) CVNET software program. "Babes-Bolyai" University, Cluj

Szefler B, Diudea MV (2012a) Polybenzene revisited. Acta Chim Slov 59:795–802

Szefler B, Diudea MV (2012b) Polybenzene multitori. Cent Eur J Chem 10:1779–1785

Szefler B, Ponta O, Diudea MV (2012) Energetics of polybenzene multi tori. J Mol Struct 1022:89–93

Valencia F, Romero AH, Hernàndez E, Terrones M, Terrones H (2003) Theoretical characterization of several models of nanoporous carbon. New J Phys 5:1231–12316

Winkler PM (1984) Isometric embedding in products of complete graphs. Discrete Appl Math 8:209–212

Chapter 13
Fullerene-Like Spheres with Faces of Negative Curvature

Michel Deza, Mathieu Dutour Sikirić, and Mikhail Shtogrin

Abstract Given $R \subset \mathbb{N}$, an (R,k)-*sphere* is a k-regular map on the sphere whose faces have gonalities $i \in R$. The most interesting/useful are (geometric) *fullerenes*, that is, $(\{5,6\},3)$-spheres. Call $\kappa_i = 1+\frac{i}{k}-\frac{i}{2}$ the *curvature* of i-gonal faces. (R,k)-spheres admitting $\kappa_i < 0$ are much harder to study. We consider the symmetries and construction for three new instances of such spheres: $(\{a,b\},k)$-spheres with $p_b \leq 3$ (they are listed), *icosahedrites* (i.e., $(\{3,4\},5)$-spheres), and, for any $c \geq 1$, *fullerene c-disks*, that is, $(\{5,6,c\},3)$-spheres with $p_c = 1$.

13.1 Introduction

Given $R \subset \mathbb{N}$, an (R,k)-*sphere* S is a k-regular map on the sphere whose faces have *gonalities* (numbers of sides) $i \in R$. Let v, e and $f = \sum_i p_i$ be the numbers of vertices, edges, and faces of S, where p_i is the number of i-gonal faces. A graph is called *m-connected* if after removing any $m-1$ vertices, it remains connected.

Clearly, k-regularity implies $kv = 2e = \sum_i i p_i$ and the *Euler formula* $2 = v - e + f$ becomes Gauss-Bonnet-like one $2 = \sum_i \kappa_i p_i$, where $\kappa_i = 1 + \frac{i}{k} - \frac{2}{2}$ is called (dualizing the definition in Higuchi (2001)) the *curvature* of the i-gonal faces.

M. Deza
Ecole Normale Superieure, 45 rue d'Ulm, 75005 Paris, France
e-mail: deza@orge.ens.fr

M. Dutour Sikirić (✉)
Department of Marine and Environmental Research, Institut Rudjer Boskovic, Bijenicka 54, 10000 Zagreb, Croatia
e-mail: Mathieu.Dutour@gmail.com

M. Shtogrin
Steklov Mathematical Institute, Demidov Yaroslavl State University, Yaroslavl, Moscow, Russia
e-mail: stogrin@mi.ras.ru

M.V. Diudea and C.L. Nagy (eds.), *Diamond and Related Nanostructures*,
Carbon Materials: Chemistry and Physics 6, DOI 10.1007/978-94-007-6371-5_13,

Let $a = \min\{i \in R\}$. Then, besides the cases $k = 2$ (a-cycle) and exotic cases $a = 1, 2$, it holds

$$\frac{2k}{k-2} > a > 2 < k < \frac{2a}{a-2},$$

that is, (a, k) should belong to the five Platonic parameter pairs $(3, 3)$, $(4, 3)$, $(3, 4)$, $(5, 3)$, or $(3, 5)$.

Call an (R, k)-sphere *standard* if $\min_{i \in R} \kappa_i = 0$, that is, $b = \frac{2k}{k-2}$, where b denotes $\max\{i \in R\}$. Such spheres have $(b, k) = (3, 6)$, $(4, 4)$, $(6, 3)$, that is, the three Euclidean parameter pairs. Exclusion of faces of negative curvature simplifies enumeration, while the number p_b of faces of curvature zero is not being restricted; there is an infinity of such (R, k)-spheres.

An $(\{a, b\}, k)$-*sphere* is an (R, k)-sphere with $R = \{a, b\}$, $1 \leq a, b$. Clearly, all possible $(a, b; k)$ for the standard $(\{a, b\}, k)$-spheres are

$$(5, 6; 3), (4, 6; 3), (3, 6; 3), (2, 6; 3), (3, 4; 4), (2, 4; 4), (2, 3; 6), (1, 3; 6).$$

Those eight families can be seen as spheric analogs of the regular plane partitions $\{6, 3\}$, $\{4, 4\}$, $\{3, 6\}$ with $p_a = \frac{2b}{b-a}$ "defects" κ_a added to get the total curvature 2 of the sphere. $(\{5, 6\}, 3)$-spheres are (geometric) *fullerenes*, important in Chemistry, while $(\{a, b\}, 4)$-spheres are minimal projections of *alternating links*, whose components are their *central circuits* (those going only ahead) and crossings are the vertices.

We considered above eight families in Deza and Dutour (2005), Deza et al. (2002, 2003), Deza and Shtogrin (2003), Dutour Sikirić and Deza (2011), Deza and Dutour Sikirić (2011), and the book Deza and Dutour Sikirić (2008), where i-faces with $\kappa_i < 0$ are allowed, mainly in Chaps. 15, 16, 17, 18, and 19. Here we consider three new natural instances of $(\{a, b, c\}, k)$-spheres, each allowing faces of negative curvature. The first section describes such $(\{a, b\}, k)$-spheres with $p_b \leq 3$. The second section concerns the *icosahedrites*, that is, $(\{3, 4\}, 5)$-spheres, in which 4-gonal faces have $\kappa_4 = -\frac{1}{5}$. The third section treats $(\{a, b, c\}, k)$-spheres with $p_c = 1$, in which unique c-gonal face can be of negative curvature, especially *fullerene c-disks*, that is, $(\{5, 6, c\}, 3)$-spheres with $p_c = 1$.

Note that all (R, k)-spheres with $1, 2 \notin R$ and $\kappa_i > 0$ for all $i \in R$ have $k = 4, 5$ or 3 and, respectively, $\kappa_i = \frac{1}{4}, \frac{1}{10}$ or $\kappa_i \in \left\{\frac{1}{6}, \frac{1}{3}, \frac{1}{2}\right\}$. So, they are only octahedron, icosahedron, and 11 $(\{3, 4, 5\}, 3)$-spheres: 8 dual deltahedra, Cube, and its truncations on one or two opposite vertices (*Dürer Octahedron*).

The work of this chapter used the program `plangraph` by the second author and relied heavily on the programs `CaGe`, `CPF`, and `plantri` (Brinkmann et al. 1997, 2003; Brinkmann and McKay 2007).

13.2 The List of $(\{a, b\}, k)$-Spheres with $p_b \leq 3$

For $a, k \geq 3$, a (a, k)-*polycycle* is a plane graph whose faces, besides some disjoint pairwisely, including exterior one and called *holes*, are a-gons and whose vertices have degree between 2 and k with vertices not on the boundary of holes being k-valent. Let us see any $(\{a, b\}, k)$-sphere, after merging its adjacent b-gons in larger faces, as a (a, k)-polycycle. For a given $(\{a, b\}, k)$-sphere, we can first remove the edges contained in two b-gons. If a vertex has a clockwise list of incident faces of the form $b^{x_1}a^{y_1} \ldots b^{x_N}a^{y_N}$ with $N \geq 2$ and $x_i, y_i \geq 1$, then we split it into N different vertices. The remaining faces are a-gonal and are organized into one or more (a, k)-polycycles with the pair (a, k) being one of $(3, 3)$, $(3, 4)$, $(4, 3)$, $(3, 5)$, and $(5, 3)$.

The $(3, 3)$-, $(3, 4)$-, and $(4, 3)$-polycycles are easily classified (see Deza and Dutour Sikirić 2008, pp. 45, 46) and this gives a method for solving the problem of this section. For the remaining two cases, we have to introduce another method. An (a, k)-polycycle is called *elementary* if it cannot be cut along an edge into two (a, k)-polycycle. An (a, k)-polycycle admits a unique decomposition into elementary (a, k)-polycycles and the list of elementary $(5, 3)$-, $(3, 5)$-polycycles is given in Deza and Dutour Sikirić (2008, pp. 75, 76).

From the set of elementary polycycles, appearing in an $(\{a, b\}, k)$-sphere, we can form a *decomposition graph* with the vertices being the occurring polycycles and two polycycles adjacent if they share an edge, a vertex, or are connected by an edge contained in two b-gons. The connecting vertices and edges are called *active*. See in Fig. 13.1 an example of such a decomposition.

See the list of polycycles used in this chapter on Fig. 13.2. Here Sq_i, Tr_i denote horizontal paths of i, respectively, squares and triangles, while series Pen_i, Sun_i are defined similarly. Note that $Tr_2 = \{3, 3\} - e$. We define *vertex-split* $\{3, 5\}$ as unique $(3, 5)$-polycycle obtained from a_3 by adjoining a Tr_1 and *face-split* $\{3, 5\}$ as unique $(3, 5)$-polycycle obtained from c_1 by adding two Tr_1 on two opposite edges.

Note that the 5-gons of unique minimal fullerene c-disk with $c = 4, 7, 8$ and $c \geq 13$ given in Fig. 13.18 are organized, respectively, into edge-split $\{5, 3\}$, $A_3 + Pen_7$, $Pen_7 + Pen_7$, and $B_2 + Pen_{c-12} + B_2$.

Theorem 13.1. *There is no* $(\{a, b\}, k)$*-sphere with* $p_b = 1$.

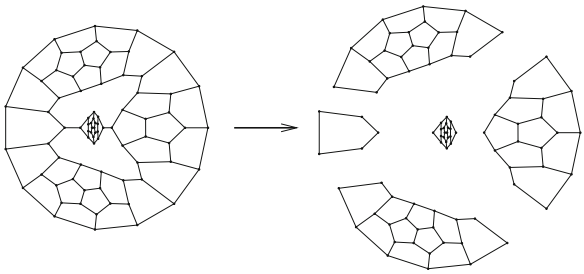

Fig. 13.1 The decomposition of a $(\{5, 15\}, 3)$-sphere seen as a $(5, 3)$-polycycle with two-, 15-, and 18-gonal holes into elementary polycycles: two edge-split $\{5, 3\}$'s, Pen_1, A_2, and $\{5, 3\} - e$ in the middle

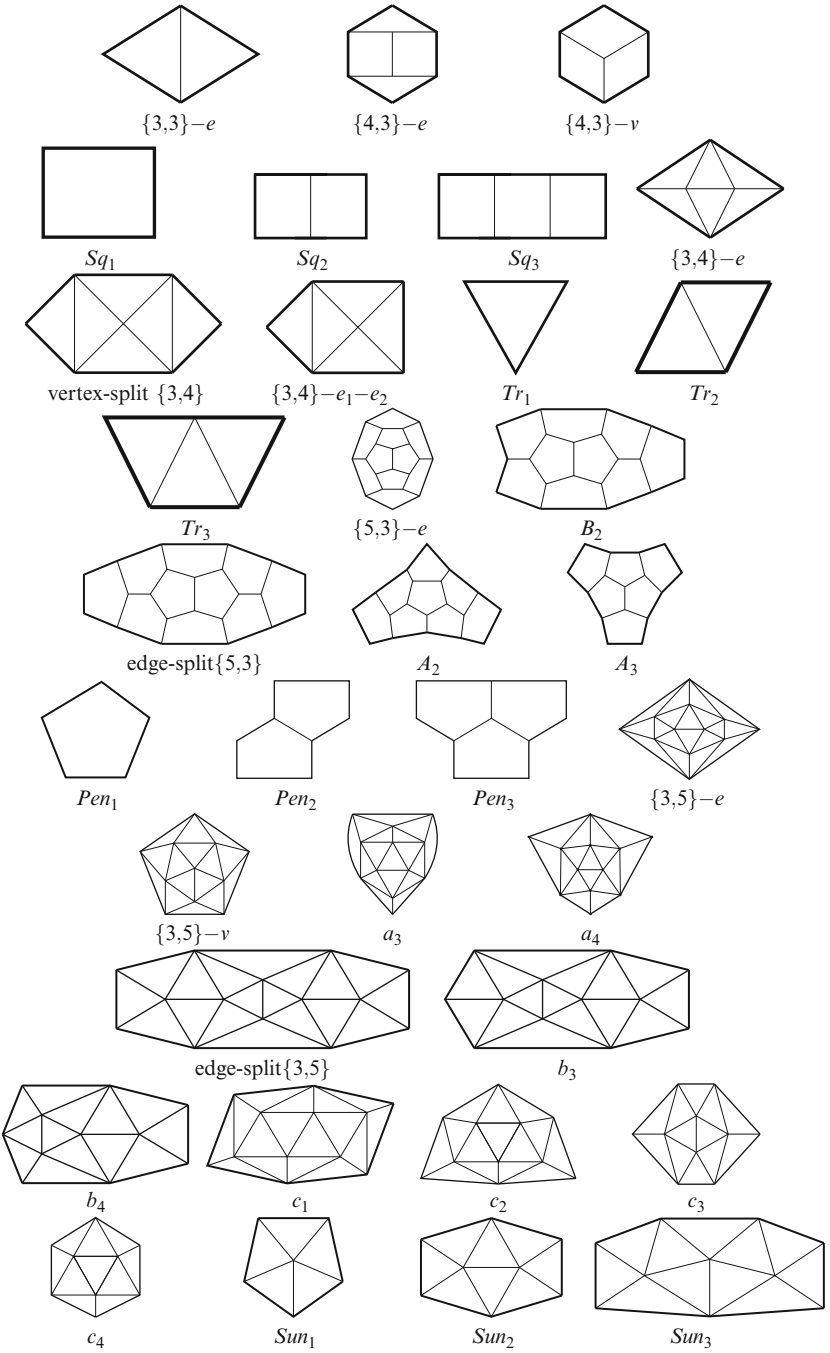

Fig. 13.2 (a, k)-polycycles from (Deza and Dutour Sikirić 2008, Chaps. 4 and 7) used in proofs of Theorems 13.2 and 13.3

Proof. The decomposition graph of such spheres is a tree. If this tree is reduced to a vertex, then the occurring polycycle has an exterior face being a b-gon and an examination of the possibilities gives $a = b$. Otherwise, we have at least one polycycle with a unique active vertex or edge. But an inspection of the list of elementary polycycles gives that no such one satisfies the condition. □

Note that $(\{6, 8\}, 3)$-maps with $p_6 = 1$ exist on an oriented surface of genus 3.

Clearly, all $(\{a, b\}, k)$-spheres with $a, k > 2$ and $p_b = 0$ are five Platonic ones denoted by $\{a, k\}$: Tetrahedron, Cube ($Prism_4$), Octahedron ($APrism_3$), Dodecahedron (snub $Prism_5$), and Icosahedron (snub $APrism_3$).

There exists unique 3-connected *trivial* $(\{a, b\}, k)$-sphere with $p_b = 2$ for $(\{4, b\}, 3)$-, $(\{3, b\}, 4)$-, $(\{5, b\}, 3)$-, and $(\{3, b\}, 5)$-: $Prism_b$ D_{bh}, $APrism_b$ D_{bd}, *snub* $Prism_b$ D_{bd}, and *snub* $APrism_b$ D_{bd}, that is, respectively, two b-gons separated by b-ring of 4-gons, $2b$-ring of 3-gons, two b-rings of 5-gons, and two $3b$-rings of 3-gons.

Clearly, for any $t \geq 2$, there are 2-connected b-vertex $(\{2, b = 2t\}, 3)$- and $(\{2, b\}, 2t)$-sphere with $p_b = 2$: a circle with t disjoint 2-gons put on it and a b-gon with every edge repeated t times.

Theorem 13.2. *Let $b > a > 2$, $k > 2$. For any nontrivial $(\{a, b\}, k)$-sphere with $p_b = 2$, the number $t = \frac{b}{a}$ is an integer. The list of such spheres (see Fig. 13.3 for pictures) consists of the following* 10 *spheres for each $t \geq 2$:*

(i) For $(a, k) = (3, 3), (4, 3), (5, 3), (3, 4), (3, 5)$, the $(\{a, ta\}, k)$-sphere D_{th} obtained by putting on a circle t polycycles $\{a, k\} - e$. Those polycycles are connected by an edge to their neighbors and so, only 2-connected.

(ii) For $(a, k) = (3, 4), (5, 3), (3, 5)$, the $(\{a, ta\}, k)$-sphere D_{th} obtained by partitioning of a circle into t polycycles: respectively, vertex-split $\{3, 4\}$, edge-split $\{5, 3\}$, edge-split $\{3, 5\}$.

(iii) The $(\{3, 3t\}, 5)$-spheres C_{th}, D_t, obtained by partitioning of a circle into t polycycles: respectively, vertex-split $\{3, 5\}$ $(Tr_1 + a_3)$ and face-split $\{3, 5\}$ $(Tr_1 + c_1 + Tr_1)$.

Proof. If the two b-gonal faces are separated by an elementary polycycle, then we are in the case of the snub $Prism_b$ or snub $APrism_b$. Otherwise, the decomposition graph should contain one cycle separating two b-gons. Any nontrivial path connected to this cycle would have a vertex of degree 1 which we have seen to be impossible. So, the decomposition graph is reduced to this cycle. Examination of the list of polycycles with exactly two connecting edges/vertices and consideration of all possibilities give the above list. □

Among the above spheres, only those coming from edge-split $\{5, 3\}$, edge-split $\{3, 5\}$, and face-split $\{3, 5\}$ are 3-connected. Those coming from vertex-split $\{3, 4\}$ and vertex-split $\{3, 5\}$ are 3-edge connected but only 2-(vertex)-connected.

Let us address now the case $p_b = 3$. Denote by $(K_3)^*$ the 2-vertex 3-edge graph. Then $(K_3)^*$ with t disjoint 2-gons put on each edge is a $(\{2, b = 2 + 4t\}, 3)$-sphere with $p_b = 3$.

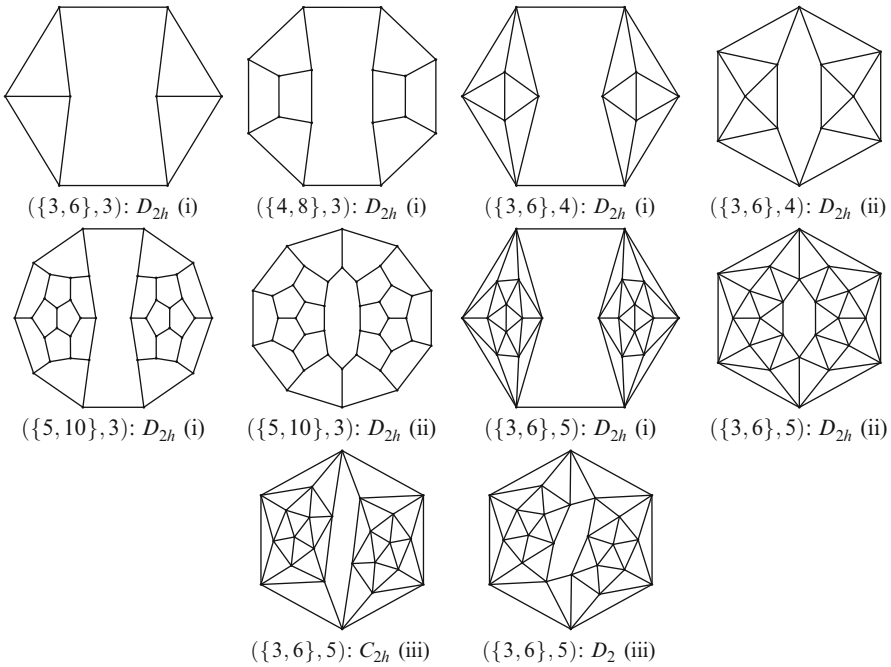

Fig. 13.3 All nontrivial $(\{a, ta\}, k)$-spheres with $p_{2a} = t = 2$; see Theorem 13.2

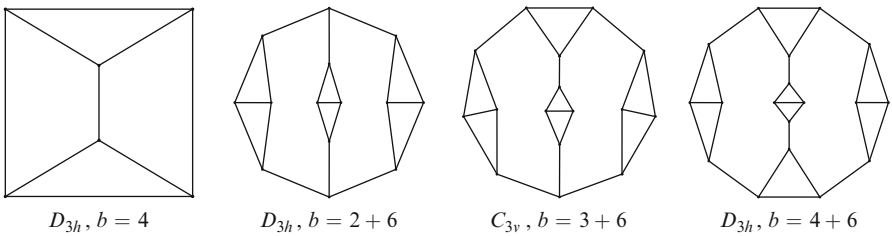

Fig. 13.4 All $(\{3, b\}, 3)$-spheres with $p_b = 3$ for $2 \le b \le 10$

Theorem 13.3. *Let $b \ge 2, b \ne a$ and let $(a, k) = (3, 3), (4, 3), (3, 4), (5, 3)$. Then $(\{a, b\}, k)$-spheres with $p_b = 3$ exist if and only if $b \equiv 2, a, 2a - 2 \pmod{2a}$ and $b \equiv 4, 6 \pmod{10}$ for $a = 5$.*

Such spheres are unique if $b \not\equiv a \pmod{2a}$ and their symmetry is D_{3h}. Let $t = \lfloor \frac{b}{2a} \rfloor$. There are seven such spheres with $t = 0$ and $3 + 4 + 5 + 9$ of them for any $t \ge 1$; see corresponding Figs. 13.4, 13.5, 13.6, 13.7 and detailed description below.

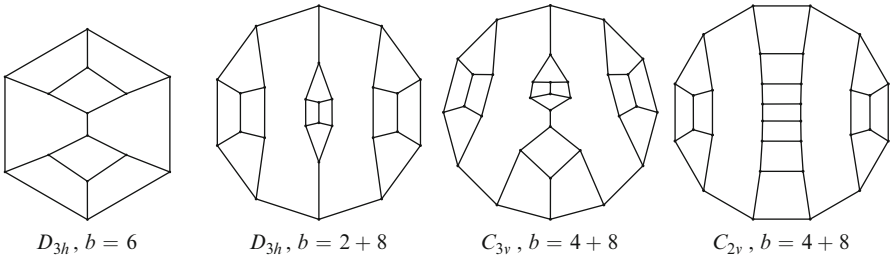

Fig. 13.5 All $(\{4, b\}, 3)$-spheres with $p_b = 3$ for $2 \leq b \leq 12$

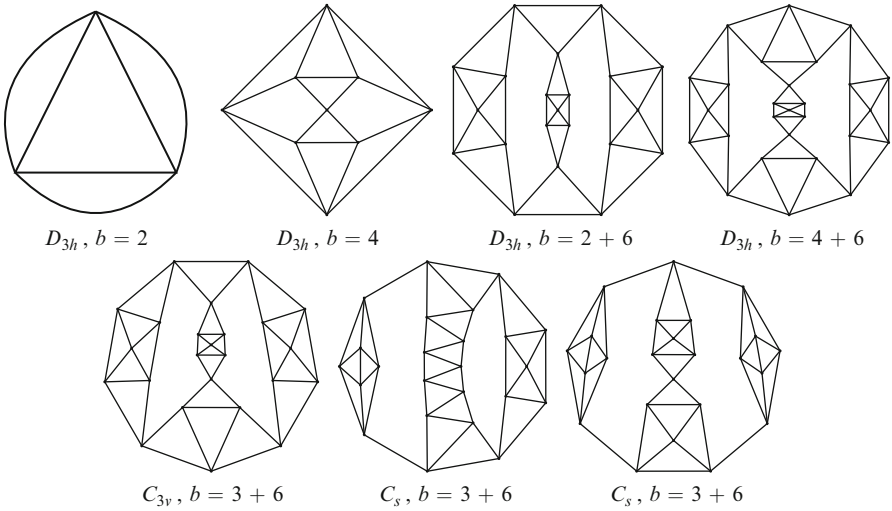

Fig. 13.6 All $(\{3, b\}, 4)$-spheres with $p_b = 3$ for $2 \leq b \leq 14$

(i) *The three* $(\{3, b\}, 3)$*-spheres with* $p_b = 3$ *and* $b = 2 + 6t$, $4 + 6t$, $3 + 6t$ *come by putting* t *polycycles* $\{3, 3\} - e$ *on* 3 *edges of, respectively,* $(K_3)^*$, $Prism_3$ *(three* 4*-*4 *edges), and Tetrahedron* $\{3, 3\}$. *Only for* $b = 2$, 4, *the graph is* 3*-connected. The symmetry is* C_{3v} *if* $b = 3 + 6t$.

(ii) *All four but one* $(\{4, b\}, 3)$*-spheres with* $p_b = 3$ *and* $b = 2 + 8t$, $6 + 8t$, $4 + 8t$ *come by putting* t *polycycles* $\{4, 3\} - e$ *on* 3 *edges of, respectively,* $(K_3)^*$, 14*-vertex* $(\{4, 6\}, 3)$*-sphere (three* 6*-*6 *edges), and Cube* $\{4, 3\}$ *(*3 *incident edges). The remaining sphere is* Sq_{8t-1} *with its two end edges connected on each of two sides by a chain of* t *polycycles* $\{4, 3\} - e$. *This graph has symmetry* C_{2v}, *while the other graph coming from Cube has symmetry* C_{3v}. *Only for* $b = 6$, *the graph is* 3*-connected.*

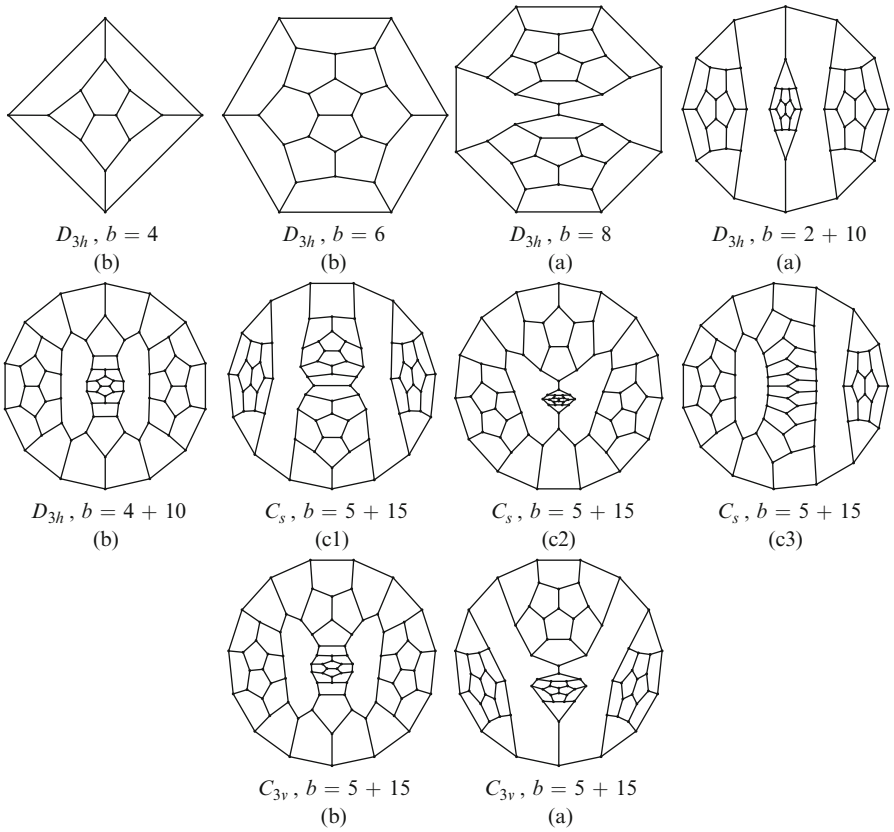

Fig. 13.7 All $(\{5, b\}, 3)$-spheres with $p_b = 3$ for $2 \leq b \leq 15$

(iii) All five but two $(\{3, b\}, 4)$*-spheres with* $p_b = 3$ *and* $b = 2 + 6t$, $4 + 6t$, $3 + 6t$ *come when replacing by* t *vertex-split* $\{3, 4\}$*'s,* 3 *vertices of, respectively, edge-doubled triangle,* 9*-vertex* $(\{3, 4\}, 4)$*-sphere* (3 *vertices common to two* 4*-gons), and Octahedron* $\{3, 4\}$ *(*3 *vertices of a triangle). The first of the remaining spheres consists of* Tr_{6t+5} *connected to its other end on one side by a chain of* t *vertex-split* $\{3, 4\}$*'s and on the other side by a chain of* t *polycycles* $\{3, 4\} - e$ *(see Fig. 13.2). The second remaining sphere consists of a vertex and* $\{3, 4\} - e_1 - e_2$ *connected by two chains of* t *polycycles* $\{3, 4\} - e$ *and one chain of* t *vertex-split* $\{3, 4\}$*'s. Those graphs have symmetry* C_s*, while the other graph coming from Octahedron has symmetry* C_{3v}*. Only for* $b = 2$ *and* $b = 4$*, the graphs are* 3*-connected.*

There are nine $(\{5,b\},3)$*-spheres with* $p_b = 3$ *for each* $t = \lfloor \frac{b}{10} \rfloor \geq 1$.

(a) Three spheres with $b = 2 + 10t$, $b = 8 + 10t$, $b = 5 + 10t$ *come by putting* t *polycycles* $\{5,3\} - e$ *on* 3 *edges of* $(K_3)^*$, *22-vertex* $(\{5,8\},3)$*-sphere (three* 8*-*8 *edges), and Dodecahedron* $\{5,3\}$ *(*3 *incident edges). Symmetry is* C_{3v} *in last case and* D_{3h} *otherwise. Only for* $b = 8$, *the graph is* 3*-connected.*

(b) Three 3*-connected spheres with* $b = 4 + 10t$, $6 + 10t$, $5 + 10t$ *come by putting* 3 *chains of* t *edge-split* $\{5,3\}$*'s between two polycycles,* $\{Pen_3, Pen_3\}$, $\{A_3, A_3\}$, *and* $\{Pen_3, A_3\}$. *Symmetry is* C_{3v} *in last case and* D_{3h} *otherwise.*

(c) Three 2*-connected* $(\{5, 5 + 10t\},3)$*-spheres of symmetry* C_s *come from, respectively:*

(c1) A chain $B_2 + t$ *times edge-split* $\{5,3\}$ *connected on both ends by* t *times* $\{5,3\} - e$

(c2) $A_2 + t(\{5,3\} - e) + Pen_1$ *connected on both ends by* t *times edge-split* $\{5,3\}$

(c3) Pen_{10t+9} *connected on one side by* t *times edge-split* $\{5,3\}$ *and on the other one by* t *times* $\{5,3\} - e$

Proof. It is not possible to have an elementary polycycle separating three b-gonal faces. Hence, the decomposition graph has three faces and is either formed of two vertices of degree 3 connected by chains of vertices of degree 2 or a vertex of degree 4 connected by two chains of vertices of degree 2 on each side. An examination of the possibilities along the same lines gives the above result. □

Note that all $(\{a,b\},k)$-spheres with $p_b = 3$ and symmetry $\neq C_s$ are bR_j (i.e., each b-gon has exactly j edges of adjacency with b-gons); see *face-regularity* in Sect. 13.3). $j = 2\lceil \frac{b}{2a} \rceil$ for $(a,k) = (3,3), (4,3)$ and $j = 0$ for $(a,k) = (3,4), (3,5)$. For $(a,k) = (5,3)$, we have $j = 0$ or $2\lceil \frac{b}{2a} \rceil$.

In case $(a,k) = (3,5)$, we have 17 infinite series of spheres but no proof that the list is complete. See below the list of $(\{3,b\},5)$-spheres obtained and in Figs. 13.8 and 13.9 their pictures for small b. All but (a) have $b = 3 + 6t$. All but (a) and (d_2) are only 2-connected. By R_e, V_{sp}, E_{sp}, and F_{sp}, we denote a chain of t polycycles P with P being $\{3,5\} - e$, vertex-split $\{3,5\}$, edge-split $\{3,5\}$, and face-split $\{3,5\}$, respectively.

(a) Three spheres with $b = 2 + 6t$, $4 + 6t$, $3 + 6t$ obtained by putting three E_{sp} between two polycycles, $\{Tr_1 + 3Tr_1, Tr_1 + 3Tr_1\}$, $\{c_4 + 3Tr_1, c_4 + 3Tr_1\}$, and $\{c_4 + 3Tr_1, Tr_1 + 3Tr_1\}$. Symmetry is C_3 in last case and D_3 otherwise.

(b_1) C_1: $c_1 + Tr_1 + F_{sp}$ with ends connected by R_e and V_{sp}.

(b_2) C_s: Sun_{6t+5} with ends connected by R_e and E_{sp}.

(b_3) C_1: $b_3 + Tr_1 + E_{sp}$ with ends connected by R_e and F_{sp}.

(b_4) C_s: $b_3 + 2Tr_1 + E_{sp}$ with ends connected by V_{sp} and E_{sp}.

(b_5) C_1: $Sun_{4+6t} + 3Tr_1$ with ends connected by V_{sp} and F_{sp}.

(c_1) C_s: a vertex and $(\{3,5\} - v) + 2Tr_1$ connected by R_e and two V_{sp}'s.

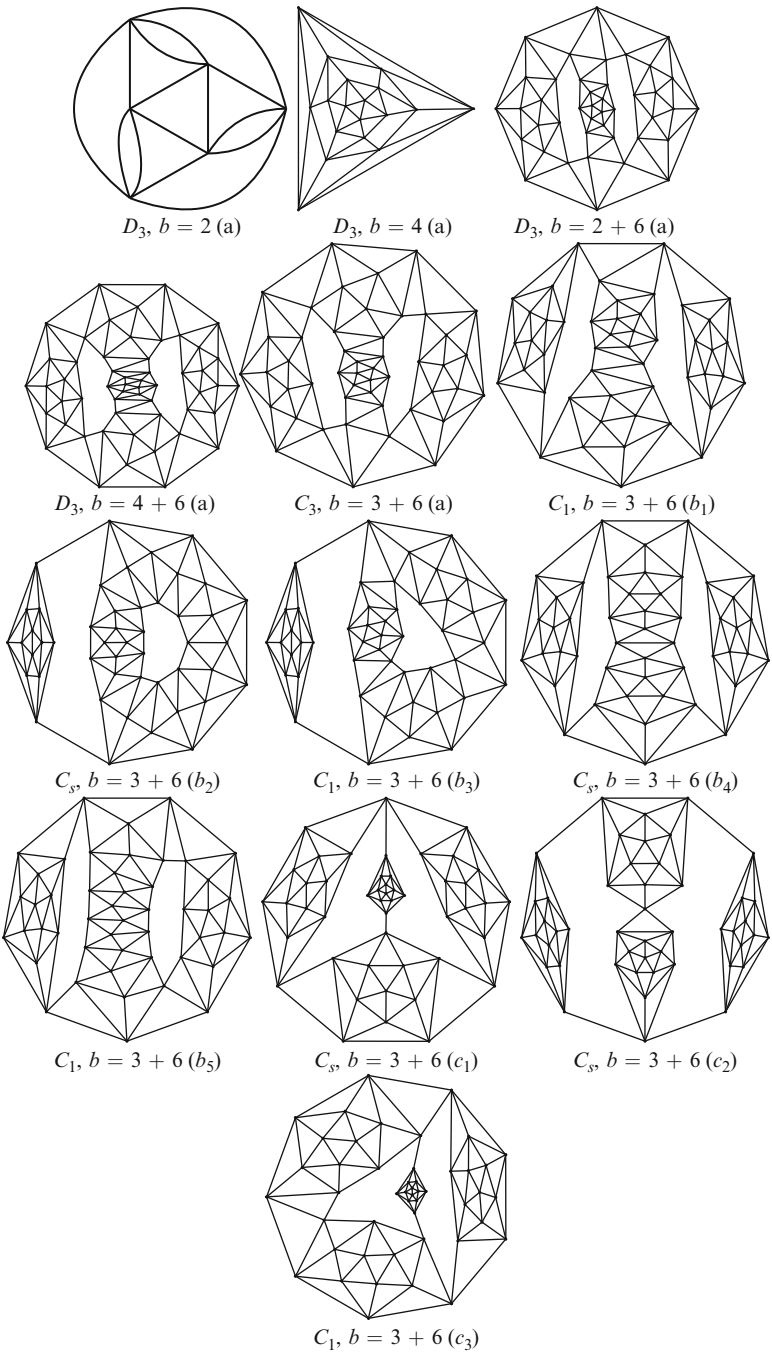

Fig. 13.8 All known $(\{3, b\}, 5)$-spheres with $p_b = 3$ and $2 \leq b \leq 10$ (part 1)

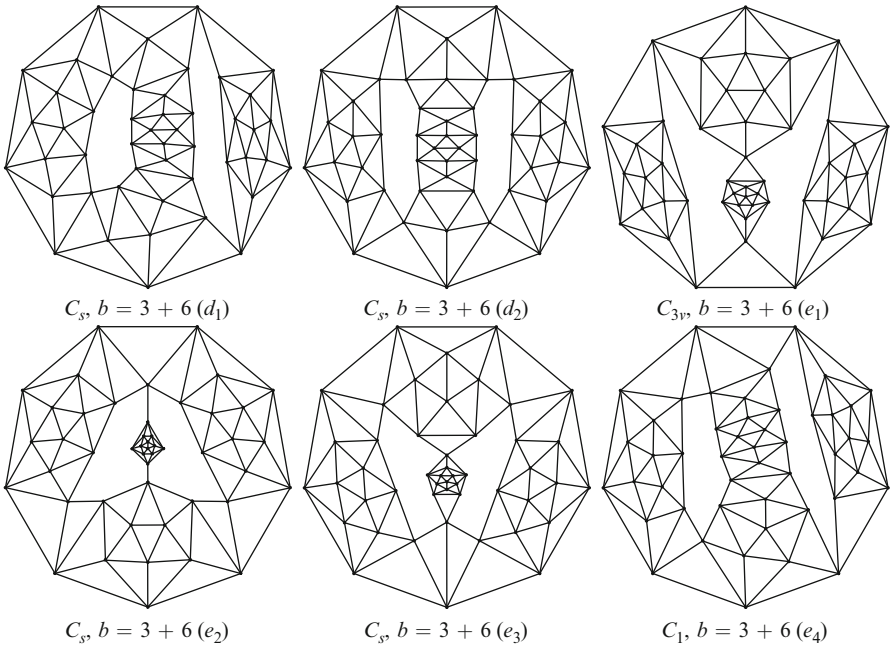

Fig. 13.9 All known $(\{3, b\}, 5)$-spheres with $p_b = 3$ and $2 \le b \le 10$ (part 2)

(c_2) C_s: a vertex and a_3 connected by two R_e's and one V_{sp}.
(c_3) C_1: a vertex and $c_2 + 2Tr_1$ connected by two V_{sp}'s and one F_{sp}.
(d_1) C_s: Sun_1 and $Sun_3 + Tr_1$ connected by V_{sp} and two E_{sp}'s.
(d_2) C_s: Sun_2 and $Sun_1 + 2Tr_1$ and connected by E_{sp} and two F_{sp}'s.
(e_1) C_{3v}: Tr_1 and a_4 connected by three V_{sp}'s.
(e_2) C_s: Tr_1 and c_2 connected by R_e and two F_{sp}'s.
(e_3) C_s: $2Tr_1$ and $c_3 + 3Tr_1$ connected by V_{sp} and two F_{sp}'s.
(e_4) C_1: $3Tr_1$ and $b_4 + Tr_1$ connected by V_{sp}, E_{sp} and F_{sp}.

Note that all 15 orbits of $(\{3, 3 + 6t\}, 5)$-spheres constructed were built from the 15 orbits of triples of triangles in Icosahedron. Note also that $\binom{20}{3} = \sum_G \frac{120}{|G|} = 5 \times 120 + 8 \times 60 + 40 + 20$, since there are 5, 8, 1, 1 cases with symmetry C_1, C_s, C_3, C_{3v}, respectively. There may be other spheres in this case and for other values of b.

13.3 Icosahedrites

We call *icosahedrite* the $(\{3, 4\}, 5)$-spheres. They are in a sense the simplest nontrivial class of 5-valent plane graphs. Clearly, for them it holds $p_3 = 20 + 2p_4$ and $v = 12 + 2p_4$. Note that all $(\{a, 3\}, 5)$-spheres with $a < 3$ are $(\{1, 3\}, 5)$-

Table 13.1 The number of v-vertex icosahedrites

v	12	14	16	18	20	22	24	26	28	30	32
Nr	1	0	1	1	5	12	63	246	1395	7,668	45,460

sphere with $(p_1, p_3; v) = (2, 6; 4)$ and four $(\{2, 3\}, 5)$-spheres with $(p_2, p_3; v) = (4, 4; 4)$ (two), $(3, 8; 6)$, $(2, 12; 8)$. Remaining $(\{1, 2, 3\}, 5)$-spheres should have $(p_1, p_2, p_3; v) = (1, 3, 1; 2)$, $(2, 1, 2; 2)$, $(1, 2, 5; 4)$, or $(1, 1, 9; 6)$; only 2nd and 3rd exist.

The simplest icosahedrite is Icosahedron, which is a $(\{3\}, 5)$-sphere of symmetry I_h. One way to obtain icosahedrite is from an *octahedrite*, that is, a $(\{3, 4\}, 4)$-sphere S. To every vertex of S, we associate a square; to every edge (coherently), a pair of adjacent triangles and faces are preserved. Only the rotational symmetries of S are preserved in the final icosahedrite. If one applies the same operation to Octahedron, then one gets the smallest (24 vertices) icosahedrite of symmetry O (see Fig. 13.13). Applying it to the infinite regular plane tiling $\{4, 4\}$ by squares, one gets the Archimedean *snub square tiling* (3.3.4.3.4). Note that there is only one other *infinite Archimedean icosahedrite*, that is, vertex-transitive 5-valent tiling of the plane by regular 3- and 4-gons only: *elongated triangular tiling* (3.3.3.4.4).

For a given icosahedrite, a *weak zigzag* WZ is a circuit of edges such that one alternates between the left and right way but never extreme left or right. The usual *zigzag* is a circuit such that one alternates between the extreme left and extreme right way.

A zigzag or weak zigzag is called *edge-simple*, respectively *vertex-simple*, if any edge, respectively vertex, of it occurs only once. A vertex-simple zigzag is also edge-simple. If WZ is vertex-simple of length l, then one can construct another icosahedrite with l more vertices.

Clearly, the weak zigzags (as well as the usual zigzags) doubly cover the edge set. For example, 30 edges of Icosahedron are doubly covered by 10 weak vertex-simple zigzags of length 6, as well as by six usual vertex-simple zigzags of length 10. Clearly, a 3-gon surrounded by nine 3-gons or a 4-gon surrounded by 12 3-gons corresponds to weak zigzags of length six or eight, respectively. In fact, no other vertex-simple weak zigzags exist.

In Table 13.1, we list the number of v-vertex icosahedrites for $v \leq 32$. From this list, it appears likely that any icosahedrite is 3-connected.

Theorem 13.4. *A $(\{3, 4\}, 5)$-sphere exists if v is even, $v \geq 12$, and $v \neq 14$. Their number grows at least exponentially with v.*

Proof. If there is a weak zigzag of length 6 in an icosahedrite G, then we can insert a *corona* (6-ring of three 4-gons alternated by three pairs of adjacent 3-gons) instead of it and get an icosahedrite with six more vertices. Since there are such icosahedrite for $n = 18, 20, 22$ (see Figs. 13.10 and 13.11), we can generate the required graphs. There is always two options when inserting the corona and so the number grows exponentially as required. □

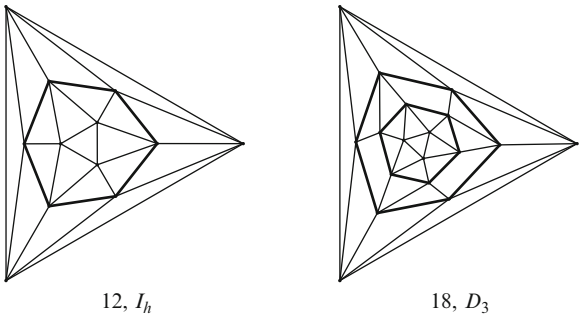

Fig. 13.10 A simple weak zigzag in an icosahedrite and the resulting expansion

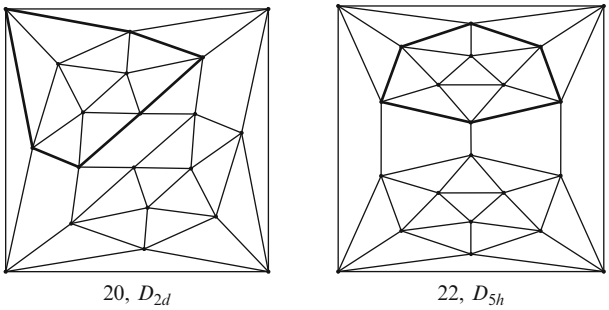

Fig. 13.11 Two icosahedrites having a simple weak zigzag of length 6

In the case of fullerenes or other standard $(\{a, b\}, k)$-spheres, the number of a-gons is fixed and the structure is made up of patches of b-gons. The parametrization of graphs, generalizing one in Thurston (1998), including the case of one complex parameter – *Goldberg-Coxeter construction* Dutour and Deza (2004) – are thus built. A consequence of this is the polynomial growth of the number of such spheres. This does not happen for the case of icosahedrites and their parametrization, if any, looks elusive.

As a consequence of this increased freedom, we can more easily build a new icosahedrite from a given one by an expansion operation, while in the case of standard $(\{a, b\}, k)$-spheres, one is essentially restricted to the Goldberg-Coxeter construction. The operation Op, respectively Op', replaces each vertex of an icosahedrite G by 6, respectively 21, vertices and gives icosahedrites Op, Op' with the same symmetries as G (see Fig. 13.14). Moreover, for any $m \geq 2$, we can define an operation OP_m that replaces every face F by a patch and add $m - 1$ rings of squares and pairs of triangles. The operation OP_2 on a 4-gon is shown in Fig. 13.14. The resulting map $OP_m(G)$ has only the rotational symmetries of G and associates, to every vertex of G, $1 + 5m(m - 1)$ vertices in $OP_m(G)$.

Theorem 13.5. *Any symmetry group of icosahedrites if one of the following* 38*:*

C_1, C_i, C_s, S_4, S_6, S_8, S_{10}. C_2, C_{2h}, C_{2v}, C_3, C_{3h}, C_{3v}, C_4, C_{4h}, C_{4v}, C_5, C_{5h}, C_{5v}, D_2, D_{2h}, D_{2d}, D_3, D_{3h}, D_{3d}, D_4, D_{4h}, D_{4d}, D_5, D_{5h}, D_{5d}, O, O_h, T, T_d, T_h, I, I_h.

Proof. By the face sizes and vertex sizes, the list of possibilities is the one indicated. We used the enumeration up to 32 vertices to find many groups and their minimal representative. If a sphere has a 3-fold axis, then it necessarily passes through two 3-gons. Those two 3-gons can be replaced by 4-gons and ipso facto we get examples of a sphere with 4-fold axis. From this we got the icosahedrites with groups C_4, C_{4h}, C_{4v}, D_4, D_{4h}, D_{4d}, and S_8. All but 40-vertex one C_4, C_{4v}, and D_{4h} are minimal.

Now, suppose that a 2-fold axis of rotation passes by two edges, which are both contained in two triangles. Then we insert a vertex on those two edges and replace the 2-fold symmetry by a 5-fold symmetry. By iterating over all known icosahedrites, and all such 2-fold axis, we get the symmetries C_5, C_{5h}, C_{5v}, S_{10} and D_{5h}, D_{5d}, and D_5; the last three are minimal. For the cases of O_h, T, T_d, and T_h, we obtained examples by hand drawing. The 132-vertex icosahedrite of symmetry I in Fig. 13.13 is obtained from Icosahedron by operation B_2. The minimal known (actually, examples are minimal whenever $v \leq 32$) are given in Figs. 13.12 and 13.13.

Aggregating groups $\mathbf{C_1}=\{C_1, C_s, C_i\}$, $\mathbf{C_m}=\{C_m, C_{mv}, C_{mh}, S_{2m}\}$, $\mathbf{D_m}=\{D_m, D_{mh}, D_{md}\}$, $\mathbf{T}=\{T, T_d, T_h\}$, $\mathbf{O}=\{O, O_h\}$, and $\mathbf{I}=\{I, I_h\}$, all 38 symmetries of $(\{3,4\},5)$-spheres are: $\mathbf{C_1}$, $\mathbf{C_m}$, $\mathbf{D_m}$ for $2 \leq m \leq 5$ and $\mathbf{T}$, $\mathbf{O}$, $\mathbf{I}$. 5-, 4- and 3-fold symmetry exists if and only if, respectively, $p_4 \equiv 0 \pmod 5$ (i.e., $v = 2p_4+12 \equiv 2 \pmod{10}$), $p_4 \equiv 2 \pmod 4$ (i.e., $v = 2p_4 + 12 \equiv 0 \pmod 8$), and $p_4 \equiv 0 \pmod 3$ (i.e., $v = 2p_4 + 12 \equiv 0 \pmod 6$).

Any group appears an infinite number of times since, for example, one gets an infinity by applying operation Op iteratively.

From the above result, it appears that the only limitations for the group are coming from the rotation axis. It seems possible that this is also true for all $(\{a,b\},k)$-spheres with b-gons being of negative curvature

A map is said to be *face-regular* or, specifically, pR_i if every face of size p is adjacent to exactly i-faces of the same size p.

Theorem 13.6. *(i) The only icosahedrite which is* $3R_i$ *is Icosahedron which is* $3R_3$

(ii) For $i = 0, 1,$ *and* 2*, there is an infinity of icosahedrites that are* $4R_i$.

Proof. Let N_{ij} denote the number of i-j edges, that is, those which are common to an i-gon and a j-gon; so, $e = N_{33} + N_{34} + N_{44}$. But $N_{34} + N_{44} \leq 4p_4$ with equality if and only if our icosahedrite is $4R_0$. So,

$$2e = 3p_3 + 4p_4 = p_3 + 2(20 + 2p_4) + 4p_4 \leq 2N_{33} + 8p_4,$$

that is, $2N_{33} \geq p_3 + 40$. It excludes the cases $3R_0$ and $3R_1$, since $2N_{33} = 0$ and p_3, respectively.

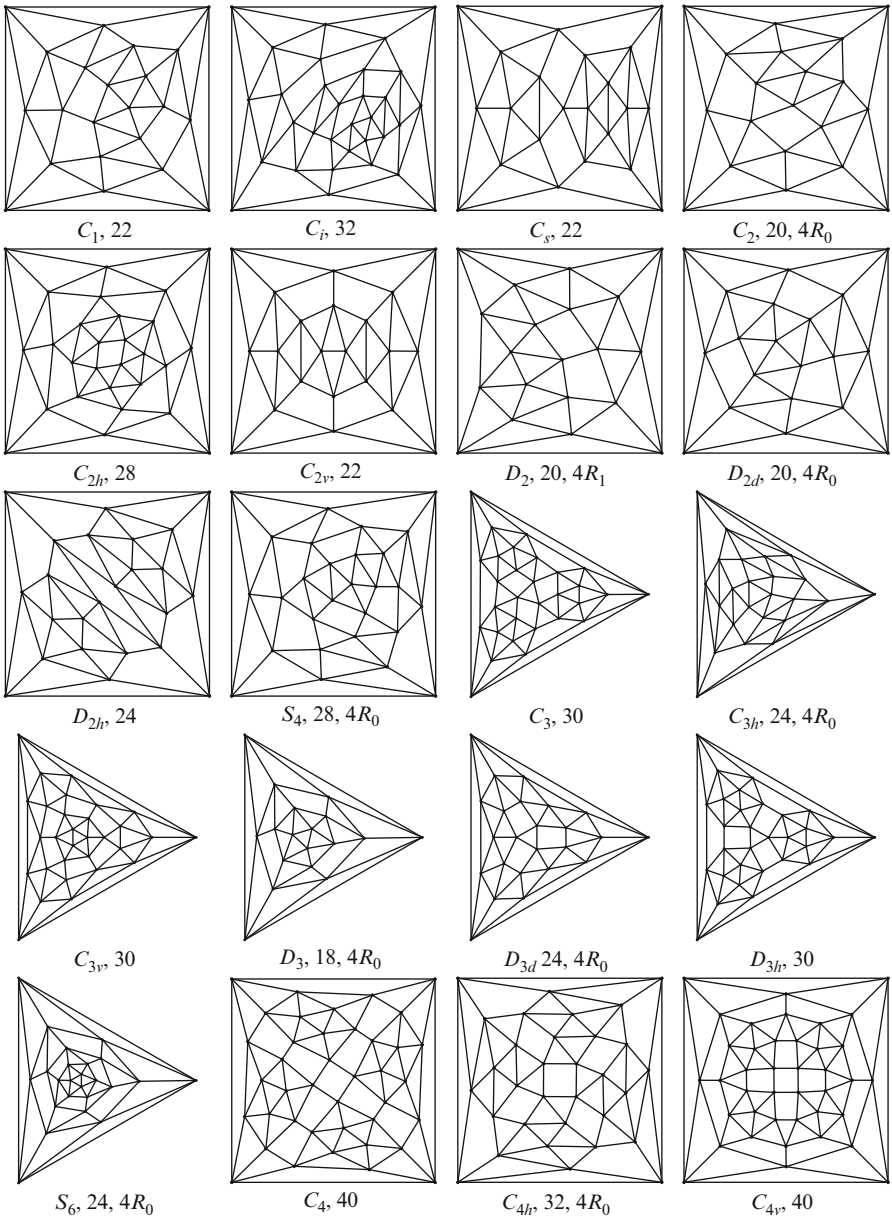

Fig. 13.12 Examples of icosahedrites for all possible symmetry groups (part 1); all 21 with at most 32 vertices are minimal ones

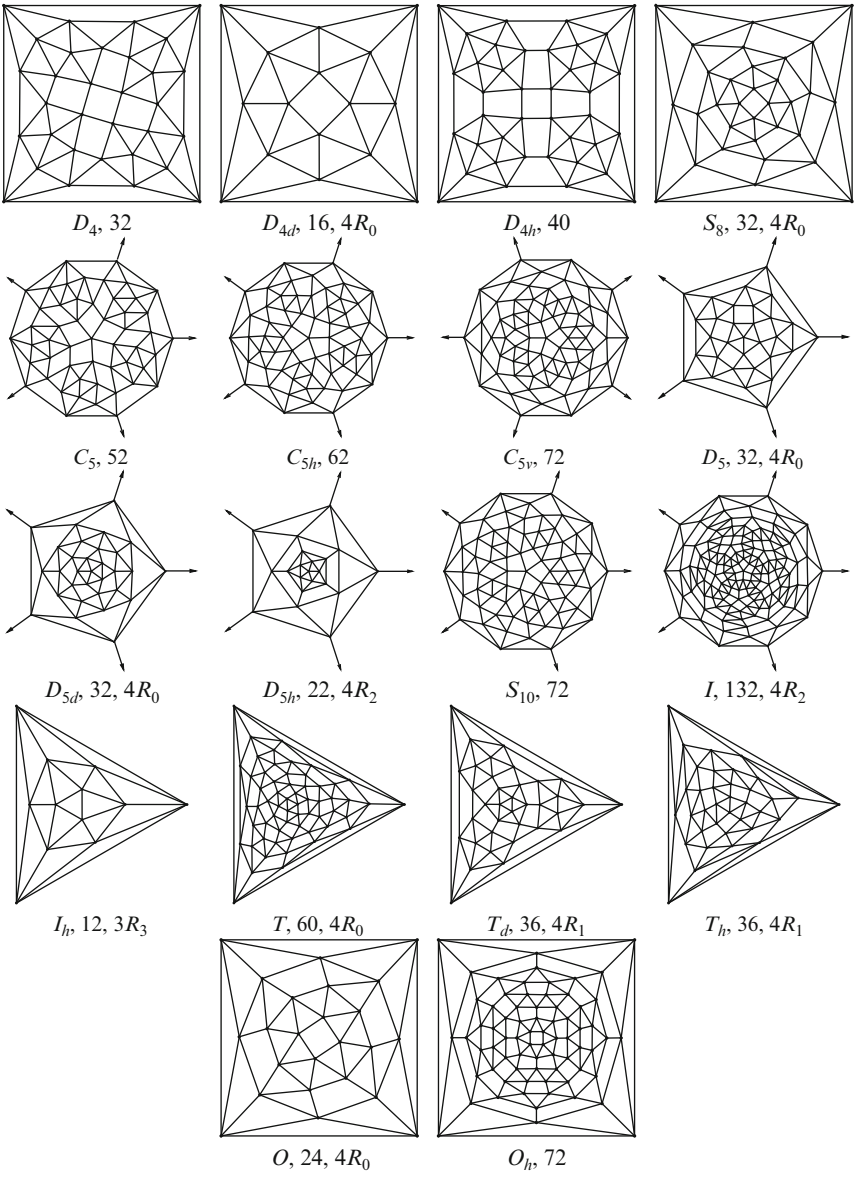

Fig. 13.13 Examples of icosahedrites for all possible symmetry groups (part 2); all 5 with at most 32 vertices are minimal ones

If our icosahedrite is $3R_2$, then $N_{33} + N_{34} = p_3 + p_3$, implying $N_{44} = p_4 - 10$. Any $4R_0$ icosahedrite with 32 vertices (i.e., with $p_4 = 10$) has $\frac{N_{33}}{p_3} = 2$, that is, it is $3R_2$ *in average*. Now, $3R_2$ means that the 3-gons are organized in rings separated by 4-gons. Such rings can be either five 3-gons with common vertex, or 12 3-gons

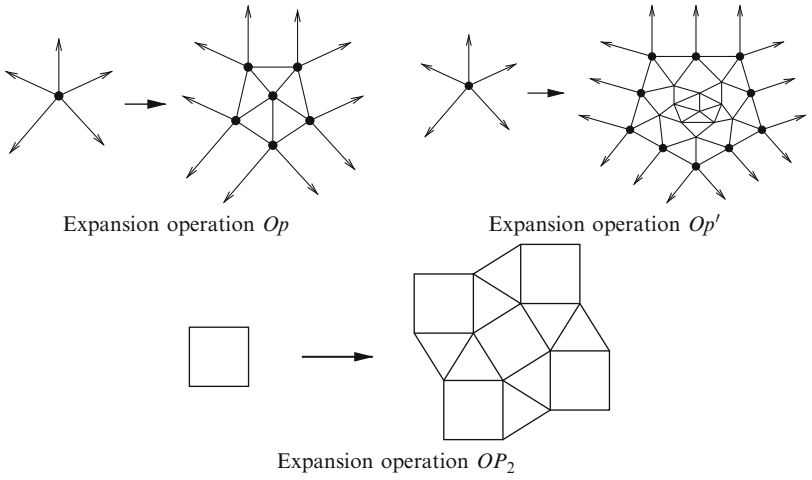

Fig. 13.14 Three expansion operations on icosahedrites

Fig. 13.15 The icosahedrite used in proof of Theorem 13.6 as the first one in an infinite series with $4R_1$

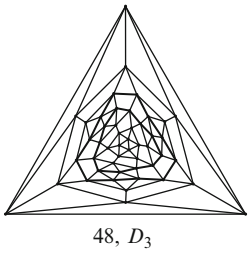

around a 4-gon, or $APrism_m$, $m > 4$. In each case, such ring should be completed to an icosahedrite by extruding edge to keep 5-regularity. In order to be isolated from other 3-gons, the ring should have a twice-longer ring of 4-gons around it. The faces touching the ring of 3-gons in a vertex only could not be 3-gonal since they have two 4-gonal neighbors. So, the isolating ring of 4-gons consists of 4-gons adjacent to the ring of 3-gons alternated by 4-gons touching it only in a vertex. It is easy to see that such a process cannot be closed.

The number of icosahedrites $4R_0$ is infinite; such series can be obtained by the operation Op (see Fig. 13.14) from, say, unique 16-vertex icosahedrite. An infinity of $4R_1$ icosahedrites can be obtained in the following way. We take the $4R_1$ icosahedrite of Fig. 13.15, and the ring bounded by two overlined circuits can be transformed into any number of concentrated rings. An infinity of icosahedrites $4R_2$ can be obtained from the 22-vertex icosahedrite of symmetry D_{5h} in Fig. 13.13. It suffices to add layers of five 4-gons alternated by layers of ten 3-gons (as in Archimedean elongated triangular plane tiling (3.3.3.4.4). □

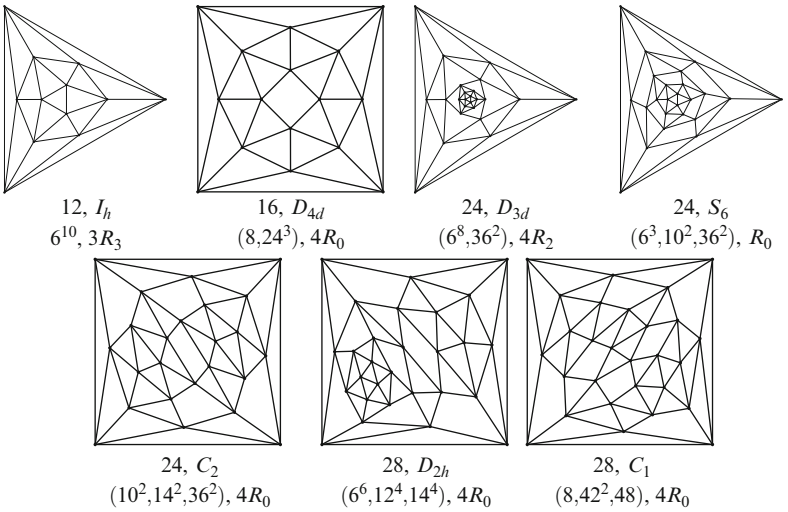

Fig. 13.16 The icosahedrites with only edge-simple weak zigzags and at most 32 vertices

Among all 54,851 icosahedrites with $v \leq 32$, there are no $4R_3$ and only four specimens $4R_2$. Those with $4R_3$ should have $2N_{33} = 3p_3 - p_4$ and v divisible by 4, but we doubt they exist. Note that part (i) of Theorem 13.6 can be easily generalized on $(\{3, b\}, 5)$-sphere with any $b \geq 4$.

All icosahedrites with only edge-simple usual zigzags and $v \leq 32$ are three of those seven (see Fig. 13.16) having only edge-simple weak zigzags: 12, I_h with (10^6); 24, D_{3d} with $(6, 10^6, 18^3)$; and 28, D_{2h} with $(10^6, 20^4)$. We expect that any icosahedrite with only edge-simple usual or weak zigzags, if such ones exist for $v \geq 34$, has v divisible by four. Also, for $v \leq 32$, the maximal number of zigzags and weak zigzags are realized only by edge-simple ones whenever they exist.

Snub $APrism_b$, Snub Cube, and Snub Dodecahedron with $(v, b) = (4b, b)$, $(24, 4)$ and $(60, 5)$, respectively, are bR_0 and only known b-gon-transitive $(\{3, b\}, 5)$-spheres. They are also, besides Icosahedron, only known $(\{3, b\}, 5)$-spheres with at most two orbits of 3-gons. The Archimedean $(\{3, b\}, 5)$-plane tilings (3.3.4.3.4), (3.3.3.4.4), and (3.3.3.3.6) have $b = 4$, 4, 6, respectively. They are transitive on b-gons and vertices. They are also, respectively, $(4R_1, 3R_1)$, $(4R_2, 3R_2)$, and $6R_0$ and have 1, 1, 2 orbits of 3-gons.

13.4 On $(\{a, b, c\}, k)$-Spheres with $p_c = 1$

Clearly, an $(\{a, b, c\}, k)$-sphere with $p_c = 1$ has

$$v = \frac{2}{k-2}(p_a - 1 + p_b) = \frac{2}{2k - a(k-2)}(a + c + p_b(b - a))$$

vertices and (setting $b'=\frac{2k}{k-2}$) $p_a = \frac{b'+c}{b'-a} + p_b\frac{b-b'}{b'-a}$ a-gons. So, $p_a = \frac{b+c}{b-a}$ if $b = b'$, that is, $(\{a, b\}, k)$-sphere is standard.

We are especially interested in *fullerene* c-disks, that is, $(\{5, 6, c\}, 3)$-spheres with $p_c = 1$. If $c \geq i$, we also impose that they are i-connected for $i \in \{1, 2, 3\}$. They have $p_5 = c + 6$, $v = 2(p_6 + c + 5)$ and there is an infinity of them for any $c \geq 1$.

In general, a $(\{5, 6, c\}, 3)$-sphere with $p_c = 1$ and a c-disk obtained from it by deleting of the c-gon are different geometrical objects. But they have the same graph. Since we consider only their combinatorial properties, we will, by abuse of language, to treat them as the same object. We will use the term *disk* but present a picture for sphere. Also, a group means here the group of a sphere, not only of its graph.

The only way to get fullerene 1-disk is to get a $(\{5, 6, r, s\}), 3)$-sphere with $p_r = p_s = 1$, $(r, s) = (3, 4), (3, 3), (2, 3), (2, 4)$ and add 4 vertices, 2-gon on the $r - s$ edge, and then erect an edge with 1-gon from the middle of $2 - r$ edge. In fact, only $(3, 4)$ is possible and minimal; such graph has 36 vertices, proving minimality of 40-vertex 1-disk.

One can check that all $(\{a, b, c\}, 3)$-spheres with $p_c = 1$, $2 \leq a, b, c \leq 6$ and $c \neq a, b$ are four series with $(a, b, c) = (4, 6, 2), (5, 6, 2), (5, 6, 3), (5, 6, 4)$ and following two 10-vertex spheres of symmetry C_{3v} having $p_a = p_b = 3$, $p_c = 1$: $(\{4, 5, 3\}, 3)$- (Cube truncated on one vertex) and $(\{3, 5, 6\}, 3)$- (Tetrahedron truncated on three vertices). There are also series of $(\{1, 4, 2\}, 4)$- and $(\{3, 4, 2\}, 4)$-spheres with $p_2 = 1$.

Theorem 13.1 implies that $(\{a, b, c\}, k)$-sphere with $p_c = 1$ and $p_b = 0$ has $c = a$, that is, it is the k-regular map $\{a, k\}$ on the sphere. We conjecture that a $(\{a, b, c\}, k)$-sphere with $p_c = p_b = 1 < a, c$ has $c = b$, that is, it is a $(\{a, b\}, k)$-sphere with $p_b = 2$. Note that the 2-vertex $(\{1, 4, 2\}, 4)$-sphere has $p_2 = p_4 = 1 = a < c < b$.

Call $(\{a, b, c\}, k)$-*thimble* any $(\{a, b, c\}, k)$-sphere with $p_c = 1$ such that the c-gon is adjacent only to a-gons and only once to each of them. *Fullerene c-thimble* is the case $(a, b, c; k) = (5, 6, c; 3)$ of above. It exists if and only if $c \geq 5$. Note that there exists a fullerene 20-disk with $p_6 = 6$, $v = 62$ with the 12-gon being adjacent only to 5-gons but adjacent twice to one of them.

Moreover, we conjecture that for odd or even $c \geq 5$, the following $(5c - 5)$- or $(5c - 6)$-vertex c-thimble is a minimal one; it holds for $5 \leq c \leq 10$ since this construction generalizes cases 7, 9−1 and 8, 10−3 in Fig. 13.18, as well as cases $c = 5$ and 6, of minimal c-disks. Take the c-ring of 5-gons, and then put inside a concentric c-ring of 5- or 6-gons: 3-path of 5-gons and, on opposite side, 3-path or 3-ring, for even or odd c, of 5-gons. Remaining $c-6$ or $c-5$ faces of interior c-ring are 6-gons. Finally, fill inside of the interior c-ring by the $\frac{c-4}{2}$- or $\frac{c-5}{2}$-path of 6-gons. Another generalization of the minimal 6-disk is, for $c = 6t$, $\frac{c(c+18)}{6}$-vertex c-thimble of symmetry (for $c > 6$) C_6 or C_{6v}. In fact, take $6t$-ring of 5-gons, then, inside of it, $6t$-ring, where six equispaced 5-gons are alternated by $(t - 1)$-tuples of 6-gons. Finally, put inside, for $i = t - 1, t - 2 \ldots, 1$, consecutively $6i$-rings of 6-gons.

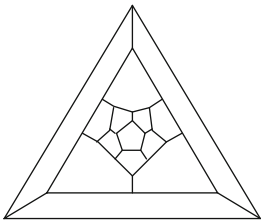

Fig. 13.17 Minimal 3-disk of type (6, 6, 5); it is also C_s-minimal 3-disk

Any such c-thimble can be elongated by adding an outside ring 5-gons along the c-gon and transforming inside ring of 5-gons along it into a ring of 6-gons. Let a $(\{5, 6, c\}, 3)$-sphere with $p_c = 1$ have a simple *zigzag* (left–right circuit without self-intersections). A *railroad* is a circuit of 6-gons, each of which is adjacent to its neighbors on opposite edges. Let us elongate the above sphere by a railroad along zigzag and then let us cut the elongated sphere in the middle of this ring. We will get two c-thimbles.

Theorem 13.7. *All simple zigzags of any elongated c-thimble are parallel and its railroads are parallel c-rings of 6-gons, forming a cylinder.*

In fact, suppose that there is a railroad in a c-thimble not belonging to the cylinder of parallel c-rings of 6-gons along the boundary c-ring of 5-gons.

Let us cut it in the middle. The thimble is separated into a smaller c-thimble with $p_5 = c$ and a $(\{5, 6, c\}, 3)$-sphere with $p_5 = 6$. But this sphere cannot contain at least $c + 1$ of $c + 6$ original 5-gons: c boundary 5-gons and, at the other side of the cylinder, at least one 5-gon. Only a railroad belonging to the cylinder can go around this 5-gon. □

Given a c-disk, call its *type*, the sequence of gonalities of its consecutive neighbors. So, any c-thimble has type $(5, \ldots, 5)$. Call an *almost c-thimble* any c-disk of type $(6, 5, \ldots, 5)$. Clearly, a $v + 2(c - 1)$-vertex almost c-thimble can be obtained from a c-thimble by inscribing a $(c - 1)$-gon into the c-gon. The minimal almost c-thimbles with $c = 4, 3, 2, 1$ come this way consecutively from Dodecahedron; they have $20 + 2 \times 4, 28 + 2 \times 3, 34 + 2 \times 2, 38 + 2$ vertices.

There are bijections between v-vertex 1-disks, $(v - 2)$-vertex 2-disks of type $(5, 6)$, and $(v - 4)$-vertex $(\{5, 6, 3, 4\}, 3)$-spheres with unique and adjacent 3 and 4-gon. Using it, we found the minimal 1-disk, given in Fig. 13.18. There is a bijection between v-vertex 3-disks of type $(6, 6, 6)$ and $(v - 2)$-vertex fullerenes with $(5, 5, 5)$-vertex (collapse the 3-gon). So, the possible types (and minimal number of vertices for examples) are (6) $(v = 40)$ for 1-disks; $(6, 6)$ $(v = 26)$, $(6, 5)$ $(v = 40 - 2)$ for 2-disks; and $(6, 6, 6)$ $(v = 22)$, $(6, 5, 5)$ $(v = 40 - 6)$, $(6, 6, 5)$ $(v = 26$; see Fig. 13.17) for 3-disks. We conjecture that the minimal 4-disk is unique, besides $c = 5, 6$, *Frank-Kasper c-disk*, that is, having no adjacent 6-gons.

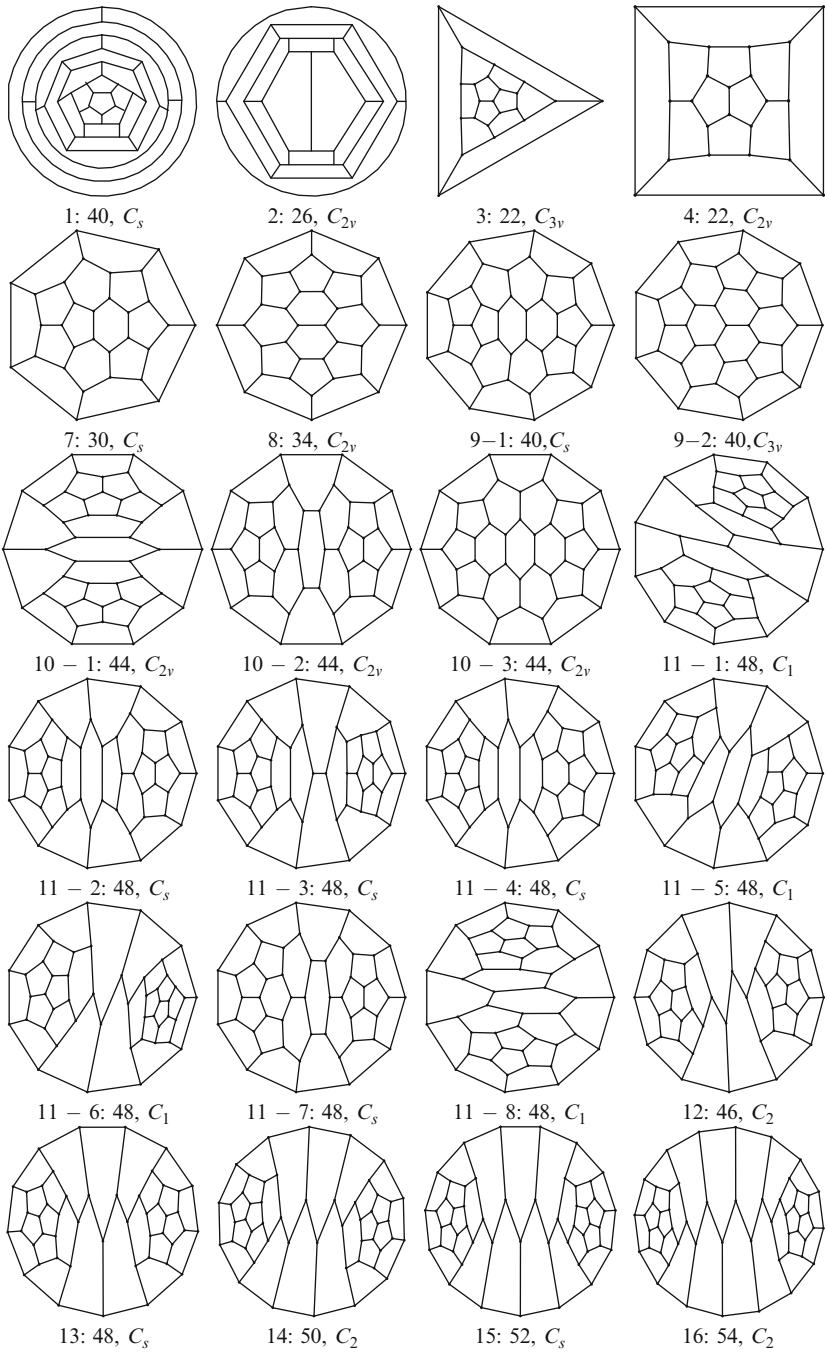

Fig. 13.18 Minimal fullerene c-disks with $1 \leq c \leq 16$, $c \neq 5, 6$

One can see unique $(\{5,6\},3)$-spheres with $v = 20, 24$ as minimal fullerene c-disks with $c = 5, 6$. Clearly, the minimal fullerene 3- and 4-disks are 22-vertex spheres obtained from Dodecahedron by truncation on a vertex or an edge. As well, minimal 3- and 4-disks with symmetry C_1 and C_2, respectively, are truncations of 28-vertex (D_2) or 24-vertex $(\{5,6\},3)$-sphere on, respectively, a vertex or an edge.

Conjecture 13.1. A v-vertex fullerene c-disk with $c \geq 1$, except the cases $(c, v) = (1, 42)$, $(3, 24)$, and $(5, 22)$, exists if and only if v is even and $v \geq 2(p(c) + c + 5)$. Here $p(c)$ denotes the minimal possible number of 6-gons (other than c-gon if $c = 6$) in a fullerene c-disk.

We have $p(1) = 14$, $p(2) = 6$, $p(3) = 3$, $p(4) = 2$, $p(5) = 0$, $p(6) = 1$, $p(7) = 3$, $p(8) = 4$, $p(9) = 6$, $p(10) = 7$, $p(11) = 8$, and $p(c) = 6$ for $c \geq 12$. For $2 \leq c \leq 20$, the conjecture was checked by computation and all minimal fullerene c-disks (2, 3, 8 for $c = 9, 10, 11$ and unique otherwise) are listed; see Fig. 13.18 for $1 \leq c \leq 16$, $c \neq 5, 6$.

The *c-pentatube* is $2(c+11)$-vertex fullerene c-disk of symmetry C_2, C_s for even, odd c, respectively. Its 5-gons are organized in two $(5,3)$-polycycles B_2 separated by Pen_{c-12}, and its six 6-gons are organized into two 3-rings each shielding a B_2 from Pen_{c-12}. The c-pentatube is unique minimal for $12 \leq c \leq 20$; we expect that it remains so for any $c \geq 12$. Note that for $c \geq 3$, we consider only 3-connected c-disks. In fact, any minimal c-disk with $3 \leq c \leq 10$ is 3-connected. But, for example, there are, among only 2-connected ones, two more minimal 11-disks and, for $c = 12, 13$, smaller 2-connected c-disks. The edges of c-pentatube with $c \geq 12$ and not divisible by 5 are doubly covered by simple zigzags Z_1, Z_2, Z_3, Z_4 of length 10 and one zigzag Z of length $6(c-1)+32$ having exactly $3(c-1)$ edges of self-intersection. Z intersects every Z_i in 8 edges. The intersections $|Z_i \cap Z_j|$ are 2 for $(i, j) = (1, 2), (3, 4)$ and 0 for other $1 \leq i < j \leq 4$.

Theorem 13.8. *The possible symmetry groups of a $(\{5,6,c\},3)$-sphere with $p_c = 1$ and $c \neq 5, 6$ are C_n, C_{nv} with $n \in \{1, 2, 3, 5, 6\}$ and n dividing c.*

In fact, any symmetry of a $(\{5,6,c\},3)$-sphere should stabilize unique c-gon. So, the possible groups are only C_n and C_{nv} with n $(1 \leq n \leq c)$ dividing c. Moreover, $n \in \{1, 2, 3, 5, 6\}$ since, on the axis it has to pass by a vertex, edge, or face. Note that $C_s = C_{1v}$. □

Cases (xi) and (xvi) in Deza et al. (2009) show that the possible symmetry groups (minimal v) of a fullerene c-disk with $c = 3$ and $c = 4$ are C_1 (30), C_s (26), C_3 (34), C_{3v} (22) and C_1 (28), C_s (24), C_2 (26) and C_{2v} (22). Minimal examples are given there. For $c = 1, 2, 7, 8, 9$, see minimal examples on Fig. 13.19. For $c = 2$, those examples are all of type $(6, 6)$ and coming from one-edge truncation of $(\{5,6\},3)$-spheres with, respectively, 28 (D_2), 26, 24, and 20 vertices.

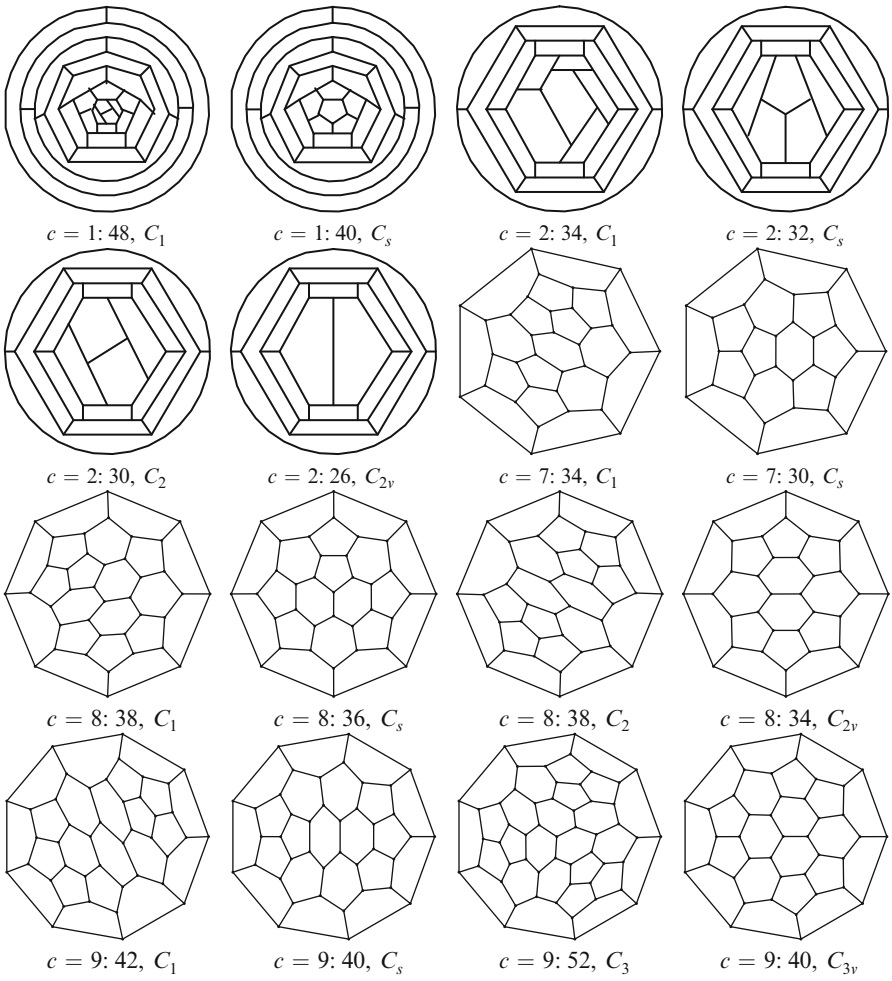

Fig. 13.19 Minimal fullerene c-disks for each possible group with $c = 1, 2, 7, 8$, and 9

References

Brinkmann G, McKay BD (2007) Fast generation of planar graphs. MATCH Commun Math Comput Chem 58:333–367

Brinkmann G, Delgado-Friedrichs O, Dress A, Harmuth T (1997) CaGe – a virtual environment for studying some special classes of large molecules. MATCH Commun Math Comput Chem 36:233–237

Brinkmann G, Harmuth T, Heidemeier O (2003) The construction of cubic and quartic planar maps with prescribed face degrees. Discrete Appl Math 128:541–554

Deza M, Dutour Sikirić M (2005) Zigzag structure of simple two-faced polyhedra. Comb Probab Comput 14:31–57

Deza M, Dutour Sikirić M (2008) Geometry of chemical graphs: polycycles and two-faced maps. Cambridge University Press, Cambridge
Deza M, Dutour Sikirić M (2012) Zigzag and central circuit structure of $(\{1, 2, 3\}, 6)$-spheres. Taiwan J Math 16:913–940
Deza M, Shtogrin M (2003) Octahedrites. Symmetry Cult Sci 11:27–64
Deza M, Huang T, Lih KW (2002) Central circuit coverings of octahedrites and medial polyhedra. J Math Res Expos 22:49–66
Deza M, Dutour Sikirić M, Shtogrin M (2003) 4-valent plane graphs with 2-, 3- and 4-gonal faces. In: Li KW (ed) Advances in algebra and related topics. World Scientific, Singapore, pp 73–97
Deza M, Dutour Sikirić M, Fowler P (2009) The symmetries of cubic polyhedral graphs with face size no larger than 6. MATCH Commun Math Comput Chem 61:589–602
Dutour Sikirić M, Deza M (2004) Goldberg-Coxeter construction for 3- or 4-valent plane graphs. Electron J Comb 11:R20
Dutour Sikirić M, Deza M (2011) 4-regular and self-dual analogs of fullerenes. In: Graovac A (ed) Mathematics and topology of fullerenes. Springer, Berlin, pp 103–116
Higuchi Y (2001) Combinatorial curvature for planar graphs. J Graph Theory 38:220–229
Thurston WP (1998) Shapes of polyhedra and triangulations of the sphere. Geom Topol Monogr 1:511–549

Chapter 14
Toward Molecules with Nonstandard Symmetry

Vladimir R. Rosenfeld

Abstract An algebraic approach to the complex problem of designing molecules with nonstandard (noncrystallographic) symmetry is proposed. Since the five-fold, seven-fold, and higher rotational symmetry are not allowed by classical crystallography, one may use some higher dimensional spaces to construct the cells for structures which are not realizable in the 3-dimensional Euclidean space. This approach makes use of the group theory, *geometric, topological, or combinatorial, symmetry, cyclic boundary conditions, k-circulant* graph, *n-cube, partial cube, etc*.. It is shown that planar projections of higher dimensional embeddings can be used to draw any partial cube, in particular, with the generalized diamond structures, the hexagonal tiling, and the diamond crystal, inclusive. Moreover, noncrystal molecules may be constructed using any graph whose automorphism group does not necessary obey the conditions imposed on the automorphism group of a k-circulant, and such a group may induce more than one orbit of atoms (orbitals).

14.1 Introduction

The problem of synthesis of novel molecules having "unusual" properties deals with many aspects, among which two are the most fundamental – namely, the topology Simmons and Maggio (1981), Paquette and Vazeux (1981), Walba et al. (1982, 1992), Merrifield and Simmons (1989), Flapan (2000), Diudea et al. (2001), Rücker and Meringer (2002), Yang et al. (2010), Jablan et al. (2011), Sciriha and Fiorini

V.R. Rosenfeld (✉)
Mathematical Chemistry Group, Department of Marine Sciences, Texas A&M University at Galveston, Galveston, TX 77553–1675, USA

Instituto de Ciencias Matematicas (ICMAT) CSIC, C/ Nicolas Cabrera, n 13–15, Campus Cantoblanco UAM, Madrid 28049, Spain
e-mail: rosenfev@tamug.edu; vladimir_rosenfeld@yahoo.com

M.V. Diudea and C.L. Nagy (eds.), *Diamond and Related Nanostructures*, Carbon Materials: Chemistry and Physics 6, DOI 10.1007/978-94-007-6371-5_14,

(1997), Rosenfeld (2007) and symmetry Rosenfeld (2007, 1999). Here, the topology means in a wider context not only how atoms are connected by chemical bonds therein but also how such molecules may be embedded on different surfaces and so be realized geometrically, recalling that, in general, surfaces may themselves be embedded in different ways in $\mathbb{E}^3$. This may also set forward some symmetry aspects, which is just a subject of special consideration in this text. However, we regard not only symmetry represented by the geometry of a molecule but also symmetry which cannot be realized in the usual Euclidean space $\mathbb{E}^3$ and pertains to the analytically given connectivity table (of chemical bonds) of a molecule. The respective space $\mathbb{E}^n$ has the dimensionality equal to the number n of atoms (valence orbitals) in a molecule and, for $n \geq 4$, cannot be visualized. But if we know symmetry of our space, this may be used for describing some properties of a designed molecule.

So, the title of this chapter refers to the synthesis of novel molecules having nonstandard topological symmetry group. By "nonstandard" we mean that it is none of point symmetry groups (and groups of nonrigid molecules either). In particular, there may be groups with many generators simultaneously having unusual orders, say $11, 29, 71, \ldots$. Accordingly, such groups cannot be realized as geometric symmetry groups in the Euclidean space $\mathbb{E}^3$ and may be regarded as topological symmetry groups in spaces of higher dimensions, while the geometric symmetry group of any molecule may solely be one of known point symmetry groups.

Hence, one task is to carry out a series of computations for graphs with nonstandard symmetries, in order to obtain *concrete coordinates* of atoms for those molecules which can topologically and geometrically be embedded in the diamond lattice (Balaban et al. 2007) or somehow otherwise realized in $\mathbb{E}^3$. In particular, nontraditional solutions (with different, earlier unknown, angles between chemical bonds) now attract chemists. They are trying to create supermolecules where the role of polyvalent atoms may be played by cage molecules, by dendrimers, or by artificial (customer) atoms (Rosenfeld 2007), among which may also be molecules that we are trying to design here. If such a task may be fulfilled, and the coordinates may be determined, this may catalyze the very synthesis of such molecules. But in fact, it is also a complex problem for several fields of mathematics, which may support such tedious work by helpful theorems. Herein, we specially consider some mathematical results which have been obtained in graph theory (Cvetković et al. 1980; Leighton 1983; Eppstein 2009; Eppstein et al. 2010; Sciriha and Fiorini 1997).

14.2 Preliminaries

First, we must prepare some auxiliary information.

14.2.1 Symmetry Groups of a Graph

Each square matrix $A = [a_{rs}]_{r,s=1}^{n}$ is the *adjacency matrix* of a (weighted) (di)graph G, where an entry a_{rs} ($r, s \in [1, n]$) is the weight of an arc rs emanating from vertex r and entering vertex s, the case $r = s$ corresponds to a selfloop (a degenerated arc whose endpoints coincide), and $a_{rs} = 0$ means that the respective arc does not exist in G. If A is symmetric, with $a_{rs} = a_{sr}$ for all pairs of indices r and s, G can be regarded also as an undirected graph having nonoriented edges $rs = sr$ instead of pairs of opposite arcs rs and sr. The case when all nonzero entries of A are equal to 1 corresponds to an unweighted graph G.

We need to consider several groups associated with an arbitrary graph G. First of all, the *automorphism group* Aut$G$ of G is the group of all operations ω which preserve both the adjacency and nonadjacency of all pairs of r and s of vertices in G, *i.e.*, $\omega r \sim \omega s$ iff $r \sim s$ and, alternatively, $\omega r \nsim \omega s$ iff $r \nsim s$. Since G can be given by its adjacency (or connectivity) matrix A, Aut$G$ is also called the *topological symmetry group* of G. Aut$G$ is practically represented by the permutation group $P(G)$ acting on the vertex set $V(G)$ (and also edge set $E(G)$) of G; for this reason, we identify the two groups below (Aut$G = P(G)$) and also write $\omega \in P(G)$ for automorphisms. Due to the permutational nature of its elements, which do not reflect the connectivity table of G, $P(G)$ is also independently called the *combinatorial symmetry group* of G. Though in part of applications, using $P(G)$ as a set of permutations is most convenient (say, for constructing orbits of P on the vertex set V), they use also the matrix representation $M(P)$ of $P(G)$ by $n \times n$ permutation $(0, 1)$-matrices (having exactly one 1 in each row and each column). In particular, the last allows to give another equivalent characterization of an automorphism $\omega \in$ Aut$G$ using its matrix representation $M_\omega \in M(G)$:

$$M_\omega A = A M_\omega \Longleftrightarrow M_\omega A M_\omega^{-1} = M_\omega A M_\omega^{T} = A \quad (\forall \omega \in \mathrm{Aut}G), \tag{14.1}$$

where M^T is the transposed of M and the last equality is regarded here as the overall one (see below). In other words, $M[P(G)]$ is the maximum subgroup of the group $M(S_n)$ of all $n \times n$ permutation matrices (representing the symmetric group S_n; $|S_n| = n!$) whose elements commute with the adjacency matrix A, as in Eq. (14.1). Lastly, G may have in general more than one geometric embedding (representation) in the Euclidean space $\mathbb{E}^n$ or any other: each representation may have its own *geometric symmetry group* $\Gamma(G)$ which may isomorphically be a not necessarily proper subgroup of Aut$G$. With some abuse of notation, we use here $\Gamma(G) \subseteq$ Aut$G$ and similar expressions to indicate such an isomorphic inclusion.

Since automorphisms are not the only possible combinatorial actions which can be performed on a graph in a general context, one may also consider *endomorphisms*. See a special subsection below.

14.2.2 Endomorphisms of a Graph

In addition to the automorphism group Aut$G$ of a graph G, one may similarly consider in a more general context the *monoid* End$G$ *of* (certain) *endomorphisms* of G Simmons and Maggio (1981), with substituting the word "monoid" for the "group" above – however, with two necessary reservations. First, not every endomorphism preserves both the adjacency and nonadjacency of vertices – just the *strict endomorphisms* preserve the two at once. Second, only strict endomorphisms can conveniently be characterized using endomorphism $(0, 1)$-matrix representations (having exactly one 1 in each row but not necessarily in each column). Namely, for the $(0, 1)$-matrix representation M_ε of a strict endomorphism $\varepsilon \in \overline{\text{End}}G$ (*monoid of strict endomorphisms*), we have (Rosenfeld 1999)

$$M_\varepsilon A M_\varepsilon^T = A \quad (\forall \varepsilon \in \overline{\text{End}}G), \tag{14.2}$$

which is poorer than the entire suite of equalities in Eq. (14.1) for automorphisms, since it adopts here only its last overall statement. But besides Eq. (14.2), for every *idempotent* ε ($\varepsilon^2 = \varepsilon$) of $\varepsilon \in \overline{\text{End}}G$, we can write (Rosenfeld 1999)

$$M_\varepsilon A = A M_\varepsilon^T = A \quad \left(\varepsilon \in \text{Id} := \left\{\varepsilon \in \overline{\text{End}}G) \mid \varepsilon = \varepsilon^2\right\}\right), \tag{14.3}$$

which is more important for $\overline{\text{End}}G$ than for Aut$G$, having a unit element as the only idempotent.

14.2.3 What Is Crucial

Consider insertion of t vertices of degree 2 in an edge to obtain a path of length $t + 1$ (with $t + 2$ vertices) therefrom. A chemical analog may be represented by the chain $\equiv \text{C} - (\text{S})_\text{t} - \text{C} \equiv$ of atoms from $\equiv \text{C} - \text{C} \equiv$ (Diudea et al. 2001; Sciriha and Fiorini 1997; Rosenfeld 2007). Graphs G_1 and G_2 are *homeomorphic* (see Diudea et al. 2001; Sciriha and Fiorini 1997; Rosenfeld 2007), if these can be produced from a third graph G_3 using such insertion of vertices of valency 2 into edges (in general, the role of G_3 may also be played by either of the two graphs).

Here, we specially note that the replacement of each edge, in G, with a simple path of the same length preserves the automorphism group (AutG^* = Aut$G$, where G^* is the homeomorphic graph obtained from G). For a chemist, this gives already a chance to try synthesize the molecule modeled by G^*, if doing directly with G fails. In a wider chemical context, one may say of homeomorphic molecules which have chains of atoms (like $-(\text{CH}_2)_\text{t}-$) substituted for ordinary C – C bonds or any similar cases (Diudea et al. 2001; Sciriha and Fiorini 1997; Rosenfeld 2007).

Moreover, recalling crystals in nature, it is also intriguing to construct larger symmetric graphs for which a given symmetric graph G is a graph divisor (Balaban

et al. 2007; see below) or, in terms of crystal physics, a *unit cell with cyclic boundary conditions*. The following subsection describes this in more detail.

14.2.4 A Graphic Crystal

As an instance, consider the simple cubic lattice $\mathcal{L}$ partitioned into cubic unit cells $\mathcal{L}_{hkl}$, where h, k, l are integers. Let each cell contain strictly inside (without points on the facets of cells) an isomorphic copy of a simple graph H. We add one essential requirement that our construction should obey the infinite translational symmetry of the host lattice $\mathcal{L}$. Accordingly, translation of an arbitrary unit cell $\mathcal{L}_{h_1k_1l_1}$ into another one $\mathcal{L}_{h_2k_2l_2}$ should induce the isomorphism of respective copies H_1 and H_2, of H, placed inside these cells, as well as automorphism of the entire construction. We call such a construction $\mathcal{C}$ a *graphic crystal*, since it is an abstract one consisting only of points and lines, rather than of real atoms linked with chemical bonds.

Numerate all vertices of $\mathcal{C}$ so that each subset of translationally equivalent points in strictly different unit cells is numbered with the same number s ($s \in [1, |H|]$). Consider the unit cell $\mathcal{L}_{000}$ together with six unit cells having common facets with it: $\mathcal{L}_{100}$, $\mathcal{L}_{010}$, $\mathcal{L}_{001}$, $\mathcal{L}_{\bar{1}00}$, $\mathcal{L}_{0\bar{1}0}$, $\mathcal{L}_{00\bar{1}}$, where $\bar{1} := -1$, and six is the (minimum) number of cells covering all facets of $\mathcal{L}_{000}$. Now, take a free isomorphic copy of H and connect an arbitrary pair of vertices u and v, therein, with μ (new) edges iff exactly μ times the vertex u pertaining $\mathcal{L}_{000}$ is connected with (copies of) vertex v in μ adjacent cells. Apparently, $\mu \in [0, 6]$ and the case $u = v$ correspond to a selfloop. Having performed this procedure for all pairs of u and v and for all six neighborhoods of $\mathcal{L}_{000}$, we obtain a derivative multigraph ("multi" ≤ 7) $\hat{H}$ which is just the *divisor of the graph* $\mathcal{C}$ (Cvetković et al. 1980), or the graph of its unit cell considered with the cyclic boundary conditions, mentioned above. This is a familiar trick, say, in the tight binding method (in quantum physics of crystals), where, in general, weighted graphs may be considered in a similar way, using summation of weights of equivalent arcs instead of merely calculating the number thereof. In particular, in quantum physics, of a special use is the phase weighting of edges, as in Klein and Rosenfeld (2011c,b).

Here, recall that the roots of the characteristic polynomial $P[A(J), x]$ of the (weighted) adjacency matrix $A(J)$ of an arbitrary graph J are also called the *spectrum of a graph* J (Cvetković et al. 1980; Sciriha and Fiorini 1997), which takes into account multiplicities of all its roots, or *eigenvalues*.

One property of the divisor $\hat{H}$ is that its spectrum includes in the spectrum of the graph $\mathcal{C}$ (*i.e.*, the entire graphic crystal). The spectra of graphs are beyond the scope of our chapter, but we want to emphasize that in the case when $\hat{H} = G$, where G is a simple graph having a "nonstandard" symmetry, our graphic crystal $\mathcal{C}$ may have some remarkable spectral properties which have not been found with the "standard" symmetry (of a unit cell) of the usual crystals.

Here, it is needed to note that the process of transforming the graph H into the multigraph $\hat{H}$ may be considered in the opposite direction. That is, one might

remove certain edges (and/or selfloops) in $\hat{H}$ and utilize "liberated valencies" for rationally connecting many copies of H (which is now produced from $\hat{H}$, rather than given ready). Similarly, we may use G (instead of $\hat{H}$). In general, one may produce many different graphic crystals from one graph G, but the spectrum of each of them will include the spectrum of G.

Note that the task to architect a graphic crystal $\mathcal{C}$ may in some (or many) cases be easier than that of creating a molecule with a graph homeomorphic to G, because, in the former case, we remove some interior edges and create respective exterior ones instead. This may decrease the congestion and strain in real molecular systems to which our graphic crystal serves as a topological template. Moreover, this may facilitate solving concomitant group-theoretical problems.

Here, one aspect should be specially emphasized. Namely, speaking of a graphic crystal, we are certainly targeted at solving some practical problems and tacitly mean that we would like to build a k-dimensional object, with $k \leq 3$. From this point of view, not every graph G may be used as a graph of a unit cell with cyclic boundary conditions, say in the case of the Euclidean space $\mathbb{E}^3$. Regrettably, not only general methods of embedding graphs on multidimensional grids are not known – the very criteria of such embeddability have not yet been found. However, there exist certain studied cases, when such criteria have been determined. In particular, we consider the so-called multidimensional circulants and some other instances, below.

14.3 The Main Part

Recall that Aut$G$ is the automorphism group of a graph $G = (V; E)$, where V and E are the vertex set and the edge set of G, respectively; $|V| = n$ and $|E| = m$. A graph G is called *vertex-transitive* (see Balaban et al. 2007; Cvetković et al. 1980) if $\forall u, v \in V\ \exists \alpha \in \text{Aut}G$, such that $\alpha u = v$. If a subgroup $R \subseteq \text{Aut}G$ acts transitively on the vertex set $|V(G)|$, it is similarly called *transitive*. If, in addition to being transitive, $|R| = |V(G)|$, then R is a *regular subgroup*. It is worth noting that each element $\omega \in R$ of order s (being the minimum number such that $\omega^s = e$) induces a permutation, of V, which has all (n/s) cycles of length s $(s \mid n)$.

14.3.1 k-Circulants

A *multidimensional circulant* (Leighton 1983), or *k-circulant* ($k \geq 1$), is a vertex-transitive graph G whose vertices can be labeled so that there exist positive integers $k, a_1, a_2, \ldots, a_k$ and a set $S \subset \mathbb{Z}^k$ such that

$$V(G) = \{(i_1, i_2, \ldots, i_k) \mid 0 \leq i_l \leq a_l \quad \text{for} \quad 1 \leq l \leq k\} \quad \text{and}$$
$$E(G) = \{\{(i_1, i_2, \ldots, i_k),\ (j_1, j_2, \ldots, j_k)\} \mid ((i_1 - j_1) \bmod(a_1), \ldots, (i_k - j_k) \bmod(a_k)) \in S\}, \tag{14.4}$$

where the second row is tantamount to determining a unit cell with cyclic boundary conditions, where all (differences of) coordinates are considered modulo $a_1, a_2, \ldots, a_k$, each one associated with its concrete coordinate (see Fig. 3 in Leighton 1983). Here, we note that k-circulants are *Cartesian products* of one-circulants; moreover, instances of such graphs are toroidal *dinormal graphs* considered in Klein and Rosenfeld (2011a).

Leighton (1983) proved remarkable theorems about one- and k-circulants, which are relevant to the topic of graphic crystals. For example, there was given the following group-theoretical characterization:

Theorem 14.1. *A graph G is a k-circulant iff* Aut$G$ *contains a regular abelian (commutative) subgroup.*

Recall that a *regular subgroup* $R \subseteq \mathrm{Aut}G$ acts faithfully on the vertex set $V(G)$; moreover, each automorphism $\omega \in R$ is represented by a permutation, all of whose cycles have the same length l (where l divides $|V|$). If we found a regular abelian subgroup $R \subseteq \mathrm{Aut}G$ and, thereby, established that G is a circulant, we need yet to make sure that we may embed G, say in the 3-dimensional integer grid. A simple criterion of such embeddability is given by the next theorem (Leighton 1983):

Theorem 14.2. *If G is a k-circulant with $n = \prod_{i=1}^{t} p_i^{b_i}$ nodes (primes $p_i \neq p_j$ for $i \neq j$), then G has dimension k for some $k \leq \max_{1 \leq i \leq t}(b_j)$.*

In particular, for n-cubes, Leighton (1983) proved:

Theorem 14.3. *The n-cube is an $\lfloor (n+1)/2 \rfloor$-dimensional circulant.*

We specially remind that all these theorems are useful for constructing graphic crystals. For "noncrystals," there are the results of other authors (Eppstein 2009; Eppstein et al. 2010; see below).

14.3.2 Isometric Diamond Subgraphs

In an *isometric* embedding, the unweighted distance $d(u, v)$ between any two vertices u and v in the graph equals the graph-theoretical distance L_1 of their placements in the grid (Eppstein 2009) (this distance is equal to the number of edges in the shortest simple path between u and v). An isometric embedding must be an induced subgraph, but not all induced subgraphs are isometric. Isometric square grid embedding may be directly used as graph drawings, while planar projections of higher dimensional embeddings can be used to draw any *partial cube* (being an isometric subgraph of a hypercube) (Eppstein 2009), a class of graphs with many applications. As a specific case, one may consider the *generalized diamond structures*, which include the hexagonal tiling and the 3-dimensional molecular structure of the diamond crystal.

The 3-dimensional points $\{(x, y, z) \mid x + y + z \in \{0, 1\}\}$, with edges connecting points at unit distance, form a 3-regular infinite graph (Fig. 1, left, in Eppstein 2009)

in which every vertex has three perpendicular edges (Eppstein 2009). Its projection onto the plane $x + y + z = 0$ is a hexagonal tiling (Fig. 1, right, in Eppstein 2009; see an alternative consideration in Balaban et al. 2007). In one higher dimension, the points $\{(w, x, y, z) \mid w + x + y + z \in \{0, 1\}\}$, with edges connecting points at unit distance, projected into the 3-dimensional subspace $w + x + y + z = 0$, form an infinite 4-regular graph embedded in space with all edges equally long and forming equal angles at every vertex (Fig. 2 in Eppstein 2009). This pattern of point placements and edges is realized physically by the crystal structure of diamonds (Balaban et al. 2007) and is often called the *diamond lattice*, although it is not a lattice in the mathematical definition of the word – it is the *diamond graph* (Eppstein 2009, see Balaban et al. 2007).

Analogously (Eppstein 2009), define a k-dimensional *generalized diamond graph* as follows. Form the set of $(k + 1)$-dimensional integer points such that the sum of coordinates is either zero or one, connect pairs of points at unit distance, and project this graph onto the hyperplane in which coordinate sum of any point is zero. The result is a highly symmetric infinite $(k + 1)$-regular graph embedded in k-dimensional space. The generalized diamond graph is an isometric subset of the $(k + 1)$-dimensional integer lattice, so any finite isometric subgraph of the generalized diamond graph is a partial cube. However, not every partial cube is an isometric subgraph of a generalized diamond graph: for instance, squares, cubes, or hypercubes are not, because these graphs contain four cycles, whereas the generalized diamonds do not.

A *cut* in a graph is a partition of the vertices into two subsets C and $V \setminus C$; an edge *spans* the cut if it has one endpoint in C and one endpoint in $V \setminus C$. If $G = (U, V; E)$ is a bipartite graph, we say that a cut $(C, (U \cup V) \setminus C)$ is *coherent* if, for every edge (u, v) that spans the cut (with $u \in U$ and $v \in V$), u belongs to C and v belongs to $(U \cup V) \setminus C$. That is, if we color the vertices black and white, all black endpoints of edges spanning the cut are on one side of a cut, and all white endpoints are on the other side (Eppstein 2009).

The *Djoković-Winkler relation* of a partial cube G determines an important family of cuts. Define a relation $\sim$ on edges of G by $(p, q) \sim (r, s)$ iff $d(p, r) + d(p, s) = d(q, r) + d(q, s)$; then, G is a partial cube iff it is bipartite and $\sim$ is an equivalence relation (see Eppstein 2009). A different version of the definition is given by Wikipedia. Namely, two edges (p, q) and (r, s) are defined to be in the relation $\overset{\diamond}{\sim}$ ($(p, q) \overset{\diamond}{\sim} (r, s)$) if $d(p, r) + d(q, s) \neq d(p, s) + d(q, r)$. The relation is reflexive and symmetric, but in general it is not transitive, *i.e.*, it is not an equivalence relation (which corrects the above assertion from Eppstein (2009)).

Each equivalence class of G spans a cut $(C, V \setminus C)$; C and $V \setminus C$ are called *semicubes* (Eppstein 2009). One may embed G into a hypercube by choosing one coordinate per Djoković-Winkler equivalence class, set to 0 within C and to 1 within $V \setminus C$. Since this embedding is determined from the distances in G, the isometric embedding of G into a hypercube is determined uniquely up to the symmetries of the cube. The *Desargues graph* is considered as an example in Fig. 3 of Eppstein (2009). But we cite below the first theorem proved by Eppstein (2009). Namely:

Theorem 14.4. *A partial cube is an isometric subgraph of a generalized diamond graph iff all cuts formed by Djoković-Winkler equivalence classes are coherent.*

For example, the Desargues graph is an isometric subgraph of a 5-dimensional generalized diamond.

Along with the *lattice dimension* k (see the subsection devoted to multidimensional circulants above), there is also the *diamond dimension* k_d of a graph G, which is the minimum dimension of a generalized diamond graph into which G may be isometrically embedded. The diamond dimension may be as low as the lattice dimension, or (*e.g.*, in the case of a path) as large as twice the lattice dimension ($k \leq k_d \leq 2k$).

In some perspective, the following part of our minisurvey may also be of synthetical chemistry interest.

14.3.3 The Optimal Angular Resolution of Graph Embeddings

Now, it is needed to cite some results from the collaborative paper by Eppstein et al. (2010). In particular, they proved (for graphs with chemical valencies):

Theorem 14.5. *Any graph G with maximum vertex degree* 4 *can be drawn in a* 3*-dimensional grid of size* $(16n/3) \times (16n/3) \times 16n$ *with angular resolution* 109.5°*, three bends per edge and no crossings.*

Eppstein et al. (2010) mean by *bends* geometric bends of lines displaying edges of an embedded graph. They consider just a few possible angles of edge bends (such as 109.5° and 120°), which they call the *angular resolution*. For a chemist, who wants to see a certain chemical relevance, such angles are just respectively classical angles of sp^2 and sp^3 hybridization of chemical bonds (say, between C atoms). Accordingly, bends may correspond to inserted divalent atoms (radicals) – exactly as this was discussed in Sect. 14.2.3 telling about the homeomorphism of graphs.

Recall that every abstract group can be represented as the automorphism group of some cubic graph, which is of paramount importance to chemistry (Rosenfeld 2007) and for this chapter. Therefore, very important is the next theorem of Eppstein et al. (2010):

Theorem 14.6. *Amy graph G of degree* 3 *has a drawing with* 120° *angular resolution and at most two bends per edge.*

In a similar spirit, they (Eppstein et al. 2010) proved also:

Theorem 14.7. *Any graph G with maximum vertex degree* 3 *can be drawn in a* 3*-dimensional grid of size* $O(n^3) \times O(n^3) \times O(n^3)$ *with angular resolution* 120°*, three bends per edge and no edge crossings.*

But we recommend the reader to see original papers (Leighton 1983; Eppstein 2009; Eppstein et al. 2010) for the other results and bibliography. Also, Lord et al. (2006) may be recommended for the further reading on this subject, in a wider context of materials science.

14.4 Conclusions

k-Circulants and not vertex-transitive graphs with commutative automorphism groups may play a role of a unit cell with cyclic boundary conditions of some real and/or graphic crystal (in general, more than one for a fixed unit cell) having one or several sublattices, respectively. Vertex-transitive graphs with a noncommutative automorphism group (*i.e.*, not k-circulants) are also of interest as potential homeomorphic models of "noncrystal" molecules. "Noncrystal" molecules may be constructed using any graph whose automorphism group does not obey the conditions imposed on the automorphism group of a k-circulant, and such a group may induce more than one orbit of atoms (orbitals). Chemical objects may homeomorphically represent all potential symmetries already observed in nature or those which are so far only "promised" by abstract automorphism groups (of graphs, etc.) (Rosenfeld 2007). A real task of chemists is to practically synthesize such molecules.

Acknowledgements We thank Prof. Douglas J. Klein (Galveston) for discussion on the subject of this chapter. Support (through grant BD-0894) from the Welch Foundation of Houston, Texas, is acknowledged.

References

Balaban AT, Klein DJ, Dahl JE, Carlson RMK (2007) Molecular descriptors for natural diamondoid hydrocarbons and quantitative structure-property relationships for their chromatographic data. Open Org Chem J 1:13–31

Cvetković DM, Doob M, Sachs H (1980) Spectra of graphs: theory and application. Academic, Berlin

Diudea MV, Gutman I, Jantschi L (2001) Molecular topology. Nova Science Publishers, New York, 332 pp

Eppstein D (2009) Isometric diamond subgraphs. In: Tollis IG, Patrignani M (eds) Proceedings of the 16th international symposium on graph drawing (GD 2008), LNCS 5417. Springer, Heidelberg, pp 384–389

Eppstein D, Löffler M, Mumford E, Nöllenburg M (2010) Optimal 3D angular resolution for low-degree graphs. arXiv:1009.0045v1 [cs.CG], 31 Aug 2010

Flapan E (2000) When topology meets chemistry: a look at molecular chemistry. Cambridge University Press, Cambridge

Jablan S, Radović L, Sazdanović R (2011) Nonplanar graphs derived from Gauss codes of virtual knots and links. J Math Chem 49:2250–2267

Klein DJ, Rosenfeld VR (2011a) Dinormal graphs. J Math Chem 49(7):1256–1262

Klein DJ, Rosenfeld VR (2011b) Phased cycles. J Math Chem 49(7):1245–1255
Klein DJ, Rosenfeld VR (2011c) Phased graphs and graph energies. J Math Chem 49(7): 1238–1244
Leighton FT (1983) Circulants and the characterization of vertex-transitive graphs. J Res Natl Bur Stand 88(6):395–402
Lord EA, Mackay AL, Ranganathan S (2006) Geometries for new materials. Cambridge University Press, Cambridge
Merrifield RE, Simmons HE (1989) Topological methods in chemistry. Wiley, New York
Paquette LA, Vazeux M (1981) Threefold transannular epoxide cyclization synthesis of a heterocyclic C17-hexaquinane. Tetrahedron Lett 22:291–294
Rosenfeld VR (1999) Endomorphisms of a weighted molecular graph and its spectrum. MATCH Commun Math Comput Chem 40:203–214
Rosenfeld VR (2007) On mathematical engineering and design of novel molecules for nanotechnological applications – review. Sci Isr Technol Adv 9(1):56–65
Rücker C, Meringer M (2002) How many organic compounds are graph-theoretically nonplanar? MATCH Commun Math Comput Chem 45:153–172
Sciriha I, Fiorini S (1997) On the characteristic polynomial of homeomorphic images of a graph. Discrete Math 174:293–308
Simmons HE, Maggio JE (1981) Synthesis of the first topologically nonplanar molecule. Tetrahedron Lett 22:287–290
Walba DM, Richards R, Haltiwanger RC (1982) Total synthesis of the first molecular Möbius strip. J Am Chem Soc 104:3219–3221
Walba DM, Zheng QY, Schilling K (1992) Topological stereochemistry. 8. Experimental studies on the hook and ladder approach to molecular knots: synthesis of a topologically chiral cyclicized hook and ladder. J Am Chem Soc 114:6259–6260
Yang W, Zhang F, Klein DJ (2010) Benzenoid links. J Math Chem 47:457–476

Chapter 15
Carbon Networks in the Solid State: A Setup Test for Computational Plane-Wave Studies of Mechanical and Electronic Properties

Jarosław J. Panek and Aneta Jezierska-Mazzarello

Abstract Computational studies of carbon networks, from simple structures (diamond, graphite) to carbon nanotubes, are usually carried out within solid-state physics frameworks. The method of choice is density functional theory coupled with periodic orbitals: plane waves, augmented plane waves, and periodicized Gaussian functions. This chapter recapitulates available approaches and describes a test of a computational setup for further use in the ab initio molecular dynamics studies. Two DFT functionals (BLYP, PBE) coupled with the DFT-D2 dispersion corrections are tested on graphite, diamond, and bct C4 networks. Convergence of energy values with respect to the supercell size and plane-wave energy cutoff, as well as optimization of structural parameters, indicates that the PBE-D2 approach is a reasonable choice for future investigations.

15.1 Introduction

Computational studies of condensed matter are nowadays dominated by the density functional theory, DFT (Hohenberg and Kohn 1964). The role of DFT in contemporary computational physics and chemistry was highlighted by the Nobel Prize awarded to Walter Kohn in 1998 (together with John A. Pople, a founding father of modern ab initio methods of chemistry). There are numerous reasons for the popularity of DFT in condensed-phase studies. First, its use of electron density as a fundamental property leads to competitive cost of calculations and good scaling with system size. Indeed, there are algorithms with linear scaling in the limit of large systems, implemented recently even for hybrid functionals (Rudberg et al. 2011).

J.J. Panek (✉) • A. Jezierska-Mazzarello
Faculty of Chemistry, University of Wrocław, ul. F. Joliot-Curie 14, 50-383 Wrocław, Poland
e-mail: jarek@elrond.chem.uni.wroc.pl

M.V. Diudea and C.L. Nagy (eds.), *Diamond and Related Nanostructures*,
Carbon Materials: Chemistry and Physics 6, DOI 10.1007/978-94-007-6371-5_15,

Second, the use of post-Hartree-Fock ab initio schemes in condensed phases is limited because of their unfavorable scaling and cost of the orbital transformation. Recently a robust implementation of the perturbative MP2 method for periodic systems was presented and successfully tested for typical semiconductors and insulators (Grüneis et al. 2010). However, for some years, the role of DFT as the method of choice for condensed-phase calculations is not endangered. Still, there are two drawbacks of DFT which limit its usefulness: lack of proper description of weak (dispersive) interactions (i.e., Van der Waals forces) and lack of systematic path to new, improved exchange-correlation functionals. Both of these reasons give rise to intensive research; recently, there appeared successful schemes of introducing dispersion corrections into the DFT framework (Wu et al. 2001). The most simple conceptually are empirical corrections of Grimme: DFT-D2 (Grimme 2006) and DFT-D3 (Grimme et al. 2011).

Static models of condensed phases are developed to calculate their electronic and mechanical properties: electronic and thermal conductivity, bulk moduli, and band structure. Recent advances in computational methods allow increasingly accurate predictions of crystal structure (Oganov 2010). However, in many cases, the dynamical nature of a system or a process must be taken into account. Molecular dynamics with classical force fields is not always a good choice, especially if we are interested in electronic structure of a material or transition metal chemistry/physics where parameterization of a force field is difficult, if at all possible. In such cases, one reverts to ab initio molecular dynamics (MD) schemes. Born-Oppenheimer MD requires complete solution of the DFT Kohn-Sham equations at each time step, while Car-Parrinello MD (CPMD) (Car and Parrinello 1985) uses a craftily designed Lagrangian to treat orbitals as dynamical variables. Thus, the orbitals are propagated without performing a complete diagonalization at each step, at a price of reduced time step (from 1–2 fs to ca. 0.1 fs) and introduction of some artifacts, e.g., CPMD "nuclear drag" which red shifts the vibrational frequencies of a studied system (Gaigeot and Sprik 2003). A development of new schemes combining the ideas of Car-Parrinello and Born-Oppenheimer MD (Kühne et al. 2007) will allow for sampling larger time scales, extending well beyond nanosecond range. Some current limitations of CPMD are difficulties for metallic and small gap systems (where maintaining adiabaticity of the orbital variables is problematic), lack of efficient Brillouin zone sampling (k-point integration) during the dynamics runs, and classical treatment of nuclear motions. The latter can be partially overcome by path integral techniques, which however give access rather to ensemble averages, not to the direct quantum dynamics of the system (Marx and Hutter 2000).

This chapter describes in the following sections a test of a computational setup for further use in the ab initio molecular dynamics studies of carbon networks. The validation of the computational setup should be carried out on well-known systems; diamond, graphite, and body-centered tetragonal (bct) C4 allotrope have been chosen as the objects of the study and will be described in the above-mentioned sequence. The next section gives rationale for the initial choice of computational tools and frameworks.

15.2 Computational Setup

Currently there is a large choice of software packages capable of solid-state DFT calculations. There are numerous commercial codes (e.g., VASP, Wien2K, Crystal09 – the last program is one of few solid-state codes using periodicized Gaussian basis functions) as well as freely available ones, at least to an academic user (e.g., CPMD, CP2K, Quantum ESPRESSO, SIESTA). The CPMD package version 3.15.3 (CPMD 2012) was chosen for our study for the following reasons:

- The source code is accessible and can be locally modified.
- The code uses plane waves as a basis set, which allows for excellent control of the basis set quality with only a few parameters (plane-wave kinetic energy cutoff for wave functions and densities).
- There is a large user community and contributed pseudopotential libraries.
- Dispersion corrections within DFT-D2 scheme (Grimme 2006) are implemented for the most popular functionals.

Two DFT functionals were chosen to provide electronic structure description: a Becke exchange scheme (Becke 1988) coupled with correlation formula of Lee, Yang, and Parr (Lee et al. 1988), denoted as BLYP, and a formula of Perdew, Burke, and Ernzerhof (Perdew et al. 1996), denoted as PBE. These two functionals are the most popular in the solid-state community due to overall good performance and long history of usage. Their role among the DFT functionals is highlighted by the fact that tedious parameterizations of DFT-D2 and DFT-D3 schemes were carried out for BLYP as well as PBE. Further, we chose Troullier-Martins norm-conserving pseudopotentials (Troullier and Martins 1991). They require larger plane-wave cutoff than ultrasoft Vanderbilt pseudopotentials, but we plan further studies of electronic structure of the carbon networks, including electron localization function (ELF) topological study (Silvi and Savin 1994). Due to a lack of charge conservation, Vanderbilt pseudopotentials are not optimal for electronic structure characterization. Use of the Troullier-Martins pseudopotentials defines the range of plane-wave cutoff values: from ca. 60 Ry to 100 Ry or more. Additionally, because the CPMD package does not allow for k-point integration during the MD runs, we employed the supercell approach to reduce the impact of a lack of reciprocal space sampling. We also consistently use DFT-D2 empirical dispersion corrections (Grimme 2006) throughout the study.

The course of the calculations for diamond and graphite is as follows: first, the optimal plane-wave cutoff value is determined at experimental structural parameters. Then, the convergence of energy per atom with the supercell size is checked to estimate the system size at which the effect of Brillouin zone sampling tends to be negligible. Finally, structural optimization of cell parameters is carried out using fractional cutoff energy values to ensure that the number of plane waves is the same for each cell size, which will avoid discontinuities in the energy curves. The computational study of the bct C4 network followed the same route except the structural optimization.

15.3 Results: Diamond

Diamond, with its cubic structure ($a = 3.567$ Å) and purely tetrahedral coordination of the sp^3 carbon atoms, is the best example of connection between structure and properties: its three-dimensional network of covalent bonds makes diamond very hard. However, simplicity of the structure makes diamond also an ideal testing object. We expect quite rapid convergence of the energy with increasing plane-wave cutoff. The results presented in Fig. 15.1 for the $2 \times 2 \times 2$ supercell (64 atoms) at experimental geometry show that the PBE functional has much better properties than BLYP with respect to the energy convergence – already the 85 Ry cutoff is close to the extrapolated "infinite cutoff" limit. For the BLYP functional, there is still no such convergence until 110 Ry. However, further studies of the diamond structure will use the 90 Ry cutoff as the compromise between accuracy and CPU usage. Diamond structure converges also very fast in terms of CPU steps: only $12 \div 14$ steps are necessary to achieve self-consistency.

The unit cell of diamond contains eight carbon atoms, which is too small number to prevent artifacts at the cell border. Adequate Brillouin zone sampling is necessary, but – since we prepare the computational setup for further use in Car-Parrinello MD simulations – there is no possibility of using integration over k points. We therefore

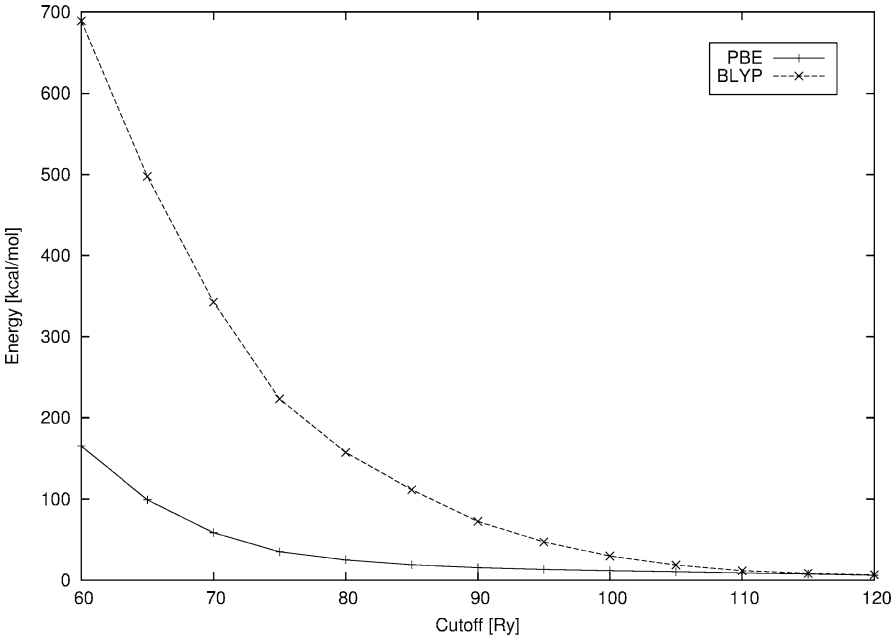

Fig. 15.1 Convergence of energies with plane-wave cutoff for diamond, $2 \times 2 \times 2$ supercell

Table 15.1 Convergence of the energy per one atom with the supercell size for diamond (experimental geometry)

Supercell	No. of atoms	E(BLYP)/1 atom [a.u.]	E(PBE)/1 atom [a.u.]
$1\times1\times1$	8	−5.58315	−5.62228
$2\times2\times2$	64	−5.65663	−5.69571
$3\times3\times3$	216	−5.66238	−5.70064
$4\times4\times4$	512	−5.66334	−5.70134

Table 15.2 Results of structural minimization of diamond lattice ($3\times3\times3$ supercell) with cell length a as the variable. Experimental value: $a = 3.567$ Å

a [Å]	E(BLYP)/1 atom [a.u.]	E(PBE)/1 atom [a.u.]
3.46	−5.66003	−5.69822
3.48	−5.66102	−5.69908
3.50	−5.66181	−5.69976
3.52	−5.66241	−5.70024
3.54	−5.66282	−5.70055
3.56	−5.66306	−5.70069
3.58	−5.66312	−5.70066
3.60	−5.66301	−5.70048
3.62	−5.66275	−5.70014
3.64	−5.66233	−5.69967
3.66	−5.66176	−5.69905

use the supercell approach to reduce this problem. The Table 15.1 provides data on the convergence of cell energy (per one atom) with respect to the cell size. The cubic structure of diamond suggests the use of proportional, cubic supercells, i.e., $2\times2\times2$, not $2\times2\times1$.

The diamond structure is rather well behaved. Already with the $3\times3\times3$ supercell ($3a = 10.18$ Å), the energy is converged to 0.001 a.u. with respect to the larger supercell (again, the PBE functional performs better than BLYP).

Choosing this $3\times3\times3$ model, we now search for the optimal lattice constant a. Such a search requires change in the cell volume, which is directly connected with number of plane waves used as a basis set. Discontinuities in the potential energy curve can arise due to uncontrolled changes of the basis set size. Avoiding this requires manual search for a cutoff value giving the same number of plane waves as in the reference state. Using the number of plane waves for the largest lattice constant used in the scan ($a = 3.66$ Å) at 90 Ry, we arrived at a range of cutoff values from 90 Ry at $a = 3.66$ Å to 100.7 Ry at $a = 3.46$ Å. This gives rise to the data grouped in Table 15.2.

It is seen that both functionals locate the optimal lattice constants within 0.01 Å of the experimental value of 3.567 Å. An interpolation suggests slightly better accuracy of PBE.

15.4 Results: Graphite

Hexagonal graphite (space group $P6_3/mmc$, $a = 2.46$ Å, $c = 6.70$ Å) is more challenging for the DFT because of interlayer stacking. This interaction is governed by weak Van der Waals forces. We will first check whether this has impact on the convergence of total energies for a chosen model ($4 \times 4 \times 1$ supercell).

The results shown in Fig. 15.2 (energies with respect to the value extrapolated to the "infinite cutoff" limit) support our earlier observations on diamond structure. The cutoff of 90 Ry seems optimal for the PBE functional, while BLYP would require larger cutoff. For consistency, we will also further use 90 Ry as the cutoff of choice. Calculations on graphite exhibit also instabilities of the SCF procedure for some cutoff values (see Fig. 15.3): 100 Ry for BLYP and 110 Ry for PBE. Generally, SCF convergence is better for the BLYP functional, but the chosen cutoff value provides good SCF convergence for both functionals.

Choosing the supercell geometry, we have now the possibility of extending the system either in the directions of the layer or in the perpendicular direction (i.e., increasing the number of layers). The results presented in Table 15.3 show that both these factors are important. The best results are achieved when the supercell has lattice constants of similar length (e.g., $4 \times 4 \times 2$, $5 \times 5 \times 2$). The $4 \times 4 \times 2$ supercell will be used further in the optimization of the interlayer spacing.

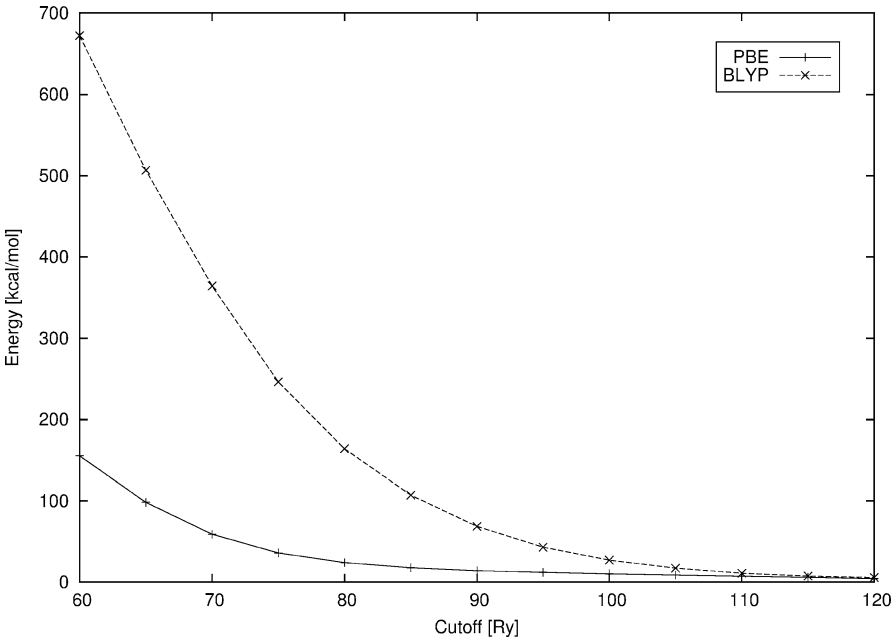

Fig. 15.2 Convergence of energies with plane-wave cutoff for graphite, $4 \times 4 \times 1$ supercell

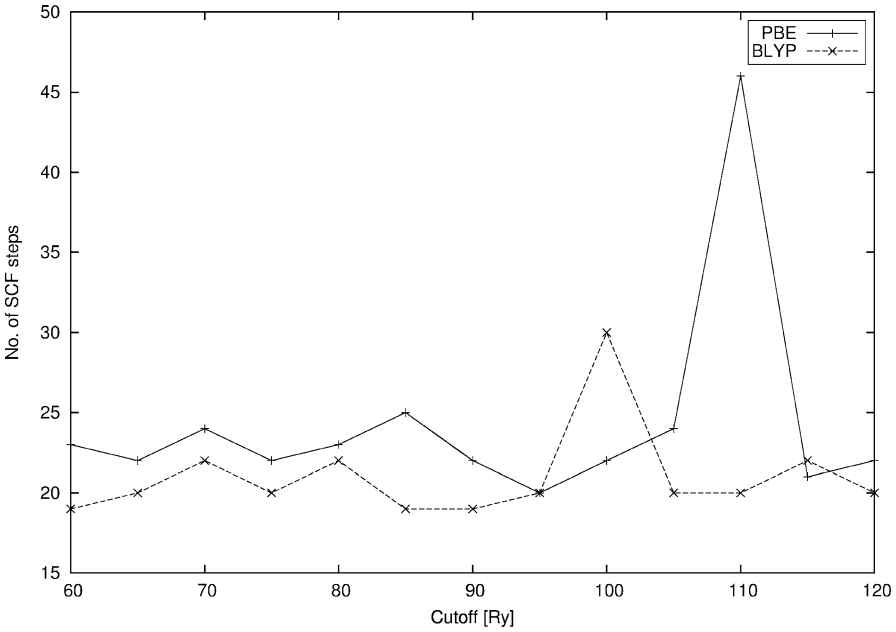

Fig. 15.3 The convergence of SCF for graphite, $4 \times 4 \times 1$ supercell

Table 15.3 Convergence of the energy per one atom with the supercell size for graphite (experimental geometry)

Supercell	No. of atoms	E(BLYP)/1 atom [a.u.]	E(PBE)/1 atom [a.u.]
$1 \times 1 \times 1$	4	−5.54457	−5.57138
$2 \times 2 \times 1$	16	−5.62763	−5.66199
$3 \times 3 \times 1$	36	−5.65618	−5.69113
$3 \times 3 \times 2$	72	−5.65758	−5.69179
$4 \times 4 \times 1$	64	−5.66594	−5.70074
$4 \times 4 \times 2$	128	−5.66861	−5.70272
$5 \times 5 \times 1$	100	−5.66554	−5.70025
$5 \times 5 \times 2$	200	−5.66813	−5.70213
$6 \times 6 \times 1$	144	−5.66527	−5.69993
$6 \times 6 \times 2$	288	−5.66783	−5.70176

The optimization of the c lattice constant is a benchmark of DFT as well as dispersion corrections. The chosen supercell size $4 \times 4 \times 2$ gave the best energy per atom in the previous test of the supercell convergence. We chose the following range of c values, again using the variable cutoff procedure: from $c = 6.816$ Å at 90 Ry down to $c = 6.576$ Å at 92.19 Ry. Optimization results are presented in Table 15.4.

Both BLYP and PBE, augmented with DFT-D2 dispersion corrections, slightly underestimate the experimental lattice constant (by 0.08 Å) predicting an optimal

Table 15.4 Results of structural minimization of graphite lattice ($4 \times 4 \times 2$ supercell) with cell length c as the variable. Experimental value: $c = 6.696$ Å

c [Å]	E(BLYP)/1 atom [a.u.]	E(PBE)/1 atom [a.u.]
6.576	−5.66888	−5.70275
6.616	−5.66891	−5.70276
6.656	−5.66884	−5.70275
6.696	−5.66877	−5.70274
6.736	−5.66870	−5.70273
6.776	−5.66863	−5.70271
6.816	−5.66855	−5.70270

interlayer spacing of 3.308 Å, too small by 0.04 Å with respect to the experiment. The accuracy provided by more rigorous treatment of dispersion forces in DFT (Dion et al. 2004) is greater: it was possible to obtain interlayer separation of 3.34÷3.35 Å, while LDA severely underestimated the separation (3.118 Å) and dispersion-uncorrected PBE yielded overestimation of the layer-layer distance (3.425 Å) (Birowska et al. 2011). In the light of these results, we conclude that the BLYP-D2 and PBE-D2 provide satisfactory description of the graphite interlayer separation.

15.5 Results: bct C4 Allotrope

Recently a new allotrope of carbon, bct C4, was characterized computationally. It is predicted to form from carbon nanotubes at 20 Gpa and possesses tetragonal structure with distinct four carbon C_4 rings, but all carbon atoms are sp^3. Computational results (Schultz et al. 1999; Umemoto et al. 2010) indicate however that this phase is stable and provide synthetic XRD patterns consistent with some experimental data.

Figure 15.4 presents the structure of the bct C4 phase. It has *I4/mmm* space group and its calculated lattice constants at 0 GPa are $a = 4.329$ Å and $c = 2.483$ Å (Umemoto et al. 2010). The steric strain associated with formation of square motifs makes the C–C bonds different in length: 1.562 Å in the ring and 1.506 Å between rings (cf. the value for diamond: 1.541 Å).

The first element of testing the computational setup is energy convergence with the cutoff. As shown on Fig. 15.5, the PBE functional again provides converged results at 90 Ry cutoff. This value will be consistently used further. We did not observe SCF difficulties within the bct C4 calculations. Further, we carry out a supercell convergence test (Table 15.5) which shows that, as in the case of graphite, the cells of shape close to cubic ($2 \times 2 \times 4$) are better converged than elongated structures ($3 \times 3 \times 3$). The $2 \times 2 \times 4$ model is of a similar size to the optimal models for diamond and graphite discussed above.

It should be mentioned here that the optimal energy values per atom for graphite (PBE: −5.70276 a.u.) and diamond (PBE: −5.70069 a.u.) are quite close, the diamond lattice is higher in energy by only 0.002 a.u. (0.06 eV) per atom, in agreement with experimental stabilities. The bct C4 phase is sterically strained, and

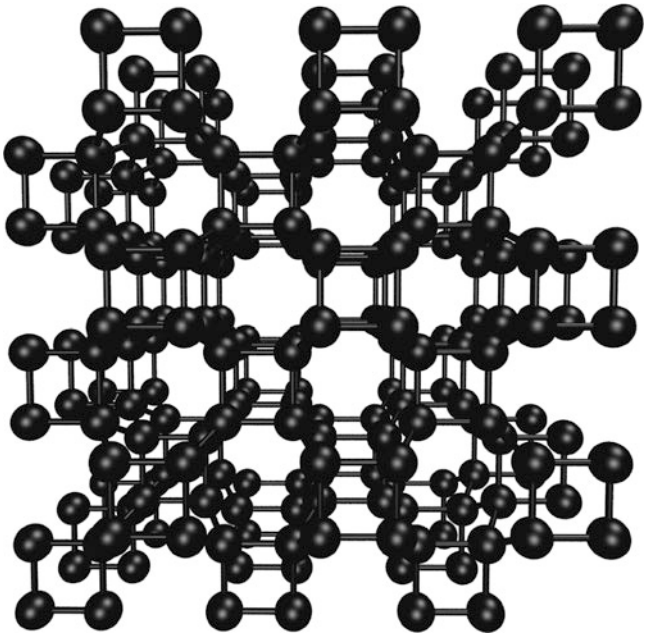

Fig. 15.4 The structure of bct C4 carbon allotrope. Drawing prepared with VMD package (Humphrey et al. 1996)

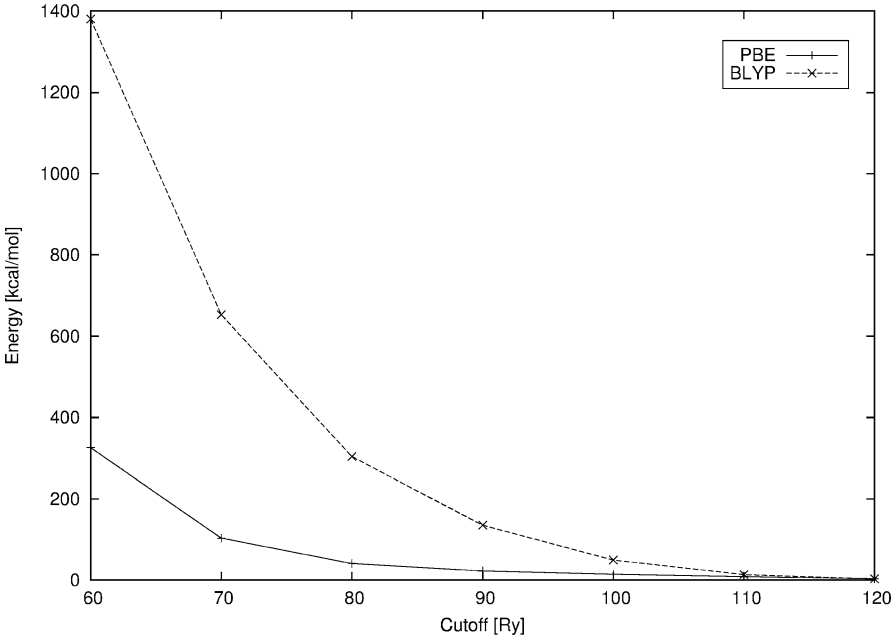

Fig. 15.5 Convergence of energies with plane-wave cutoff for bct C4, $2 \times 2 \times 4$ supercell

Table 15.5 Convergence of the energy per one atom with the supercell size for bct C4

Supercell	No. of atoms	E(BLYP)/1 atom [a.u.]	E(PBE)/1 atom [a.u.]
$1 \times 1 \times 1$	8	−5.53529	−5.57273
$1 \times 1 \times 2$	16	−5.63453	−5.67525
$2 \times 2 \times 2$	64	−5.64225	−5.68113
$2 \times 2 \times 3$	96	−5.65227	−5.69080
$2 \times 2 \times 4$	128	−5.65410	−5.69245
$3 \times 3 \times 3$	216	−5.65304	−5.69115

its energy is higher by 0.01 a.u. (0.3 eV) per atom; this value obtained with the PBE-D2 approach is in a very good agreement with the results of Umemoto et al. (0.22 eV/atom).

15.6 Conclusions

This study covered characterization of an exemplary computational setup for further use in calculations on large carbon networks. Possible applications in Car-Parrinello MD studies suggested the use of a supercell model rather than Brillouin zone sampling via k-point techniques. Availability of empirical dispersion corrections to the most popular functionals was also considered.

The computational method suggested within this study turned out to be the PBE functional augmented with the DFT-D2 dispersion corrections and a plane wave energy cutoff of 90 Ry. Despite slower SCF convergence than BLYP, it provided better convergence properties. The proposed methodology successfully predicts quantitative stability of graphite, diamond, and body-centered tetragonal C4 carbon phase, and it will be employed in future studies of carbon nanostructures, including recently proposed toroidal allotropic forms (Diudea and Szefler 2012) and "superhard" phases (He et al. 2012).

References

Becke AD (1988) Density-functional exchange-energy approximation with correct asymptotic behavior. Phys Rev A 38:3098–3100

Birowska M, Milowska K, Majewski JA (2011) Van der Waals density functionals for graphene layers and graphite. Acta Phys Pol A 120:845–848

Car R, Parrinello M (1985) Unified approach for molecular dynamics and density-functional theory. Phys Rev Lett 55:2471–2474

CPMD (2012) The CPMD Consortium page. http://www.cpmd.org. Accessed 30 Nov 2012

Dion M, Rydberg H, Schröder E, Langreth DC, Lundqvist BI (2004) Van der Waals density functional for general geometries. Phys Rev Lett 92:246401

Diudea M, Szefler B (2012) Nanotube junctions and genus of multi-tori. Phys Chem Chem Phys 14:8111–8115

Gaigeot MP, Sprik M (2003) Ab initio molecular dynamics computation of the infrared spectrum of aqueous uracil. J Phys Chem B 107:10344–10358

Grimme S (2006) Semiempirical GGA-type density functional constructed with a long-range dispersion correction. J Comput Chem 27:1787–1799

Grimme S, Antony J, Ehrlich S, Krieg H (2011) A consistent and accurate ab initio parametrization of density functional dispersion correction (DFT-D) for the 94 elements H-Pu. J Chem Phys 132:154104

Grüneis A, Marsman M, Kresse G (2010) Second-order Møller-Plesset perturbation theory applied to extended systems. II. Structural and energetic properties. J Chem Phys 133:074107

He C, Sun L, Zhang C, Peng X, Zhang K, Zhong J (2012) Phys Chem Chem Phys 14:8410–8414

Hohenberg P, Kohn W (1964) Inhomogeneous electron gas. Phys Rev 136:B864–B871

Humphrey W, Dalke A, Schulten K (1996) VMD – visual molecular dynamics. J Mol Graph 14:33–38

Kühne T, Krack M, Mohamed F, Parrinello P (2007) Efficient and accurate Car-Parrinello-like approach to Born-Oppenheimer molecular dynamics. Phys Rev Lett 98:066401

Lee C, Yang W, Parr RG (1988) Development of the Colle-Salvetti correlation-energy formula into a functional of the electron density. Phys Rev B 37:785–789

Marx D, Hutter J (2000) Ab initio molecular dynamics: theory and implementation. In: Grotendorst J (ed) NIC series: modern methods and algorithms of quantum chemistry proceedings, vol 3. John von Neumann Institute for Computing, Jülich, pp 329–477

Oganov AR (ed) (2010) Modern methods of crystal structure prediction. Wiley-VCH, Berlin

Perdew JP, Burke K, Ernzerhof M (1996) Generalized gradient approximation made simple. Phys Rev Lett 77:3865–3868

Rudberg E, Rubensson EH, Salek P (2011) Kohn–Sham density functional theory electronic structure calculations with linearly scaling computational time and memory usage. J Chem Theory Comput 7:340–350

Silvi B, Savin A (1994) Classification of chemical bonds based on topological analysis of electron localization functions. Nature 371:683–686

Schultz PA, Leung K, Stechel EB (1999) Small rings and amorphous tetrahedral carbon. Phys Rev B 59:733–741

Troullier N, Martins JL (1991) Efficient pseudopotentials for plane-wave calculations. Phys Rev B 43:1993–2006

Umemoto K, Wentzcovitch RE, Saito S, Miyake T (2010) Body-centered tetragonal C_4: a viable sp^3 carbon allotrope. Phys Rev Lett 104:125504

Wu X, Vargas MC, Nayak S, Lotrich V, Scoles G (2001) Towards extending the applicability of density functional theory to weakly bound systems. J Chem Phys 115:8748–8757

Chapter 16
Drawing Diamond Structures with Eigenvectors

István László, Ante Graovac[†], and Tomaž Pisanski

Abstract Very often the basic information about a nanostructure is a topological one. Based on this topological information, we have to determine the Descartes coordinates of the atoms. For fullerenes, nanotubes and nanotori, the topological coordinate method supplies the necessary information. With the help of the bilobal eigenvectors of the Laplacian matrix, the position of the atoms can be generated easily. This method fails, however, for nanotube junctions and coils and other nanostructures. We have found recently a matrix W which could generate the Descartes coordinates for fullerenes, nanotubes and nanotori and also for nanotube junctions and coils as well. Solving, namely, the eigenvalue problem of this matrix W, its eigenvectors with zero eigenvalue give the Descartes coordinates. There are nanostructures however, whose W matrices have more eigenvectors with zero eigenvalues than it is needed for determining the positions of the atoms in 3D space. In this chapter, we have studied this problem in the case of diamond structures. We have found that this extra degeneracy is due to the fact that the first and second neighbour interactions do not determine the geometry of the structure. It was found that including the third neighbour interaction as well, diamond structures were described properly.

[†]deceased

I. László (✉)
Department of Theoretical Physics, Institute of Physics, Budapest University of Technology and Economics, H-1521 Budapest, Hungary
e-mail: laszlo@iek.bme.hu

T. Pisanski
Department of Mathematics, Faculty of Mathematics and Physics, University of Ljubljana, Jadranska 19, SI-1000 Ljubljana, Slovenia

M.V. Diudea and C.L. Nagy (eds.), *Diamond and Related Nanostructures*, Carbon Materials: Chemistry and Physics 6, DOI 10.1007/978-94-007-6371-5_16,

16.1 Introduction

The recovering of geometry from topology corresponds to embedding the graph into the Euclidean space R^3 or R^2. In many cases only the topological structure of the molecules or atomic arrangements are given, but in order to make deeper study of the substance, we need the Descartes coordinates of the atoms as well. Here we describe the topological structure with the help of a graph, where its vertices represent the atoms and the edges the pairs of neighbouring atoms. In most of the cases, the edges are the chemical bonds. There are many methods for geometric representation and visualization of graphs (Hall 1970; Di Battista et al. 1999; Godsil and Royle 2001; Kaufmann and Wagner 2001; Koren 2005; Lovász and Vesztergombi 1999; Pisanski et al. 1995; Tutte 1963). Here we study the possibility to generate Descartes coordinates for atoms in nanostructures by using graph spectra and eigenvectors of selected graph matrices (Biyikoglu et al. 2007; Colin de Verdière 1998; Godsil and Royle 2001; Graovac et al. 2008a, b; van der Holst 1996; László 2005, 2008; Rassat et al. 2003). In the present study, we shall pay special attention to diamond nanostructures. In our previous publication (László et al. 2001), we have examined the possibilities of drawing graphs with eigenvectors of the adjacency matrix A, the Laplacian L and the Colin de Verdière matrix M. We have also suggested the matrix W for drawing graphs. While the applications of the matrices A, L and M are restricted to spherical structures, the matrix W can be used for any atomic arrangement. In order to show the applicability of W, we have applied it for the construction of 130 various clusters (László et al. 2012). These clusters were cut out from simple cubic (sc), basis-centred cubic (bcc), face-centred cubic (fcc) and diamond (diam) lattice systems. It turned out that the first and second neighbour matrix elements were sufficient for the structures sc, bcc and fcc, but for the diamond structures, we had to take into account the third neighbours as well. In this chapter, we shall study this special property of the diamond structure.

First basic notations and definitions will be given, and then, algorithms based on the matrices A, L and C_{17} will be presented. Then, we generate the matrix W based on harmonic potentials, and we shall apply it for diamond structures.

16.2 Basic Notions and Definitions

The topological structure of the atomic arrangement will be represented by a graph G(V, E), where V is the set of vertices and E is the set of edges. Molecular graphs are graphs which represent the constitution of molecules (Trinajstić 1992) or atomic arrangements, that is, each vertex $v \in \mathrm{V}$ represent an atom of the structure under study, and each edge $(u, v) \in \mathrm{E}$ means that the atoms u and v are in some way related to each other, that is, they are chemically bonded. The value $n = |\mathrm{V}|$ equals the number of vertices or atoms in the structure studied.

The matrix $\mathrm{A} = \mathrm{A}(\mathrm{G}) = (a_{uv})$ is the adjacency matrix of the graph G(V, E), where $a_{uv} = 1$ if $(u, v) \in \mathrm{E}$ and $a_{uv} = 0$ if u is not adjacent to v or $u = v$.

The identity matrix and the all-1 matrix (where $J_{ij} = 1$ for all i and j) will be denoted by I and J, respectively. If the graph G is a weighted graph, the values a_{uv} equal the corresponding weights on edges. The Laplacian matrix Q of graph G is defined by $\mathrm{Q} = \mathrm{Q(G)} = \mathrm{Q(A)} = \mathrm{D} - \mathrm{A}$, where $\mathrm{D} = (d_{vv})$ is the diagonal matrix with $d_{vv} = \sum_{u:(u,v)\in E} a_{uv}\, d_{vv}$. Note that d_{vv} represents the degree of vertex v. The eigenvalues of the adjacency matrix A and those of the Laplacian matrix Q are numbered in descending and in ascending order, respectively. It can be proved easily that $\mathrm{Qc} = 0$ if the components of the eigenvector **c** are the same, for example, $c_i = \frac{1}{\sqrt{n}}$, that is, **c** is the eigenvector corresponding to the zero eigenvalue. While the adjacency matrix and the Laplace matrix depend on the order of vertices, their spectra are graph invariants and are preserved under any automorphism of a graph.

We now define lobality of eigenvectors. Let c be an eigenvector of G and let us label each vertex of i by c_i. Let $\mathrm{G_c}$ denote the graph obtained from G by removing all vertices i if $c_i = 0$ and all edges (i, j) if $c_i c_j < 0$. In general G_c is disconnected, but each of its connected components has induced labels of the same sign. It is either positive or negative. An eigenvector c of G is m-lobal if the graph $\mathrm{G_c}$ consists of m-connected components.

In our graph drawing procedures, the bi-lobal eigenvectors ($m = 2$) will be the most important. For the nodal properties of graph Laplacians, see the reference (Biyikoglu et al. 2004).

Under embedding a graph G(V, E) into R^k, we mean a mapping

$$\tau : \mathrm{V(G)} \to R^k. \tag{16.1}$$

In Godsil and Royle (2001) and Pisanski and Žitnik (2009), such an embedding is called a graph representation.

Note that τ may be viewed as a matrix with k columns, each of length n. We will denote by τ_i the n-dimensional vector formed by taking the ith column of the matrix τ. Rows of this matrix correspond to the vertices of the graph. The matrix element is denoted by $\tau(u)_i$ while $\tau(u)$ is a k-dimensional row vector for each $u \in \mathrm{V}$. Thus, τ_i is an n-dimensional vector with entries corresponding to the vertices of the graph G(V, E).

16.3 Algorithms for Generating Eigenvectors in Graph Drawing

The methods used in generating eigenvectors in graph drawing can be divided into two groups. In the first group are the methods based on extremal values and in the second group are the methods based on analogy. Let us turn first to the methods based on extremal values. There are two methods in this group, the method invented by Pisanski and Shawe-Taylor (Pisanski and Shawe-Taylor 1993, 2000) and the method developed by Lovász and Schrijver (Lovász and Schrijver 1999).

Pisanski and Shawe-Taylor (Pisanski and Shawe-Taylor 1993, 2000; Fowler et al. 1995) defined the optimal embedding of the weighted graph G(V, E) by minimizing the following energy function:

$$E(\tau) = \sum_{(u,v)\in E} a_{uv}\|\tau(u) - \tau(v)\|^2 - \beta \sum_{(u,v)\notin E} \|\tau(u) - \tau(v)\|^2, \tag{16.2}$$

and it was subjected to the constraints

$\|\tau_i\| = 1, \tau_i^T \mathrm{c}^1 = 0$ for $i = 1, \ldots, k$
$\tau_i^{\mathrm{T}} \tau_j = 0$ for $1 \le i < j \le k$, and β is a positive constant.

It was proven in Pisanski and Shawe-Taylor (1993, 2000) that the optimal embedding for this problem is given by $\tau_i = \mathrm{c}^{i+1}$ for $i = 1, \ldots, k$ and the minimal value of $E(\tau)$ is

$$\sum_{l=2}^{k+1} \lambda_l - \beta n k. \tag{16.3}$$

Here the corresponding Laplacian $\mathrm{Q} = \mathrm{Q}(\mathrm{B})$ for the eigenvalues and eigenvectors was constructed from the matrix B with the matrix elements $b_{uv} = a_{uv} + \beta$ if $(u, v) \in E$ and $b_{uv} = 0$ otherwise. It was proved also that in the case where the graph is not weighted, the optimal embedding does not depend on the parameter β.

Lovász and Schrijver (Lovász and Schrijver 1999) defined a symmetric $n \times n$ matrix M for the 3-connected planar graph G(V, E) with the following properties:

1. M has exactly one negative eigenvalue of multiplicity 1.
2. For all $(u, v) \in \mathrm{E} m_{uv} < 0$ and if $u \neq v$ and $(u, v) \notin \mathrm{E} m_{uv} = 0$.
3. M has rank $n - 3$.

They have proved that if we have a matrix M with the above mentioned conditions, then the null space of M (the eigenvectors c^2, c^3 and c^4 of the eigenvalue $\lambda = 0$) gives a proper embedding of G(V, E) in the sphere S^2 as $\tau_i = \mathrm{c}^{i+1}$ for $i = 1, \ldots, 3$ and $||\tau_i||^2 = 1$. Thus, the relation $(x_u, y_u, z_u) = (\tau(u)_1, \tau(u)_2, \tau(u)_3)$ is valid for each vertex. It was also proved that this null space contains bi-lobal eigenvectors (van der Holst 1996). In the scientific literature, the matrix M is often called Colin de Verdière matrix (Lovász and Schrijver 1999).

Now we continue with the methods based on analogy. There are also two methods in this group. The method developed for spherical clusters (Manolopoulos and Fowler 1992, Fowler and Manolopulos 1995) and the method applicable for toroidal structures (Graovac et al. 2000; László et al. 2001).

The idea of using eigenvectors (molecular orbitals) for drawing molecular graphs was used first in chemical setting by Fowler and Manolopoulos (Manolopoulos and Fowler 1992; Fowler and Manolopulos 1995). Their idea is based on Stone's tensor

surface harmonic theory (Stone 1981). Stone has found a good approximation for eigenvectors of spherical metallic clusters by calculating the values of spherical harmonics at the atomic positions. Fowler and Manolopoulos constructed the coordinates from eigenvectors attributed to spherical harmonics. They have found that the first few Hückel molecular orbitals of fullerenes invariably contain three bi-lobal eigenvectors which are discrete version of the continuous p_x, p_y and p_z orbitals. Since the p_x, p_y and p_z orbitals on a sphere are proportional to the x, y and z coordinates, the three lowest bi-lobal eigenvectors $\mathtt{c}^{k_1}$, $\mathtt{c}^{k_2}$ and $\mathtt{c}^{k_3}$ determine the (x_i, y_i, z_i) topological coordinates of the ith atom by the relations:

$$x_i = S_1 c_i^{k_1}, \tag{16.4}$$

$$y_i = S_2 c_i^{k_2}, \tag{16.5}$$

$$z_i = S_3 c_i^{k_3}, \tag{16.6}$$

with the scaling factors

$$S_\alpha = S_0 \tag{16.6a}$$

or

$$S_\alpha = \frac{S_0}{\sqrt{\lambda_1 - \lambda_{k_\alpha}}}, \tag{16.6b}$$

where S_0 is a constant (Manolopoulos and Fowler 1992; Fowler and Manolopulos 1995).

The most realistic picture of fullerenes (Dresselhaus et al. 1996) can be obtained by choosing (16.6b) for the scaling factor $S_\alpha = \frac{S_0}{\sqrt{\lambda_1 - \lambda_{k_\alpha}}}$ (Manolopoulos and Fowler 1992; Fowler and Manolopulos 1995; László 2004a, b; Pisanski and Shawe-Taylor 1993).

Graovac et al. (2000) generated the Descartes coordinates of nanotori using three eigenvectors $\mathtt{c}^2$, $\mathtt{c}^3$ and $\mathtt{c}^{\mathrm{opt}}$ of the adjacency matrix $\mathtt{A}$ describing a 3-valent toroidal structure. The second and third eigenvectors are $\mathtt{c}^2$ and $\mathtt{c}^3$. The eigenvector $\mathtt{c}^{\mathrm{opt}}$ was selected in a way to obtain optimal drawing. The toroidal structures, however, obtained from three eigenvectors usually are distorted or flattened in some way (Graovac et al. 2000; László et al. 2001). This problem was solved using four eigenvectors of the adjacency matrix (László et al. 2001). In this method the position of a point on the surface of a torus is given as the sum of two vectors $\mathtt{R}$ and $\mathtt{r}$, where the vector $\mathtt{R}$ is in the xy plane and $\mathtt{r}$ is in the planes perpendicular to the plane of $\mathtt{R}$. These two vectors are two-dimensional planar vectors; each of them can be described by two bi-lobal eigenvectors. If $\mathtt{c}^{k_1}$, $\mathtt{c}^{k_2}$, $\mathtt{c}^{k_3}$ and $\mathtt{c}^{k_4}$ are for bi-lobal eigenvectors of the adjacency matrix $\mathtt{A}$, then using basic geometrical construction,

the (x_i, y_i, z_i) topological coordinates of the ith atom on the torus is given by the relations (László et al. 2001; László and Rassat 2003):

$$x_i = S_1 c_i^{k_1} \left(1 + S_4 c_i^{k_4}\right), \tag{16.7}$$

$$y_i = S_2 c_i^{k_2} \left(1 + S_4 c_i^{k_4}\right), \tag{16.8}$$

$$z_i = S_3 c_i^{k_3}. \tag{16.9}$$

The coefficients S_α are calculated with Eq. (16.6b).

16.4 Embedding of Any molecular Arrangement

In the previous paragraph, we have seen that the applicability of three eigenvectors is restricted only to spherical structures and nanotubes. In László et al. (2011), it was shown that there exist a matrix W which can reproduce practically exactly the (x_i, y_i, z_i) Descartes coordinates with the help of three eigenvectors. This matrix was obtained by minimizing the total energy

$$E(r) = E\left(r_{12}, r_{21}, \ldots r_{ij}, r_{ji} \ldots\right) \tag{16.10}$$

of the system, and it was proved that

$$\mathrm{WX} = 0, \quad \mathrm{WY} = 0, \quad \mathrm{WZ} = 0. \tag{16.11}$$

The matrix elements of W are calculated as

$$w_{ij} = -\frac{\partial E(r)}{r_{ij}\partial r_{ij}} - \frac{\partial E(r)}{r_{ji}\partial r_{ji}} \tag{16.12}$$

for the off-diagonal elements and as

$$w_{ii} = \sum_{j \neq i}^{n} \left(\frac{\partial E(r)}{r_{ij}\partial r_{ij}} + \frac{\partial E(r)}{r_{ji}\partial r_{ji}}\right) = -\sum_{j \neq i}^{n} w_{ij} \tag{16.13}$$

for the diagonal elements, and r_{ij} are the interatomic distances. We have found further that

$$\mathrm{WU} = 0 \tag{16.14}$$

with $u_i = \frac{1}{\sqrt{n}}$.

Other details can be found in reference (László et al. 2011).

If the centre of mass of the molecule is in the origin and the molecule is directed in such a way that the eigenvectors of its tensor of inertia are showing to the directions of the x, y and z axis, then the vectors X, Y, Z and U are orthogonal eigenvectors of the matrix W. That is,

$$\mathrm{X} = S_x \mathrm{C}^{\mathrm{x}}, \quad \mathrm{Y} = S_y \mathrm{C}^{\mathrm{y}} \quad \text{and} \quad \mathrm{Z} = S_z \mathrm{C}^{\mathrm{z}}, \tag{16.15}$$

where C^{x}, C^{y}, C^{z} and U are orthogonal and normalized eigenvectors of W with zero eigenvalue and S_x, S_y and S_z are appropriate scaling factors.

The question arises if we have any orthogonal and normalized eigenvectors A^{x}, A^{y}, A^{z} and U of W with zero eigenvalue, are there any appropriate scaling factors S_x, S_y and S_z for obtaining the Descartes coordinates with a relation

$$\mathrm{X} = S_x \mathrm{A}^{\mathrm{x}}, \quad \mathrm{Y} = S_y \mathrm{A}^{\mathrm{y}} \quad \text{and} \quad \mathrm{Z} = S_z \mathrm{A}^{\mathrm{z}} \tag{16.16}$$

If the number of eigenvectors with zero eigenvalue is four, the answer is yes, but in Eq. (16.16), we obtain a rotation of the molecule as the vectors A^{x}, A^{y} and A^{z} can be obtained as linear combination of the vectors C^{x}, C^{y} and C^{z}. If the vectors C^{x}, C^{y} and C^{z} are mixed with the vector U, it means arbitrary translation and a rotation of the molecule. As the vector U is known, it can be easily subtracted from the linear combinations in the case of mixings. If the degeneracy of the zero eigenvalue is higher than four, the Descartes coordinates of the atoms can be obtained with the help of a projection from a higher-dimensional space. The purpose of the present study is to show this phenomenon in the case of diamond structures.

Usually the first neighbour distances in a molecule do not determine the positions of the atoms, but the full structure can be described if we know the second neighbour distances as well. We introduce a secondary graph $\mathrm{G}^{(2)}$ obtained from G by adjoining new edges, corresponding to the second neighbours in G. Therefore, the edges of the graph $\mathrm{G}^{(2)}$ correspond to the first and second neighbours of a molecule or its molecular graph $\mathrm{G} = \mathrm{G}(\mathrm{V}, \mathrm{E})$.

The matrix W can be generated from a total energy $\boldsymbol{E}(\boldsymbol{r})$ which depends only on the first and second neighbours of the molecule. If the dimension of the null space of W is four, then this null space contains three eigenvectors which give a proper embedding of $\mathrm{G}(\mathrm{V}, \mathrm{E})$ into R^3.

16.5 Construction of Matrix W from Harmonic Potential

In our previous publication, we tested application of the matrix W for several structures, as nanotube junctions nanotori and helical nanotubes (László et al. 2011). In that work the interatomic interactions and the matrix W were calculated with the help of the Brenner potential (Brenner 1990) and harmonic potential as well. From our point of view, the harmonic potential is simpler and more general than the Brenner one; as in the case of harmonic potential, there is no limitation for the

number of first neighbours. In our preliminary calculations, we have found further that in some cases the multiplicity of the zero eigenvectors was greater than four. In our previous publication (László et al. 2012), we have calculated the matrix W for harmonic potential and then applied it for several clusters taken out of simple cubic, face-centred cubic, body-centred cubic and diamond structures.

The total energy of Eq. (16.10) was in the form of

$$E(r) = E\left(r_{12}, r_{21}, \ldots r_{ij}, r_{ji} \ldots\right) = \sum_{i,j=1}^{n} \frac{1}{2} k_{ij} \left(r_{ij} - a_{ij}\right)^2. \tag{16.17}$$

Here $k_{ij} = k_{ji}$ are the spring constants and $a_{ij} = a_{ji}$ are parameters. The summation goes for all the pairs $(\boldsymbol{i,j})$ which are sufficient for determining the equilibrium positions of the atoms.

From Eqs. (16.12) and (16.17), it follows that

$$w_{ij} = -\frac{\partial E(r)}{r_{ij}\partial r_{ij}} - \frac{\partial E(r)}{r_{ji}\partial r_{ji}} = -2k_{ij}\left(1 - \frac{a_{ij}}{r_{ij}}\right). \tag{16.18}$$

As it is stated above in Eq. (16.18), the values r_{ij} minimize the total energy $E(r)$ of Eq. (16.17). The eigenvalue problem of matrix W has meaning only if it is not the zero matrix. From this it follows that the parameters a_{ij} must be different of the corresponding interatomic distance r_{ij}.

16.6 Descartes Coordinates for Diamond Clusters Obtained from the Eigenvectors of Matrix W Based on Harmonic Potentials

We have studied altogether 130 clusters in ref. (László et al. 2012). These cluster were cut out from simple cubic, basis-centred cubic, face-centred cubic and diamond lattice systems. The spherical clusters had a maximal number of shells 20, and each of them contained an atom in the centre of the cluster. These clusters contained all of the atoms inside the sphere given by the corresponding radius. The first neighbour interatomic distance was 1.54 Å for each structure. The nonspherical structures were given by the number of unit cells n_x, n_y and n_z in the direction of the axes X, Y and Z (László et al. 2012). We have found that for many diamond structures, the degeneracy of the zero eigenvalue of the second neighbour matrix W was greater than four.

In Fig. 16.1, 16.2, and 16.3, we present three structures to explain this problem. In Fig. 16.1a, we can see the graph of a diamond carbon cluster of six atoms C_6. The white vertices mark the two carbon atoms with four neighbours. Let us suppose that the centre of mass of the molecule is in the origin and the molecule is directed in such a way that the eigenvectors of its tensor of inertia are showing to

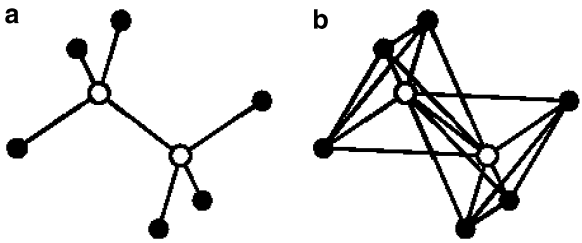

Fig. 16.1 The graphs of the diamond carbon cluster C_6. The graph of first neighbours (**a**) and second neighbours (**b**). The two *white vertices* determine the axis of tetrahedron rotation in (**b**)

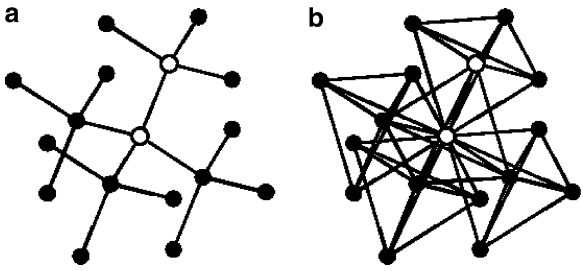

Fig. 16.2 The graphs of the diamond carbon cluster C_{17}. The graph of first neighbours (**a**) and second neighbours (**b**). The two *white vertices* determine one of the axes of tetrahedron rotation in (**b**)

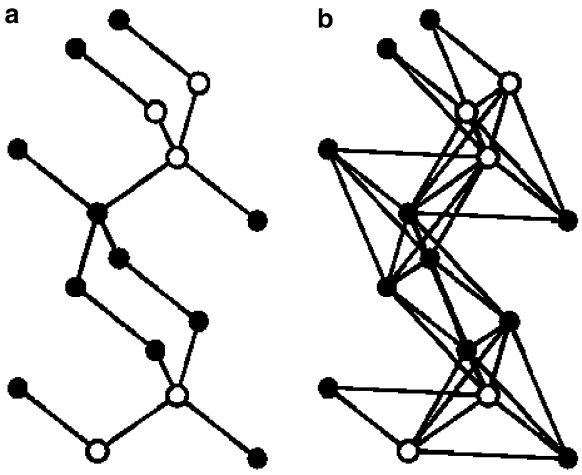

Fig. 16.3 The graphs of the diamond carbon cluster C_{16}. The graph of first neighbours (**a**) and second neighbours (**b**). Any two neighbouring *white vertices* in (a) determine the axis of triangle rotation in (**b**)

the directions of the x, y and z axis, then the vectors X, Y, Z and U are orthogonal eigenvectors of the matrix W. The off-diagonal matrix elements of W correspond to the first and second neighbour pairs of vertices as they are shown in Fig. 16.1b. The second neighbour vertices of graph in Fig. 16.1a are determined in the graph theoretical definition. That is, they are the pairs of vertices with a distance of 2. The structure of Fig. 16.1b is obtained by minimizing the total energy of Eq. (16.17). In Fig. 16.1b, we can see two tetrahedrons constructed by three black vertices and one white vertex of the tetrahedron. Each of these tetrahedrons contains inside the other white vertex. Let us rotate one of the tetrahedron around the axis of the bond

with white atoms. Using this rotation we obtain new atomic coordinates X′, Y′ and Z′. As this rotation does not change the bond distances of Fig. 16.1b, the minimal value of total energy of Eq. (16.17) will not change. From this follows that X′, Y′ and Z′ are eigenvectors of matrix W with zero eigenvalue. If $\mathbf{X}'$, $\mathbf{Y}'$ and $\mathbf{Z}'$ are linearly independent of X, Y, Z and U, we generated new eigenvectors of the matrix W taking into account first and second neighbour interactions. We have obtained that degeneracy of the matrix with graph of Fig. 16.1b is six instead of four. But if we take into account the third neighbour interactions as well, the position of the previous tetrahedrons will be fixed, and we cannot generate new eigenvectors with zero eigenvalue. In reference (László et al. 2012), we have found that the degeneracy of the zero eigenvalue was four if the matrix W was constructed with the help of first, second and third neighbour interactions.

In Fig. 16.2 we have presented the case of a C_{17} molecule. In Fig. 16.2b it is shown that the second neighbour graph has four tetrahedrons which can generate new eigenvectors with zero eigenvalue for the matrix W with first and second interactions. We have calculated that the degeneracy was 12 instead of four.

The structure C_{16} in Fig. 16.3 has three atoms with undefined positions. Namely, there are three triangles having two white and one black vertex in Fig. 16.3b which can be rotated around the side of two white vertices. These rotations can also produce new eigenvectors with zero eigenvalue. For this structure we have found ten degenerated eigenvectors with zero eigenvalue.

As there are some numerical uncertainties for this structure, it is not excluded that this degeneracy is even higher, that is, 13.

16.7 Conclusions

After revising the algorithms for generating eigenvectors in graph drawing, we studied the problems of constructing Descartes coordinates with the help of the matrix W. In three examples we have shown that the extra degeneracy of the zero eigenvalue of matrix W was due to the fact that the first and second neighbour interactions do not determine the position of the atoms in diamond structures. With the help of first, second and third neighbour interactions, the relative position of the atoms is given, and the Descartes coordinates of the atoms can be determined from the eigenvectors of the matrix W. With the help of third neighbour interactions, the degeneracy was 4 in each case we were studying. Even in the case of four eigenvector, in general case, the final structure will undergo rotation translation and some affine transformation. But, in this case, the scaling factors can be determined using some given interatomic distances.

The drawback of W is that at present there is not a simple algorithm for its construction. There is a hope, however, that using appropriate approximations for the matrix elements of W, a method can be found for constructing topological

coordinates of complicated nonspherical structures as well**.** According to our present results, the harmonic potential looks to be a promising tool for resolving these problems.

Acknowledgments I. László thanks for the support of grants TAMOP-4.2.1/B-09/1/KONV-2010-0003, TAMOP-4.2.1/B-09/1/KMR-2010-0002 and for the support obtained in the frame work of bilateral agreement between the Croatian Academy of Science and Art and the Hungarian Academy of Sciences. The research of T. Pisanski has been financed by ARRS project P1-0294 and within the EUROCORES Programme EUROGIGA (project GReGAS N1-0011) of the European Science Foundation.

References

Biyikoglu T, Hordijk W, Leydold J, Pisanski T, Stadler PF (2004) Graph Laplacians, nodal domains, and hyperplane arrangements. Linear Algebra Appl 390:155–174

Biyikoglu T, Leydold J, Stadler PF (2007) Laplacian eigenvectors of graphs. Perron-Frobenius and Faber-Krahn type theorems. LNM 1915. Springer, Berlin/Heidelberg

Brenner DW (1990) Empirical potentials for hydrocarbons for use in simulating the chemical vapor deposition of diamond films. Phys Rev B 42:9458–9471

Colin de Verdière Y (1998) Spectres de graphes. Cours spécialisés 4. Société Mathématique de France, Paris

Di Battista G, Eades P, Tamassia R, Tollis IG (1999) Graph drawing: algorithms for the visualization of graphs. Prentice Hall, Upper Saddle River

Dresselhaus MS, Dresselhaus G, Eklund PC (1996) Science of fullerenes and carbon nanotubes: their properties and applications. Academic, New York/London

Fowler PW, Manolopulos DE (1995) An atlas of fullerenes. Clarendon, Oxford

Fowler PW, Pisanski T, Shawe-Taylor JS (1995) Molecular graph eigenvectors for molecular coordinates. In: Tamassia R, Tollis EG (eds) Graph drawing. DIMACS international workshop, GD'94, Princeton, New Jersey, USA, 10–12 October 1994. Lecture Notes in Computer Science 894. Springer, Berlin

Godsil CD, Royle GF (2001) Algebraic graph theory. Springer, Heidelberg

Graovac A, Plavšić D, Kaufman M, Pisanski T, Kirby EC (2000) Application of the adjacency matrix eigenvectors method to geometry determination of toroidal carbon molecules. J Chem Phys 113:1925–1931

Graovac A, Lászlo I, Plavšić D, Pisanski T (2008a) Shape analysis of carbon nanotube junctions. MATCH Commun Math Comput Chem 60:917–926

Graovac A, László I, Pisanski T, Plavšić D (2008b) Shape analysis of polyhex carbon nanotubes and nanotori. Int J Chem Model 1:355–362

Hall KM (1970) An r-dimensional quadratic placement algorithm. Manag Sci 17:219–229

Kaufmann M, Wagner D (eds) (2001) Drawing graphs. Methods and models. LNCS 2025. Springer, New York

Koren Y (2005) Drawing graphs by eigenvectors: theory and practice. Comput Math Appl 49:1867–1888

László I (2004a) Topological coordinates for nanotubes. Carbon 42:983–986

László I (2004b) The electronic structure of nanotubes and the topological arrangements of carbon atoms. In: Buzaneva E, Scharff P (eds) Frontiers of multifunctional integrated nanosystems. NATO Science Series, II. Mathematics, Physics and Chemistry, 152. Kluwer Academic Publishers, Dordrecht, p 11

László I (2005) Topological coordinates for Schlegel diagrams of fullerenes and other planar graphs. In: Diudea MV (ed) Nanostructures: novel architecture. Nova, New York, pp 193–202
László I (2008) Hexagonal and non-hexagonal carbon surfaces. In: Blank V, Kulnitskiy B (eds) Carbon nanotubes and related structures. Research Singpost, Kerala, pp 121–146
László I, Rassat A (2003) The geometric structure of deformed nanotubes and the topological coordinates. J Chem Inf Comput Sci 43:519–524
Lovász L, Schrijver A (1999) On the null space of the Colin de Verdière matrix. Annales de l'Institute Fourier (Grenoble) 49:1017–1026
Lovász L, Vesztergombi K (1999) Representation of graphs. In: Halász G, Lovász L, Simonovits M, Sós VT (eds) Paul Erdős and his mathematics. Bolyai Society. Springer, New York
László I, Rassat A, Fowler PW, Graovac A (2001) Topological coordinates for toroidal structures. Chem Phys Lett 342:369–374
László I, Graovac A, Pisanski T, Plavšić D (2011) Graph drawing with eigenvectors. In: Putz MV (ed) Carbon bonding and structures. Advances in physics and chemistry. Springer, Dordrecht, pp 95–115
László I, Graovac A, Pisanski T (2012) Nanostructures and eigenvectors of matrices. In: Ashrafi AR, Cataldo F, Graovac A, Iranmanesh A, Ori O, Vukicevic D (eds) Carbon materials chemistry and physics: topological modelling of nanostructures and extended systems. Springer, Dordrecht/Heidelberg/London/New York
Manolopoulos DE, Fowler PW (1992) Molecular graphs, point groups, and fullerenes. J Chem Phys 96:7603–7614
Pisanski T, Shawe-Taylor JS (1993) Characterising graph drawing with eigenvectors. In: Technical report CSD-TR-93-20, Royal Holloway, University of London, Department of Computer Science, Egham, Surrey TW200EX, England
Pisanski T, Shawe-Taylor JS (2000) Characterising graph drawing with eigenvectors. J Chem Inf Comput Sci 40:567–571
Pisanski T, Žitnik A (2009) Representing graphs and maps. In: Beineke LW, Wilson RJ (eds) Encyclopedia of mathematics and its applications, 128. Cambridge University Press, Cambridge, pp 151–180
Pisanski T, Plestenjak B, Graovac A (1995) NiceGraph and its applications in chemistry. Croat Chim Acta 68:283–292
Rassat A, László I, Fowler PW (2003) Topological rotational strengths as chirality descriptors for fullerenes. Chem Eur J 9:644–650
Stone AJ (1981) New approach to bonding in transition-metal clusters and related compounds. Inorg Chem 20:563–571
Trinajstić N (1992) Chemical graph theory. CRC Press, Boca Raton/Ann Arbor/London/Tokyo
Tutte WT (1963) How to draw a graph. Proc Lond Math Soc 13:743–768
van der Holst H (1996) Topological and spectral graph characterizations. Ph.D. thesis, University of Amsterdam, Amsterdam

Chapter 17
On the Structure of Quasicrystals in a Higher-Dimensional Space

V.Ya. Shevchenko, G.V. Zhizhin, and A.L. Mackay

The scatter of sparrows works out the space where they were.

R. Hoffmann/selected poems. 1985

Abstract Categories of the generalized crystallography, where structures are tiled by a large number of identical cells, include quasi-identity and quasi-equivalence. The hierarchy of the organization levels is considered, involving the *n*-D space. In the theory of proportions, the irrational numbers, such as e, $\acute{\imath}$, π, and τ, play an important role. The golden-ratio number $\boldsymbol{\tau}$ is fundamental for the geometry of structures with five- or tenfold symmetry, eventually called quasicrystals. The fact that these numbers are irrational suggests that in the Euclidean space E_3, we observe the projections of the fundamental polyhedra from a higher-dimensional space. Thus, complex crystal (or quasicrystal) structures are only cells of some much more complex assemblies of higher dimensionality.

17.1 Motivation

In 2011, D. Shehtman was awarded the Nobel Prize in chemistry for the discovery of quasicrystals. He was the first who noticed the unusual symmetry (5–10) in electron-diffraction patterns of quenched Al-Mn alloys. This observation was noticed in April 8, 1982.

V.Ya. Shevchenko (✉) • G.V. Zhizhin
Institute of Silicate Chemistry RAS, nab.Makarova, 2, Saint-Petersburg 199034, Russia
e-mail: shevchenko@isc.nw.ru

A.L. Mackay
Lanchester Road, 22, London N6 4TA, UK

Birkbeck College, University of London, Malet Street, Bloomsbury,
London WC1E 7HX, England

M.V. Diudea and C.L. Nagy (eds.), *Diamond and Related Nanostructures*,
Carbon Materials: Chemistry and Physics 6, DOI 10.1007/978-94-007-6371-5_17,

The recognition of this event and its assessment went on rather dramatically.

Suffice it to say that the outstanding structural chemist, Nobel Prize winner L. Pauling sharply criticized that work (Pauling 1985). He received from D. Shehtman an x-ray diffraction pattern obtained at NIST, USA, with CuK_α radiation and carried out its computational processing. A model of a $MnAl_6$ icosahedral twinning cubic crystal was constructed, which could produce the pattern that was assumed to be icosahedral reflexes. For comparison, L. Pauling used the electron-diffraction patterns of $NaCd_2$, a structure he studied long time ago (Pauling 1923). This structure appeared to be so complex that it could not be identified for more than 40 years, until S. Samson determined its parameters (Samson 1962). At present, several more polyatomic structures with large cell parameters are known. However, we constructed the structure of $NaCd_2$ in 2009, on different new principles (Shevchenko et al. 2009). In conclusion of his paper, Pauling (1985) reassured the crystallography community and reiterated the basic laws of classical crystallography. However, some authors (including the authors of the discovery) responded unambiguously: Pauling's model is contradictory.

Experimental data obtained using high-resolution transmission electron microscopy (HRTEM), field-ion microscopy, Mössbauer spectroscopy, etc. (Cahn et al. 1986) have proven the presence of real fivefold axes and the existence of quasicrystals with icosahedral symmetry.

John Maddox called L. Pauling a cat among doves; authors of Cahn et al. (1986) asserted that the cat died, whereas the pigeons survived despite a turmoil. The letter of A. Mackay, in the same issue of Nature, substantially extended the structural capabilities that could provide reflexes of the icosahedral type.

The most important is the suggestion of the existence of quasicrystals in the *n*-dimensional space that A. Mackay pointed out long time ago (Mackay 1981, 1982). Mackay published a chart, which he named "domains associated with generalized crystallography—conceptual-associative approach." One of the associations that demonstrate the development of classical crystallography reads as follows: quasi-equivalence, local symmetry, pentagonal symmetry, Penrose patterns, aperiodic crystals, and fractal dimensionality.

The idea of the generalized crystallography was first put forward by J.D. Bernal in the 1960s (Bernal 1967). The basic concepts of his notion consist in a more generalized approach to the basic problem of classical crystallography, that is, tiling of structures into larger number of identical cells. The generalized crystallography suggests the quasi-identity and quasi-equivalence. The hierarchy of the organization levels is considered involving the *n*-D space. It is suggested that initial structures contain primary information about the evolution mechanisms, a kind of "genes" that govern the further buildup. In essence, Bernal's suggestions reflect the variety of objects in nature, as investigated by crystallographers at that time, not only by using x-ray analysis. The mathematical tools for this generalization were developed by Delone in 1920, on the ground of Voronoi's dissections rather than on the concept of Fedorov's unit cell. If a local ordering covers several tens of atomic radii, it is necessary that the whole volume be crystalline (and, accordingly, have its spatial group). The ordering at smaller distances (e.g., the icosahedral ordering) may give

rise to quasicrystals. Basically, this is the definition of the nanospace and nanoworld as a specific region in which a chemical substance is formed.

The fundamental characteristic of the substance is its structure. The structure (constitution, arrangement, order) is a combination of stable interconnections of an object that provide its integrity and self-identity. Analysis of this definition calls for the space to be defined in the nanosize domain. The space is not a passive receptacle, as it was considered by B. Riemann. Rather, it is a scene in which chemical processes develop. The numerical characteristic of the space that defines the set of its properties and features is referred to as its regularity. Another fundamental characteristic of the space, associated with the structure, is the symmetry. This notion enabled a mathematical definition of the space by means of the simple finite groups.

17.2 Main Results

In the 1980s, more than 100 prominent mathematicians, under the guidance of D. Gorenstein, established a consortium aimed to provide a complete classification of the simple finite displacement groups consisting of three infinite countable families and 26 so-called sporadic groups with special properties, the "monster" highest order included. The order of this group amounts to about 10^{53}, which, probably, indicates the total number of compounds (including chemical ones) in nature (note that the total number of protons in the universe is about 10^{80}). Thus, the symmetry underlies almost all structures and regularities of the living and nonliving nature. The formation of a specific substance originates in the nanoworld, in the space partitioned into various displacement groups of fundamental domains.

The functional domain of each displacement group, together with its congruent domain specified by that group, obviously, provides the filling of the space without voids. (Hereby we cited the beginning of the Hilbert problem No. 18.) Next, the following question can be put: How an infinite set of identical bodies, for example, spheres of a given size, can be arranged in the space most closely or be arranged so that the filled-to-unfilled regions ratio should be as large as possible?

In the theory of proportions and structural properties of the nature, the irrational numbers, such as e, $\acute{\imath}$, π, and τ, play an important role. The golden-ratio number $\boldsymbol{\tau}$ is fundamental in the geometry of bodies with five- or tenfold symmetry in the 3-D space; it is the ratio of the length of the diagonal to the edge of a regular pentagon and also the radius of a circle circumscribed about a regular decagon to its edge. The fact that these numbers are irrational suggests that, in the Euclidean space, we observe projections of the fundamental polyhedra from a higher-dimensional space. This is exemplified by a regular icosahedron, with the center located at the origin of coordinates. Let the coordinates of its 12 vertices be $\pm r_1, \ldots r_6$. If the icosahedron is formed so that r_i lie on a unit sphere, then, at $\acute{\imath} \neq j$, the scalar products are equal to $\left(r_i r_j\right) = \pm 1/\sqrt{5}$.

The irrationality of $\sqrt{5}$ results in the fact that the "lattice" produced by the vectors r_i (icosahedron vertices) will not be a real lattice, that is, the set of points of the form $m_1 r_1 + m_2 r_2 + \cdots m_6 r_6$, where m_i are the arbitrary integers, will be a dense subgroup in E_3 isomorphic to z^6 rather than a discrete subgroup in E_3.

It appears that this set is a lattice over the ring of integers in the quadratic field $Q\left(\sqrt{5}\right)$ rather than that over the ring of integers z. It can also be treated as a real lattice in the six-dimensional space E_6. Therefore, the regular icosahedron, which is often found in structural chemistry, naturally leads to the E_6 lattices (Conway and Sloane 1998). The case of a regular 4-D polyhedron, with 120 dodecahedral cells, can be similarly described.

Several fundamental problems of the substance structure had been considered in various studies preceding Shechtman's discovery, in 1982. In the same year, cka had published a paper (Mackay 1982, private communication) in which he demonstrated that the Penrose covering is unique and nonperiodic. Then, by the involved fivefold symmetry, it falls beyond the limits accepted by the classical crystallography formalism and can be referred to as a quasi-lattice.

In a later paper, analyzing the $AlMn_6$ structure, Mackay (1987) asserted that this is a texture of icosahedral symmetry, mentioned by K. Herman in 1931. The same reflexes were revealed in six other alloys as well; hence, this phenomenon is general.

The Mackay's quasi-lattice is a set of points, each point having integral indices with respect to the N-base vectors, N being larger than the space dimensionality. In this chapter, Mackay transferred the paradigm of structural analysis based on x-ray diffraction patterns to the direct research methods; then, the unit cell should not necessarily be a translation invariant.

It should be noted that, in 1975, several years prior to R. Penrose, the amateur mathematician R. Ammann discovered coverings with rhombic tiles, which also provide aperiodic structures (Ammann et al. 1992). Independently, F. Beenker obtained similar results (Beenker 1982). All these studies provided a kind of tiling that is a plane cut of a 4-D lattice, then projected on the plane.

Let us consider two electron-diffraction patterns, a "classical" one obtained by D. Shechtman for the Al_6Mn_4 quasicrystal (Fig. 17.1, Cahn et al. 1986) and another one provided by the $Al_{72}Ni_{20}Co_8$ alloy (Fig. 17.2, Abe et al. 2004). Both these patterns do not show a translational symmetry but tenfold and fivefold symmetry axes. It can be seen that (1) the bright points spread out from the center of the diffraction pattern along the radii with an increasing step; (2) inside each regular pentagon in the diffraction pattern, there is a smaller-sized pentagon wherein a next smaller pentagon arises; and so forth. This self-similarity by scaling can also be assigned to the Penrose tiling and icosahedral symmetry.

Let us fill a plane with regular polygons of increasing size (a hierarchical filling of a plane; Zhizhin 2010). The similarity factor depends only on the number of sides of the polygon in question. The plane is filled by means of extending the sides of the polygon of the previous generation until the sides intersect. The sides of the polygon of the subsequent generation pass through the obtained intersection points. The lengths of the sides of the increasing polygons make up a geometric progression.

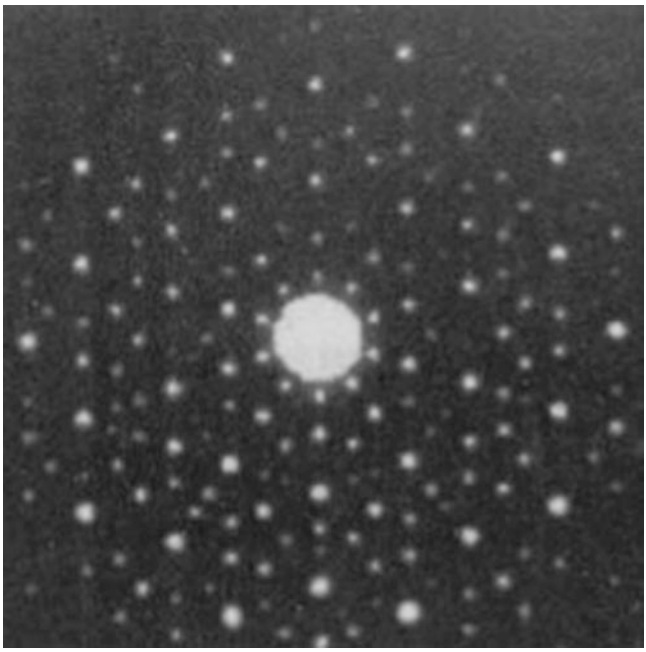

Fig. 17.1 The electron-diffraction pattern of alloy Al_6Mn_4 (Cahn et al. 1986)

The value of the geometric progression factor as a function of the number of the sides of the polygon is determined in Zhizhin (2010). When a plane is hierarchically filled with a regular polygon (e.g., a pentagon), the distance between the vertices of the pentagons increases fast.

More realistic results are obtained when the plane is filled with twinned polygons. Let us consider two regular convex pentagons with the common center, which are rotated with respect to each other by an angle of 36°. To hierarchically fill the plane with this complex, we prolong from the center outward the radii that pass through all the vertices of the complex and also all the lines parallel to each of the radii. Thereby five sets of parallel lines are formed. In this case, the parallel lines of one of the sets naturally intersect all the lines of the other sets of the parallel lines. As a result, a set of regular pentagons, which lie on the sides of the decagon of the source complex and surround the decagon without gaps, is built up. By extending the sides of the constructed pentagons up to the intersection, a new layer of the pentagons of larger size lying on the diagonals of the pentagons is formed.

By continuing this process, we obtain a grid of vertices of the pentagons, as depicted in Fig. 17.3. Obviously, this grid exactly coincides with the diffraction pattern in Fig. 17.2. By connecting the nodes in the grid with the straight lines, we obtain the hierarchical dense filling of the plane with the regular pentagon. A set of similar pentagons is formed (Fig. 17.3) so that beside the pentagons embedded into each other, with the similarity factor from Zhizhin (2010), sets of pentagons lying

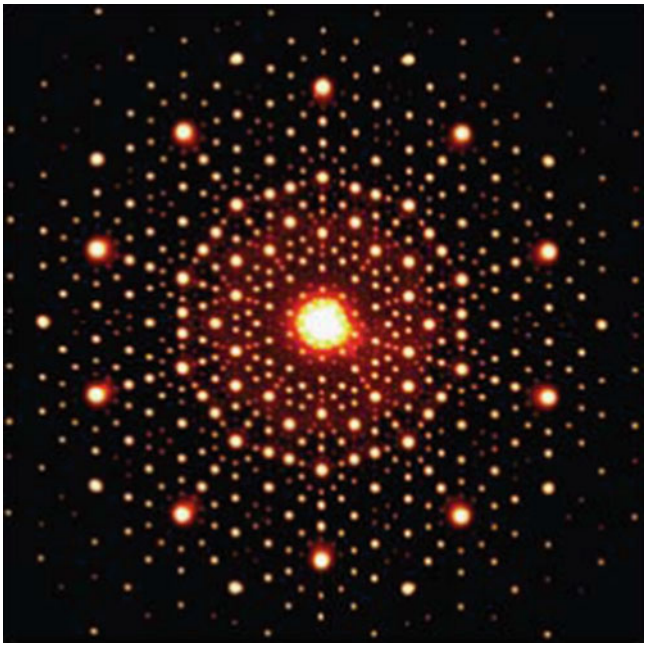

Fig. 17.2 The electron-diffraction pattern of alloy $Al_{72}Ni_{20}Co_8$ (Abe et al. 2004)

on the diagonal of a pentagon of smaller size are formed. It can be demonstrated that the similarity factor in these sets of pentagons equals to $\sqrt{\left(3+\sqrt{3}\right)/2}$.

As the larger-sized pentagons propagate away from the center, in addition to the concentric pentagons of smaller size, there appear pentagons between the central pentagons and lateral sides of the larger-sized pentagons. In this system, the density of arrangement of the vertices of the pentagons, in principle, may increase to infinity in each local area of the plane. It should be noted that certain similarity factors are independent of any external parameters and are fundamental numbers that characterize the geometry of the structure in question.

Attempts to transfer the results obtained in Zhizhin (2010) to the 3-D space have shown that such a transfer is impossible—first, because the 3-D space can be filled without gaps and clearances only by cubes or truncated octahedra and, second, filling the 3-D space with other convex polyhedra calls for concurrent involvement of polyhedra of different shapes. In this case, finite clusters of polyhedra of identical shapes are not formed.

The situation basically changes with moving to a multidimensional space, in particular, the 4-D space. In a multidimensional space, the polytopes are sets of polyhedra adjacent to each other over the whole faces. This is consistent with the notion that a substance is formed in the nanoworld in the multidimensional space (Shevchenko et al. 2009).

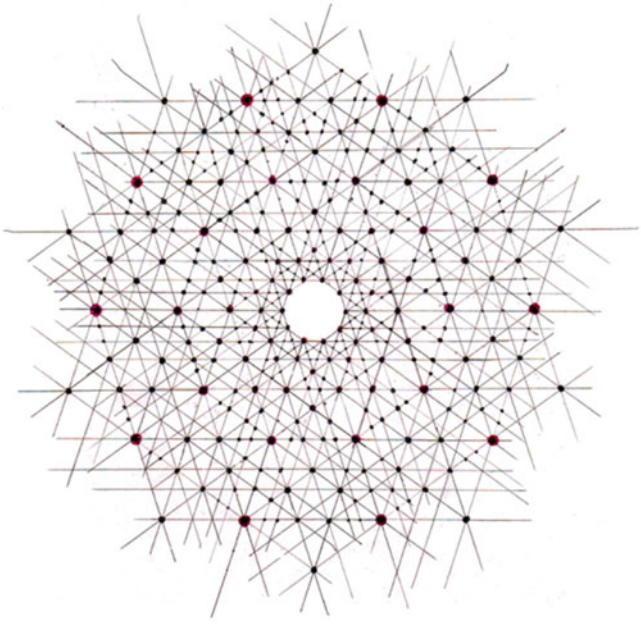

Fig. 17.3 The hierarchical dense filling of the plane by regular pentagons

As mapped on a plane, a regular simplex in the 4-D space is a set of five regular tetrahedra, each face of which represents a set of five regular tetrahedra, each face of any of those being covered by some face of a certain tetrahedron from that set. Let us superimpose two regular simplexes on each other so that the centers of the simplexes should coincide and each vertex of the simplex lies in the middle between two nearest vertices of the other simplex. Then we hierarchically fill the 4-D space with the obtained twinned regular simplex. The result of such filling projected on a plane is shown in Fig. 17.4. The nonperiodic lattices observed in the electron-diffraction patterns of various substances are the projection on a plane of the hierarchical filling of the 4-D space with the twinned regular simplex. It is essential that there is no golden ratio in the division of a regular simplex by a segment. The golden ratio appears on the plane only as a result of the projection from the 4-D space to the 2-D space whereby the segments loose the commensurability. The intersections of the straight lines of these sets create on the plane a system of regular pentagons of different sizes. Moreover, the pattern of the intersections of these lines coincides with that arising from the hierarchical dense filling of the plane with the twinned regular pentagon (Fig. 17.4) and, therefore, describes the arrangement of the quasicrystal lattice sites observed in the plane diffraction patterns.

Hence, the structure of quasicrystals observed in the plane diffraction patterns is based on the system of five sets of parallel lines, that is, the periodicity along five directions on the plane is hidden in these structures. The multiplicity of the

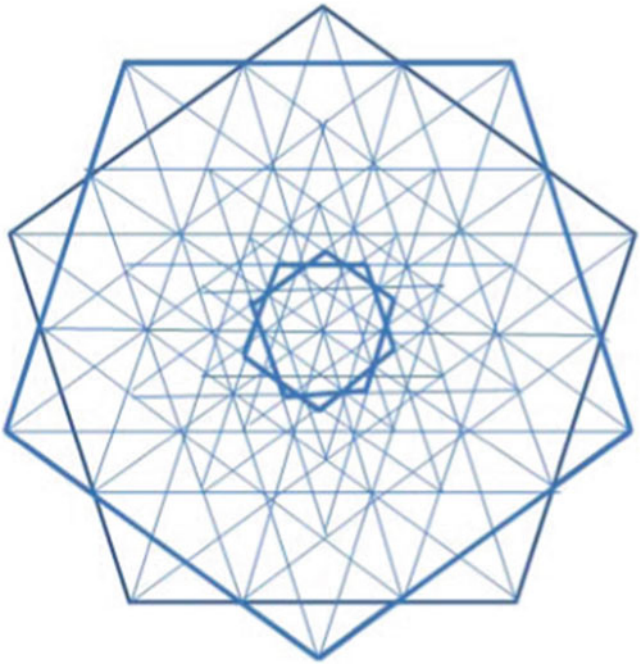

Fig. 17.4 The projection of 4-D space on 2-D plane of the hierarchical filling by the regular simplex

directions on the plane along which the periodicity occurs is the consequence of the multidimensionality of the real space of the nanoworld.

It should be noted that the idea of presentation of the multidimensional space as a scene of chemical interaction had originated long before the experimental discovery of quasicrystals. In particular, it arose from publications of the Penrose tilings and attempts to comprehend the aperiodic structures.

In the early twentieth century, Kowalewski (1921) had considered polyhedra, such as triacontahedron or rhombic triacontahedron. These polyhedra constructed from rhombs (Kowalewski named them Keplerian) show the property of the golden ratio of their diagonals $\tau = \left(\sqrt{5}+1\right)/2$. Then G. Kowalewski demonstrated that the use of a 6-D cube makes it possible to fill the whole space with figures derived from the base polyhedron. (Later, in 2008, S. Andersson constructed virus structures in a similar way.)

In 1993, J. Sadoc and R. Mosseri studied quasiperiodic structures based on the 8-D lattice. A formula was proposed that allows one to calculate the location of points on the bundle shell. Such 4-D quasicrystals show interesting properties, which ultimately provide the transfer to the 3-D space of the icosahedral or tetrahedral symmetry (Sadoc and Mosseri 1993).

A plane tiling with the regular decahedron was proposed (Lord et al. 2011). An original approach to the analysis of structures of compounds in the Bi-Se system was developed by Lind and Lidin (2003). By using a [3 + 1]-dimensional space model, the authors succeeded in overcoming contradictions associated to the incommensurable phases (which is known to be essential in the building up of aperiodic quasicrystals) and in understanding of the formation of such layered structures.

17.3 Conclusion

Dealing with objects in n-dimensional spaces is nowadays more accessible, and, owing to the capabilities of the computer technology, the structure representation in structural chemistry is possible in its deep complexity (Molnar and Prok 2012).

In conclusion, it should be said that the brilliant discovery of the quasicrystals was perceived and predicted by great mathematicians and chemists, starting with Euclid, Kepler, Haüy, and the outstanding generation of structural chemists of the twentieth century, whose studies we endeavored to overview.

References

Abe E, Yan Y, Pennycook SJ (2004) Quasicrystals as cluster aggregates. Nat Mater 3:759–767
Ammann R, Grünbamm B, Shephard G (1992) Aperiodic tiles. Discret Comput Colum 8:1–25
Andersson S (2008) The structure of virus Capsids. Z Anorg Allg Chem 634(12–13):2161–2170
Beenker F (1982) Algebraic theory of nonperiodic tilings of the plane by two simple building blocks: a square & a rhombus. TM report 82- WSKO4, 1982
Bernal JD (1967) Generalized crystallography. In: In the origin of life. World Publishing Company, Wenatchee
Cahn J, Gratias D, Shechtman D (1986) Pauling's model not universally accepted. Nature 319:102–103
Conway JH, Sloane N (1998) Sphere packings, lattices & the groups. Springer, New York
Kowalewski G (1921) Mathematica Delecting and, Magishe Quadrate und Magishe Parkette Der Keplersche Körper. Von Wilhelm Engelmann, Leipzig (in German)
Lind H, Lidin S (2003) A general structure model for Bi-Se phases using a superspace formalism. Solid State Sci 5:47–57
Lord E, Ranganathan S, Kulkarni U (2011) Quasicrystals: tiling versus clustering. Phil Mag A 81:2645–2651
Mackay A (1981) De nive quinquangula. Krystallografiya 26:910–919
Mackay A (1982) Crystallography & the Penrose pattern. Physica A 114:609–613
Mackay A (1987) What has Penrose tiling to do with the icosahedral phases? Geometrical aspects of the icosahedral quasicrystal problem. J Microsc 146:233–243
Molnar E, Prok I (2012) Animation of the 4-dimentional regular solids moving in the computer 2-screen with visibility and shading of 2-faces. Build Caused Saf 41:89–92
Pauling L (1923) The crystal structure of magnesium stannide. J Am Chem Soc 45:2777–2780

Pauling L (1985) Apparent icosahedral symmetry is due to directed multiple twinning of cubic crystals. Nature 317:512–514
Sadoc J, Mosseri R (1993) The E_8 lattice and quasicrystals. J Non-Cryst Solid 153–154:247–252
Samson S (1962) Crystal structure of $NaCd_2$. Nature 195:259–262
Shevchenko V, Blatov V, Zhizhin G (2009) Intermetallic compounds of the $NaCd_2$ family perceived as assemble of nanoclusters. Struct Chem 20:975–982
Zhizhin G (2010) Geometrical basis of the dissipative structures. Politechnika, Saint-Petersburg, p 120

Chapter 18
Mathematics of D_5 Network

A.R. Ashrafi, F. Koorepazan-Moftakhar, Mircea V. Diudea, and M. Stefu

Abstract Diamond D_5 is the generic name proposed by Diudea for hyperdiamonds constructed mostly from pentagons and hexagons. There are known several allotropes of D_5; within this chapter only the clathrate II structure (the basic diamond D_5) and the spongy D_5 structure are considered. A topological index is a single number representation of the topology of a given structure. Topological indices are calculated on the graphs associated to the chemical structure and were extensively used in QSAR/QSPR studies. The aim of this chapter is to apply some group theoretical algorithms to compute symmetry and topological indices of this important class of nanostructured materials.

A.R. Ashrafi (✉)
Department of Nanocomputing, Institute of Nanoscience and Nanotechnology, University of Kashan, Kashan 87317-51167, I.R. Iran

Department of Mathematics, Faculty of Mathematical Sciences, University of Kashan, Kashan 87317-51167, I.R. Iran
e-mail: Ashrafi@kashanu.ac.ir

F. Koorepazan-Moftakhar
Department of Mathematics, Faculty of Mathematical Sciences, University of Kashan, Kashan 87317-51167, I.R. Iran

M.V. Diudea • M. Stefu
Faculty of Chemistry and Chemical Engineering, Babes-Bolyai University, Arany Janos street 11, 400028 Cluj, Romania

M.V. Diudea and C.L. Nagy (eds.), *Diamond and Related Nanostructures*, Carbon Materials: Chemistry and Physics 6, DOI 10.1007/978-94-007-6371-5_18,

18.1 Introduction and Definitions

A *graph* is a pair $G=(V,E)$ of *points* and *lines*. The points and lines of G are also called *vertices* and *edges* of the graph, respectively. If e is an edge of G, connecting the vertices u and v, then we write $e=uv$ and say "u and v are adjacent." A *path* P in G is a sequence $v_1, v_2, \ldots, v_r$ of vertices such that v_i and v_{i+1} are adjacent, $1 \le i \le r-1$. A path graph is a graph consisting of a single path. A *cycle* graph C_n of order n is a graph with $V(G) = \{v_1, v_2, \ldots, v_n\}$ and $E(G) = \{v_1v_2, v_2v_3, \ldots, v_{n-1}v_n, v_nv_1\}$. A graph with the property that each pair of vertices can be connected by a path is called a *connected graph*. A *chemical graph* is a graph in which the degree of each vertex is at most four. Chemical graphs are models of molecules in which atoms are represented by vertices and chemical bonds by edges of a graph. This theory had an important effect on the development of the chemical sciences (Trinajstić 1992).

By IUPAC terminology, a *topological index* is a numerical value associated with chemical constitution purporting for correlation of chemical structure with various physical properties, chemical reactivity, or biological activity. There is not a one-to-one correspondence between chemical structures and topological indices, because several graphs may have the same topological index. The *distance* $d(u,v) = d_G(u,v)$ between two vertices u and v in a graph G is the length of a shortest path in G connecting u and v. This defines a meter on the set of all vertices of the graph. A topological index is called distance-based if it is related to the distance function $d(-,-)$.

The first reported distance-based topological index is the *Wiener index* (Wiener 1947). It is defined as the summation of all distances over all edges of G. This interpretation of the Wiener index was introduced by Haruo Hosoya, who used the name "topological index" for such numbers (Hosoya 1988).

In the year 2000, a molecular structure descriptor, named the *Padmakar-Ivan index* (PI index for short), was put forward by Padmakar Khadikar (Khadikar 2000; Khadikar et al. 2001a, b). Eventually, in a series of papers (Sabaghian-Bidgoli et al. 2011; Ashrafi and Ghorbani 2010; Ashrafi et al. 2008, 2009a, b, 2010; Khadikar et al. 2001a, b, 2002a, b, 2003; Gutman and Ashrafi 2008) and books (Diudea et al. 2006; Ashrafi et al. 2009a, b; Ashrafi and Ghorbani 2009), the preliminary properties of the PI index were determined and examples were offered for its applicability in QSPR/QSAR studies. In Ashrafi and Rezaei (2007), Ashrafi and Loghman (2006a, b, c), and Xu and Deng (2006), exact formulas for PI index of some classes of nanotubes are reported.

The PI index is defined as follows: Let G have exactly m edges, $e=uv$ be an edge, and $w \in V(G)$. Define $d(e,w) = \mathrm{Min}\{d(u,w),d(v,w)\}$. If $f=ab \in E(G)$, then f is said to be parallel with e and we write $f \,||\, e$, if $d(e,a) = d(e,b)$. Define $m_u(e)$ to be the number of edges of the graph G whose distance to the vertex u is smaller than the distance to the vertex v. Analogously, let $m_v(e)$ be the number of edges of the graph G whose distance to the vertex v is smaller than the distance to the vertex u. Then

$$\mathrm{PI}(G) = \sum_{e=uv} \Big[m_u(e) + m_v(e) \Big] \tag{18.1}$$

In Khalifeh et al. (2008), the authors proposed a vertex version of the PI index. If G is a graph, then this topological index is defined as

$$\mathrm{PI}_v(G) = \sum_{e=uv \in E(G)} \Big[n_u(e) + n_v(e) \Big] \tag{18.2}$$

where $n_u(e)$ is the number of vertices of G lying closer to u and $n_v(e)$ is the number of vertices of G lying closer to v. The Szeged index is another topological index introduced by Ivan Gutman (1994). This topological index G is defined as

$$\mathrm{Sz}(G) = \sum_{e=uv \in E(G)} n_u(e) n_v(e) \tag{18.3}$$

Notice that in computing PI, PI_v, and Sz, the vertices and edges equidistant to u and v are not taken into account.

The eccentricity of a given vertex u in a graph G, $\varepsilon(u)$, is the largest distance between u and any other vertex v of G. The maximum eccentricity over all vertices of G is called the diameter, $\mathrm{diam}(G)$, and the minimum eccentricity among the vertices of G is called the radius of G, denoted by $R(G)$. The set of vertices whose eccentricity is equal to the radius of G is called the center of G. The eccentric connectivity index $\xi^c(G)$ of a graph G, (Sharma et al. 1997), is defined as

$$\xi^c(G) = \sum_{u \in V(G)} \deg(u) \varepsilon(u) \tag{18.4}$$

The mathematical properties of this topological index are studied in some recent papers (Ashrafi et al. 2011; Gupta et al. 2002; Zhou and Du 2010; Sardana and Madan 2001).

Throughout this chapter, our notation is standard and taken mainly from Trinajstić (1992) and Diudea et al. (2006). Our calculations are done by the aid of TopoCluj (Diudea et al. 2002), GAP (The GAP Team 1995), MAGMA (Bosma et al. 1997), and HyperChem (HyperChem package Release 7.5 for Windows 2002).

18.2 Symmetry of Some D_5 Networks

We first describe some group theoretical notions. We start by definition of the symmetry. To do this, we use the notion of a group action in which every element of the group acts like a one-to-one map. To clarify this notion, we assume that G is a group and X is a set. The group G is said to act on a set X when there is a map ϕ such that ϕ: $G \times X \to X$ and for all elements $x \in X$:

1. If e denotes the identity element of the group, then $\phi(e,x) = x$
2. For all $g,h \in G$, $\phi(g, \phi(h,x)) = \phi(gh,x)$

To simplify our arguments, we usually write gx as $\phi(g,x)$. The set X is called a G-set and ϕ is a group action. The set $\{gx \mid g \in G\}$ is called the orbit of x. The subgroup that fixes is called the isotropy subgroup of x.

For a permutation σ on n objects, the corresponding permutation matrix is an $n \times n$ matrix P_σ given by $P_\sigma = [x_{ij}]$, $x_{ij} = 1$ if $i = \sigma(j)$ and 0 otherwise. It is easy to see that $P_\sigma P_\tau = P_{\sigma\tau}$, for each permutation σ and τ on n objects, and so the set of all $n \times n$ permutation matrices is a group isomorphic to the symmetric group S_n on n symbols. It is well known that a permutation σ of the vertices of a graph G belongs to its automorphism group if it satisfies $P_\sigma^t A P_\sigma = A$, where A is the adjacency matrix of G. Suppose $\mathrm{Aut}(G) = \{\sigma_1, \ldots, \sigma_m\}$. The matrix $S_G = [s_{ij}]$, where $s_{ij} = \sigma_i(j)$ is called a solution matrix for G. Clearly, to compute the automorphism group of G, it is enough to calculate a solution matrix for G.

The Diamond D_5 is a name proposed by Diudea for hyperdiamonds containing mostly pentagonal rings (Diudea 2010; Diudea et al. 2011a, b, 2012; Kyani and Diudea 2012; Diudea and Nagy 2012; Szefler and Diudea 2012). There are known several allotropes of D_5; within this chapter, six types of substructures, belonging to the clathrate II structure (the basic D_5 allotrope) and to the spongy D_5, are considered. These are D_5-20(16)Ada_198, D_5-Spongy_504, C_{57}, D_5-20(12)Ada_158, D_5-20(18)Dia_226, and D_5-20(20)Dia_246 (Fig. 18.1a–f).

Suppose G is a graph, A is a subgroup of its automorphism group, $x \in V(G)$, and $f \in A$. Then $xf := (x)f$ defines an action of A on G. This action is called the natural action of G on $V(G)$. The subgroup A has also a natural action on $E(G)$. These actions are called transitive if they have one orbit. In Darafsheh (2010), the following useful result is proved:

Theorem *Suppose that $G = (V,E)$ is a simple connected graph and the orbits of the natural action of* $\mathrm{Aut}(G)$ *on $E(G)$ are $\Delta_i = \Delta_i(e_i)$, $1 \le i \le s$, where $e_i = u_i v_i$ is an edge of G. Then,*

1. *If $N_u(e) = \{w \in V \mid d(w,u) < d(w,v)\}$ and $N_v(e) = \{w \in V \mid d(w,v) < d(w,u)\}$, then $n_u(e) = |N_u(e)|$ and $n_v(e) = |N_v(e)|$. In particular, the Szeged index of G can be computed by the following formula*:

$$\mathrm{Sz}(G) = \sum |\Delta_i| n_{u_i}(e_i|G) \times n_{v_i}(e_i|G).$$

2. *The PI index of G is computed as follows:*

$$\mathrm{PI}(G) = \sum_{i=1}^{r} |E_i| \Big(n_{e_i u_i}(e_i|G) + n_{e_i v_i}(e_i|G) \Big).$$

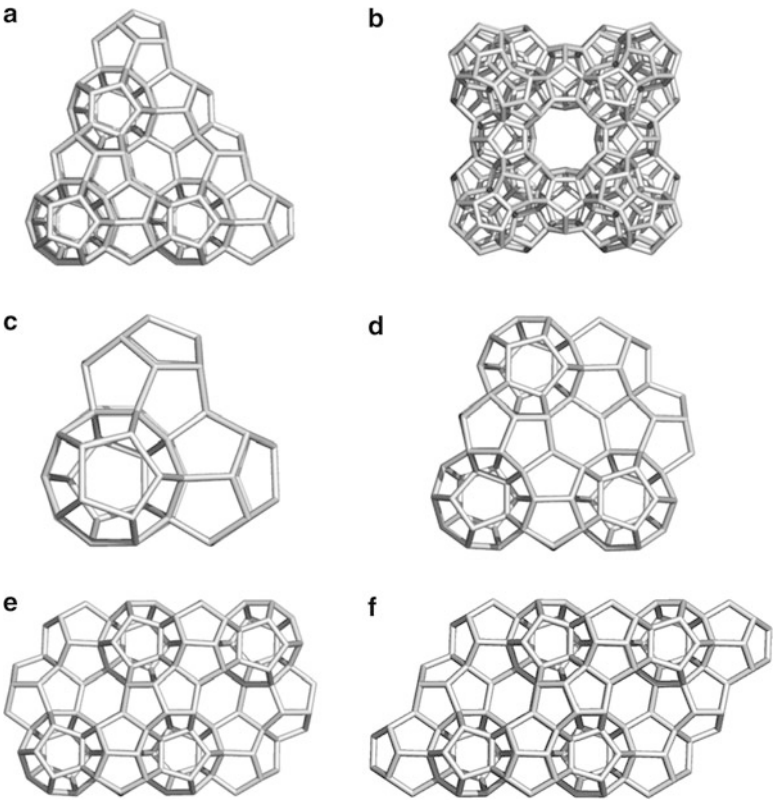

Fig. 18.1 The molecular graph of D_5 networks: (**a**) D_5-20(16)Ada_198; (**b**) D_5-Spongy_504; (**c**) C_{57}; (**d**) D_5-20(12)Ada_158; (**e**) D_5-20(18)Dia_226; (**f**) D_5-20(20)Dia_246

3. *If for* $v \in V$ *we defined* $(v) = \sum_{x \in V} d(v, x)$, *then* $\mathrm{W}(G) = \frac{1}{2} \sum_{v \in V} d(v)$. *If the action is transitive, then* $\mathrm{W}(G) = \frac{1}{2}|V|d(v)$, *for any* $v \in V$.

By a similar argument as above, one can prove that if $V_1, \ldots, V_r$ are orbits of the natural action of $\mathrm{Aut}(G)$ on $V(G)$, then

$$\mathrm{PI}_v(G) = \sum_{i=1}^{r} |V_i| \Big(n_{u_i}(e_i) + n_{v_i}(e_i) \Big).$$

In our method, we have to first compute the automorphism group of the graph under consideration and then the orbits of the action of the automorphism group on the set of vertices and edges. Finally, by applying the above theorem,one can

Table 18.1 Computing symmetry and some topological indices of D_5 networks

Struct	D_5 network	PI	PI_e	W	Sz	$\xi^c(G)$	Aut(G)
(a)	D_5-20(16)Ada_198	51,372	89,532	126,621	1,257,482	7,768	S_4
(b)	D_5-spongy_504	335,856	595,064	1,189,908	21,564,496	31,384	$C_2 \times S_4$
(c)	C_{57}	4,080	6,696	6,294	35,486	1,244	S_4
(d)	D_5-20(12)Ada_158	32,684	56,352	71,629	645,298	5,324	S_4
(e)	D_5-20(18)Dia_226	67,478	118,202	168,997	1,859,040	9,236	D_{12}
(f)	D_5-20(20)Dia_246	80,022	140,444	213,129	2,428,978	11,840	D_{12}

compute these topological indices. To describe our calculations, we have to draw the molecules by HyperChem and then compute the distance matrix of these molecular graphs by TopoCluj. We next prepare some GAP and MAGMA pseudocodes to compute the automorphism group and then orbits of the automorphism group under natural action. Finally, we apply our main theorem to compute PI, PI_v, Sz, W, and ξ^c, for six D_5 networks. These programs are accessible from the authors upon request.

The Cauchy-Frobenius Lemma states that if G is a finite group acting on a finite set A, then G has m orbits on A, where $|G| = \Sigma_{x \in G} |fix(x)|$. Here, $fix(x)$ denotes the set of all elements $y \in A$ such that $xy = y$. On the other hand, according to our main theorem, the values $d(x) = \Sigma_{y \in V(G)} d(x,y)$, $[n_u(e) \times n_v(e)]$, and $[n_u(e) + n_v(e)]$ on each orbits of the natural actions of Aut(G) are constant. Therefore, to compute these quantities, it is enough to compute all orbits of the natural actions and then obtain a representative set for orbits. Then by applying our theorem, we can calculate our mentioned graph invariants.

Our calculations with the aid of GAP and MAGMA show that in each case there is just one orbit of length four and other orbits are singleton. Applying our algorithm mentioned above, we can compute in Table 18.1 the values of PI, PI_v, Sz, W, and ξ^c for six types of D_5 networks that are computed.

Our calculations on six D_5 networks suggest the following conjecture:

Conjecture The natural action of the automorphism groups in each D_5 networks has exactly n – 3 orbits containing n – 2 singletons and one orbit of length 4, where n is the number of vertices.

In Table 18.2, a generator set for the symmetry group of all D_5-type networks is presented. Using these generator sets and a simple GAP program, one can prove that the symmetry groups of these D_5 networks are isomorphic to S_4, $C_2 \times S_4$ or a dihedral group of order 12.

Table 18.2 Generators of symmetry groups

X_a = (1, 5) (2, 4) (6, 41) (7, 42) (8, 16) (9, 17) (10, 15) (13, 14) (21, 23) (22, 24) (25, 32) (26, 31) (27, 30) (28, 33) (29, 34) (36, 37) (38, 39) (43, 154) (44, 155) (45, 196) (46, 198) (47, 197) (48, 142) (49, 143) (50, 170) (51, 169) (52, 158) (53, 159) (54, 166) (55, 161) (56, 162) (57, 163) (58, 172) (59, 171) (60, 160) (61, 168) (62, 167) (63, 157) (64, 156) (65, 165) (66, 164) (67, 178) (68,174) (69, 182) (70, 181) (71, 177) (72, 173) (73, 180) (74, 179) (75, 176) (76, 175) (77, 152) (78, 153) (79, 188) (80, 190) (81, 189) (82, 145) (83, 146) (84, 149) (85, 150) (86, 151) (87, 144) (88, 148) (89, 147) (90, 141) (91, 140) (92, 136) (93, 137) (94, 138) (95, 126) (96, 127) (97, 183) (98, 184) (99, 113) (100, 112) (103, 109) (107, 115) (108, 114) (110, 111) (116, 121) (118, 125) (119, 124) (122, 123) (128, 131) (132, 133) (134, 186) (135, 187) (139, 185)

Y_a = (1, 27, 34) (2, 26, 33) (3, 25, 32) (4, 28, 31) (5, 29, 30) (6, 39, 42) (7, 38, 41) (8, 20, 16) (9, 19, 17) (10, 18, 15) (13, 22, 23) (14, 21, 24) (36, 37, 40) (43, 152, 137) (44, 153, 138) (45, 188, 136) (46, 190, 140) (47, 189, 141) (48, 150, 126) (49, 151, 127) (50, 167, 112) (51, 168, 113) (52, 160, 109) (53, 159, 102) (54, 166, 101) (55, 164, 115) (56, 165, 114) (57, 163, 106) (58, 172, 104) (59, 171, 105) (60, 158, 103) (61, 169, 99) (62, 170, 100) (63, 156, 110) (64, 157, 111) (65, 162, 108) (66, 161, 107) (67, 178, 120) (68, 174, 117) (69, 180, 124) (70, 179, 125) (71, 173, 121) (72, 177, 116) (73, 182, 119) (74, 181, 118) (75, 175, 123) (76, 176, 122) (77, 154, 93) (78, 155, 94) (79, 196, 92) (80, 198, 91) (81, 197, 90) (82, 145, 129) (83, 146, 130) (84, 144, 131) (85, 142, 95) (86, 143, 96) (87, 149, 128) (88, 147, 133) (89, 148, 132) (97, 194, 183) (98, 195, 184) (134, 191, 186) (135, 192, 187) (139, 193, 185)

Z_a = (1, 43) (2, 44) (3, 45) (4, 46) (5, 47) (6, 48) (7, 49) (8, 50) (9, 51) (10, 52) (11, 53) (12, 54) (13, 55) (14, 56) (15, 57) (16, 58) (17, 59) (18, 60) (19, 61) (20, 62) (21, 63) (22, 64) (23, 65) (24, 66) (25, 67) (26, 69) (27, 70) (28, 73) (29, 74) (30, 77) (31, 78) (32, 79) (33, 80) (34, 81) (35, 82) (36, 83) (37, 84) (38, 85) (39, 86) (40, 87) (41, 88) (42, 89) (71, 72) (75, 76) (90, 152) (91, 153) (92, 188) (93, 189) (94, 190) (95, 147) (96, 148) (97, 175) (98, 176) (99, 171) (100, 172) (101, 166) (102, 159) (103, 163) (104, 167) (105, 168) (106, 160) (107, 165) (108, 164) (109, 158) (110, 161) (111, 162) (112, 170) (113, 169) (114, 156) (115, 157) (116, 192) (117, 191) (118, 154) (119, 155) (120, 196) (121, 193) (122, 194) (123, 195) (124, 198) (125, 197) (126, 143) (127, 142) (128, 146) (129, 145) (130, 144) (131, 149) (132, 150) (133, 151) (134, 174) (135, 173) (136, 178) (137, 179) (138, 180) (139, 177) (140, 182) (141, 181) (183, 184) (185, 187)

X_b = (1, 7) (2, 6) (5, 8) (9, 10) (12, 17) (13, 16) (18, 20) (19, 21) (22, 23) (24, 37) (25, 38) (26, 35) (27, 34) (28, 33) (29, 31) (30, 32) (36, 41) (39, 40) (42, 45) (43, 47) (44, 46) (48, 49) (51, 52) (54, 57) (58, 191) (59, 192) (60, 188) (61, 181) (62, 180) (63, 189) (64, 190) (65, 182) (66, 179) (67, 178) (68, 185) (69, 184) (70, 183) (71, 194) (72, 193) (73, 186) (74, 187) (75, 211) (76, 210) (77, 209) (78, 208) (79, 218) (80, 203) (81, 196) (82, 195) (83, 198) (84, 213) (85, 212) (86, 214) (87, 215) (88, 200) (89, 199) (90, 217) (91, 216) (92, 207) (93, 206) (94, 204) (95, 205) (96, 202) (97, 201) (98, 197) (99, 224) (100, 225) (101, 223) (102, 220) (103, 219) (104, 221) (105, 226) (106, 228) (107, 227) (108, 119) (109, 222) (110, 120) (111, 234) (112, 233) (113, 235) (114, 236) (115, 240) (116, 237) (117, 238) (118, 239) (121, 443) (122, 442) (123, 439) (124, 440) (125, 444) (126, 438) (127, 437) (128, 441) (129, 446) (130, 445) (131, 447) (132, 453) (133, 452) (134, 450) (135, 451) (136, 449) (137, 448) (138, 456) (139, 457) (140, 454) (141, 455) (142, 459) (143, 458) (144, 473) (145, 474) (146, 471) (147, 470) (148, 469) (149, 467) (150, 468) (151, 465) (152, 466) (153, 464) (154, 463) (155, 462) (156, 477) (157, 460) (158, 461) (159, 476) (160, 475) (161, 472) (162, 481) (163, 482) (164, 302) (165, 478) (166, 480) (167, 479) (168, 484) (169, 483) (170, 485) (171, 487) (172, 486) (173, 488) (174, 504) (175, 502) (176, 503) (177, 501) (229, 489) (230, 490) (231, 491) (232, 492) (246, 254) (247, 255) (248, 251) (249, 253) (250, 252) (256, 257) (258, 277) (259, 278) (260, 275) (261, 276) (262, 267) (263, 268) (264, 266) (265, 281) (269, 280) (270, 279)

(continued)

Table 18.2 (continued)

(271, 272) (273, 274) (282, 284) (285, 291) (286, 292) (287, 293) (288, 290) (294, 494) (295, 493) (296, 495) (297, 496) (298, 299) (303, 309) (304, 308) (307, 310) (311, 312) (314, 319) (315, 318) (320, 322) (321, 323) (324, 325) (326, 339) (327, 340) (328, 337) (329, 336) (330, 335) (331, 333) (332, 334) (338, 343) (341, 342) (344, 347) (345, 349) (346, 348) (350, 351) (353, 354) (356, 357) (358, 363) (359, 364) (360, 361) (362, 367) (365, 366) (368, 371) (372, 416) (373, 417) (374, 380) (375, 379) (378, 381) (382, 383) (385, 390) (386, 389) (391, 393) (392, 394) (395, 396) (397, 410) (398, 411) (399, 408) (400, 407) (401, 406) (402, 404) (403, 405) (409, 414) (412, 413) (415, 418) (419, 420) (422, 423) (425, 426) (427, 500) (428, 499) (429, 497) (430, 498) (431, 432) (433, 436)

Y_b = (1, 74) (2, 73) (3, 65) (4, 61) (5, 68) (6, 64) (7, 63) (8, 60) (9, 72) (10, 71) (11, 62) (12, 70) (13, 69) (14, 67) (15, 66) (16, 59) (17, 58) (18, 96) (19, 97) (20, 79) (21, 80) (22, 77) (23, 78) (24, 90) (25, 91) (26, 88) (27, 86) (28, 87) (29, 84) (30, 85) (31, 83) (32, 98) (33, 81) (34, 82) (35, 95) (36, 94) (37, 93) (38, 92) (39, 75) (40, 76) (41, 89) (42, 110) (43, 109) (44, 108) (45, 107) (46, 106) (47, 105) (48, 104) (49, 103) (50, 102) (51, 101) (52, 100) (53, 99) (54, 117) (55, 118) (56, 115) (57, 116) (111, 112) (113, 114) (119, 485) (120, 483) (121, 257) (122, 256) (123, 248) (124, 244) (125, 251) (126, 247) (127, 246) (128, 243) (129, 255) (130, 254) (131, 245) (132, 253) (133, 252) (134, 250) (135, 249) (136, 242) (137, 241) (138, 279) (139, 280) (140, 262) (141, 263) (142, 260) (143, 261) (144, 273) (145, 274) (146, 271) (147, 269) (148, 270) (149, 267) (150, 268) (151, 266) (152, 281) (153, 264) (154, 265) (155, 278) (156, 277) (157, 276) (158, 275) (159, 258) (160, 259) (161, 272) (162, 293) (163, 292) (164, 291) (165, 290) (166, 289) (167, 288) (168, 287) (169, 286) (170, 285) (171, 284) (172, 283) (173, 282) (174, 300) (175, 301) (176, 298) (177, 299) (178, 449) (179, 448) (180, 447) (181, 440) (182, 441) (183, 451) (184, 450) (185, 439) (186, 437) (187, 438) (188, 444) (189, 446) (190, 445) (191, 453) (192, 452) (193, 442) (194, 443) (195, 468) (196, 467) (197, 470) (198, 469) (199, 462) (200, 477) (201, 463) (202, 464) (203, 466) (204, 475) (205, 476) (206, 459) (207, 458) (208, 473) (209, 474) (210, 471) (211, 472) (212, 457) (213, 456) (214, 455) (215, 454) (216, 460) (217, 461) (218, 465) (219, 479) (220, 480) (221, 478) (222, 484) (223, 488) (224, 486) (225, 487) (226, 481) (227, 482) (228, 302) (229, 494) (230, 493) (231, 496) (232, 495) (233, 492) (234, 491) (235, 490) (236, 489) (237, 503) (238, 501) (239, 502) (240, 504) (294, 295) (296, 297) (303, 382) (304, 383) (305, 381) (306, 377) (307, 378) (308, 389) (309, 390) (310, 384) (311, 386) (312, 385) (313, 376) (314, 375) (315, 374) (316, 380) (317, 379) (318, 388) (319, 387) (320, 411) (321, 410) (322, 409) (323, 408) (324, 403) (325, 402) (326, 412) (327, 413) (328, 395) (329, 397) (330, 398) (331, 414) (332, 399) (333, 392) (334, 391) (335, 394) (336, 393) (337, 406) (338, 407) (339, 404) (340, 405) (341, 400) (342, 401) (343, 396) (344, 417) (345, 415) (346, 416) (347, 422) (348, 424) (349, 423) (350, 373) (351, 418) (352, 372) (353, 420) (354, 421) (355, 419) (356, 430) (357, 429) (358, 431) (359, 432) (360, 425) (361, 499) (362, 500) (363, 497) (364, 498) (365, 427) (366, 428) (367, 426) (368, 434) (369, 435) (370, 433) (371, 436)

Z_b = (6, 14) (7, 15) (8, 11) (9, 13) (10, 12) (16, 17) (18, 37) (19, 38) (20, 35) (21, 36) (22, 27) (23, 28) (24, 26) (25, 41) (29, 40) (30, 39) (31, 32) (33, 34) (42, 44) (45, 51) (46, 52) (47, 53) (48, 50) (54, 55) (58, 389) (59, 390) (60, 384) (61, 377) (62, 381) (63, 388) (64, 387) (65, 376) (66, 380) (67, 379) (68, 378) (69, 382) (70, 383) (71, 385) (72, 386) (73, 375) (74, 374) (75, 403) (76, 402) (77, 400) (78, 401) (79, 408) (80, 409) (81, 407) (82, 406) (83, 405) (84, 413) (85, 412) (86, 395) (87, 396) (88, 397) (89, 398) (90, 399) (91, 414) (92, 392) (93, 391) (94, 394) (95, 393) (96, 410) (97, 411) (98, 404) (99, 372) (100, 373) (101, 418) (102, 419) (103, 420) (104, 421) (105, 424) (106, 423) (107, 422) (108, 415) (109, 416) (110, 417) (111, 432) (112, 431) (113, 425) (114, 426) (115, 435) (116, 436) (117, 434) (118, 433) (119, 223) (120, 225) (121, 303) (122, 304) (123, 305) (124, 306) (125, 307) (126, 316) (127, 317) (128, 313) (129, 315) (130, 314) (131, 310) (132, 312) (133, 311) (134, 308) (135, 309) (136, 319) (137, 318) (138, 339)

(continued)

Table 18.2 (continued)

(139, 340) (140, 337) (141, 338) (142, 329) (143, 330) (144, 328) (145, 343) (146, 326) (147, 324) (148, 325) (149, 342) (150, 341) (151, 334) (152, 333) (153, 336) (154, 335) (155, 322) (156, 323) (157, 320) (158, 321) (159, 332) (160, 331) (161, 327) (162, 346) (163, 345) (164, 344) (165, 353) (166, 354) (167, 355) (168, 352) (169, 351) (170, 350) (171, 347) (172, 348) (173, 349) (174, 369) (175, 368) (176, 370) (177, 371) (178, 186) (179, 187) (180, 185) (183, 184) (191, 193) (192, 194) (195, 208) (196, 209) (197, 210) (198, 211) (199, 201) (200, 202) (203, 216) (204, 207) (205, 206) (212, 213) (214, 215) (217, 218) (219, 220) (222, 224) (227, 228) (229, 361) (230, 362) (231, 363) (232, 364) (233, 234) (235, 236) (237, 239) (241, 247) (242, 246) (245, 248) (249, 250) (252, 257) (253, 256) (258, 260) (259, 261) (262, 263) (264, 277) (265, 278) (266, 275) (267, 274) (268, 273) (269, 271) (270, 272) (276, 281) (279, 280) (282, 285) (283, 287) (284, 286) (288, 289) (291, 292) (294, 365) (295, 366) (296, 357) (297, 356) (298, 301) (302, 487) (358, 429) (359, 430) (360, 428) (367, 427) (442, 450) (443, 451) (444, 447) (445, 449) (446, 448) (452, 453) (454, 473) (455, 474) (456, 471) (457, 472) (458, 463) (459, 464) (460, 462) (461, 477) (465, 476) (466, 475) (467, 468) (469, 470) (478, 480) (481, 486) (482, 488) (483, 485) (489, 499) (490, 500) (491, 497) (492, 498) (493, 494) (495, 496) (501, 502)

X_c = (1, 9) (2, 10) (3, 8) (6, 7) (14, 16) (15, 17) (18, 31) (19, 32) (20, 33) (21, 34) (22, 24) (23, 25) (26, 39) (27, 30) (28, 29) (35, 36) (37, 38) (40, 41) (42, 43) (45, 49) (46, 50) (47, 48) (52, 53) (54, 56)

Y_c = (1, 13) (2, 12) (3, 11) (6, 17) (7, 16) (14, 15) (18, 19) (20, 21) (22, 39) (23, 40) (24, 30) (25, 29) (26, 27) (28, 41) (31, 38) (32, 37) (33, 36) (34, 35) (43, 44) (46, 47) (48, 52) (49, 51) (50, 53) (55, 56)

Z_c = (1, 7) (2, 6) (5, 8) (9, 10) (12, 17) (13, 16) (18, 20) (19, 21) (22, 23) (24, 37) (25, 38) (26, 35) (27, 34) (28, 33) (29, 31) (30, 32) (36, 41) (39, 40) (42, 45) (43, 47) (44, 46) (48, 49) (51, 52) (54, 57)

X_d = (1, 3) (4, 7) (5, 8) (10, 13) (11, 12) (16, 60) (17, 69) (18, 20) (21, 153) (24, 39) (25, 40) (26, 41) (27, 42) (28, 43) (29, 50) (30, 51) (31, 49) (32, 46) (33, 48) (34, 47) (35, 44) (36, 45) (37, 53) (38, 52) (54, 145) (55, 144) (56, 135) (57, 136) (58, 141) (59, 138) (61, 139) (62, 147) (63, 146) (64, 137) (65, 143) (66, 142) (67, 134) (68, 133) (70, 140) (74, 82) (75, 83) (76, 79) (77, 81) (78, 80) (84, 85) (86, 94) (87, 95) (88, 93) (91, 92) (99, 101) (100, 102) (103, 118) (104, 119) (105, 120) (106, 121) (107, 122) (108, 129) (109, 130) (110, 128) (111, 125) (112, 127) (113, 126) (114, 123) (115, 124) (116, 132) (117, 131) (148, 149) (150, 152) (155, 158) (156, 157)

Y_d = (1, 3) (4, 11) (5, 10) (6, 9) (7, 12) (8, 13) (14, 15) (16, 54) (17, 66) (18, 86) (19, 90) (20, 94) (21, 95) (22, 97) (23, 98) (24, 103) (25, 104) (26, 105) (27, 106) (28, 107) (29, 108) (30, 109) (31, 110) (32, 111) (33, 112) (34, 113) (35, 114) (36, 115) (37, 116) (38, 117) (39, 118) (40, 119) (41, 120) (42, 121) (43, 122) (44, 123) (45, 124) (46, 125) (47, 126) (48, 127) (49, 128) (50, 129) (51, 130) (52, 131) (53, 132) (55, 138) (56, 135) (57, 136) (58, 139) (59, 144) (60, 145) (61, 141) (62, 146) (63, 147) (64, 137) (65, 140) (67, 134) (68, 133) (69, 142) (70, 143) (71, 73) (74, 81) (75, 80) (76, 79) (77, 82) (78, 83) (84, 85) (87, 153) (88, 150) (89, 151) (91, 149) (92, 148) (93, 152) (96, 154) (99, 157) (100, 158) (101, 156) (102, 155)

Z_d = (1, 28, 122) (2, 27, 121) (3, 31, 128) (4, 24, 126) (5, 25, 127) (6, 26, 125) (7, 30, 132) (8, 29, 131) (9, 32, 120) (10, 38, 129) (11, 37, 130) (12, 34, 118) (13, 33, 119) (14, 35, 124) (15, 36, 123) (16, 148, 94) (17, 156, 98) (18, 91, 145) (19, 88, 141) (20, 87, 147) (21, 86, 146) (22, 100, 143) (23, 99, 142) (39, 77, 109) (40, 78, 108) (41, 76, 105) (42, 72, 106) (43, 73, 110) (44, 84, 114) (45, 85, 115) (46, 79, 111) (47, 81, 116) (48, 80, 117) (49, 71, 107) (50, 75, 104) (51, 74, 103) (52, 83, 112) (53, 82, 113) (54, 63, 59) (55, 62, 60) (56, 58, 61) (65, 70, 68) (66, 69, 67) (89, 136, 151) (90, 139, 152) (92, 144, 153) (93, 135, 150) (95, 138, 149) (96, 137, 154) (97, 140, 155) (101, 134, 157) (102, 133, 158)

(continued)

Table 18.2 (continued)

X_e = (1, 201) (2, 200) (3, 199) (4, 207) (5, 206) (6, 205) (7, 208) (8, 209) (9, 204) (10, 203) (11, 202) (12, 133) (13, 134) (14, 211) (15, 210) (16, 178) (17, 177) (18, 167) (19, 168) (20, 184) (21, 185) (22, 186) (23, 187) (24, 188) (25, 189) (26, 190) (27, 191) (28, 192) (29, 193) (30, 194) (31, 195) (32, 196) (33, 217) (34, 197) (35, 218) (36, 215) (37, 214) (38, 198) (39, 219) (40, 216) (41, 213) (42, 212) (43, 220) (44, 224) (45, 223) (46, 225) (47, 226) (48, 222) (49, 221) (50, 123) (51, 82) (52, 98) (53, 97) (54, 91) (55, 87) (56, 94) (57, 90) (58, 89) (59, 86) (60, 96) (61, 95) (62, 88) (63, 93) (64, 92) (65, 85) (66, 84) (67, 124) (68, 121) (69, 120) (70, 131) (71, 132) (72, 126) (73, 129) (74, 130) (75, 122) (76, 118) (77, 119) (78, 83) (79, 125) (80, 127) (81, 128) (99, 108) (100, 109) (101, 161) (102, 162) (103, 182) (104, 183) (105, 179) (106, 172) (107, 176) (110, 173) (111, 171) (112, 174) (113, 175) (114, 181) (115, 180) (116, 169) (117, 170) (135, 150) (136, 151) (137, 152) (138, 153) (139, 154) (140, 163) (141, 164) (142, 160) (143, 157) (144, 159) (145, 158) (146, 155) (147, 156) (148, 166) (149, 165)

Y_e = (1, 22) (2, 21) (3, 25) (4, 28) (5, 27) (6, 26) (7, 31) (8, 32) (9, 20) (10, 23) (11, 24) (12, 18) (13, 19) (14, 30) (15, 29) (16, 159) (17, 158) (33, 34) (35, 37) (38, 41) (39, 42) (44, 47) (45, 46) (50, 51) (52, 60) (53, 61) (54, 59) (57, 58) (63, 65) (64, 66) (67, 69) (70, 73) (71, 74) (76, 79) (77, 78) (82, 177) (83, 169) (84, 195) (85, 196) (86, 190) (87, 185) (88, 189) (89, 194) (90, 193) (91, 184) (92, 188) (93, 187) (94, 186) (95, 191) (96, 192) (97, 168) (98, 167) (99, 132) (100, 131) (101, 148) (102, 149) (103, 165) (104, 166) (105, 160) (106, 153) (107, 157) (108, 161) (109, 162) (110, 154) (111, 152) (112, 155) (113, 156) (114, 164) (115, 163) (116, 150) (117, 151) (118, 174) (119, 175) (120, 176) (121, 172) (122, 171) (123, 178) (124, 173) (125, 170) (126, 179) (127, 181) (128, 180) (129, 182) (130, 183) (133, 207) (134, 206) (135, 147) (136, 146) (139, 143) (144, 145) (197, 198) (202, 208) (203, 209) (204, 205) (210, 211) (212, 213) (214, 216) (217, 219) (221, 224) (222, 223)

Z_e = (4, 12) (5, 13) (6, 9) (7, 11) (8, 10) (14, 15) (16, 50) (17, 51) (18, 52) (19, 53) (20, 54) (21, 55) (22, 56) (23, 63) (24, 64) (25, 62) (26, 59) (27, 61) (28, 60) (29, 57) (30, 58) (31, 66) (32, 65) (33, 39) (34, 38) (37, 40) (41, 42) (44, 49) (45, 48) (67, 110) (68, 106) (69, 107) (70, 109) (71, 108) (72, 105) (73, 103) (74, 104) (75, 111) (76, 112) (77, 113) (78, 116) (79, 117) (80, 114) (81, 115) (82, 123) (83, 119) (84, 92) (85, 93) (86, 91) (89, 90) (95, 97) (96, 98) (99, 101) (100, 102) (118, 125) (120, 124) (129, 131) (130, 132) (133, 167) (134, 168) (135, 169) (136, 170) (137, 171) (138, 172) (139, 173) (140, 180) (141, 181) (142, 179) (143, 176) (144, 178) (145, 177) (146, 174) (147, 175) (148, 183) (149, 182) (150, 156) (151, 155) (154, 157) (158, 159) (161, 166) (162, 165) (184, 204) (185, 200) (186, 201) (187, 203) (188, 202) (189, 199) (190, 205) (191, 206) (192, 207) (193, 210) (194, 211) (195, 208) (196, 209) (197, 217) (198, 213) (212, 219) (214, 218) (223, 225) (224, 226)

X_f = (1, 239) (2, 240) (3, 241) (4, 242) (5, 243) (6, 244) (7, 245) (8, 246) (9, 222) (10, 223) (11, 189) (12, 188) (13, 219) (14, 218) (15, 232) (16, 233) (17, 231) (18, 227) (19, 228) (20, 230) (21, 229) (22, 226) (23, 224) (24, 225) (25, 234) (26, 178) (27, 177) (28, 237) (29, 238) (30, 235) (31, 236) (32, 108) (33, 109) (34, 115) (35, 116) (36, 117) (37, 118) (38, 119) (39, 120) (40, 121) (41, 122) (42, 98) (43, 99) (44, 123) (45, 124) (46, 125) (47, 126) (48, 127) (49, 61) (50, 60) (51, 100) (52, 101) (53, 102) (54, 103) (55, 104) (56, 105) (57, 106) (58, 107) (59, 110) (62, 111) (63, 112) (64, 113) (65, 114) (66, 92) (67, 93) (68, 179) (69, 180) (70, 181) (71, 182) (72, 183) (73, 184) (74, 185) (75, 186) (76, 160) (77, 161) (78, 187) (79, 190) (80, 191) (81, 170) (82, 171) (83, 169) (84, 165) (85, 166) (86, 168) (87, 167) (88, 164) (89, 162) (90, 163) (91, 172) (94, 175) (95, 176) (96, 173) (97, 174) (128, 215) (129, 216) (130, 214) (131, 210) (132, 211) (133, 213) (134, 212) (135, 209) (136, 207) (137, 208) (138, 217) (139, 220) (140, 221) (141, 155) (142, 154) (143, 200) (144, 201) (145, 199) (146, 195) (147, 196) (148, 198) (149, 197) (150, 194) (151, 192) (152, 193) (153, 202) (156, 205) (157, 206) (158, 203) (159, 204)

(continued)

Table 18.2 (continued)

Y_f = (1, 9) (2, 10) (3, 8) (6, 7) (11, 13) (12, 14) (15, 16) (17, 19) (20, 23) (21, 24) (26, 29) (27, 28) (32, 33) (34, 42) (35, 43) (36, 41) (39, 40) (45, 47) (46, 48) (49, 67) (50, 66) (51, 57) (52, 56) (55, 58) (60, 65) (61, 64) (68, 136) (69, 137) (70, 135) (71, 131) (72, 132) (73, 134) (74, 133) (75, 130) (76, 128) (77, 129) (78, 138) (79, 139) (80, 140) (81, 144) (82, 143) (83, 147) (84, 146) (85, 145) (86, 151) (87, 152) (88, 150) (89, 148) (90, 149) (91, 153) (92, 157) (93, 156) (94, 155) (95, 154) (96, 158) (97, 159) (98, 161) (99, 160) (100, 170) (101, 171) (102, 169) (103, 165) (104, 166) (105, 168) (106, 167) (107, 164) (108, 162) (109, 163) (110, 172) (111, 175) (112, 176) (113, 173) (114, 174) (115, 185) (116, 184) (117, 181) (118, 182) (119, 186) (120, 180) (121, 179) (122, 183) (123, 187) (124, 190) (125, 191) (126, 189) (127, 188) (192, 200) (193, 201) (194, 199) (197, 198) (203, 205) (204, 206) (207, 208) (209, 211) (212, 215) (213, 216) (218, 221) (219, 220) (222, 223) (224, 232) (225, 233) (226, 231) (229, 230) (235, 237) (236, 238) (239, 245) (240, 244) (243, 246)

Z_f = (1, 7) (2, 6) (5, 8) (9, 10) (11, 47) (12, 48) (13, 139) (14, 140) (15, 23) (16, 24) (17, 22) (20, 21) (28, 30) (29, 31) (32, 89) (33, 90) (34, 74) (35, 73) (36, 70) (37, 71) (38, 75) (39, 69) (40, 68) (41, 72) (42, 77) (43, 76) (44, 78) (45, 79) (46, 80) (49, 113) (50, 114) (51, 81) (52, 82) (53, 83) (54, 84) (55, 85) (56, 86) (57, 87) (58, 88) (59, 91) (60, 92) (61, 93) (62, 94) (63, 95) (64, 96) (65, 97) (66, 206) (67, 205) (98, 115) (99, 116) (100, 106) (101, 105) (104, 107) (108, 109) (117, 122) (120, 121) (124, 126) (125, 127) (128, 134) (129, 133) (132, 135) (136, 137) (141, 175) (142, 176) (143, 151) (144, 152) (145, 150) (148, 149) (156, 158) (157, 159) (160, 215) (161, 216) (162, 198) (163, 197) (164, 194) (165, 195) (166, 199) (167, 193) (168, 192) (169, 196) (170, 201) (171, 200) (172, 202) (173, 203) (174, 204) (177, 237) (178, 238) (179, 207) (180, 208) (181, 209) (182, 210) (183, 211) (184, 212) (185, 213) (186, 214) (187, 217) (188, 218) (189, 219) (190, 220) (191, 221) (222, 239) (223, 240) (224, 230) (225, 229) (228, 231) (232, 233) (241, 246) (244, 245)

References

Ashrafi AR, Ghorbani M (2009) Mathematics of fullerenes. Part II: counting problems. University of Kashan Press, Kashan

Ashrafi AR, Ghorbani M (2010) PI and omega polynomials of IPR fullerenes. Fuller Nanotub Carbon Nanostruct 18:198–206

Ashrafi AR, Loghman A (2006a) Padmakar-Ivan index of $TUC_4C_8(S)$ nanotubes. J Comput Theor Nanosci 3:378–381

Ashrafi AR, Loghman A (2006b) PI index of Zig-Zag polyhex nanotubes. MATCH Commun Math Comput Chem 55:447–452

Ashrafi AR, Loghman A (2006c) PI index of armchair polyhex nanotubes. Ars Comb 80:193–199

Ashrafi AR, Rezaei F (2007) PI index of polyhex nanotori. MATCH Commun Math Comput Chem 57:243–250

Ashrafi AR, Jalali M, Ghorbani M, Diudea MV (2008) Computing PI and omega polynomials of an infinite family of fullerenes. MATCH Commun Math Comput Chem 60:905–916

Ashrafi AR, Ghorbani M, Jalali M (2009a) Study of IPR fullerene by counting polynomials. J Theor Comput Chem 8:451–457

Ashrafi AR, Ghorbani M, Jalali M (2009b) Mathematics of fullerenes. Part I: topological indices. University of Kashan Press, Kashan

Ashrafi AR, Ghorbani M, Jalali M (2010) The PI and edge Szeged polynomials of an infinite family of fullerenes. Fuller Nanotub Carbon Nanostruct 18:107–116

Ashrafi AR, Saheli M, Ghorbani M (2011) The eccentric connectivity index of nanotubes and nanotori. J Comput Appl Math 235:4561–4566

Bosma W, Cannon J, Playoust C (1997) The Magma algebra system. I. The user language. J Symb Comput 24:235–265

Darafsheh MR (2010) Computation of topological indices of some graphs. Acta Appl Math 110:1225–1235

Diudea MV (2010) Diamond D_5, a novel allotrope of carbon. Studia Univ Babes-Bolyai Chemia 55:11–17

Diudea MV, Nagy CL (2012) All pentagonal ring structures related to the C_{20} fullerene: diamond D_5. Diamond. Relat Mater 23:105–108

Diudea MV, Ursu O, Nagy LCs (2002) TOPOCLUJ. Babes-Bolyai University, Cluj

Diudea MV, Florescu MS, Khadikar PV (2006) Molecular topology and its applications. EFICON, Bucharest

Diudea MV, Ilić A, Medeleanu M (2011a) Hyperdiamonds: a topological view. Iran J Math Chem 2:7–29

Diudea MV, Nagy CL, Ilić A (2011b) Diamond D_5, a novel class of carbon allotropes. In: Putz MV (ed) Carbon bonding and structures. Advances in physics and chemistry, vol 5. Springer, Berlin, pp 273–289

Diudea MV, Nagy CL, Bende A (2012) On diamond D_5. Struct Chem 23:981–986

Gupta G, Singh M, Madan AK (2002) Application of graph theory: relationship of eccentric connectivity index and Wiener's index with anti-inflammatory activity. J Math Anal Appl 266:259–268

Gutman I (1994) A formula for the Wiener number of trees and its extension to graphs containing cycles. Graph Theory Notes New York 27:9–15

Gutman I, Ashrafi AR (2008) On the PI index of phenylenes and their hexagonal squeezes. MATCH Commun Math Comput Chem 60:135–142

Hosoya H (1988) On some counting polynomials in chemistry. Discret Appl Math 19:239–257

HyperChem package Release 7.5 for Windows (2002) Hypercube Inc., Florida, USA

Khadikar PV (2000) On a novel structural descriptor PI. Nat Acad Sci Lett 23:113–118

Khadikar PV, Kale PP, Deshpande NV, Karmarkar S, Agrawal VK (2001a) Novel PI indices of hexagonal chains. J Math Chem 29:143–150

Khadikar PV, Karmarkar S, Agrawal VK (2001b) A novel PI index and its applications to QSPR/QSAR studies. J Chem Inf Comput Sci 41:934–949

Khadikar PV, Karmarkar S, Varma RG (2002a) On the estimation of PI index of polyacenes. Acta Chim Slov 49:755–771

Khadikar PV, Karmarkar S, Singh S, Shrivastava A (2002b) Use of the PI index in predicting toxicity of nitrobenzene derivatives. Bioorg Med Chem 10:3163–3170

Khadikar PV, Mandloi D, Bajaj AV, Joshi S (2003) QSAR study on solubility of alkanes in water and their partition coefficients in different solvent system using PI index. Bioorg Med Chem Lett 13:419–422

Khalifeh MH, Yousefi-Azari H, Ashrafi AR (2008) Vertex and edge PI indices of Cartesian product graphs. Discret Appl Math 156:1780–1789

Kyani A, Diudea MV (2012) Molecular dynamics simulation study of the diamond D_5 substructures. Central Eur J Chem 10(4):1028–1033

Sabaghian-Bidgoli H, Ashrafi AR, Fathy M (2011) Study of IPR fullerenes by PI index. J Comput Theor Nanosci 8:1259–1263

Sardana S, Madan AK (2001) Application of graph theory: relationship of molecular connectivity index, Wiener's index and eccentric connectivity index with diuretic activity. MATCH Commun Math Comput Chem 43:85–98

Sharma V, Goswami R, Madan AK (1997) Eccentric connectivity index: a novel highly discriminating topological descriptor for structure-property and structure-activity studies. J Chem Inf Comput Sci 37:273–282

Szefler B, Diudea MV (2012) On molecular dynamics of the diamond D_5 seeds. Struct Chem 23:717–722

The GAP Team (1995) GAP, groups, algorithms and programming. Lehrstuhl De für Mathematik, RWTH, Aachen

Trinajstić N (1992) Chemical graph theory. CRC Press, Boca Raton
Wiener H (1947) Structural determination of paraffin boiling points. J Am Chem Soc 69:17–20
Xu L, Deng H (2006) PI indices of tori Tp, q[C4;C8] covering C4 and C8. MATCH Commun Math Comput Chem 57:485–502
Zhou B, Du Z (2010) On eccentric connectivity index. MATCH Commun Math Comput Chem 63:181–198

Chapter 19
Quasicrystals: Between Spongy and Full Space Filling

Mircea V. Diudea

Abstract Quasicrystals are structures showing long-range ordering rather than translational periodicity and could be either spongy or filled ones. Spongy structures are hollow-containing materials, encountered either in natural zeolites or in synthesized spongy carbon. Filled structures consist of small cages and/or tiles that can fill a given space. The design and topological study of some hypothetical structures is presented in terms of map operations and genus calculation of their associated graphs, respectively. Among the discussed structures, one remarks some novel spongy hyper-dodecahedra that can evolve with 1 periodicity. Other spherical multi-shell cages represent aggregates of smaller cages, the classical C_{60} fullerene included. A whole gallery of nanostructures is presented in the Appendices.

19.1 Introduction

Matter is widely polymorphic and a classification into crystalline to amorphous can depend in some extent on the measurement method. A sample, appearing crystalline (to a selected area) in electron diffraction, may appear amorphous to powder X-ray diffraction. Steinhardt (1990) classified the matter into crystals, glasses, and quasicrystals, according to several characteristics, as follows:

Crystals: Highly ordered, with atomic clusters repeated periodically (a crystal shows an essentially discrete diffraction diagram). The underlying feature of crystals is their pure periodicity in three independent directions of the space. The symmetry of crystal lattices is completely described by the 230 symmetry groups of the space.

Glasses: Materials highly disordered, with atoms arranged in a dense but random array.

M.V. Diudea (✉)
Faculty of Chemistry and Chemical Engineering, Babes-Bolyai University,
400028 Cluj, Romania
e-mail: diudea@chem.ubbcl

M.V. Diudea and C.L. Nagy (eds.), *Diamond and Related Nanostructures*,
Carbon Materials: Chemistry and Physics 6, DOI 10.1007/978-94-007-6371-5_19,

Quasicrystals: Highly ordered, with atomic clusters repeated in a complex, nonperiodic pattern. Electron diffraction shows sharp patterns, as first reported in experiment by Shehtman et al. (1984). They discovered sharp diffraction patterns of icosahedral symmetry in Al-Mn alloy rapidly solidified, and this phase is metastable and resistant to crystallization up to 350 °C.

An icosahedron is locally the most densely packed arrangement and has been observed in aperiodic materials such as liquids and amorphous. The icosahedral rotational symmetry contradicts the translational periodicity and it was thought that a long-range order of icosahedral symmetry is unlikely to be found in condensed matter, even though a famous two-dimensional pentagonal tiling, called Penrose tiling, has been discovered (Penrose 1978; Grünbaum and Shephard 1987; Danzer 1989; Mikhael et al. 2008). Alan Mackay (1982), transposing the Penrose tiling into 3D, modeled a possible atomic structure and next simulated a diffraction pattern showing a tenfold local symmetry. Thus, he theoretically predicted the quasicrystals, notion introduced by Levine and Steinhardt (1984) (see also Steinhardt 1987, 1990; Mackay 1987), on the ground of the quasiperiodic translational order (Hargittai 1992; Hargittai and Hargittai 2010; Fujiwara and Ishii 2008).

Quasicrystals occur in many different systems, such as metal alloys (Shechtman et al. 1984; Tsai et al. 1987, 2000), binary systems (Fe_2O_3, Fe_3O_4, PbS, etc.) (Shevchenko et al. 2006a, b; Talapin et al. 2009), liquid crystal dendrimers (Zeng et al. 2004), and tri-block copolymers (Hayashida et al. 2007). Colloidal particles subjected to laser fields are forced into the direction of highest light intensity. Therefore, interfering laser beams can be used to induce quasiperiodic complex structures in a charge-stabilized colloidal suspension (Burns et al. 1990; Schmiedeberg and Stark 2012). Very recently, the naturally occurring quasicrystalline mineral icosahedrite, $Al_{63}Cu_{24}Fe_{13}$, has been identified in a sample from the Khatyrka River in Chukhotka, Russia (Bindi et al. 2009, 2011).

In quasicrystal, the thermal and electronic transports manifest more like in glasses than in normal crystals. The low surface energy of quasicrystals makes them resistant to corrosion and adhesion and determines low friction coefficients.

The mathematics of quasicrystals provided classification of aperiodic tilings by using advanced topological tools or studies on diffraction beyond the crystallographic domain (Baake and Moody 2000; Baake et al. 2002; Baake and Kösters 2011). Quasicrystals are aperiodic structures; however, they still possess long-range positional and orientational order. Among the rotational symmetries, 2-, 3-, 4-, and 6-fold axes are allowed in crystals, while 5-, 7-, and all higher rotations are disallowed. Unlike crystals, quasicrystals can, in principle, possess any non-crystallographic rotational symmetry. In lieu of translational periodicity, quasicrystals exhibit self-similarity by scaling and this is related to the golden ratio $\tau = (\sqrt{5} + 1)/2$ (i.e., the ratio of the diagonal to the edge of the regular pentagon) and further to the Fibonacci sequence. This feature is clearly apparent in direct-space models and diffraction patterns.

Icosahedral symmetry is allowed together with translational symmetry in 6-dimensional space (Hermann 1949; Bak 1986; Mackay 1990). Application of the projection matrix to the vertices of a 6-dimensional hypercube provides a regular

icosahedron. The 3-dimensional direct-space approach and the 6-dimensional reciprocal-space approach are complementary, and they are often used together. The higher-dimensional approach yields numerical data directly comparable to results from microscopy (Deloudi and Steurer 2007).

This chapter is organized as follows. After an introductory part, some concepts related to the spongy structures and the negative curvature, encountered therein, are presented in the second section. The third section is devoted to map operations useful in the design of molecular structures. The fourth section lists several classes of structures, with their construction and genus calculation. The chapter ends with references and an appendices.

19.2 Spongy Structures

In the synthesis of fullerenes, it is well known that a mixture of nanostructures appears: single- and multi-walled nanotubes, nanotubes capped by fullerene halves, onion-fullerenes, and others. It is expected that in the experimental conditions, fullerenes can be spanned, thus resulting open cages, of which open faces (i.e., windows) can fit to the eventually present nanotubes of various chirality and tessellation (most probably being the graphitic hexagonal structure). Such spanned fullerenes, joined with nanotubes consisting of 0, 1, ..., n rows of atoms, can be assimilated to nanotube junctions. According to their symmetry, tetrahedral, octahedral, and icosahedral junctions can be distinguished (Diudea and Nagy 2007).

Tetrahedral junctions are particularly interesting due to their similarity with the tetrahedral sp^3 hybridized carbon atom: the valences are now nanotubes, while the atom is an opened cage embedded in a surface of genus 2 (see below). Like the single C atom, a tetrapodal junction can be used to build various nanostructures, particularly diamondoids.

Octahedral junctions appear in zeolites, in natural aluminosilicates with spongy structure, or in the already synthesized spongy carbon (Benedek et al. 2003, 2011; Valencia et al. 2003); their associated graphs can be embedded in the P-surface. Icosahedral junctions are also possible, for example, in multi-tori and zeolites (Nagy and Diudea 2005a; Diudea and Petitjean 2008).

Graphitic structures, with rings larger than the hexagon, needed to induce negative Gaussian curvature, have been proposed since the early papers published twenty years ago (Schoen 1970; Mackay 1985; Mackay and Terrones 1991, 1993; Terrones and Mackay 1993; Townsend et al. 1992; Lenosky et al. 1992; O'Keeffe et al. 1992; Vanderbilt and Tersoff 1992). These have been called schwarzites, in the honor of H. A. Schwarz (1865, 1890), who first investigated the differential geometry of such surfaces. Next, the molecular junctions have been "in silico" assembled in various networks and experimental evidences for such junctions have been reported (Ricardo-Chavez et al. 1997; Terrones and Mackay 1997; Terrones et al. 2002; Terrones and Terrones 1997, 2003; Ceulemans et al. 1999; Romo-Herrera et al. 2007).

Schwarzite associate graphs are assumed to be embedded in triply periodic (intersection-free) minimal surfaces and are related to labyrinth graphs, also involving nanotube junctions. A surface S can be characterized by calculating its genus (O'Keeffe and Hyde 1996; Hyde and Ramsden 2000), defined in terms of the integral Gaussian curvature according to the Gauss–Bonnet (Bonnet 1853) theorem:

$$\chi(S) = (1/2\pi) \int_S K \, \mathrm{d}S \tag{19.1}$$

with $\chi(S)$ being the Euler–Poincaré characteristic. From this, the surface genus g is calculated by

$$\chi(S) = n(1 - g) \tag{19.2}$$

where $n = 1$ for non-orientable (Moebius) surfaces and $n = 2$ for orientable surfaces. Recall that an embedding is a representation of a graph on a surface S such that no edge crossings occur (Harary 1969). The surface characteristic is also related to the graph elements by the well-known Euler–Poincare formula (Euler 1758):

$$\chi(S) = v - e + f \tag{19.3}$$

where $v = |V(G)|$ is the number of vertices/atoms, $e = |E(G)|$ is the number of edges/bonds, while f is the number of faces of the graph/molecule.

The genus of the surface S is thus related to the Euler's characteristic $\chi(S)$:

(i) case of the sphere: $g = 0$ and $\chi(S) > 0$ (objects positive curvature);
(ii) case of the torus: $g = 1$ and $\chi(S) = 0$,
(iii) $g > 1$ and $\chi(S) < 0$ (objects of negative curvature)

In other words, the genus can be seen as the number of holes to be performed in the sphere to make it homeomorphic to the surface embedding a given graph. Also, it can be seen as the number of simple tori composing a given graph.

The generalization of a polygon (2D) or a polyhedron (3D) to n-dimensions is a polytope. By using the Schläfli symbols, the Platonic solids, tetrahedron, octahedron, icosahedron, cube, and dodecahedron, can be written as [3,3], [3,4], [3,5], [4,3], and [5,3]. The three regular tessellations [3,6], [4,4], and [6,3] represent the coverings of the plane by triangles, squares, and hexagons, respectively. Next, the space filling by cubes can be written as [4,3,4], with four cubes meeting at every edge; in general, the [p,q,r] symbol means that r cages (of [p,q] type, p being the size of polygon, while q is the vertex degree) meet at any edge of the net. For example, the polytope [3,3,5], which can be considered a 4D analogue of icosahedron, consists of 600 tetrahedral cells. Its dual is the regular polytope [5,3,3], the analogue of dodecahedron, whose 120 cells are dodecahedra. These 4D polytopes, also called polychora, have been first described by Swiss mathematician Ludwig Schläfli (1901).

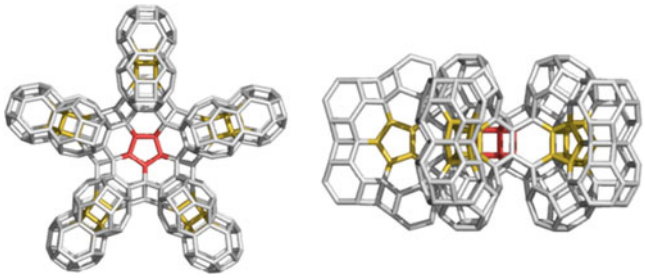

Fig. 19.1 Multi-torus 24Cy$_5$_420, $v = 420$; $e = 720$; $f_4 = 150$ $f_5 = 12$; $f_6 = 170$; by Euler formula, $g = -((420 - 720) + (150 + 0 + 140) - 2)/2 = 6$; by our formula, $g = 5(2 - 1) + 1 = 6$

To investigate the n-dimensional polytopes, a generalization of Euler's formula, also due to Schläfli, is used:

$$\sum_{i=0}^{n-1} (-1)^i f_i = 1 - (-1)^n \tag{19.4}$$

In the above formula, f_i are elements of the f-vector $(f_0, f_1, \ldots, f_{n-1})$ of a convex polytope. In case $n = 4$, f_i are identified to vertices, edges, rings, and cages/voids, respectively, and (19.4) is written as

$$f_0 - f_1 + f_2 - f_3 = 0 \tag{19.5}$$

In case $n = 3$, the above formula is the well-known Euler (1758) formula:

$$v - e + f = 2 \tag{19.6}$$

Either related to the number of holes in spongy structures (i.e., multi-tori) by genus or counting the constituting figures (i.e., polytopes) in space-filling structures, the above relations are useful in description of the spatiality of rather complex structures. In spongy structures, built up by tube junctions, the following theorem holds (Diudea and Schefler 2012):

Theorem 19.1 *The genus of a structure, built up from u-tube junction units, of genus g_u, is calculated as $g = u(g_u - 1) + 1$, irrespective of the unit tessellation.*

Demonstration comes out from construction and is illustrated on the multi-torus in Fig. 19.1: there are five units open to be inserted in exactly five simple tori and one more torus that joins all the above five units, thus demonstrating the first part of the theorem.

For the second part of the theorem, the proposed formula will be confirmed, by counting formulas (19.5) or (19.6) on numerous examples, in the following sections.

19.3 Operations on Maps

Structures discussed in this study are represented by simple, nondirected (molecular) graphs. Their design is based on "operations on maps," merely applied on the Platonic solids: tetrahedron (T), cube (C), octahedron (Oct), dodecahedron (Do), and icosahedron (Ico). A map M is a discretized surface domain, while the operations on maps are topological modifications of a parent map. All the parameters herein presented refer to regular maps (i.e., having all vertices and faces of the same valence/size). The symmetry of parents is preserved by running these operations. Several operations on maps are known and are currently used to decorate a surface domain. The reader is invited to consult some recent publications in this respect (Diudea 2010a, MCM). In the following, only the most important operations will be detailed.

19.3.1 Dual Du

Dual: Put a point in the center of each face of the map; next, join two such points if their corresponding faces share a common edge (Pisanski and Randić 2000). It is the (Poincaré) *dual* $Du(M)$. The vertices of $Du(M)$ represent faces in M and vice versa. In the transformed map, the following relations exist: $Du(M)$, $v = f_0$, $e = e_0$, and $f = v_0$. Dual of the dual returns the original map: $Du(Du(M)) = M$. Tetrahedron is self-dual, while the other Platonic polyhedra form pairs: Du(Cube) = Octahedron and Du(Dodecahedron) = Icosahedron (see Fig. 19.2 for symbols hereafter used). It is also known as the Petrie dual.

19.3.2 Medial Med

Medial: Put new vertices in the middle of the original edges and join two vertices if the edges span an angle (and are consecutive). Medial is a 4-valent graph and

Fig. 19.2 The five Platonic polyhedra

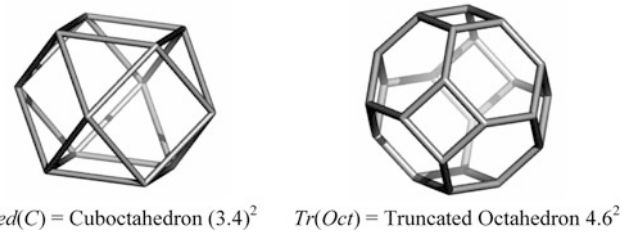

Fig. 19.3 Medial and truncation

$Med(M) = Med(Du(M))$, as illustrated in Fig. 19.3, left. The transformed map parameters are $Med(M)$, $v = e_0$, $e = 2e_0$, and $f = f_0 + v_0$. The medial operation rotates parent s-gonal faces by π/s (Pisanski and Randić 2000). Points in the medial represent original edges; thus, this property can be used in topological analysis of edges in the parent polyhedron. Similarly, the points in dual give information on the parent faces.

19.3.3 Truncation Tr

Truncation: Cut off the neighborhood of each vertex by a plane close to the vertex, such that it intersects each edge meeting the vertex. Truncation is similar to the medial, the transformed map parameters being $Tr(M)$, $v = 2e_0 = d_0v_0$, $e = 3e_0$, and $f = f_0 + v_0$ (Pisanski and Randić 2000). This was the main operation used by Archimedes in building its well-known 13 solids. Figure 19.3, right, illustrates a transform by this operation.

19.3.4 Polygonal Mapping P_n

Add a new vertex in the center of each face. Put n-3 points on the boundary edges. Connect the central point with one vertex on each edge (the end points included). Thus, the parent face is covered by triangles ($n = 3$), quadrilaterals ($n = 4$), and pentagons ($n = 5$). The P_3 operation is also called *stellation* or *triangulation*.

The transformed map parameters are $P_n(M)$, $v = v_0 + (n-3)e_0 + f_0$, $e = ne_0$, and $f = s_0 f_0$. Figure 19.4 gives examples of the P_n operations realization (Diudea and Nagy 2007).

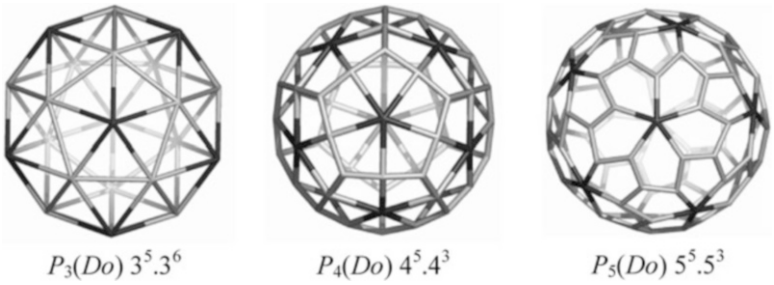

Fig. 19.4 Polygonal P_n operations on the dodecahedron *Do*

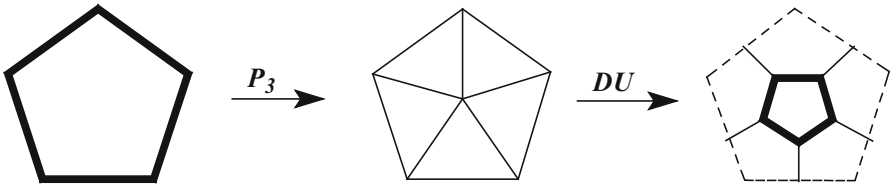

Fig. 19.5 The leapfrog *Le* operation on a pentagonal face

19.3.5 Leapfrog Le

Leapfrog (*tripling*) is a composite operation (Eberhard 1891; Fowler 1986; Diudea et al. 2006) that can be written as

$$Le(M) = Du(P_3(M)) = Tr(Du(M)) \tag{19.7}$$

A sequence of stellation–dualization rotates the parent s-gonal faces by π/s. Leapfrog operation is illustrated, on a pentagonal face, in Fig. 19.5.

A bounding polygon, of size $2d_0$, is formed around each original vertex. In the most frequent cases of 4- and 3-valent maps, the bounding polygon is an octagon and a hexagon, respectively.

If the map is a d_0 regular graph, the following theorem holds (Diudea and John 2001):

Theorem 19.2 *The number of vertices in Le(M) is d_0 times larger than in the original map M, irrespective of the tessellation type.*

Demonstration follows from the observation that for each vertex of M, d_0 new vertices result in $Le(M)$: $v/v_0 = d_0v_0/v_0 = d_0$. The transformed parameters are $Le(M)$, $v = s_0 f_0 = d_0v_0$, $e = 3e_0$, and $f = v_0 + f_0$.

Note that in $Le(M)$ the vertex degree is *always* 3, as a consequence of the involved triangulation P_3. In other words, the dual of a triangulation is a *cubic net*. It is also

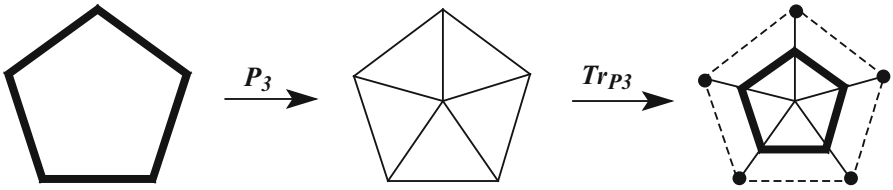

Fig. 19.6 The quadrupling Q operation on a pentagonal face

true that truncation always provides a trivalent lattice. A nice example of using *Le* operation is *Le*(Dodecahedron) = Fullerene $C_{60,}$ $(5.6^2)_{60}$.

19.3.6 Quadrupling/Chamfering Q

Quadrupling (Eberhard 1891; Diudea and John 2001) is another composite operation (cf. sequence):

$$Q(M) = E_{-}(Tr_{P_3}(P_3(M))) \tag{19.8}$$

where E_{-} denotes the (old) edge deletion (dashed lines, in Fig. 19.6) in the truncation Tr_{P3} of each central vertex of the P_3 operation. The Q operation leaves unchanged the initial orientation of the polygonal faces.

Theorem 19.3 *The vertex multiplication ratio in a Q transformation is* $d_0 + 1$ *irrespective of the original map tessellation.*

With the observation that for each vertex of M, d_0 new vertices appear in $Q(M)$ and the old vertex is preserved, the demonstration is immediate: $v = d_0 v_0 + v_0$; $v/v_0 = d_0 + 1$. The transformed parameters are $Q(M)$, $v = (d_0 + 1)v_0$, $e = 4e_0$, and $f = f_0 + e_0$.

Q operation involves two π/s rotations, so that the initial orientation of the polygonal faces is preserved. Note that the quadrupling transform of a 4-valent map is not a regular graph anymore (because of mixing the new trivalent vertices with the parent 4-valent ones). Only $Q(M)$ of a 3-valent map is a 3-regular graph. Q insulates the parent faces always by hexagons. An example of this operation is: Q (Dodecahedron) = Fullerene C_{80}, $(5.6^2)_{60}(6^3)_{20}$. It is also called "chamfering" (edge chamfering being equivalent to vertex truncation).

19.3.7 Septupling

Two operations on maps are known: the septupling S_1 and S_2 (Diudea 2004, 2005a, b; Diudea et al. 2006; Diudea and Nagy 2007). The S_1 operation was also

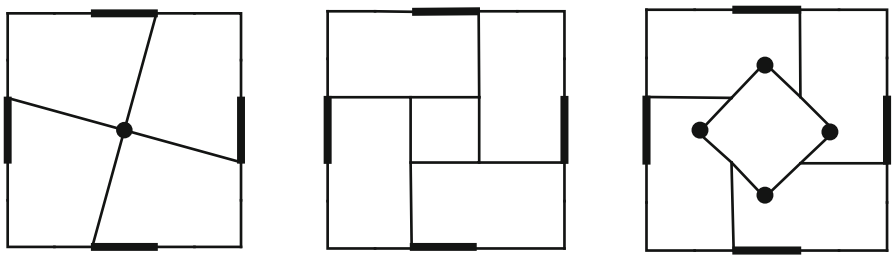

Fig. 19.7 Septupling S_1 operation on a square face, up to the open structure

called (Diudea 2003) Capra *Ca* – the goat, by the Romanian name of the English *leapfrog* children game. It is a composite operation that can be written as

$$S_1(M) = Tr_{P_5}(P_5(M)) \tag{19.9}$$

with Tr_{P5} meaning the truncation of the new, face-centered, vertices introduced by P_5 operation, which involves an E_2 (i.e., two new points put on each edge) operation.

The nuclearity of the Goldberg (1937) polyhedra is given by

$$m = \left(a^2 + ab + b^2\right); a \geq b; a + b > 0 \tag{19.10}$$

which provides the multiplication factor $m = v/v_0$. In a 3-valent map, *Le* (1,1); $m = 3$; *Q* (2,0); $m = 4$ and *S*(2,1); $m = 7$. An example of this operation is S_I (Dodecahedron) = Fullerene C_{140}, $(5.6^2)_{60}(6^3)_{80}$.

S_1 insulates any face of M by its own hexagons, which are not shared with any old face. It is an intrinsic chiral operation: it rotates the parent edges by $\pi/(3/2)s$. Since P_5 operation can be done either clockwise or counterclockwise, it results in an enantiomeric pair of objects, $S_{1S}(M)$ and $S_{1R}(M)$, with the subscript *S* and *R* referring to *sinister*/*rectus* stereochemical isomery.

S_1 can continue with the *open* operation, $O\,p_k(S_i(M))$, where k represents the number of points added on the boundary of the parent faces that become the *open* faces. The resulting open objects have all the polygons of the same $(6 + k)$ size. The above operation sequence enables the construction of negatively curved networks. Figure 19.7 gives the steps of S_1 realization on a square face in a trivalent lattice, up to the open structure.

Theorem 19.4 *The vertex multiplication ratio in an S transformation is* $2d_0 + 1$ *irrespective of the original map tiling.*

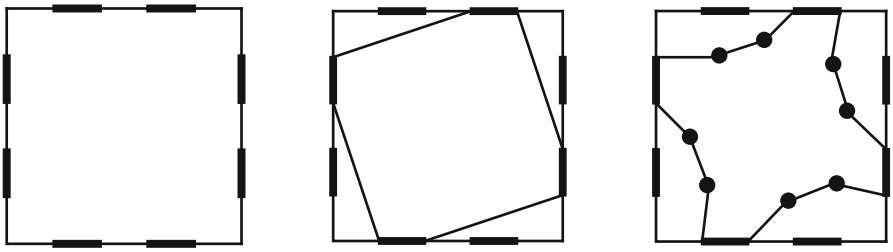

Fig. 19.8 Septupling S_2 operation on a square face, up to the open structure

For demonstration, observe that for each old vertex, $2d_0$ new vertices (Fig. 19.7) appear and the old vertex is preserved in the transformed map. Thus, $v = 2d_0v_0 + v_0$ and $v/v_0 = 2d_0 + 1$.

The S_2 operation (Diudea 2005b) is a simpler one (Fig. 19.8); it can be achieved by putting four vertices on each edge of the parent map M (e_4 operation), and next join these new vertices in order $(-1, +3)$:

$$S_2 = J_{(-1,+3)}(E_4(M)) \tag{19.11}$$

It insulates the double-sized parent faces by pentagons and parent vertices by pentagon d_0-multiples; the transformed objects are non-chiral ones.

Chirality in S_2 is brought by the Op operation Op_{2a}, achieved by adding two points on alternative edges of the double-sized parent face boundary (Fig. 19.8).

The transformed lattice parameters are identical to those provided by S_1 (Eq. 19.9). Note that both the septupling operations keep the parent vertices. The transformed parameters are $S_1(M)\&S_2(M)$, $v = v_0(2d_0 + 1)$, $e = 7e_0$, and $f = f_0(s_0 + 1)$. An example of this operation is: S_2 (Tetrahedron) = Fullerene C_{28} $(5^3)(5^2.6)$.

Peter John (Diudea et al. 2006) has proposed a generalization of operations on maps, inspired from the work of Goldberg (1937) and the representation of polyhedra in the (*a*,*b*) "inclined coordinates" (60° between axes).

TOPO GROUP CLUJ has developed several software programs dedicated to polyhedral tessellation and embedment in surfaces of various genera, either as finite or infinite structures: TORUS, CageVersatile_CVNET, JSCHEM, OMEGA counter, and NANO-Studio (Diudea et al. 2003; Stefu and Diudea 2005; Nagy and Diudea 2005a, b, 2009; Cigher and Diudea 2006).

Note that structures of quasicrystals can also be designed by inflation–deflation operation, matching rules, the grid method, strip projection, cut projection, or generalized dual method (de Bruijn 1981; Kramer 1982; Bak 1986; Socolar et al. 1986). These methods are closely related to each other.

19.4 Design of Structures

19.4.1 Structures Including C_{20} and C_{28} Fullerenes

Spongy structures are basically designed by using small cages/units, eventually called fullerenes, of tetrahedral, octahedral, or icosahedral symmetry. Here we are interested in the design of structures (either spongy or dense ones) with icosahedral symmetry, as encountered in quasicrystals.

Let us start the construction of some complex (yet hypothetical) structures by using two of the smallest fullerenes: C_{20} and C_{28}. In view of achieving the fivefold symmetry, a pentagonal hyper-ring (i.e., a torus) is designed, as shown in Fig. 19.9. Note that structures herein discussed will be presented in three different views, two-, three-, and fivefold symmetry (added as a suffix to their name), in the Appendices gallery. The number of atoms is given at the end of structure name, eventually before symmetry specification. For the sake of simplicity, we write, for example, 20 instead of C_{20} and 28 instead of C_{28}.

A dodecahedron having in lieu of its pentagonal faces some kind of hyper-pentagons (e.g., the R_5 hyper-faces in Fig. 19.9) is a spongy structure, generically

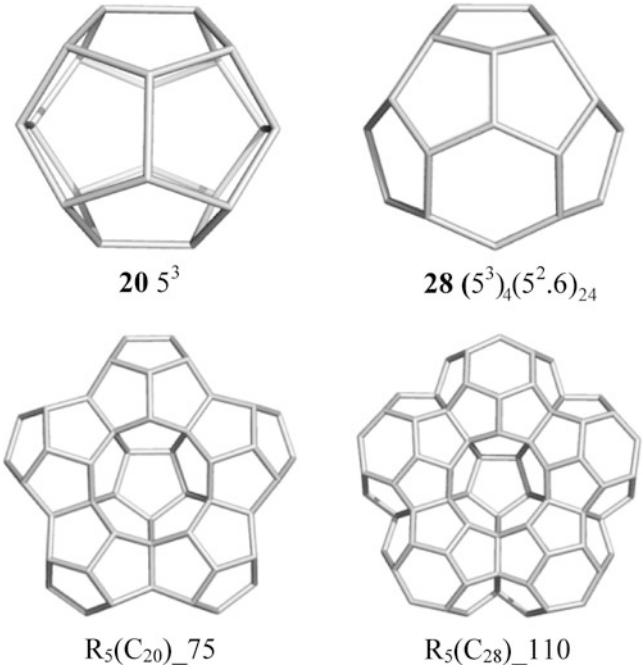

Fig. 19.9 Small cages/units (*top row*) used in the building of pentagonal hyper-rings R_5 (*bottom row*)

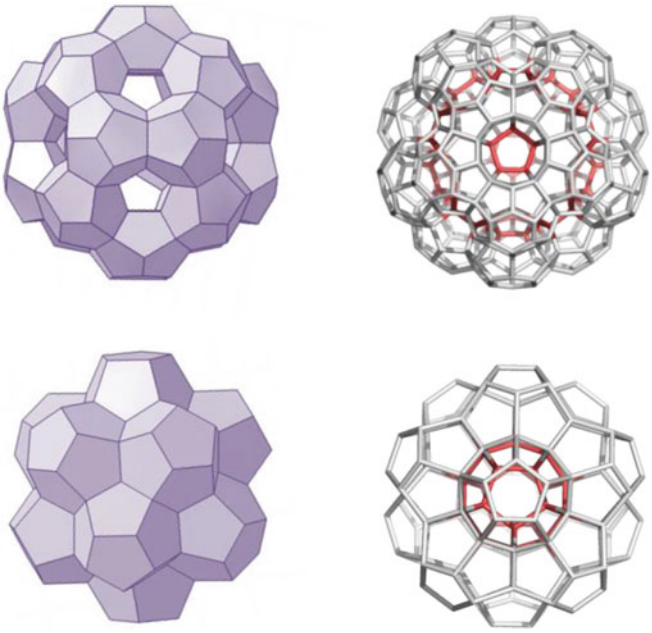

Fig. 19.10 Spongy U_{20}, **20**(20)_250 (*top*, *left*) and **28**(20)_380 (*top*, *right*), and their common core (the 110-keplerate, *bottom left*); the filled object **20**(1)(12)_130 (*bottom*, *right*)

named in the following U_{20}, to remind the 20 simple cages/units composing it. Figure 19.10 illustrates the U_{20} units derived from cages 20 and 28. Remark that both U_{20} units, **20**(20)_250 and **28**(20)_380, have the same hollow core, DoP_4TRS_110, designed by applying the P_4 map operation on the dodecahedron, followed by the selective truncation "TRS" of the five-connected vertices. The structure DoP_4TRS_110 is the "envelope" of twelve dodecahedra, having as the core a 13th dodecahedron, named in our notation **20**(1)(12)_130 (also 13Do_130), a structure consisting of $20 + 110$ atoms. Note that DoP_4TRS_110 is the 110-vertex icosahedral keplerate, possibly designed by sequential cross section of the (5, 3, 3) polytope with 3D hyperplanes, sections denoted 2_3, 3_3, and 4_3 (Shevchenko 2011; Müller et al. 2001). In case of **20**(20)_250, it can be seen that its envelope is (the transformed by S_2 map operation of the dodecahedron) DoS_2_140. Next, the two cages, DoP_4TRS_110 (inside) and DoS_2 (outside), are interconnected to give $DoS_2\&P_4TRSDo\_250$, that is, **20**(20)_250. The procedure can be extended to the other Platonics, tetrahedron (T) and cube (C), to obtain similar spongy (or filled, by the Platonic corresponding object) structures: $TS_2\&P_4TRS\_50$ and $TS_2\&P_4TRST\_54$; $CS_2\&P_4TRS\_100$ and $CS_2\&P_4TRSC\_108$.

Construction can continue, either linearly or radially. For the moment let us focus on linear evolution and let us coalesce two such U_{20} units by identifying the two opposite of their hyper-pentagons R_5. The process results in a rodlike structure, as

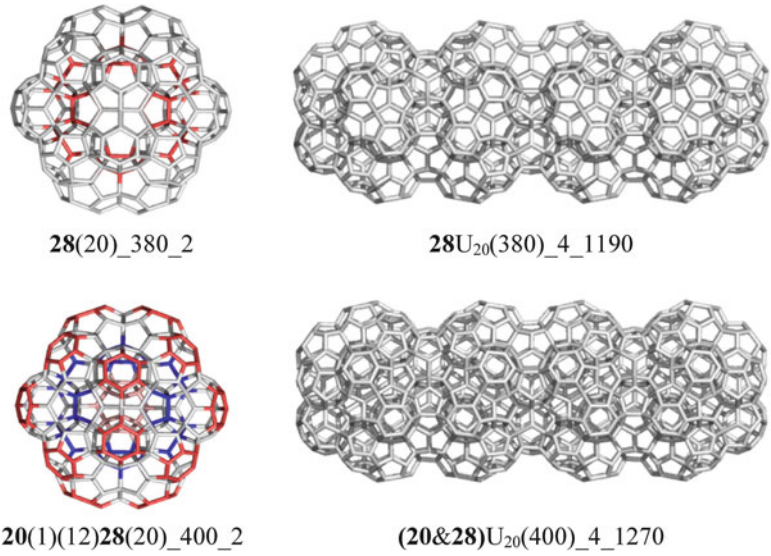

Fig. 19.11 Linear evolution of spongy (*top row*) and filed (*bottom row*) U_{20} units

shown in Fig. 19.11. In case of **20**(20)_250, any unit is involved in 3 windows (i.e., open faces, also pentagons) and 3 unit connections, so there is no free face/ring to continue a U_{20}_k rod by a hyper-pentagon R_5 identification.

Note that **28**U_{20}(380)_*k* is a new 1-periodic 21-nodal 3,4-c net, belonging to the Pmma group; the point symbol for this net is $\{5^2.6\}12\{5^3\}12\ \{5^4.6.8\}19\ \{5^5.6\}11$.

To the same Pmma group also belongs the filled 1-periodic net 28U_{20}(400)_*k*, which is a new 23-nodal 3,4-c net and has the point symbol $\{5^2.6\}12\{5^3\}8\{5^4.6.8\}13\ \{5^5.6\}17\{5^6\}8$. The crystallographic data are acknowledged to Prof. Davide Proserpio, University of Milan, Italy, and TOPOS databases (http://www.topos.ssu.samara.ru/index.html).

There is a clear experimental support for the above rodlike structures. In alloys like AlMn, AlFe, AlCuCo, and AlCoNi, a decagonal phase, with a diffraction pattern of tenfold rotational symmetry, having a 1-dimensional translational periodicity along the tenfold rotational axis, has been observed (Bendersky 1985). Also oxomolybdate clusters can form rodlike structures (Müller and Roy 2003; Shevchenko 2011). Table 19.1 lists the genus calculation by (19.6) and tube junction formula (Theorem 19.1).

Resuming to the U_{20} units, it is conceivable to ask if the central hollow can be filled with the "missed" blocks, keeping in mind some geometric considerations. It is the well-known problems of space filling by polyhedral cells (Frank and Kasper 1958; Haji-Akbari et al. 2010) and sphere packing (Mackay 1962; Coxeter 1958,

Table 19.1 Genus calculation on U_{20}-k rod-like structures; $g = u(g_u - 1) + 1$

Spongy_structure	v	e	f_5	f_6	f	χ	g	g_u	u	$g = f_{op} - 1$
$20U_{20}$_1_250	250	450	180	0	180	−20	11	1.5	20	11
$28U_{20}$ _1_380	380	660	240	20	260	−20	11	1.5	20	11
$28U_{20}$ _2_650	650	1,140	420	30	450	−40	21	11	2	21
$28U_{20}$ _3_920	920	1,620	600	40	640	−60	31	11	3	31
$28U_{20}$ _4_1190	1, 190	2,100	780	50	830	−80	41	11	4	41

1961; Goldberg 1971; Zong and Talbot 1999; Hales 1992, 2006). According to Ulam conjecture (Gardner 2001), all hard convex shapes pack more densely than the spheres, which have a maximum packing fraction of $\varphi = \pi/\sqrt{18} \approx 0.7405$. This happens in the face-centered cubic *fcc* array and was conjectured by Kepler but only recently demonstrated by Hales (2005).

Remark the spongy structure **20**(20)_250 (Fig. 19.10): it is a 6-nodal 3,4-c $\{(5^6)_{60}[(5^5)_{30}(5^5)_{60}][(5^3)_{20}(5^3)_{20}(5^3)_{60}]\}$ spongy hyper-dodecahedron, made from 20 cells all dodecahedral, a face-regular $5R_5$ map of genus $g = 11$, its core being the 110-keplerate. The packing fraction $\phi = 20/33 \approx 0.6060$ is calculated with respect to the 33 dodecahedra needed for the radial space filling (see **20**(1)(12)(20)_270, Fig. 19.12). Comparing with the spheres' maximum fraction (0.7405, see above), it is clearly a spongy, non-convex structure. Its fivefold symmetry is evident; even the pentagons show some distortion (and strain) to the regular pentagon. The topological symmetry data of this structure, with Platonic-like tiling, not yet referred in the literature, in our best knowledge, are illustrated in Appendix 19.1. For the general regular polytopes, the reader is invited to consult refs. Grünbaum (1967), Coxeter (1973), Wells (1977), and Ziegler (1995).

Filling the space can be achieved eventually by self-assembling of nanoparticles. "Self-assembly is a non-trivial process whereby a system explores its configuration space and eventually settles into a local minimum" (Shevchenko and Mackay 2008). The rules for self-assembly may be more apparent in the N-dimensional reciprocal space than in the real space.

For example, the 120 cells of the 4D regular polytope [5,3,3], the analogue of dodecahedron, to be realized in 3D, flattening by distortion must occur. It is the case of structures growing radially, as shown in Fig. 19.12. Their name includes the type of cages (the occurrence), shell by shell, and the number of atoms, as a suffix. Table 19.2 lists the figures calculation (cf. (19.5)) while Table 19.3 shows the genus calculation in diamond D_5.

Multi-shell icosahedral/dodecahedral structures have been designed earlier by several authors (Dandoloff et al. 1980; Zeger and Kaxiras 1993; Shevchenko 2011). A rodlike structure for filled structures could also be designed (Fig. 19.11).

The case of arrays 20&28 (Fig. 19.13) is related to the *mtn* network, called ZSM-39, or clathrate II, or *fcc*_C_{34} or diamond D_5 (Benedek and Colombo 1996; Deza and Shtogrin 2003; Blasé et al. 2010; Diudea 2010b; Diudea and Nagy 2012).

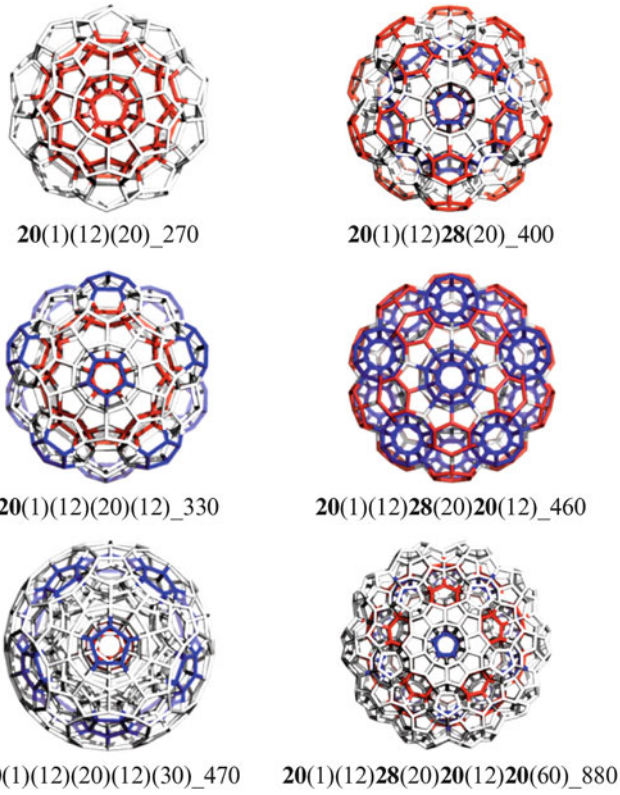

Fig. 19.12 Radial space filling by C_{20} and C_{28} fullerenes

Table 19.2 Figures calculation in radial space-filling structures; cf. $f = f_0 - f_1 + f_2 - f_3 = 0; f_3 = c = u + 2$

Shell	Filled structure	v	e	r_5	r_6	$u = v - e + r - 2$	f
0	20(1)(12)_130	130	230	114	0	12	0
1	20(20)_250	250	450	222	0	20	0
2	20(1)(12)(20)_270	270	500	264	0	32	0
3	20(1)(12)(20)(12)_330	330	620	336	0	44	0
4	20(1)(12)(20)(12)(30)_470	470	910	516	0	74	0
1	28(20)_380	380	660	252	50	20	0
2	20(1)(12)28(20)_400	400	710	294	50	32	0
3	20(1)(12)28(20)20(12)_460	460	830	366	50	44	0
4	20(1)(12)28(20)20(12)20(60)_880	880	1,640	816	50	104	0

Remark the space filling in D_5_anti is 3-periodic, while in the rodlike 1-periodic structure D_5_sin (Fig. 19.13, bottom), it is radially filled, as in quasicrystals (see also Appendix 19.2). D_5_sin is a 27-nodal 3,4-c net, of the Pm group, with the point symbol $\{5^3\}18\{5^5.6\}18\{5^5.8\}16\{5^6\}13$.

Table 19.3 Genus calculation in diamond D_5-related structures

Hollow structure	v	e	$g = 1 + u(g_u - 1)$	g_u	u	$g = f_{op} - 1$
20(12)_28(1)ada	158	274	3	1.5	4	3
20(18)28(2)dia_sin	226	398	5	2;1.5	3 + 2	5
20(18)28(2)dia_anti	226	398	5	1.5	8	5

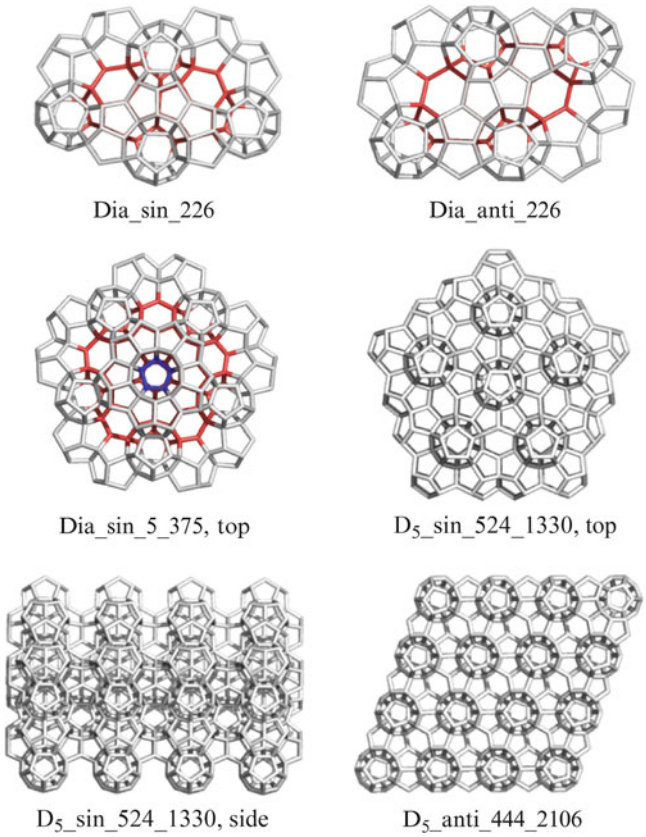

Fig. 19.13 Diamond D_5-related structures

19.4.2 Structures Including Tetrahedra

Space filling by tetrahedra (C_4) and truncated tetrahedra (C_{12}) is well known (Haji-Akbari et al. 2010; Pearson 1972; Conway and Torquato 2006; Kallus et al. 2009). Tetrahedrally close packed structures are encountered in Frank and Kasper (1958) phases (of intermetallic compounds) and in zeolites as well (with SiO_4 or $SiAlO_4$ tetrahedra). A cell of the 600-cell icosahedron-like 4D [3,3,5] polytope consists of five tetrahedra joined around a line (denoted here **4**(5)). Figure 19.14 illustrates arrays of such cells with five- and tenfold symmetry, disposed in hyper-layers (see also Deza et al. 2013). Structure **12**(1)**12′**(20)_84_5 (Fig. 19.15) shows more clear

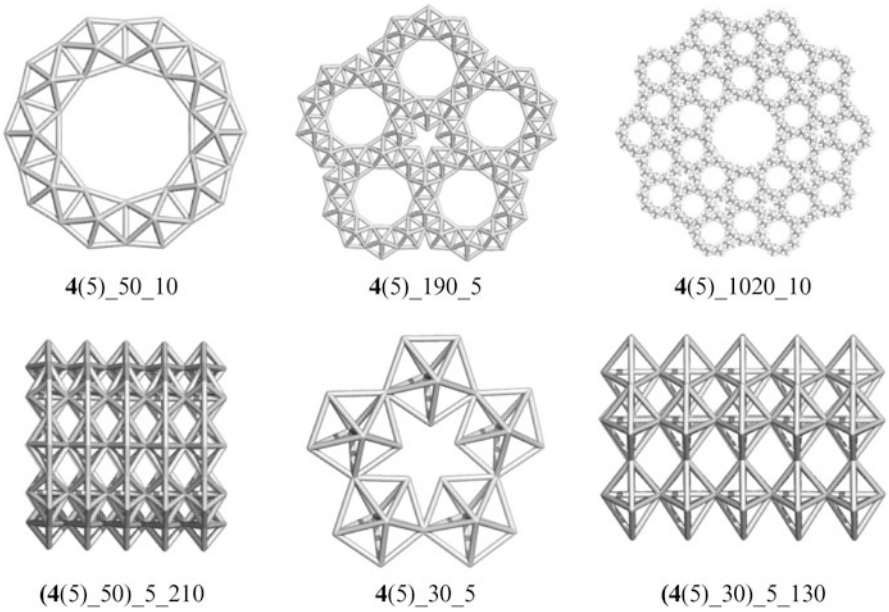

Fig. 19.14 Tetrahedron hyper-sheet layers in ten- and fivefold symmetry

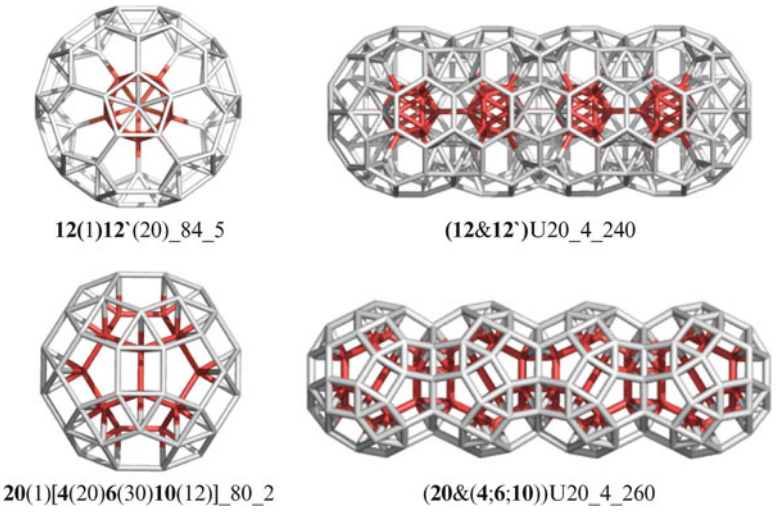

Fig. 19.15 Icosahedral diamonds and corresponding rodlike structures

Table 19.4 Space-filling figures calculation in rodlike (**12**&**12'**)U_{20}_k structures (cf. $f = f_0 - f_1 + f_2 - f_3 = 0$)

k	Atoms	v	e	r_3	r_6	$u = v - e + r - 2$	$c = v - e + r$	f
1	84	84	192	80	50	20	22	0
2	136	136	323	140	85	36	38	0
3	188	188	454	200	120	52	54	0
4	240	240	585	260	155	68	70	0

Table 19.5 Figures calculation in rodlike (**20**&(**4**;**6**;**10**))U_{20}_k structures (cf. $f = f_0 - f_1 + f_2 - f_3 = 0$)

k	Atoms	v	e	r_3	r_4	r_5	$C_4 = 20k - 5(k-1)$	u	c	f
1	80	80	210	80	90	24	20	62	64	0
2	140	140	375	140	165	46	35	114	116	0
3	200	200	540	200	240	68	50	166	168	0
4	260	260	705	260	315	90	65	218	220	0

the cell [3,3,5]: 12 stands for the core icosahedron, while "prime" 12 denotes the truncated tetrahedron. An experimental realization of this cell was brought by Breza et al. (2004) with a beautiful icosahedral diamond. A rodlike structure (**12**&**12'**)U_{20}_4_240 was designed in this respect (Fig. 19.15, top, right; see also Shevchenko 2011).

The dual of **12**(1)**12'**(20)_84 is **20**(1)[**4**(20)**6**(30)**10**(12)]_80 (Fig. 19.15, bottom). Observe its core is the dodecahedron, while the cover is the rhombicosidodecahedron (Med(Med(Ico))); the corresponding rodlike structure is also shown.

Tables 19.4 and 19.5 list figures calculation for the rodlike structures of Fig. 19.15. Note (**12**&**12'**)U_{20}_k is a new 1-periodic net, of the group $P21/m$. The point symbol for this 5-nodal 4,5,6-c net is $\{3^2.4.6^3\}10\ \{3^3.4^2.5.6^4\}5\{3^5.4^5.6^5\}11$. The same group $P21/m$ was assigned for the 5-nodal 5,6-c net (**20**&(**4**;**6**;**10**))U_{20}_k, with the point symbol $\{3^3.4^4.5^3\}3\ \{3^3.4^6.5^5.6\}\ \{3^3.4^6.5^6\}2$.

19.4.3 Structures Including Fullerene C_{60}

By applying the map/net operations on dodecahedral filling space structures like 20(1)(12)_130 and the others illustrated in Fig. 19.12, a mixed tiling system was revealed.

C_{60} can aggregate with itself and some additional carbon atoms, disposed in radial or linear geometries as (1) truncated octahedron C_{24} shares hexagons with itself and the fullerene, while the pentagonal prism C_{10} keeps the distance between the pentagonal faces of fullerene (symbol **60**&**24**&**10**), and (2) fullerene shares with itself a pentagon, while the hexagons are all covered by truncated tetrahedra C_{12} (symbol **60**&**12**). Figure 19.16 illustrates the radial aggregates of **60**&**24**&**10,** while a linear one is shown in Fig. 19.17, top. In the bottom of this figure, the rodlike structure (**60**&**12**)U_{20}_k, $k = 4$ is presented (see also Appendix 19.3).

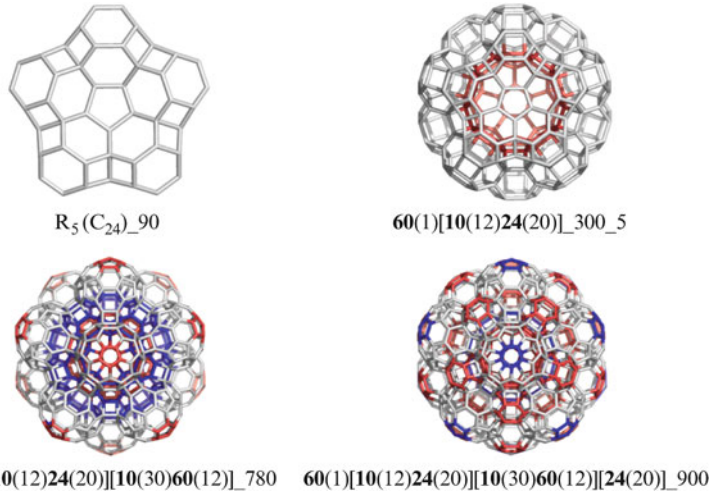

Fig. 19.16 Radial aggregation of **60**&**24**&**10**

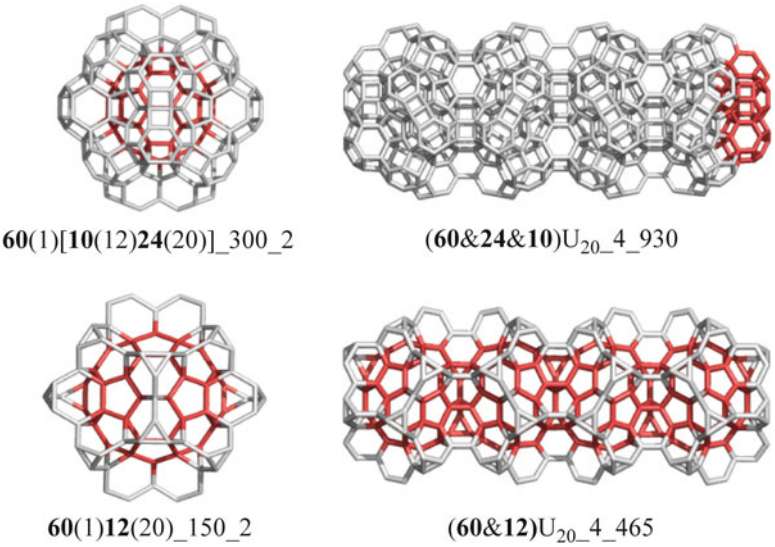

Fig. 19.17 Linear aggregation of **60**&**24**&**10** (*top*) and **60**&**12** (*bottom*) systems

Radial aggregation of **60**&**12** can be easily designed by applying the map operations, for example, *Le*, on the shell structures (see Fig. 19.18). The consistency of these structures was checked as shown in Tables 19.6, 19.7, 19.8.

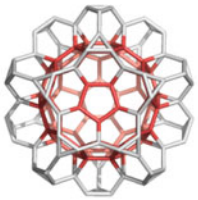

60(1)**12**(20)_150_5

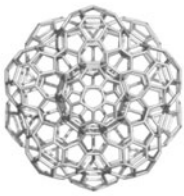

Le(**20**(1)(12))_570 or
60(1)**12**(20)[**12**(20)**60**(12)]_570

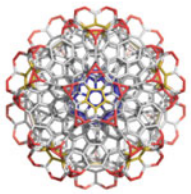

LeX(**20**(1)(12)(20))_870 or
60(1)**12**(20)[**12**(20)**60**(12)]
[**12**(30)**12**(60]_870

Le(**20**(1)(12)(20))_1320 or
60(1)**12**(20)[**12**(20)**60**(12)][**12**(30)**12**(60]
[**60**(20)]_1320

Fig. 19.18 Radial aggregation by **60**&**12**, within leapfrog *Le* map operation

Table 19.6 Radial space filling by **60**&**24**&**10**; structures: (0 = C_{60}); (1 = **60**(1)[**10**(12)**24**(20)]); (2 = **60**(1)[**10**(12)**24**(20)][**10**(30)**60**(12)]); (3 = **60**(1)[**10**(12)**24**(20)][**10**(30)**60c**(12)][**24**(20)])

Shell	v	e	r_4	r_5	r_6	r	24	10	c	c_{60}	$c+1$	f
0	60	90	0	12	20	32	0	0	0	1	2	0
1	300	540	120	24	130	274	20	12	32	1	34	0
2	780	1,380	210	156	310	676	20	42	62	13	76	0
3	900	1,620	270	156	390	816	40	42	82	13	96	0

Table 19.7 Radial space filling by **60**&**12**; structures: (1 = **60**(1)**12**(20)_150); (2 = Le(**20**(1)(12))_570); (3 = LeX(**20**(1)(12)(20))_870); (4 = Le(**20**(1)(12)(20))_1320)

Struct	v	e	r_3	r_5	r_6	$c = v-e+r$	60	$12 = r_6/4$	c(sum)	f
1	150	270	50	12	80	22	1	20	20 + 2	0
2	570	1,020	110	114	280	54	1 + 12	40	40 + 12 + 2	0
3	870	1,650	290	114	520	144	1 + 12	130	130 + 12 + 2	0
4	1,320	2,460	320	264	720	164	1 + 12 + 20	130	130 + 12 + 20 + 2	0

Table 19.8 Linear space filling by (**60**&**12**)U_{20}_k

k	Atoms	v	e	r_3	r_5	r_6	$u = v-e+r-2$	$c = v-e+r$	f
1	150	150	270	50	12	80	20	22	0
2	255	255	465	85	23	140	36	38	0
3	360	360	660	120	34	200	52	54	0
4	465	465	855	155	45	260	68	70	0

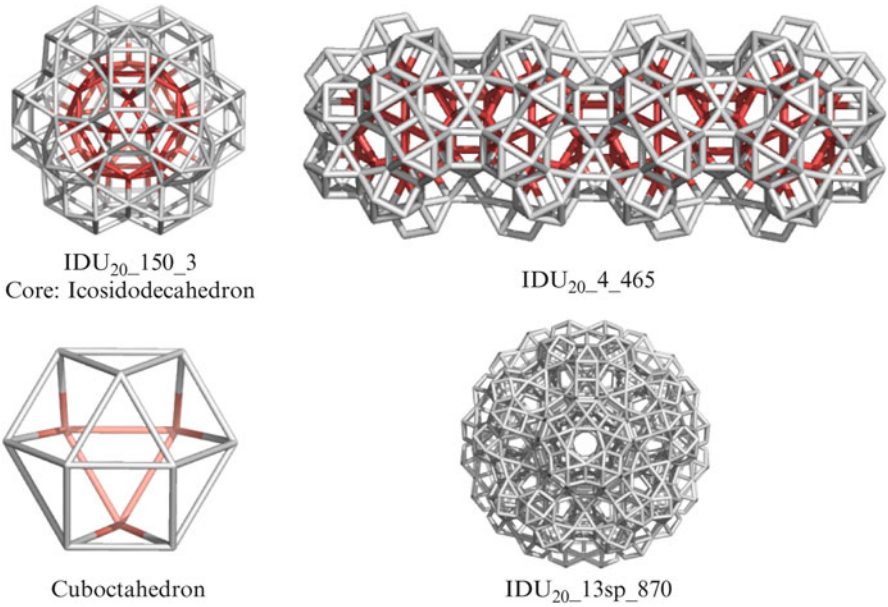

Fig. 19.19 Spongy structure built up by cuboctahedron

The (**60**&**12**)U_{20}_k is a new 8-nodal 3,4-c net and belongs to the Pmma group; it has the symbol net $\{3.5.6^4\}11\{3.6^2\}6\{3.6^4.10\}4$. Also, the 12-nodal 3,4-c 1-periodic (**60**&**24**&**10**)U_{20}_*k* net is a new one and belongs to the Cmcm group; its net symbol is $\{4.6^2\}6\{4^2.5.6^3\}11\{4^2.6^4\}4$.

The energy of carbon structures designed by (**60**&**24**&**10**) and (**60**&**12**) (Figs. 19.16, 19.17, 19.18) has been computed by the DFTB + method (Aradi et al. 2007) and evidenced the most stabilization by aggregation (reference molecule C_{60}) among all the spongy and space-filling structures herein discussed (see Chap. 6, Attila and Diudea, this book).

19.4.4 Other Structures with Icosahedral Symmetry

1. *ID net*. The structures in Fig. 19.19 have as the cage unit the cuboctahedron; the unit IDU_{20} is built up by the sequence *Med*(*Med*(IP)), the iterative medial operation performed on the centered icosahedron, by operating all the rings. Its core is the Archimedean icosidodecahedron, ID = *Med*(Ico)_30. Next, by identifying R_5 of IDU_{20}, one can design either a rodlike or a sphere-like array. The rodlike structure is a new 8-nodal 4,6-c net, of the group *Pmm*2. Its point symbol is $\{3^2.4^2.5^2\}6\{3^3.4^4.5^5.6^3\}8\{3^3.4^4.5^6.6^2\}7$. Genus calculation in these spongy structures is shown in Table 19.9.

Table 19.9 Genus calculation in spongy rod-like U_{20}_k built up by $IDU_{20} =$ Med(Med(IcoP))

IDU_{20}	v	e	f_3	f_4	g	$u = f_4/6$	u^a	g_u	$g = u(g_u - 1) + 1$
IDU_{20}op	150	390	80	120	21	20		2	21
IDU_{20}cl	150	390	100	120	11	20		1.5	11
IDU_{20}_4	465	1,245	260	390	66	65	4(65/80)	21	66
IDU_{20}_13sp	870	2,430	520	780	131	130	13(130/260)	21	131

[a]Ratio in brackets comes out from $u = f_4/6$ (calculated with the counted f_4 faces) and $u = 20$ k, $k = 4;13$, calculated in case of non-coalesced U_{20} units

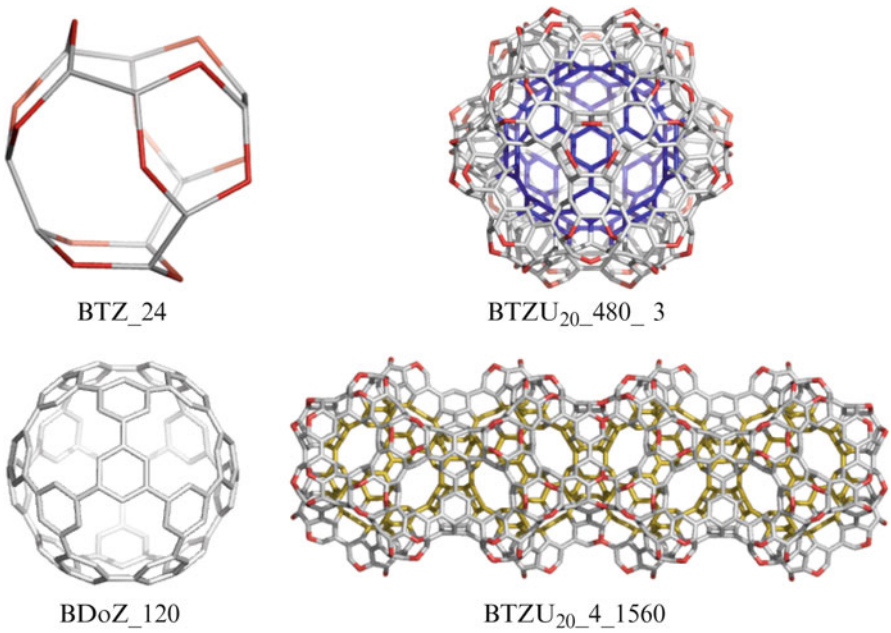

Fig. 19.20 BTZ_24-related structures: U_{20} and its rodlike derivative

2. *Polybenzenes*. The polybenzene unit BTZ_24 can form a hyper-ring R_5 that further arranges in a U_{20} unit (Fig. 19.20, top row); by identifying R_5, either rodlike $BTZU_{20}\_k$ (Fig. 19.20, bottom row) or spherical, both closed (BTZC_1920) or open ($BTZU_{20}$_12sp_3120) structures of fivefold symmetry can be formed (Fig. 19.21, bottom). Figure 19.21 also details the steps to the closed-cage BTZC_1920 (Diudea and Nagy 2007).

The number of tetrahedral units BTZ_24 $= U_1$ in the linear array of BTZ20_k (Table 19.10, entries 3–6) is $u = 20\,k - 5(k-1) = 15\,k + 5$, according to the construction mode. Also, it can be counted as $u = f_6/4$.

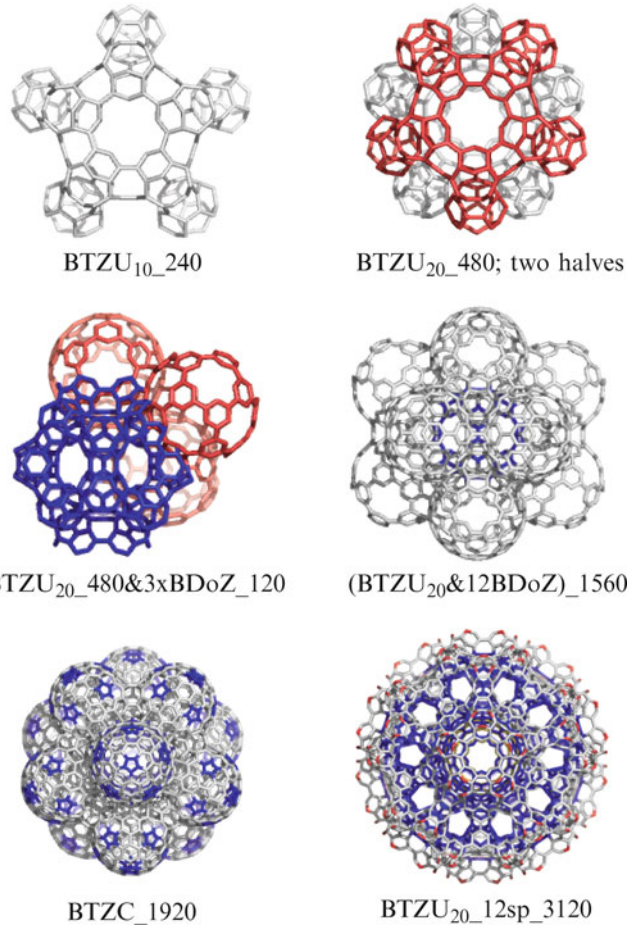

Fig. 19.21 BTZ_24-related structures: U_{20} construction (*top row*); U_{20} coalescence with BDoZ_120 (*middle row*) and the double-shell (*closed-left*; *open-right*) derivatives (*bottom row*)

The data in the last four rows of Table 19.10 prove the following:

Theorem 19.5 *The genus in multi-tori shows the lower bound value in structures of icosahedral symmetry, while the upper bound value is shown in linear structures, providing the same number of identical units.*

$BTZU_{20}\_k$ is a new 1-periodic 20-nodal 3-c net of the group *Pmc*21. Its point symbol is $\{5.6.8\}2\{5.8^2\}3\{6.8^2\}6$.

3. *Penrose-like 3D structures*. The importance of Penrose tiling (Penrose 1978) in the history of icosahedral quasicrystal discovery and in structure elucidation is nowadays well demonstrated (Fujiwara and Ishii 2008).

Table 19.10 Genus calculation in spongy structures built up by polybenzene BTZ_24 unit

BTZ	v	e	f_6	f_8	g	$u = f_6/4$	u^a	g_u	$g = 1 + u(g_u - 1)$
U_1	24	30	4	–	2	1	–	2	2
U_{20}	480	690	80	90	21	20	–	2	21
U_{20}_5	1,920	2,790	320	390	81	80	5(80/100)	21	81
C_1920	1,920	2,880	620	210	30	–	–	–	–
U_{20}_12	4,440	6,465	740	915	186	185	12(185/240)	21	186
U_{20}_12sp	3,120	4,590	520	690	131	130	13(130/260)	21	131

[a]Ratio in brackets comes from $u = f_6/4$ (calculated with the counted f_4 faces) and $u = 20$ k, $k = 5;12;13$, calculated in case of non-coalesced U_{20} units

In this section we present some 3D structures with icosahedral Penrose-type covering designed by the aid of map operations. Two map operations are important in this respect, medial *Med* and dual *Du*, and they work as a "twin" operator. The pair operations can be preceded by any map operation; also the iterative *Med* can be used. Another operation providing rhombohedra is P_4 (as the above pair does); however, in multi-shell structures, it works somehow different.

The dodecahedral star (DoMedˆ2Du_62) and other smaller rhombic cages (e.g., rhombic triacontahedron, rhombic icosahedron) appear as shapes in the icosahedral metallic alloy quasicrystals and were used in modeling (Blatov 2012; De Boissieu 2012; Ishimasa 2008; Yamamoto and Takakura 2008) some high-dimensional complex structures (see also Figs. 19.22, 19.23, 19.24).

The cage DoQMedDu_122 (Fig. 19.22) accommodates twelve rhombic icosahedra, that is, Rico-cages, to build the structure {(DoMedˆ2Du_62)@ DoQMedDu_122)}_164. In the name of complex cages, the first substructure is the core, the last one being the "covering" cage. The complementary smaller cages needed to fill the space = envelope will be specified. The Med-part cage (in the sense of Med&Du operations) of the above one is {(DoMedˆ2_60)@ DoQMed_120 +30)}_210, and all its substructures are in the same Med&Du relation with the substructures of {(DoMedˆ2Du_62)@ DoQMedDu_122)}_164 (even some small differences exists – Fig. 19.22). The equivalence classes of figures in these complex structures are given in Table 19.11 (and illustrated in Appendix 19.4), while the genus calculation in Table 19.12.

The *equivalence classes* of the polytope figures, vertices, edges, faces/rings, and cages, were calculated by our software Nano-Studio (Nagy and Diudea 2009). The routine for vertex classes has two subroutines: (1) one calculates a discriminating topological index for vertices irrespective of their degree or local environment and (2) the second one looks for the (hard) rings that surround each verte20. In this respect, the initially possible degenerate classes given by ring counting were split according to the global topological index discrimination. For edge classes, one provides the medial *Med*(G) of which vertices represent the edges in the parent graph. For faces, one dualizes the parent graph, of which faces are vertices in *Du*(G).

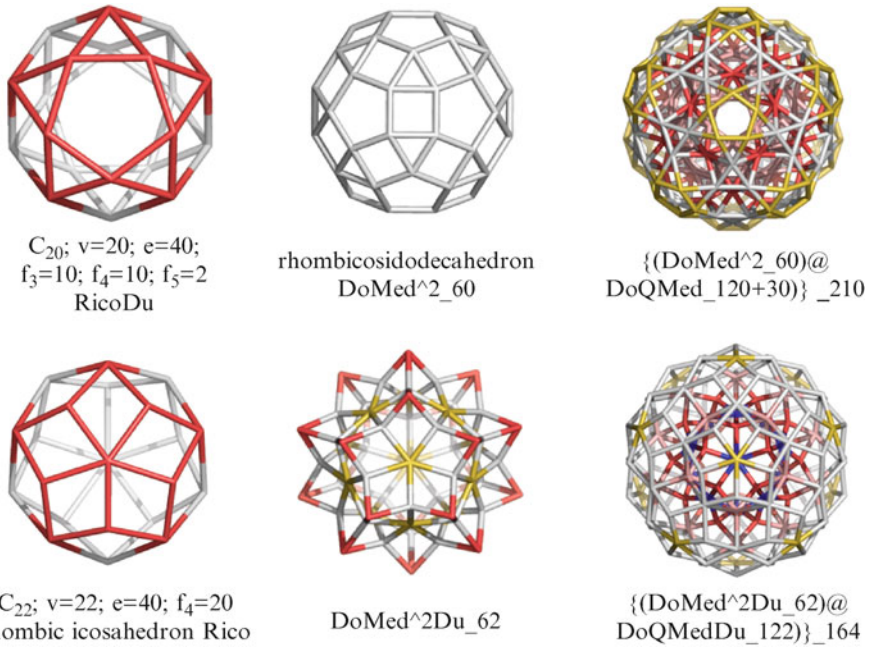

Fig. 19.22 Penrose-like tiling on structures derived from rhombic icosahedron

The pair structures 13DoMed_230 and 13DoMedDuX_374 (Fig. 19.23) were designed by applying the map/net operations (see their name) on the double-shell structure of 13 dodecahedra 13Do_130 (also named here **20**(1)(12)_130). Dualization of a multi-shell cage provides a rather complicated structure. In view of a clear illustration of the involved relation Med-Du, we deleted some additional bonds (see "X" letter), as in the case of 13DoMedDuX_374. This structure suggests a way of aggregation (see Shevchenko 2012) of 13 units of rhombic triacontahedra (a spongy cage of genus $g = 9$, Table 19.12), by identifying atoms of connectivity 5. By deleting the central cage, the remained empty cage 13DoMedDuXc_354 shows $g = 4$.

Finally, by applying the Med-operation on all edges of the triple-shell 33Do_270 cage (also named above **20**(1)(12)(20)_270), a beautiful structure is obtained (Fig. 19.24). It is an aggregate of icosidodecahedra, as is the above-mentioned double-shell cage 13DoMed_230. For these multi-shell structures, the figure equivalence classes include the vertex classification by their surrounding hard rings (given, in these two cases, in decreasing order of vertex centrality). Such complex structures can also be understood as arrays of tetrahedral units, as shown in Fig. 19.24, right (see also Sects. 19.4.2 and 19.4.3).

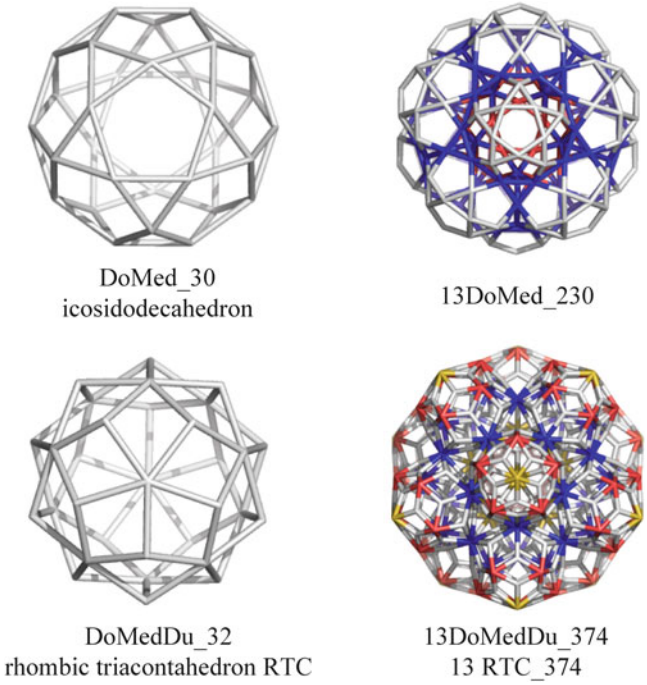

Fig. 19.23 Penrose-like tiling on structures derived from icosahedron

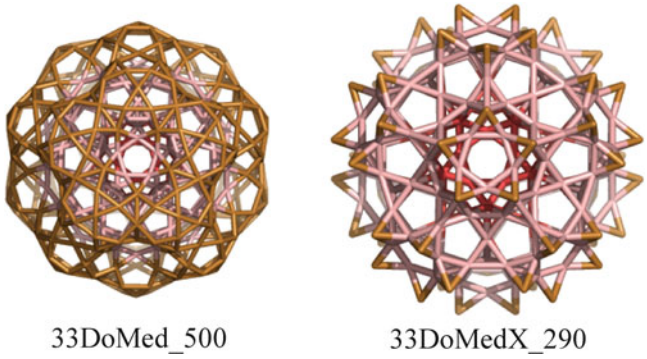

Fig. 19.24 Medial transform of the 33Do multi-shell dodecahedron (*left*) and its multi-tetrahedron structure

Table 19.11 Equivalence classes for the figures of Penrose-like multi-shell cages

Structure	*v*	*e*	*f*
{(DoMedˆ2_60) @DoQMed_120 + 30)}_210	210: $\{30.(60)^3\}$	600: $\{(60)^4.(120)^3\}$	454: $\{(12)^2.(20)^2.30.(60)^6\}$
{(DoMedˆ2Du_62) @DoQMedDu_122)}_164	164: $\{(12)^2.20.(30)^2.60\}$	360: $\{(60)^4.120\}$	210: $\{30.(60)^3\}$
	By rings: $4^9(20).4^7(30).4^5(12.12.30).4^3(60)$		
13DoMed_230	230: $\{20.30.(60)^3\}$	570: $\{30.(60)^5.(120)^2\}$	394: $\{(12)^2.(20).^2 30.(60)^5\}$
{DoMed@12DoMed}_230	By rings: (in decreasing centrality): $3^6.5^3 = 50$: {30.20} $3^5.5^3 = 60$: {60} $3^2.5^2 = 120$: {60.60}		
13DoMedDuX_374	374: $\{(12)^2.20.30.(60)^5$	780: $\{(60)^5.(120)^4\}$	390: {390}
{DoMedDu@12DoMedDu}_374			
33DoMed_500	500: $\{20.(30)^2.(60)^5.120\}$	1,320: $\{(30)^2.(60)^9.(120)^6\}$	984: $\{(12)^2.(20)^3.(30)^2.(60)^{10}.(120)^2\}$
{DoMed@12DoMed@20DoMed}_500	By rings: (in decreasing centrality): $3^6.5^3 = 230$: $\{30.20.(60)^3\}$ $3^5.5^3 = 60$: {60} $3^4.5^3 = 30$: {30} $3^2.5^2 = 180$: {120.60}		

19.5 Conclusions

Quasicrystals can be seen as aperiodic crystals of which symmetry is incompatible with lattice translation. However, the herein permitted rotational symmetry enables a kind of periodicity, along the rotational axis, a result found in experiments. They could be either spongy or filled structures. In this chapter, the design of some hypothetical structures, in terms of map operations, was presented. We focused on the topology of spongy or filled structures in view of elucidating their (atomic) structure, known being this problem in quasicrystal experimental studies, due to the lack of periodicity. Genus calculation and topological symmetry were the main goals of this study, while the versatile operations on maps, as implemented in our "Cage

Table 19.12 Genus calculation in Penrose-like 3D structures; the name of cages seen as filled ones are given in bold; the only rhombic faces are italicized

Structure	v	e	r_3	r_4	r_5	r_6	$v-e+f-c$	g	Cages c
RicoMed	20	40	10	10	2	0	2	0	
RicoDu	22	40	0	20	0	0	2	0	
DoMed	30	60	20	0	12	0	2	0	
DoMedDu	32	60	0	30	0	0	2	0	
DoMedMed	60	120	20	30	12	0	2	0	
DoMedMedDu	62	120	0	60	0	0	2	0	
DoQMed	120	240	80	0	12	30	2	0	
DoQMedDu	122	240	0	120	0	0	2	0	
DoQMed + 30c12	210	600	280	150	24	0	0	–	12 + 30 + 20 + 2
DoQMedc12	210	480	120	120	24	0	−6	4	–
DoQMedc12_ filled	210	480	120	120	24	20	0	–	12 + 2
DoQMedDuc12_ filled	164	360	0	210	0	0	0	–	12 + 2
13DoMed_ filled	230	570	280	0	114	0	0	–	40 + 12 + 2
13DoMedDuX	374	780	0	390	0	0	−16	9	–
13DoMedDuXc	354	720	0	360	0	0	−6	4	–
13DoMedDuXc_ filled	354	720	0	360	0	20	0	–	12 + 2
33DoMed_ filled	500	1, 320	720	0	264	0	0	–	130 + 34

Versatile" CVNET software, were the useful tool enabling the structure design. The study on topology and structure assembling was performed by the Nano-Studio software package. In the Appendices, a whole gallery of nanostructures was listed.

Appendices

Appendix 19.1. C_{20} Patterned Structures

Equivalence classes of **20**(20)_250

Vertices (250): **5^6** {60}; **5^5** {30; 60}; **5^3** {20; 60; 20}

(given in decreasing centrality, from top to bottom and from left to right, in the figure below)

Edges (450): {60^5; 30; 120}; *rings/faces* (222): {60^3; 30(tubes); 12 (windows)}

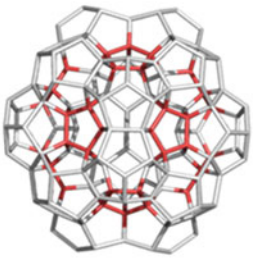

20(20)_250_2
cls 5^6 {60}

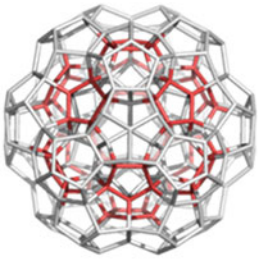

20(20)_250_3

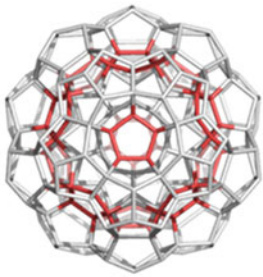

20(20)_250_5

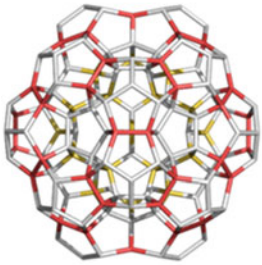

20(20)_250_2
cls 5^5 {30; 60}

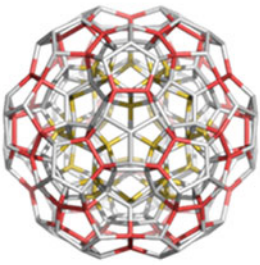

20(20)_250_3

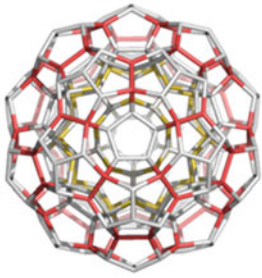

20(20)_250_5

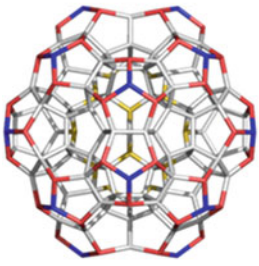

20(20)_250_2
cls 5^3 {20; 60; 20}

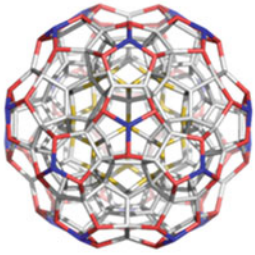

20(20)_250_3

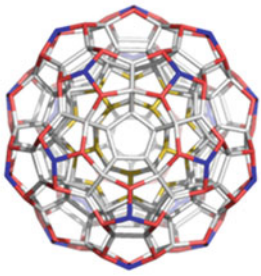

20(20)_250_5

Vertex equivalence classes of **20**(1)(12)(20)_270: 5^6{20; 20; 30; 60}; 5^5 {60}; 5^3 {60; 20}

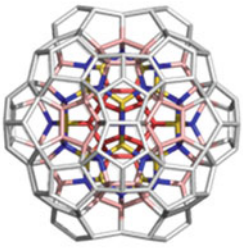

20(1)(12)(20)_270_2
cls 5^6
{20; 20; 30; 60}

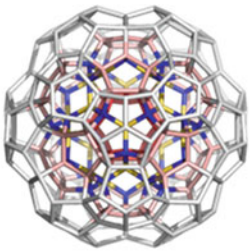

20(1)(12)(20)_270_3

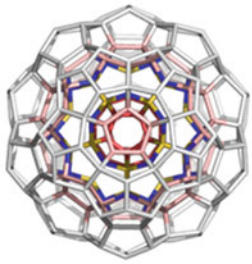

20(1)(12)(20)_270_5

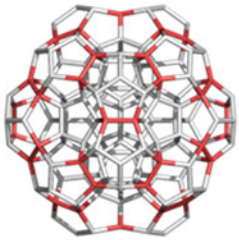

20(1)(12)(20)_270_2
cls 5^5 {60}

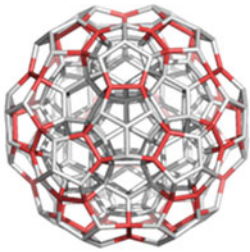

20(1)(12)(20)_270_3

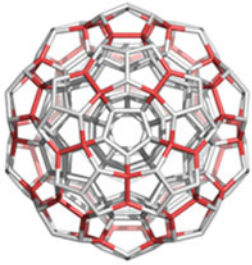

20(1)(12)(20)_270_5

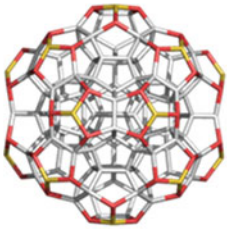

20(1)(12)(20)_270_2
cls 5^3 {60; 20}

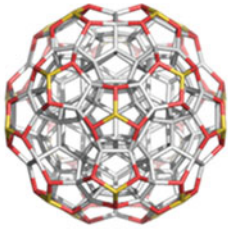

20(1)(12)(20)_270_3

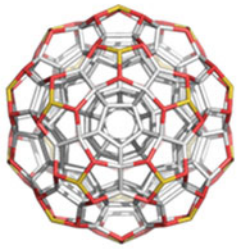

20(1)(12)(20)_270_5

C_{20} patterned structures_1

20(1)_20_2

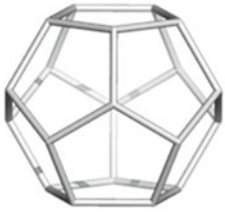

20(1)_20_3

20(1)_20_5

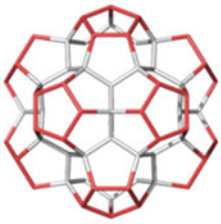

DoP4TRS_110_2

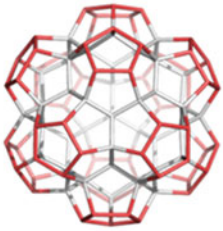

DoP4TRS_110_3

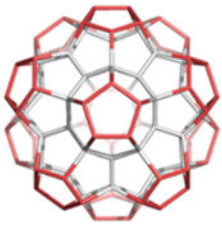

DoP4TRS_110_5

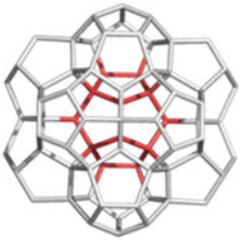

20(1)(12)_130_2

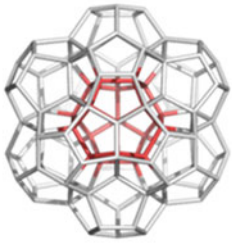

20(1)(12)_130_3

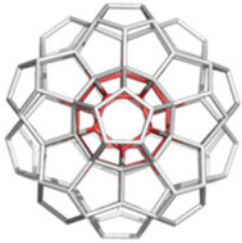

20(1)(12)_130_5

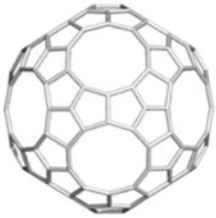

DoS_2_140_2

DoS_2_140_3

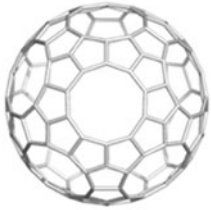

DoS_2_140_5

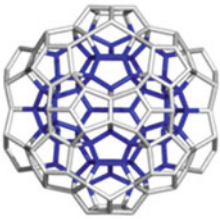

20(20)_250_2; also
(DoS_2_140+ DoP4TRS_110)

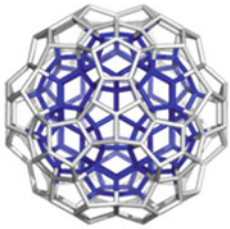

20(20)_250_3

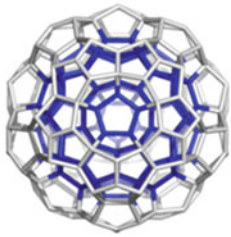

20(20)_250_5

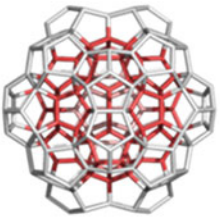

20(33)_270_2; also
(DoS_2_140÷ **20**(1)(12)_130)
(**20**(1)_20÷**20**(20)_250)

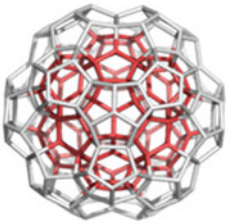

20(33)_270_3
also 33Do_270_3

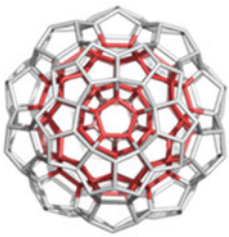

20(33)_270_5
also 33Do_270_5

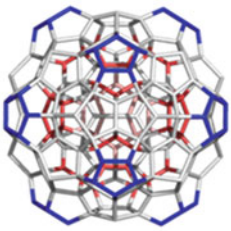

20(1)(12)(20)(12)_330_2

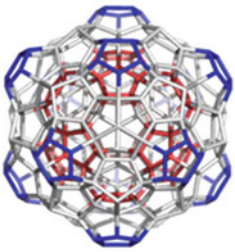

20(1)(12)(20)(12)_330_3

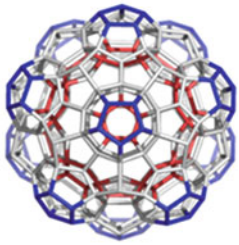

20(1)(12)(20)(12)_330_5

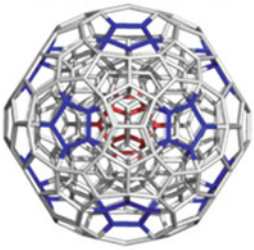

20(1)(12)(20)(12)(30)_470_2
5^6; {350}
({20^2; 30; 60^3;20;60;20})
5^5; {60}
5^3; {60}

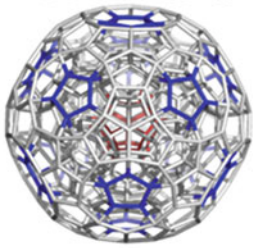

20(1)(12)(20)(12)(30)_
470_3

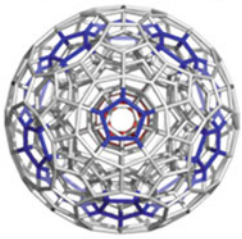

20(1)(12)(20)(12)(30)_
470_5

C_{20} – transformed structures_2

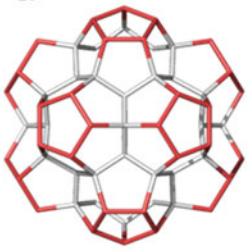

DoP4TRS1_110_2

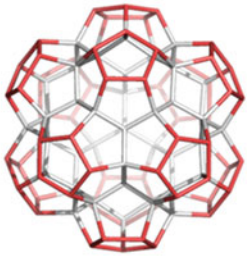

DoP4TRS1_110_3

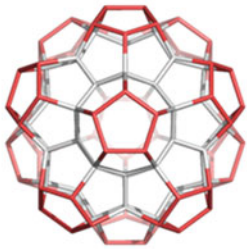

DoP4TRS1_110_5

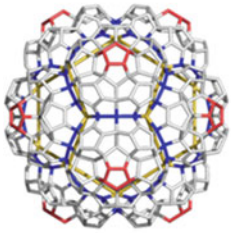

DoP4TRS2_650_2

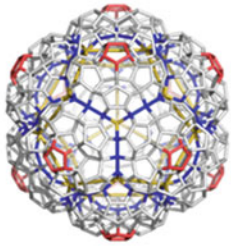

DoP4TRS2_650_3

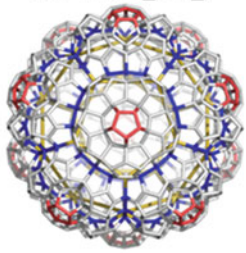

DoP4TRS2_650_5

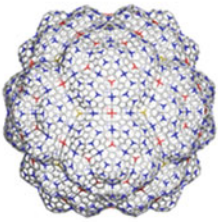

DoP4TRS3_3890_2

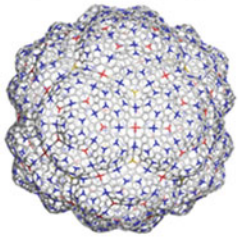

DoP4TRS3_3890_3

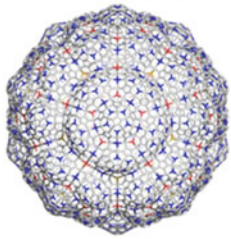

DoP4TRS3_3890_5

C_{20} – transformed structures_2

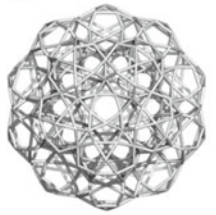

20(20)_Med_450

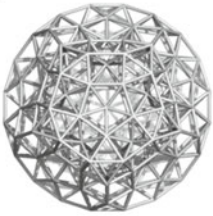

20(20)_Du_222

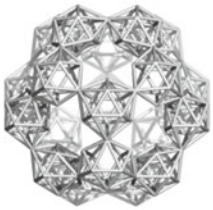

20(20)_Dux_210

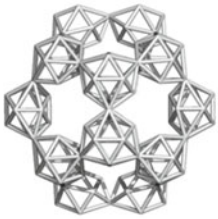

20(20)_DuX_210_2

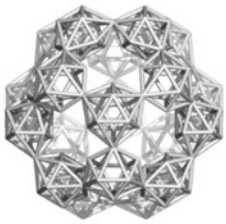

20(20)_DuX_210_3

20(20)_DuX_210_5

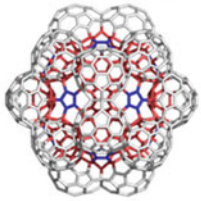

20(20)_250_Le_1110_2

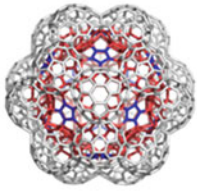

20(20)_250_Le_1110_3

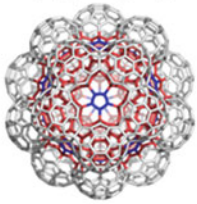

20(20)_250_Le_1110_5

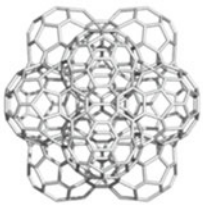

20(1)(12)_130_Le_570_2

20(1)(12)_130_Le_570_3

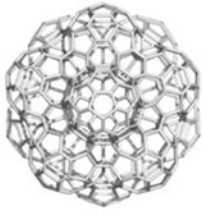

20(1)(12)_130_Le_570_5

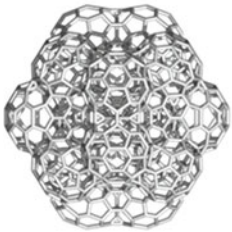

20(1)(12)(20)_270_
Le_1320_2

20(1)(12)(20)_270_
Le_1320_3

20(1)(12)(20)_270_
Le_1320_5

Appendix 19.2. C_{28} Patterned Structures

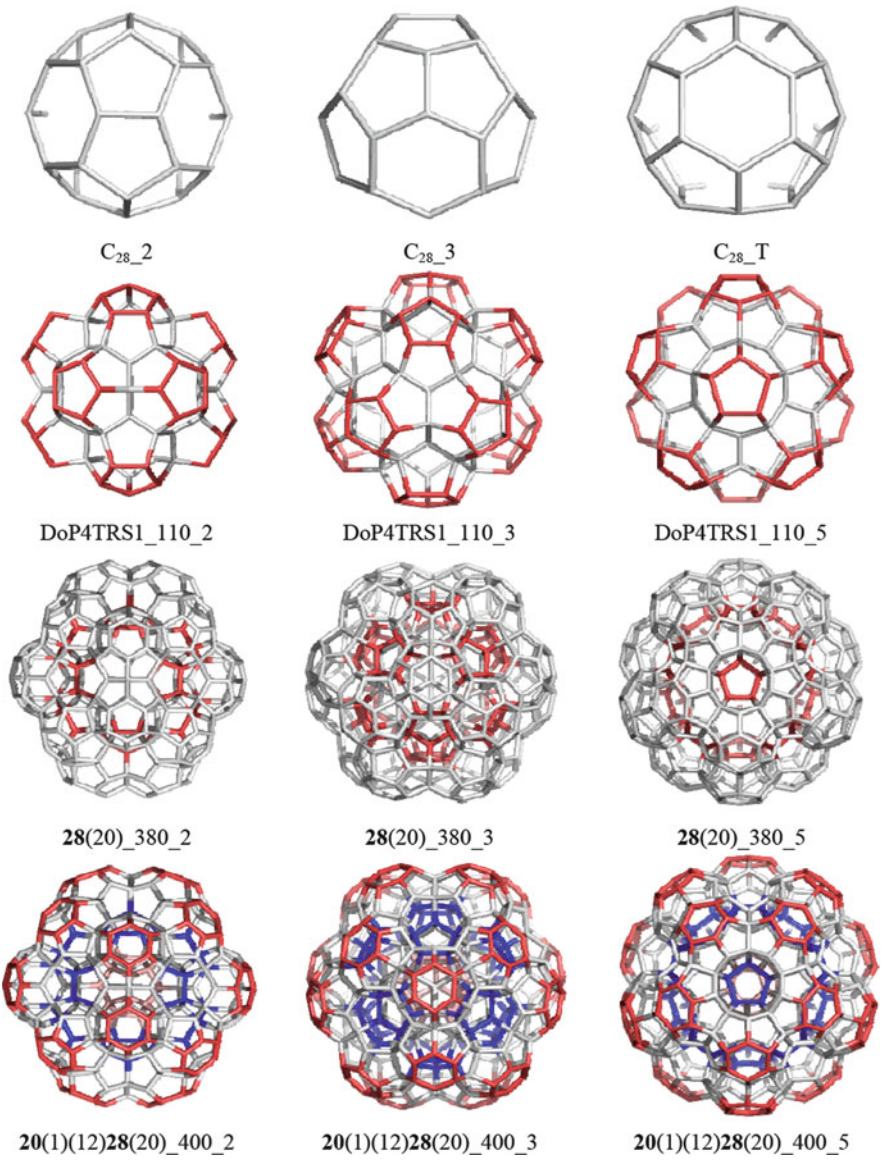

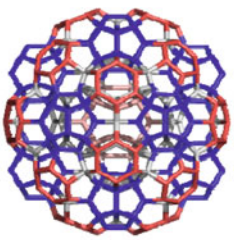

20(1)(12)**28**(20)**20**(12)
_460_2

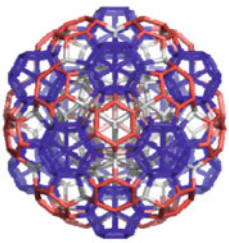

20(1)(12)**28**(20)**20**(12)
_460_3

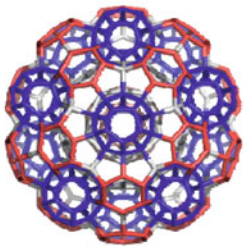

20(1)(12)**28**(20)**20**(12)
_460_5

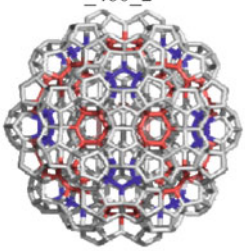

20(1)(12)**28**(20)**20**(12)
20(60)_880_2

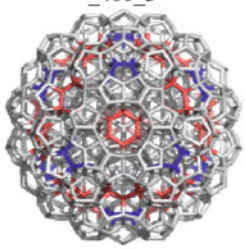

20(1)(12)**28**(20)**20**(12)
20(60)_880_3

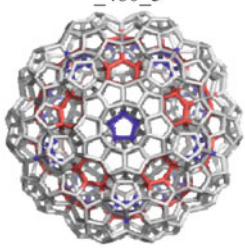

20(1)(12)**28**(20)**20**(12)
20(60)_880_5

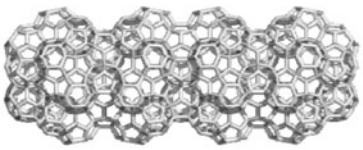

28(20)_U_{20}_4_1190

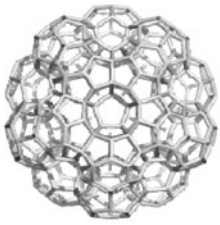

28(20)_U_{20}_1_380

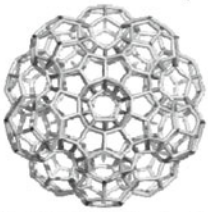

20(1)(12)**28**(20)U_{20}_1_400

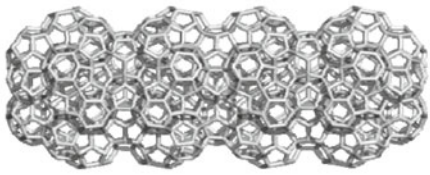

20(1)(12)**28**(20)_U_{20}_4_1270

C_{20} and C_{28} patterned structures: Diamond D_5

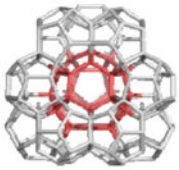

Ada_158

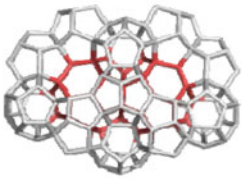

Dia_sin_226

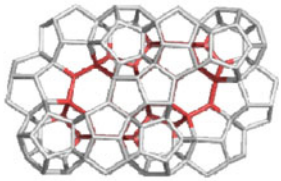

Dia_anti_226

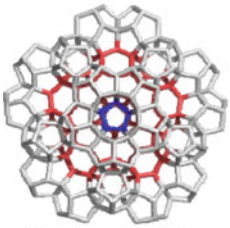

Dia_sin_5_375, top

D_5_sin_411_1330, top

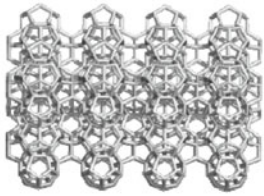

D_5_sin_411_1330, side

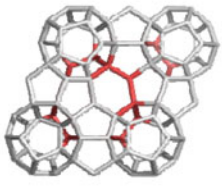

Dia_anti_226, top

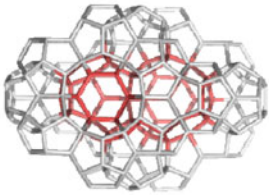

Dia_anti, side_226

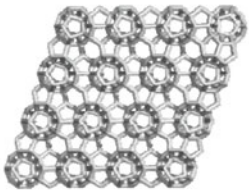

D_5_anti_444_2106

Appendix 19.3. Truncated Octahedron 24 = C_{24} Patterned Structures

24_2

24_3

24_4

C_{60}_2

C_{60}_3

C_{60}_5

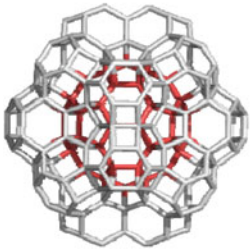

60(1)**24**(20)**10**(12)_300_2

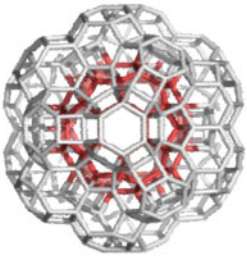

60(1)**24**(20)**10**(12)_300_3

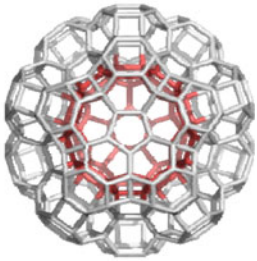

60(1)**24**(20)**10**(12)_300_5

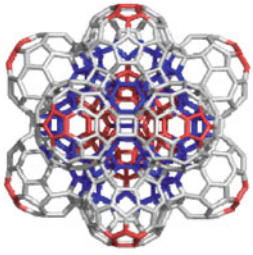

60(1)**24**(20)**10**(12)**60**(12)
_780_2

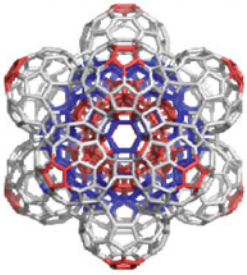

60(1)**24**(20)**10**(12)**60**(12)
_780_3

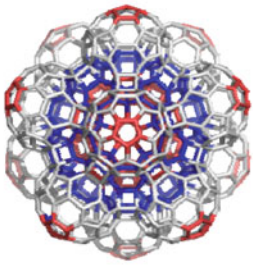

60(1)**24**(20)**10**(12)**60**(12)
_780_5

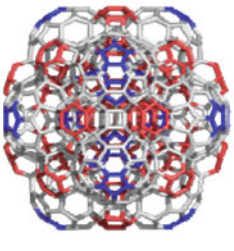

60(1)**24**(20)**10**(12)**60**(12)
24(20)_900_2

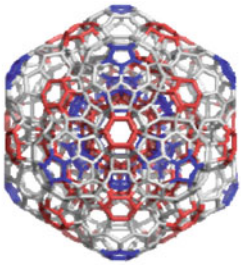

60(1)**24**(20)**10**(12)**60**(12)
24(20)_900_3

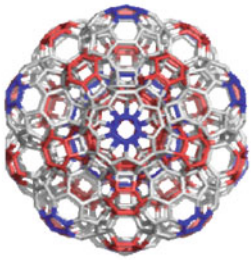

60(1)**24**(20)**10**(12)**60**(12)
24(20)_900_5

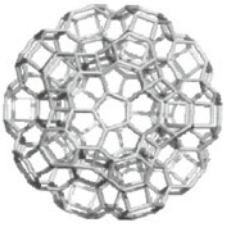

60(1)**24**(20)**10**(12)U_{20}
_1_300

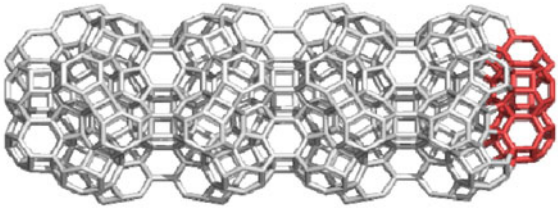

60(1)**24**(20)**10**(12)_ U_{20}_4_930

Truncated Tetrahedron 12 Patterned Structures

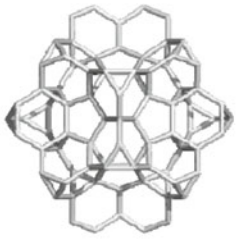

60(1)**12**(20)_150_2

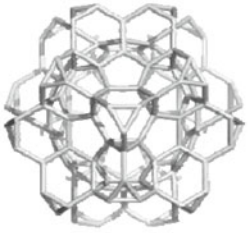

60(1)**12**(20)_150_3

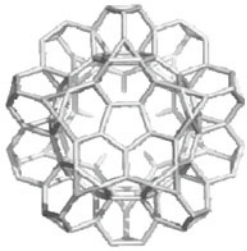

60(1)**12**(20)_150_5

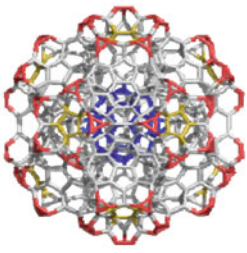

60_12_870_2

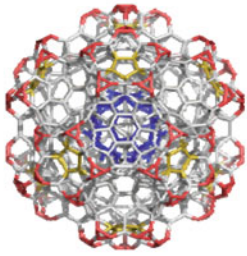

60_12_870_3

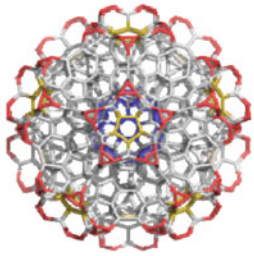

60_12_870_5

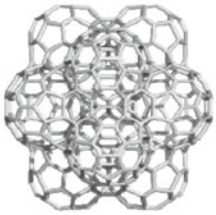

Le(**20**(1)(12))_570_2

Le(**20**(1)(12)_570_3

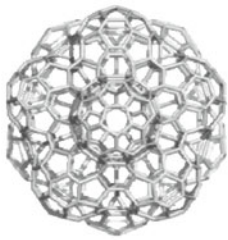

Le(**20**(1)(12)_570_5

Le(**20**(1)(12)(20))_1320_2

Le(**20**(1)(12)(20))_1320_3

Le(**20**(1)(12)(20))_1320_5

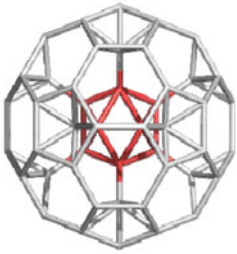

12(1)**12**`(20)_84_2

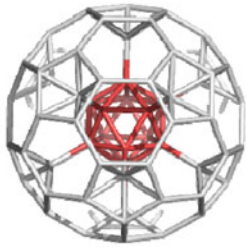

12(1)**12**`(20)_84_3

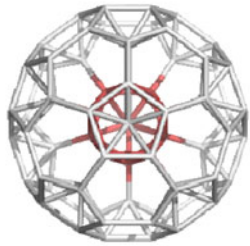

12(1)**12**`(20)_84_5

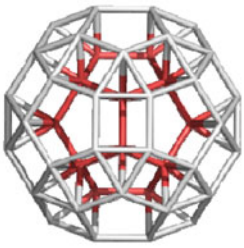

20(1)[**4**(20)**6**(30)**10**(12)]_80_2

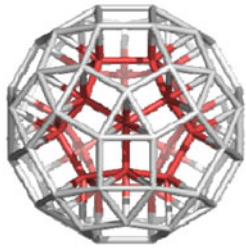

20(1)[**4**(20)**6**(30)**10**(12)]_80_3

20(1)[**4**(20)**6**(30)**10**(12)]_80_5

Appendix 19.4. Penrose-Like 3D Structures: Designed by Dualization of Medials Du(Med(M))

DoMed_30_2

DoMed_30_3

DoMed_30_5

DoMedDu_32_2

DoMedDu_32_3

DoMedDu_32_5
Rhombic Triacontahedron

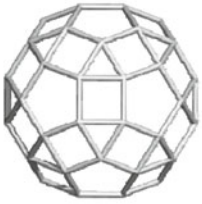

DoMed^2_60_2
Rhombicosi
dodecahedron RID

DoMed^2_60_3

DoMed^2 _60_5

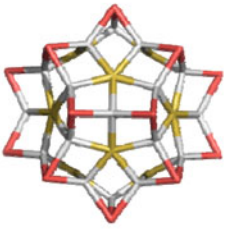

DoMed^2 Du_62_2

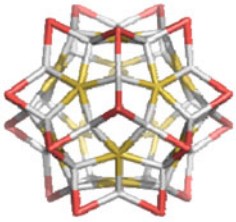

DoMed^2 Du_62_3

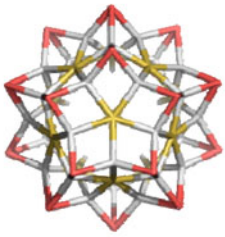

DoMed^2Du_62_5

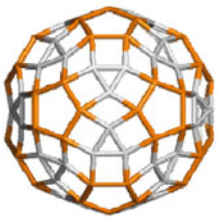

DoMed^3_120_2

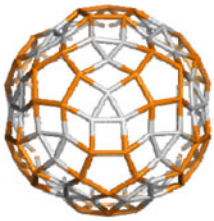

DoMed^3_120_3

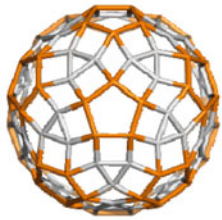

DoMed^3_120_5

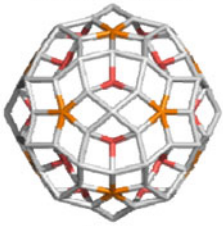

DoMed^3Du_122_2

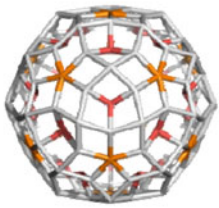

DoMed^3Du_122_3

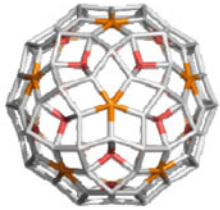

DoMed^3Du_122_5

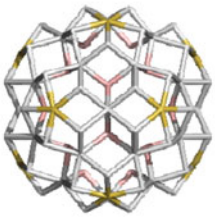

DoQMedDu_122_2

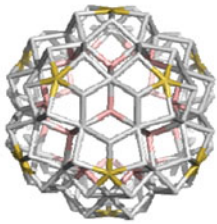

DoQMedDu_122_3

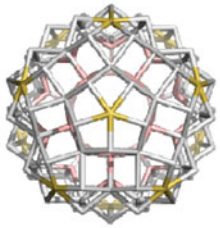

DoQMedDu_122_5

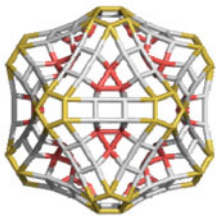

DoMed^4_240_2

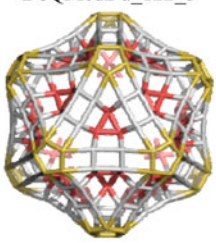

DoMed^4_240_3

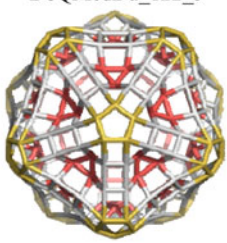

DoMed^4_240_5

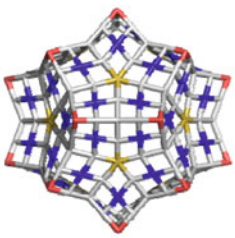

DoMed^4Du _242_2

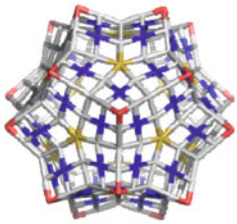

DoMed^4Du _242_3

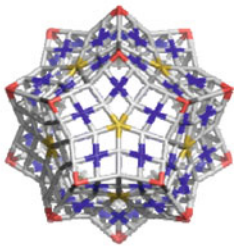

DoMed^4Du_242_5

Equivalence classes of: {(DoMed^2Du_62)@DoQMedDu_122)}_**164**

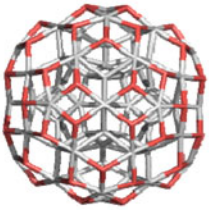

Class 1: (4^3(60))_2

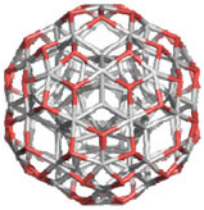

Class 1: (4^3(60))_3

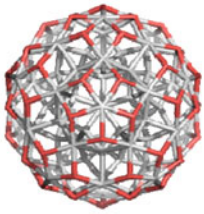

Class 1: (4^3(60))_5

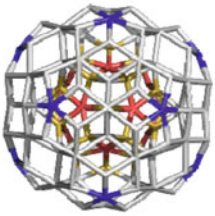

Class 2: (4^5(12.12.30))_2

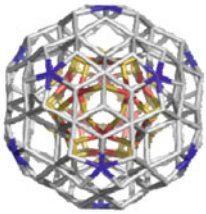

Class 2: (4^5(12.12.30))_3

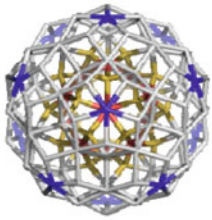

Class 2: (4^5(12.12.30))_5

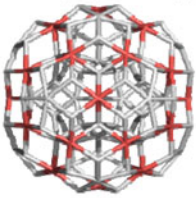

Class 3: (4^7(30))_2

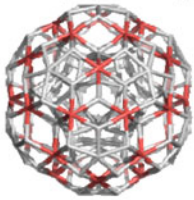

Class 3: (4^7(30))_3

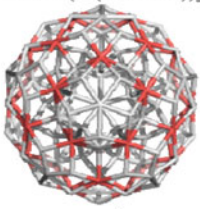

Class 3: (4^7(30))_5

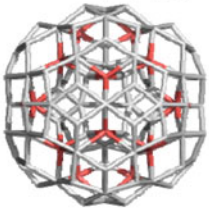

Class 4:(4^9(20))_2

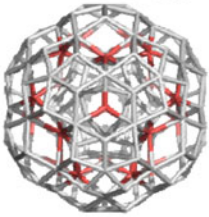

Class 4:(4^9(20))_3

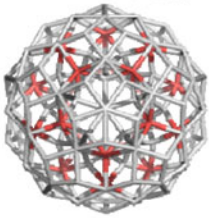

Class 4:(4^9(20))_5

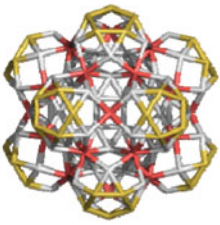

{(DoMed^2_60)@ DoQMed_120+30)} **_210_2**

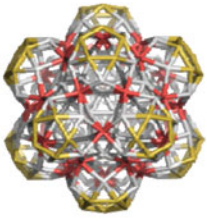

{(DoMed^2_60)@ DoQMed_120+30)} **_210_3**

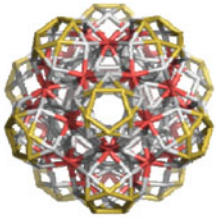

{(DoMed^2_60)@ DoQMed_120+30)} **_210_5**

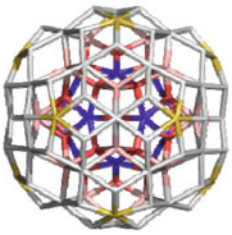

{(DoMed^2Du_62)@ DoQMedDu_122)}_**164_2**

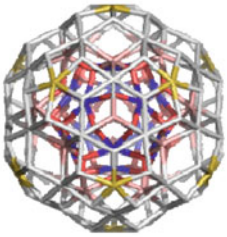

{(DoMed^2Du_62)@ DoQMedDu_122)}_**164_3**

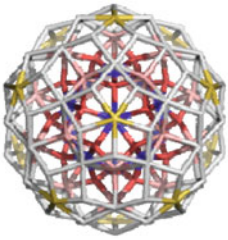

{(DoMed^2Du_62)@ DoQMedDu_122)}_**164_5**

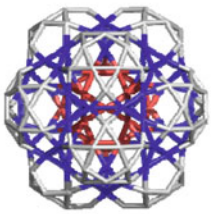

13DoMed_230_2

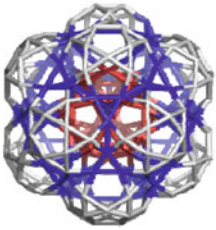

13DoMed_230_3

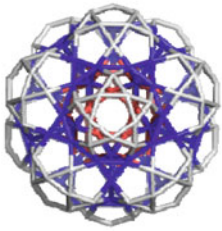

13DoMed_230_5

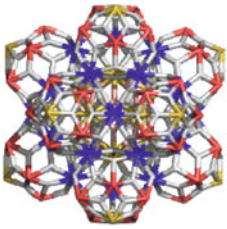

13 RTC_374_2

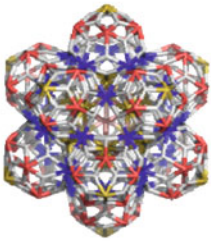

13 RTC_374_3

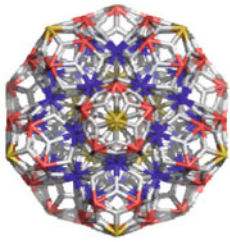

13 RTC_374_5
13DoMedDu_374_5

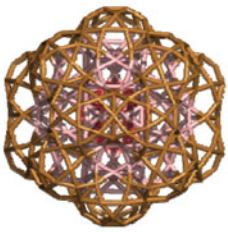

33DoMed_500_2

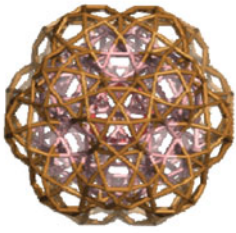

33DoMed3500_5

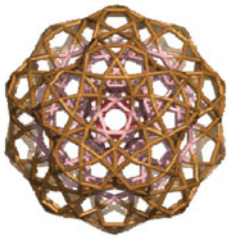

33DoMed_500_5

Equivalence classes of: 13DoMed_**230 (in increased atom centrality)**

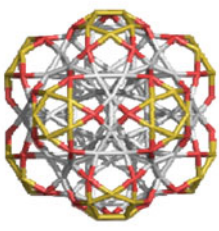

Class 1: $3^2.5^2$; {60.60})_2

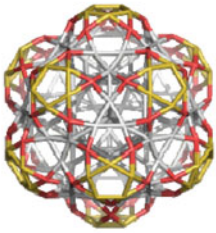

Class 1: _3

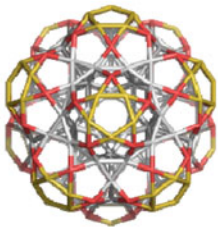

Class 1:_5

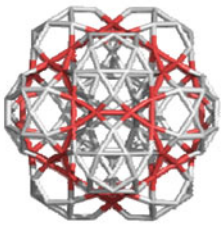

Class 2: $3^5.5^3$; {60}_2

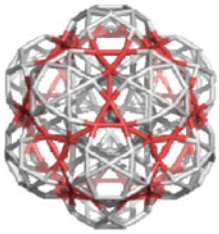

Class 2_3

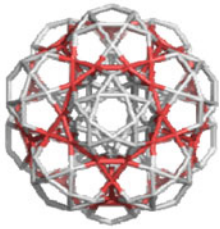

Class 2_5

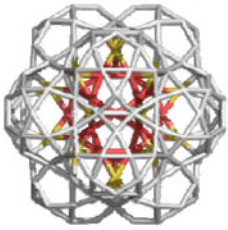

Class 3: $3^6.5^3$;{30.20}_2

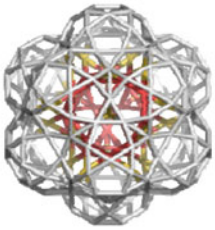

Class 3_3

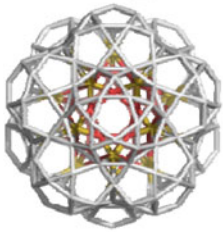

Class 3_5

Equivalence classes of : 33DoMed_**500**

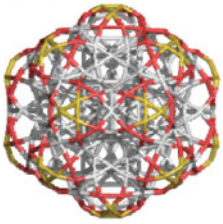

Class 1: $3^2.5^2$; {120.60}_2

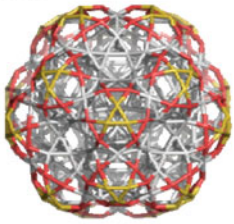

Class 1: _3

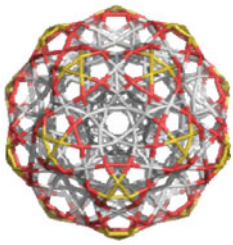

Class 1:_5

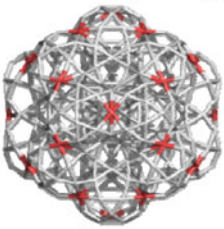

Class 2: $3^4.5^3$; {30}_2

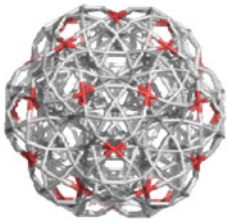

Class 2: _3

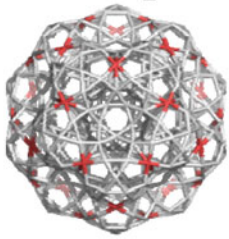

Class 2:_5

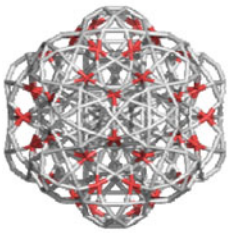

Class 3: $3^5.5^3$; {60}_2

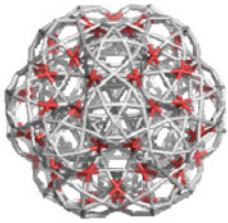

Class 3: _3

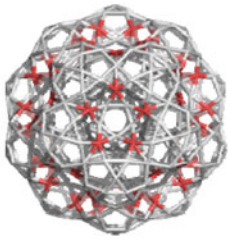

Class 3:_5

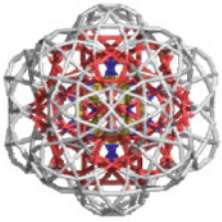

Class 4: $3^6.5^3$; $\{30.20.(60)^3\}$_2

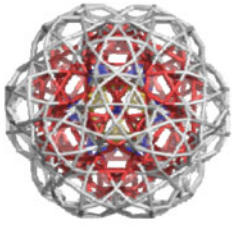

Class 4: _3

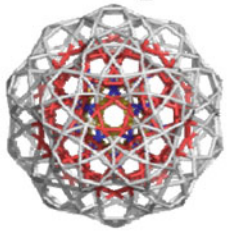

Class 4:_5

References

Aradi B, Hourahine B, Frauenheim T (2007) DFTB$^+$, a sparse matrix-based implementation of the DFTB method. J Phys Chem A 111:5678–5684

Baake M, Kösters H (2011) Random point sets and their diffraction. Philos Mag 91:2671–2679

Baake M, Moody RV (2000) Directions in mathematical quasicrystals. American Mathematical Society, Providence

Baake M, Grimm U, Moody RV (2002) What is aperiodic order? arXiv:math/0203252

Bak P (1986) Icosahedral crystals: where are the atoms? Phys Rev Lett 56:861–864

Bendersky L (1985) Quasicrystal with one–dimensional translational symmetry and a tenfold rotation axis. Phys Rev Lett 55:1461–1463

Benedek G, Colombo L (1996) Hollow diamonds from fullerenes. Mater Sci Forum 232:247–274

Benedek G, Vahedi-Tafreshi H, Barborini E, Piseri P, Milani P, Ducati C, Robertson J (2003) The structure of negatively curved spongy carbon. Diam Relat Mater 12:768–773

Benedek G, Bernasconi M, Cinquanta E, D'Alessio L, De Corato M (2011) The topological background of schwarzite physics. In: Cataldo F, Graovac A, Ori O (eds) The mathematics and topology of fullerenes. Springer, Dordrecht, pp 217–247

Bindi L, Steinhardt PJ, Yao N, Lu PJ (2009) Natural quasicrystals. Science 324:1306–1309

Bindi L, Steinhardt PJ, Yao N, Lu PJ (2011) Icosahedrite, $Al_{63}Cu_{24}Fe_{13}$, the first natural quasicrystal. Am Mineral 96:928–931

Blasé X, Benedek G, Bernasconi M (2010) Structural, mechanical, and superconducting properties of clathrates. In: Colombo L, Fasolino A (eds) Computer-based modeling of novel carbon systems and their properties. Carbon materials: chemistry and physics 3. Springer, Dordrecht

Blatov VA (2012) Nanocluster analysis of intermetallic structures with the program package TOPOS. Struct Chem 23:955–963

Bonnet O (1853) Note sur la therorie generale des surfaces. C R Acad Sci Paris 37:529–532

Breza J, Kadlečikova M, Vojs M, Michalka M, Vesely M, Danis T (2004) Diamond icosahedron on a TiN-coated steel substrate. Microelectron J 35:709–712

Burns MM, Fournier J-M, Golovchenko JA (1990) Optical matter: crystallization and binding in intense optical fields. Science 249:749–754

Ceulemans A, King RB, Bovin SA, Rogers KM, Troisi A, Fowler PW (1999) The heptakisoctahedral group and its relevance to carbon allotropes with negative curvature. J Math Chem 26:101–123

Cigher S, Diudea MV (2006) Omega counter. Babes-Bolyai Univ, Cluj

Conway JH, Torquato S (2006) Packing, tiling and covering with tetrahedral. Proc Natl Acad Sci 103:10612–10617

Coxeter HSM (1958) Close-packing and so forth. Ill J Math 2:746–758

Coxeter HSM (1961) Close packing of equal spheres. In: Coxeter HSM (ed) Introduction to geometry, 2nd edn. Wiley, New York, pp 405–411

Coxeter HSM (1973) Regular polytopes, 3rd edn. Dover Publications, New York

Dandoloff R, Döhler G, Bilz H (1980) Bond charge model of amorphous tetrahedrally coordinated solids. J Non-Cryst Solids 35–36:537–542

Danzer L (1989) Three-dimensional analogs of the planar Penrose tiling and quasicrystals. Discret Math 76:1–7

De Boissieu M (2012) Atomic structure of quasicrystals. Struct Chem 23:965–976

de Bruijn NG (1981) Algebraic theory of Penrose's non-periodic tilings of the plane, I. Kon Nederl Akad Wetensch Proc Ser A 84:39–66

Deloudi S, Steurer W (2007) Systematic cluster-based modeling of the phases in the stability region of decagonal Al-Co-Ni. Philos Mag 87:2727–2732

Deza M, Shtogrin MI (2003) Octahedrites. Symmetry: Cult Sci Spec Issue Polyhedra Sci Art 11:27–64

Deza M, Dutour-Sikirić M, Shtogrin MI (2013) Fullerene-like spheres with faces of negative curvature, Chapter 13. In: Diamond and related nanostructures. Springer, Dordrecht, pp 249–272
Diudea MV (2003) Capra-a leapfrog related operation on maps. Studia Univ "Babes-Bolyai" 48: 3–16
Diudea MV (2004) Covering forms in nanostructures. Forma (Tokyo) 19:131–163
Diudea MV (2005a) Covering nanostructures. In: Diudea MV (ed) Nanostructures-novel architecture. NOVA, New York, pp 203–242
Diudea MV (2005b) Nanoporous carbon allotropes by septupling map operations. J Chem Inf Model 45:1002–1009
Diudea MV (2010a) Nanomolecules and nanostructures – polynomials and indices. MCM, No 10. University of Kragujevac, Serbia
Diudea MV (2010b) Diamond D_5, a novel allotrope of carbon. Studia Univ Babes-Bolyai Chemia 55:11–17
Diudea MV, John PE (2001) Covering polyhedral tori. MATCH Commun Math Comput Chem 44:103–116
Diudea MV, Nagy CL (2007) Periodic nanostructures. Springer, Dordrecht
Diudea MV, Nagy CL (2012) All pentagonal ring structures related to the C_{20} fullerene: diamond D_5. Diam Relat Mater 23:105–108
Diudea MV, Petitjean M (2008) Symmetry in multi tori. Symmetry Cult Sci 19:285–305
Diudea MV, Schefler B (2012) Nanotube junctions and the genus of multi-tori. Phys Chem Chem Phys 14:8111–8115
Diudea MV, Parv B, Ursu O (2003) TORUS. Babes-Bolyai University, Cluj
Diudea MV, Ştefu M, John PE, Graovac A (2006) Generalized operations on maps. Croat Chem Acta 79:355–362
Eberhard V (1891) Zur Morphologie der polyeder. B. G. Teubner, Leipzig
Euler L (1758) Elementa doctrinae solidorum. Novi Comm Acad Sci Imp Petrop 4:109–160
Fowler PW (1986) How unusual is C_{60}? Magic numbers for carbon clusters. Chem Phys Lett 131:444–450
Frank FC, Kasper JS (1958) Complex alloy structures regarded as sphere packings. Definitions and basic principles. Acta Cryst 11:184–190
Fujiwara T, Ishii Y (2008) Quasicrystals. Elsevier, Amsterdam
Gardner M (2001) Packing spheres. In: The colossal book of mathematics: classic puzzles, paradoxes, and problems. W.W. Norton, New York, pp 128–136
Goldberg M (1937) A class of multi-symmetric polyhedral. Tôhoku Math J 43:104–108
Goldberg M (1971) On the densest packing of equal spheres in a cube. Math Mag 44:199–208
Grünbaum B (1967) Convex polytopes. Wiley, New York
Grünbaum B, Shephard GS (1987) Tilings and patterns. W.H. Freeman, New York
Haji-Akbari A, Engel M, Keys AS, Zheng X, Petschek RG, Palffy-Muhoray P, Glotzer ShC (2010) Disordered, quasicrystalline and crystalline phases of densely packed tetrahedral. arXiv:10125138
Hales TC (1992) The sphere packing problem. J Comput Appl Math 44:41–76
Hales TC (2005) A proof of the Kepler conjecture. Ann Math 162:1065–1185
Hales TC (2006) Historical overview of the Kepler conjecture. Discret Comput Geom 36:5–20
Harary F (1969) Graph theory. Addison-Wesley, Reading
Hargittai I (ed) (1992) Fivefold symmetry. World Scientific, Singapore
Hargittai M, Hargittai I (2010) Symmetry through the eyes of a chemist. Springer, Dordrecht
Hayashida K, Dotera T, Takano T, Matsushita Y (2007) Polymeric quasicrystal:mesoscopic quasicrystalline tiling in ABS star polymers. Phys Rev Lett 98:195502
Hermann C (1949) Kristallographie in Raumen Beiliebiger Dimenzionszahl 1 Die Symmetrieoperationen. Acta Crystallogr 2:139–145
Hyde ST, Ramsden S (2000) Chemical frameworks and hyperbolic tilings. In: Hansen P, Fowler P, Zheng M (eds) Discrete mathematical chemistry. DIMACS series in discrete mathematics and theoretical computer science, vol 51. American Mathematical Society, Providence, pp 203–224

Ishimasa T (2008) New group of icosahedral quasicrystals. In: Fujiwara T, Ishii Y (eds) Quasicrystals. Elsevier, Amsterdam, pp 49–74
Kallus Y, Elser V, Gravel S (2009) A dense periodic packing of tetrahedra with a small repeating unit. arXiv:09105226
Kramer P (1982) Non-periodic central space filling with icosahedral symmetry using copies of seven elementary cells. Acta Cryst A 38:257–264
Lenosky T, Gonze X, Teter M, Elser V (1992) Energetics of negatively curved graphitic carbon. Nature 355:333–335
Levine D, Steinhardt PJ (1984) Quasicrystals: a new class of ordered systems. Phys Rev Lett 53:2477–2480
Mackay AL (1962) A dense non-crystallographic packing of equal spheres. Acta Crystallogr 15:916–918
Mackay AL (1982) Crystallography and the Penrose pattern. Physica 114A:609–613
Mackay AL (1985) Periodic minimal surfaces. Nature 314:604–606
Mackay AL (1987) Quasi-crystals and amorphous materials. J Non-Cryst Solids 97–98:55–62
Mackay AL (1990) Quasicrystals turn to the sixth-dimension. Nature 344:21–21
Mackay AL, Terrones H (1991) Diamond from graphite. Nature 352:762–762
Mackay AL, Terrones H (1993) Hypothetical graphite structures with negative Gaussian curvature. Philos Trans R Soc A 343:113–127
Mikhael J, Roth J, Helden L, Bechinger C (2008) Archimedean-like tiling on decagonal quasicrystalline surfaces. Nature 454:501–504
Müller A, Roy S (2003) En route from the mystery of molybdenum blue via related manipulatable building blocks to aspects of materials science. Coord Chem Rev 245:153–166
Müller A, Kögerler P, Dress AWM (2001) Giant metal-oxide-based spheres and their topology: from pentagonal building blocks to keplerates and unusual spin systems. Coord Chem Rev 222:193–218
Nagy CL, Diudea MV (2005a) Nanoporous carbon structures. In: Diudea MV (ed) Nanostructures – novel architecture. NOVA, New York, pp 311–334
Nagy CL, Diudea MV (2005b) JSChem. Babes-Bolyai University, Cluj
Nagy CL, Diudea MV (2009) NANO-Studio. Babes-Bolyai University, Cluj
O'Keeffe M, Hyde BG (1996) Crystal structures: I. Patterns and symmetry. BookCrafters, Inc, Celsea
O'Keeffe M, Adams GB, Sankey OF (1992) Predicted new low energy forms of carbon. Phys Rev Lett 68:2325–2328
Pearson WB (1972) The crystal chemistry and physics of metals and alloys. Wiley, New York
Penrose R (1978) Pentaplexity. Eureka 39:16–22
Pisanski T, Randić M (2000) Bridges between geometry and graph theory. In: Geometry at work. MAA Notes 53. Mathematical Association of America, Washington, DC, pp 174–194
Ricardo-Chavez JL, Dorantes-Dávila J, Terrones M, Terrones H (1997) Electronic properties of fullerenes with nonpositive Gaussian curvature: finite zeolites. Phys Rev B 56:12143–12146
Romo-Herrera JM, Terrones M, Terrones H, Dag S, Meunier V (2007) Covalent 2D and 3D networks from 1D nanostructures: designing new materials. Nano Lett 7:570–576
Schläfli L (1901) Theorie der vielfachen Kontinuität Zürcher und Furrer, Zürich (Reprinted in: Ludwig Schläfli, 1814–1895, Gesammelte Mathematische Abhandlungen, Band 1, 167–387, Verlag Birkhäuser, Basel, 1950)
Schmiedeberg M, Stark H (2012) Comparing light-induced colloidal quasicrystals with different rotational symmetries. J Phys Condens Matter 24:284101–284106
Schoen AH (1970) Infinite periodic minimal surfaces without self-intersections. NASA Technical Note D–5541
Schwarz HA (1865) Über minimalflächen. Monatsber Berlin Akad, Berlin
Schwarz HA (1890) Gesammelte Matematische Abhandlungen. Springer, Berlin
Shechtman D, Blech I, Gratias D, Cahn JW (1984) Metallic phase with long-range orientational order and no translational symmetry. Phys Rev Lett 53:1951–1953

Shevchenko VY (2011) Search in chemistry, biology and physics of the nanostate. Lema, St Petersburg
Shevchenko VY (2012) What is a chemical substance and how is it formed? Struct Chem 23: 1089–1101
Shevchenko VY, Mackay AL (2008) Geometrical principles of the self-assembly of nanoparticles. Glass Phys Chem 34:1–8
Shevchenko EV, Talapin DV, Kotov NA, O'Brien S, Murray CB (2006a) Structural diversity in binary nanoparticle superlattices. Nature 439:55–59
Shevchenko EV, Talapin DV, Murray CB, O'Brien S (2006b) Structural characterization of self-assembled multifunctional binary nanoparticle superlattices. J Am Chem Soc 128:3620–3637
Socolar JES, Steinhardt PJ, Levine D (1986) Quasicrystals with arbitrary orientational symmetry. Phys Rev B 32:5547–5551
Stefu M, Diudea MV (2005) CageVersatile_CVNET. Babes-Bolyai University, Cluj
Steinhardt PJ (1987) Icosahedral solids: a new phase of matter? Science 238:1242–1247
Steinhardt PJ (1990) Quasi-crystals – a new form of matter. Endeavour 14:112–116
Talapin DV, Shevchenko EV, Bodnarchuk MI, Ye X, Chen J, Murray CB (2009) Quasicrystalline order in self-assembled binary nanoparticle superlattices. Nature 461:964–967
Terrones H, Mackay AL (1993) Triply periodic minimal surfaces decorated with curved graphite. Chem Phys Lett 207:45–50
Terrones H, Mackay AL (1997) From C_{60} to negatively curved graphite. Prog Cryst Growth Charact 34:25–36
Terrones H, Terrones M (1997) Quasiperiodic icosahedral graphite sheets and high-genus fullerenes with nonpositive Gaussian curvature. Phys Rev B 55:9969–9974
Terrones H, Terrones M (2003) Curved nanostructured materials. New J Phys 5:1261–12637, http://www.topos.ssu.samara.ru/index.html
Terrones M, Banhart F, Grobert N, Charlier J-C, Terrones H, Ajayan PM (2002) Molecular junctions by joining single-walled carbon nanotubes. Phys Rev Lett 89:075505(1–4)
Townsend SJ, Lenosky TJ, Muller DA, Nichols CS, Elser V (1992) Negatively curved graphite sheet model of amorphous carbon. Phys Rev Lett 69:921–924
Tsai AP, Inoue A, Masumoto T (1987) A stable quasicrystal in Al-Cu-Fe system. Jpn J Appl Phys 26:L1505–L1507
Tsai AP, Guo JQ, Abe E, Takakura H, Sato TJ (2000) A stable binary quasicrystal. Nature 408:537–538
Valencia F, Romero AH, Hernàndez E, Terrones M, Terrones H (2003) Theoretical characterization of several models of nanoporous carbon. New J Phys 5:1231–12316
Vanderbilt D, Tersoff J (1992) Negative-curvature fullerene analog of C_{60}. Phys Rev Lett 68:511–513
Wells AF (1977) Three-dimensional nets and polyhedral. Wiley, New York
Yamamoto A, Takakura H (2008) Recent development of quasicrystallography. In: Fujiwara T, Ishii Y (eds) Quasicrystals. Elsevier, Amsterdam, pp 11–47
Zeger L, Kaxiras E (1993) New model for icosahedral carbon clusters and the structure of collapsed fullerite. Phys Rev Lett 70:2920–2923
Zeng X, Ungar G, Liu Y, Percec V, Dulcey AE, Hobbs JK (2004) Supramolecular dendritic liquid quasicrystals. Nature 428:157–160
Ziegler GM (1995) Lectures on polytopes. Springer, New York
Zong C, Talbot J (1999) Sphere packings. Springer, New York

Index

M.V. Diudea and C.L. Nagy (eds.), *Diamond and Related Nanostructures*, Carbon Materials: Chemistry and Physics 6, DOI 10.1007/978-94-007-6371-5,